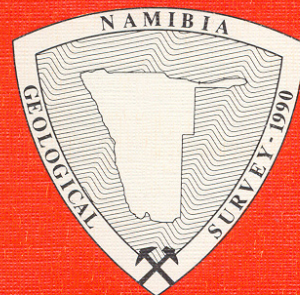


GEOLOGICAL SURVEY OF NAMIBIA

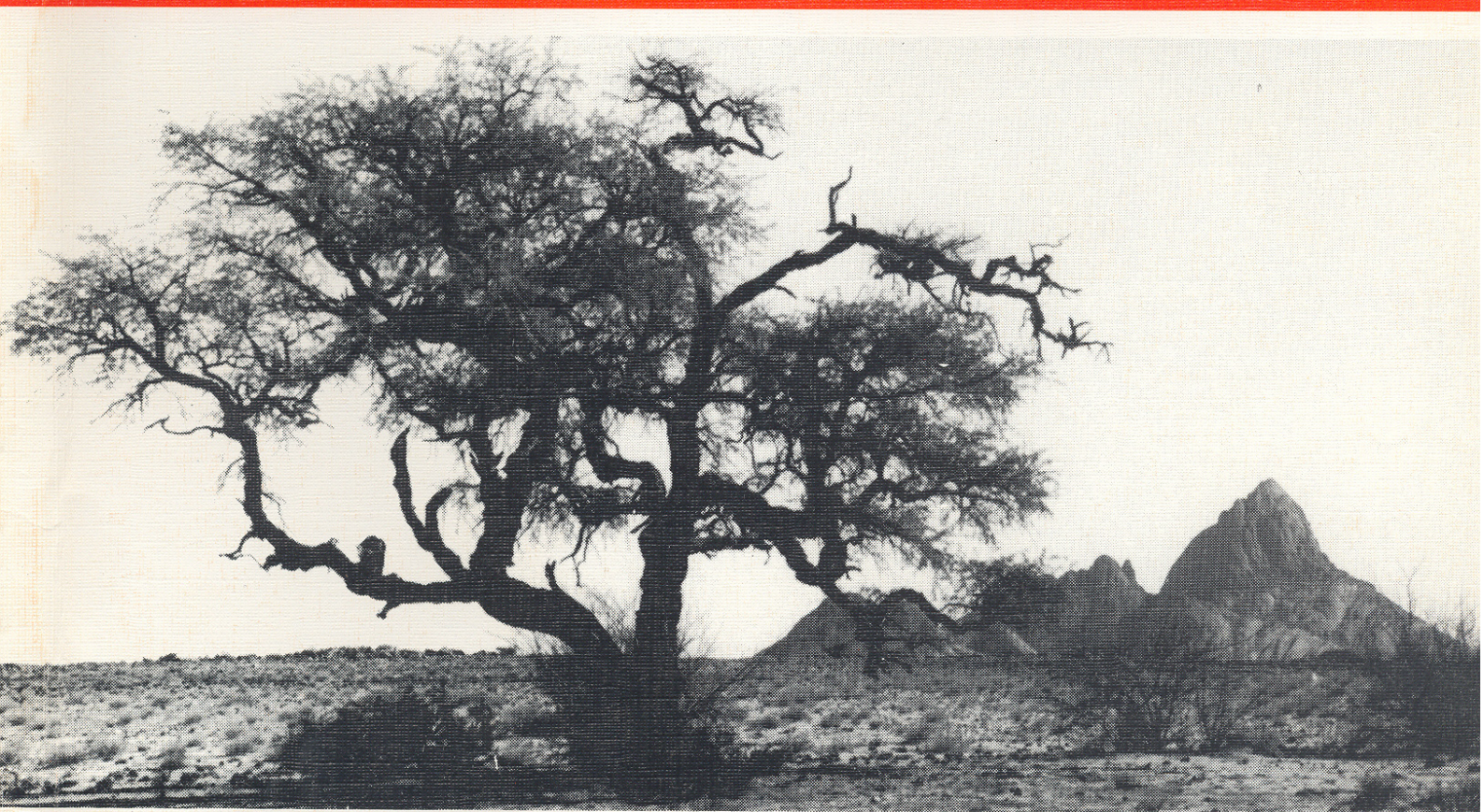
MINISTRY OF MINES AND ENERGY



**A STUDY OF EPIGENETIC MINERALISATION IN THE CENTRAL  
ZONE OF THE DAMARA OROGEN, NAMIBIA, WITH SPECIAL  
REFERENCE TO GOLD, TUNGSTEN, TIN AND RARE EARTH  
ELEMENTS**

by

**N.M. STEVEN**



MEMOIR 16

1993

**Front cover:** View of the Klein Spitzkoppe mountains looking northwards. This post-Karoo granite intrusion into the Central Zone of the Damara Orogen crops out some 60 km west of Usakos (*Photograph by K.Faure*).

**MINISTRY OF MINES AND ENERGY**

**GEOLOGICAL SURVEY OF NAMIBIA**

Director: B. G. Hoal

**MEMOIR 16**

**A study of epigenetic mineralisation in the Central Zone of the Damara Orogen, Namibia, with special reference to gold, tungsten, tin and rare earth elements**

**by**

**Nicholas M. Steven**

Editor: Clare Kennedy Galloway

Obtainable from the Geological Survey  
P.O. Box 2168, Windhoek, Namibia

	Price
Local	(+GST) R20.00
Abroad (Post Free)	R25.00

ISBN 0-86976-264-8

*Copyright reserved*  
**1993**



---

## ABSTRACT

Epigenetic, rare earth element, gold, tin and tungsten, mineralisation in the northeast-trending, intracratonic branch of the deeply eroded, late Proterozoic/early Palaeozoic, Pan-African Damara Orogen is hosted by meta-arkoses, marbles and metaturbidites in the magmatic arc (Central Zone; CZ) of the orogen, a tectono-stratigraphic entity characterised by multiple deformation, green-schist/amphibolite-facies, low-pressure/high-temperature metamorphism and numerous granitic and pegmatitic intrusions. This memoir integrates regional and detailed geological mapping with petrographic studies, whole-rock geochemistry (obtained by X-ray fluorescence spectrometry, atomic absorption spectrometry, fire assay and infrared spectroscopy), mineral chemistry studies (electron microprobe and X-ray diffraction) and geochronological work (Rb-Sr whole-rock and mineral age determinations and Pb-Pb model ages) to examine six examples of metasediment-hosted epigenetic mineralisation in the Usakos-Karibib-Omaruru district, central Namibia. The investigated area straddles the magnetically defined Omaruru Lineament, which divides the CZ into southern (SCZ) and northern (NCZ) portions. Geological mapping and lithostratigraphic work support the geophysical evidence for this subdivision: in the SCZ, predominantly continental and shallow marine Damaran metasediments are floored by a 1.7-2.0 Ga granite gneiss basement inlier, that is transected by numerous east-northeast-trending auriferous megashears. These structures controlled late Proterozoic mafic dyke emplacement, Damaran rifting and sedimentation, alkaline volcanism and the localisation of hydrothermal fluids in the overlying cover rocks. In the NCZ, where basement inliers are not exposed, the metamorphosed equivalents of Damaran shallow marine carbonates are overlain by deeper water sediments and turbidites. Sedimentation was controlled by rifting, facies belts being oriented parallel to the axis of the orogen. Felsic and mafic volcanic rocks comprise only a fraction (<5 %) of the Damara Sequence.

Isoclinal folds in the Damara Sequence provide evidence for extensive crustal shortening across the CZ during early Damaran deformation ( $D_1$  and  $D_2$ ), but not for significant lateral displacement: facies belts remained essentially where they evolved.  $D_3$  deformation ( $F_3$  folding) and concomitant granite intrusion were responsible for the northeast-trending structural grain and domal structures of the CZ. Late orogenic semi-ductile and brittle  $D_4$  deformation was confined to the vicinity of major structural breaks such as the north-north east-trending Abbabis and Welwitschia lineament zones. Buchan-type metamorphic assemblages are described for the first time from central Namibia. Mineral assemblages of metapelitic units have been used to construct a petrogenetic grid for the CZ: results agree well with PIT estimates made from calcite-graphite geothermometry and dolomite-calcite solvus thermometry. Peak metamorphic conditions of -3 kbar and 650°C were attained in the field area at 520 Ma; the geothermal gradient was 55-65°C/km.

The majority of Damaran intrusions in the CZ are granitic in composition: the economically significant late-orogenic suite is dominated by leucogranites and pegmatites. No Damaran granitoid in the CZ contains any significant sulphide or precious metal mineralisation. Early and late orogenic granites are mildly peraluminous, those granites intruded at the peak of regional metamorphism are strongly peraluminous; most intrusions are S-type, have high ( $^{87}\text{Sr}/^{86}\text{Sr}$ )<sub>i</sub> ratios and  $\delta^{18}\text{O}$  values, and do not have a calc-alkaline chemistry. Most plutons have trace element signatures of intraplate granites. Three rare-element pegmatite provinces are present in the CZ: the lithium pegmatite province of the SCZ and the stanniferous pegmatites of the Sandamap-Davib Ost and Nainais-Kohero tin belts in the NCZ. New Rb-Sr whole-rock dates refute recent suggestions that Damaran stanniferous pegmatites have been modified by Jurassic-Cretaceous or post-Karoo greisenising fluids.

At the enigmatic Eureka rare earth occurrence west of Usakos, disseminated magnetite and monazite, both minerals part of a high-temperature assemblage in a dolomite-carbonate rock, are hosted by Etusis Formation quartzites. The monazite mineralisation formed at  $500 \pm 20$  Ma, slightly after the peak of metamorphism, but the carbonate enclosing the monazite has a mantle ( $^{87}\text{Sr}/^{86}\text{Sr}$ )<sub>i</sub> signature. There is no field or petrographic evidence for the presence of a carbonatite intrusion of any size.

The Eureka occurrence bears some similarities with the middle Proterozoic Bayan Obo iron-rare earth-niobium deposits in Inner Mongolia, China, that were formed by the hydrothermal replacement of syn-rift sedimentary dolomite by fluids from a hidden alkaline-carbonatite in an intracontinental rift setting. Mineralising fluids at Eureka probably ascended via deep-seated tectonic breaks such as the Omaruru Lineament and the Welwitschia lineament zone during Etusis times.

At the Otjua Tungsten Prospect north of Omaruru, the largest scheelite-fluorite replacement skarn in Namibia is developed within Okawayo Formation marble in the aureole of the late-tectonic, highly fractionated but unmineralised Otjua leucogranite. Three zones or facies of skarn, successively vesuvianite facies, scheelite-bearing garnet facies and tungsten-barren pyroxene facies, represent increasing degrees of replacement of calcitic marble. Systematic changes in mineralogy, mineral chemistry and whole-rock compositions of the skarn facies show that the subvertical calcitic marble acted as a reactive conduit for a channelised mineralising fluid that emanated from a point source at depth. The presence of widely distributed, pre-existing, tungsten/scheelite mineralisation in the metamorphosed marls (scheelite-bearing granofels) of the lower Swakop Group suggests that the Otjua granite, rather than being the source of the fluids as previously suggested, may merely have acted as a 'heat-engine' and mobilised fluids from the metasediments within its thermal aureole.

Carbonate-hosted auriferous quartz veins and associated alteration of hydrothermal origin that can broadly be referred to as distal skarn are widespread in the Karibib Formation in the Karibib area. Gold mineralisation is not spatially associated with a particular type of igneous rock: only the ubiquitous lithium pegmatites contain minor sulphide and gold-bearing phases. In the skarn, sulphide minerals include chalcopyrite, sphalerite, pyrrotite, bismuth and silver tellurides, while silicate alteration commonly comprises massive tremolite and more rarely vesuvianite, garnet and pyroxene. Mineralisation is hosted by late-tectonic, brittle deformation structures and locally thrust faults. The style of alteration and the Au-Bi-As-Te association bears certain similarities to the gold skarns of the western United States. Previous models for the origin of the gold skarn mineralisation of the Karibib area have stressed the importance of the relatively minor mafic volcanic rocks of the Daheim Member as a gold source. New geological mapping and geochemistry emphasise the auriferous nature of the megashears in the underlying granitic basement. Largely circumstantial evidence suggests that the sources for the gold-bismuth mineralisation are hidden, late-/post-tectonic felsic intrusions, specifically lithium pegmatites and/or hydrothermal fluids derived from the basement.

Metaturbidite-hosted gold mineralisation discovered during the course of field work is believed to be of a style previously unknown in southern Africa. A 2500-metre-long zone of gold mineralisation is hosted by altered Kuiseb Formation schist, quartz veins and mylonite rocks in the aureole of a leucogranite and rare-element pegmatite dome on the farm Sandamap Noord, west of Usakos. Au/As fluids, either mobilised from the metasediments by and/or expelled from the stanniferous pegmatites, were concentrated in north-northeast-trending structures. The three main types of alteration/mineralisation are: a kaolinite-alunite rock (advanced argillic alteration) that contains < 1 g/t Au, a jarosite schist that contains up to 46 g/t Au and a massive grunerite rock that contains up to 0.5 g/t Au. Associated alteration includes a massive calcite-graphite-tourmaline rock and galena- and pyrite-bearing quartz veins. Some of the high-strain zones surrounding the domal structure formed during the diapiric intrusion of the granites and pegmatites and are thus unrelated to the regional tectonism, but only the north-northeast-trending portions are mineralised with gold. The gold zone lies within 10 km of the north-northeast-trending Welwitschia lineament zone which played an important role in the localisation of late-/post-tectonic uraniferous alaskites at the Rössing Uranium Mine. The mineralisation on Sandamap Noord has similarities with Archaean mesothermal gold deposits: epigenetic Au-As-W mineralisation is structurally controlled in late-tectonic ( $D_3/D_4$ ) structures; the wallrock alteration is retrograde with respect to peak metamorphism; the mineralisation is 'gold-only' with high gold enrichment factors ( $10^3$ - $10^4$ ) moderate enrichments of As, Band Wand low enrichment of Cu, Zn and Pb.

---

A structural analysis of metaturbidite-hosted tourmalinites on the farm Ohere, west of Omaruru, revealed that although tourmalinite is a stratiform rock on the decimetre scale, this type of mineralisation is confined to the hinge of an  $F_2$  fold. Elsewhere tourmalinites are oriented parallel to an axial planar  $S_2$  fabric and commonly occupy kink bands. The sub-vertical  $S_2$  cleavage in the aureole of a granitoid provided a channel way for boron-rich fluids resulting in the selective replacement of schist and formation of crosscutting tourmalinites. Subsequent replacement of the metaturbidites along the essentially bedding-parallel  $S_1$  fabric in the hinge zone led to the formation of stratiform tourmalinites. Tourmalinites contain significant B-F-W-Sn mineralisation: scheelite is present, but no tin or fluorine phases have been identified. A mass balance calculation shows that the elements Si and Zr remained stationary during boron metasomatism, there was a net introduction of the elements B, C, Al, Mg, Na, Ca, F, S, Sr and V and a net loss of the elements H, K, Fe, Ba and Rb. The amount of transfer of elements (in  $\mu\text{mol g}^{-1}$ ) during the tourmalinisation on Ohere was not too dissimilar from that reported in North America and was caused by a fluid derived from a granitic or pegmatitic melt. An exhalative origin for the CZ tourmalinites, a currently popular model for tourmalinites in general, is rejected.

Scheelite-bearing vesuvianite-quartz skarnoid rocks in the Kuiseb Formation on the farm Ohere represent a significant stratiform tungsten reserve that has certain characteristics in common with the Corruga-type, scheelite-bearing, bedded calc-silicate lithologies of the Broken Hill District, Australia. In Namibia, they are regional metamorphic rocks with a skarn-like mineral assemblage occurring as poorly layered to massive, discontinuous lenses several hundreds of metres in length and contain significant concentrations of W, Sn, Zn and F. Petrography and electron microprobe analysis of small ( $<50 \mu\text{m}$ ) reddish-brown inclusions in sphene revealed the presence of stanniferous rutile and an unidentified zirconium titanium mineral. This lithology is a type of metamorphogenic skarn whose development is related to the Buchan-style metamorphism that affected the area. There is no evidence that vesuvianite rocks are metamorphosed coticule rocks as has been suggested for the morphologically similar Australian examples.

The currently fashionable Andean-type collision model involving the northwestward subduction of the Kalahari Craton below the Congo Craton is unsuccessful in explaining the continental nature and paucity of the CZ magmato-hydrothermal deposits. The epigenetic mineral occurrences of the CZ have a strong intracratonic signature and bear some similarities with the Sn, W, Mo and U deposits of back-arc magmatic belts of the Eastern Cordillera of Bolivia and the Western Tin Belt of Thailand and Burma. Partial melting of pre-Damaran crust and the mobilisation of fluids from these inliers and the Damaran metasediments played the most important role in producing the relatively small, epigenetic gold, tin and tungsten deposits of the CZ. Late-tectonic, dextral movement on the Omaruru Lineament is believed to have been the underlying control on the localisation of late- $D_3/D_4$  epigenetic mineralisation. Peak metamorphic temperatures increased along the axis of the orogen from northeast to southwest: the Usakos-Karibib-Omaruru area lay within the  $400^\circ\text{C}$ - $700^\circ\text{C}$  'window', spanning the greenschist-amphibolite facies transition. Thermal conditions were ideal for the emplacement and preservation of late-tectonic pegmatites and high-temperature skarns ( $400$ - $650^\circ\text{C}$ ) and at a later stage, because of the rapid uplift, lower temperature ( $<300^\circ\text{C}$ ), epigenetic vein-type mineralisation.



---

**CONTENTS**

<b>1. INTRODUCTION.....</b>	<b>1</b>	OF THE NCZ IN THE USAKOS AREA.....	<b>50</b>
1.1 INTRODUCTORY COMMENTS.....	1	3.3.1 Sandamap Noord peraluminous leucogranite .....	50
1.2 RECENT SCIENTIFIC DEVELOPMENTS IN CENTRAL NAMIBIA.....	1	3.3.2 Ketelbank leucogranite.....	51
1.3 THE SIGNIFICANCE OF THESE RECENT DEVELOPMENTS AND THE IMPLICATIONS FOR GOLD METALLOGENY .....	1	3.4 SYN- AND LATE-TECTONIC GRANITOIDS OF THE NCZ IN THE OMARURU AREA.....	53
1.4 REASONS FOR UNDERTAKING THIS STUDY.....	5	3.4.1 Ohere Oos Salem granitoid .....	53
1.5 AIMS AND OBJECTIVES OF THIS STUDY.....	5	3.4.2 Ohere leucogranite .....	53
1.6 PREVIOUS WORK IN CENTRAL NAMIBIA.....	6	3.4.3 Otjua leucogranite .....	54
1.7 STUDY AREA.....	7	3.5 TECTONIC CONTROLS ON THE LOCATION OF GRANITES IN THE NCZ .....	56
1.8 METHODS EMPLOYED .....	8	3.6 PEGMATITES .....	56
1.9 A NOTE ON THE DIFFERENCE BETWEEN THE PhD THESIS AND THIS MEMOIR.....	8	3.6.1 Magnetite-bearing pegmatites hosted by lower Swakop Group meta- sediments in the SCZ.....	56
1.10 ACKNOWLEDGEMENTS .....	8	3.6.2 Lithium pegmatites of the SCZ in the Karibib area .....	57
<b>2. LITHOSTRATIGRAPHY AND LITHOGEO- CHEMISTRY .....</b>	<b>11</b>	3.6.3 Pegmatites hosted by lower Swakop Group metasediments in the NCZ .....	58
2.1 INTRODUCTION .....	11	3.6.4 Pegmatites hosted by upper Kuiseb Formation metasediments in the NCZa and NCZe.....	58
2.1.1 Pre-Damara basement.....	11	3.6.5 Summary of pegmatites within field area .....	60
2.1.2 Damara Sequence.....	14	3.7 GEOCHEMISTRY OF THE GRANITOID INTRUSIONS .....	60
2.1.3 Post-Damara geology .....	16	3.7.1 Introduction .....	60
2.2 THE LITHOSTRATIGRAPHY OF THE DAMARA SEQUENCE .....	17	3.7.2 Geochemical classification of the NCZ granites and a comparison with other Damara granitoids .....	60
2.2.1 Nosib Group.....	17	3.7.3 The tectonic setting of the NCZ granites as deduced from trace element geochemistry .....	61
2.2.2 Swakop Group .....	20	3.8 CONCLUSION.....	63
2.2.3 Summary of the Damara depositional episode .....	43		
2.3 THE GEOCHEMISTRY OF THE CLASTIC METASEDIMENTS OF THE DAMARA SEQUENCE .....	45		
2.3.1 Introduction.....	45		
2.3.2 Geochemical classification of the clastic rocks.....	47		
<b>3. INTRUSIVE ROCKS.....</b>	<b>49</b>	<b>4. STRUCTURE.....</b>	<b>65</b>
3.1 INTRODUCTION .....	49	4.1 INTRODUCTION .....	65
3.2 EARLY TECTONIC LEUCOGRANITES ALONG THE OMARURU LINEAMENT.....	49	4.2 STRUCTURE OF THE ABBABIS COMPLEX ON THE FARMS ABBABIS AND NARUBIS.....	66
3.3 SYN- AND LATE-TECTONIC GRANITOIDS			

---

4.2.1 Introduction .....	66	5.3.2 Metamorphism in the core of the Schönfeld Dome in NCZd .....	83
4.2.2 Megashear Zones.....	66	5.3.3 Metamorphism on the farm Ohere 106 in NCZe.....	84
4.2.3 Structural control on the emplacement of (Gannakouriep?) metadolerites .....	67	5.4 THERMOBAROMETRY .....	86
4.2.4 Structural control on emplacement of Damaran pegmatites and Karoo dykes .....	67	5.4.1 Barometry.....	87
4.2.5 The significance of sheared early Proterozoic rocks underlying the Damara Sequence of the SCZ.....	68	5.4.2 Thermometry.....	87
4.3 DAMARAN DEFORMATION - INTRODUCTORY COMMENTS .....	68	5.5 CONCLUDING COMMENTS ON THE DAMARAN TECTONOTHERMAL HISTORY OF THE FIELD AREA .....	88
4.3.1 Damaran deformation across the Omaruru Lineament west of Usakos .....	68	<b>6. GEOCHRONOLOGY.....</b>	<b>91</b>
4.3.2 Damaran deformation of the middle Swakop Group in NCZd.....	72	6.1 INTRODUCTION .....	91
4.3.3 Damaran deformation of the upper Kuseb Formation in NCZe .....	73	6.2 Rb-Sr WORK.....	91
4.4 CONCLUSION.....	74	6.2.1 Analytical Procedure.....	91
<b>5. METAMORPHISM.....</b>	<b>77</b>	6.3 THE RELATIONSHIP BETWEEN LEUCOGRANITE AND PEGMATITES .....	97
5.1 INTRODUCTION .....	77	6.4 MINERALISATION AND THE YOUNGER INTRUSIONS .....	99
5.2 METAMORPHISM ON THE FARM SANDAMAP NOORD 115 IN NCZa.....	79	6.5 GRANITE AND PEGMATITE PETRO- GENESIS AND THE ISOTOPIC EVOLUTION OF THE CZ.....	99
5.2.1 Introduction.....	79	6.6 Pb-Pb WORK.....	100
5.2.2 Regional metamorphism .....	79	<b>7. MINERALISATION.....</b>	<b>103</b>
5.2.3 Early kinematic cordierite and late- kinematic andalusite growth in aluminous schists.....	79	7.1 INTRODUCTION .....	103
5.2.4 Contact metamorphism associated with the D <sub>3</sub> /D <sub>4</sub> leucogranite/pegmatite dome .....	80	7.2 MAGNETITE-MONAZITE OCCURRENCE HOSTED BY THE ETUSIS FORMATION ON EUREKA .....	104
5.2.5 Cataclastic metamorphism associated with the D <sub>3</sub> /D <sub>4</sub> leucogranite/pegmatite dome .....	80	7.2.1 Introduction.....	104
5.2.6 Metamorphic effects associated with the F <sub>4</sub> folds.....	81	7.2.2 Geological setting.....	105
5.2.7 Mylonitisation on the northwest side of the D <sub>3</sub> /D <sub>4</sub> leucogranite/pegmatite dome .....	81	7.2.3 Petrography of the monazite rock.....	105
5.2.8 Summary .....	82	7.2.4 Geochemistry of the monazite rock.....	105
5.3 METAMORPHISM ACROSS THE OMARURU LINEAMENT NORTH OF OMARURU .....	82	7.2.5 Discussion.....	105
5.3.1 Metamorphism on the farm Kassandara 40 in NCZa.....	82	7.2.6 Conclusion .....	108
		7.3 TUNGSTEN SKARN MINERALISATION IN THE OKAWAYO FORMATION AT OTJUA.....	108
		7.3.1 Introduction.....	108
		7.3.2 Geological setting.....	109
		7.3.3 Morphology and petrography of the skarn ....	110
		7.3.4 Skarn mineral chemistry .....	113
		7.3.5 Marble and skarn bulk rock chemistry .....	114
		7.3.6 Genesis of the Otjua skarn.....	115

7.3.7 Conclusion .....	118	ROCKS IN THE KUISEB FORMATION ON OHERE.....	140
7.4 GOLD SKARN MINERALISATION IN THE KARIBIB FORMATION IN THE KARIBIB DISTRICT.....	118	7.7.1 Introduction .....	140
7.4.1 Introduction .....	118	7.7.2 Geological setting.....	141
7.4.2 Onguati Copper Mine.....	119	7.7.3 Characteristics of vesuvianite skarnoid rocks.....	141
7.4.3 Habis Gold Prospect silicate skarn.....	123	7.7.4 Petrography of the vesuvianite skarnoid rocks.....	142
7.4.4 Summary of the gold skarns of the Karibib area.....	124	7.7.5 Geochemistry.....	144
7.4.5 Origin of the gold mineralisation .....	124	7.7.6 Discussion .....	144
7.4.6 Conclusion.....	126	7.7.7 Conclusion.....	144
7.5 TURBIDITE-HOSTED GOLD MINERALISATION IN THE KUISEB FORMATION ON SANDAMAP NOORD .....	126	<b>8. SYNTHESIS .....</b>	<b>147</b>
7.5.1 Introduction .....	126	8.1 CENTRAL ZONE MINERALISATION IN THE LIGHT OF GEODYNAMIC CONSIDERATIONS.....	147
7.5.2 Geological setting.....	127	8.2 REGIONAL STRUCTURAL CONTROLS ON THE LOCALISATION OF EPIGENETIC MINERALISATION IN THE CZ .....	149
7.5.3 The auriferous zone .....	128	8.3 CONCLUDING THOUGHTS ON GOLD METALLOGENESIS IN CENTRAL NAMIBIA .....	150
7.5.4 Gold and the 'pathfinder' elements .....	130	8.4 PELITE/TURBIDITE-HOSTED GOLD MINERALISATION IN THE DALRADIAN AND THE DAMARAN CZ COMPARED.....	151
7.5.5 Summary .....	130	8.5 CONCLUDING COMMENTS .....	152
7.5.6 Genesis of the gold mineralisation .....	131	REFERENCES .....	153
7.5.7 Conclusion.....	133	APPENDIX.....	161
7.6 TOURMALINITE MINERALISATION IN THE KUISEB FORMATION ON OHERE ....	133		
7.6.1 Introduction .....	133		
7.6.2 Geological setting.....	133		
7.6.3 Nature and petrography of the tourmalinite ..	134		
7.6.4 Structural investigation of tourmalinite mineralisation .....	134		
7.6.5 Structural summary .....	135		
7.6.6 Geochemistry of the tourmalinites .....	137		
7.6.7 Genesis of the tourmalinites .....	137		
7.6.8 Conclusion.....	140		
7.7 SCHEELITE-VESUVIANITE SKARNOID			

#### LIST OF MAPS ACCOMPANYING MEMOIR

- Map 1: Geological map of an area north of Omaruru
- Map 2: Geological map of Ohere 106, Omaruru District
- Map 3: Geological map of Sandamap Noord 115
- Map 4: Geological map of Sandamap 64
- Map 5: Geological map of Eureka 99
- Map 6: Geological map of Lukasbank 63

For financial reasons these maps have been reduced for this publication.  
Paper or ammonia prints of the originals can be obtained from the  
Geological Survey of Namibia, 45 Robert Mugabe Avenue, P.O. Box 2168, Windhoek



# 1. INTRODUCTION

## 1.1 INTRODUCTORY COMMENTS

West-central Namibia is a major mineral-producing province where a diverse range of commodities such as uranium, tin, tantalum, niobium, lithium, gold and tourmaline are mined (Fig. 1.1). All of these commodities with the exception of gold are extracted from pegmatitic intrusions. Between 1975 and 1984, the mining industry contributed between 26.1 and 46% of the Gross Domestic Product of Namibia (Chamber of Mines of SWA/Namibia report, 1985). If the diamondiferous alluvial and raised-beach deposits of southern Namibia are excluded, then it is apparent that a substantial proportion of the country's mineral revenue is derived from the district bounded by Swakopmund, Uis and Windhoek (Fig. 1.1). The region is essentially underlain by the intracontinental branch of the Pan-African Damara Orogen (Miller, 1983a). This contains a late-Proterozoic succession of meta-arkoses, marbles, calc-silicate rocks and metapelites with very minor meta-volcanic rocks, and rests unconformably on early Proterozoic granitic basement. Basement lithologies crop out in a series of inliers in the vicinity of the Abbabis geanticline which extends from east of Swakopmund to south of Karibib (Fig. 1.2). The Damara Sequence and underlying basement lithologies were subsequently deformed, meta-morphosed and intruded by predominantly granitic intrusions during the late Precambrian/early Palaeozoic Damaran orogeny. The exact nature of the orogenic event has been the subject of much discussion. An ensialic aulacogen model has been proposed by Martin and Porada (1977) to account for the various features of the Damara Orogen, while various plate tectonic models (Kasch, 1983a; Miller, 1983a) and subsequent modifications (Martin, 1983) have been put forward. Both the basement gneisses and the Damara Sequence have subsequently been intruded by Karoo-age mafic dyke swarms and post-Karoo volcanic complexes.

## 1.2 RECENT SCIENTIFIC DEVELOPMENTS IN CENTRAL NAMIBIA

In recent years exploration and scientific interest has shifted from the relatively well-documented intrusion-hosted uranium (Berning *et al.*, 1976; Marlow, 1983) and tin deposits (Richards, 1986) to mineral occurrences in the Damaran metasediments. Some of these occurrences are amenable to opencast mining and have the potential to be significant earners of revenue. During the 1980s several discoveries of epigenetic metasediment-hosted mineralisation were made near the towns of Usakos, Karibib and Omaruru (Fig. 1.3). This area is underlain by the Central Zone (CZ) of the Damara Orogen (Miller, 1983a), where the Damaran metasediments have been multiply deformed, have undergone greenschist-amphibolite facies metamorphism and been intruded by numerous syn-/late-tectonic felsic igneous intrusions. The scheelite-bearing skarn at the Otjua Tungsten Prospect (Steven, 1987) is one of the few documented tungsten skarns on the African continent.

Finely disseminated scheelite mineralisation, apparently unrelated to igneous intrusions, is widely distributed in calc-silicate rocks of the Damara Sequence. Scheelite-bearing tourmalinites and scheelite-bearing vesuvianite rocks, initially believed to represent meta-exhalites, have also been discovered in the Omaruru and Usakos areas (Steven, 1987; Badenhorst, 1988a). Several of the tourmalinite rocks were found to contain anomalous gold contents (500 ppb Au). Interest in the gold potential of central Namibia was further stimulated by the discovery of gold bearing skarn mineralisation in the marbles of the Karibib Formation near Karibib during 1985-1987 (Navachab Gold Mine Field Guide, 1989) and the subsequent opening of the Navachab opencast gold mine in 1989. Prior to this date, only small-scale gold mining had been conducted in Namibia, notably in the Rehoboth area (Fig. 1.1) from early Proterozoic lithologies. At the time of its discovery, the Navachab occurrence was believed to be the first record of skarn-hosted gold mineralisation in southern Africa and was thus particularly exciting.

## 1.3 THE SIGNIFICANCE OF THESE RECENT DEVELOPMENTS AND THE IMPLICATIONS FOR GOLD METALLOGENY

Some of these discoveries were slightly unexpected because of the essentially ensialic nature of the Central Zone and the generally lithophilic character of the associated mineral deposits. The tungsten skarn mineralisation at Otjua is notable because of the lack of accompanying sulphide mineralisation in contrast to skarn deposits of the Circum-Pacific region (Einaudi *et al.*, 1981). Steven (1987) considered that the presence of two types of tungsten mineralisation, one characteristic of the Proterozoic (the disseminated scheelite mineralisation) and one which is more representative of the Phanerozoic (the tungsten replacement skarn mineralisation) emphasised the transitional nature of the Damaran orogeny which spans the Precambrian-Cambrian boundary. The recognition of tourmalinite mineralisation in the Central Zone was regarded as significant because of the extensive literature describing, *inter alia*, tourmalinites as hosts to gold mineralisation (Fleischer and Routhier, 1973); the association between tourmalinites and exhalative massive sulphide mineralisation (Plimer, 1988); and the use of tourmalinites as prospecting guides for massive sulphide deposits (Slack, 1982) and gold mineralisation (McArdle *et al.*, 1989). The scheelite-bearing vesuvianite lithologies of central Namibia have features similar to Corruga-style mineralisation (Slack, 1987, pers. comm.), which is considered by Plimer (1983) to represent the distal exhalative facies of the Broken Hill massive sulphide deposit in Australia. The discovery of economic concentrations of gold in the Damara Orogen is important because there is a notable paucity of gold mineralisation in middle and late Proterozoic rocks (Woodall, 1979). Moreover, other than the turbidite-hosted gold deposit at Ondundo (Fig. 1.4; Reuning, 1937), relatively few significant occurrences of the precious metal have been located in central Na-

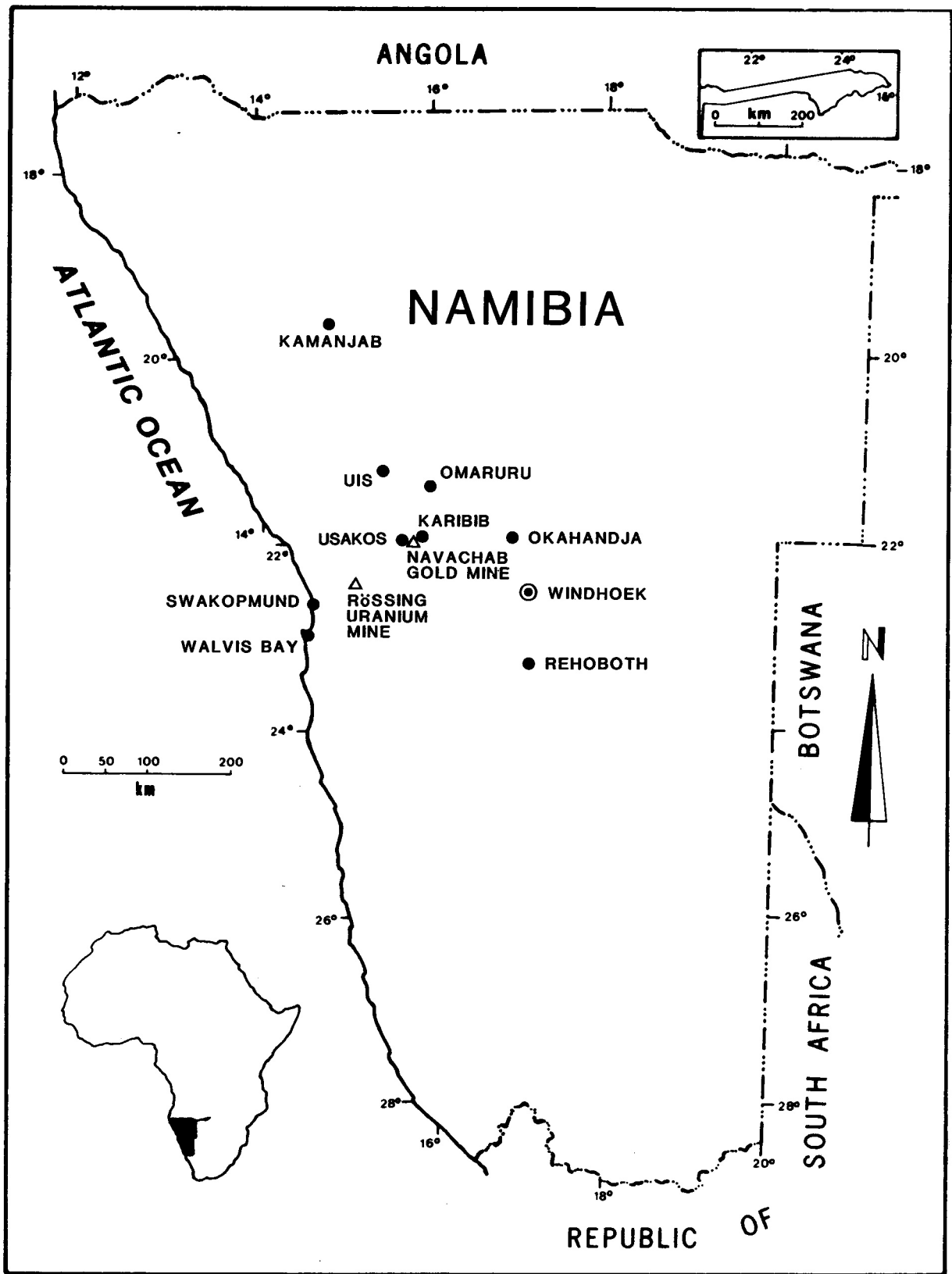


Figure 1.1: Locality map for Namibia

mibia (Haughton *et al.*, 1939; Frommurze *et al.*, 1942; Smith, 1965; Miller, 1983a) in spite of a 125-year prospecting history. Gold has only been mined profitably on a small scale at the Epako and Ondundo Prospects (Haughton *et al.*, 1939). Although production figures are not available for these two prospects, it is unlikely that the combined gold production

from all the prospects shown in Fig. 1.4 exceeded one metric ton prior to 1989. The proportion of mafic volcanic rocks and banded iron formations (BIF), both well-documented hosts to gold mineralisation, within the Central Zone is extremely small. Moreover, there are very few occurrences of those elements that are well known (Boyle, 1979) to accompany gold

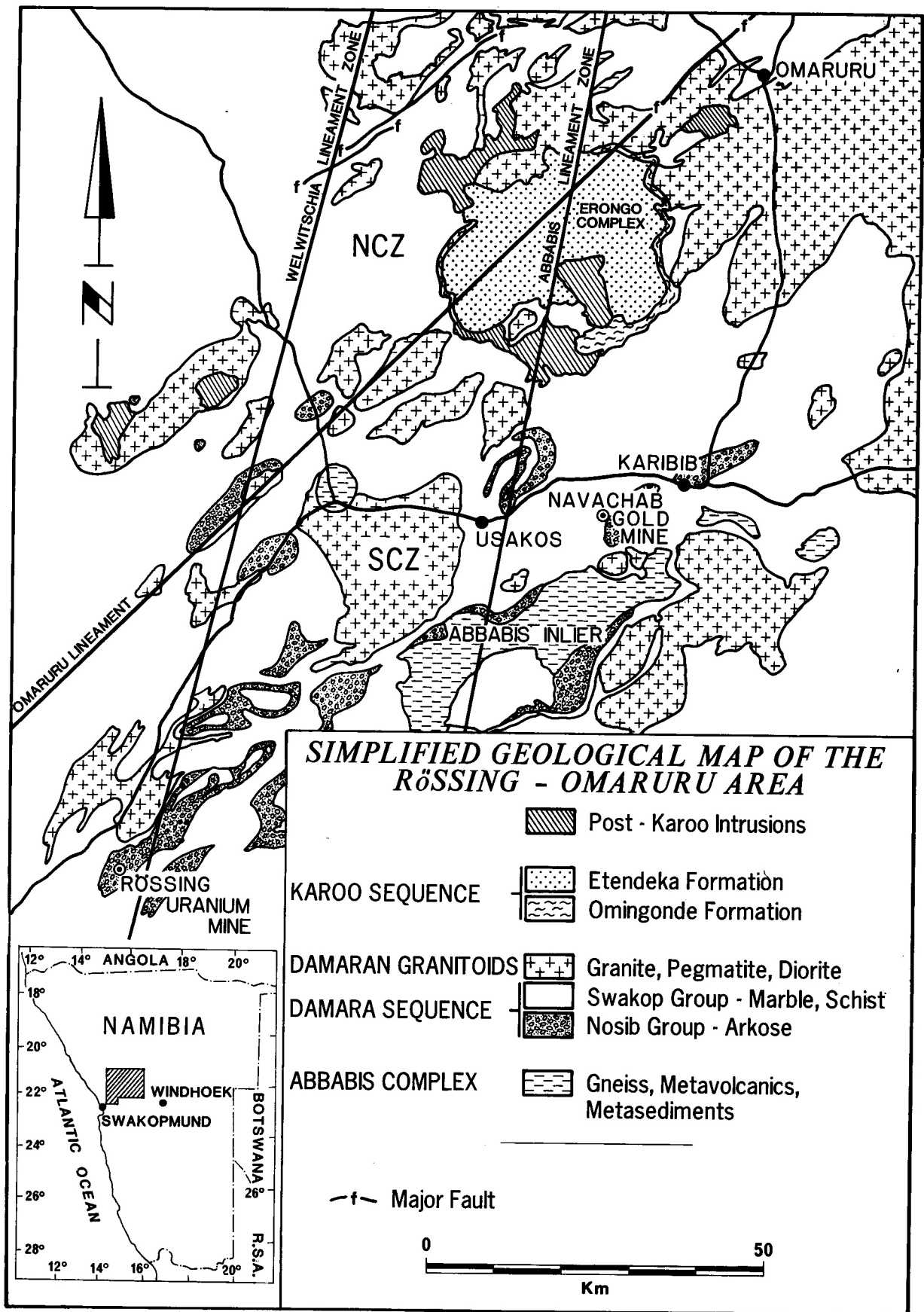
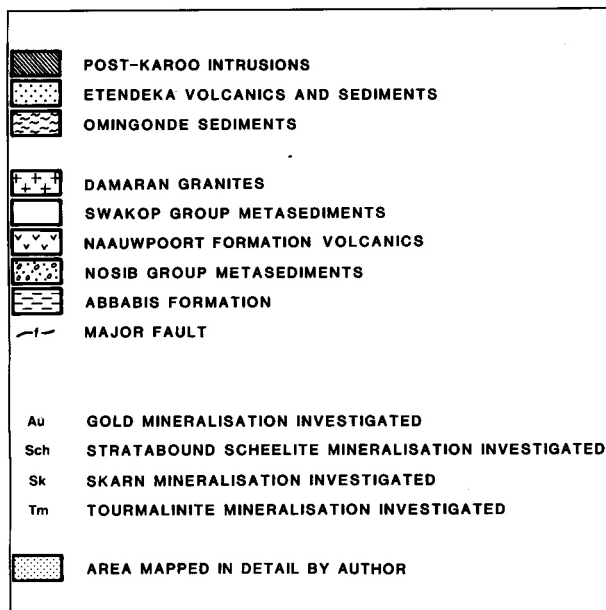


Figure 1.2: Regional geology of central Namibia.





Key to Figure 1.3 (left)

pegmatites of the Usakos-Karibib district, in areas directly underlain by early Proterozoic basement. Furthermore, there were reports of gold mineralisation within early Damaran quartzites that underlie the Chuos Mountains southwest of Usakos (Smith, 1965). Moreover, the gold potential of the metapelites and metagreywackes at the top of the Damara Sequence had never been seriously investigated. Woodall (1979) noted that the majority of Australian Proterozoic gold deposits were hosted by orogenic sequences, namely successions containing abundant turbidites, or where deformation had been intense. The Kuiseb Formation, the uppermost Damaran stratigraphic unit, represents a Proterozoic orogenic sequence and, in early 1987, it was considered that, in spite of the presence of auriferous quartz veins at Ondundu, the various turbidite-hosted gold models had not been properly investigated in central Namibia. Furthermore, the concept that thick accumulations of metagreywackes and pyritic schists within the grabens of the northern portion of the Central Zone might represent a substantial gold reservoir had not been considered.

#### 1.4 REASONS FOR UNDERTAKING THIS STUDY

This memoir is largely based on a Ph.D. thesis (Steven, 1992) presented at the University of Cape Town. One of the prime motivating factors behind the thesis was the desire to describe several newly discovered, poorly documented styles of mineralisation from a relatively unknown terrain. Because of the common close spatial association between many of these mineral occurrences and granitic and pegmatitic intrusions, it was suspected that these styles of mineralisation would be restricted to those parts of the orogen, such as the CZ, where such plutons are abundant. The CZ was subjected to low-pressure/high-temperature metamorphism during the Damaran orogeny (Miller, 1983a) and it was thought that a high geothermal gradient, itself probably related to the widespread granite intrusions, may also have played a key role in the formation of these essentially hydrothermal deposits.

Secondly, although the plate tectonic model for the Damara Orogen has gained acceptance amongst many geologists (Miller, 1983a), direct analogy with present-day collisional settings such as the Circum-Pacific reveals significant differences in the types of mineral deposits in the two terrains. In my experience, plate tectonic models which invoke the large-scale subduction of oceanic crust are unsuitable as a predictive tool for mineral exploration in central Namibia. In this regard it was felt that Miller's (1983b) review of the economic implications of a plate tectonic model for the Damara with its strong mobilist flavour was only partly correct and, in the CZ in particular, was out of date. According to Miller's (1983a) interpretation, the CZ represents the magmatic arc generated above a northwestward-dipping subduction zone during the collision between the Kalahari and Congo Cratons. Although Miller (1983a) has considered the Damaran granitic rocks to be calc-alkaline in composition, there is an almost complete lack of intrusion-hosted base arid precious metal mineralisation similar to that developed in active continental margin batholiths such as in the Circum-Pacific region. In fact, there is a preponderance of highly fractionated S-type granites and pegmatites in the late orogenic suite of Damaran intrusions. All the intrusion-hosted mineralisation in the CZ occurs in these late-tectonic plutons. The majority of the uraniumiferous alaskites have been derived from the large-scale anatectic melting of the granitic basement and the basal part of the Damara Sequence (Marlow, 1983; Hawkesworth and Marlow, 1983). The Otjua tungsten skarn was formed as the result of the intrusion of an S-type granite with abnormally high  $(^{87}\text{Sr}/^{86}\text{Sr})_i$  and  $\delta^{18}\text{O}$  values (Steven, 1987). Many of the stanniferous pegmatites also have crustal signatures and Haack and Gohn (1988) envisaged large-scale partial melting of Damaran metapelites to explain the high  $(^{87}\text{Sr}/^{86}\text{Sr})_i$  of these intrusions. It was suspected that if the intrusion-hosted mineralisation shows such a strong lithophilic signature, then the metasediment-hosted deposits, which are commonly developed in the aureoles of these plutons, would exhibit a similar character.

Thirdly, ideas that I thought needed urgent addressing were suggestions that the pegmatite-hosted tin mineralisation of the CZ is of Jurassic-Cretaceous age (Diehl, 1986) or alternatively that stanniferous pegmatites have been modified by post-Karoo "greisenising fluids" (Pirajno *et al.*, 1988). Because much of the tourmalinite mineralisation occurs in the immediate vicinity of tin pegmatites and geochronological investigations of these intrusions had been planned, it was felt that a contribution could be made in resolving this contentious issue.

#### 1.5 AIMS AND OBJECTIVES OF THIS STUDY

The main aim of this regional metallogenic investigation is therefore to describe six examples of metasediment-hosted epigenetic mineralisation from central Namibia and place them within the existing tectono-stratigraphic framework of the CZ. More specifically, this memoir aims to discuss what is believed to be epigenetic rare earth, gold, tungsten and tourmaline mineralisation hosted by the metamorphosed equivalents of the quartzites of the Nosib Group

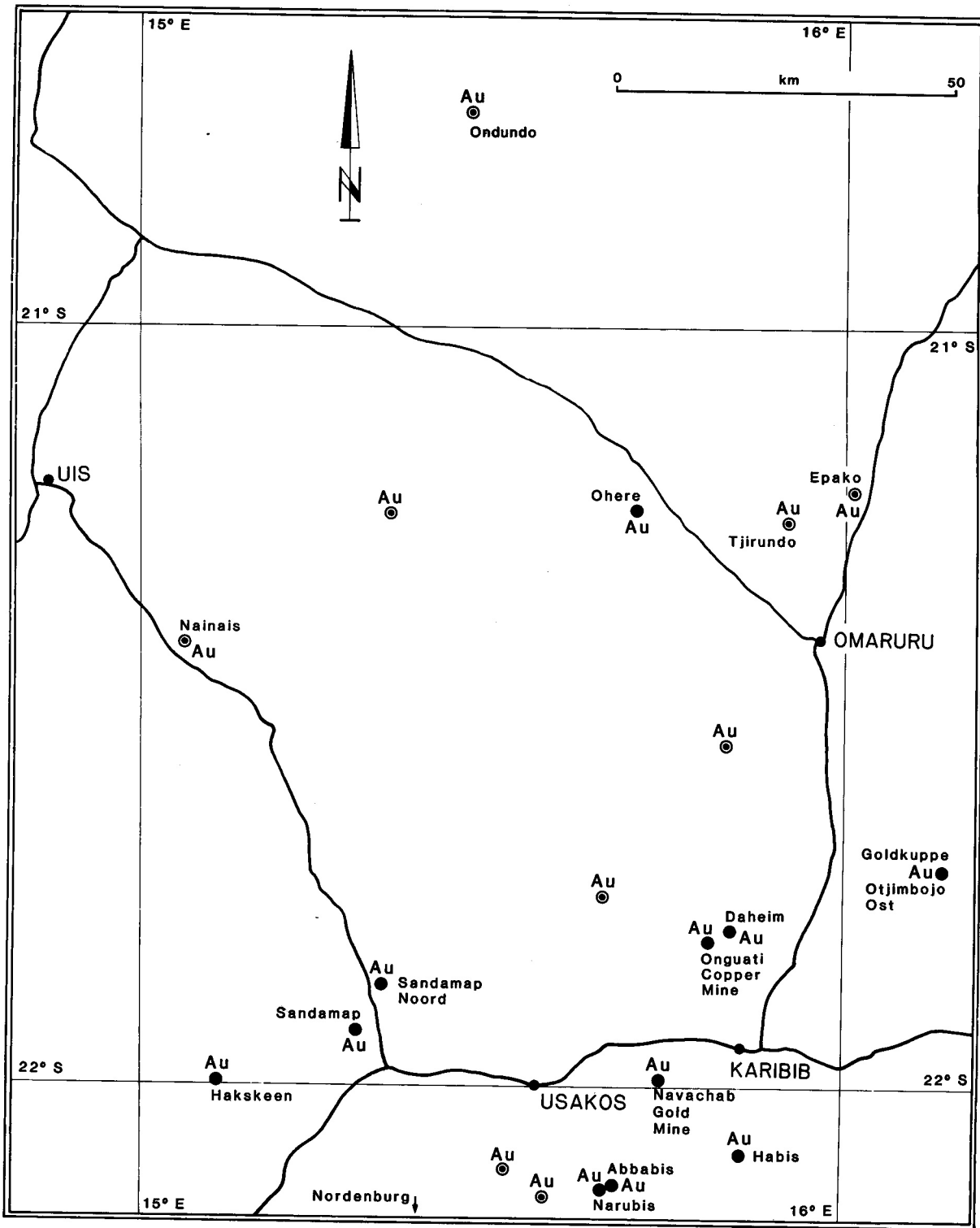
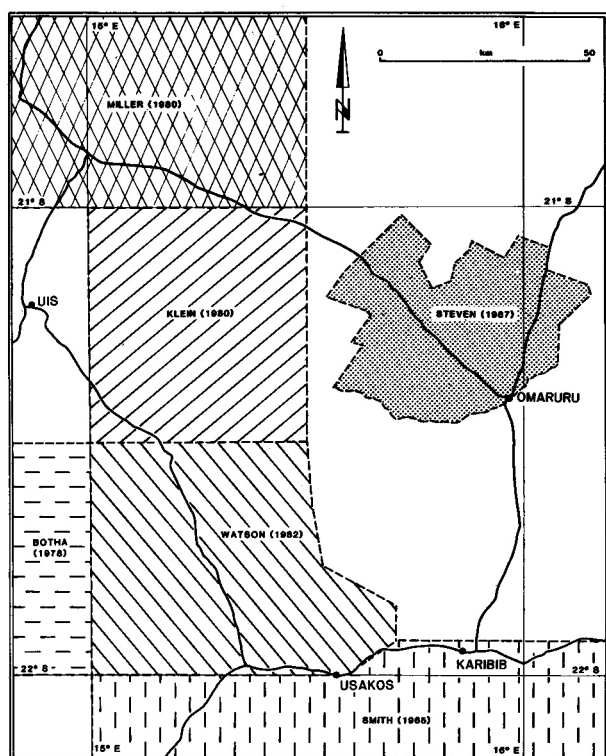


Figure 1.4: Occurrences of gold in central Namibia (ringed occurrences after Martin, 1963)

and the carbonates and the turbidites of the Swakop Group. The relationship of these occurrences to the surrounding granitic and pegmatitic intrusions will be described. Particular emphasis will be placed on the relationship between the mineralisation and the tectonothermal history of the CZ. It is hoped that this regional metallogenic study of the well-exposed, high-temperature zone of a Pan-African belt will have applications elsewhere in southern Africa.

### 1.6 PREVIOUS WORK IN CENTRAL NAMIBIA

Previous work in the Central Zone has concentrated on describing the regional geology. The areas covered by Smith (1965), Botha (1978), Klein (1980), Miller (1980), Watson (1982) and Steven (1987) are shown in Fig. 1.5. During reconnaissance work conducted for a mining company, the author compiled the most recent geological map of the



**Figure 1.5:** Areas covered by previous workers in central Namibia

Omaruru area at a scale of 1:50 000 in 1985. A reduced version of this map (Steven, 1987; Map 1) was the first geological map of the Omaruru area to be published since Haughton *et al.* (1939). A provisional petrographic study of the granites in Area 2115B was completed by Badenhorst (1986a), who has been responsible for regional mapping of the Karibib and Omaruru areas in recent years (Badenhorst, 1987). Much of our knowledge of the underlying structure of the western portion of the CZ is based on an interpretation of the aeromagnetic data that was completed by Corner (1983). This study was undertaken primarily to determine if there is a structural control on the localisation of uraniumiferous alaskites such as are developed at the Rössing Uranium Mine. Corner (1983) was able to identify several lineaments and lineament zones which he interpreted as gentlinal ridges and he concluded that these faults controlled sedimentation. One of his most significant discoveries was that the CZ is divided into two portions, a northern one (NCZ) and a southern one (SCZ), by the magnetically defined Omaruru Lineament (Fig. 1.2). The SCZ is underlain by basement lithologies and Damaran meta-arkoses and marbles, while the magnetically quieter NCZ is characterised by Damaran marbles and overlying thick (4-10 km) accumulations of pelitic metasediments that were deposited in grabens. Badenhorst (1987) confirmed that the Omaruru Lineament is a major tectono-stratigraphic boundary. A scientific discovery of note made during the mid-1980s was that continental, alkaline, mafic volcanic rocks in the Karibib District, first recognised by Miller (1983a), were more widespread than originally thought (Badenhorst, 1989, pers. comm.). Several gold prospects, notably Onguati (Fig. 1.4), are developed in the immediate vicinity of these volcanic

rocks (Pirajno *et al.*, 1990a). Relatively little attention has been paid to the Karoo geology of central Namibia. The most recent description of the post-Karoo Erongo volcanic complex was given by Pirajno (1990).

Little has been published on the metasediment-hosted mineralisation of the area. The nature of the Otjua Tungsten Prospect was described by Steven (1987) and a note on the stratiform tourmalinites of the Kuiseb Formation was presented by Badenhorst (1988a). Short descriptions of general geological features of economic interest noted during their regional work are given by Smith (1965) and Watson (1982). Most investigations into the economic geology of the area have concentrated on the tin and lithium pegmatites. Memoirs on the tin fields were compiled by Haughton *et al.* (1939) and Frommurge *et al.* (1942). The lithium pegmatites of the Karibib area were the subject of detailed studies by Roering (1963, 1966) and Von Knorring (1985). Late-tectonic lithium pegmatites from the Rubicon Mine and cassiterite-bearing pegmatites from the Uis Tin Mine have recently been dated by Haack and Gohn (1988). The most recent description of the alteration-mineralisation of the Krantzberg wolframite deposit on the northeast side of the post-Karoo Erongo Complex has been given by Pirajno and Schlögl (1987).

## 1.7 STUDY AREA

For the purposes of this memoir the term "central Namibia" refers to the Usakos-Karibib-Omaruru area (Fig. 1.3). It was decided at the outset that the study should focus on the mineralisation/alteration features within two districts that straddle the Omaruru Lineament as defined by Corner (1983). In the first area, located to the north of Omaruru, the various tectono-stratigraphic assemblages on the northern side of the Omaruru River including tourmalinite and scheelite-bearing skarnoid rocks (defined as lithologies with a coarse-grained calc-silicate gangue whose development is not obviously related to a granitic pluton) on the farm Ohere, the Epako Gold Prospect and the tungsten skarn mineralisation on the farm Otjua (Fig. 1.3), are investigated. The second area, covering the farms Sandamap Noord, Sandamap, Eureka and Lukasbank, lies to the west of Usakos (Fig. 1.3) and was not only selected because of the recently discovered tourmalinite and scheelite mineralisation, but also because of the good exposure of a representative stratigraphic section of the Central Zone within a relatively small area. Moreover, this second area covers the important tectono-stratigraphic boundary between the Southern Central Zone and the Northern Central Zone near the intersection of the Omaruru Lineament and Welwitschia lineament zone (Fig. 1.2). As the project evolved it was evident that a discussion of the gold skarn mineralisation in the Karibib Formation marbles would be meaningless without at least a preliminary investigation of the gold mineralisation in the underlying basement. For this reason a third area surrounding known gold mineralisation in the early Proterozoic inlier on the farms Abbabis and Narubis was examined (Fig. 1.3). In addition several occurrences of epigenetic gold mineralisation hosted by Damaran lithologies within the Usakos-Karibib-Omaruru area have been investigated.

## 1.8 METHODS EMPLOYED

In order that limited funds should be spent cost-effectively, extensive use was made of pre-existing regional maps and information that could be gained from the published literature. However, it was realised that the regional investigation of a poorly known area would require a considerable amount of detailed mapping. In the Omaruru area (Map 1) the farm Ohere was mapped at 1 :20 000 (Map 2), not only because of the mineralisation, but also because of the unusually good exposure of the upper portion of the Damara Sequence. A structural study of the tourmalinite mineralisation and the scheelite skarnoid rocks on Ohere was conducted at a scale of 1: 1000. To the west of Usakos, the four farms Sandamap Noord 115, Sandamap 64, Eureka 99 and Lukasbank 63 were mapped at a scale of 1 :25 000 (Maps 3 to 6). Immediately south of the Navachab Gold Mine (Fig. 1.3), an area surrounding known gold mineralisation in the early Proterozoic Abbabis Inlier was geologically mapped at a scale of 1:20 000. The geology of these three areas, where no detailed work had previously been conducted, has been integrated within the existing lithostratigraphic framework compiled by the geological community over the last twenty-five years.

To aid interpretation, a total of 138 samples of Damaran metasediments, intrusive rocks and alteration zones and a limited number of Karoo intrusive rocks were analysed by x-ray fluorescence (XRF) and combined with 35 whole-rock analyses from a previous study (Steven, 1987) to provide a comprehensive lithochemical database for the Usakos and Omaruru areas. Gold concentrations were determined by atomic absorption spectrometry and by fire assay. The overwhelming majority of whole-rock analyses were selected from areas that were mapped in detail by the author. Basement lithologies (Abbabis Complex) were not analysed. Emphasis was placed on obtaining information on elements of economic interest and the pathfinder elements associated with the base and precious metal mineralisation developed in the area. The analytical methods used are discussed in the Appendix.

The results of petrographic studies have been integrated with the text. Certain silicate, oxide, sulphate and arsenate phases were identified by x-ray diffraction (XRD). Sulphide phases from the various skarns were analysed by electron microprobe and representative analyses are given in tables. Various silicate phases were also analysed by electron microprobe for confirmatory purposes. Whole-rock and mineral age determinations (Rb-Sr method) were conducted on granitic and pegmatitic intrusions that either host or crop out in the immediate vicinity of mineralisation. The isotopic composition of galena samples from two gold prospects was also investigated.

## 1.9 A NOTE ON THE DIFFERENCE BETWEEN THE PH.D. THESIS AND THIS MEMOIR

There are three main differences between the thesis (Steven, 1992) and this memoir. Firstly, the colour maps of a portion of the Abbabis Inlier (1:20 000), the tourmalinite mineralisation on Ohere (1:1 000) and the scheelite skar-

noid rocks on Ohere (1:1 000) have not been reproduced here for financial reasons. Secondly, further Rb-Sr data (Steven *et al.*, 1992) has been obtained for the granitoids and pegmatites that were dated for the thesis. Consequently the Rb-Sr whole-rock dates presented in this memoir are more accurate and the errors in ( $^{87}\text{Sr}/^{86}\text{Sr}$ )<sub>i</sub> ratios are smaller. Thirdly, a more comprehensive interpretation of the litho-geochemistry of the Damaran metasediments is given here.

## 1.10 ACKNOWLEDGEMENTS

This memoir is based on a Ph.D. thesis that was presented in the Department of Geology, University of Cape Town (Steven, 1992). The thesis was generously supported by Gold Fields South Africa and Gold Fields Namibia to whom I am very grateful. Richard Viljoen, Erhardt Kostlin and Pat Vickers are particularly thanked for their assistance. Louis Kruger, and especially Volker Petzel, are thanked for logistical help in Namibia. Without Gold Field's financial support this project would never have got off the ground. I also acknowledge the receipt of a CSIR doctoral bursary from the South African government.

In Namibia, many thanks to Franco Pirajno, Volker Petzel, Frikkie Badenhorst, Roger Swart, Dudley Corbett and Le Roux van Schalkwyk for the exchange of geological ideas over the years. Gabi Schneider of the Geological Survey of Namibia is thanked for XRD work. Rob Carr and the management of Anglo American Prospecting Services Namibia are thanked for permission to sample the Epako borehole. The management of Navachab Gold Mine are thanked for granting permission to take four samples (NS324-327) of the Karibib Formation during a mine visit in May 1989 and for allowing publication of the geochemical data on the Etusis Formation. Ted Grobicki and the management of Randex are thanked for permission to sample the Habis Gold Prospect. John Twidale and Genmin Namibia are thanked for providing logistical support on a field trip in 1991. I wish to thank the farmers Klaus Byrne and his family of the farm Ehuero, Frau Gladys of Abbabis and Frau Arnold of Otjua for allowing us to camp on their properties and making our field work so pleasant. A very special thank you to Dieter and Thea Lauenstein for accommodating us in Windhoek and for financial support.

At Scientific Services Pty, Cape Town, I would like to thank Stuart Moir and, particularly, Ralph Freese for help with various analytical problems. At the Geological Survey of South Africa, Pretoria, I wish to thank Mr Trojak for help with the CO<sub>2</sub> and H<sub>2</sub>O determinations and Dr Edge, Frikkie Snyman and Peter for their assistance with the gold analyses.

At the University of Cape Town I am indebted to many people. In the Department of Geology, a special thank you to my thesis supervisors John Moore and Chris Hartnady. Huw Humphreys is thanked for help with microscopy in general and for commenting on Chapter 5. Rose Kovats is thanked for help with draughting. Rob Oliver and Henry Hendricks are thanked for their efforts in cutting thin sections. In the Department of Geochemistry, I would like to thank Bruce Cairns and Dave Wilson for technical assistance. Andy Duncan and Dave Hill are thanked for ex-

plaining the intricacies of UNIX and help with computing in general. Dave Reid, and especially James Willis, answered numerous questions on the analysis of rocks in general and XRF in particular. I am particularly grateful to Richard Armstrong and Chandra Harris for their help in the radiogenic isotope laboratory and to Dick Rickard and Marshall Otter for their assistance with electron microprobe analysis.

In the Department of Analytical Chemistry, Bruno Pougnet and Gary Gabriels are thanked for their help with the boron analyses. Kevin Faure is thanked for the front cover photo-

graph.

A very special thank you to Move, my wife, for her fantastic support and encouragement over the years in the field and the laboratory and especially her work in draughting the maps and diagrams.

Finally, although this memoir overlaps with my Ph.D. thesis, it has benefited considerably from the critical reviews of Roger Jacob and Judith Kinnaird. Dave Reid and Richard Armstrong commented on the revised Chapter 6.



## 2. LITHOSTRATIGRAPHY AND LITHOGEOCHEMISTRY

### 2.1 INTRODUCTION

#### 2.1.1 Pre-Damaran basement

The oldest rocks in central Namibia are the pre-Damaran basement gneiss lithologies of the Abbabis Inlier (Fig. 1.2). Gevers (1931) recognised the unconformity with the overlying basal conglomerate of the Damaran Nosib Formation on the farm Abbabis 70 and proposed the name Abbabis System for this early Proterozoic assemblage. The term Abbabis Complex was accepted by SACS (1980). The first U-Pb age determination on the Narubis Granitoid Complex of the Abbabis Inlier (nomenclature of Brandt, 1987a) was conducted by Jacob *et al.* (1978). Zircons from "granite-gneiss" yielded a concordia age of  $1925^{+330}_{-280}$  Ma. These granitoids have intruded basement metasedimentary and metavolcanic host rocks and thus provide minimum ages for the inlier. The Narubis Granitoid Complex comprises various granite gneisses with subordinate hornblende gneiss, quartz-feldspar-biotite-andalusite-garnet gneiss, biotite-sillimanite-garnet schist, quartzite and amphibolite (Fig. 2.1). Granite gneisses, formerly granitoids, comprise more than 95% of the Abbabis-age rocks in the mapped area. Other lithologies are preserved as metre-size xenoliths or fragments, up to one hundred metres in length.

Two notable discoveries made during the course of field work are that the Abbabis Inlier in the Usakos-Karibib area is locally cut by major east-northeast-trending shear zones and an east-northeast-trending metadolerite dyke swarm (Fig. 2.1) that shows similarities with the late Proterozoic Gannakouriep mafic dykes of southern Namibia. The Narubis Granitoid Complex is transected by a number of sub-

vertical east-northeast-trending megashear zones that show evidence for significant lateral displacement. These shear zones are cut by undeformed pegmatites almost certainly of late Damaran age. Associated rocks include biotite phyllites (metamorphosed fault gouge?) with east-northeast-trending (Damaran?) foliations. South of Karibib the Abbabis Inlier has been intruded by a swarm of mafic dykes that were possibly intruded between 900 and 1000 Ma during the rifting that initiated the Damaran episode. The metadolerites bear similarities to the mafic dyke swarm in the Abbabis Inlier near Swakopmund (Jacob, 1988, pers. comm.). These subvertical dykes postdate the development of the megashears and, as far as the author is aware, nowhere in the Usakos-Karibib area do they crosscut the overlying Damaran lithologies. The metadolerites, which have not been identified in the NCZ, may be up to several tens of metres wide, have undergone greenschist facies metamorphism and minor post-crystallisation deformation. The term metadolerite is preferred over amphibolite because their subvertical intrusive nature can readily be seen in the field. A small number of dykes possess a faint foliation but the majority are unfoliated and comprise actinolitic hornblende, plagioclase, minor quartz, K-feldspar, opaque minerals, and traces of epidote, chlorite and malachite. In what appears to be an older generation of metadolerite dyke (as determined from crosscutting relationships), biotite comprises up to ten modal per cent, but no primary mica was noted. In these earlier dykes, strained, primary (igneous) andesine-labradorite laths up to 5 mm long are surrounded by randomly oriented metamorphic amphibole and biotite. Whether this relatively high potassium content is a reflection of the alkaline affinity of the magma from which the dolerite crystallised or results

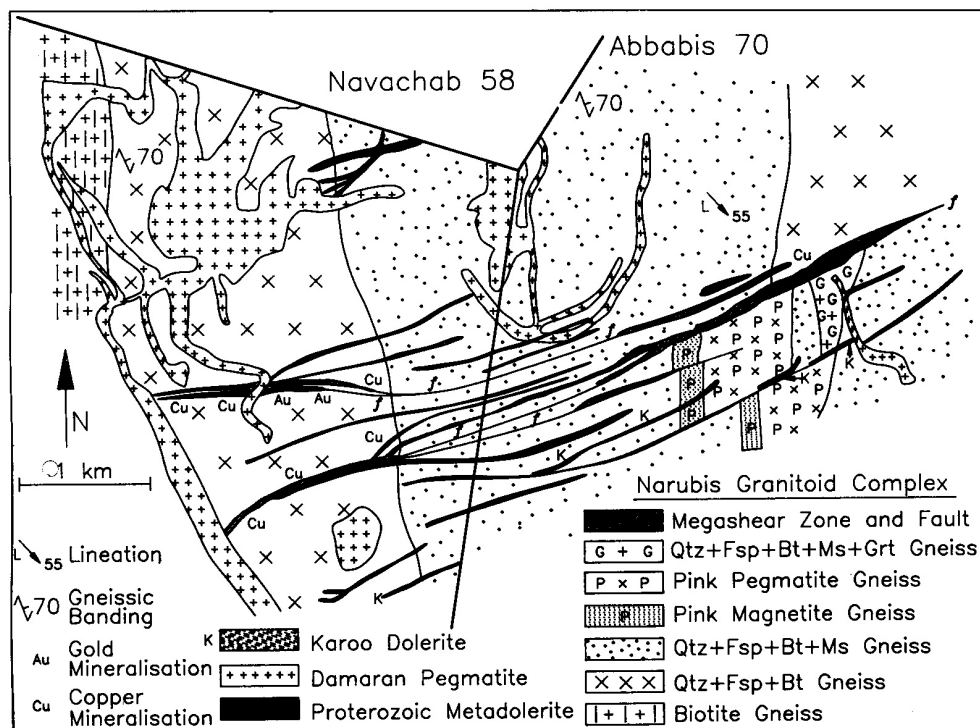


Figure 2.1: Simplified geological map of a portion of the Abbabis Inlier

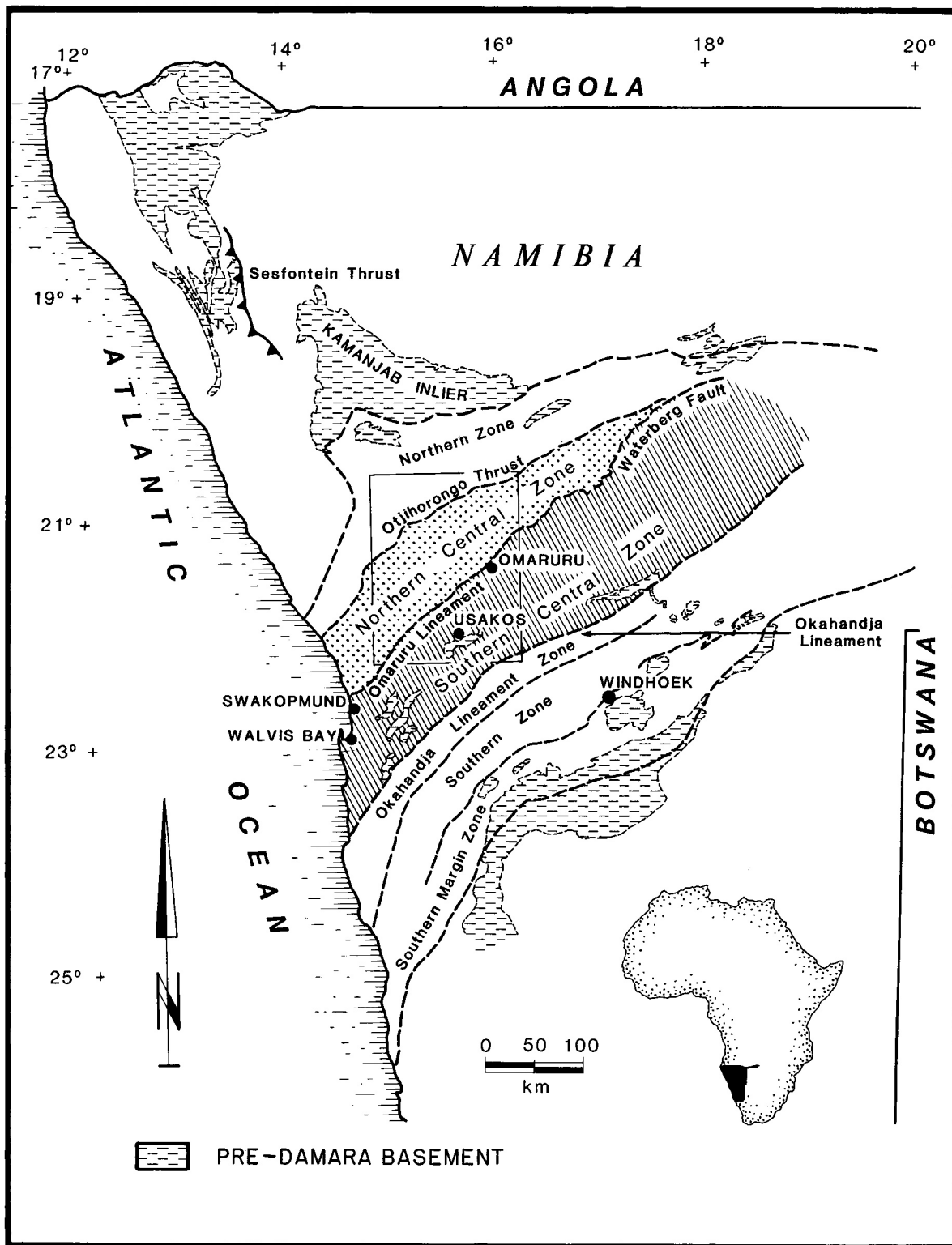
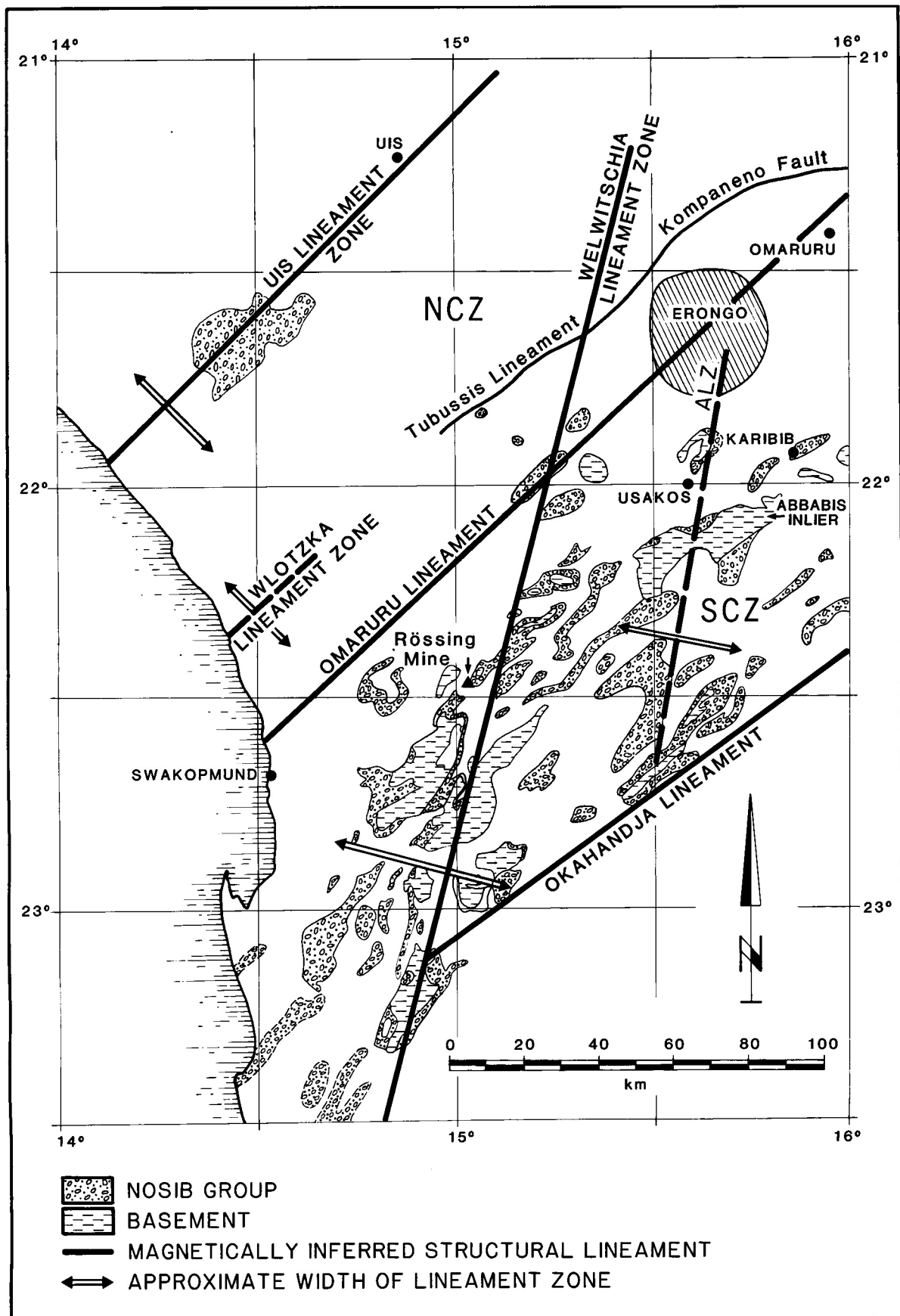


Figure 2.2: Tectonostratigraphic zones of the Damara Orogen (after Miller, 1983a) with Figure 1.3 outlined

from metasomatism is difficult to say. A distinctive lithology intimately connected with the metadolerites in the vicinity of shear zones is coarse-grained, orbicular aggregates of anthophyllite, chlorite and magnetite. This unusual rock type may represent altered immiscibility products formed from the stopping of granite-gneiss wallrocks by the intrud-

ing mafic magma. In common with the shear zones, these anthophyllite-chlorite-magnetite rocks possess anomalous gold contents. Numerous xenoliths of magnetite-amphibolite (hornblendite) in undeformed late-tectonic magnetite-bearing pegmatites found on the northern edge of the SCZ on the farm Lukasbank (Fig. 1.3; Map 6) are interpreted as frag-



**Figure 2.3:** Structural lineaments and exposures of basement inliers and Nosib Group metasediments in central Namibia (modified after Corner, 1983)

Group	Formation	Lithologies
Swakop	Kuiseb	Metaturbidites and Biotite Schists and minor Calc-silicate Rocks and Marble
	Onguati	Quartzite, Schist, Calc-silicate Rock, Marble
	Karibib	Calcitic and Dolomitic Marble and minor Calc-silicate Rocks and Schist
		Daheim Member Continental Mafic Volcanics (only present in SCZ)
		Omusema Member Amphibolites (only present in SCZ)
	Oberwasser	Biotite Schist, Calc-silicate Rocks and very minor Felsic Volcanics
	Okawayo	Calcitic Marble
	Spes Bona	Biotite Schist, Calc-silicate Rocks and very minor Felsic Volcanics
Chuoss	Glaciogenic Mixtite, Banded Iron Formation	
	Rössing	Dolomitic Marble, minor Calc-silicate Rocks and Calcitic Marble
Nosib	Khan	Pyribole Calc-silicate Rocks, minor Biotite Schist, Graphite Schist and Marble
	Etusis	Feldspathic Quartzite, Grit and minor Calc-silicate Rocks and Schist

**Table 2.1:** Damaran stratigraphy of the Central Zone in the Usakos—Karibib—Omaruru area

ments of pre- or early Damaran mafic dykes.

### 2.1.2 Damara Sequence

The intracontinental branch of the overlying Pan-African Damara Orogen, which contains only minor volcanic rocks, has been divided by Miller (1983a) into several tectono-stratigraphic zones (Fig. 2.2). The Usakos-Karibib-Omaruru area is underlain by the Central Zone (CZ) of the Damara Orogen, which, according to Miller (1983a), is characterised by sillimanite-cordierite metamorphic assemblages, widespread granite intrusions and northeasterly trending  $D_3$  domal structures. However, recent mapping has shown that certain areas in the CZ have been metamorphosed to only greenschist grade. The CZ is divided into a northern portion (NCZ) and a southern one (SCZ) by the northeast-trending Omaruru Lineament-Waterberg Fault (Fig. 2.2). The term Omaruru Lineament (Fig. 2.3) was introduced by Corner (1983) to distinguish between the “magnetically quiet domain of the northern portion of the Central Zone (NCZ) and the disturbed part of the rest of the Central Zone to the south (SCZ)” (the lineament is best observed on the aeromagnetic colour composite map of central Namibia; Corner, 1981). There are significant sedimentological facies changes across the Omaruru Lineament and Badenhorst (1986b) considered the structure to be a major tectono-stratigraphic boundary. However, the structure is commonly difficult to pinpoint in the field: for example to the east and south of the Erongo Complex the boundary between the SCZ and the NCZ is diffuse and marked by a series of east-northeast-trending magnetic features. Moreover, the extensive granite intrusions and poor exposure on the eastern side of the Erongo Complex hamper interpretation. That there is a major tectonic break between the NCZ and the SCZ to the northeast of the Erongo Complex is evident

near Omaruru where several northeast-trending megafaults, that are southwestward extensions of the Waterberg Fault, are clearly visible (Map 1). Some of these faults were re-activated during Karoo times. Corner (1983) also identified two north-northeast-trending magnetic features named the Welwitschia and Abbabis lineament zones (ALZ; Fig. 2.3). Corner considered these zones to correspond to exposures of basement and the former to have had an important influence on the localisation of uraniferous alaskitic granites such as are developed at the Rössing Uranium Mine. More recently, Hoffman (1989) has referred to the Central Zone as the ‘Swakop Tectono-stratigraphic Terrane’. Because Hoffman’s work concentrates on the southern Damara and the southern foreland and he did not subdivide the Swakop Terrane into northern and southern portions, the term Central Zone (CZ) has been retained for this memoir.

The lithostratigraphy of the Damara Sequence in the CZ has been reviewed and significantly revised by Badenhorst (1981), who has also correlated the stratigraphy across the Omaruru Lineament. Badenhorst’s (1987) review integrated his work with the regional geology compiled by Smith (1965), Botha (1978), Klein (1980), Watson (1982) and Brandt (1985). The stratigraphy of the CZ (slightly modified after Badenhorst, 1987 and 1988a, p.67) is given in Table 2.1. The SCZ is characterised by granitic gneisses of the Abbabis Complex and Damaran Nosib Group arkoses and lower Swakop Group shelf carbonates, mantled gneiss domes and amphibolite facies metamorphism. One of the best stratigraphic sections in the northern SCZ is exposed on the farm Okawayo (Fig. 1.3; Steven and Badenhorst, 1988).

The NCZ is underlain by very minor Nosib Group sediments and upper Swakop Group shelf carbonates (including the important marker marbles of the Karibib Formation) and overlying pelagic sediments (Kuiseb Formation), which have

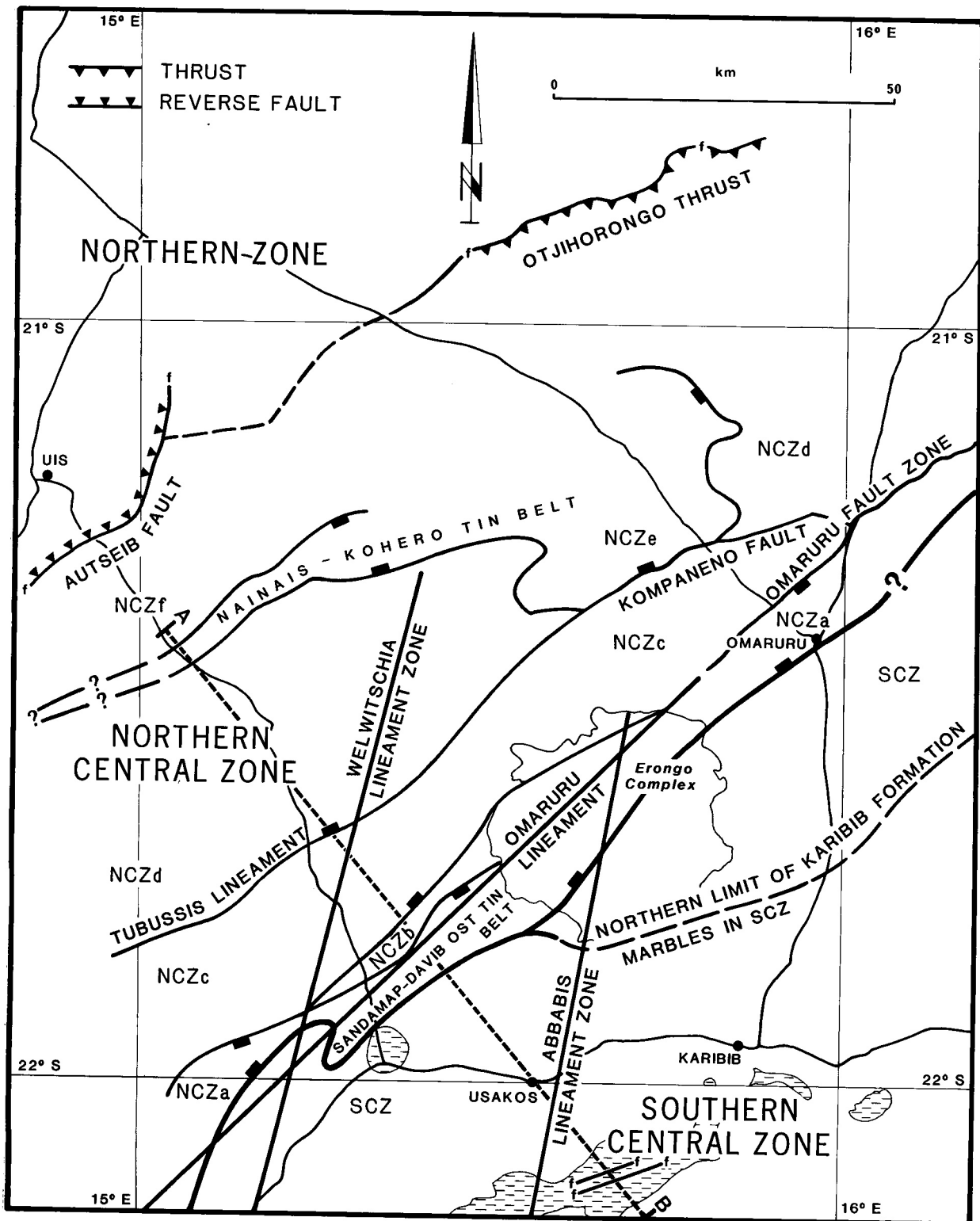


**Figure 2.4:** Tectonostratigraphic zones of the Usakos—Karibib—Omaruru area (modified after Badenhorst, 1987). Block on side of fault/lineament that on aggregate was downthrown during Damaran sedimentation. A-B marks section line shown in Figure 2.5

generally been metamorphosed at lower grades than the SCZ and intruded by a number of syn- and late-tectonic granites and pegmatites. Badenhorst (1987) has divided the NCZ itself into six tectono-stratigraphic zones (NCZa-f; Figs. 2.4 and 2.5) and the distribution of the formations within the zones is given in Table 2.2. This division is based on differences in stratigraphy, structure, grade of metamorphism, age of intrusive rocks and geophysical characteristics (Klein, 1980;

Watson, 1982; Badenhorst, 1986a; Steven, 1987). Boundaries between these subzones form major east-north east- or northeast-trending linear features and are either faults, stratigraphic boundaries or combinations of these. Northeast-trending faults are considered to have played a major role in controlling sedimentation in the NCZ. In NCZa (which includes the Sandamap-Davib Ost Tin Belt) and NCZe (the

SCZ	NCZa	NCZb	NCZc	NCZd West of Erongo	NCZd North of Omaruru	NCZe
L. Kuiseb Karibib Oberwasser (Okawayo) (Spes Bona) Chuos Rössing Khan Etusis	U.Kuiseb	L. Kuiseb Karibib Oberwasser  Etusis	L. Kuiseb Karibib Oberwasser (Okawayo) (Spes Bona)  Etusis	L. Kuiseb Karibib Oberwasser	L. Kuiseb Karibib Oberwasser Okawayo Spes Bona	U. Kuiseb

**Table 2.2:** Distribution of Damaran formations in the SCZ and NCZ (formations in brackets only present east of Abbabis lineament zone)

SCZ	NCZa	NCZb	NCZc	NCZd West of Erongo	NCZd North of Omaruru	NCZe
L. Kuiseb Karibib UM Karibib US (Karibib LM) (Karibib LS)  Chuos Rössing Khan Etusis	U.Kuiseb	L. Kuiseb Karibib UM  Oberwasser  Etusis	L. Kuiseb Karibib UM (Karibib US) (Karibib LM) (Karibib LS) Oberwasser  Etusis	L. Kuiseb Karibib UM  Oberwasser	L. Kuiseb Karibib UM Karibib US Karibib LM Karibib LS	U. Kuiseb

**Table 2.2a:** Distribution of Damaran formations in the SCZ and NCZ - an alternative stratigraphy. UMU= Upper Marble Unit; USU = Upper Schist Unit; LMU = Lower Marble Unit; LSU = Lower Schist Unit (formations in brackets only present east of Abbabis lineament zone)

Nai-nais-Kohero Tin Belt) only the higher levels of the Kuiseb Formation crop out (Fig. 2.5). The absence of Nosib Group sediments in the tin belts (Corner, 1983) suggests that these were basement highs during Nosib times; reverse displacement probably occurred along the listric faults during Kuiseb times (Fig. 2.5). In NCZe the peak regional metamorphic grade is significantly lower (i.e. greenschist) than in the other zones. In NCZb, Nosib Group sediments crop out locally and the Karibib Formation comprises several thin marble horizons which rarely attain a thickness of more than 100 metres. Only the lower levels of the Kuiseb Formation crop out in NCZb. In NCZc only very minor Nosib Group sediments are present, the thickness of the Karibib-Formation is highly variable and the lower Kuiseb Formation metapelites and calcareous lithologies are well developed. Syntectonic garnetiferous leucogranite intrusions in the Kuiseb Formation are widespread in NCZc. On the northern side of the Tubussis Lineament (the strike extension of the Wlotzka lineament zone; Fig. 2.3) in NCZd there is a pronounced thickening of the calcareous lithologies of the Swakop Group (the several-hundred-metre-thick Karibib Formation marbles

in particular) and these are overlain by pelagic sediments of the Kuiseb Formation. To the north of Omaruru, NCZd is underlain by Swakop Group calcareous and calc-silicate lithologies, some of which may represent meta-evaporites. Large volumes of late- to post-tectonic granites commonly crop out in the cores of domal structures in NCZd north of Omaruru. NCZf lies outside the field area. In this chapter the important regional, tectonically controlled variations in the sediments are emphasised and the various styles of metasediment-hosted mineralisation are introduced (Table 2.3).

### 2.1.3 Post-Damaran geology

Post-Damaran activity in the CZ included considerable faulting, movement on the Omaruru Lineament-Waterberg Fault in the vicinity of Omaruru and the intrusion of a large number of Karoo dolerite dykes. In the Abbabis Inlier the dykes are oriented east-northeast (Fig. 2.1), in the vicinity of Omaruru a number of dykes have intruded parallel to major northeast-trending faults (Map 1) and west of Usakos a north-

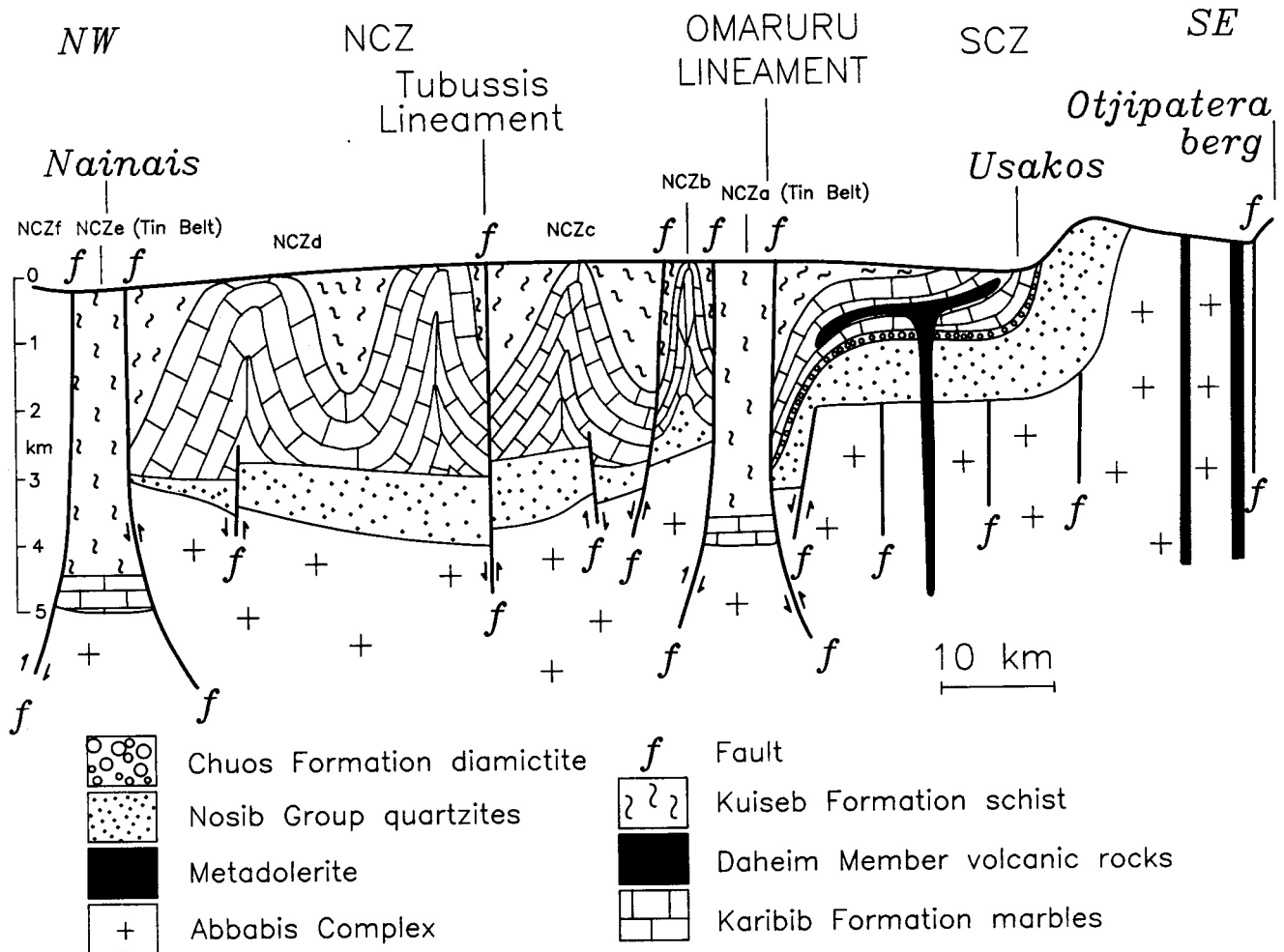


**Figure 2.5:** Schematic cross-section through the CZ showing monoclinial downfold across Omaruru Lineament. Basement profile and thickness of Nosib Group in NCZ taken from Corner's (1983) computer-model section. Granitoids have been omitted

northeast-trending dyke swarm, approximately 25 kilometres wide, has intruded along the Welwitschia lineament zone (Fig. 2.3). In post-Karoo times (approximately 130-120 Ma) the Gross and Klein Spitzkoppe, Otjhorongo and Omaruru Hills granites and the Okonjeje and the Erongo complexes were intruded. A poorly exposed, undeformed hornblende-diorite plug with gabbroic and lamprophyric portions on the farm Eausiro West 101 (Map 1) may be of post-Karoo age. The Tertiary to Quaternary Kalahari Group in the CZ is represented by sand and calcrete, the major river beds possessing coarse- to fine-grained fill.

## 2.2 THE LITHOSTRATIGRAPHY OF THE DAMARA SEQUENCE

### 2.2.1 Nosib Group

The sediments of the Nosib Group in the CZ are dominated by the meta-arkoses of the Etusis Formation and the calc-silicate lithologies of the Khan Formation. Evidence for the existence of minor metamorphosed felsic volcanic rocks in the Nosib Group elsewhere in the CZ was presented by Jacob (1974) and Blaine (1977).

#### 2.2.1.1 Etusis Formation

Smith (1965) has described the nature of the "Nosib Formation" in the southern SCZ in detail. The arkosic metasediments of the Etusis Formation are best developed in the vicinity of the Abbabis Inlier, where they attain a maximum thickness of 3300 m. The Etusis Formation is only locally developed in the NCZ and its most northerly occurrence in the area under review is just south of the Tubussis Lineament in NCZc (Fig. 2.3). In NCZb a sequence of pink-weathering feldspathic quartzites, approximately 1000 m thick, is poorly exposed in the core of a northeasterly trending domal structure in the northwest corner of Sandamap Noord (Map 3). The metaquartzites are locally cross bedded and possess a number of bedding-parallel ferruginous stringers which give a diagnostic pinkish colour to this lithology. A characteristic feature of the Etusis Formation where it has undergone upper amphibolite facies metamorphism is the presence of oblate spheroids of fibrolite usually less than 2 cm in diameter. Similar concentrations of fibrolite were noted in the Etusis Formation by Blaine (1977) in the vicinity of the Waldau Ridge (op. cit., p.11-12). Very subordinate marble, calc-silicate rocks and quartz-biotite schists are also developed within the Etusis Formation on Sandamap Noord, which has been extensively intruded by quartzo-feldspathic intrusive rocks.

This style of intrusion is confined to the Nosib Group and facilitates mapping in areas of poor exposure.

Samples of Etusis Formation quartzite from NCZb, namely the core of the Sandamap Noord dome and the northern SCZ in the Okawayo Section (Badenhorst, 1987), were examined microscopically and geochemically. The peak metamorphic conditions at these localities were upper amphibolite and lower amphibolite facies respectively. The quartzite comprises quartz (70-90%), altered feldspar (20-30%), muscovite (0-5%), biotite (0-2%) and traces of pyrite, sphene and zircon. Interstitial iron oxides, primarily haematite and goethite (locally after pyrite) are concentrated in 1-cm-long stringers and may comprise 5% of the rock. The quartz grains are embayed or lobate and locally granoblastic and oriented muscovite overgrows altered interstitial feldspar. The composition of the feldspar cannot always be determined optically on account of the alteration, but the proportions of alkalis in the bulk-rock analyses (Table 2.4) indicate that the majority was K-feldspar. The Etusis Formation quartzites are subarkoses (locally arkoses) according to the classification of Folk (1968). The fibrolite spheroids comprise fine-grained sillimanite with traces of muscovite, graphite and sphene.

Although no sedimentological facies analysis has been conducted, the Etusis Formation of the NCZ and the northern SCZ is distinctly thinner and more mature than in the southern SCZ. For example, at the Nordenburg Gold Prospect (Fig. 1.4) on the flanks of the Abbabis Inlier, the Etusis Formation is several thousand metres thick and possesses numerous grit layers. Concentrations of detrital iron minerals on bedding planes may be 5 mm thick. Conglomeratic bands are common in the Etusis Formation of the southern SCZ and crossbedding was noted near the SJ Claims (now Rössing Uranium Mine) by Smith (1965). In contrast, pebbly or gritty layers are absent and planar crossbedding is rare on Sandamap Noord and in the Okawayo Section. Iron minerals are important accessories, but concentrations are not as high as in the southern SCZ. The Etusis Formation is considered to represent a sequence of fluvio-deltaic sediments derived from pre-existing granitic basement (Miller, 1983a) and, from the limited data available, it would indeed seem that, in the CZ, this formation was derived from lithotypes similar to those found in the Abbabis Inlier. No further volcanic rocks in the Etusis Formation were discovered during the course of field work.

The Etusis Formation is known to host two styles of epigenetic mineralisation (Table 2.3). At the Nordenburg Gold

Formation	Syngenetic Mineralisation	Epigenetic Mineralisation and Host Rock	Table
U. Kuiseb	W in Calc-Silicate Rocks	W in Vesuvianite Skarnoid Rocks Tourmaline Alteration in Schist	7/7-1
L. Kuiseb	W in Calc-Silicate Rocks	Shear-hosted Gold-Arsenic in Schist Tungsten Skarn in Marble	7/5-1
Onguati		Tourmaline Alteration in Quartzite	
Karibib		Gold Skarn in Marble Tin Skarn in Marble	7/4-1,8
Oberwasser	W in Calc-Silicate Rocks	Gold Quartz Veins hosted by Schist	
Okawayo		Tungsten Skarn in Marble Gold Skarn in Marble	7/3-1
Spes Bona	W in Calc-Silicate Rocks		
Chuos	BIF in Glaciogenic Mixtite Massive Sulphide		
Rössing	Cu-Ironstone, Magnetite Quartzite		
Khan	Cp, Po, Py, W in Calc-Silicate Rocks		
Etusis		Magnetite-Monazite Skarn(?) in Marble Gold Quartz Veins in Metaquartzite	7/2-1
Abbabis Complex		Gold Quartz Veins in Granitic Basement	

Table 2.3: Syngenetic and epigenetic metasediment-hosted mineralisation in the CZ. W = Scheelite

Prospect, quartzitic metasediments host minor auriferous quartz veins where they directly overlie basement lithologies. Folded dolomitic marbles at the top of the Etusis Formation host unusual magnetite-monazite mineralisation on the farm Eureka (Map 5). This occurrence has variously been described as a skarn and an unusual carbonatite and will be discussed in detail in Chapter 7. The lithology that encloses this carbonate is a quartzo-feldspathic gneiss with minor biotite, carbonate, graphite, muscovite, zircon and iron oxides and is considered to represent a metapsammite (Table 2.4).

### 2.2.1.2 Khan Formation

The term Khan Formation was first used by Nash (1971) to describe a sequence of quartz-feldspar-clinopyroxene-amphibole gneisses which overlie the Etusis Formation. This is the equivalent of the calc-granulite facies of the 'Nosib Formation' of Smith (1965). Miller (1983a) described the Khan Formation as a succession of marly sediments now consisting of pyroxene-amphibole-bearing feldspathic quartzite and Watson (1982) discussed the nature of the Khan Formation to the northwest of Usakos. The Khan Formation is confined to the SCZ (Table 2.2) and is best developed to the southwest of Usakos in the Khan River near the Rössing Uranium Mine (Smith, 1965). The most northerly outcrops are on the farms Sandamap and Eureka (Maps 4 and 5). Here the formation is dominated by a 1500-m-thick sequence of pyroxene-amphibole calc-silicate rocks with a characteristic streaky, almost gneissic, texture. Very subordinate quartz-biotite schist, graphite schist and calcitic and dolomitic marbles are also present. Although poorly exposed, the sequence does not appear to be duplicated. As with the underlying Etusis Formation, the Khan Formation thins with increasing distance from the Abbabis Inlier and is less than 20 m thick in the Okawayo Section (Badenhorst, 1987).

The calc-silicate rocks of the Khan Formation in the Sandamap area were examined in detail. No sedimentary features were noted in the calc-silicate gneiss which comprises quartz (35-45%), plagioclase (20-40%), hornblende (5-20%), clinopyroxene (5-10%), biotite (1-5%), chlorite (trace-5%), sphene (trace-4%), muscovite (0-3%), carbonate (<1%), apatite (trace), graphite (trace), zircon (trace) and hematite (trace). Sulphides are a prominent accessory in almost all specimens and include subhedral pyrite and anhedral pyrrhotite and chalcopyrite. The plagioclase is extensively altered and microcline may also be present. The grain size is usually less than 0.7 mm, locally up to 2 mm. A poorly developed fabric in the gneiss is defined by the long axes of the micas. Textural features of note are the lobate or cusped and even angular nature of the quartz grains. Anhedral hornblende exhibits a poikiloblastic texture and appears to overgrow pyroxene. Chlorite is locally associated with amphibole. A point of note is the absence of scapolite in the Khan Formation on Eureka, in contrast to the formation in the type area (Smith, 1965). Geochemical analyses of the Khan Formation calc-silicate rocks are listed in Table 2.5. Graphite schist on Eureka may be the strike equivalent of the graphite deposits on Black Range (Fig. 1.3) and comprises quartz ( $\pm 40\%$ ), altered K-feldspar ( $\pm 40\%$ ), graphite

	NS256	NS257	NS328	NS348
SiO <sub>2</sub> (wt%)	85.97	84.93	85.73	78.87
TiO <sub>2</sub>	.18	.25	.29	.36
Al <sub>2</sub> O <sub>3</sub>	6.53	7.47	6.97	10.64
Fe <sub>2</sub> O <sub>3</sub>	.28	.19	.16	.44
FeO	.89	.61	.43	.79
MnO	.01	.03	<.01	.04
MgO	.26	.24	.08	.37
CaO	.09	.16	.12	1.00
Na <sub>2</sub> O	1.09	1.66	.68	4.32
K <sub>2</sub> O	3.29	3.40	5.01	2.22
P <sub>2</sub> O <sub>5</sub>	.04	.07	.09	.10
H <sub>2</sub> O-	.11	.06	.08	.15
H <sub>2</sub> O+	.55	.50	.27	.61
CO <sub>2</sub>	.32	.45	.09	.44
TOTAL	99.62	100.02	99.99	100.33
F (ppm)	235	355	340	370
S	6	772	505	163
Rb	108	116	171	71
Ba	858	768	980	621
Sr	62	110	55	252
Th	7	8	21	6
U	2	2	1	<1.2
Zr	123	164	222	281
Nb	8	12	9	14
Mo	<.5	<.5	1	1
Sn	2	3	<1.3	<1.3
W	<3.9	<3.9	16	13
V	12	13	28	18
Cr	16	15	18	25
Co	<1.8	<1.7	<1.6	4
Ni	7	5	4	8
Cu	6	7	6	8
Zn	9	6	8	18
Ga	6	7	5	9
Pb	18	15	12	13
Ge	<.8	<.8	<.8	<.8
As	.9	1.0	.8	<.7
Sb	<1.1	<1.1	<1.1	<1.1
Bi	<2.5	<2.5	<2.5	<2.5
Se	<.7	<.7	<.7	<.7
Te	<1.8	<1.8	<1.8	<1.8
Sc	2	3	2	4
Y	13	13	15	13
La	15	17	23	20
Ce	27	35	45	41
Nd	14	16	28	22
Au (ppb)	<5	<5	<5	7

**Table 2.4:** Whole-rock analyses of the Etusis Formation metaquartzites on Sandamap Noord, Okawayo and Eureka  
 NS256: Sandamap Noord 115, Usakos District: 4 km NW of Sandamap Tin Mine  
 NS257: Sandamap Noord 115, Usakos District: 4.2 km NW of Sandamap Tin Mine  
 NS328: Okawayo Section, Okawayo 46, Karibib District  
 NS348: Eureka 99, Usakos District: vicinity of magnetite-monazite occurrence

( $\pm 10\%$ ), altered mica and traces of hematite. Quartz is arranged granoblastically and enveloped by the feldspar, while the graphite flakes do not exceed 1 mm in length.

	NS258	NS259	NS260	NS261
SiO <sub>2</sub> (wt%)	69.34	68.57	69.14	70.41
TiO <sub>2</sub>	.68	.67	.73	.68
Al <sub>2</sub> O <sub>3</sub>	10.15	9.69	10.46	10.40
Fe <sub>2</sub> O <sub>3</sub>	.22	.26	.16	.30
FeO	3.97	4.25	4.49	4.14
MnO	.13	.12	.15	.14
MgO	2.80	3.15	2.86	2.69
CaO	8.30	9.31	8.31	7.79
Na <sub>2</sub> O	1.08	.54	.52	.89
K <sub>2</sub> O	1.10	1.33	.86	.43
P <sub>2</sub> O <sub>5</sub>	.16	.16	.17	.16
H <sub>2</sub> O-	.05	.18	.12	.14
H <sub>2</sub> O+	.74	1.18	.78	.66
CO <sub>2</sub>	.95	.64	.62	1.00
TOTAL	99.66	100.32	99.37	99.82
F (ppm)	466	255	1052	431
S	<5.1	212	1388	262
Rb	44	68	92	26
Ba	288	400	359	326
Sr	200	166	199	184
Th	9	9	10	9
U	3	2	4	3
Zr	229	224	229	225
Nb	11	10	12	10
Mo	<.5	.6	.7	<.5
Sn	8	5	11	6
W	7	<4.9	<4.9	<4.8
V	98	95	107	99
Cr	95	88	100	90
Co	9	12	13	12
Ni	30	31	40	29
Cu	12	22	93	11
Zn	70	62	84	64
Ga	12	12	13	12
Pb	18	5	8	14
Ge	<1.0	<1.0	<1.0	<1.0
As	1.0	<.9	1	<.9
Sb	<1.3	<1.3	<1.3	<1.3
Bi	<3.0	<3.1	<3.1	<3.0
Se	<.9	<.9	2	<.9
Te	<2.1	<2.1	<2.1	<2.1
Sc	13	13	14	14
Y	33	35	33	33
La	28	27	26	28
Ce	56	53	55	54
Nd	30	31	30	30
Au (ppb)	<5	<5	12	<5

**Table 2.5:** Whole-rock analyses of the Khan Formation calc-silicate rocks on the farm Sandamap 64, Usakos District  
 NS258: 3.5 km ENE of Vaalkop, Qtz+Plag+Hbl+Cpx+Bt calc-silicate rock  
 NS259: 3.1 km ENE of Vaalkop, Qtz+Plag+Hbl+Bt+Cpx calc-silicate rock  
 NS260: 2.2 km ENE of Vaalkop, Qtz+Plag+Hbl+Bt calc-silicate rock  
 NS261: 2.2 km ENE of Vaalkop, Qtz+Plag+Hbl+Cpx+Bt calc-silicate rock

The Khan Formation is of economic interest for a number of reasons. Firstly, bedding-parallel copper-bearing layers are present in coarse-grained calc-silicate rocks at the Khan Mine (Ramdohr, 1938). Miller (1983b) suggested that these were derived from the metamorphism of evaporitic layers rather than as the result of igneous intrusion. Thus the presence of disseminated pyrrhotite-chalcopyrite-pyrite mineralisation in the Khan Formation of the Eureka dome is noteworthy. Secondly, large amounts of ironstone float in areas underlain by the Khan Formation were noted on Eureka (Map 5). No outcrop of ironstone was discovered, but this concentration of ironstone float is unusual. Thirdly, stream sediment sampling of the farm Black Range by Johannesburg Consolidated Investment Co. in the early 1980s revealed the presence of a number of tungsten anomalies in areas underlain by the Khan Formation. Because of the lack of mineralised pegmatites at this stratigraphic level and in this area (Frommurge *et al.*, 1942) it is considered unlikely that these anomalies are derived from degraded wolframite. Although this area has not been examined by the author, the presence of a style of mineralisation similar to the calc-silicate-hosted scheelite of the Swakop Group (Steven, 1987) seems likely (Table 2.3).

## 2.2.2 Swakop Group

The Swakop Group comprises calcareous and overlying pelitic lithotypes (Table 2.1) and hosts several styles of epigenetic gold, tin and tungsten mineralisation (Table 2.3). In addition, sulphide and scheelite mineralisation that can broadly be described as syngenetic will be reviewed.

### 2.2.2.1 Rössing Formation

The Rössing Formation is confined to the SCZ (Table 2.2) and is not developed east of the Abbabis lineament zone (Fig. 2.4). The large number of lithologies which constitute the Rössing Formation in the type area in the southern SCZ have been discussed by Jacob (1974). In the northern SCZ west of Usakos, the Rössing Formation is represented by dolomitic marble (Watson, 1982). The outcrops in the Sandamap-Goabeb area, immediately south of the Omaruru Lineament, represent the northern limit of its distribution. Here dolomitic marble with very subordinate calcitic marble and calc-silicate rocks is exposed within the core of the Eureka, dome (Maps 4 and 5). The original thickness of the formation is probably in the order of 300 m, but assessments are complicated by the folding. A pale yellow or buff colour and the presence of coarse-grained crystals of tremolite, forsterite, serpentine and phlogopite clearly distinguish this carbonate from the more calcareous marbles higher up in the Swakop Group. This marble is extracted as an ornamental stone on the farm Namibfontein. The Rössing Formation hosts a number of predominantly scapolitic skarns with subordinate garnet and pyroxene. Watson (1982) attributed the development of these skarn minerals to the metamorphism of a type of evaporite deposit, though in many instances pegmatitic bodies are present in close proximity to the skarn and a magmatic origin or modification by magmatic fluids appears more plausible.

The Rössing Formation in the Sandamap-Eureka area was examined microscopically and geochemically (Table 2.6). The dolomitic marble comprises dolomite (30-95%), calcite (2-40%), forsterite (trace-20%), serpentine (trace-8%), tremolite (trace-5%) and phlogopite (trace-3%) and the grain size varies from a few microns to 4 mm. In general the marble has a granoblastic polygonal mosaic texture with some dolomite grains having a lobate nature and locally serrated grain boundaries. Calcite is anhedral and interstitial to the larger dolomite grains. Forsterite and phlogopite are universally associated with calcite suggesting that they grew during dedolomitisation. A good example of dedolomitisation can be seen in sample NS265 which contains nearly 8 wt% H<sub>2</sub>O. In this rock very fine-grained (<20 µm) rounded, subhedral dolomite is enveloped by a calcitic groundmass. Approximately ten per cent of the rock comprises aggregates of a colourless mineral that may be brucite or hydromagnesite. A cupriferous ironstone/gossan horizon has been discovered at the base of the Rössing Formation near Vaalkop on the farm Sandamap (Map 4). This horizon is traceable for a distance of approximately 700 metres and varies in thickness from two to five metres. Graphite and pyrite-bearing magnetite quartzites and an unusual malachite-stained hornblende rock are also present. In addition several small copper showings were noted in the Rössing Formation in the core of the Eureka dome (Map 5).

#### 2.2.2.2 Chuos Formation

The glaciogenic mixtite and associated Banded Iron Formation (BIF) of the Chuos Formation in the CZ have been exhaustively discussed by Gevers (1931), Smith (1965), Jacob (1974), Schermerhorn (1974), Martin *et al.* (1985) and Henry *et al.* (1986). Badenhorst (1987) reviewed the suitability of the Chuos Formation as a stratigraphic marker in the CZ. In the SCZ the Chuos Formation is well developed in the vicinity of the Abbabis Inlier (Smith, 1965) and is 220 m thick in the Okawayo Section, but is absent in the Sandamap-Eureka area (Maps 4 and 5). In the area of the NCZ investigated, the Chuos Formation is not present (Table 2.2), but Badenhorst (1987) has mentioned the presence of a pebbly schist below the Okawayo Formation in the NCZ to the southeast of the Messum Complex (in Area 2114C, Tsaun). The Chuos Formation comprises interbedded mixtite and magnetite-rich quartzite, the latter best developed close to basement highs (Martin, 1978). The only other known mineralisation hosted by this formation is the massive sulphide mineralisation in the vicinity of Rössing Mountain (Jacob, 1992, pers. comm.).

#### 2.2.2.3 Spes Bona Formation

The term Spes Bona Formation was first used by Badenhorst (1988a) to describe an intercalated sequence of biotite schist and calc-silicate rock below the Okawayo Formation marble. The formation is named after a farm in the Okawayo Section (Fig. 1.3), where it is approximately 30 metres thick. The Spes Bona Formation has not been recognised west of the Abbabis lineament and its distribution in the SCZ appears to be limited. On the northern side of the Erongo Complex the Spes Bona Formation is commonly the lower-most stratigraphic unit developed in NCZc and NCZd (Table 2.2). To

	NS262	NS263	NS264	NS265
SiO <sub>2</sub> (wt%)	.81	8.71	2.95	1.65
TiO <sub>2</sub>	.53	<.01	.03	.02
Al <sub>2</sub> O <sub>3</sub>	.07	.02	.23	.16
Fe <sub>2</sub> O <sub>3</sub>	.00	.06	.07	.00
FeO	.08	.11	.11	.21
MnO	.00	.04	.02	.02
MgO	20.85	18.97	19.48	23.53
CaO	31.46	33.42	32.36	34.86
Na <sub>2</sub> O	<.02	<.02	<.02	<.02
K <sub>2</sub> O	.03	.01	.13	<.00
P <sub>2</sub> O <sub>5</sub>	.11	.55	.09	<.00
H <sub>2</sub> O-	.05	.22	.14	.10
H <sub>2</sub> O+	.20	2.27	.88	7.79
CO <sub>2</sub>	45.36	34.90	42.20	30.68
TOTAL	99.55	99.27	98.69	99.02
F (ppm)	386	488	500	651
S	<3.7	<4.0	<3.6	<3.8
Rb	3	3	7	2
Ba	18	<2.0	57	12
Sr	88	144	163	171
Th	<1.8	<1.9	<1.9	<1.9
U	<1.4	<1.5	<1.4	<1.5
Zr	3	1	5	5
Nb	<.6	<.6	1	<.6
Mo	<.5	<.5	<.5	<.5
Sn	<1.4	<1.5	<1.5	<1.5
W	<4.3	12	<4.4	15
V	<1.7	<1.8	4	<1.8
Cr	2	3	2	3
Co	<1.7	<1.8	<1.8	<1.8
Ni	4	<1.6	<1.5	<1.6
Cu	<1.1	<1.2	<1.2	<1.2
Zn	11	46	8	8
Ga	<.9	<.9	<.9	<.9
Pb	2	<2.2	<2.1	<2.2
Ge	<.9	<.9	<.9	<.9
As	<.8	<.9	<.8	<.8
Sb	<1.3	<1.3	<1.3	<1.3
Bi	<2.7	<2.9	<2.8	<2.9
Se	<.8	<.9	<.8	<.9
Te	<2.0	<2.1	<2.0	<2.1
Sc	<2.3	<2.4	<2.3	<2.4
Y	.8	1	2	<.7
La	<2.4	<2.6	<2.5	<2.7
Ce	<4.4	<4.6	<4.4	<4.7
Nd	<2.7	3	<2.8	3
Au (ppb)	<5	<5	<5	<5

**Table 2.6:** Whole-rock analyses of the Rössing Formation marbles on the farm Sandamap 64, Usakos District  
 NS262: 3.3 km ENE of Vaalkop, dolomite marble  
 NS263: 3.3 km ENE of Vaalkop, dolomite-forsterite-serpentinite marble  
 NS264: 3.2 km ENE of Vaalkop, dolomite-forsterite marble  
 NS265: 1.2 km ENE of Vaalkop, dolomite marble

the north and west of Omaruru, the formation is at least 500 metres thick (Map 1) and here calc-silicate layers host finely disseminated scheelite mineralisation. Because of the essentially identical nature of the Spes Bona and the Oberwasser

Formation metasediments and metavolcanic rocks, they will be discussed together.

#### 2.2.2.4 Okawayo Formation

Due to the lack of detailed mapping in the Omaruru area in the mid-1980s, Steven (1987) referred to the first carbonate unit below the Karibib Formation marbles proper as the Rössing Formation. Badenhorst (1987) subsequently named this marble the Lower Marble Unit (LMU) of the Karibib Formation and, after he had recognised a more complete stratigraphic section in the Okawayo area, introduced the term Okawayo Formation (Badenhorst, 1988a). The formation is now recognised in the NCZ and the SCZ, but it has not been identified west of the Abbabis lineament zone. In the Oka-

wayo Section it attains a thickness of 15 metres (Steven and Badenhorst, 1988) and in the Omaruru area, in NCZc and NCZd, the marble is 0.7-4 metres thick. The marble comprises calcite (95-98%), plagioclase (0-2%), clinopyroxene (0-2%), pyrrhotite (0-2%), graphite (0-2%), and trace amounts of apatite, sphene, sericite and clinozoisite. Calcite grains vary in size from 1-5 mm, other minerals being interstitial and very fine-grained. A granoblastic texture is ubiquitous and plagioclase locally exhibits a poikiloblastic nature. Geochemical analyses of the marble reveal its calcitic nature (Table 2.7). The extensive areal distribution of the relatively thin Okawayo Formation points to considerable crustal stability (at least locally) at the time of sedimentation. This marble hosts the Otjua Tungsten Prospect (Map 1), the largest scheelite skarn found to date in the Damara Orogen (Steven, 1987), and gold-bearing skarn at the Navachab Gold Mine (Badenhorst, 1989, pers. comm.).

	OT101	OT124	OT125	OT126
SiO <sub>2</sub> (wt%)	2.85	3.77	3.01	4.67
TiO <sub>2</sub>	.03	.01	.02	.05
Al <sub>2</sub> O <sub>3</sub>	.61	.38	.42	.84
FeO	.45	.37	.25	.51
MnO	.10	<.01	<.01	<.01
MgO	.89	.77	.71	.92
CaO	53.28	53.14	53.58	51.58
Na <sub>2</sub> O	<.02	<.02	<.02	<.02
K <sub>2</sub> O	.07	.08	.03	.12
P <sub>2</sub> O <sub>5</sub>	.16	.10	.09	.10
H <sub>2</sub> O-	.06	.21	.11	.23
LOI	42.09	41.57	41.32	40.58
TOTAL	100.59	100.40	99.54	99.60
F (ppm)	<490	<490	<490	<490
S	97	25	377	637
Rb	<2.0	<2.0	<2.0	5
Ba	8	9	13	18
Sr	1616	1541	1446	1355
Th	<5.2	<5.2	<5.2	<5.2
U	<4.3	<4.3	<4.3	5
Zr	9	6	10	13
Nb	<1.9	<1.9	<1.9	<1.9
Mo	14	14	87	30
Sn	<4.0	<4.0	<4.0	<4.0
W	<5.6	<5.6	<5.6	<5.6
V	<2.9	4	4	9
Cr	<2.7	3	<2.7	6
Co	<1.9	<1.9	<1.9	<1.9
Ni	<1.7	<1.7	<1.7	<1.7
Cu	<1.7	<1.7	11	24
Zn	4	4	12	11
Pb	10	<5.8	<5.8	<5.8
As	<7.0	<7.0	<7.0	<7.0
Sb	<5.0	<5.0	<5.0	<5.0
Sc	<3.4	<3.4	<3.4	<3.4
Y	<2.1	<2.1	3	3
Au (ppb)	<5	<5	<5	<5

**Table 2.7:** Whole-rock analyses of the Okawayo Formation marbles at the Otjua Tungsten Prospect, Omaruru District

N.B. All iron expressed as FeO

OT101: Grid 49W/137S

OT124: Borehole OT1, 66.11-67.60 m

OT125: Borehole OT20, 79.07-80.03 m

OT126: Borehole OT8, 54.00-57.02 m

#### 2.2.2.5 Oberwasser Formation

##### 2.2.2.5.1 Metasediments

The term Oberwasser Formation was first used by Botha (1978) to describe a 700-m-thick sequence of intercalated calc-silicate rocks, biotite schists and minor marbles that underlie the Karibib Formation carbonates in NCZd on the farm Oberwasser in the lower Omaruru River (Fig. 1.3). In the NCZ the Oberwasser Formation (or the Spes Bona Formation) is usually the lower-most stratigraphic unit developed (Table 2.2). The Oberwasser Formation thins and becomes more calc-silicate-dominated as one moves south-eastwards from the type area towards the Omaruru Lineament. In the northern SCZ, the Oberwasser Formation attains a maximum thickness of 300 m in the Sandamap area (Map 4) and is of the order of 70 m in the Okawayo Section (Badenhorst, 1987). Closer to the Abbabis Inlier the formation is thinner. Martin (cited in Watson, 1982) suggested that the Oberwasser Formation is a facies equivalent of the Khan Formation on account of the interfingering of the Nosib and Swakop Groups elsewhere in the CZ. However, the two formations can be seen on Sandamap (Map 4) and, as Watson (1982) has stated, a clear distinction can be made between the Khan Formation which interfingers with meta-quartzite and the Oberwasser Formation which is associated with calc-silicate rocks and marbles. Moreover, the two formations can easily be distinguished in the field, the Khan Formation being a dark green, streaky calc-silicate gneiss, the Oberwasser calc-silicate rocks being a paler colour with no amphibole. North of Omaruru in NCZd, the Oberwasser Formation is notably more calcareous than in the type area, contains numerous scapolite-bearing calc-silicate rocks (which may represent meta-evaporites), and hosts syn-genetic tungsten and epigenetic gold mineralisation (Table 2.3). The nature of the formation in the northern SCZ at Sandamap and in NCZc and NCZd in the Omaruru area has been investigated and will be compared with the unmineralised type area and the Khan Formation.

On the farm Sandamap, the Oberwasser Formation comprises alternating horizons of calc-silicate rocks, quartz-biotite schist and very subordinate marble. This contrasts with the type area where the formation can more accurately

	NS268	NS269
SiO <sub>2</sub> (wt%)	48.56	52.90
TiO <sub>2</sub>	.67	.75
Al <sub>2</sub> O <sub>3</sub>	14.58	15.31
Fe <sub>2</sub> O <sub>3</sub>	.06	.13
FeO	7.00	5.48
MnO	.41	.24
MgO	5.28	4.10
CaO	20.63	17.82
Na <sub>2</sub> O	.64	.93
K <sub>2</sub> O	.55	.61
P <sub>2</sub> O <sub>5</sub>	.17	.19
H <sub>2</sub> O-	.14	.14
H <sub>2</sub> O+	.69	.76
CO <sub>2</sub>	.98	.92
TOTAL	100.37	100.28
F (ppm)	393	403
S	<5.0	<4.9
Rb	40	43
Ba	60	47
Sr	482	452
Th	11	11
U	3	4
Zr	133	157
Nb	13	14
Mo	.8	3
Sn	28	19
W	<5.8	<5.4
V	140	157
Cr	98	107
Co	22	15
Ni	43	63
Cu	<1.6	3
Zn	405	97
Ga	26	29
Pb	4	9
Ge	<1.2	<1.1
As	<1.1	<1.0
Sb	<1.6	<1.5
Bi	9	<3.4
Se	<1.1	<1.0
Te	<2.5	<2.4
Sc	18	19
Y	19	18
La	24	31
Ce	41	61
Nd	24	36
Au (ppb)	10	<5

**Table 2.8:** Whole-rock analyses of the Oberwasser Formation calc-silicate rocks on the farm Sandamap 64, Usakos District NS268: 2.9 km ESE of Cilliers Workings, Plag+Cpx calc-silicate rock  
NS269: 2.9 km ESE of Cilliers Workings, Plag+Cpx+Qtz calc-silicate rock

be described as a succession of biotitic calc-silicate rocks suggesting deposition in deeper water. At Sandamap, the calc-silicate rocks are fine-grained granofelses (<0.5 mm)

containing plagioclase (40-50%), clinopyroxene (20-40%), sphene (1-2%), quartz (0-10%), hornblende (0-5%), sericite (0-5%) and traces of potash feldspar, zoisite, calcite, graphite, pyrrhotite, pyrite and iron oxides. The rocks generally granoblastic in texture, but grain size is variable and the clinopyroxene is locally poikiloblastic. The calc-silicate rocks are notably less siliceous than those of the Khan Formation (compare Tables 2.5 and 2.8). The Oberwasser Formation schist is composed of quartz (40-50%), untwinned plagioclase and potash feldspar (~30%), biotite (20-30%), tourmaline (0.5%) and traces of pyrite, hematite and zircon. The grain size rarely exceeds 0.4 mm, the tourmalines being only tens of microns in length. These tourmalines are unrelated to the pegmatitic intrusions in the area. Geochemical analyses of the schist are given in Table 2.9.

On the northwest side of the Omaruru Lineament in NCZc and NCZd near Omaruru, the Oberwasser Formation is developed in the cores of several domal structures (Map 1). The minimum thickness of the formation is estimated at 500 metres and comprises an alternating sequence of quartz-biotite schists, calc-silicate rocks, scheelite-bearing granofels and minor carbonate units. The proportion of carbonaceous units decreases from the basal contact and facies changes, both along and across strike, are a feature of this formation. The calc-silicate rocks represent metamorphosed marls and their intercalation with thin calcareous lithologies and a close association with the calcitic Okawayo Formation suggest their deposition in a shallow marine environment. The top of the sequence was deposited in deeper water. The extensive areal distribution of the relatively thin Okawayo Formation points to considerable crustal stability (at least locally) at the time of sedimentation. This contrasts with the Oberwasser Formation in the type area.

The base of the formation in the Omaruru area is best exposed in the core of the Schönfeld Dome at the Otjua Tungsten Prospect (Map 1). Schist comprises 60-70% of the sequence and is composed of quartz and feldspar (60-80%), biotite (15-40%), clinopyroxene (2-3%) and traces of apatite, chlorite, calcite, pyrite and chalcopyrite. Equant quartz and feldspar crystals (<2 mm) are arranged granoblastically, while the schistosity is defined by fine-grained biotite. Pyroxene locally exhibits a poikiloblastic texture. Geochemical analyses indicate higher Al<sub>2</sub>O<sub>3</sub> and alkali contents in the schists from the Otjua Tungsten Prospect and hence a higher abundance of clay minerals in the original sediment than in the more siliceous schists from the Sandamap area (compare Tables 2.9 and 2.10). The calc-silicate rocks contain a very fine-grained granoblastic mosaic of quartz and untwinned plagioclase comprising 80% of the modal abundance, diopside (5-20%), biotite (0-20%) and traces of scapolite and sphene. Diopside is commonly poikiloblastic in texture. Geochemical analyses of the calc-silicate rocks from Otjua are given in Table 2.11.

The most distinctive feature of the Oberwasser Formation in the Omaruru area in both NCZc and NCZd, however, is the presence of scheelite-bearing granofelses (SBG). At the Otjua Tungsten Prospect, SBG comprise approximately 2-3% of the Spes Bona and Oberwasser Formation meta-sediments and are developed as thin, discontinuous interca-

	NS266	NS267
SiO <sub>2</sub> (wt%)	68.12	71.13
TiO <sub>2</sub>	.71	.63
Al <sub>2</sub> O <sub>3</sub>	12.67	11.18
Fe <sub>2</sub> O <sub>3</sub>	.15	.38
FeO	5.38	5.27
MnO	.08	.10
MgO	3.67	3.66
CaO	1.80	1.64
Na <sub>2</sub> O	2.07	1.25
K <sub>2</sub> O	2.83	2.83
P <sub>2</sub> O <sub>5</sub>	.22	.21
H <sub>2</sub> O-	.13	.13
H <sub>2</sub> O+	.96	1.15
CO <sub>2</sub>	1.03	.13
TOTAL	99.82	99.69
F (ppm)	721	862
S	<5.3	<5.3
Rb	114	117
Ba	432	390
Sr	99	77
Th	9	9
U	3	2
Zr	186	192
Nb	14	13
Mo	1	.9
Sn	5	3
W	8	<4.7
V	123	102
Cr	87	66
Co	17	16
Ni	40	36
Cu	34	60
Zn	108	97
Ga	16	14
Pb	2	3
Ge	<.9	<.9
As	<.9	2
Sb	<1.3	<1.3
Bi	<2.9	<2.9
Se	<.9	1
Te	<2.1	<2.0
Sc	14	11
Y	32	27
La	20	12
Ce	41	20
Nd	25	14
Au (ppb)	<5	<5

**Table 2.9:** Whole-rock analyses of the Oberwasser Formation schists on the farm Sandamap 64, Usakos District  
 NS266: 550 m NE of Vaalkop, Qtz+Plag+Bt schist  
 NS267: 550 m NE of Vaalkop, Qtz+Plag+Bt schist

lations within the calc-silicate rocks. These granofelses vary in thickness from a few centimetres to several metres, but are more commonly in the 10-50 cm range and comprise quartz (0-40%), plagioclase feldspar (0-40%), diopsidic py-

roxene (10-60%), scapolite (0-60%), hornblende (0-10%), clinozoisite (0-15%), sericite (0-10%), sphene (1-4%), biotite (0-20%), apatite (1-2%), carbonate (0-5%), scheelite (0-2%) and traces of pyrite, pyrrhotite and chalcopyrite. SBG are equally well developed in the core of the Schönfeld Dome, which has been intruded by several types of granite, and the Okakombo horst block, where felsic intrusions are essentially absent. Geochemical analyses of SBG from the Otjua Tungsten Prospect and the Okakombo horst block are given in Table 2.12.

Schists of the middle Oberwasser Formation host a swarm of auriferous quartz veins at the Epako Gold Prospect (Fig 1.3 and Table 2.3). Calc silicate lithologies comprise only a minor component of the formation at this level but commonly contain scheelite. The schist contains quartz (15-30%), K-feldspar (20-30%), plagioclase (10-15%), biotite (25-30%), opaque minerals (probably graphite, 2-3%), cordierite (0-15%), muscovite (trace-3%), andalusite (0-3%), sillimanite (0-3%) and traces of tourmaline. The schist is considerably less calcareous than at Otjua (compare Tables 2.13 and 2.10). Here the close proximity (<100 m) of granites and pegmatites has resulted in the "schist" losing its lepidoblastic nature. The biotite is randomly oriented in the granoblastic mosaic. Porphyroblasts (up to 3 mm) and poikiloblasts of K-feldspar contain numerous inclusions of quartz and biotite. Another textural feature of note is the development of porphyroblasts of pyrite and loellingite rimmed by arseno-pyrite (up to 4 mm). Coarse-grained aggregates of chalcopyrite and pyrrhotite are also present in the schists. The schists are locally chloritised, bleached and contain secondary carbonate (Table 2.13). However, the alteration described above is confined to the immediate vicinity of the gold prospect and is atypical of the Oberwasser Formation. It is thus evident that the Oberwasser Formation close to the Omaruru Lineament both in the Usakos and Omaruru areas is considerably different from the type area.

#### 2.2.2.5.2 Metavolcanic rocks in the Spes Bona and Oberwasser Formations

There is evidence for minor felsic volcanism in both the Spes Bona and Oberwasser Formations north of Omaruru. At the Otjua Tungsten Prospect, several boreholes intersected a well-foliated, laterally impersistent, quartzofeldspathic rock (referred to as a sulphidic tonalite by Steven, 1987) that varies in thickness from a few tens of centimetres to several metres. Unfortunately, this lithology is not exposed on surface and from the limited information available it is unclear whether these are intrusive or extrusive rocks. The very fine-grained nature of these rocks suggests an extrusive origin and thus the term dacite would be more appropriate than tonalite (Streckeisen, 1976). Locally these lithologies interfinger on a centimetre scale with the schist and comprise an anhedral mosaic of quartz and plagioclase with microcline (5-15%), biotite (0-5%), muscovite (0-2%), clinozoisite (0-2%), pyrrhotite (0-3%) and traces of chalcopyrite and pyrite. The rock is granoblastic in texture, the grain size being approximately 250 µm. Jacob (1974), Blaine (1977) and Miller (1980) have described similar quartzofeldspathic rocks from the Etusis Formation or

	OT117	OT123
SiO <sub>2</sub> (wt%)	56.70	54.66
TiO <sub>2</sub>	.79	.85
Al <sub>2</sub> O <sub>3</sub>	16.86	17.76
Fe <sub>2</sub> O <sub>3</sub>	7.87	8.34
MnO	.08	.07
MgO	5.00	4.89
CaO	4.56	4.31
Na <sub>2</sub> O	1.79	2.17
K <sub>2</sub> O	3.79	4.28
P <sub>2</sub> O <sub>5</sub>	.20	.20
H <sub>2</sub> O-	.10	.18
LOI	1.20	1.08
TOTAL	98.94	98.79
F (ppm)	2200	1070
S	193	546
Rb	340	210
Ba	630	740
Sr	183	198
Th	11	11
U	<4.0	6
Zr	165	171
Nb	14	15
Mo	3	<1.4
Sn	<4.0	<4.0
W	15	10
V	183	198
Cr	111	121
Co	26	24
Ni	66	73
Cu	40	64
Zn	146	151
Pb	13	8
As	<7.0	<7.0
Sb	<5.0	<5.0
Sc	21	24
Y	31	33
Au (ppb)	<5	<5

**Table 2.10:** Whole-rock analyses of the Oberwasser Formation schists at the Otjua Tungsten Prospect

N.B. All iron expressed as Fe<sub>2</sub>O<sub>3</sub>

OT117: Borehole OT23, 118.9-120.5 m, biotite schist

OT123: Borehole OT20, 79.07-80.03 m, biotite schist

	OT118	OT121	OT122
SiO <sub>2</sub> (wt%)	54.74	65.20	63.28
TiO <sub>2</sub>	.64	.73	.72
Al <sub>2</sub> O <sub>3</sub>	11.23	11.17	11.21
FeO	5.37	4.36	5.03
MnO	.28	.15	.22
MgO	3.58	3.62	3.61
CaO	18.73	9.23	10.97
Na <sub>2</sub> O	1.09	2.43	1.67
K <sub>2</sub> O	.60	1.71	1.83
P <sub>2</sub> O <sub>5</sub>	.21	.24	.22
H <sub>2</sub> O-	.10	.09	.16
LOI	3.61	1.24	1.01
TOTAL	100.18	100.17	99.93
F (ppm)	535	1508	973
S	8	<7	<6.5
Rb	36	137	152
Ba	189	288	346
Sr	343	411	448
Th	32	8	10
U	6	<4.0	<4.0
Zr	151	226	229
Nb	11	12	13
Mo	3	<1.4	3
Sn	<4.0	<4.0	<4.0
W	21	10	17
V	94	91	91
Cr	66	74	76
Co	17	12	15
Ni	36	34	37
Cu	<1.5	<1.5	<1.5
Zn	146	76	110
Pb	<5	7	8
As	<7.0	<7.0	<7.0
Sb	<5.0	<5.0	<5.0
Sc	14	13	14
Y	35	36	35
Au (ppb)	<5	8	<5

**Table 2.11:** Whole-rock analyses of the Oberwasser Formation calc-silicate rocks at the Otjua Tungsten Prospect

N.B. All iron expressed as FeO

OT118: Borehole OT23, 66.05-67.54 m

OT121: Borehole OT20, 167.4-168.8 m

OT122: Borehole OT20, 173.0-174.6 m

(after Steven, 1987)

stratigraphic equivalent which they considered to represent metamorphosed felsic volcanic rocks. The textures of the recrystallised Naauwpoort rhyolite (Miller, 1980, p.13, Fig. 4.8) and the samples of Etusis Formation examined by Jacob (1974, samples 8400, 8401, 8402, 8411) are similar to those from Otjua. A geochemical analysis of a more siliceous sample (Table 2.14) reveals a rhyolitic composition. The high calcium content of this sample (which was extruded onto or deposited within a marly sequence) relative to the analyses of Nosib alkaline to peralkaline rhyolites listed by Miller

(1983a) may be the result of alteration. The Spes Bona/Okawayo/Oberwasser sediments to the northwest of Omaruru are considered to have been deposited on the margin of a basin whose southeastern edge was defined by the Omaruru Lineament. If this is correct then the rhyolitic and dacitic volcanic rocks described above are confined to the graben margins as are the Nosib extrusive centres (Miller, 1983a, p. 438).

	OT130	OT131	OT132	OT133	OT134	OT135	OT136	OT137	OT138	OT139
SiO <sub>2</sub> (wt%)	60.45	51.58	58.63	49.59	49.70	60.07	67.61	65.35	66.77	63.56
TiO <sub>2</sub>	.63	.46	.73	.54	.60	.64	.55	.58	.71	.63
Al <sub>2</sub> O <sub>3</sub>	11.80	12.83	12.16	13.07	12.04	9.44	9.60	9.51	10.54	9.56
FeO	5.78	9.15	6.52	9.16	9.69	5.12	4.94	5.57	4.47	4.78
MnO	.20	.57	.43	.55	.63	.15	.20	.25	.12	.17
MgO	3.45	4.32	4.11	3.48	3.72	3.73	2.38	2.93	2.78	2.26
CaO	15.18	18.81	14.91	19.94	20.83	16.56	12.41	12.84	11.53	14.02
Na <sub>2</sub> O	.66	.72	.48	.77	.83	.69	.31	.20	.60	.67
K <sub>2</sub> O	.14	.14	.62	.57	.18	.13	.32	.57	.46	.30
P <sub>2</sub> O <sub>5</sub>	.17	.14	.24	.15	.19	.22	.19	.16	.24	.19
H <sub>2</sub> O-	.13	.10	.13	.08	.09	.10	.09	.11	.04	.07
LOI	1.28	1.03	1.24	1.60	1.10	2.95	1.43	2.15	1.99	2.71
TOTAL	99.87	99.85	100.20	99.50	99.60	99.80	100.03	100.22	100.25	98.92
F (ppm)	<490	1071	827	<490	<490	150	140	150	220	170
S	14	<7.0	9	<6.0	<6.0	28	1636	343	825	29
Rb	19	12	55	49	22	9	18	31	34	20
Ba	19	15	84	69	15	44	73	276	100	30
Sr	190	184	116	226	225	286	186	183	138	160
Th	<4.5	23	15	12	9	14	<4.0	8	<5.0	<5.0
U	<3.5	7	8	<4.0	<3.5	<4.0	<3.5	<4.0	<4.0	<4.0
Zr	158	98	240	114	147	279	168	175	183	185
Nb	12	37	38	38	38	25	11	12	19	67
Mo	3	6	5	8	6	5	3	4	5	9
Sn	14	32	72	26	61	<4.0	<4.0	<4.0	<4.0	<4.0
W	879	2258	2078	14274	2009	34	86	525	25	2406
V	88	119	112	107	106	79	72	89	103	82
Cr	67	63	80	70	68	64	62	63	79	72
Co	17	20	24	16	20	12	12	13	12	12
Ni	37	47	47	40	43	57	29	37	21	33
Cu	4	<1.5	<1.5	<1.6	<1.5	29	15	33	47	7
Zn	140	198	128	200	274	278	112	123	62	169
Pb	14	19	18	9	16	16	<5.0	9	9	8
As	<7.0	<7.0	<7.0	<7.0	<7.0	<7.0	<7.0	<7.0	<7.0	<7.0
Sb	<5.0	<5.0	<5.0	<5.0	<5.0	<5.0	<5.0	<5.0	<5.0	<5.0
Sc	13	17	18	19	17	12	11	13	14	11
Y	47	78	88	64	52	92	37	36	60	40
Au (ppb)	<5	<5	27	27	<5	<5	<5	<5	<5	<5

**Table 2.12:** Whole-rock analyses of the Spes Bona and Oberwasser Formations scheelite-bearing granofels on the farms Otjua, Tjirundo and Okakambo, Omaruru District

N.B. All iron expressed as FeO

OT130: Otjua Tungsten Prospect: Borehole OT16, Assay No. 43316

OT131: Otjua Tungsten Prospect: Borehole OT16, Assay No. 43322

OT132: Otjua Tungsten Prospect: Borehole OT22, Assay No. 24191

OT133: Otjua Tungsten Prospect: Borehole OT22, Assay No. 24192

OT134: Otjua Tungsten Prospect: Borehole OT22, Assay No. 24219

OT135-139: Tjirundo Süd/Okakambo fence

(after Steven, 1987)

### 2.2.2.5.3 The Oberwasser Formation problem

The correlation of Oberwasser Formation from the type area with the calc-silicate lithologies immediately below the Karibib Formation in the Usakos-Omaruru area is problematic. Within the study area the only rocks which appear to be the direct equivalents of the Oberwasser Formation as described by Botha (1978) are found west of Usakos in NCZb, NCZc and NCZd in the area examined by Watson (1982). To the east of the Abbabis lineament zone and its northern extension, the lithologies below the Karibib Formation are more calcareous, marbles are present and the calc-silicate rocks commonly contain disseminated scheelite mineralisation. An alternative stratigraphy has been proposed by Badenhorst

(1989, pers. comm.) for the area to the east of the Abbabis lineament zone. The new names are given in Table 2.2a. The thick sequence of Karibib Formation marbles is now referred to as the Karibib Formation Upper Marble Unit (UMU). In the two tectono-stratigraphic zones where a thick sequence of predominantly schistose rocks has been identified immediately below the Karibib Formation marble (to the east of the Abbabis lineament zone and its extensions), the schist/calc-silicate rock package is referred to as the Karibib Formation Upper Schist Unit (USU). The thin marble (formerly Okawayo Formation) becomes the Karibib Formation Lower Marble Unit (LMU) and the underlying schist is now referred to as the Karibib Formation Lower Schist Unit (LSU).

## 2.2.2.6 Karibib Formation

	NS359	NS360	NS361	NS358
SiO <sub>2</sub> (wt%)	57.83	54.42	58.28	41.21
TiO <sub>2</sub>	.93	.91	.88	.92
Al <sub>2</sub> O <sub>3</sub>	17.44	18.87	17.26	16.13
Fe <sub>2</sub> O <sub>3</sub>	.00	.00	.01	.98
FeO	7.97	7.45	6.42	5.79
MnO	.11	.09	.09	.12
MgO	4.69	4.52	4.24	3.97
CaO	2.52	1.89	2.05	10.92
Na <sub>2</sub> O	1.87	1.57	1.63	2.24
K <sub>2</sub> O	3.73	4.86	4.35	1.70
P <sub>2</sub> O <sub>5</sub>	.20	.16	.19	.25
H <sub>2</sub> O-	.26	.16	.15	.52
H <sub>2</sub> O+	1.82	2.14	1.88	4.47
CO <sub>2</sub>	1.34	2.16	2.22	8.47
TOTAL	100.70	99.22	99.65	97.68
F (ppm)	1151	1025	979	947
S	471	2400	540	744
Rb	155	168	155	173
Ba	634	1116	1008	59
Sr	121	131	128	67
Th	14	13	14	14
U	4	4	5	7
Zr	185	182	179	342
Nb	15	15	14	17
Mo	1	10	1	<.6
Sn	6	6	5	15
W	14	15	17	30
V	209	225	204	175
Cr	132	145	131	118
Co	22	37	9	15
Ni	47	60	29	48
Cu	20	92	18	<1.4
Zn	148	159	140	140
Ga	23	27	24	31
Pb	27	47	38	9
Ge	<1.0	<1.0	<1.0	<1.0
As	49	1189	121	8
Sb	<1.4	<1.4	<1.3	<1.4
Bi	<3.1	<3.2	<3.0	<3.1
Se	<.9	<.9	<.9	<.9
Te	<2.2	<2.2	<2.2	<2.2
Sc	23	24	22	18
Y	39	36	39	51
La	32	31	36	40
Ce	71	69	72	79
Nd	38	37	39	42
Au (ppb)	<5	<5	5	13

**Table 2.13:** Whole-rock analyses of the Oberwasser Formation schists at the Epako Gold Prospect

NS359: Borehole ED-1, 223.31-223.77 m, Qtz+Plag+Bt(+Ms) schist

NS360: Borehole ED-1, 270.25-270.71 m, Qtz+Plag+Bt+Ms+Sil schist

NS361: Borehole ED-1, 273.06-273.63 m, Qtz+Plag+Bt+Ms+Sil schist

NS358: Borehole ED-1, 136.4-136.72 m, highly altered Qtz+Plag+Chl schist

## 2.2.2.6.1 Mafic Volcanic Rocks

The first report of mafic volcanic rocks in the Karibib Formation of the SCZ was given by Miller (1983c). Massive amphibolites (Omusema Member) and amphibolitic pillow lavas (Daheim Member) from the base of the Karibib Formation were described. The Omusema Member is up to 500 metres thick and is best developed to the south and east of Karibib (De Kock, 1985). Recent geological mapping north of Karibib has confirmed that the volcanic rocks of the Daheim Member, which may be several hundred metres thick, are confined to a geographically small area, south of the Erongo Complex and east of the Abbabis lineament zone (Badenhorst, 1988, pers. comm.). Both members were interpreted, on the basis of their geochemical signatures, to be alkaline volcanic rocks associated with a continental (rifting?) environment (Miller, 1983c, p.131). Damaran mafic volcanic rocks or the metamorphosed equivalents thereof are essentially absent from the NCZ (Steven, 1987). The volcanic rocks of the Daheim Member are known to contain minor gold mineralisation (Petzel, 1988, pers. comm.) and Pirajno *et al.* (1990a) have suggested that the carbonate-hosted gold mineralisation at the Onguati Mine was derived from metals that had been leached out of the orthoamphibolites. This model for the origin of gold deposits, which involves the derivation of auriferous fluids from mafic volcanic rocks during prograde regional metamorphism, has gained widespread attention (Keays *et al.*, 1989). It was thus considered important during the course of field work to pay particular attention to the nature of the Karibib Formation elsewhere in the CZ and, more specifically, near gold prospects. The Sandamap-Eureka area, on the SCZ/NCZ boundary, was chosen for an examination of the Karibib Formation because of the detailed mapping available in the vicinity of significant gold mineralisation (Maps 3 and 4).

A thick sequence of mafic volcanic rocks that could represent the equivalent of the Omusema or Daheim Members is not developed in the Sandamap area. However, several minor horizons (less than 10 cm thick) of fine-grained ferruginous cherts with ovoid structures and several greenish carbonate layers were discovered within calcitic marbles on a low knoll west of Hill 1166 in the northwest corner of Sandamap 64 (Map 4). It was initially thought that these horizons might represent tuffaceous material that would have been broadly contemporaneous with the Daheim Member. Petrographic study reveals that the 'chert' is a scapolite-plagioclase-tremolite calc-silicate rock. The green carbonate is a tremolitic marble. No patches of meta-igneous material that could represent volcanic bombs were identified. Several unusually dark green calc-silicate horizons (up to one metre thick) are developed within the Karibib Formation on the Sandamap-Sandamap Noord boundary (Maps 3 and 4). It was also thought that these might have a tuffaceous component. Geochemical analyses are given in Table 2.15. The more mafic nature of the calc-silicate rocks is evident from the presence of actinolitic amphibole rather than tremolite,

	OT120
SiO <sub>2</sub> (wt%)	75.67
TiO <sub>2</sub>	.01
Al <sub>2</sub> O <sub>3</sub>	13.74
Fe <sub>2</sub> O <sub>3</sub>	0.94
MnO	<0.01
MgO	<0.01
CaO	3.50
Na <sub>2</sub> O	3.65
K <sub>2</sub> O	1.85
P <sub>2</sub> O <sub>5</sub>	.02
H <sub>2</sub> O-	0.06
LOI	0.58
<b>TOTAL</b>	<b>100.02</b>
F (ppm)	<490
S	1992
Rb	143
Ba	97
Sr	254
Th	34
U	15
Zr	109
Nb	37
Mo	2
Sn	<4.0
W	17
V	<2.8
Cr	3
Co	2
Ni	<1.7
Cu	140
Zn	12
Pb	12
As	<7.0
Sb	<5.0
Sc	2
Y	16
Au (ppb)	13

**Table 2.14:** Whole-rock analyses of the sulphidic rhyolite in the Oberwasser Formation at the OtjuaTungsten Prospect, Omaruru District

N.B. All iron expressed as Fe<sub>2</sub>O<sub>3</sub>

OT120: Borehole OT14, 181.12-184.16 m (after Steven, 1987)

	NS312	NS313	NS314	NS316
SiO <sub>2</sub> (wt%)	56.54	53.74	54.44	49.86
TiO <sub>2</sub>	.70	.67	.71	1.57
Al <sub>2</sub> O <sub>3</sub>	14.10	13.59	13.57	11.16
Fe <sub>2</sub> O <sub>3</sub>	.22	.40	.64	.00
FeO	2.05	2.97	4.15	7.80
MnO	.06	.05	.06	.76
MgO	5.75	6.10	5.69	12.62
CaO	9.07	12.06	9.54	11.67
Na <sub>2</sub> O	2.23	1.37	1.61	.41
K <sub>2</sub> O	5.49	4.23	5.22	1.59
P <sub>2</sub> O <sub>5</sub>	.14	.15	.16	.20
H <sub>2</sub> O-	.04	.06	.12	.14
H <sub>2</sub> O+	.28	.52	.64	.00
CO <sub>2</sub>	2.10	3.21	2.73	.00
<b>TOTAL</b>	<b>98.78</b>	<b>99.12</b>	<b>99.28</b>	<b>99.46</b>
F (ppm)	1843	1966	1084	1623
S	<5.2	921	<5.0	<4.9
Rb	110	163	141	135
Ba	988	387	412	205
Sr	439	405	303	148
Th	11	10	11	10
U	8	3	2	<1.7
Zr	149	144	151	120
Nb	15	13	12	29
Mo	<.5	<.6	<.6	<.6
Sn	4	12	6	13
W	6	<4.9	<5.0	<5.4
V	93	98	114	72
Cr	79	80	80	56
Co	4	10	6	23
Ni	13	28	46	46
Cu	2	14	<1.4	12
Zn	9	5	11	173
Ga	17	19	19	18
Pb	4	<2.3	10	13
Ge	1	<1.0	<1.0	2
As	3	6	1	1
Sb	<1.3	<1.4	<1.4	<1.5
Bi	<3.0	<3.1	<3.2	<3.4
Se	<.9	<.9	<.9	<1.0
Te	<2.1	<2.2	<2.2	<2.4
Sc	17	18	19	16
Y	11	12	30	41
La	28	39	32	26
Ce	51	73	64	65
Nd	24	37	34	40
Au (ppb)	<5	<5	<5	<5

**Table 2.15:** Whole-rock analyses of mafic calc-silicate rocks of the Karibib Formation on the farms Sandamap Noord 115, and Lukasbank 63, Usakos District

NS312: 2.5 km SW of Sandamap Tin Mine, tremolite-plagioclase-microcline rock

NS313: 1.8 km SW of Sandamap Tin Mine, tremolite-plagioclase-microcline rock

NS314: 3.0 km SW of Sandamap Tin Mine, hornblende-plagioclase-microcline rock

NS316: Lukasbank 63

but the presence of microcline and scapolite suggest that the rock was derived from a clayey marl. It has thus not been possible to state unequivocally that minor tuffaceous material is absent from the Karibib Formation west of the Abbabis lineament zone. However, the lack of metalavas in the Sandamap area is important because it is considered unlikely that the very minor volume of (possibly) tuffaceous material could have significantly contributed to the gold budget at the Sandamap Noord Gold Prospect (see Chapter 7). Moreover,

	Habis	Onguati	Sandamap
Zone	SCZ	SCZ	NCZ
Regional Nature	Dolomitic marble	Calcitic (CM) and dolomitic marble (DM)	Calcitic marble
Mineralisation Host	Dolomitic marble	Calcitic marble	Calcitic marble
Grain Size	100 $\mu\text{m}$ -2 mm	CM 300-500 $\mu\text{m}$ ; DM 100 $\mu\text{m}$	2-5 mm
Major Minerals	dolomite (90-97%)	CM-calcite (97-98%) DM-dolomite (95%)	calcite (95-98%)
Minor Minerals	quartz (1-5%) tremolite (0-5%) calcite (0-5%) muscovite (trace)	<div style="display: inline-block; vertical-align: middle;">           muscovite (1%) graphite (0-2%) phlogopite (0-1%) quartz (trace) tremolite (trace) apatite (trace) chlorite (trace)         </div> <div style="display: inline-block; vertical-align: middle; margin-left: 10px;">} CM</div> <div style="display: inline-block; vertical-align: middle;">           phlogopite (2-3%) tremolite (trace) chlorite (trace) muscovite (trace)         </div> <div style="display: inline-block; vertical-align: middle; margin-left: 10px;">} DM</div>	quartz (1-2%) graphite (0-2%) diopside (0-1%) muscovite (0-1%) pyrite (trace) chlorite (trace) K-feldspar (trace) sphene (trace) goethite (trace) hematite (trace)
Textural Features	annealed polygonal mosaic with interstitial or microcrystalline quartz	CM-polygonal mosaic and interstitial quartz DM-as above with cross-cutting dolomite	polygonal mosaic, but deformed calcite lamellae indicate late-tectonic deformation
Tremolite nature	poikiloblastic (<2 mm)	poikiloblastic (<500 $\mu\text{m}$ )	None
WRA Numbers	NS355-357	NS367-369	NS270-273

**Table 2.16:** Petrographic details of the Karibib Formation in the vicinity of the Habis, Navachab, Onguati and Sandamap Gold Prospects

the presence of gold mineralisation in an area where there are no significant mafic volcanic rocks means that alternative models to the one proposed by Pirajno *et al.* (1990a) for the origin of some of the gold mineralisation in the CZ must be considered.

#### 2.2.2.6.2 Metasediments

The most prominent stratigraphic marker in the CZ is the sequence of Karibib Formation marbles, but an assessment of its true thickness is complicated by the tectonism. In the SCZ, in the vicinity of the Abbabis Inlier, the formation attains a maximum thickness of 660 metres and comprises mainly dolomitic marble with subordinate calcitic marble, calc-silicate rocks and biotite schists (Smith, 1965). On the northern side of the Omaruru Lineament there is a marked increase in the proportion of calc-silicate lithologies at the base of the formation and dolomites are replaced by calcitic marbles. In NCZb the formation consists of calcitic marble with minor calc-silicate rocks that may be less than 100 metres thick (Map 3), while in NCZc the formation may attain a thickness of several hundreds of metres (for example immediately south of the Gross Spitzkop). On the northwest

side of the Tubussis Lineament (Fig. 2.4) there is a notable thickening of the Karibib Formation (Watson, 1982) and Klein (1980) has divided the formation into three members. The Harmonie Member (calc-silicate dominated with rare stromatolites), the Otjongeama Member (marble dominated) and the Arises River Member (pure coarse-grained calcitic marble) attain a maximum thickness of 1560 metres in NCZd north of Omaruru (Badenhorst, 1987). The Karibib Formation is an important host of gold-bearing skarn in the CZ and an unusual tin skarn at the Gross Spitzkop in NCZc (Fig. 1.3 and Table 2.3). The nature of the formation near the Navachab Gold Mine and the Habis, Onguati and Sandamap Gold Prospects has been investigated (Fig. 1.3). At the four localities, the Karibib Formation was sampled several hundred metres from the nearest known/visible gold mineralisation and its nature is discussed in order of increasing distance from the Abbabis Inlier. No unequivocal sedimentary features were recorded in the carbonates which have undergone amphibolite facies metamorphism. Estimates of the modal carbonate abundances were made after staining the thin sections with Alizarin Red S.

The Habis Gold Prospect is located near the centre of the Abbabis Inlier where metasediments of the Chuos and Ka-

Zone	SCZ		
Regional Nature	Calcitic marble (CM) and dolomitic marble (DM)		
Mineralisation Host	Calcitic (CM), dolomitic marble (DM) and calc-silicate marble (MC)		
	CM	DM	MC
Grain Size	50-400 $\mu\text{m}$	50-400 $\mu\text{m}$	groundmass (<200 $\mu\text{m}$ ) tremolites (200 $\mu\text{m}$ -3 mm)
Major Minerals	calcite (80-90%) dolomite (0-10%)	calcite (60-80%) dolomite (10-30%)	K-feldspar (20-40%) tremolite (10-30%) diopside (10-30%) calcite (2-20%)
Minor Minerals	quartz (0-2%) muscovite (0-2%) opaques (<1%) feldspar (trace) sphene (trace)	tremolite (1-2%) muscovite (0-4%) quartz (trace) chlorite (trace)	opaques (2%) sphene (1%) quartz (trace) plagioclase (trace) epidote (trace) clinozoisite (trace) phlogopite (trace) tourmaline (trace)
Textural Features	annealed polygonal	annealed polygonal mosaic with dolomite restricted to discrete areas, but no evidence for replacement of one carbonate type by another	annealed polygonal mosaic
Tremolite Nature (maximum size)	none	poikiloblastic (<1 mm)	prismatic or poikiloblastic (<2 mm)
WRA Numbers	NS324	NS325	NS326-327

Table 16 continued

ribib Formations overlie basement gneisses (Smith, 1965). A sequence of fine-grained white carbonates (lower marble), several hundred metres thick, is overlain by schistose sediments which are in turn succeeded by a several-hundred-metre-thick sequence of fine-grained, light grey and grey dolomitic carbonates (upper marble). Zones of massive tremolite associated with auriferous gossan are present in the upper marble approximately 500 metres north-northeast of the Habis farmhouse (Chapter 7.4). The dolomitic nature of the lower and upper marbles is evident from Tables 2.16 and 2.17. The marbles generally possess an annealed metamorphic texture. However, approximately 10% of the lower marble comprises randomly oriented fractures and cavities filled with very fine-grained carbonate and microcrystalline quartz. In the upper marble there is a concentration of coarse-grained (2 mm) dolomite crystals with quartz in lensoid stringers up to several centimetres long. Minor poikiloblastic tremolite is an integral part of the metamorphic assemblage in both the lower and upper marbles.

The Navachab Gold Mine is situated on the northern flank of the Abbabis Inlier, where sediments of the Swakop

Group have been deformed into a northeasterly trending domal structure (Smith, 1965). Gold skarn mineralisation is primarily hosted by calc-silicate marble (MC) and dolomitic marble (DM) of the Karibib Formation, and to a much lesser extent by the calcitic marble (CM; Anglo American nomenclature, Navachab Gold Mine Field Guide, 1989). Petrographic and geochemical analyses reveal that the so-called dolomitic marble is in fact highly calcitic (Tables 2.16 and 2.18). All the marbles possess an annealed polygonal mosaic and, although dolomite grains tend to cluster together, there is no evidence for the replacement of one carbonate by another. Small poikiloblasts of tremolite derived during regional metamorphism are common in the dolomitic and calc-silicate marbles.

The Onguati Copper Mine is located towards the northern edge of the SCZ. Auriferous copper skarn and quartz veins are hosted by calcitic marbles of the lower portions of the Karibib Formation in the core of a major east-northeast-trending anticlinal structure, the Onguati-Otjimbojo anticline (1:1 000 000 Geological Map of Namibia). The calcitic marble (Tables 2.16 and 2.19) that hosts the majority of the miner-

	NS355	NS356	NS357
SiO <sub>2</sub> (wt%)	2.40	.35	2.18
TiO <sub>2</sub>	<.01	.00	.00
Al <sub>2</sub> O <sub>3</sub>	.02	.05	.04
Fe <sub>2</sub> O <sub>3</sub>	<.00	.02	<.15
FeO	.08	.13	.18
MnO	.01	.01	<.01
MgO	21.13	21.72	20.52
CaO	30.10	30.61	28.82
Na <sub>2</sub> O	<.02	<.02	<.02
K <sub>2</sub> O	<.00	.02	.01
P <sub>2</sub> O <sub>5</sub>	.04	.00	.02
H <sub>2</sub> O-	.03	.01	.05
H <sub>2</sub> O+	.08	.07	.08
CO <sub>2</sub>	45.28	46.27	47.80
TOTAL	99.19	99.28	99.70
F (ppm)	521	534	536
S	<3.7	<3.6	<3.6
Rb	<.7	2	<.7
Ba	<1.8	3	<1.8
Sr	57	52	82
Th	<1.8	<1.8	<1.8
U	<1.4	<1.4	<1.4
Zr	.7	.8	<.6
Nb	<.6	<.6	<.6
Mo	<.5	<.5	<.5
Sn	<1.4	<1.4	<1.4
W	<4.2	<4.2	<4.2
V	<1.6	3	2
Cr	<1.6	2	<1.5
Co	<1.6	<1.7	<1.6
Ni	<1.4	<1.4	<1.4
Cu	<1.1	<1.1	<1.1
Zn	4	5	6
Ga	<.9	<.9	<.9
Pb	2	2	<2.0
Ge	<.8	<.8	<.8
As	<.8	<.8	<.8
Sb	<1.2	<1.2	<1.2
Bi	<2.7	<2.7	<2.7
Se	<.8	<.8	<.8
Te	<2.0	<2.0	<2.0
Sc	<2.2	<2.2	<2.1
Y	<.7	1	<.7
La	<2.4	<2.4	<2.3
Ce	<4.3	<4.3	<4.0
Nd	<2.6	4	3
Au (ppb)	<5	14	<5

**Table 2.17:** Whole-rock analyses of the Karibib Formation marbles from the Habis Gold Prospect, Karibib District  
 NS355: white marble 900 m N of Habis farmhouse  
 NS356: light grey marble 800 m NE of Habis farmhouse  
 NS357: grey marble 550 m NNE of Habis farmhouse

	NS324	NS325	NS326	NS327
SiO <sub>2</sub> (wt%)	2.75	2.47	43.05	49.41
TiO <sub>2</sub>	.03	.03	.57	.67
Al <sub>2</sub> O <sub>3</sub>	.51	.58	10.89	11.44
Fe <sub>2</sub> O <sub>3</sub>	.16	.24	<.12	5.83
FeO	.25	.09	3.70	.01
MnO	.01	.06	.11	.39
MgO	2.93	5.36	3.52	8.16
CaO	51.41	48.90	22.93	18.10
Na <sub>2</sub> O	.03	.02	.64	.76
K <sub>2</sub> O	.21	.16	2.78	2.37
P <sub>2</sub> O <sub>5</sub>	.06	.03	.20	.16
H <sub>2</sub> O-	.08	.08	.06	.08
H <sub>2</sub> O+	.13	.18	.69	.63
CO <sub>2</sub>	41.47	41.44	9.82	2.54
TOTAL	100.04	99.64	98.95	100.54
F (ppm)	605	572	493	1048
S	<4.2	<4.0	344	6670
Rb	6	6	92	114
Ba	120	<2.0	328	404
Sr	301	692	795	1032
Th	3	<2.2	10	13
U	<1.7	<1.7	4	3
Zr	5	2	112	134
Nb	<.7	1	10	11
Mo	<.6	3	.7	<.6
Sn	2	<1.7	4	3
W	<5.4	<5.4	7	11
V	4	6	89	121
Cr	7	7	69	84
Co	<2.3	<2.2	18	11
Ni	<1.9	<1.9	46	21
Cu	4	5	42	165
Zn	19	6	23	59
Ga	<1.1	<1.1	15	18
Pb	7	5	10	11
Ge	<1.1	<1.1	<1.1	<1.1
As	1	<1.0	<1.0	<1.0
Sb	<1.5	<1.5	<1.5	<1.5
Bi	<3.4	<3.4	<3.4	11
Se	<1.0	<1.0	<1.0	<1.0
Te	<2.4	<2.4	<2.3	<2.4
Sc	<3.5	<3.4	9	15
Y	2	3	20	18
La	<3.7	<3.5	25	27
Ce	12	8	51	58
Nd	7	8	28	29
Au (ppb)	12	18	33	355

**Table 2.18:** Whole-rock analyses from the Karibib Formation marbles and calc-silicate rocks from the Navachab Gold Mine, Karibib District  
 NS324: Section 2600, contorted marble (CM)  
 NS325: Section 2600, dolomite marble (DM)  
 NS326: Section 2600, banded calc-silicate marble (MC)  
 NS327: Section 2600, banded calc-silicate rock (MC)

	NS367	NS368	NS369
SiO <sub>2</sub> (wt%)	.23	.64	1.43
TiO <sub>2</sub>	.01	.01	.03
Al <sub>2</sub> O <sub>3</sub>	.08	.37	.31
Fe <sub>2</sub> O <sub>3</sub>	.14	.19	3.73
FeO	.00	.00	.00
MnO	.04	.02	.68
MgO	.77	.18	18.38
CaO	55.31	55.51	30.28
Na <sub>2</sub> O	<.02	<.02	<.02
K <sub>2</sub> O	.04	.05	.10
P <sub>2</sub> O <sub>5</sub>	.06	.02	.05
H <sub>2</sub> O-	.04	.04	.02
H <sub>2</sub> O+	.00	.00	.00
CO <sub>2</sub>	.00	.00	.00
TOTAL	100.19	100.38	99.33
F (ppm)	442	343	388
S	<4.2	<4.3	<3.6
Rb	4	4	4
Ba	<2.2	<2.2	10.3
Sr	1111	2360	235
Th	<3.2	<3.3	<2.7
U	<3.8	<4.0	<3.2
Zr	<3.5	<4.4	4
Nb	4	5	<2.1
Mo	3	7	<2.3
Sn	<1.8	<1.8	<1.6
W	<5.6	<5.7	<4.7
V	<2.6	<2.6	3
Cr	3	3	4
Co	<2.4	<2.4	<2.4
Ni	<1.9	<1.9	<1.6
Cu	<1.5	13.7	2.1
Zn	5.1	4.4	18.4
Ga	<1.1	<1.2	<1.0
Pb	<4.6	<4.7	<3.9
Ge	<1.1	<1.2	<1.0
As	<1.0	3	<.9
Sb	<1.5	<1.6	<1.4
Bi	<3.6	<3.6	<3.0
Se	<1.0	<1.1	<.9
Te	<2.5	<2.5	<2.2
Sc	<4.0	<4.0	<2.3
Y	<2.7	<2.7	3
La	<3.9	<3.9	3
Ce	<6.6	8	<5.2
Nd	6	8	5
Au (ppb)	<5	8	<5

**Table 2.19:** Whole-rock analyses of the Karibib Formation marbles from the Onguati Copper Mine, Karibib District  
 NS367: calcitic marble  
 NS368: upper marble (grey)  
 NS369: dolomitic marble

	NS270	NS271	NS272	NS273
SiO <sub>2</sub> (wt%)	.96	1.44	3.98	1.66
TiO <sub>2</sub>	.00	.01	.04	.03
Al <sub>2</sub> O <sub>3</sub>	.06	.10	.28	.52
Fe <sub>2</sub> O <sub>3</sub>	.00	.00	.13	.17
FeO	.13	.19	.61	.08
MnO	.02	<.01	.10	.01
MgO	.16	.05	1.47	.40
CaO	54.63	54.74	51.69	54.10
Na <sub>2</sub> O	<.02	<.02	.06	.03
K <sub>2</sub> O	.01	.02	.00	.14
P <sub>2</sub> O <sub>5</sub>	.04	.06	.92	.04
H <sub>2</sub> O-	.03	.06	.05	.04
H <sub>2</sub> O+	.06	.07	.07	.12
CO <sub>2</sub>	43.18	42.87	40.46	42.26
TOTAL	99.28	99.61	99.88	99.60
F (ppm)	316	330	303	426
S	<4.3	<4.3	<4.5	<4.4
Rb	<.9	1	<.9	4
Ba	<2.1	<2.1	<2.2	6
Sr	1960	2332	714	1040
Th	<2.4	<2.4	<2.3	<2.4
U	<1.9	<1.9	<1.8	<1.8
Zr	<1.3	<1.4	2	3
Nb	<.8	1	<.8	<.8
Mo	<.6	<.6	<.6	<.6
Sn	<1.8	<1.8	<1.7	<1.8
W	<5.8	<5.8	<5.6	<5.7
V	<2.5	<2.5	<2.5	3
Cr	<2.3	<2.2	<2.2	<2.3
Co	<2.3	<2.3	<2.4	<2.3
Ni	<2.1	<2.0	<2.0	<2.0
Cu	<1.6	<1.6	<1.5	<1.6
Zn	11	<1.0	<1.0	2
Ga	<1.2	<1.2	<1.1	<1.2
Pb	3	<2.8	<2.7	<2.7
Ge	<1.2	<1.2	<1.1	<1.1
As	<1.1	<1.1	2	<1.0
Sb	<1.5	<1.5	<1.5	<1.5
Bi	<3.7	<3.7	<3.6	<3.6
Se	<1.1	<1.1	<1.0	<1.1
Te	<2.5	<2.5	<2.4	<2.4
Sc	<3.8	<3.8	<3.6	<3.8
Y	2	<.9	8	2
La	<3.9	<3.9	9	<3.8
Ce	<6.4	<6.3	17	<6.4
Nd	7	8	16	6
Au (ppb)	<5	<5	<5	<5

**Table 2.20:** Whole-rock analyses of the Karibib Formation marbles on the farms Sandamap 64 and Sandamap Noord 115, Usakos District  
 NS270: 1.8 km SE of Cilliers Workings, calcite marble (Sandamap 64)  
 NS271: 2.5 km N of Sandamap farmhouse, calcite marble (Sandamap 64)  
 NS272: 2.5 km N of Sandamap farmhouse, calcite marble (Sandamap 64)  
 NS273: 300 m W of Sandamapberg, calcite marble (Sandamap Noord 115)

	NS362	NS363	NS364
SiO <sub>2</sub> (wt%)	68.35	66.78	62.06
TiO <sub>2</sub>	.74	.65	.82
Al <sub>2</sub> O <sub>3</sub>	12.97	12.21	15.43
Fe <sub>2</sub> O <sub>3</sub>	5.68	2.83	6.87
FeO	1.51	3.72	.74
MnO	.05	.09	.12
MgO	1.90	2.35	3.19
CaO	.56	1.18	.68
Na <sub>2</sub> O	.81	1.65	2.38
K <sub>2</sub> O	3.01	3.00	2.46
P <sub>2</sub> O <sub>5</sub>	.24	.18	.44
H <sub>2</sub> O-	.52	.30	.22
H <sub>2</sub> O+	3.59	3.43	3.53
CO <sub>2</sub>	.28	.98	.17
TOTAL	100.22	99.36	99.11
F (ppm)	1785	1035	992
S	64	330	68
Rb	144	124	120
Ba	443	338	351
Sr	42	105	88
Th	11	10	13
U	3	2	3
Zr	216	191	202
Nb	15	13	17
Mo	1	.7	.7
Sn	4	4	18
W	13	11	10
V	108	88	119
Cr	72	73	96
Co	19	22	17
Ni	44	38	40
Cu	39	49	17
Zn	73	115	139
Ga	18	15	19
Pb	10	27	72
Ge	<.9	<.9	<.9
As	128	13	27
Sb	<1.3	<1.3	<1.3
Bi	<2.9	<2.9	<2.9
Se	<.9	<.9	<.9
Te	<2.1	<2.1	<2.1
Sc	14	12	18
Y	33	25	50
La	30	27	49
Ce	59	55	100
Nd	32	31	54
Au (ppb)	<5	<5	<5

**Table 2.21:** Whole-rock analyses of the Onguati Formation quartzite on the farm Onguati 52, Karibib District  
 NS362: Banks of Khan River, Hill 1066, muscovite-chlorite-quartzite  
 NS363: Banks of Khan River, Hill 1046, muscovite quartzite  
 NS364: Banks of Khan River, Hill 1067

	NS338	NS339	NS340
SiO <sub>2</sub> (wt%)	58.06	66.82	69.69
TiO <sub>2</sub>	.66	.72	.75
Al <sub>2</sub> O <sub>3</sub>	11.57	11.32	10.59
Fe <sub>2</sub> O <sub>3</sub>	<.19	<.10	<.01
FeO	5.84	4.29	4.11
MnO	.39	.20	.23
MgO	3.10	2.35	1.78
CaO	16.90	12.30	11.63
Na <sub>2</sub> O	.81	.49	.40
K <sub>2</sub> O	.29	.05	.05
P <sub>2</sub> O <sub>5</sub>	.26	.17	.17
H <sub>2</sub> O-	.13	.11	.09
H <sub>2</sub> O+	.90	.76	.68
CO <sub>2</sub>	.49	.50	.50
TOTAL	99.42	100.07	100.67
F (ppm)	574	384	414
S	56	257	268
Rb	11	3	3
Ba	52	81	45
Sr	367	218	216
Th	5	9	6
U	2	4	2
Zr	149	191	203
Nb	18	16	11
Mo	3	.9	1
Sn	73	25	30
W	453	14	18
V	64	78	70
Cr	66	67	65
Co	12	7	9
Ni	28	15	21
Cu	2	4	3
Zn	602	57	95
Ga	20	14	13
Pb	<2.5	<2.2	<2.2
Ge	<1.1	<1.0	<1.0
As	2	<.9	1
Sb	<1.5	<1.4	<1.3
Bi	<3.4	<3.1	<3.1
Se	<1.0	<.9	<.9
Te	<2.3	<2.2	<2.1
Sc	11	12	11
Y	23	40	41
La	19	33	31
Ce	38	57	61
Nd	23	31	34
Au (ppb)	<5	<5	<5

**Table 2.22:** Whole-rock analyses of the Kuiseb Formation calc-silicate rocks on the farm Pforte 65, Usakos District  
 NS338: RUL grid, PA 52.03/1140  
 NS339: RUL grid, PA 52.05/1145  
 NS340: RUL grid, E of main road

	NS332	NS333
SiO <sub>2</sub> (wt%)	2.31	6.95
TiO <sub>2</sub>	.03	.06
Al <sub>2</sub> O <sub>3</sub>	.37	1.34
Fe <sub>2</sub> O <sub>3</sub>	.12	.22
FeO	.33	.93
MnO	.13	.17
MgO	.78	1.27
CaO	55.11	50.74
Na <sub>2</sub> O	<.02	.03
K <sub>2</sub> O	.00	.02
P <sub>2</sub> O <sub>5</sub>	.14	.24
H <sub>2</sub> O-	.03	.09
H <sub>2</sub> O+	.16	.20
CO <sub>2</sub>	40.76	37.57
TOTAL	100.27	99.81
F (ppm)	443	454
S	<4.3	<4.6
Rb	<.9	1
Ba	<2.2	<2.2
Sr	762	959
Th	<2.3	2
U	<1.8	<1.8
Zr	<1.0	6
Nb	<.7	2
Mo	.7	.9
Sn	4	3
W	<5.6	7
V	<2.6	6
Cr	3	7
Co	<2.4	<2.4
Ni	<2.0	<2.0
Cu	7	10
Zn	12	46
Ga	<1.1	2
Pb	3	3
Ge	<1.1	<1.1
As	<1.0	<1.0
Sb	<1.5	<1.6
Bi	<3.6	<3.6
Se	<1.0	<1.1
Te	<2.4	<2.5
Sc	<3.8	<3.6
Y	6	10
La	12	10
Ce	18	15
Nd	12	16
Au (ppb)	8	<5

**Table 2.23:** Whole-rock analyses of the Kuiseb Formation marbles on the farm Pforte 65, Usakos District  
 NS332: RUL grid, PA 52.10/1135  
 NS333: RUL grid, PA 52.15/1130

alisation is overlain by virtually pure dolomitic marble. Both lithologies possess an annealed mosaic of carbonate grains with minor interstitial quartz. The dolomitic marble has several crosscutting zones of recrystallised coarse-grained

dolomite as well as small poikiloblastic tremolite.

Minor gold mineralisation in quartz veins is hosted by the calcitic marbles of the Karibib Formation at Hill 1166 on Sandamap. This prospect is located in the core of an F<sub>4</sub> fold on the northern edge of the SCZ near the intersection of the Omaruru Lineament and the Welwitschia lineament zone. The thickness of the Karibib Formation varies between 80 and several hundred metres due to the tectonism (Maps 3 and 4). The formation comprises calcitic marble with very subordinate calc-silicate rocks and biotite schist (Steven, 1988). Petro-graphic and geochemical analyses (Tables 2.16 and 2.20) reveal the purity of the marble, which has an annealed metamorphic texture. However, many of the calcite grains have deformed cleavages and twin lamellae indicating that a major deformational event postdated the annealing process which was probably the peak of metamorphism. The significance of this late-tectonic F<sub>4</sub> deformation will be discussed in Chapter 4.

In summary, the Karibib Formation comprises carbonate units with very subordinate calc-silicate and biotite schist. In the SCZ close to the Abbabis Inlier dolomitic marble predominates over calcitic marble, but the proportion of the latter increases in a northerly direction. In the NCZ the Karibib Formation is represented by calc-silicate rocks and calcitic marble. Gold mineralisation in the CZ is hosted by both calcitic and dolomitic marble and appears to be confined to the SCZ. The origin of the dolomite is of particular interest because Pirajno *et al.* (1990a) have stated that dolomitisation of the Karibib Formation was one of the 'ore-forming processes' that led to the development of gold skarn mineralisation in central Namibia. However, near the Abbabis Inlier dolomitic marble forms the bulk of the Karibib Formation (Smith, 1965, p.29). No evidence (such as crosscutting veins) for late-stage dolomitisation of the Karibib Formation could be found in any of the samples examined in this study. Since it is unlikely that the entire Karibib Formation was dolomitised at the time of the formation of the late-Damara hydrothermal gold veins, a primary or syndiagenetic origin for the dolomites of this formation appears more plausible (see discussion in Chapter 7.4).

#### 2.2.2.7 Onguati Formation

The term Onguati Formation was introduced by Badenhorst (1988a) to describe an intercalated sequence of schist, marble and quartzites (up to 800 m thick) that represents a transitional zone between the shelf carbonates of the Karibib Formation and the pelagic sediments of the Kuiseb Formation in the northern SCZ. In the type area, quartzites are the most predominant lithology and comprise quartz (50-55%), sericite and chlorite (30-40%), altered feldspar (0-5%), limonite (5%), and traces of tourmaline and zircon. The overall texture is fine-grained (the grain size seldom exceeding 150 µm) and equigranular with quartz crystals granoblastically arranged. Chlorite and limonite are intimately related and randomly oriented micas overgrow feldspar. Geochemical analyses of the Onguati Formation are listed in Table 2.21. On the farm Onguati 52 (Fig. 1.3) on the south bank of the Khan River quartzites host tourmaline rocks which are broadly stratabound, but are crosscutting within that zone (Table 2.3). The area has been intruded by several Damara pegmatites and the development of these

	NS274	NS275	NS276	NS277	NS278	NS281	NS282	NS283
SiO <sub>2</sub> (wt%)	63.52	63.40	57.90	57.78	57.77	57.98	61.72	75.47
TiO <sub>2</sub>	.81	.82	.77	.77	.77	.83	.83	.75
Al <sub>2</sub> O <sub>3</sub>	15.68	15.75	17.55	17.34	17.70	19.08	17.82	10.98
Fe <sub>2</sub> O <sub>3</sub>	1.04	.93	.65	.70	.24	2.64	2.01	.51
FeO	5.25	5.40	6.28	6.31	6.34	4.67	5.21	3.21
MnO	.11	.10	.11	.11	.11	.09	.08	.05
MgO	3.12	3.09	4.62	4.63	4.40	3.59	3.37	1.43
CaO	1.54	1.37	3.54	3.52	2.96	.85	.51	1.17
Na <sub>2</sub> O	2.86	3.45	1.74	1.74	1.83	1.47	.70	3.35
K <sub>2</sub> O	2.97	2.91	4.38	4.27	4.81	4.38	4.61	1.63
P <sub>2</sub> O <sub>5</sub>	.31	.16	.19	.20	.17	.29	.22	.28
H <sub>2</sub> O-	.18	.21	.21	.26	.12	.28	.14	.07
H <sub>2</sub> O+	1.32	1.13	.97	1.19	.90	2.30	1.98	.67
CO <sub>2</sub>	.73	.87	.15	.18	.63	.44	.48	.38
TOTAL	99.43	99.60	99.08	99.00	98.76	98.88	99.68	99.95
F (ppm)	1777	1667	1349	1355	1169	844	827	441
S	<5.2	<5.0	<5.1	<5.0	<5.5	<5.2	20	39
Rb	150	160	191	194	188	206	194	80
Ba	508	600	934	904	1515	638	800	247
Sr	168	146	309	304	233	105	58	140
Th	14	15	18	17	14	14	14	16
U	4	4	3	4	3	4	4	5
Zr	217	209	167	168	159	187	190	377
Nb	16	17	17	16	16	18	16	14
Mo	.7	<.5	<.6	<.6	<.6	<.5	.6	<.5
Sn	58	37	8	8	7	6	8	5
W	<4.8	<4.7	5	6	<5.0	11	7	<4.3
V	125	131	134	134	141	138	145	66
Cr	99	96	98	97	102	122	113	59
Co	7	9	20	22	17	27	21	10
Ni	37	38	50	52	41	57	42	19
Cu	11	4	9	6	28	2	28	6
Zn	119	120	151	158	146	145	138	59
Ga	20	24	26	26	26	28	26	13
Pb	34	29	18	16	31	21	14	9
Ge	<1.0	<.9	<1.0	<1.0	<1.0	<1.0	<1.0	<.9
As	51	30	1	<1.0	<1.0	44	6	13
Sb	<1.3	<1.3	<1.4	<1.4	<1.4	<1.3	<1.3	<1.2
Bi	<3.0	<3.0	<3.2	<3.2	<3.1	<3.0	<3.0	<2.7
Se	<.9	<.9	<.9	<.9	<.9	<.9	<.9	<.8
Te	<2.1	<2.1	<2.2	<2.2	<2.2	<2.1	<2.1	<1.9
Sc	18	17	22	21	22	23	22	11
Y	47	35	41	40	37	37	39	42
La	29	31	43	41	28	30	30	33
Ce	64	62	84	79	55	61	56	74
Nd	37	34	48	47	32	37	36	42
Au (ppb)	4	<5	<5	<5	<5	<5	10	7

**Table 2.24:** Whole-rock analyses of Kuiseb Formation schist on the farms Sandamap 64 and Sandamap Noord 115, Usakos District  
 NS274: Sandamap Noord, 1.2 km N of Sandamap Tin Mine, biotite-muscovite schist  
 NS275: Sandamap Noord, 1.2 km N of Sandamap Tin Mine, biotite-muscovite schist  
 NS276: Sandamap Noord, 1.5 km WSW of Sandamap Tin Mine, biotite schist  
 NS277: Sandamap Noord, 1.5 km WSW of Sandamap Tin Mine, biotite schist  
 NS278: Sandamap, 200 m E of Cilliers Workings, biotite-muscovite schist  
 NS281: Sandamap Noord, 300 m N of Sandamap Tin Mine, biotite-andalusite-muscovite schist  
 NS282: Sandamap Noord, 300 m N of Sandamap Tin Mine, biotite-andalusite-muscovite schist  
 NS283: Sandamap Noord, 300 m N of Sandamap Tin Mine, biotite-muscovite schist

	NS284	NS285	NS286	NS287	NS288	NS289	NS290	NS291
SiO <sub>2</sub> (wt%)	71.25	59.85	62.66	65.89	64.05	54.27	56.71	55.87
TiO <sub>2</sub>	.73	.81	.81	.78	.77	.82	.85	.84
Al <sub>2</sub> O <sub>3</sub>	12.69	16.84	15.98	14.61	15.81	17.60	18.07	18.24
Fe <sub>2</sub> O <sub>3</sub>	.65	.43	.38	.33	.36	.81	.43	.28
FeO	3.90	6.38	5.90	5.27	5.46	5.70	7.24	7.46
MnO	.09	.10	.17	.08	.11	.12	.12	.12
MgO	1.92	4.27	3.76	2.87	3.28	4.66	4.28	4.33
CaO	1.88	2.54	2.33	1.64	1.96	4.08	2.12	1.85
Na <sub>2</sub> O	3.08	2.38	2.52	3.32	2.71	1.91	3.22	3.66
K <sub>2</sub> O	1.96	3.83	3.23	2.95	3.06	4.93	3.69	3.78
P <sub>2</sub> O <sub>5</sub>	.22	.20	.16	.24	.16	.19	.26	.22
H <sub>2</sub> O-	.10	.15	.12	.32	.11	.23	.16	.16
H <sub>2</sub> O+	.76	1.01	.93	.79	.93	1.77	1.16	1.14
CO <sub>2</sub>	.45	1.04	1.04	.68	.59	2.22	.47	.13
TOTAL	99.68	99.84	100.00	99.77	99.36	99.31	98.77	98.07
F (ppm)	561	848	1126	770	866	1131	4051	3966
S	<5.5	<5.3	<5.4	<5.3	10	<5.0	<5.4	<5.2
Rb	96	156	158	139	157	195	926	1013
Ba	463	627	794	435	468	859	425	441
Sr	198	135	192	184	182	202	134	130
Th	12	11	12	12	13	18	13	12
U	4	3	2	3	4	4	4	4
Zr	236	168	201	210	175	176	176	172
Nb	14	15	17	16	17	16	15	15
Mo	<.5	.6	<.5	<.5	<.5	<.6	<.6	.8
Sn	4	4	5	4	3	7	348	368
W	<4.5	<4.9	<4.8	<4.7	<4.7	6	8	5
V	88	155	112	101	122	135	181	184
Cr	70	109	88	79	90	95	127	129
Co	15	19	21	15	15	23	23	24
Ni	30	50	40	34	28	50	58	62
Cu	2	35	18	11	9	49	6	5
Zn	92	129	116	101	117	140	173	194
Ga	17	24	22	20	21	26	25	27
Pb	12	23	28	27	31	32	23	22
Ge	<.9	<1.0	<1.0	<.9	<.9	<1.0	<1.0	<1.0
As	6	11	<.9	9	4	<1.0	8	9
Sb	<1.3	<1.4	<1.3	<1.3	<1.3	<1.4	<1.4	<1.4
Bi	<2.8	<3.1	<3.0	<2.9	<3.0	<3.1	<3.2	<3.2
Se	<.8	<.9	<.9	<.9	<.9	<.9	<.9	<.9
Te	<2.0	<2.2	<2.1	<2.0	<2.1	<2.2	<2.2	<2.2
Sc	14	21	18	15	19	20	24	24
Y	32	34	35	39	39	42	34	33
La	27	25	29	29	28	42	23	27
Ce	57	48	59	60	54	86	49	54
Nd	33	29	30	34	31	48	31	29
Au (ppb)	<5	11	<5	7	<5	<5	<5	<5

Table 2.24 (continued):

- NS284: Sandamap Noord, 300 m N of Sandamap Tin Mine, biotite schist  
NS285: Sandamap Noord, 1.9 km NW of Sandamap Tin Mine, biotite-muscovite schist  
NS286: Sandamap Noord, 2.0 km NW of Sandamap Tin Mine, biotite-muscovite schist  
NS287: Sandamap Noord, 1.8 km NNW of Sandamap Tin Mine, biotite-muscovite schist  
NS288: Sandamap Noord, 1.9 km WNW of Sandamap Tin Mine, biotite-muscovite schist  
NS289: Sandamap 64, 500 m NE of Cilliers Workings, biotite-muscovite schist  
NS290: Sandamap Noord, 1.2 km S of Sandamap Tin Mine, biotite schist  
NS291: Sandamap Noord, 1.2 km S of Sandamap Tin Mine, biotite-muscovite schist

	NS351	NS352	NS353	NS354
SiO <sub>2</sub> (wt%)	81.71	60.99	63.00	61.56
TiO <sub>2</sub>	.30	.89	.81	.82
Al <sub>2</sub> O <sub>3</sub>	9.22	15.94	16.82	16.17
Fe <sub>2</sub> O <sub>3</sub>	.36	4.16	1.01	1.46
FeO	1.44	1.72	4.78	4.43
MnO	.03	.08	.12	.12
MgO	.71	2.75	3.09	3.10
CaO	.43	.80	.90	.73
Na <sub>2</sub> O	3.62	1.69	1.47	2.25
K <sub>2</sub> O	1.82	6.80	5.18	6.50
P <sub>2</sub> O <sub>5</sub>	.08	.35	.38	.24
H <sub>2</sub> O-	.08	.46	.16	.14
H <sub>2</sub> O+	.83	2.06	2.18	1.64
CO <sub>2</sub>	.13	1.02	.08	.13
TOTAL	100.76	99.71	99.98	99.29
F (ppm)	225	854	1080	1083
S	99	<5.3	<5.4	<5.5
Rb	54	208	201	248
Ba	503	874	965	837
Sr	95	80	73	78
Th	5	13	12	14
U	2	4	45	3
Zr	109	241	180	173
Nb	6	16	16	16
Mo	.6	.6	.9	1
Sn	<1.3	7	8	7
W	13	11	14	12
V	43	114	128	128
Cr	37	97	104	107
Co	3	17	16	22
Ni	10	37	38	40
Cu	3	<1.3	5	5
Zn	56	88	107	111
Ga	9	22	23	22
Pb	11	22	14	41
Ge	<.8	<1.0	<1.0	<1.0
As	3	3	4	<1.0
Sb	<1.1	<1.3	<1.3	<1.3
Bi	<2.5	<3.0	<3.0	<3.0
Se	<.7	<.9	<.9	<.9
Te	<1.8	<2.1	<2.1	<2.1
Sc	6	17	18	19
Y	16	45	53	38
La	15	34	37	32
Ce	34	67	88	70
Nd	18	40	48	37
Au (ppb)	14	<5	<5	<5

**Table 2.25:** Whole-rock analyses of Kuseib Formation meta-sediments on the farm Kassandara 40, Omaruru District  
 NS351: Kassandara/Epako Süd fence, 3.5 km NNE of Swartberg, feldspathic metaquartzite  
 NS352: Kassandara/Epako Süd fence, 3.5 km NNE of Swartberg, biotite-muscovite-K-feldspar schist  
 NS353: Kassandara/Epako Süd fence, 3.2 km NNE of Swartberg, biotite-muscovite-K-feldspar schist  
 NS354: Kassandara/Epako Süd fence, 3.2 km NNE of Swartberg, biotite-muscovite-K-feldspar schist

zones of tourmalinisation is probably related to these intrusions or possibly to the Erongo Complex.

#### 2.2.2.8 Kuseib Formation

The sediments of the Kuseib Formation are widely distributed throughout the CZ. In the SCZ, the formation is represented by quartz-biotite schists, but sedimentary features have been destroyed during metamorphism and deformation and the top of the formation is not seen. Smith (1965) noted a minimum thickness of 3300 metres for the formation south of the Abbabis Inlier and Badenhorst (1987) recorded a minimum thickness of 40 metres in the Okawayo Section. A complete section through the Kuseib Formation is nowhere exposed in the NCZ. Klein (1980) considered the contact with the underlying Karibib Formation to be commonly faulted and he divided the formation into two levels (Table 2.2). In general, the lower levels found in NCZb, NCZc and NCZd are characterised by pelagic metasediments that have undergone amphibolite-facies metamorphism and have been intruded by syn- and late-tectonic granites. Calc-silicate lithologies possess finely disseminated scheelite, and marble horizons host tungsten skarn mineralisation in NCZc (Table 2.3). The upper levels of the Kuseib Formation (Klein's informal Uis Formation) are found in NCZa and NCZe and, in the latter, the formation exceeds 4000 metres in thickness (cf 10 000 metres near Ondundo in the NZ; Miller, 1980). The upper Kuseib is dominated by metaturbidites that have been regionally metamorphosed to greenschist facies in NCZe and amphibolite facies in NCZa. The metasediments have been intruded by late/post-tectonic granites and stanniferous pegmatites that have caused a thermal metamorphic overprint of the metasediments. Thus two metamorphic episodes can clearly be distinguished in NCZe. The upper Kuseib Formation is of economic interest for a number of reasons (Table 2.3). Firstly, this stratigraphic level hosts the Sandamap-Davib Ost, Nainais-Kohero (Fig. 2.4) and Strathmore-Uis tin belts. Secondly, the Kuseib Formation schists of NCZa host gold-arsenic mineralisation where they have been sheared (Chapter 7.5). Thirdly, tourmaline schists and zones of tourmalinised schist (discussed in Chapter 7.6) and scheelite-bearing vesuvianite calc-silicate rocks (discussed in Chapter 7.7) are present in both NCZa and NCZe.

In NCZb, NCZc and NCZd the lower levels of the Kuseib Formation are represented by biotite schist which is locally garnetiferous (for example on Pforte; Fig. 1.3). The mineralogy of the schist varies with composition and metamorphic grade. Due to the deformation and metamorphism no sedimentary features can be identified. In both NCZb and NCZc, the base of the formation is notably calcareous and contains a high proportion of calc-silicate rocks, some of which possess finely disseminated scheelite mineralisation (Table 2.22). Minor marble horizons, usually less than five metres thick, are present at the base of the formation in NCZc and host tungsten skarn mineralisation on Pforte. These marble bands are comprised largely of calcite (Table 2.23).

In NCZa the upper levels of the Kuseib Formation are represented by biotite ± andalusite ± sillimanite schists.

	NS213	NS214	NS215	NS216	NS217	NS218	NS219	NS220
SiO <sub>2</sub> (wt%)	58.33	58.53	57.59	58.45	57.16	63.42	60.71	61.74
TiO <sub>2</sub>	.85	.86	.77	.76	.84	.87	.93	.79
Al <sub>2</sub> O <sub>3</sub>	18.18	18.35	17.98	16.71	18.21	17.41	17.78	16.89
Fe <sub>2</sub> O <sub>3</sub>	3.45	4.76	7.24	.00	7.22	3.79	5.58	5.88
FeO	3.78	2.70	.25	6.81	.06	2.31	1.19	.72
MnO	.08	.09	.11	.20	.08	.05	.06	.06
MgO	3.75	3.79	4.23	4.04	3.40	2.64	3.24	3.50
CaO	.39	.71	3.13	6.90	.34	.15	.42	.25
Na <sub>2</sub> O	.29	.88	2.12	.45	1.00	.77	.63	.26
K <sub>2</sub> O	6.02	4.85	4.20	3.03	5.72	5.07	5.79	5.76
P <sub>2</sub> O <sub>5</sub>	.19	.13	.19	.16	.11	.05	.22	.14
H <sub>2</sub> O-	.34	.46	.32	.12	.35	.47	.37	.24
H <sub>2</sub> O+	3.16	3.02	1.47	.72	4.59	3.01	2.69	2.48
CO <sub>2</sub>	1.25	.46	.24	1.09	.70	.92	1.01	1.20
TOTAL	100.04	99.59	99.83	99.44	99.77	100.94	100.61	99.91
F (ppm)	916	706	1274	1267	1040	742	625	957
S	<5.3	<5.7	30	5220	<5.6	<4.9	<5.5	1066
Rb	243	167	203	139	232	199	293	335
Ba	693	705	1090	566	784	715	744	821
Sr	31	60	363	150	58	41	40	30
Th	15	16	19	17	16	15	15	13
U	5	3	4	5	4	4	6	4
Zr	185	183	164	140	179	172	214	172
Nb	16	17	16	16	18	16	17	16
Mo	.6	<.5	<.6	1	<.5	<.5	<.5	<.5
Sn	4	7	6	23	16	13	10	75
W	8	10	8	5	6	8	8	6
V	159	147	137	163	130	147	169	158
Cr	116	110	101	100	109	119	114	115
Co	21	22	18	19	14	22	18	12
Ni	53	45	47	37	34	41	39	23
Cu	24	41	41	22	4	2	12	23
Zn	141	129	143	146	140	110	113	95
Ga	26	27	27	25	27	25	26	24
Pb	15	18	52	11	12	8	4	4
Ge	<1.0	<1.0	1	<1.0	<1.0	<.9	<1.0	<1.0
As	12	43	3	12	38	68	19	25
Sb	<1.4	<1.3	<1.4	<1.4	<1.3	<1.3	<1.3	<1.3
Bi	<3.1	<3.0	<3.1	4	<3.1	<2.9	<3.0	<3.0
Se	<.9	<.9	<.9	<.9	<.9	<.9	<.9	<.9
Te	<2.2	<2.2	<2.2	<2.2	<2.2	<2.1	<2.1	<2.1
Sc	21	22	20	22	21	22	23	22
Y	38	37	39	39	36	33	40	29
La	34	34	38	33	32	33	38	27
Ce	66	69	71	72	62	63	81	54
Nd	38	39	44	39	34	35	42	30
Au (ppb)	N/A	<5	<5	<5	<5	N/A	N/A	<5

**Table 2.26:** Whole-rock analyses of Kuiseb Formation metasediments on the farm Ohere 106, Omaruru District

NS213: RUL grid 9000/8900, biotite-muscovite phyllite  
 NS214: RUL grid 9200/9400, biotite-muscovite phyllite  
 NS215: RUL grid 7600/8700, biotite-muscovite phyllite  
 NS216: RUL grid 9600/7700, biotite-muscovite phyllite  
 NS217: 2 km NW of farmhouse, biotite-muscovite schist  
 NS218: Grid 1, biotite-muscovite-cordierite schist  
 NS219: Grid 2, biotite-muscovite-cordierite schist  
 NS220: Grid 2, biotite-muscovite schist  
 N/A = Not analysed

	NS252	NS253	NS254
SiO <sub>2</sub> (wt%)	78.58	80.79	80.98
TiO <sub>2</sub>	.58	.49	.58
Al <sub>2</sub> O <sub>3</sub>	9.78	9.66	9.56
Fe <sub>2</sub> O <sub>3</sub>	.05	.17	.18
FeO	1.10	.87	.98
MnO	.01	.00	.01
MgO	.54	.37	.41
CaO	.56	.25	.26
Na <sub>2</sub> O	1.46	2.52	1.93
K <sub>2</sub> O	6.03	3.82	4.23
P <sub>2</sub> O <sub>5</sub>	.13	.12	.14
H <sub>2</sub> O-	.08	.08	.05
H <sub>2</sub> O+	.62	.57	.56
CO <sub>2</sub>	.35	.29	.18
TOTAL	99.88	100.01	100.06
F (ppm)	235	265	247
S	<5.1	<5.2	95
Rb	137	103	104
Ba	680	751	823
Sr	68	61	64
Th	10	8	9
U	3	1	2
Zr	304	226	286
Nb	10	9	10
Mo	<.5	<.5	<.5
Sn	4	3	4
W	<4.2	4	<4.0
V	40	36	41
Cr	36	33	40
Co	4	5	4
Ni	5	11	10
Cu	2	5	5
Zn	26	20	21
Ga	10	10	10
Pb	22	23	17
Ge	<.8	<.8	<.8
As	7	11	19
Sb	1	1	<1.1
Bi	<2.6	<2.5	<2.6
Se	<.8	<.7	<.8
Te	<1.9	<1.8	<1.8
Sc	7	7	8
Y	20	18	18
La	22	23	22
Ce	56	53	52
Nd	31	28	28
Au (ppb)	<5	<5	10

**Table 2.27:** Whole-rock analyses of Kuiseb Formation quartzite on the farm Sandamap Noord 115, Usakos District  
 NS252: 3.4 km WNW of Sandamap Tin Mine  
 NS253: 3.4 km WNW of Sandamap Tin Mine  
 NS254: 3.4 km WNW of Sandamap Tin Mine

	NS221	NS222	NS224
SiO <sub>2</sub> (wt%)	84.64	86.39	83.70
TiO <sub>2</sub>	.52	.14	.46
Al <sub>2</sub> O <sub>3</sub>	7.10	5.59	7.81
Fe <sub>2</sub> O <sub>3</sub>	.33	.66	1.63
FeO	1.19	.16	.21
MnO	.06	.04	.06
MgO	.48	.23	.47
CaO	.99	1.54	.52
Na <sub>2</sub> O	2.89	2.39	3.93
K <sub>2</sub> O	1.34	1.75	1.17
P <sub>2</sub> O <sub>5</sub>	.08	.04	.07
H <sub>2</sub> O-	.04	.03	.09
H <sub>2</sub> O+	.48	.24	.57
CO <sub>2</sub>	.88	1.29	.36
TOTAL	101.02	100.49	101.06
F (ppm)	156	122	223
S	11	123	<5.0
Rb	37	29	41
Ba	371	387	388
Sr	145	97	130
Th	8	4	7
U	3	1	2
Zr	392	90	283
Nb	10	3	8
Mo	<.5	<.5	<.5
Sn	6	3	2
W	4	<3.8	<3.9
V	24	9	28
Cr	30	15	28
Co	4	<1.7	4
Ni	6	7	8
Cu	3	4	2
Zn	19	10	23
Ga	6	4	7
Pb	17	15	16
Ge	<.8	<.8	<.8
As	5	1	5
Sb	<1.1	<1.1	<1.1
Bi	<2.5	<2.5	<2.5
Se	<.7	<.7	<.7
Te	<1.8	<1.7	<1.8
Sc	5	2	5
Y	24	10	21
La	25	12	18
Ce	52	27	41
Nd	28	16	23
Au (ppb)	5	<5	<5

**Table 2.28:** Whole-rock analyses of the Kuiseb Formation quartzites on the farm Ohere 106, Omaruru District  
 NS221: RUL grid 8200/8890, quartzite from metaturbidite sequence  
 NS222: RUL grid 8200/9650, quartzite from metaturbidite sequence  
 NS224: RUL grid 10000/9800, quartzite from metaturbidite sequence

	NS206
SiO <sub>2</sub> (wt%)	51.74
TiO <sub>2</sub>	.54
Al <sub>2</sub> O <sub>3</sub>	8.76
Fe <sub>2</sub> O <sub>3</sub>	.11
FeO	3.23
MnO	.48
MgO	1.60
CaO	22.27
Na <sub>2</sub> O	.19
K <sub>2</sub> O	.28
P <sub>2</sub> O <sub>5</sub>	.14
H <sub>2</sub> O-	.08
H <sub>2</sub> O+	.88
CO <sub>2</sub>	10.51
<b>TOTAL</b>	<b>100.81</b>
F (ppm)	282
S	<5.2
Rb	11
Ba	224
Sr	835
Th	8
U	3
Zr	137
Nb	10
Mo	<.6
Sn	78
W	<5.3
V	50
Cr	44
Co	8
Ni	18
Cu	6
Zn	66
Ga	12
Pb	13
Ge	<1.1
As	1
Sb	<1.4
Bi	<3.3
Se	<1.0
Te	<2.3
Sc	7
Y	64
La	24
Ce	42
Nd	26
Au (ppb)	<5

**Table 2.29:** Whole-rock analysis of the Kuseb Formation marble on the farm Ohere 106, Omaruru District  
NS206: RUL grid 8800/7800, tremolite-calc-silicate marble

A locally rapid alternation in the grain size of the schist: suggests the presence of graded bedding (as in a Bouma sequence), but no unequivocal sedimentary features can be identified. The mineralogy of the schist varies with composition and metamorphic grade and will be discussed in detail in Chapter 5. For the sake of completeness, bulk-rod analyses of upper Kuseb Formation schists from the farm! Sandamap Noord and Kassandara (both in NCZA) and Ohere (NCZE) are presented in Tables 2.24, 2.25 and 2.26. Minor muscovite-bearing quartzites with planar crossbedding (which are not representative of the Kuseb Formation in general) are developed in the west-central portion of Sandamap Noord (Map 3) and comprise quartz (60-75%), feldspar (15-25%), muscovite (trace-5%), chlorite (trace-5%), biotite (0-4%), sillimanite (0-3%) and tourmaline (0-2%) and traces of calcite and opaque minerals. Much of the feldspar is untwinned and altered making compositional determination difficult. The quartzite has a fine-grained (approximately 300 µm) granoblastic texture with porphyroblasts of muscovite up to several millimetres in diameter. This mica invariably contains numerous randomly oriented fibrolite needles. Geochemical analyses of these quartzites are listed in Table 2.27.

In NCZE the Kuseb Formation comprises a sequence of metaturbidites with subordinate phyllite (Chapter 5) and minor arsenopyrite-pyrite-pyrrhotite-bearing schist, scheelite-bearing calc-silicate rocks, marble, tourmaline schist and zones of tourmalinisation (Chapter 7.6) and scheelite-bearing vesuvianite rocks (Chapter 7.7). A section through the upper Kuseb Formation in NCZE is best exposed on Ohere (Map 2). Bouma sequences are well-developed in the turbidites. Other sedimentary features of note include rip-up clasts, flame structures and scours. The proximal turbidites are represented by metaquartzites (greywackes) which comprise quartz (± 75%), untwinned plagioclase and K-feldspar (± 20%), muscovite (3%), chlorite (2-3%), sphene (trace-1 %), opaque minerals (probably haematite and possibly rutile-1 %) and traces of biotite, tourmaline, calcite and zircon. The quartz and feldspar are arranged in a granoblastic mosaic with interstitial calcite and poikiloblastic or ragged muscovite. The grain size seldom exceeds 200 µm. Geochemical analyses are given in Table 2.28. The graphitic marble, which is usually less than one metre thick, contains quartz (± 40%), calcite (± 20%), untwinned feldspar (± 15%), tremolite (± 10%), clinopyroxene (± 10%), clinozoisite (3-4%), graphite (± 2-3%) and sphene (± 1%). The rock possesses a polygonal mosaic texture and the grain size is usually less than 150 µm. A single geochemical analysis is given in Table 2.29.

The calc-silicate rocks of the upper Kuseb Formation in NCZA and NCZE possess a diverse mineralogy and are of interest because, in both the Sandamap Noord and Ohere areas, they host finely disseminated scheelite mineralisation (Table 2.3). Calc-silicate horizons or lenses are usually in the order of several tens of centimetres thick and, on account of the tectonism, commonly have a lensoid or spindle-

	NS243	NS244	NS245	NS246	NS247	NS248	NS249	NS250	NS251	NS279	NS280
SiO <sub>2</sub> (wt%)	62.85	74.26	71.42	71.30	61.69	75.11	72.34	61.77	69.74	66.46	66.85
TiO <sub>2</sub>	.59	.33	.20	.53	.64	.24	.53	.62	.70	.81	.81
Al <sub>2</sub> O <sub>3</sub>	9.87	10.91	6.43	9.60	9.37	8.45	10.68	12.23	11.60	12.38	12.44
Fe <sub>2</sub> O <sub>3</sub>	1.18	.66	.20	.17	.51	.10	.71	.59	1.09	.50	.35
FeO	2.07	1.44	.69	1.63	1.98	2.30	2.56	3.15	1.09	3.60	3.75
MnO	.14	.13	.08	.06	.11	.06	.12	.87	.09	.74	.74
MgO	.38	.44	.26	.46	.52	1.18	.69	1.38	.44	1.60	1.61
CaO	17.01	9.02	15.78	11.57	16.69	6.63	9.15	14.42	11.55	11.80	11.85
Na <sub>2</sub> O	.48	.82	.04	.20	.10	.17	.32	.74	.61	.65	.14
K <sub>2</sub> O	.10	.25	3.09	.22	.13	3.53	.22	1.21	.26	.07	.07
P <sub>2</sub> O <sub>5</sub>	.16	.07	.06	.12	.20	.07	.20	.42	.20	.24	.24
H <sub>2</sub> O-	.17	.11	.05	.10	.08	.09	.08	.14	.10	.03	.04
H <sub>2</sub> O+	.62	.64	.09	.31	.38	.57	.56	.90	.82	.62	.46
CO <sub>2</sub>	5.04	1.34	1.82	4.32	8.15	2.52	2.01	1.94	2.39	.65	.63
TOTAL	100.66	100.43	100.21	100.58	100.56	101.02	100.17	100.39	100.68	100.14	99.99
F (ppm)	318	253	262	271	231	186	276	559	355	351	352
S	<4.8	52	<5.1	<5.2	<4.9	<5.2	<5.1	76	48	2996	131
Rb	6	14	119	12	6	109	10	62	18	7	.9
Ba	56	141	579	338	318	606	177	369	170	<3.9	<3.8
Sr	161	295	864	701	715	219	376	185	271	304	326
Th	10	8	5	9	13	5	8	7	11	19	16
U	3	2	2	3	5	<1.4	3	3	4	5	5
Zr	249	110	80	190	330	90	286	167	344	433	335
Nb	7	7	5	10	12	5	10	12	12	17	14
Mo	.6	.6	<.5	<.5	<.6	<.5	2	<.6	<.5	<.6	<.6
Sn	25	34	88	72	7	2	142	65	15	14	9
W	<5.0	5	<4.9	<4.5	5	6	4913	12	38	271	8
V	78	46	11	40	47	23	68	51	52	67	62
Cr	42	33	18	41	42	25	50	45	42	63	59
Co	6	6	3	9	8	6	10	5	6	9	9
Ni	11	11	4	10	7	7	17	13	10	19	19
Cu	<1.3	1	<1.3	<1.2	<1.3	2	<1.4	2	<1.2	34	3
Zn	226	230	91	96	169	176	223	78	159	30	65
Ga	14	12	5	10	11	9	15	16	14	15	15
Pb	10	31	60	65	60	61	62	5	101	4	4
Ge	6	1	<1.0	<.9	<1.0	<.9	<1.2	2	1	<1.0	<1.0
As	9	8	3	5	18	5	39	<.9	22	6	49
Sb	4	2	3	2	2	2	3	<1.4	5	<1.4	<1.4
Bi	<3.1	<2.8	<3.1	<2.9	<3.1	<2.8	<3.2	<3.2	<2.9	<3.1	<3.2
Se	<.9	<.8	<.9	<.8	<.9	<.8	<1.0	<.9	<.9	<.9	<.9
Te	<2.2	<2.0	<2.1	<2.0	<2.1	<2.0	<2.1	<2.2	<2.0	<2.1	<2.2
Sc	9	6	3	9	9	5	10	12	8	13	12
Y	44	20	23	32	40	15	38	96	40	72	52
La	39	19	10	24	31	15	31	34	32	53	39
Ce	78	40	23	49	70	33	63	70	67	104	83
Nd	42	21	22	30	41	19	40	40	38	60	47
Au (ppb)	<5	7	<5	7	15	<5	<5	<5	8	<5	<5

**Table 2.30:** Whole-rock analyses of the Kuiseb Formation calc-silicate rocks on the farm Sandamap Noord 115, Usakos District  
 NS243, NS244, NS251: 2.6 km NW of Sandamap Tin Mine  
 NS245, NS246, NS247, NS249: 1.2 km N of Sandamap Noord farmhouse  
 NS248: 3.3 km WNW of Sandamap Tin Mine  
 NS250: 300 m S of Cilliers Workings  
 NS279, NS280: 250 m N of Sandamap Tin Mine

shaped geometry. These lenses, which represent boudinaged horizons, are notably flatter in NCZa than in NCZe, attesting to the more intense deformation closer to the Omaruru Lineament. The mineralogy of these equigranular calc-silicate rocks comprises quartz (35.80%), plagioclase feldspar (2-25%), clinopyroxene (trace-35%), hornblende (trace-20%), garnet (trace-10%), chlorite (0-10%), tremolite (0-5%), clinozoisite (0-3%), biotite/phlogopite (0-2%), calcite (trace-10%), microcline (0-3%), scapolite (0-2%), scheelite (0-2%), sphene (trace-2%), epidote (0-1%), pyrrhotite (0-1%), pyrite (0-1%), chalcopyrite (0-0.5%), graphite (trace) and iron oxides

(trace). The quartz and feldspar form a granoblastic mosaic that is poikiloblastically enveloped by pyroxene and hornblende in particular. Garnet is poikiloblastic or xenoblastic and may be several millimetres in diameter. The grain size of the mosaic seldom exceeds 400 µm. The scheelite crystals are usually only several hundred microns in size, but may have a poikiloblastic habit up to one centimetre across. The sulphides are clustered in elongate aggregates which lie parallel to the metamorphic banding. Bulk-rock analyses of calc-silicate rocks from Sandamap Noord and Ohere are given in Tables 2.30 and 2.31.

	NS200	NS201	NS202	NS203	NS204	NS205
SiO <sub>2</sub> (wt%)	72.68	57.96	68.79	70.13	62.47	72.74
TiO <sub>2</sub>	.70	.65	.64	.81	.66	.74
Al <sub>2</sub> O <sub>3</sub>	11.80	11.49	11.13	11.31	10.69	11.27
Fe <sub>2</sub> O <sub>3</sub>	.28	.52	1.22	.29	.51	.35
FeO	3.89	8.52	3.45	4.34	2.92	3.85
MnO	.28	1.29	.37	.62	.27	.31
MgO	1.62	2.46	1.48	1.75	1.45	1.63
CaO	6.60	14.69	11.15	8.78	15.79	6.89
Na <sub>2</sub> O	.20	.44	.46	.37	.26	.33
K <sub>2</sub> O	.04	.31	.05	.11	.08	.05
P <sub>2</sub> O <sub>5</sub>	.18	.22	.17	.21	.17	.17
H <sub>2</sub> O-	.10	.15	.07	.03	.05	.04
H <sub>2</sub> O+	1.07	.47	.63	.30	.25	.32
CO <sub>2</sub>	.29	.78	.14	.39	4.86	1.35
TOTAL	99.73	99.95	99.77	99.43	100.44	100.05
F (ppm)	189	289	275	2214	250	237
S	2430	4770	2483	1657	1058	3080
Rb	2	16	4	2	4	2
Ba	6	14	<3.6	12	<3.5	13
Sr	204	213	333	185	318	183
Th	11	10	11	24	9	11
U	3	3	3	3	3	2
Zr	199	187	208	260	186	233
Nb	11	11	11	14	11	12
Mo	<.5	<.6	<.6	.8	<.6	<.5
Sn	2	79	194	512	201	7
W	133	8	<5.0	16	6	<4.7
V	59	100	68	77	67	62
Cr	62	75	69	65	58	67
Co	10	21	9	5	8	16
Ni	26	38	21	4	19	45
Cu	253	159	69	78	23	56
Zn	50	147	145	203	59	51
Ga	14	16	13	15	13	13
Pb	3	4	14	9	12	7
Ge	<.9	2	<1.0	6	<1.0	<.9
As	36	15	5	2	9	31
Sb	<1.3	<1.6	<1.4	<1.4	<1.4	<1.3
Bi	<3.0	<3.7	10	46	<3.2	<3.0
Se	<.9	<1.1	<.9	<.9	<.9	<.9
Te	<2.1	<2.5	<2.2	<2.2	<2.2	<2.1
Sc	15	15	14	14	11	15
Y	55	68	47	49	52	54
La	30	32	31	33	30	36
Ce	63	64	62	69	60	72
Nd	40	38	37	40	36	41
Au (ppb)	<5	<5	10	<5	6	<5

**Table 2.31:** Whole-rock analyses of the Kuiseb Formation calc-silicate rocks on the farm Ohere 106, Omaruru District  
 NS200: RUL grid, 7400/6800  
 NS201: RUL grid, 7000/7100  
 NS202: RUL grid, 8800/7500  
 NS203: RUL grid, 7400/8000  
 NS204: RUL grid, 2700/5000

Particular attention was paid during field work to the possible presence of mafic volcanic rocks in the Kuiseb Formation of the CZ which would represent equivalents of the Matchless Member amphibolite of the SZ (Miller, 1983c). No such volcanic horizons have previously been reported in the Omaruru-Usakos area. Two instances of possible volcanic horizons were noted during field work. Neither is more than five metres thick, nor do they comprise more than a fraction of the stratigraphy of the area. In NCZa a two-metre-thick zone of pale-green schist with extensive ferruginous staining on the northwest of Sandamap Noord (Map 3) was initially considered to represent a metamorphosed tuffaceous horizon. This lithology (sample NS255) comprises sericite ( $\pm$  35%), quartz ( $\pm$  20%), green biotite ( $\pm$  15%), plagioclase ( $\pm$  10%),

	NS255	NS240
SiO <sub>2</sub> (wt%)	58.96	66.36
TiO <sub>2</sub>	.81	.79
Al <sub>2</sub> O <sub>3</sub>	17.85	13.31
Fe <sub>2</sub> O <sub>3</sub>	2.63	.00
FeO	4.07	5.02
MnO	.08	.24
MgO	3.55	2.50
CaO	.47	10.73
Na <sub>2</sub> O	.64	.27
K <sub>2</sub> O	4.68	.06
P <sub>2</sub> O <sub>5</sub>	.19	.20
H <sub>2</sub> O-	.47	.09
H <sub>2</sub> O+	4.26	.35
CO <sub>2</sub>	1.17	.14
TOTAL	99.95	100.06
F (ppm)	1121	565
S	157	78
Rb	250	1
Ba	863	302
Sr	146	300
Th	12	11
U	4	2
Zr	166	205
Nb	14	14
Mo	.7	<0.6
Sn	7	174
W	<4.8	13
V	205	102
Cr	129	88
Co	16	15
Ni	49	26
Cu	43	6
Zn	82	112
Ga	26	16
Pb	26	6
Ge	<1.0	<1.0
As	18	2
Sb	<1.3	<1.4
Bi	<3.0	<3.1
Se	1	<.9
Te	<2.1	<2.2
Sc	25	17
Y	30	44
La	21	35
Ce	43	70
Nd	25	42
Au (ppb)	<5	10

**Table 2.32:** Whole-rock analysis of the Kuiseb Formation mafic schists on the farms Sandamap Noord 115, Usakos District and Ohere 106, Omaruru District  
 NS255: 4.6 km NW of Sandamap Tin Mine  
 NS240: Grid 7

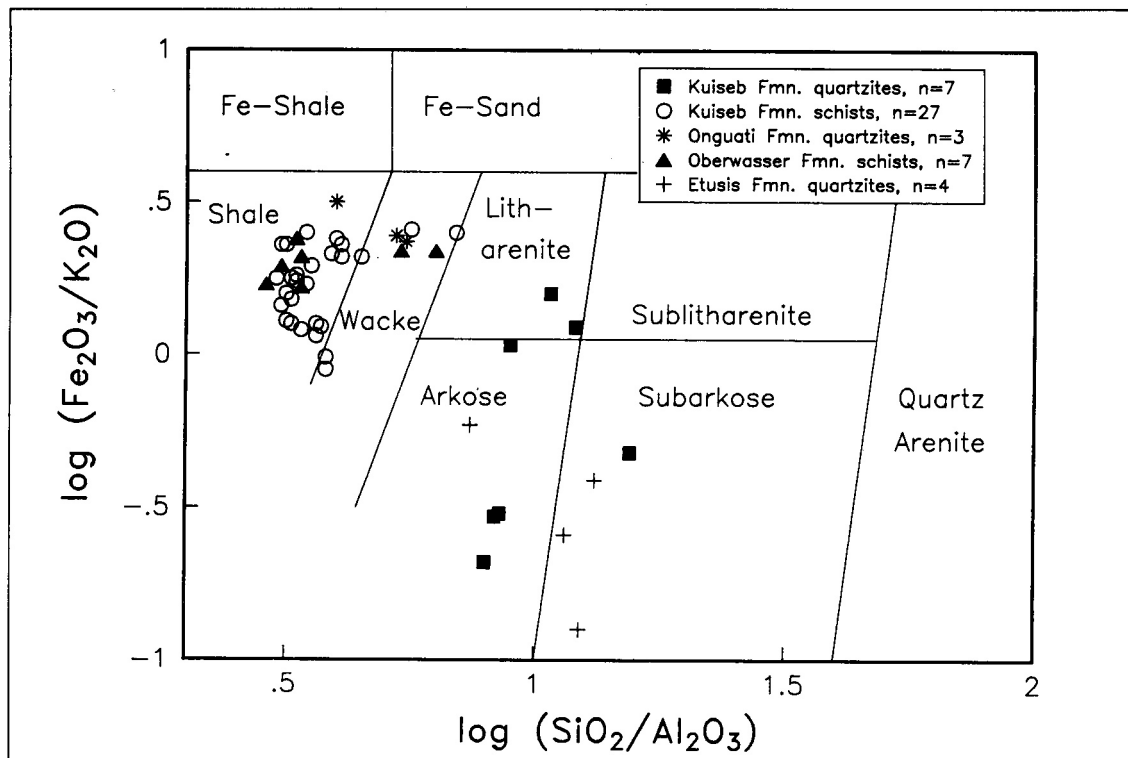


Figure 2.6: Geochemical classification of CZ clastic metasediments

K-feldspar ( $\pm 10\%$ ), muscovite ( $\pm 5\%$ ) and traces of sphene, zircon, serpentine and iron oxides. The sericite has entirely replaced a poikiloblastic feldspar. No volcanic textures were noted in thin section. Moreover, the bulk composition of this lithology (Table 2.32) is similar to unaltered Kuseib Formation schists on Sandamap Noord.

In NCZe on Ohere (Map 2) on Grid 7 an amphibole-bearing rock (sample NS240) that is several metres thick is traceable for over 150 metres. The lithology contains quartz (45-60%), tremolitic amphibole with possibly a significant hornblende component ( $\pm 25\%$ ), plagioclase (15-25%), microcline (0-10%), sphene ( $\pm 1\%$ ) and ore minerals ( $\pm 1\%$ ). The fabric of the rock is defined by oriented amphibole which locally assumes a poikiloblastic habit and envelops the granoblastic mosaic of quartz and feldspar. A single geochemical analysis of this rock (Table 2.32) reveals a bulk composition similar to the calc-silicate rocks (for example NS202) and it is unlikely that NS240 contains a significant tuffaceous component. To conclude, there is no evidence for significant volcanic activity in the CZ which could be equated with the Matchless Member volcanism in the Southern Zone of the orogen (Fig. 2.2).

### 2.2.3 Summary of the Damaran depositional episode

The Damaran sedimentary package in central Namibia can now be related to the formation of the northern Nosib graben (Miller, 1983a) and subsequent basin development in the CZ. Major facies changes in both the Nosib and Swakop Groups across the Omaruru Lineament (Fig. 2.5) testify to the strong control exerted by this structure on Damaran sedimentation (see also Henry *et al.*, 1990 and Stanistreet *et al.*, 1991). In general, the SCZ comprises continental, shallow

marine and minor pelagic sediments, while the NCZ contains shallow marine sediments overlain by pelagic sediments up to 4 km thick. Deposition of fluvio-deltaic quartzites of the Etusis Formation occurred during rifting of granitic basement between 1000 and 900 Ma. This rifting was followed by spreading and gradual basin subsidence resulting in the deposition of shallow marine (or possibly lacustrine) calcareous lithologies during Khan times. An evaporitic or lacustrine depositional environment is indicated for at least some of the Khan Formation. The development of massive ironstone, sulphide mineralisation and graphite schists at the top of the Khan Formation and the base of the Rössing Formation appears to be localised in the vicinity of a major rift, namely the Omaruru Lineament. As far as the author is aware, the Sandamap-Eureka occurrence is unique in the CZ. The Rössing Formation BIF may be the chronostratigraphic equivalent of the Chuos Formation which is not developed in the Sandamap-Eureka area. These lithological associations invite comparison with a similar situation in the Pan-African Gariep belt in southern Namibia at the Hilda Subgroup/Numees Formation contact in the Dabie River (Hartnady *et al.*, 1990 p.35). Immediately below the Numees Formation (a diamictite with associated BIF) massive dolomite, ironstones, graphite schist and grunerite rocks of the Dabie River Formation are developed. Hoffman (1989) correlated the Numees Formation diamictite and BIF with the Naos pebbly schists rather than the Chuos Formation diamictites and BIF. However, the BIF-sulphide-graphite association immediately below a glaciogenic unit may be more widespread in Pan-African belts than was originally thought. Although the Chuos Formation mixtite is considered to be a glaciomarine deposit (Badenhorst, 1988b), the large variations in thickness are attributed to syn-sedimentary faulting associated with deposi-

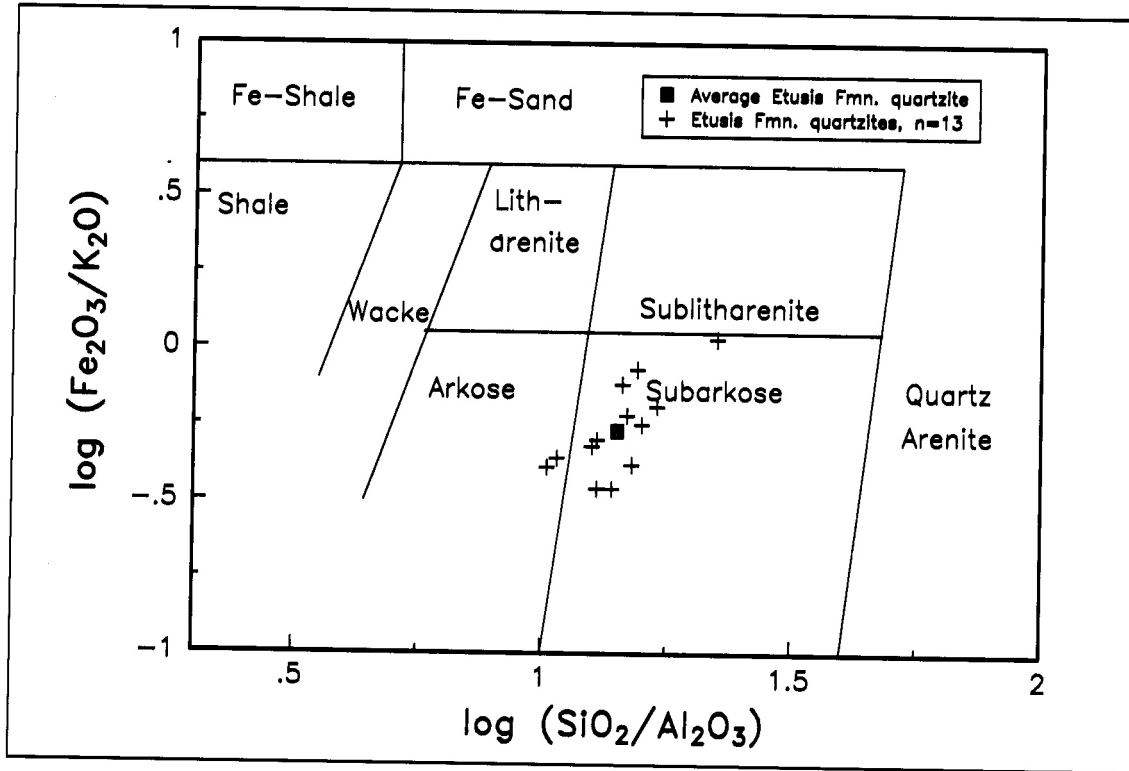


Figure 2.7: Geochemical classification of Etusis Formation quartzites at Navachab

tion of the sediments in half-grabens (Henry *et al.*, 1986). In mid-Swakop times the presence of possible evaporites in the Spes Bona and Oberwasser Formations and stromatolites in the carbonates of the Karibib Formation imply shallow marine sedimentation. Crustal instability is indicated by felsic volcanism in Spes Bona and Oberwasser times close to the Omaruru Lineament. The extension of mafic alkaline pyroclastic rocks and lavas on the basin margins (Daheim Member) point to the presence of deeper-seated fractures near granitic basement in the SCZ. Syn-sedimentary breccias at

the top of the Karibib Formation in the Arises River Member marbles (Klein, 1980) are indicative of further syndepositional faulting related to spreading. A transition to more pelagic sedimentation during lower Kuiseb times implies an increase in the rate of basin subsidence which culminated in localised rifting with accompanying deposition of the upper Kuiseb Formation turbidites. On the basis of a westward increase in sediment maturity, Miller (1983a) argued that these flysch deposits were derived from Kibaran and Katangan rocks to

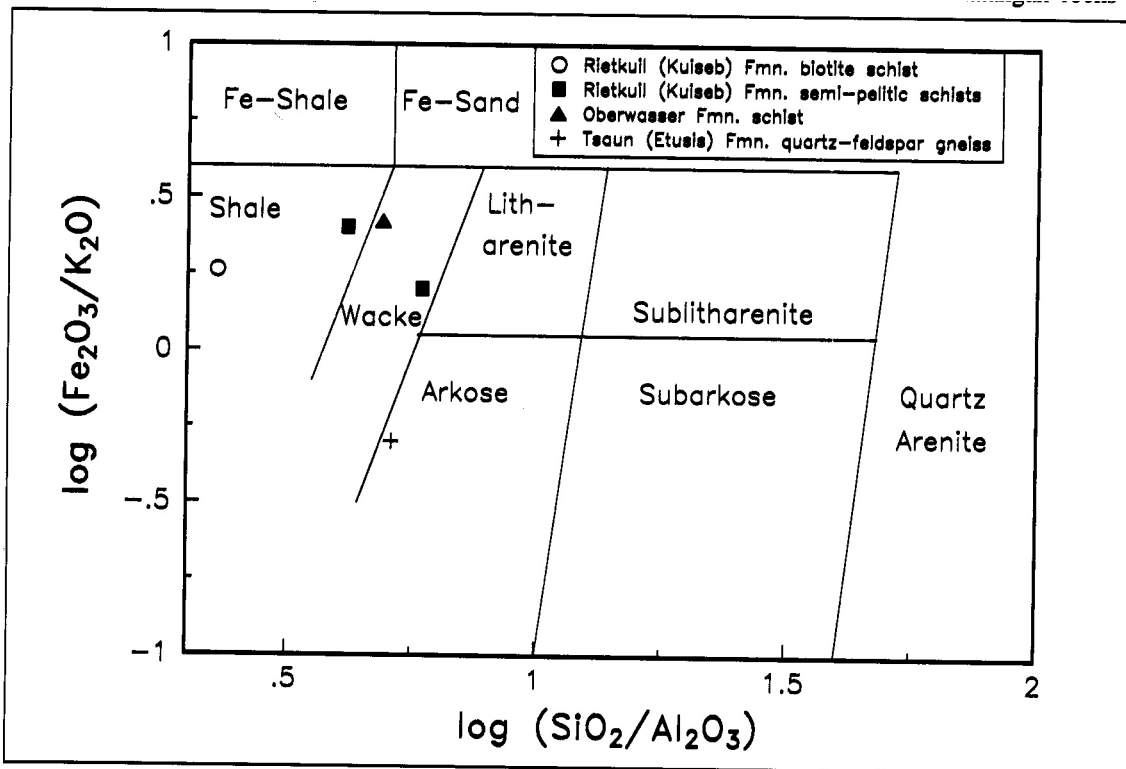


Figure 2.8: Geochemical classification of CZ clastic metasediments southwest of Uis

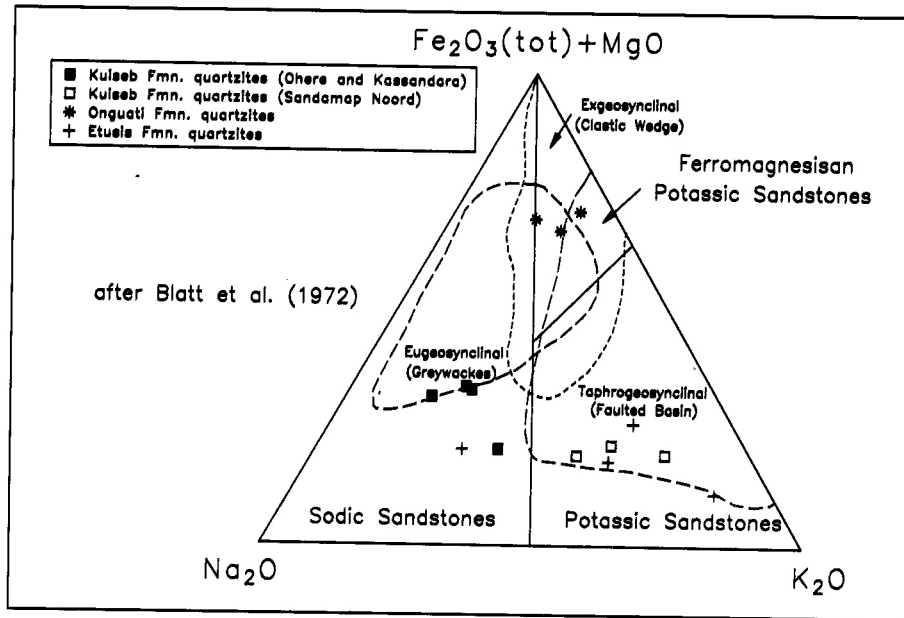


Figure 2.9: Chemical composition of CZ quartzites in relation to tectonic setting

	Etusis Fmn.	Onguati Fmn.	Kuiseb Fmn.	Kuiseb Fmn.
	A	B	C	D
	n=4	n=3	n=3	n=4
SiO <sub>2</sub>	83.87	65.73	80.12	84.11
TiO <sub>2</sub>	.27	.74	.55	.36
Al <sub>2</sub> O <sub>3</sub>	7.90	13.53	9.67	7.43
Fe <sub>2</sub> O <sub>3</sub>	.27	5.13	.13	.75
FeO	.68	1.99	.98	.75
MnO	.03*	.09	.01*	.04
MgO	.24	2.48	.44	.47
CaO	.34	.81	.36	.87
Na <sub>2</sub> O	1.94	1.61	1.97	3.21
K <sub>2</sub> O	3.48	2.82	4.70	1.52
P <sub>2</sub> O <sub>5</sub>	.08	.29	.13	.06
H <sub>2</sub> O-	.10	.35	.07	.06
H <sub>2</sub> O+	.48	3.52	.58	.53
CO <sub>2</sub>	.32	.48	.27	.67
TOTAL	99.99	99.56	99.98	100.83
F	325	1271	249	181
S	362	154	95*	78*
Rb	117	129	114	40
Ba	807	377	751	412
Sr	120	78	64	117
Th	10	12	9	6
U	2*	3	2	2
Zr	197	203	272	218
Nb	11	15	10	7
Mo	1*	.9	<.5	.6*
Sn	2*	9	4	3*
W	14*	11	4*	9*
V	18	105	39	26
Cr	19	80	36	28
Co	4*	19	4	4*
Ni	6	40	9	7
Cu	7	35	4	3
Zn	10	109	22	27
Ga	7	18	10	7
Pb	15	36	20	15
Ge	<.8	<.9	<.8	<.8
As	.9*	56	12	4
Sb	<1.1	<1.3	1*	<1.1
Bi	<2.5	<2.9	<2.6	<2.5
Se	<.7	<.9	<.8	<.7
Te	<1.8	<2.1	<1.8	<1.8
Sc	3	15	7	5
Y	13	36	19	18
La	19	35	23	18
Ce	37	71	53	39
Nd	20	39	29	21

the northeast. The evidence from the proximal turbidites on Ohere suggests that the sediments were more locally derived. In the CZ, rupture of the crust did not occur and thus the graben has an ensialic intracratonic nature.

### 2.3 THE GEOCHEMISTRY OF THE CLASTIC METASEDIMENTS OF THE DAMARA SEQUENCE

#### 2.3.1 Introduction

A comprehensive treatment of the geochemical data presented here is beyond the scope of this memoir. Thus this section only highlights some features of the major element geochemistry. Nomenclature is a key problem when discussing and comparing the geochemistry of metasediments and has recently been addressed by Moore (1989). Consequently the terms “clastic”, “greywacke” (taken to mean a sandstone), “metasediment”, “quartzite” and “schist” have been used *sensu* Bates and Jackson (1987). The word schist has the prefix metapsammitic or metapelitic (*sensu* Moore, 1989; upper-amphibolite-facies terrane) depending on the whether the “pelitic” components (biotite, muscovite and garnet) make up <20% or >20% of the rock respectively. A fundamental assumption made in the discussion below is that the com-

Table 2.33 (left): Average composition of Damaran quartzites from the CZ

A = Etusis Formation arkoses and subarkoses (SandClass); B = Onguati Formation quartzites (classified as wackes, locally shales by SandClass); C = Kuiseb Formation muscovite quartzites (classified as arkoses by SandClass); D = Kuiseb Formation greywackes (classified as litharenites, locally arkoses by SandClass)

\* Averages have only been calculated for those samples (given below) containing concentrations of the element in excess of the LLD. True values for the populations are lower.

A: MnO (3), U (3), Mo (2), Sn (2), W (2), Co (1), As (3);

C: MnO (2), S (1), W (1), Sb (2);

D: S (3), Mo (1), Sn (3), W (2), Co (3)

	Sandamap Noord (NCZa)		Kassandara (NCZa)		Ohere (NCZe)	
	n=16		n=3		n=8	
	Mean	S.D.	Mean	S.D.	Mean	S.D.
SiO <sub>2</sub>	61.63	5.70	61.85	1.04	59.49	2.22
TiO <sub>2</sub>	.80	.04	.84	.04	.83	.06
Al <sub>2</sub> O <sub>3</sub>	16.36	2.14	16.31	.45	17.69	.63
Fe <sub>2</sub> O <sub>3</sub>	.78	.66	2.21	1.70	5.41*	1.51*
FeO	5.62	1.10	3.64	1.67	2.23	2.26
MnO	.10	.03	.10	.02	.09	.05
MgO	3.60	.97	2.98	.20	3.57	.50
CaO	2.12	1.01	.81	.09	1.54	2.38
Na <sub>2</sub> O	2.49	.85	1.80	.40	.80	.60
K <sub>2</sub> O	3.59	.98	6.16	.86	5.05	1.02
P <sub>2</sub> O <sub>5</sub>	.22	.05	.32	.07	.15	.05
H <sub>2</sub> O-	.18	.07	.26	.18	.34	.11
H <sub>2</sub> O+	1.18	.46	1.96	.28	2.64	1.16
CO <sub>2</sub>	.65	.50	.41	.53	.86	.36
TOTAL	99.32	-	99.66	-	100.02	-
F	1422	1073	1006	132	941	246
S	23*	15*	<5	-	2105*	2747*
Rb	263	279	219	25	226	64
Ba	666	302	892	66	765	151
Sr	176	66	77	4	96	114
Th	14	2	13	.9	16	2
U	4	.7	4	.4	4	.7
Zr	199	52	198	37	176	21
Nb	16	1	16	.1	17	.6
Mo	.7*	.1*	.9	.2	.9*	.4*
Sn	55	119	8	.6	19	24
W	7*	2*	13	1	7	2
V	131	30	123	8	151	13
Cr	98	19	102	5	111	7
Co	18	6	18	3	18	4
Ni	43	12	38	2	40	9
Cu	14	14	5*	.0*	21	15
Zn	131	32	102	13	127	19
Ga	23	4	22	.8	26	1
Pb	23	8	26	14	16	15
Ge	<1.0	-	<1.0	-	1*	-
As	16*	16*	3*	1*	28	21
Sb	<1.3	-	<1.3	-	<1.3	-
Bi	<3.0	-	<3.0	-	4*	-
Se	<.9	-	<.9	-	<.9	-
Te	<2.1	-	<2.1	-	<2.1	-
Sc	19	4	18	.9	22	.7
Y	38	4	45	7	36	4
La	31	6	34	3	34	3
Ce	63	12	75	12	67	8
Nd	36	7	42	6	38	5
Au (ppb)	<5	-	<5	-	<5	-

Table 2.34: Average composition of Kuiseb Formation schists from the CZ

\* Averages and S.D.s have been calculated for those samples (given below) containing concentrations of the element in excess of the LLD. True averages and S.D.s for the population are lower.

Sandamap Noord: S (3), Mo (4), W (7), As (12); Kassandra: Cu (2), As (2); Ohere: Fe<sub>2</sub>O<sub>3</sub> (7), S (3), Mo (2), Ge (1), Bi (1)

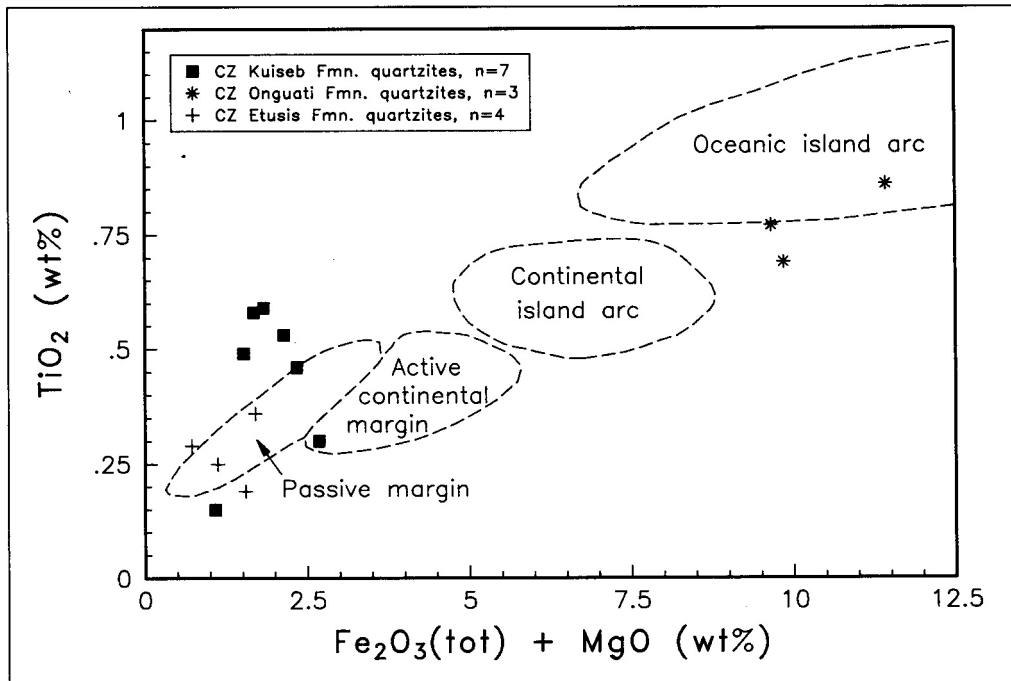


Figure 2.10:  $\text{TiO}_2$  vs  $\text{Fe}_2\text{O}_3(\text{tot}) + \text{MgO}$  for CZ quartzites

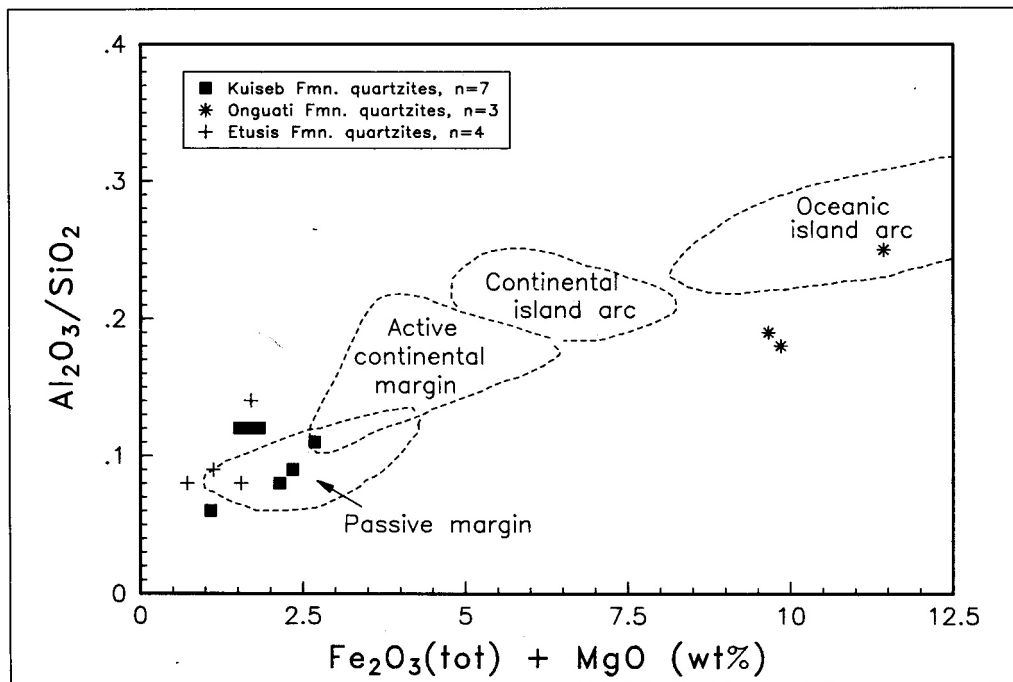


Figure 2.11:  $\text{Al}_2\text{O}_3/\text{SiO}_2$  vs  $\text{Fe}_2\text{O}_3(\text{tot}) + \text{MgO}$  for CZ quartzites

positions of the metasediments are dehydrated equivalents of the original sediments, i.e. there has been no significant loss of material or migration of elements during metamorphism (see Moore, 1989 for a discussion).

### 2.3.2 Geochemical classification of the clastic rocks

Numerous systems for the classification of clastic rocks exist (Pettijohn *et al.*, 1972; Blatt *et al.*, 1980). More recent-

ly, Herron (1988) has reviewed the various shortcomings of these schemes and proposed the SandClass system for the geochemical classification of sands and shales. The ratio of total iron expressed as  $\text{Fe}_2\text{O}_3$  to  $\text{K}_2\text{O}$  (an indicator of mineralogical stability) is plotted against the ratio  $\text{SiO}_2/\text{Al}_2\text{O}_3$  (an indicator of mineralogical maturity). The main advantage of this system over Pettijohn *et al.*'s (1972) is that it does not make use of the relatively mobile element Na. Moreover, the ratio  $\text{Na}_2\text{O}/\text{K}_2\text{O}$  used by Pettijohn *et al.* (1972) is not well

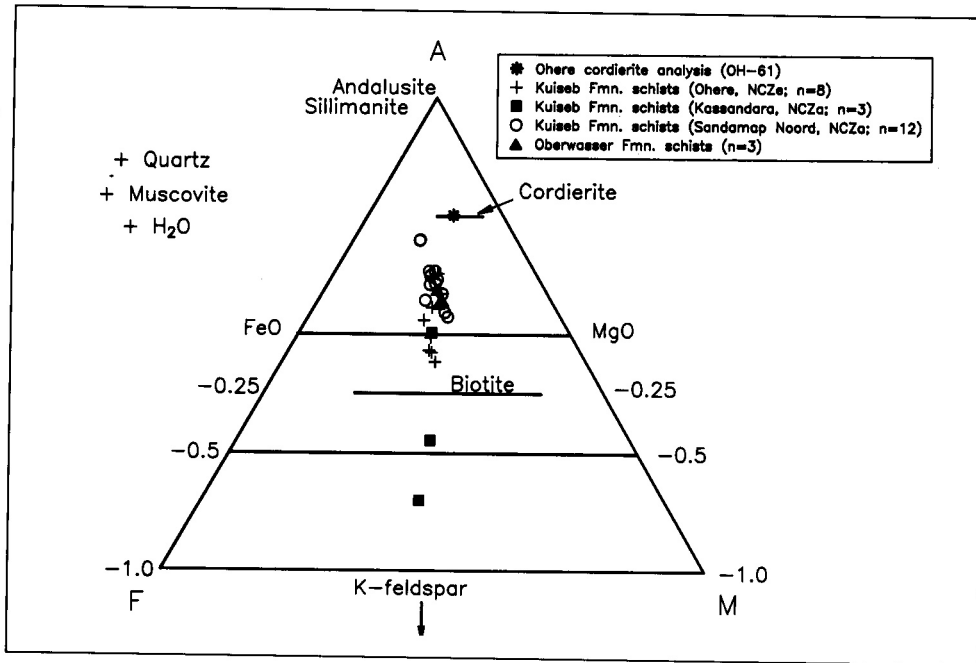


Figure 2.12: AFM plot for Oberwasser and Kuiseb Formations schists

suiting to distinguishing lithic fragments from feldspars. The 48 analyses of clastic metasediment presented in this memoir are plotted in Fig. 2.6. Quartzites of the Etusis Formation are classified as subarkoses or arkoses, those of the Onguati Formation as wackes or shale, and quartzites of the Kuiseb Formation as litharenites, arkoses or subarkoses. The majority of the Kuiseb schists are classified as shales; the four schists classified as wackes are the only two schists that are metapsammitic and two metapelites with K<sub>2</sub>O contents in excess of 6.5 wt%. The data presented in Fig. 2.6 can be compared with the few other whole-rock analyses available for the CZ. Thirteen analyses of Etusis Formation quartzite from the immediate vicinity of the Navachab Gold Mine are predominantly subarkoses (Fig. 2.7). Five analyses of metasediment from southwest of Uis (Botha, 1978) are given in Fig. 2.8. The Tsaun Formation (Etusis equivalent) is classified as an arkose, the Oberwasser Formation from the type area as a wacke and the Rietkuil formation (Kuiseb equivalent) as a wacke or a shale.

2.2.3.1 Geochemistry of the quartzitic rocks and determination of the tectonic setting of deposition

Sandstone composition is a function of the interplay between provenance, weathering, transportation and diagenesis, but the primary control is tectonism (Bhatia, 1983). Blatt *et al.* (1972, 1980) were some of the first authors to relate sandstone composition to tectonic setting. Average compositions of the 14 samples of Damaran quartzite (Table 2.33) have been plotted on a Fe<sub>2</sub>O<sub>3</sub> (total)+MgO-Na<sub>2</sub>O-K<sub>2</sub>O ternary diagram (Fig. 2.9) which includes the three tectonic environments recognised by Blatt *et al.* (1980). The first point of note is that the CZ metasediments with the exception of the Onguati Formation have low total iron and MgO contents. This emphasises the intracratonic nature of the source areas for the CZ sediments. The majority of the Etusis quartzites and the Kuiseb Formation quartzites from Sandamap Noord, having been deposited closest to the granitic basement inlier, have compositions similar to the taphrogeo-synclinal (or

faulted cratonic basin) types. The Onguati Formation quartzites are exogeosynclinal in nature: their ferromagnesian nature is probably a result of the presence of mafic volcanic detritus from the underlying Daheim Member. In contrast, those Kuiseb quartzites (essentially greywackes) from Ohere and Kassandara which were deposited furthest from the Abbabis Inlier are sodic sandstones and compositionally similar to eu-geosynclinal sediments.

Bhatia (1983) has attempted to classify the sandstones of Australian Palaeozoic sequences in terms of four plate tectonic settings: oceanic island arc, continental island arc, active continental margin and passive margin. The 14 analyses of CZ quartzite have been recalculated on a volatile-free basis, normalised to 100 wt% and plotted on two of Bhatia's (1983) diagrams (Figs. 2.10 and 2.11). The quartzites of the Etusis and Kuiseb Formation show most affinities with passive margin sandstones, while those of the Onguati Formation show certain similarities with oceanic island-arc sandstones.

2.3.2.2 Geochemistry of the schists

Thirty-four analyses of unaltered Oberwasser and Kuiseb Formation schist are given in the memoir; average compositions of the latter are given in Table 2.34. Only two samples (NS283 and NS284) are metapsammitic; the remainder are metapelitic. Those schists which contain muscovite have been plotted on an AFM diagram (Thompson, 1957) where the coordinates are given as follows (element oxides in molecular proportions):

$$A = ([Al_2O_3] - 3 [K_2O] / Al_2O_3] - 3 [K_2O] + [MgO] + FeO),$$

F = (FeO/MgO+FeO) and M = (MgO/MgO+FeO). The ranges in cordierite and biotite composition are taken from Winkler (1976): a single cordierite analysis from Ohere is given, but tie-lines have not been drawn. The two features of note in Fig. 2.12 are the highly potassic nature of the Kuiseb Formation schists on Kassandara and the relatively constant FeO: MgO ratio in both Oberwasser and Kuiseb Formation metapelites and metapsammites.

### 3. INTRUSIVE ROCKS

#### 3.1 INTRODUCTION

Information on the predominantly granitic intrusions of the Central Zone is available from the regional studies of Smith (1965) and Miller (1973). One of the most intriguing aspects is the marked confinement of granite and pegmatite types to specific stratigraphic levels. Miller (1983a) divided the various syn- to post-tectonic granitic rocks of the CZ into three groups:

1) Red, medium- to fine-grained granites which intrude basement or Nosib Group lithologies and are thus concentrated near the Abbabis Inlier,

2) syn- to late-tectonic coarsely porphyritic, biotite monzogranites and associated biotite dioritic rocks of the Salem Granite Suite which are essentially restricted to the Kuiseb Formation,

3) late- to post-tectonic, fine- to coarse-grained leucogranites, pegmatitic alaskites and pegmatites.

This subdivision has been widely used by workers in the Damara Orogen. Other minor groups of intrusions are present within central Namibia, two of which crop out within the field area. Firstly, hornblende-magnetite rocks (hornblendite of Miller, 1983a), which may be xenoliths of Gannakouriep(?) age metadolerites (see Chapter 2), are present as inclusions in undeformed, younger magnetite-bearing pegmatites on Eureka (Map 5) and Lukasbank (Map 6). Secondly, a small number of hornblende diorites crop out south of Karibib (Smith, 1965). The nature of the uraniumiferous granitic intrusions of the SCZ has been discussed by Marlow (1983), who proposed a fourfold subdivision of the CZ granitoids into red granites, Salem granites, leucogranites and alaskites. All of these lithologies, with the exception of the Salem granite, may host uranium mineralisation in the SCZ. Marlow (1983) concluded that the intrusion of uraniumiferous leucogranites and alaskites was restricted to a late- to post-tectonic event.

The distribution and petrographic characteristics of the granites of the NCZ, where red granites are essentially absent, have been described by Badenhorst (1986a). Members of the Salem Granite Suite, both syn- and late-tectonic, are essentially restricted to the Kuiseb Formation and, within the field area, are concentrated in NCZa and NCZc near Omaruru and in NCZe. Several types of late-/post-tectonic leucogranite crop out in the NCZ, but there are differences between those hosted by the Kuiseb Formation schists and those hosted by the more carbonaceous lithologies of the lower Swakop Group. Similarly, the late-tectonic stanniferous muscovite pegmatites hosted by the upper Kuiseb Formation in NCZa and NCZe can easily be distinguished in the field from the relatively anhydrous biotite-garnet-tourmaline pegmatites hosted by the lower Swakop Group formations.

There is a close spatial relationship between mineralisation and the younger granites in the CZ and in this chapter particular attention is given to the late- to post-tectonic intrusions. For example, Steven (1987) concluded that the development of skarn-hosted tungsten mineralisation at the Otjua Tungsten Prospect was caused by the intrusion of a late-tec-

tonic leucogranite. Tin mineralisation in the NCZ is hosted by late-/post-tectonic pegmatites (Richards, 1986; Haack and Gohn, 1988; this work). An important aim of this chapter will be to assess Miller's (1983b) claim that the granitic plutons are calc-alkaline in nature (op. cit. p.391) and thus determine the tectonic environment in which these magmas were generated. This has important implications for the styles of mineralisation that one might expect to be developed in the CZ. It was decided to focus on the intrusions of the NCZ, which have not been investigated in detail, in contrast to the SCZ where a large amount of mineralogical and geochemical data is available on the mineralised pegmatites of the Karibib area (Roering, 1963, 1966) and the uraniumiferous intrusions (Marlow, 1983). To illustrate the different types of granite intrusion in the NCZ, six examples of early, syn- and late-tectonic intrusions (three from the Usakos area, three from Omaruru area) have been selected and are discussed in order of decreasing age in each subsection. The nature of the four main types of pegmatite within the field area is subsequently examined. Emphasis has been placed on a stratigraphic overview. The geochronological work that has been completed by the author will be discussed in Chapter 6, though the Rb-Sr whole-rock ages are presented here. All lithological names and the "leuco-" prefix are used *sensu* Streckeisen (1976).

#### 3.2 EARLY TECTONIC LEUCOGRANITES ALONG THE OMARURU LINEAMENT

On the northern side of the Omaruru Lineament in NCZc, early tectonic, foliated, garnetiferous leucogranites possessing a penetrative foliation are common in the lower Kuiseb Formation. On the southern side of the Kompaneno Fault on Gross Okandjou (Fig. 3.1), garnetiferous leucogranites have been isoclinally folded indicating an early orogenic age at the youngest. This type of (possibly lopolithic) intrusion is common at this stratigraphic level elsewhere in the CZ (Miller, 1983a). However, because of the intensity of the deformation and the poor exposure it is impossible to determine whether these were intruded as sills or dykes. Miller (1983a) has contended that the base of the Kuiseb Formation formed a barrier to intrusion of these granites to higher levels. The characteristics of a garnetiferous leucogranite that is several tens of metres wide on Pforte (Fig. 3.1) are listed in Table 3.1 and a geochemical analysis is given in Table 3.2.

On the eastern side of the Omaruru Fault Zone on Kasandara (Fig. 3.1), foliated leucogranites without garnet are particularly common in the upper Kuiseb Formation. To the southwest, on Sandamap Noord, the local presence of thin (from approximately one centimetre to several tens of centimetres) foliated quartz-feldspar-biotite rocks in the schists suggests the presence of minor syntectonic granite intrusions. These rocks have a broadly granitic composition (as determined from petrographic study) comprising quartz, untwinned K-feldspar, albite, biotite (5-10%), opaque minerals (1-2%) and traces of muscovite, apatite and zircon. These aplites have an equigranular granoblastic texture, the grain

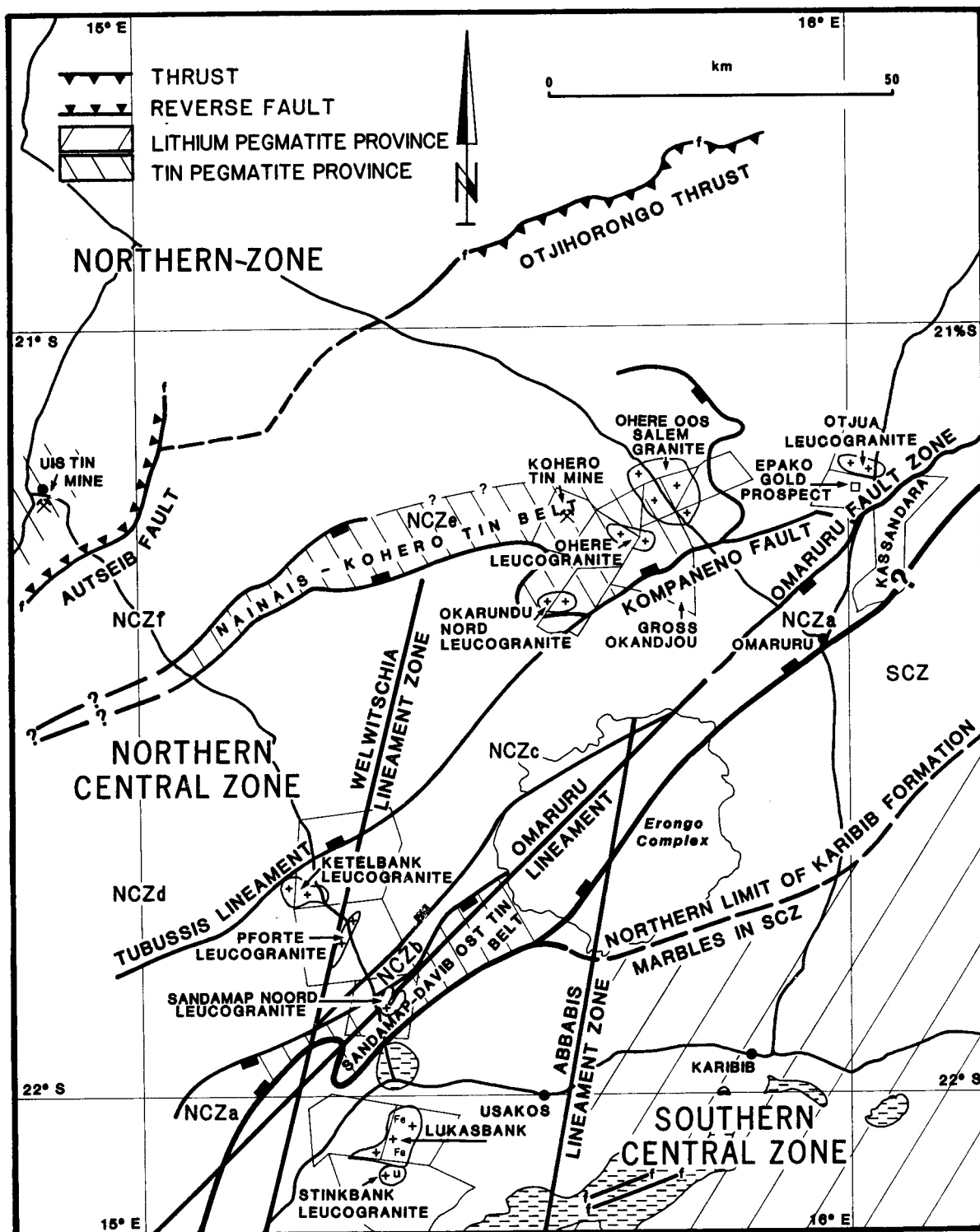


Figure 3.1: Localities and granitoids referred to in Chapter 3

size seldom exceeding 250  $\mu\text{m}$ .

### 3.3 SYN- AND LATE-TECTONIC GRANITOIDS OF THE NCZ IN THE USAKOS AREA

#### 3.3.1 Sandamap Noord peraluminous leucogranite

In the immediate vicinity of the Omaruru Lineament in NCZa on the farm Sandamap Noord (Fig. 3.1), a folded, lens-shaped, leucogranite phacolith lies in the core of a  $D_3/D_4$  domal structure (Map 3). The presence of significant (~5%)

primary muscovite is unusual amongst granites of the NCZ. Peraluminous granites are comparatively rare in the Damara Orogen, the largest being the well-known Donkerhuk intrusion (Miller, 1979, 1983a) which also intruded along and immediately to the south of a major tectonic break, namely the Okahandja Lineament. The term 'phacolith' (defined by Bates and Jackson [1987] as a minor syntectonic concordant, concavo-convex intrusion within folded strata) for the Sandamap Noord intrusion is preferred over 'laccolith' (a concordant igneous intrusion with a known or assumed flat floor). However, the formation of the domal structure was

	Garnetiferous Leucogranite	Peraluminous Leucogranite	Leucogranite
Orogenic Phase	Early Tectonic	Syn-Metamorphic Peak	Late Tectonic
Type Locality	Pforte	Sandamap Noord	Ketelbank
Zone	NCZc	NCZa	NCZc
Stratigraphic Level	Lower Kuiseb Formation	Upper Kuiseb Formation	Lower Kuiseb Formation
Intrusion Shape	Sheet-like Lopolith/Dyke	8000m long Folded Phacolith	Oval-shaped Stock
Tectonic Fabric	Penetrative Foliation	Banded-Not Foliated	None
Major Minerals	Quartz, Microcline Oligoclase	Quartz, Microcline Oligoclase	Quartz, Orthoclase Oligoclase, Perthite
Minor Minerals (<5%)	Garnet, Muscovite	Muscovite, Biotite, Garnet Tourmaline	Biotite, Muscovite, Fe-Oxides, Possible Anti-Perthite
Accessory Minerals (<0.5%)	Biotite, Zircon, Iron Oxides	Zircon, Chlorite, Iron Oxides	Tourmaline, Garnet, Chlorite, Zircon
Alteration Minerals	Sericite after Feldspar Secondary Yellow Mineral	Sericite after Feldspar	Sericite after Feldspar Chlorite after Biotite
Muscovite Status	Some may be Primary, Much is Secondary	Majority is Magmatic Minor amount is secondary	Poikilitic Grains appear Primary, but Majority after Altered Feldspar
Textural Features	Round, Lobate Grains, Round Quartz in Feldspar, Local Triple Junctions, Much Feldspar Alteration	Round, Lobate Grains, Round Quartz in Feldspar, Minor Feldspar Alteration, Quartz-Undulose Extinction	Igneous Texture, Oligoclase Very Sericitised, Feldspars and Quartz have Undulose Extinction
Age of Intrusion	Unknown	512±19 Ma (Rb-Sr WR)	Unknown
WRA Numbers	NS341	NS292-295	NS342-345

**Table 3.1:** Granites of the Northern Central Zone - Usakos area

partly related to this intrusion and thus the term lopolith as originally described by Hatch *et al.* (1972) where ‘the intrusion causes the arching of the roof’ may be more appropriate. The morphological and mineralogical characteristics of this 8-km-long intrusion are listed in Table 3.1. The phacolith possesses banding rather than a true foliation indicating that this syntectonic granite postdates the early, more intense deformational phases. In thin section the grains are somewhat rounded and are commonly lobate suggesting minor metamorphic recrystallisation. The leucogranite comprises quartz, microcline, oligoclase, muscovite, biotite, garnet, tourmaline, zircon and chlorite. The feldspars are universally fresh, though slight sericitisation of the microcline has occurred locally. The micas tend to be preferentially oriented. The muscovite in the Sandamap Noord leucogranite is magmatic according to the criteria of Miller *et al.* (1981). A notable feature of the Sandamap Noord leucogranite is the presence of local accumulations of apatite in stringers. Within these zones, pale green, fine-grained apatite crystals, which may comprise 60% of the rock, are enveloped in anhedral quartz (30%). Accessory minerals in these zones include

oligoclase, garnet, biotite, muscovite and zircon. Lepidolite-cassiterite-phosphate-bearing pegmatites are particularly clustered around this domal structure (see discussion on the genetic relationship between the dome and the pegmatites in chapters 6 and 7.5). Geochemical analyses of the Sandamap Noord leucogranite are given in Table 3.3.

### 3.3.2 Ketelbank leucogranite

The late-tectonic Ketelbank leucogranite intrudes lower Kuiseb Formation schists immediately south of the Tubusis Lineament in the NCZc (Fig. 3.1). This unfoliated, leucocratic stock is best exposed in the river immediately east of the Ketelbank farmhouse. The pluton is unusual in that it is one of the few late-tectonic granites to contain muscovite visible in hand specimen. The granite also contains minor garnet and tourmaline and the feldspars have a slightly preferred orientation which is interpreted as a flow texture. The intrusion contains local concentrations of biotite and minor biotite-rich xenoliths up to one metre long and 10 cm thick

	NS341
SiO <sub>2</sub> (wt%)	74.72
TiO <sub>2</sub>	.04
Al <sub>2</sub> O <sub>3</sub>	13.75
Fe <sub>2</sub> O <sub>3</sub>	.12
FeO	1.30
MnO	.08
MgO	.14
CaO	.89
Na <sub>2</sub> O	3.30
K <sub>2</sub> O	5.18
P <sub>2</sub> O <sub>5</sub>	.04
H <sub>2</sub> O-	.14
H <sub>2</sub> O+	.50
CO <sub>2</sub>	.06
TOTAL	100.27
F (ppm)	352
S	<5.3
Rb	225
Ba	61
Sr	25
Th	34
U	5
Zr	66
Nb	24
Mo	1
Sn	4
W	15
V	4
Cr	15
Co	<1.8
Ni	3
Cu	4
Zn	15
Ga	23
Pb	54
Ge	1
As	<.9
Sb	<1.2
Bi	<2.6
Se	<.8
Te	<1.9
Sc	5
Y	73
La	24
Ce	58
Nd	28
Au (ppb)	<5

**Table 3.2:** Whole-rock analyses of the garnetiferous leucogranite on the farm Pforte 65, Usakos District  
NS341: RUL grid PA 51.85/1128

and is locally crosscut by minor pegmatitic veins. The morphological and petrographic characteristics of this intrusion are listed in Table 3.1. One of the most notable features of the Ketelbank leucogranite is the widespread development of perthite and anti-perthite. The feldspars are strained and

	NS292	NS293	NS294	NS295
SiO <sub>2</sub> (wt%)	73.60	74.32	73.73	73.77
TiO <sub>2</sub>	.17	.07	.11	.18
Al <sub>2</sub> O <sub>3</sub>	13.99	14.00	14.28	13.60
Fe <sub>2</sub> O <sub>3</sub>	.27	.21	.23	.83
FeO	1.33	1.15	1.56	.97
MnO	.03	.06	.08	.02
MgO	.31	.19	.25	.26
CaO	.76	.63	.74	1.07
Na <sub>2</sub> O	3.03	3.60	2.71	3.42
K <sub>2</sub> O	5.67	5.18	5.67	4.76
P <sub>2</sub> O <sub>5</sub>	.20	.17	.21	.15
H <sub>2</sub> O-	.12	.09	.09	.11
H <sub>2</sub> O+	.43	.40	.54	.38
CO <sub>2</sub>	.08	.06	.09	.11
TOTAL	99.97	100.12	100.27	99.62
F (ppm)	517	542	581	334
S	<5.4	<5.5	<5.3	273
Rb	286	282	285	229
Ba	213	127	145	255
Sr	68	47	52	82
Th	39	21	29	50
U	6	4	4	8
Zr	129	65	83	151
Nb	16	18	25	16
Mo	<.5	<.5	<.5	<.5
Sn	7	8	8	8
W	<4.2	6	7	<4.2
V	2	2	2	5
Cr	5	7	22	9
Co	<1.9	<1.8	<1.9	<1.9
Ni	2	1	<1.4	2
Cu	2	3	<1.1	2
Zn	29	27	32	33
Ga	18	18	23	17
Pb	46	45	42	50
Ge	<.8	1	<.8	<.8
As	<.8	<.8	<.8	.9
Sb	<1.2	<1.1	<1.2	<1.2
Bi	<2.6	4	5	<2.6
Se	<.8	<.8	<.8	<.8
Te	<1.9	<1.8	<1.9	<1.9
Sc	4	3	5	4
Y	25	23	28	37
La	45	17	27	50
Ce	98	36	61	104
Nd	47	18	30	47
Au (ppb)	12	<5	10	<5

**Table 3.3:** Whole-rock analysis of the Sandamap Noord leucogranite phacolith  
NS292: Sandamap Noord, Usakos District  
NS293: Sandamap Noord, Usakos District  
NS294: Sandamap Noord, Usakos District  
NS295: Sandamap Noord, Usakos District

highly fractured K-feldspar exhibits the patchy development of gridiron twinning so characteristic of microcline. The occurrence of these apparently structurally induced exsolution features is surprising in a supposedly late-tectonic granite and may be related to movement on the Welwitschia lineament zone. The feldspars in the leucogranite are more extensively

	NS342	NS343	NS344	NS345
SiO <sub>2</sub> (wt%)	73.02	73.54	72.54	73.77
TiO <sub>2</sub>	.22	.18	.15	.15
Al <sub>2</sub> O <sub>3</sub>	13.82	13.83	14.46	13.64
Fe <sub>2</sub> O <sub>3</sub>	.20	.09	.24	.33
FeO	1.37	1.43	1.03	.92
MnO	.03	.02	.02	.02
MgO	.33	.35	.26	.30
CaO	.81	1.03	1.18	1.03
Na <sub>2</sub> O	2.58	2.84	3.05	2.59
K <sub>2</sub> O	6.57	6.01	5.81	5.89
P <sub>2</sub> O <sub>5</sub>	.08	.07	.09	.08
H <sub>2</sub> O-	.17	.19	.15	.08
H <sub>2</sub> O+	.71	.68	.61	.54
CO <sub>2</sub>	.07	.11	.11	.08
TOTAL	99.98	100.38	99.67	99.42
F (ppm)	486	543	476	556
S	63	95	127	224
Rb	264	261	238	250
Ba	357	305	291	280
Sr	76	78	81	77
Th	42	36	34	36
U	4	5	5	5
Zr	149	145	116	136
Nb	15	15	13	15
Mo	1	1	1	.7
Sn	4	5	4	4
W	14	18	15	12
V	9	9	7	7
Cr	15	18	17	11
Co	3	<1.9	<1.8	2
Ni	3	4	3	<1.4
Cu	3	3	3	3
Zn	31	33	34	74
Ga	17	16	18	17
Pb	57	55	49	57
Ge	<.8	<.8	<.8	<.8
As	<.9	<.9	<.8	<.9
Sb	<1.2	<1.2	<1.2	<1.2
Bi	<2.6	<2.7	<2.6	<2.6
Se	<.8	<.8	<.8	<.8
Te	<1.9	<1.9	<1.9	<1.9
Sc	4	4	4	5
Y	35	43	76	52
La	50	46	38	42
Ce	109	98	85	86
Nd	51	48	41	42
Au (ppb)	<5	<5	<5	<5

**Table 3.4:** Whole-rock analyses of the leucogranite on the farm Ketelbank 66, Usakos District  
 NS342: 200 m SE of the farmhouse  
 NS343: 200 m SE of the farmhouse  
 NS344: 200 m SE of the farmhouse  
 NS345: 200 m SE of the farmhouse

sericitised than any of the other late-tectonic granites investigated. Geochemical analyses of the Ketelbank leucogranite are given in Table 3.4.

### 3.4 SYN- AND LATE-TECTONIC GRANITOIDS OF THE NCZ IN THE OMARURU AREA

The two granites on the farms Ohere and Ohere Oos are particularly important because well-exposed thermal aureoles surrounding the plutons can be observed (see Chapter 5).

#### 3.4.1 Ohere Oos Salem granitoid

The unfoliated Ohere Oos Salem granitoid in the NCZe (Fig. 3.1) exhibits the classic porphyritic texture of the Salem Suite (Miller, 1983a). Good exposures of this pluton can be seen on the Omaruru-Khorixas road (Map 1). Feldspars are commonly aligned suggesting a flow texture. The granitoid does not possess a tectonic fabric and clearly postdates the isoclinal folding of the surrounding Kuiseb Formation metasediments. The core of this intrusion is granitic in composition and its characteristic features are listed in Table 3.5. Locally the granite loses its porphyritic nature, is medium-grained, is more leucocratic and contains minor tourmaline nests. The marginal phase of this intrusion is distinctly more mafic and tongues of granodioritic, and even dioritic, material with numerous schist xenoliths can be seen intruding the metasediments on Ohere Oos. However the contact between the truly granitic and mafic phases appears gradational and there seems little doubt that they belong to the same intrusion. It would appear that differentiation of the pluton occurred after intrusion, the more highly fractionated core of the pluton crystallising last. Geochemical analyses of the granitic and granodioritic phases are given in Table 3.6.

#### 3.4.2 Ohere leucogranite

The Ohere leucogranite (Fig. 3.1) intrudes Kuiseb Formation metasediments in NCZe. The pluton is oval in shape, the long axis running east-southeast. This granite can easily be distinguished from the early, more deformed leucogranites found in NCZa and NCZc (Map 1), but the local presence of a subvertical east-southeast-trending foliation indicates that this is not a post-tectonic intrusion. The foliated portions of the granite appear to be concentrated in discrete zones suggesting a possible relationship to late-tectonic regional shearing on the Kompaneno Fault and Omaruru Fault Zone (Map 1; see discussion in Chapter 4). The long axes of feldspars are also oriented approximately east-southeast: the randomly oriented biotite indicates that this is a magmatic feature. The composition of this fractionated leucogranite is more uniform than the Salem granite. The pluton contains a small number of biotite-rich xenoliths and is locally crosscut by tourmaline-bearing pegmatites. The characteristic features of the Ohere leucogranite are summarised in Table 3.5 and geochemical analyses are given in Table 3.7. There is a prominent total count radiometric anomaly over the Ohere leucogranite (1:50 000 airborne radiometric map) as there is with the Ketelbank, Okarundu Nord and Otjua leucogranites (Fig. 3.1).

	Salem Granite	Leucogranite	Leucogranite
Orogenic Phase	Syn-Tectonic	Syn-/Late Tectonic	Late Tectonic
Type Locality	Ohere Oos/Etendero	Ohere/Ehuuro/Gr. Okandjou	Otjua
Zone	NCZe	NCZe	NCZd
Stratigraphic Level	Upper Kuiseb Formation	Upper Kuiseb Formation	Lower Swakop Group
Intrusion Shape	Slightly folded Stock	Oval-shaped Stock	Oval-shaped Stock
Tectonic Fabric	None	Fabric Related to Shearing	None
Major Minerals	Quartz, Orthoclase Oligoclase	Quartz, Microcline Oligoclase	Quartz, Microcline (locally Perthitic), Oligoclase
Minor Minerals	Biotite, Microcline	Biotite	Biotite, Orthoclase
Accessory Minerals (<0.5%)	Muscovite, Chlorite, Iron Oxides, Zircon, Apatite Very Minor Tourmaline	Muscovite, Iron Oxides Zircon, Very Minor Tourmaline	Muscovite, Iron Oxides Garnet, Tourmaline Zircon, Apatite, Calcite
Alteration Minerals	Sericite after Feldspar Chlorite after Biotite Secondary Yellow Mineral	Sericite after Feldspar	Sericite after Feldspar Chlorite after Biotite
Muscovite Status	Majority is Secondary after Feldspar	Some is Primary, Majority is Secondary	Some is Primary, Majority is Secondary
Textural Features	Igneous Texture Locally Myrmekitic Quartz-Undulose Extinction Oligoclase highly Sericitised	Igneous Texture Myrmekitic Intergrowths Quartz-Undulose Extinction Oligoclase locally Sericitised	Igneous Texture Myrmekitic Intergrowths Quartz-Undulose Extinction Oligoclase locally Sericitised
Age of Intrusion	542 ± 11 Ma (Rb-Sr WR)	506 ± 135 Ma (Rb-Sr WR)	478 ± 4 Ma (Rb-Sr WR)
WRA Numbers	NS232-235	NS236-239	OT112, 113, 127, 128

**Table 3.5:** Granites of the Northern Central Zone - Omaruru area

### 3.4.3 Otjua leucogranite

The Otjua leucogranite is an unfoliated, locally porphyritic intrusion that intrudes lower Swakop Group meta-sediments in the core of the Schönfeld Dome (Fig. 3.1). The dominant mafic mineral is biotite. Muscovite is very rarely observed in hand specimen, garnet is locally present and schorl is fairly common within quartz-tourmaline nests that range in size from 5-15 cm in diameter. The granite contains a small number of biotite-rich xenoliths, but on the whole this appears to be a highly fractionated intrusion. The petrographic features of the Otjua leucogranite are summarised in Table 3.5 and the reader is referred to Steven (1987) for a more detailed description. Perhaps the most notable petrographic feature of the Otjua leucogranite is the widespread development of a myrmekitic texture, which is common in the younger leucogranites of the NCZ. This texture is rarely observed in the leucocratic portions of the Ohere Oos Salem granite. The major difference between the leucogranites of the Omaruru area and the leucogranites to

the southwest of the Erongo, such as the Ketelbank intrusion and those described by Marlow (1983), is that the latter contain a significant amount of muscovite (compare Tables 3.1 and 3.5) and can be classified as two-mica granites. Significantly, all three late-tectonic leucogranites discussed above crop out within 5 km of the Tubussis Lineament and its northeastern extension. The Otjua leucogranite has an Rb-Sr whole-rock age of 478 ± 4 Ma and a high  $\delta^{18}\text{O}$  value of 15.1‰ (Haack *et al.*, 1983). Other leucogranites in the CZ have similar late-tectonic ages. The youngest uraniumiferous leucogranite in the SCZ, the Stinkbank pluton, has an Rb-Sr whole-rock age of 484 ± 24 Ma (Marlow, 1983) and is also spatially associated with, and believed to be responsible for, tungsten skarn mineralisation (Steven, 1987). The Otjua leucogranite, and indeed all the other intrusions under discussion, contain neither scheelite nor wolframite nor any sulphide minerals. Geochemical analyses of the Otjua leucogranite and a fine-grained granite that is thought to be cogenetic (Steven, 1987) are given in Table 3.8.

	NS232	NS233	NS234	NS235
SiO <sub>2</sub> (wt%)	64.26	73.16	72.59	64.49
TiO <sub>2</sub>	.81	.24	.20	.72
Al <sub>2</sub> O <sub>3</sub>	15.72	13.48	14.16	15.80
Fe <sub>2</sub> O <sub>3</sub>	1.08	1.95	1.85	3.52
FeO	3.81	.10	.13	1.34
MnO	.07	.03	.04	.07
MgO	1.85	.32	.28	1.64
CaO	3.62	1.52	1.52	3.11
Na <sub>2</sub> O	3.05	2.67	2.86	3.14
K <sub>2</sub> O	4.00	5.64	5.92	4.33
P <sub>2</sub> O <sub>5</sub>	.23	.04	.04	.21
H <sub>2</sub> O-	.12	.11	.10	.11
H <sub>2</sub> O+	.67	.50	.52	.50
CO <sub>2</sub>	.11	.08	.13	.11
TOTAL	99.40	99.84	100.32	99.09
F (ppm)	1081	1569	1064	1010
S	<5.2	<5.2	<5.2	<5.3
Rb	137	334	318	165
Ba	1183	412	422	1005
Sr	372	110	112	324
Th	12	38	51	14
U	3	6	12	3
Zr	262	181	170	256
Nb	20	27	26	21
Mo	.8	<.5	<.5	.7
Sn	4	16	15	5
W	<4.8	4	<4.3	<4.8
V	69	6	4	66
Cr	25	6	5	30
Co	13	2	<2.0	12
Ni	10	2	<1.5	12
Cu	8	<1.1	<1.1	9
Zn	62	32	32	63
Ga	19	20	20	19
Pb	33	39	52	27
Ge	<1.0	<.9	<.9	<1.0
As	1	2	1	2
Sb	<1.3	<1.2	<1.2	<1.3
Bi	<3.0	<2.8	<2.7	<3.0
Se	<.9	<.8	<.8	<.9
Te	<2.1	<1.9	<1.9	<2.1
Sc	12	5	5	11
Y	31	42	52	34
La	57	66	76	42
Ce	106	127	142	80
Nd	50	61	67	41
Au (ppb)	<5	<5	10	<5

**Table 3.6:** Whole-rock analyses of the Ohere Oos Salem granitoid, Omaruru District.

NS232: Ohere Oos, main road, granodioritic phase

NS233: Ohere Oos, main road, granitic phase

NS234: Gross Okandjou, granitic phase

NS235: Ohere Oos, granodioritic phase

	NS236	NS237	NS238	NS239
SiO <sub>2</sub> (wt%)	72.80	73.07	73.01	73.09
TiO <sub>2</sub>	.23	.21	.22	.22
Al <sub>2</sub> O <sub>3</sub>	13.88	13.74	13.99	13.88
Fe <sub>2</sub> O <sub>3</sub>	.00	.00	.10	.00
FeO	1.84	1.79	1.64	1.79
MnO	.03	.03	.03	.03
MgO	.30	.28	.28	.30
CaO	1.29	1.38	1.29	1.42
Na <sub>2</sub> O	2.76	2.84	2.52	2.91
K <sub>2</sub> O	5.91	5.56	6.15	5.60
P <sub>2</sub> O <sub>5</sub>	.05	.05	.04	.04
H <sub>2</sub> O-	.08	.07	.12	.08
H <sub>2</sub> O+	.52	.51	.46	.47
CO <sub>2</sub>	.19	.29	.09	.28
TOTAL	99.90	99.84	99.93	100.10
F (ppm)	1263	901	727	949
S	<5.2	<5.3	<5.2	<5.2
Rb	363	355	358	344
Ba	346	321	384	337
Sr	88	88	94	96
Th	39	50	37	50
U	6	6	5	5
Zr	177	164	184	181
Nb	31	30	28	29
Mo	<.5	<.5	<.5	.6
Sn	11	11	8	9
W	5	<4.3	<4.3	<4.3
V	5	5	5	5
Cr	10	6	9	9
Co	<2.0	<2.0	3	<2.0
Ni	<1.4	<1.4	8	<1.4
Cu	1	<1.1	1	2
Zn	31	37	31	30
Ga	20	20	20	19
Pb	55	46	44	52
Ge	<.9	<.9	<.9	<.9
As	<.9	<.9	<.9	<.9
Sb	1	<1.2	<1.2	<1.2
Bi	<2.7	<2.7	<2.7	<2.7
Se	<.8	<.8	<.8	<.8
Te	<1.9	<1.9	<1.9	<1.9
Sc	5	4	5	4
Y	48	55	45	47
La	77	63	64	76
Ce	151	124	122	150
Nd	67	56	55	66
Au (ppb)	<5	<5	<5	<5

**Table 3.7:** Whole-rock analyses of the Ohere leucogranite, Omaruru District

NS236: Ohere 106

NS237: Gross Okandjou 187

NS238: Ohere 106

NS239: Gross Okandjou 187

	OT112	OT113	OT127	OT128	OT129
SiO <sub>2</sub> (wt%)	72.80	73.17	73.44	71.66	73.44
TiO <sub>2</sub>	.25	.25	.26	.35	.28
Al <sub>2</sub> O <sub>3</sub>	13.49	13.41	13.84	14.80	13.46
Fe <sub>2</sub> O <sub>3</sub>	2.25	2.19	2.24	1.89	2.49
MnO	<.01	<.01	<.01	<.01	<.01
MgO	.34	.30	.34	.47	.39
CaO	1.54	1.54	1.32	.82	1.49
Na <sub>2</sub> O	2.49	2.53	2.36	2.60	2.44
K <sub>2</sub> O	5.52	5.56	5.66	6.36	5.47
P <sub>2</sub> O <sub>5</sub>	.10	.07	.08	.41	.07
H <sub>2</sub> O-	.04	.09	.14	.20	.17
LOI	.44	.54	.58	.90	.60
TOTAL	99.26	99.65	100.26	100.46	100.30
F (ppm)	487	730	<490	<490	<490
S	99	<6	<6	12	<6
Rb	353	358	348	302	310
Ba	278	307	306	280	314
Sr	73	81	79	61	83
Th	41	70	40	19	46
U	8	9	5	7	6
Zr	207	195	208	162	223
Nb	38	35	39	11	38
Mo	<1.2	<1.2	<1.2	<1.2	<1.2
Sn	65	<4.0	16	<4.0	41
W	14.0	8.0	8.0	<5.6	9
V	9	9	10	7	10
Cr	8	5	4	4	6
Co	3	4	4	3	4
Ni	<1.2	<1.2	<1.2	<1.2	<1.2
Cu	<1.2	<1.2	<1.2	<1.2	<1.2
Zn	31	28	32	91	29
Pb	32	34	30	46	38
As	<7.0	<7.0	<7.0	<7.0	<7.0
Sb	<5.0	<5.0	<5.0	<5.0	<5.0
Sc	6	5	5	1	6
Y	63	85	57	6	52
Au (ppb)	<5	10	<5	<5	<5

**Table 3.8:** Whole-rock analyses of the Otjua leucogranite and fine-grained granite, Otjua Tungsten Prospect, Omaruru District

N.B All iron expressed as Fe<sub>2</sub>O<sub>3</sub>

OT112: OM6 survey beacon, leucogranite

OT113: OM6 survey beacon, leucogranite

OT127: 1.2 km E of prospect, leucogranite

OT128: 200 m W of tar road, leucogranite

OT129: Epako/Otjua boundary fence S of prospect, fine-grained granite

### 3.5 TECTONIC CONTROLS ON THE LOCATION OF GRANITES IN THE NCZ

Marked lithostratigraphic changes across the Omaruru and Tubussis Lineaments attest to the controls these major structures exerted on sedimentation. There is also evidence that these tectonic breaks played a role in the localisation of granites throughout the orogeny. Syntectonic leucogranites with an elongate outcrop pattern are particularly concentrated along the northern side of the Omaruru Lineament in NCZa, and to a lesser extent NCZc, near Omaruru (Map 1). There is a concentration of late-tectonic leucogranites along the Tubussis Lineament. The Ketelbank, Okarundu Nord, Ohere and Otjua plutons all crop out within 5 km of this major structural break (Fig. 3.1). Evidence for late-tectonic strike-slip movement on the Omaruru Lineament will be discussed

in Chapter 4. It is believed that this lateral movement generated pull-apart structures which assisted in the localisation of intrusions, most notably immediately north of the Omaruru flower structure (Map 1) in the Schönfeld Dome. Geophysical evidence from northern Scotland suggests that such major faults as the Walls Boundary Fault can extend to the base of the crust, i.e. approximately 35 km (Coward, 1990). The emplacement of plutons in the Damara in the vicinity of major subvertical faults, which presumably also extend deep into the crust, begs the question as to whether these tectonic breaks were zones of melting. Leake (1990) has discussed how strike-slip movements on major faults, which pushed large crustal blocks into the mantle, triggered large-scale crustal melting during the Acadian and Hercynian orogenies. The author considers that there is substantial evidence to indicate that the Omaruru Lineament was an important zone of melting in the early stages of the Damara Orogen. In the latter stages of the orogeny, the Tubussis Lineament played a more important role in the generation of granitic melts. This topic will be discussed more extensively once the isotopic data has been presented in Chapter 6.

### 3.6 PEGMATITES

Late-tectonic pegmatitic intrusions are widely distributed in central Namibia. Although a spatial relationship with late-tectonic granitic intrusions is not uncommon, in few cases do the pegmatites appear to be differentiates of the granitoid. None of the pegmatites examined exhibits migmatitic features. There is a marked restriction of pegmatite types to certain tectono-stratigraphic zones. The three main types of undeformed, late-tectonic pegmatite within the field area, namely the magnetite-bearing pegmatites hosted by the lower Swakop Group in the SCZ, the tourmaline-bearing pegmatites of the lower Swakop Group in the NCZ and the muscovite-rich pegmatites of the Kuiseb Formation, are discussed below. A fourth type, the lithium pegmatites of the Karibib district, the subject of detailed investigations by Roering (1963, 1966) and Miller (1969), is mentioned briefly. Emphasis is placed in this section on a regional overview.

#### 3.6.1 Magnetite-bearing pegmatites hosted by lower Swakop Group metasediments in the SCZ

Homogenous, magnetite-bearing pegmatites that have intruded calc-silicate and carbonate lithologies of the lower Swakop Group are best exposed on the farms Eureka and Lukasbank (Fig. 3.1) where they cover an area of approximately 50 km<sup>2</sup> (Maps 5 and 6). The pink-red pegmatites locally have a granitic phase and commonly contain xenoliths of hornblende-magnetite rocks and biotite gneiss. The petrographic features of the magnetite-bearing pegmatite are summarised in Table 3.9. This lithology is confined to the SCZ and does not contain tourmaline, a fact which distinguishes these pegmatites from those of the NCZ. Other pegmatites of the SCZ such as those which have intruded Abbabis Complex lithologies are also deficient in tourmaline.

Type Locality	Eureka, Lukasbank; Usakos District
Zone	SCZ
Stratigraphic Level	Rössing and Oberwasser Formation
Tectonic Fabric	None
Major Minerals	Quartz, microcline and microperthite, plagioclase, magnetite
Minor Minerals	Muscovite
Accessory Minerals	Hematite, limonite, sericite
Alteration Minerals	Sericite after plagioclase
Degree of Alteration	Very Minor
Textural Features	Alteration of Plagioclase

**Table 3.9:** Late-orogenic magnetite-bearing pegmatite hosted by the Lower Swakop Group on the farm Eureka

### 3.6.2 Lithium pegmatites of the SCZ in the Karibib area

Several of the lithium pegmatites in the Karibib area (Fig. 3.1) are located within Abbabis Complex gneisses and Damaran granites, but the majority of these intrusions are

hosted by the carbonate lithologies of the Karibib Formation in the SCZ. Smith (1965) attributed this to the 'damming effect on volatiles' by the marbles. These pegmatites have been exploited for their lithium minerals, tourmaline, beryl, feldspar, columbite-tantalite and bismuth (Roering, 1963; Smith,

Type Locality	Epako Gold Prospect	Otjua Tungsten Prospect
Zone	NCZd	NCZd
Stratigraphic Level	Oberwasser Formation	Spes Bona, Okawayo, Oberwasser Fmn.
Tectonic Fabric	None	None
Major Minerals	Quartz, Microcline (locally Perthitic), Oligoclase	Quartz, Microcline, Oligoclase
Minor Minerals (<5%)	Biotite, Garnet, Tourmaline	Biotite, Garnet, Tourmaline
Accessory Minerals (<0.5%)	Muscovite, Iron Oxides, Calcite	Muscovite, Chlorite, Zircon Iron Oxides, Calcite
Alteration Minerals	Sericite after Feldspar	Chlorite after Biotite and Garnet Sericite after Feldspar
Degree of Alteration	Very Minor	Very Minor
Muscovite Status	Majority is Sericite after Feldspar, Some Crystals Appear Primary	Sericite after Feldspar
Textural Features	Graphic Quartz-Feldspar Intergrowth, Quartz has Slightly Undulose Extinction Oligoclase Slightly Sericitised,	Graphic Quartz-Feldspar and Quartz-Tourmaline Intergrowth, Myrmekitic Texture, Quartz has Slightly Undulose Extinction, Very Minor Feldspar Alteration
Age of Intrusion	Unknown-probably late-tectonic	Unknown-probably late-tectonic

**Table 3.10:** Late-orogenic pegmatites hosted by the Lower Swakop Group in the Omaruru area

Type Locality	Sandamap Noord (NST8)	Sandamap Noord (NST9)	Kohero (NST12)
Pegmatite Type	Non-Stanniferous Pegmatite	Stanniferous Pegmatite	Stanniferous Pegmatite
Zone	NCZa	NCZa	NCZe
Tectonic Fabric	None	None	None
Major Minerals	Quartz, Microcline, Albite/Oligoclase	Quartz, Albite/Oligoclase	Quartz, Albite/Oligoclase
Minor Minerals (<5%)	Muscovite, Garnet	Microcline, Muscovite, Tourmaline	Muscovite, Tourmaline
Accessory Minerals (<0.5%)	Biotite, Tourmaline Apatite, Zircon, Chlorite	Lepidolite, Cassiterite, Columbite, Ferberite, Purperite, Loellingite, Petalite, Triphylite, Zircon	Lepidolite, Cassiterite Columbite, Zircon, Sphene
Alteration Minerals	Chlorite, Sericite	Sericite	Sericite
Degree of Alteration	Very Minor	Muscovite Greisen is Very Well Developed	Muscovite Greisen is Very Well Developed
Muscovite Status	Majority is Primary, Sericite Overgrows Plagioclase	Sericite is Secondary after Plagioclase	Very Minor Sericite, Majority is Coarse-grained and Pokilitic
Textural Features		Albitisation of Microcline, Quartz-Many Inclusions, Oligoclase Highly Cloudy and Overgrown by Sericite Undulose Extinction of Qtz	Two Generations of Plagioclase-Early One Highly Altered, Later One Result of Albitisation (?)
Age of Intrusion	473 ± 23 Ma (Rb-Sr WR)	468 ± 14 Ma (Rb-Sr WR)	492 ± 11 Ma (Rb-Sr WR)

**Table 3.11:** Late-orogenic pegmatites hosted by the Kuiseb Formation in the tin belts of the Northern Central Zone

1965; Miller, 1969; Von Knorring, 1985). Significantly, the lithium pegmatites of the SCZ do not contain tin mineralisation.

### 3.6.3 Pegmatites hosted by lower Swakop Group metasediments in the NCZ

The most notable feature of the pegmatites that intrude the marine sediments of the lower Swakop Group is that they contain significant schorl. The best examples can be seen in the Schönfeld Dome in NCZd (Map 1) on the Otjua Ridge (Steven, 1987) where pegmatites have intruded the subvertically dipping metasediments in a *lit-par-lit* manner. The pegmatitic intrusions appear to be derived from the large number of late-tectonic granites within the core of this dome such as the Otjua leucogranite. The pegmatites commonly possess a mineralogical banding that parallels lithological contacts and exhibit a graphic quartz-feldspar and quartz-tourmaline intergrowth. The petrographic characteristics of pegmatites from the vicinity of the Otjua Tungsten and Epako Gold Prospects (Fig. 1.3) are summarised in Table 3.10. The essential features are the presence of garnet and biotite, the very minor amount of muscovite and the lack of significant

feldspar alteration. The pegmatites of the NCZd do not contain cassiterite or wolframite, but are known to contain traces of sulphide mineralisation (Haughton *et al.*, 1939, p.113).

### 3.6.4 Pegmatites hosted by upper Kuiseb Formation metasediments in NCZa and NCZe

The muscovite-bearing pegmatites of the upper Kuiseb Formation have been well studied, because they commonly host cassiterite mineralisation and local concentrations of Nb, Ta, Li and Cs (Haughton *et al.*, 1939; Frommurge *et al.*, 1942; Wagener, 1989). The stanniferous pegmatites of the NCZ are located within the tin belts (Fig. 3.1) and examples have been selected from two localities in NCZa and NCZe, namely on Sandamap Noord in the Sandamap-Davib Ost tin belt and from the Kohero Tin Mine in the Nainais-Kohero tin belt (Fig. 3.1). This provides an opportunity to compare stanniferous pegmatites hosted by metasediments that have been metamorphosed to upper amphibolite and greenschist facies respectively. Key petrographic and mineralogical features of these pegmatites have been identified and can be compared with pegmatites hosted at other stratigraphic levels. For de-

tailed morphological descriptions of individual tin prospects, the reader is referred to Haughton *et al.* (1939) and Frommurze *et al.* (1942). In most cases the pegmatites occur near granitic intrusions, either leucogranites (as in NCZa) or leucogranites and Salem granites (as in NCZe), but, although there is commonly a spatial relationship between the two, the pegmatites do not appear to be derived from the granitoids. Tin mineralisation is notably hosted by muscovite greisen zones, zones of albitisation and areas of muscovite and topaz development. It is noteworthy that the best mineralised pegmatites are usually developed in the centre of the tin belts and that unmineralised, unaltered, garnet and tourmaline-bearing pegmatites are concentrated close to the Salem Granite intrusions. Stanniferous pegmatites are the only intrusive rocks in the CZ which contain notable concentrations of sulphides (Haughton *et al.*, 1939).

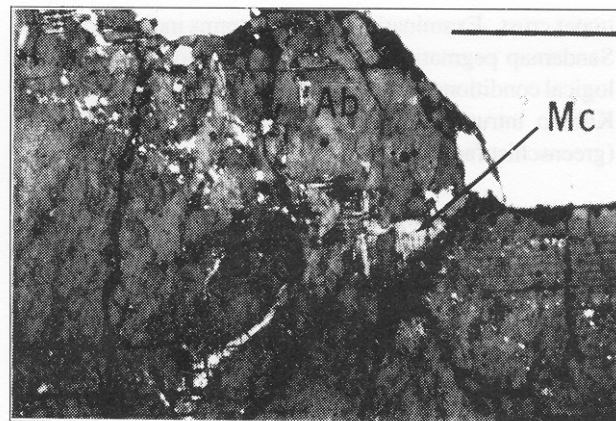


Plate 3.1: Extensively albitised (Ab) microcline (Mc) in stanniferous pegmatite at the Sandamap Tin Mine (NST9; XL); scale bar = 1 mm

#### 3.6.4.1 Pegmatites in the Sandamap-Davib Ost tin belt

On Sandamap Noord, the leucogranite in the core of the D<sub>3</sub>/D<sub>4</sub> domal structure is immediately surrounded by undeformed, late-/post-tectonic pegmatites (Map 3). The non-stanniferous pegmatite from the edge of the domal structure contains quartz, microcline and albite/oligoclase with minor muscovite and garnet and traces of tourmaline and biotite altering to chlorite (Table 3.11). The majority of the muscovite is primary, but some small white micas overgrow sericitised microcline. However, feldspar alteration is generally very minor. The pegmatite is igneous in texture and has not been recrystallised by metamorphic processes. This pegmatite has a late Damaran Rb-Sr whole-rock age of 473 ± 23 Ma (Chapter 6). Several circular or lenticular cassiterite-bearing pegmatites, hosted by the Kuiseb Formation, are arranged concentrically around the Sandamap Noord domal structure (Map 3). These pegmatites vary in length from a metre to over 1 km and most are conformable with the schistosity of the enclosing schists. The majority of the larger stanniferous pegmatites (such as at the Sandamap Tin Mine) are zoned and have quartz cores many tens of metres in diameter. Cassiterite mineralisation is particularly concentrated in a Li-rich greisen which contains purperite, petalite, triphylite and lithiophyllite (Von Knorring, 1985, pers. comm.). The outer zone of the pegmatite comprises quartz, albite/oligoclase, minor microcline, tourmaline, lepidolite and muscovite and traces of chlorite (Table 3.11). The microcline is almost completely albitised (plate 3.1).

There is a notable correlation between cassiterite mineralisation and albitised K-feldspar elsewhere in the Damara Orogen, such as at the Uis Tin Mine (Richards, 1986). In contrast to the non-stanniferous pegmatites on Sandamap Noord, the plagioclase is cloudy and extensively altered, being overgrown by tiny muscovite laths concentrated in fractures. The stanniferous pegmatites have an unequivocal igneous texture that has not been recrystallised. Locally the pegmatite contains columbite, ferberite and minor pockets of auriferous (determined by fire assay) arsenic mineralisation. Large (3 mm) crystals of loellingite have largely been replaced by scorodite and are commonly surrounded by a skeletal framework of small, euhedral arsenopyrite rhombs. This stanniferous pegmatite has an Rb-Sr whole-rock age of 468 ± 14 Ma (Chapter 6). The genetic relationship

between the leucogranite and the various types of pegmatite will be discussed in chapters 6 and 7.5.

#### 3.6.4.2 Pegmatites in the Nainais-Koheron tin belt

At the Kohero Tin Mine (Map 1), in contrast, a subvertical swarm of north-northeast-trending stanniferous pegmatite dykes cut across the schistosity of phyllites and schists of the Kuiseb Formation. The pegmatite dykes attain a maximum length of 600 metres and a maximum thickness of 40 metres. The consistent strike of the intrusions suggests their *en echelon* emplacement in a regional shear couple similar to that described from the Uis Tin Mine (Richards, 1986). The intrusion of pegmatites into rocks undergoing brittle deformation in NCZe contrasts with the higher metamorphic grade and associated ductile deformation during pegmatite emplacement in NCZa. The stanniferous pegmatite at the Kohero Tin Mine comprises quartz and plagioclase with minor muscovite and tourmaline (Table 3.11). There appear to be two generations of plagioclase, the early one being extensively altered and a younger, fresher variety, which may have formed from the albitisation of K-feldspar. Cassiterite mineralisation is concentrated in those portions of the pegmatites that have been altered to a muscovite greisen. A notable feature is the local tourmalinisation of the country rock on the margin of the pegmatite intrusions (see discussion in Chapter 7.6). A similar style of wallrock alteration on the edge of stanniferous pegmatites was noted by Richards (1986) at the Uis Tin Mine (Fig. 3.1).

#### 3.6.4.3 Stanniferous pegmatite morphology

The morphology of the stanniferous pegmatites in the two tin belts is markedly different. In the southern tin belt, pegmatites are lens-shaped or bulbous and are compositionally zoned with a quartz core. In the Nainais-Kohero tin belt in contrast, pegmatites do not bear such a close spatial relationship to leucogranites, are not zoned and have been emplaced as a swarm of steeply dipping or subvertical dykes. These significant differences reflect the differing metamorphic conditions that prevailed in the two tin belts during pegmatite emplacement and are discussed in Chapter 5. Brisbin (1986) has recently reviewed the mechanics of pegmatite intrusion. He distinguished various patterns of pegmatite intrusions representing distinct levels within the upper crust. Examina-

tion of his diagrams indicates that the Sandamap pegmatites were emplaced under ductile rheological conditions (amphibolite facies), while the Nainais-Kohero intrusions were emplaced in the brittle domain (greenschist facies).

### 3.6.5 Summary of pegmatites within field area

The pegmatites within the field area can be divided into two groups, namely those in the SCZ and the NCZ. In the southwest of the field area (Eureka-Lukasbank) in the SCZ, anhydrous, magnetite-bearing pegmatite bodies with very minor mica intrude lower Swakop metasediments in areas that are underlain by basement and Nosib Group lithologies. It would appear that these magnetite-bearing pegmatites were derived from the melting of large volumes of basement and Etusis Formation sediments in areas that have undergone (at least?) upper amphibolite facies metamorphism in a similar manner to the uraniferous alaskites (Hawkesworth and Marlow, 1983). Sixty kilometres to the east in the Karibib district, in an area underlain by basement lithologies and where the Nosib Group is not so well developed, more hydrous lithium-bearing pegmatites have intruded both Abbabis Complex and Damaran lithologies. These lithium pegmatites exhibit the characteristics of rare-element pegmatites (Cerny, 1982a) that consolidated between 3.5 and 7 km (0.9-2.2 kbars) in the crust. Derivation of these intrusions from basement lithologies appears to be the most plausible explanation at this stage. Peak metamorphic conditions around Karibib were lower amphibolite facies (Puhan, 1983), markedly lower than in the Eureka-Lukasbank area. Neither of the above-mentioned types of pegmatite is spatially associated with, nor appears to be derived from, granitic intrusions.

In the NCZ, schorl-bearing, but essentially anhydrous and otherwise unmineralised, pegmatites intrude calcareous and semi-pelitic lithologies of the lower Swakop Group: The best examples are in the core of the Schönfeld Dome north of Omaruru and the pegmatites appear to be derivatives of the leucogranites that have formed this structure. In the former graben structures that were filled with upper Kuiseb Formation turbidites and are now represented by the tin belts (NCZa and NCZe), stanniferous muscovite-bearing pegmatites, which are only rarely associated with granites, are developed. These tin pegmatites, which exhibit extensive hydrothermal alteration and are another type of rare-element pegmatite (as defined by Cerny, 1982a), are essentially confined to this stratigraphic level.

None of the pegmatites within the field area exhibits migmatitic features and the sheer size of the pegmatite bodies precludes a local, *in situ* derivation. For the purposes of this investigation the pegmatites can thus be divided into two groups: those that are derivatives of granitic intrusions and those that, if they are not derivatives of partially melted crustal lithologies, were masses of magma that interacted and were significantly modified by fluids from the enclosing metasediments. It is this interaction with the country rock that is believed to have resulted in the strong stratigraphic control on pegmatite type in the CZ. Possible precursor rocks for the partial melts can be subdivided into three

types; firstly, the granitic gneisses of the Abbabis Complex and the arkoses and quartzites of the Etusis Formation (derived from that basement), secondly, the carbonates of the lower Swakop Group and thirdly, the hydrous metapelites of the upper Swakop Group. The carbonate lithologies can be ruled out as having contributed significant volumes of partial melt on compositional grounds and because the metamorphic conditions were not high enough (see discussion in Chapter 5). Thus the two main precursors for partial melts within the field area are the "granitic" lithologies of the SCZ and the hydrous Kuiseb pelites in the NCZ. This would account for the schorl-rich nature of the pegmatites that have intruded the Swakop Group: marine sediments are a large reservoir of boron (Wedepohl, 1978). In contrast, the pegmatites that have intruded the basement and Damaran continental meta-sediments are deficient in schorl.

## 3.7 GEOCHEMISTRY OF THE GRANITOID INTRUSIONS

### 3.7.1 Introduction

That the intrusive rocks of the CZ are essentially granitic in composition is well documented: Miller (1983a) records the proportion of gabbro/diorite:tonalite/granodiorite: granite as 2:2:96. Within that portion of the NCZ examined in this study gabbros and tonalites are unknown and pegmatites are numerous. On the basis of petrographic study, all the granitoids that were examined in detail were determined to be granites (s.s.), with the exception of the marginal phase of the Ohere Oos Salem granite. The leucogranites examined have a minimum SiO<sub>2</sub> content of 71.66 wt%. Thus the granites of the NCZ cannot be referred to as a calc-alkaline suite (defined as "a series of rocks in which the weight percentage of silica is between 56 and 61"; Bates and Jackson, 1987) as suggested by Miller (1983a). All intrusions examined were analysed geochemically to determine whether something more specific could be determined about the nature of the granitoids. Other than the new analyses presented in this memoir, only Steven (1987) has published trace element data for the granitoids of the Usakos-Karibib-Omaruru area. Thus the data set for the NCZ in central Namibia (22 samples) is small.

### 3.7.2 Geochemical classification of the NCZ granites and a comparison with other Damaran granitoids

#### 3.7.2.1 Major element classification

Several geochemical schemes have been proposed for the classification of granites. Shand (1943) was the first to suggest the use of an index of alumina saturation. Various modifications of this index have been employed by Clarke (1981) and more recently Zen (1986, 1988) who proposed the use of the aluminum saturation index (ASI), which is defined as the molar ratio of Al<sub>2</sub>O<sub>3</sub> to the sum of CaO, K<sub>2</sub>O and Na<sub>2</sub>O. Zen (1988) distinguished between ASI<sub>bulk</sub> and ASI<sub>corr</sub>, the latter being corrected for the CaO content of apatite (and invariably exceeding the former). To avoid confusion only ASI<sub>bulk</sub> are quoted in this memoir. Subaluminous granites have ASI values less than 1, mildly peraluminous between

Intrusion	Orogenic Phase	ASI <sub>bulk</sub>
Pforte garnetiferous leucogranite	early tectonic	1.09
Ohere Salem granite (granitic phase)	syn-tectonic	1.00
Ohere Salem granite (dioritic phase)	syn-tectonic	1.02
Sandamap Noord leucogranite	syn-metamorphic peak	1.12
Ohere leucogranite	syn-/late-tectonic	1.05
Ketelbank leucogranite	late-tectonic	1.08
Otjua leucogranite	late-tectonic	1.09
Otjua fine-grained granite	late-tectonic	1.07

**Table 3.12:** Alumina saturation indices (Zen, 1988) for CZ granites

I and 1.1 and strongly peraluminous granites have ASI numbers exceeding 1.1. This classification system is preferred to the S-type/I-type scheme (Chappell and White, 1974; Hine *et al.*, 1978) because of the absence of the genetic implication that all S-type granites are derived from sediments and that I-type granites are derived from rocks that have not been involved in weathering processes: many S-type granites, which are peraluminous by definition, need not be derived exclusively from the anatexis of pelites (Clarke, 1981). All the granites of the NCZ sampled are at least mildly peraluminous as defined by Zen (1986; Table 3.12). The synmetamorphic peak Sandamap Noord leucogranite, the only intrusion to contain significant magmatic muscovite, is strongly peraluminous. This is noteworthy because strongly peraluminous granites are comparatively rare in the Damara Orogen, the largest being the Donkerhuk intrusion which also intruded along a major tectonic break, namely the Okahandja Lineament. Blaxland *et al.* (1979) determined Rb-Sr whole-rock ages of  $523 \pm 8$  Ma and  $521 \pm 15$  Ma for the Donkerhuk granite, which compare with  $512 \pm 19$  Ma for the Sandamap Noord leuco-granite. This indicates contemporaneous intrusion of peraluminous granites at the peak of metamorphism on both margins of the SCZ (Fig. 2.2).

### 3.7.2.2 Rb, Ba and Sr contents of the granitoids

Many authors have made use of the elements Rb, Ba and Sr as indicators of magmatic fractionation, alteration and accompanying mineralisation (Nockolds and Allen, 1953; Exley, 1957; McCarthy and Hasty, 1976; Plimer and Elliot, 1979). During magmatic differentiation Rb is concentrated in residual melts and both Ba and Sr tend to be depleted because of their incorporation in crystallising feldspar. All the leucogranites of the NCZ (Tables 3.13 and 3.14) are enriched in Rb and depleted in Ba compared to the average granitic rocks quoted by Turekian and Wedepohl (1961). On the Rb-Ba-Sr diagram of El Bouseily and El Sökkary (1975) all the granitoids of the NCZ, with the exception of the granodioritic marginal phase of the Ohere Oos Salem granite, plot either in or on the margins of strongly differentiated granites (Fig. 3.2). Further evidence for the highly fractionated nature of the NCZ granitoids is provided by their relatively high Rb/Sr ratios (Fig. 3.3): average low-calcium granites (Turekian and Wedepohl, 1961) have ratios of 1.7. Rb/Sr ratios of NCZ granitoids are indistinguishable from those of the uraniumiferous alaskites of central Namibia (Marlow, 1981).

	Mean	Minimum	Maximum	N
SiO <sub>2</sub> (wt%)	73.38	72.54	74.72	15
TiO <sub>2</sub>	.19	.11	.24	13
Al <sub>2</sub> O <sub>3</sub>	13.90	13.48	14.46	15
Fe <sub>2</sub> O <sub>3</sub>	.53	.10	1.95	12
FeO	1.22	.10	1.84	15
MnO	<.01	<.01	<.01	0
MgO	.28	.14	.35	15
CaO	1.10	.63	1.52	15
Na <sub>2</sub> O	2.91	2.52	3.60	15
K <sub>2</sub> O	5.70	4.76	6.57	15
P <sub>2</sub> O <sub>5</sub>	.09	.04	.21	15
H <sub>2</sub> O-	.11	.07	.19	15
H <sub>2</sub> O+	.52	.38	.71	15
CO <sub>2</sub>	.12	.06	.29	15
F (ppm)	724	334	1569	15
S	157	63	273	5
Rb	293	225	363	15
Ba	284	61	422	15
Sr	78	25	112	15
Th	39	21	51	15
U	6	4	12	15
Zr	140	65	184	15
Nb	22	13	31	15
Mo	1	.6	1	6
Sn	8	4	16	15
W	11	5	18	9
V	5	2	9	15
Cr	11	5	22	15
Co	3	2	3	4
Ni	3	2	8	9
Cu	3	1	4	11
Zn	33	16	74	15
Ga	19	16	23	15
Pb	50	39	58	15
Ge	1	1	1	2
As	1	.9	2	3
Sb	1	1	1	1
Bi	5	4	5	2
Se	<0.8	<0.8	<0.8	0
Te	<1.9	<1.9	<1.9	0
Sc	4	3	5	15
Y	46	23	76	15
La	51	17	77	15
Ce	104	36	151	15
Nd	48	18	67	15
Au (ppb)	11	10	12	3

**Table 3.13:** Average NCZ leucogranite analyses excluding Otjua (n = 15)

### 3.7.3 The tectonic setting of the NCZ granites as deduced from trace element geochemistry

Several authors have used trace element discrimination diagrams to determine the tectonic setting at the time of granite emplacement, though strictly speaking discriminant fields reflect source regions rather than tectonic regimes. Pearce *et al.* (1984) divided granites on the basis of intrusive settings into four main groups: ocean-ridge granites (ORG), volcanic-arc granites (VAG), within-plate-granites (WPG) and collision-

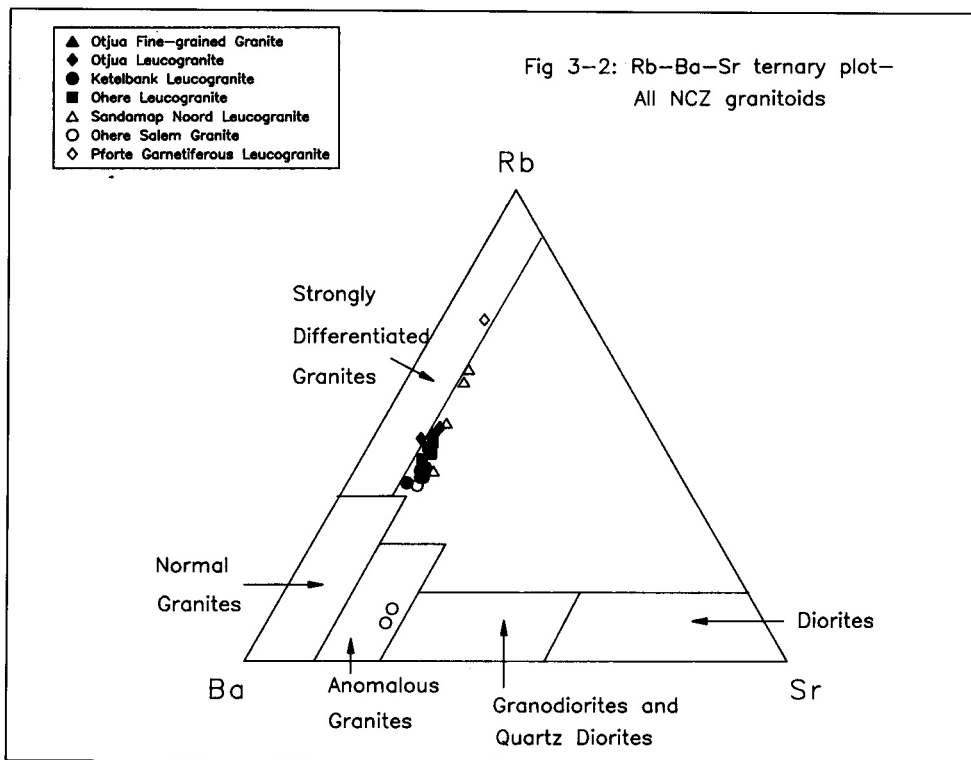


Figure 3.2: Rb-Ba-Sr ternary plot - all NCZ granitoids

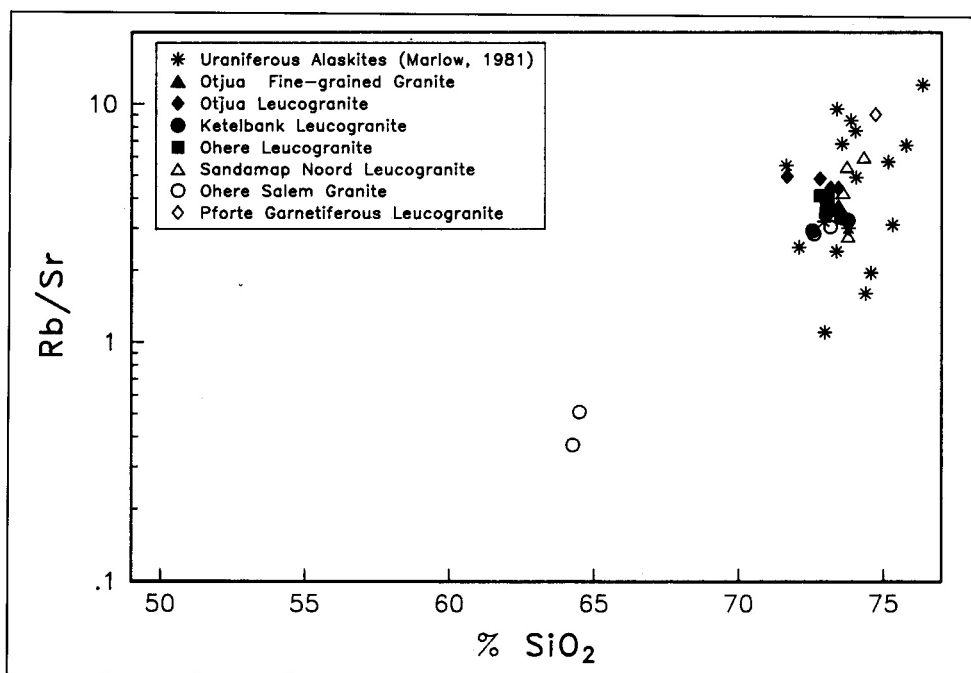


Figure 3.3: Rb/Sr-SiO<sub>2</sub> (wt%) - all NCZ granitoids

granites (COLG). Although the discrimination boundaries are empirically drawn, they do have a theoretical basis in the different petrogenetic histories of the granite groups. On the Nb-Y discriminant diagram (Fig. 3.4), the granites analysed are listed in presumed chronological order. The early tectonic garnetiferous leucogranite and the younger Salem granitoids plot in the WPG field. In contrast the synmetamorphic peak Sandamap Noord leucogranite straddles the VAG/syn-COLG and WPG fields. All the late-tectonic leu-

cogranites (with the exception of two samples) have a within-plate-granite not a volcanic-arc or collision-granite signature. On the Rb-(Y+Nb) discriminant diagram (Fig. 3.5) the early tectonic leucogranite plots in the WPG field. The Sandamap Noord leucogranite samples in contrast plot within the boundaries of the VAG and syn-COLG. All the late-tectonic leucogranites with the exception of two samples have a within-plate-granite signature. Of all the granites examined by Pearce *et al.* (1984), the WPG of the Nigerian suite bear

	Mean	Minimum	Maximum	N
SiO <sub>2</sub> (wt%)	72.90	71.66	73.44	5
TiO <sub>2</sub>	.28	.25	.35	5
Al <sub>2</sub> O <sub>3</sub>	13.80	13.41	14.80	5
Fe <sub>2</sub> O <sub>3</sub>	2.21	1.89	2.49	5
MnO	<.01	<.01	<.01	0
MgO	.37	.30	.47	5
CaO	1.34	.82	1.54	5
Na <sub>2</sub> O	2.48	2.36	2.60	5
K <sub>2</sub> O	5.71	5.47	6.36	5
P <sub>2</sub> O <sub>5</sub>	.15	.07	.41	5
H <sub>2</sub> O-	.13	.04	.20	5
LOI	.61	.44	.90	5
F (ppm)	609	487	730	2
S	55	12	99	2
Rb	334	302	358	5
Ba	297	278	314	5
Sr	75	61	83	5
Th	43	19	70	5
U	7	5	9	5
Zr	199	162	223	5
Nb	32	11	39	5
Mo	<1.2	<1.2	<1.2	0
Sn	41	16	65	3
W	10	8	14	4
V	9	7	10	5
Cr	6	4	8	5
Co	4	3	4	5
Ni	<1.2	<1.2	<1.2	0
Cu	<1.2	<1.2	<1.2	0
Zn	42	28	91	5
Pb	36	30	46	5
As	<7.0	<7.0	<7.0	0
Sb	<5.0	<5.0	<5.0	0
Sc	5	1	6	5
Y	53	6	85	5
Au (ppb)	10	10	10	1

Table 3.14: Average Otjua granite analyses (n = 5)

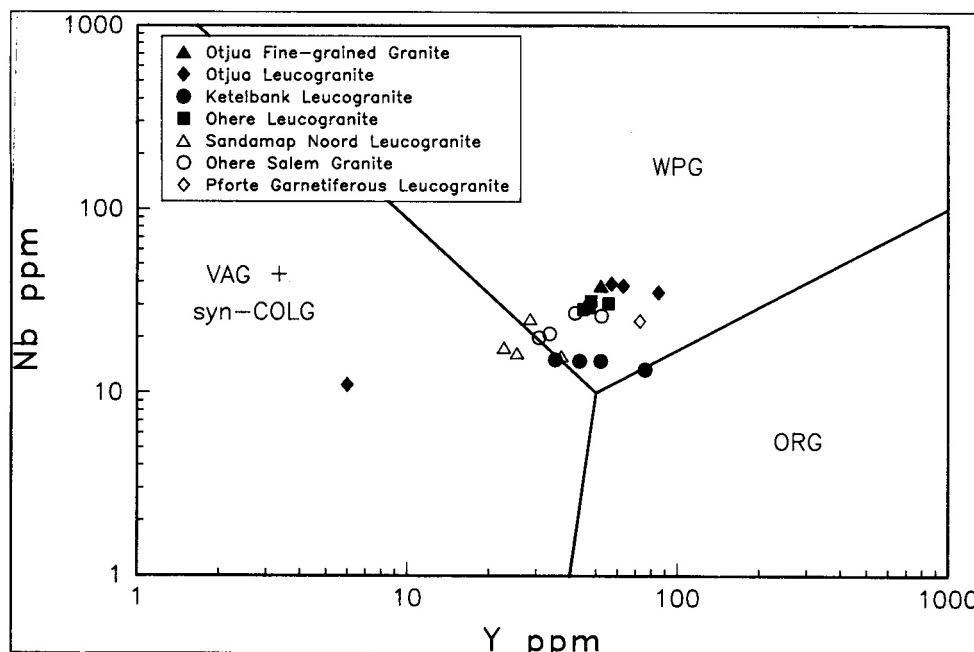
the closest resemblance to the early and late orogenic granitoids of the Central Zone. The petrogenetic pathway for the Nigerian WPG was explained by the existence of an enriched mantle source and combined assimilation-fractionation at intermediate and acidic compositions (Pearce *et al.*, 1984).

### 3.8 CONCLUSION

The overwhelming majority of early, syn- and late-tectonic Damaran intrusions in the Central Zone are granitic in composition. The late-orogenic suite in particular is dominated by leucogranites and pegmatites. Because of the composition of the associated granitoids, and partly because of the extensive erosion (approximately 10 km of the orogen has been eroded), no volcanic rocks have been identified in the aureole of any Damaran pluton in the CZ. The early and late orogenic granites are mildly peraluminous; those granites intruded at the peak of regional metamorphism are strongly peraluminous (Blaxland *et al.*, 1979; see chapter 6). All the granites examined, with the exception of some members of the Salem suite, can be classified as S-type granites. Leucogranites of all ages are more common in the NCZ than the SCZ which is characterised by granitic material in the cores and on the edges of reactivated basement domes and lithium pegmatites. Three rare-element pegmatite provinces can be distinguished in the CZ, namely the lithium pegmatite province of the Karibib area and the stanniferous pegmatites of the two tin belts in the NCZ (Fig. 3.1).

The granitoids of the NCZ do not have a calc-alkaline chemistry. Only the Salem granitoids could be considered to be part of a calc-alkaline suite, but active continental margin magmatic suites (Wilson, 1989) are not dominated by leucogranites and pegmatites in the manner of the CZ. All the granitoids examined, with the exception of the synmetamorphic peak intrusions, have trace element signatures which

Figure 3.4 (below): Nb-Y discriminant diagram - all NCZ granitoids



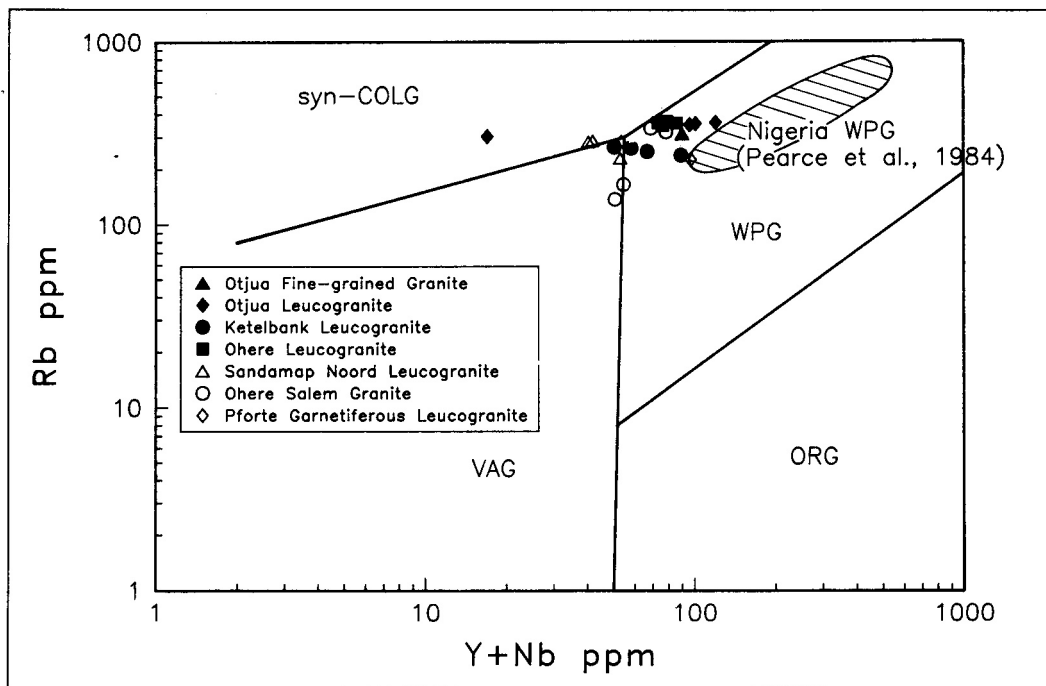


Figure 3.5: Rb-(Y+Nb) discriminant diagram - all NCZ granitoids

bear similarities with intraplate granites. In the CZ there is a complete lack of intrusion-hosted base and precious metal mineralisation similar to that developed in active continental-margin batholiths such as in the Circum-Pacific region. None of the Damaran granites in the area examined hosts any sulphide or cassiterite mineralisation. With the exception of the Stinkbank leucogranite, uranium mineralisation is restricted to pegmatites and alaskites. The relatively minor arsenic and bismuth deposits of the CZ are either hosted by, or concentrated near, late-tectonic pegmatites. Antimony and mercury deposits or showings are unknown in central Namibia. No precious metal mineralisation nor significant hydrothermal alteration of the type normally associated with gold mineralisation has been recorded in any of the Damaran granitic intrusions. The small degree of deuteric alteration in the Damaran granites is noteworthy and gives an indication of the anhydrous nature of the plutons. Moreover, Haack *et al.* (1983) noted that oxygen isotope fractionations between minerals in the CZ granites were normal, “especially no quartz-feldspar reversals were noted”, indicating very little interaction between meteoric water and felsic intrusions in the CZ. This lack of alteration, either deuteric or meteoric, is considered to be one of the prime reasons why there is an essential absence of granite-hosted mineralisation in central

Namibia.

Miller (1983a) and Kasch (1983a) have interpreted the Central Zone granitoids as the magmatic arc generated during the northward-directed subduction of the Kalahari Craton. Although some of the early intrusions, notably those of the unmineralised Salem Suite, do have an I-type chemistry (Miller, 1983a), there is little other evidence for the presence of a calc-alkaline magmatic arc at a plate boundary. These early intrusions were almost certainly responsible for a significant input of heat and triggered large-scale partial melting of the overlying continental crust. In the NCZ the majority of continental collision (570-530 Ma) and all the post-collision (530-460 Ma) intrusions have S-type chemistries and high  $(^{87}\text{Sr}/^{86}\text{Sr})_i$  and  $\delta^{18}\text{O}$  ratios. The CZ is floored by early Proterozoic basement that is essentially granitic in nature. Haack *et al.* (1983) concluded that the majority of CZ intrusions are crustal remelts. Isotopic data presented by Hawkesworth and Marlow (1983) indicate derivation of the uraniumiferous intrusions from crustal material. The author considers that the leucogranites in particular were generated by melting of the crust as a result of movement on major structural breaks such as the Omaruru and Tubussis Lineaments. These petrogenetic considerations will be discussed more fully once the new isotopic data has been presented in Chapter 6.

## 4. STRUCTURE

## 4.1 INTRODUCTION

The structure of the west-central portion of the CZ was investigated by Smith (1965) and Watson (1982) as part of their regional studies and a review has been given by Miller (1983a). An examination of the aeromagnetic signature of the western portion of the orogen and an interpretation of the regional structure has been conducted by Corner (1983). In the Damaran orogeny, two phases of isoclinal folding, during which some recumbent folds were formed, were followed

by the formation of northeast-trending  $F_3$  folds. These folds have been extensively modified by granite diapirs to form domal structures and have given rise to the distinctive outcrop pattern of the CZ. Miller (1983a) has mentioned three relatively minor phases of post- $D_3$  deformation. The Omaruru Lineament, which separates the SCZ from the NCZ, is clearly visible on the aeromagnetic composite of the orogen (Corner, 1983), but, near the Erongo Complex, is difficult to pinpoint in the field. Interpretation of this northern part of the SCZ (Fig. 4.1) is further complicated by the magnet-

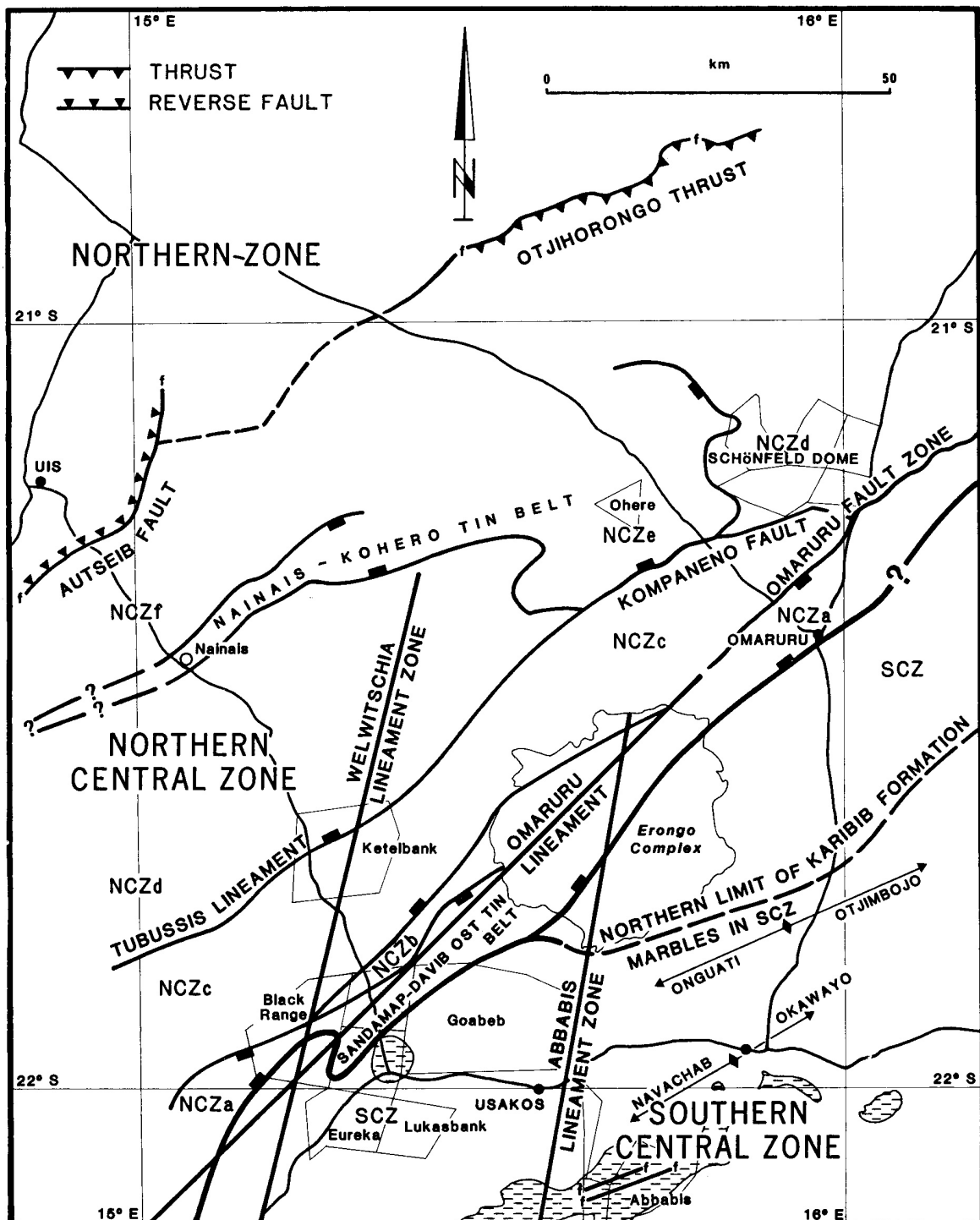


Figure 4.1: Localities referred to in Chapter 4

ic shadow of the Erongo Complex (Hartnady, 1991, pers. comm.). West of the Welwitschia lineament zone, the SCZ has a northeast-trending magnetic fabric; to the east the SCZ has an east-northeast-trending magnetic grain. The Omaruru Lineament probably marks the northern boundary of the Abbabis basement inlier and “constitutes a line of monoclinical downfolding of the stratigraphy to the north” (Corner, 1983). In the author’s opinion, the influence of the Omaruru Lineament on Damaran geology was almost as profound as that of the better known Okahandja Lineament (Miller, 1979). Structural styles change markedly across this structure. In the SCZ, the Damara Sequence is underlain by an inlier of granitic gneisses that, in the Karibib area, is believed to have behaved as a relatively rigid block during the Damaran orogeny. Consequently the lower portion of the Damara Sequence, comprising the mechanically competent Nosib Group quartzites and calc-silicate rocks, is not as intensely deformed as the carbonate units higher up in the sequence. The primarily dolomitic carbonates of the Karibib Formation in the SCZ appear to have a simpler, less complicated deformational history than their counterparts in the NCZ. Another characteristic feature of the SCZ is the presence of mantled gneiss domes which are absent north of the Omaruru Lineament. In the NCZ, which is not floored by relatively competent granite gneisses and arkoses (at least not at the presently exposed level), mechanically weaker (Heard, 1976) calcitic carbonate units and an overlying thick (up to 10 km) sequence of schists with differing mechanical properties have been multiply deformed in different manners. The degree of ductile deformation in the NCZ increases as one approaches the Omaruru Lineament. For example, phases of isoclinal and tight folding in the Sandamap-Davib Ost tin belt (NCZa; Fig. 4.1) distinguish this tectono-stratigraphic zone from the less intensely deformed, but compositionally similar, Nainais-Kohero tin belt (NCZe) further to the northwest (compare sections 4.3.1 and 4.3.3).

It is not the intention here exhaustively to review the structure of the CZ, but to highlight those features that have played a crucial role in localising epigenetic mineralisation in the CZ. Much of the mineralisation is developed in close proximity to late-tectonic intrusions and, because the former lacks a pervasive fabric, appears to be of late-Damaran age. Thus particular attention has been paid to the Damaran late-tectonic ( $D_3$  and  $D_4$ ) structures. The structural geology of the pre-Damaran basement has also been examined for two reasons. Firstly, basement reactivation was proposed by Kröner (1984) as having played a major role in the development of Damaran domal structures. Secondly, a discussion of the apparently epigenetic gold mineralisation in the Karibib Formation marbles of the SCZ would be meaningless without an appreciation of the underlying pre-Damaran lithologies, and at least a cursory investigation of the gold occurrences in the Abbabis basement. For this reason a portion of the Abbabis Inlier containing shear zone-hosted gold mineralisation was mapped, with particular emphasis on structural features. Four areas have been selected to illustrate the different styles of deformation in the CZ:

1) the Abbabis Complex in the SCZ on the farms Abbabis

70 and Narubis 67 (Figs. 2.1 and 4.1)

2) the Abbabis Complex and Damara Sequence across the Omaruru Lineament on the farms Sandamap Noord 115 (Map 3), Sandamap 64 (Map 4), Eureka 99 (Map 5) and Lukasbank (Map 6)

3) the middle Swakop Group in the Schönfeld dome in NCZd (Map 1)

4) the upper Swakop Group on the farm Ohere 106 in NCZe (Map 2).

The various deformational events ( $D_1$ - $D_n$ ), associated folding phases ( $F_1$ - $F_n$ ) and accompanying foliations ( $S_1$ - $S_n$ ) have been assigned following the conventions of Hobbs *et al.* (1976). Sedimentary layering is abbreviated by  $S_0$ . The subscript ‘A’ has been used to distinguish deformational events and fabrics in the Abbabis Inlier from those in the Damaran cover rocks. A summary of the structural control on the localisation of mineralisation is given in Chapter 8.

## 4.2 STRUCTURE OF THE ABBABIS COMPLEX ON THE FARMS ABBABIS AND NARUBIS

### 4.2.1 Introduction

The basement inlier on the farms Abbabis and Narubis (Fig. 4.1) comprises various granite gneisses with subordinate hornblende gneiss, quartz-feldspar-biotite-andalusite-garnet gneiss, biotite-sillimanite-garnet schist, quartzite and amphibolite (Fig. 2.1). This assemblage is now referred to as the Narubis Granitoid Complex and represents “intrusive rocks of granitic composition” (Brandt, 1987a). The granite gneisses (locally augen gneisses) possess a gneissic layering (as defined by Hobbs *et al.*, 1976) and, although rocks of this nature are not ideal for determining the deformational history of an area, the following has been elucidated. The granitoids were deformed by at least one phase of isoclinal folding ( $A_1F_1$ ), which probably formed the gneissic fabric, and an upright closed to tight folding phase ( $A_2F_2$ ).  $A_2F_2$  fold axes have a prominent accompanying lineation that plunges steeply southeast. The complex has subsequently been deformed by two relatively minor folding phases,  $A_3F_3$  and  $A_4F_4$ . These last two phases are characterised by relatively open, upright folds that plunge steeply southwards and to the northeast respectively. The  $A_3F_3$  folds commonly have veinlets of undeformed pegmatitic material intruded parallel to their axial planes. The comparatively rare  $A_4F_4$  folds possess a vertical axial-planar fracture cleavage and may be of Damaran age. Several minor deformed pegmatite layers within isoclinally folded granite gneiss suggest that granulite facies metamorphism with associated partial melting accompanied the early phases of deformation.

### 4.2.2 Megashear Zones

The Narubis Granitoid Complex is transected by a number of subvertical east-northeast-trending auriferous (determined by fire assay) megashear zones that show evidence for significant lateral displacement (Fig. 2.1). Final significant strike-slip movement on these major fractures is thought to have occurred prior to 900 Ma because the spa-

tially associated, but undeformed mafic dykes are thought to have intruded contemporaneously with the rifting that initiated the Damaran episode (see discussion below). Shear zones form topographic ridges, up to several tens of metres wide, and have a “pinch and swell” (anastomosing) outcrop pattern which is believed to arise from the stacking of faulted slices within duplexes. Recrystallised siliceous cataclases comprise quartz (65-95%), plagioclase (0-20%), magnetite (2-10%), chalcopryrite (0-3%) and traces of biotite, muscovite and zircon. Minerals are arranged in a polygonal granular mosaic, a recrystallised fabric that may have developed during the Damaran orogeny. In the vicinity of the megashear zones, the predominantly north-northwest-striking foliation of the gneisses has been rotated and crenulated. Porphyroclasts of gneiss are common within mylonitic zones. A localisation of sheared pink pegmatitic rocks of quartzo-feldspathic composition near these shears suggests that movement on these zones induced small-scale partial melting of the granite gneisses. There is evidence for considerable lateral displacement on the shear zones, but determination of the direction of movement on these structures has proved problematic. Intrafolial folds (commonly non-cylindrical) within the shears generally, but not exclusively, indicate sinistral displacement. However, mylonitic fabrics within the main shear zone strike  $090^\circ$ , that is between  $10^\circ$  to  $25^\circ$  to the southeast of the shear zone. These may represent Riedel shears and, if so, indicate dextral displacement on the main structure. The series of east-northeast-striking shears on the Narubis/Abbabis boundary (bottom centre of Fig. 2.1) probably represents a contractional duplex (Woodcock and Fischer, 1986).

#### 4.2.3 Structural control on the emplacement of (Gannakouriep?) metadolerites

The megashears probably extend to the base of the earth's crust and have exerted a strong control on the orientation of the metadolerite dyke swarm. The fact that some of the dykes are foliated and some not suggests either the tapping of mantle magmas over a long period of time (the foliated ones perhaps being contemporaneous with final movements on the shear zones) or alternatively the local development of a Damaran fabric. The majority of the dykes are subvertical, but there are conjugate sets dipping  $60^\circ$  north-northwest and  $60^\circ$  south-southeast. If these dykes have occupied a conjugate set of fractures, then  $\sigma_1$  was vertical and  $\sigma_3$ , oriented north-northwest/south-southeast, was horizontal. This brittle failure of the Abbabis basement in an extensional stress field probably occurred as a result of rifting in pre-Nosib/Nosib times. The shear zones and the metadolerite dyke swarm in particular are almost certainly responsible for the east-northeast-trending magnetic grain of the Abbabis Inlier.

#### 4.2.4 Structural control on emplacement of Damaran pegmatites and Karoo dykes

Undeformed, probably late-Damaran, muscovite pegmatite dykes and sills with minor concentrations of beryl and columbite crosscut all other lithologies and the megashear

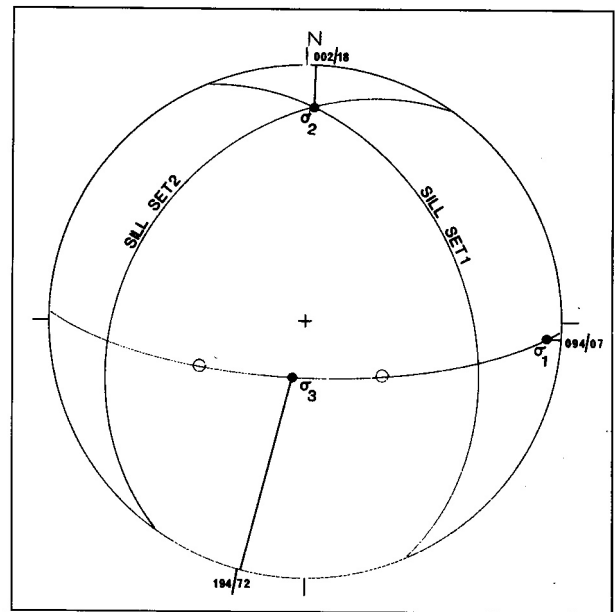


**Figure 4.2:** Conjugate pegmatite sills in the Abbabis Inlier and the theoretical stress field under which similarly oriented fractures would develop

zones (Fig. 2.1). Shallowly dipping sills predominate over dykes and possess a prominent igneous banding. The majority of pegmatite sills strike northerly and dip at a shallow angle ( $5^\circ$ - $30^\circ$ ) to the west (the mountainous terrain gives rise to the outcrop pattern). In the northwest corner of Abbabis, sills are arranged in conjugate sets, the one set oriented  $157^\circ/37^\circ$  east and the other  $035^\circ/35^\circ$  west (Fig. 4.2). The theoretical compressional stress field under which similarly oriented fractures would develop has an essentially horizontal  $\sigma_1$  ( $094^\circ/7^\circ$ ), a shallowly plunging  $\sigma_2$  ( $002^\circ/18^\circ$ ) that lies almost in the plane of the Abbabis lineament zone, and an essentially vertical  $\sigma_3$  ( $194^\circ/72^\circ$ ). This is interesting because the Damaran  $F_4$  fold structures of the SCZ developed in a similar stress field (see section 4.3.1.4) and suggests contemporaneous brittle deformation of the Abbabis basement. Moreover, north-northeast-trending structures such as the Welwitschia and Abbabis lineament zones (Fig. 4.1) were envisaged by Corner (1983) to have played an important role in the emplacement of late-tectonic (syn- $F_4$ ) pegmatites. This most certainly seems to be the case on the farms Narubis and Abbabis, situated within 10 km of the Abbabis lineament zone. A small number of vertical east-northeast-trending pegmatite dykes have intruded parallel to, and locally crosscut, the megashear zones. Immediately west of the Narubis-Abbabis fence, pegmatite dykes appear to be arranged *en echelon*. These pegmatitic dykes may have been emplaced in extensional fractures that formed as a result of minor dextral movement on the megashear zones during late Damaran times. It is quite probable that this minor reactivation of the megashear zones occurred as a result of the Damaran west-northwest-directed compression which controlled sill emplacement. The pegmatites are locally crosscut by auriferous (determined by fire assay) chalcopryrite-bearing quartz veins. In Karoo times several east-northeast-trending dolerite dykes were intruded parallel to the megashears (Fig. 2.1).

#### 4.2.5 The significance of sheared early Proterozoic rocks underlying the Damara Sequence of the SCZ

The previously unknown auriferous megashear zones, which parallel the long axis of the Abbabis Inlier, are important for a number of reasons. Firstly, these megashears are developed over a distance of at least 6 km across strike. Photogeological interpretation indicates that they are developed in the southern portion of the farm Navachab 58. Thus a substantial portion of the Abbabis Inlier is transected by such structures. Secondly, in the region of these shears have evidently been zones of crustal weakness from the Proterozoic until Karoo times and, of most relevance to this investigation, during the latter stages of the Damaran orogeny. Thirdly, Corner (1983) suggested, on the basis of aeromagnetic evidence, that the northern edge of the Abbabis geanticlinal ridge was marked by a zone of monoclinical downfolding of Damaran sediments to the north. This downfolding may well have occurred because of reactivation of these east-northeast-trending basement megashears. Fourthly, similar east-north east-trending auriferous megashear zones transect 1.7 to 2.0 Ga (Burger *et al.*, 1976) basement gneisses in the Kamanjab Inlier (Fig. 2.2; for example at the Huab River Gold Prospect on the farm Mesopotamie 504). Weber *et al.* (1983) recorded sinistral movement on these megashear zones. In contrast to the CZ, the Kamanjab Inlier, located on the northern margin of the Damara Orogen, is surrounded by Damaran lithologies that have a relatively simple deformational history and have undergone greenschist facies metamorphism. The megashears in the Kamanjab Inlier have not been sealed by subsequent tectonism and the circulation of ground waters has resulted in substantial accumulations of gold at the present-day erosional level. Gold mineralisation is also known from the pre-Damara basement inliers of the Southern Margin Zone of the Damara Orogen (Fig. 2.2). This suggests a contemporaneous pre-Damara gold mineralising event within the Proterozoic inliers that floor the continental branch of the Damara. Fifthly, the Navachab-Okawayo and the Onguati-Otjimbojo anticlines (Fig. 4.1) have long axes trending east-northeast. Gold skarn mineralisation is essentially restricted to carbonate units in the core of these structures. The geophysical evidence (Corner, 1983) suggests that this northern portion of the SCZ is also underlain by Abbabis Inlier lithologies. There is considered to be enough evidence to suggest that these gneisses on the northern boundary of the SCZ have also been cut by east-northeast-trending (auriferous?) megashears which:

1) provided access for the magma which formed the Daheim Member alkaline lavas and pyroclastics rocks. These continental volcanic rocks are considered to have been extruded along east-northeast-trending rifts (Pirajno, 1988, pers. comm.). There is a possibility that the mafic dyke swarm on Abbabis/Narubis is younger than Gannakouriep age and was the feeder zone for the Daheim Member volcanic rocks;

2) provided access for hydrothermal auriferous fluids. This would explain the close association between gold skarn mineralisation and the anticlinal structures. More specifically, the damming up of hydrothermal fluids by a

relatively thin skin of overlying Karibib Formation over a deep-seated fracture zone would account for the approximately 50-km-long, linear, east-northeast-trending zone of gold-bismuth-arsenic skarn mineralisation between Onguati and Otjimbojo (Fig. 4.1);

3) provided access/focal points for the lithium-beryl pegmatites of the Karibib area.

It can be concluded that an understanding of the structure of the Abbabis basement is essential for locating gold mineralisation in the Damaran cover rocks. The idea that major fractures within the basement acted as important access/focusing points for hydrothermal fluids during the Damaran orogeny will be expanded upon in Chapter 8.

### 4.3 DAMARAN DEFORMATION - INTRODUCTORY COMMENTS

The most recent synthesis of the structural history of the CZ has been provided by Kröner (1984) who recognised four main deformation phases. Although largely based on work conducted in the SCZ to the southwest of Eureka (Fig. 4.1) near the Rössing Uranium Mine, this summary holds true for most of the field area, with the exception of NCZe. Because of the flat topography, evidence for the first two deformational events is commonly scanty within the field area (cf. the mountainous terrain in the vicinity of the Rössing Uranium Mine; Kröner, 1984).

1)  $D_1$  deformation produced large-scale, recumbent  $F_1$  folds and thrusts,

2)  $D_2$  deformation, the most intense phase, caused isoclinal  $F_2$  folds, prominent elongate mineral lineations and formed the regional, bedding-parallel fabric. The peak of regional metamorphism occurred syn- $D_2$  at ~520 Ma (Haack *et al.*, 1980).

3)  $D_3$  deformation generated large-scale, open to tight  $F_3$  folds with upright axial planes. These  $F_3$  folds commonly have a northeasterly-plunging mineral lineation. Diapiric rise of granite intrusions into  $F_3$  antiforms and synforms resulted in the formation of the elliptical  $D_3$  domes (elongate northeastward). On the basis of geochronological evidence, Kröner contended that  $D_3$  domes formed in the period 510-460 Ma ( $F_3$  folding in the NCZ occurred ~480-460 Ma; Haack *et al.*, 1980).

4)  $D_4$  deformation produced two distinct orientations in different areas: open northwest-trending folds that are usually represented by kink bands (Kröner, 1984) and a north-northeast-striking foliation (Jacob, 1974). In certain areas, notably the immediate vicinity of major structural breaks such as the north-north east-trending Welwitschia Lineament Zone,  $D_4$  deformation is characterised by reclined, almost flat-lying folds and a prominent east-southeast-plunging mineral lineation.

#### 4.3.1 Damaran deformation across the Omaruru Lineament west of Usakos

##### 4.3.1.1 Introduction

The structure of a section across the Omaruru Lineament extending from Sandamap Noord in the north to

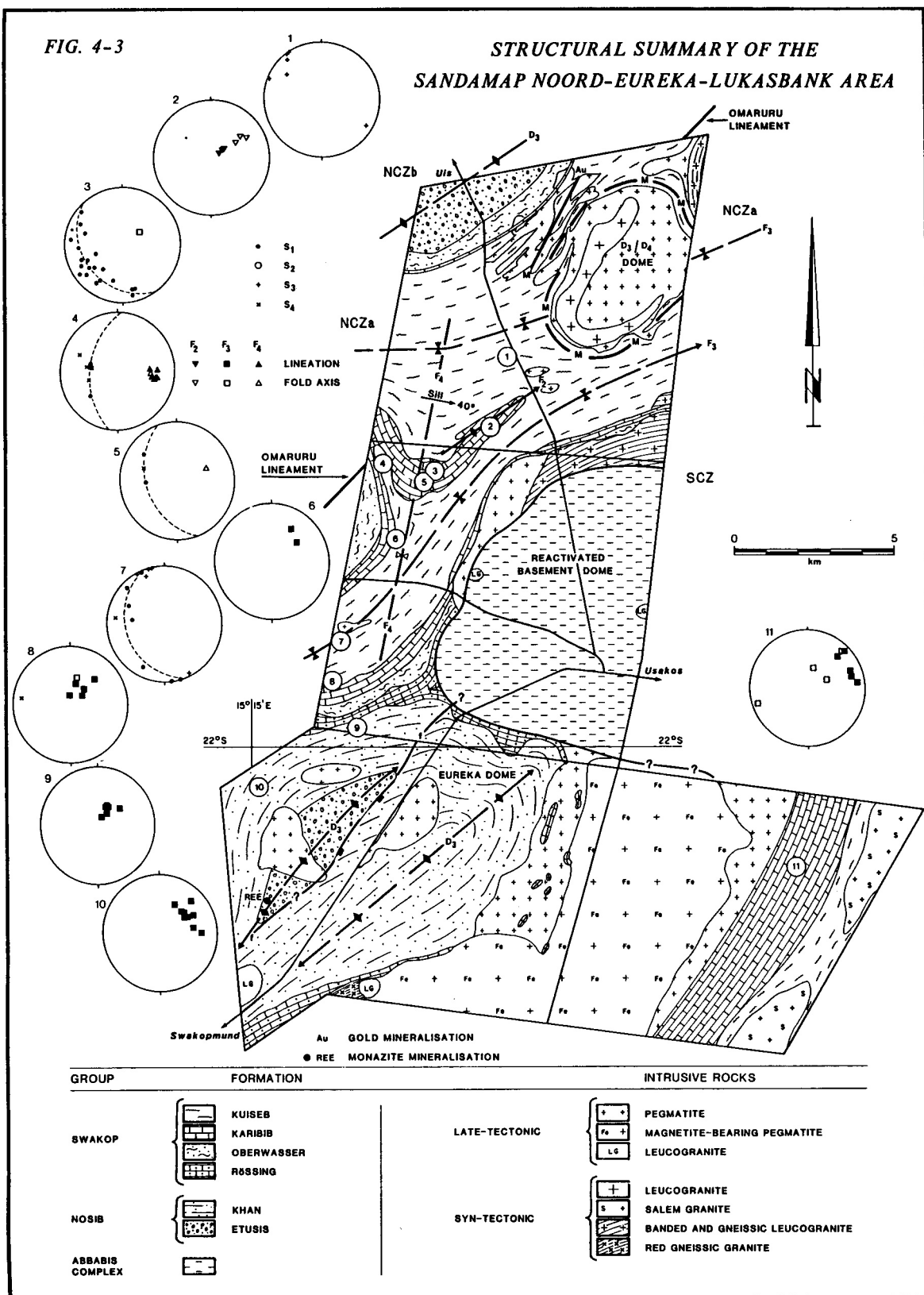


Figure 4.3: Structural summary of the Sandamap Noord—Eureka—Lukasbank area

Eureka in the south (Figs. 4.1 and 4.3) will now be examined. Multiply deformed rocks correlated with the Abbabis Complex lithologies are poorly exposed in a basement inlier on Sandamap (Map 4). Rocks of the Damara Sequence in this portion of the CZ were affected by three major ( $D_1$ - $D_3$ ) and at least one minor deformational phase ( $D_4$ ) during the Damaran orogeny. The overall northeasterly trending struc-

tural grain of the area is apparent from Smith's (1965) and Watson's (1982) regional mapping, with the  $D_3$  deformation and the concomitant granite intrusion being responsible for the oval to elongate domal structures (Miller, 1983a). Younging directions in the Sandamap-Eureka area are difficult to determine and it must be emphasised that the stratigraphic sequence has largely been derived from regional correla-

tions. In the Damaran metasediments there are few way-up indicators and interpretational problems are compounded by the two-dimensional exposure in the area. Further complications in interpreting the Damaran tectonism are caused by the fact that the basement inlier on Sandamap is probably a reactivated basement dome (the best explanation for the trifurcation of the Rössing Formation marbles; Map 4), though the inlier may have behaved as a rigid block during the latter phases of Damaran deformation. Moreover, there are large competency contrasts (and hence deformational characteristics) between the three groups of metasediment, namely the quartzites, calc-silicate rocks and dolomites of the Nosib and lower/middle Swakop Groups, the calcitic carbonates of the middle Swakop Group and the metapelites of the upper Swakop Group. Finally, there is a major problem in identifying different fabric generations in a multiply deformed schistose sequence. However, the Sandamap-Eureka section is one of the best areas to see the various styles of deformation of the Damara Sequence across a major tectonic boundary. Because of the limited number of structural features of interest in the lower part of the sequence, this investigation focuses on the Karibib and Kuiseb Formations.

#### 4.3.1.2 $D_1$ and $D_2$ Structures

Nosib Group rocks with an apparently simple deformation history almost universally occupy the cores of structural domes, while multiply deformed Kuiseb Formation schists lie in structural basins. The metasediments possess a planar fabric ( $S_1$ ), which can be seen to be essentially bedding-parallel in all lithologies except the schists, where bedding is very rarely preserved. The  $S_1$  fabric is represented by a mineral foliation or locally a segregation, which tends to wrap around domal structures. Throughout the Sandamap Noord-Eureka area, fold closures have only locally been observed in the Karibib and Kuiseb Formations and are quite possibly not present in the lower portions of the Damara Sequence. Isoclinal folds, interpreted as the first folding phase ( $F_1$ ) are present within the calcitic Karibib Formation marbles. To the southwest of the Sandamap Tin Mine the Karibib Marbles have been further deformed by upright, tight  $F_2$  folds, whose axes and associated lineations plunge steeply and consistently on a bearing  $058^\circ$  (Fig. 4.3, Stereo. 2). These latter folds are interpreted as being  $F_2$  closures because of the presence of poorly exposed  $F_1$  isoclinal folds with much shorter wavelengths in the Kuiseb Formation to the west. The  $F_2$  fold on Sandamap Noord is of particular interest because of the development of tourmalinites in the core of the structure (see Map 3 and discussion in Chapter 7.6).

Thus, in the Sandamap-Eureka area, one isoclinal and one tight folding phase are recognised, which may belong to one isoclinal, deformational event. This contradicts Miller's (1983a, p.459) contention that  $F_1$  and  $F_2$  were isoclinal. No evidence for recumbent folding (as suggested by Miller, 1983a) could be found. The sequence below the Karibib Formation is rarely overturned and, where so, dips steeply, for example on the south of Eureka (Map 5). This localised overturning is related to the development of the  $D_3$  Eureka dome. Throughout the field area, the  $S_1$  fabric is essentially

steeply dipping or vertical. Flat-lying duplications of the sequence are confined to  $F_4$  structures. However, it must be emphasised that the rarity of preserved early fold closures, the transposition of foliations by subsequent deformation phases, the abundant granite intrusions and the two-dimensional exposure combine to obscure the early deformational history.

#### 4.3.1.3 $D_3$ Structures

The  $D_3$  deformation is characterised by the development of large-scale northeast-trending  $F_3$  antiforms and synforms with upright axial planes and good examples are exposed on Sandamap and Sandamap Noord (Fig. 4.3). A northeasterly plunging mineral lineation commonly accompanies these folds. Granite intrusions have disturbed the  $F_3$  folds and thus comments are confined to the metasediments at some distance from the intrusions.  $F_3$  folds are more open and have significantly longer wavelengths than the tighter  $F_2$  folds. The best example of a northeast/east-north east-plunging  $F_3$  fold is exposed in the western portion of Sandamap in the vicinity of the Cilliers Workings (Map 4 and Stereo. 7). A prominent, east-northeast-trending, axial-planar  $S_3$  schistosity is developed in the Kuiseb Formation near the hinge zone of this fold.

An  $S_3$  fabric, a pervasive schistosity, is developed in the Kuiseb Formation schists in the west-central portion of Sandamap Noord (Map 3). This subvertical fabric strikes between  $023^\circ$  and  $060^\circ$  (Stereo. 1), consistently  $10^\circ$ - $30^\circ$  to the north of  $S_1$  in this area. The intersection lineation between this  $S_3$  foliation and the more pronounced  $S_1$  plunges almost vertically, lending a characteristic 'pencil-shaped' weathering to the schists in the area. Another example of a northeast-plunging  $F_3$  fold is present near Hill 1166 on Sandamap (Stereo. 3). The large spread of  $S_1$  around the great circle indicates that this is a relatively open, upright fold in contrast to the  $F_2$  folds. The majority of lineations within the Sandamap-Eureka area plunge at  $40^\circ$ - $70^\circ$  to the northeast or east-northeast and are considered to be  $D_3$  in age. Examples from the calc-silicate rocks of the Khan Formation in the core of the Eureka Dome, where no fold axes are visible, are shown in Stereo 10. Comparison of Stereos 1, 3, 7 and 10 indicates that a  $D_3$  age for the lineations of the more competent lithologies of the Damara Sequence is likely. This is of interest because one of the most characteristic features of the CZ is the presence of a moderately to steeply northeast/east-northeast-plunging lineation in the calc-silicate rocks and more quartzitic lithologies;

The  $F_3$  folds have been modified by domal structures cored by granite (Sandamap Noord) or pegmatite (Eureka) or both or reactivated basement (Sandamap; Fig. 4.3). These  $D_3$  domes have an elliptical outcrop pattern, elongate northeast. Because the leucogranite-cored dome on Sandamap Noord is elongate north-northeast, it is assigned a slightly younger,  $D_3/D_4$  age (see below). A mineral lineation commonly plunges down the surface of these domes (see southern side of domal structure on Sandamap Noord, Map 3). In the author's opinion, there is no evidence in the Sandamap Noord-Eureka area for the derivation of domal structures by cross-folding as suggested by Smith (1965).

The domes appear to be the result of diapiric rise of granite and reactivated basement. Of the three domes shown in Fig. 4.3, overturning of the stratigraphy, which may be related to ballooning during diapirism (Talbot, 1977), is confined to the southern side of the Eureka Dome (Map 5). As far as can be ascertained,  $D_3$  doming postdated  $F_3$  folding.

#### 4.3.1.4 $D_4$ Structures

A fourth folding phase has been recognised in a zone that extends from the southwest corner of Sandamap to the northern part of Sandamap Noord (Fig. 4.3). The style of deformation along the axial trace of this north-northeast-trending  $F_4$  structure varies from in the south, where fold axes plunge steeply north-northeast and the axial plane dips steeply eastward, to the Sandamap/Sandamap Noord boundary where the fold is essentially reclined, the axial plane dipping shallowly eastwards. Mylonitic structures intimately associated with gold mineralisation in the northern portion of Sandamap Noord possibly developed as a result of  $D_4$  deformation. The zone will now be examined from south to north (Fig. 4-3).

At the Cilliers Workings (Map 4), the Kuiseb Formation schists possess a spaced, locally pervasive, fracture cleavage ( $S_4$ ). This  $F_4$  fabric strikes north-northeast and dips steeply eastwards (Stereo. 8). Immediately north of the Sandamap-Eureka fence, near the  $F_4$  hinge zone, lineations in the Khan Formation, thought to be of  $F_3$  age, plunge steeply north-northeast (Stereo. 9). Thus  $F_3$  structures appear to have been rotated by the  $F_4$  deformation. One kilometre north of the Henties Bay - Usakos road, lineations in the Oberwasser and Kuiseb Formations plunge moderately to the northeast (Stereo. 6). Further north, at Hill 1166, both limbs of closed, reclined  $F_4$  folds dip moderately eastwards, while the fold axis plunges east-northeast (Stereo. 5). Thus  $F_4$  folds verge northwestwards. In the northwest corner of Sandamap, the fold axes of reclined  $F_4$  folds plunge eastwards (Stereo. 4). These folds locally possess an axial-planar,  $S_4$  foliation. A very prominent sillimanite lineation developed here and in the southwest of Sandamap Noord (Map 3) plunges shallowly on a bearing of approximately 1000, parallel to the  $F_4$  fold axis. Prominent sillimanite lineations are confined to the Kuiseb Formation in the core of this  $F_4$  structure suggesting a thermal event at the time of its development. This localised tectonothermal event was possibly associated with the younger granite and pegmatite intrusions (see discussion in Chapter 5).

Continuing the traverse northwards, the Kuiseb Formation schists in the west-central part of Sandamap Noord possess the previously described  $S_3$  foliation. The main reason for ascribing this to a  $D_3$  rather than a  $D_4$  event is its northeasterly, rather than north-northeast, orientation and subvertical attitude (Stereo. 1). In the north of Sandamap Noord late-tectonic mylonitic structures have sheared aluminous schists and metaturbidites of the Kuiseb Formation. The intrusion of late-tectonic pegmatites into a metaturbidite sequence has resulted in the development of high strain zones in schists that are concentrically arranged around the  $D_3/D_4$  domal structure (Map 3). However, a 2500-metre-long north-northeast-trending, eastward dipping ( $50-80^\circ$ )

zone of Au-As-W mineralisation is located in an area of particularly intense mylonite development on the north-west side of the dome. Moreover, mylonite zones that cut late-tectonic pegmatites are only present on the northwest side of the dome and are thus thought to be younger ( $D_4$ ) than the concentrically arranged mylonites. The nature of these mylonitic structures is discussed in detail in Chapter 5. The change in style and increase in intensity of  $F_4$  deformation across the Omaruru Lineament is believed to result from uneven, scissor-like displacement along the fold hinge. This occurred because of the different mechanical properties of the Nosib and lower Swakop Groups on the one hand and the upper Swakop group on the other. Westward-directed compression resulted in the development of reclined folds in the relatively ductile Karibib Formation marbles and Kuiseb Formation schists. Further north, in an area of higher strain,  $F_4$  deformation sheared out the Kuiseb Formation resulting in the development of mylonitic structures. At the south end of the  $F_4$  structure, closer to the core of the Eureka dome, deformation of the more quartzitic metasediments of the lower Swakop Group merely resulted in local reorientation of  $F_3$  lineations.

#### 4.3.1.5 Summary of the regional distribution and importance of $D_4$ structures

Northwestward-verging, late-tectonic  $F_4$  folds with north-northeast-trending axial traces are common on Sandamap and Sandamap Noord, but on a regional basis are localised in the vicinity of the north-northeast-trending Welwitschia lineament zone (Fig. 4.1). Jacob (1974) recorded the local presence of upright  $F_4$  structures with predominantly north-northeast-striking axial planes in the southern SCZ near Langer Heinrich. Watson (1982) mapped a number of Damaran-age northerly and north-northeast-trending faults in the calc-silicate rocks and marbles of the middle Swakop Group on Black Range and Goabeb (to the west and east of Sandamap respectively; Fig. 4.1). This suggests that late-tectonic ( $D_4$ ) ductile and brittle deformation, controlled to a large extent by the mechanical properties of the various lithologies, occurred contemporaneously on the northern margin of the SCZ. Gold mineralisation on Sandamap Noord is hosted by quartz veins associated with mylonitic rocks that parallel a north-northeast-trending late-tectonic shear structure which is interpreted as being of  $D_4$  age. Poor exposure precludes an assessment as to whether these structures actually host gold mineralisation or whether the relationship is coincidental. Some of the high strain zones surrounding the domal structure on Sandamap Noord formed during intrusion of the granites and pegmatites and are thus unrelated to the regional tectonism, but only the north-northeast-trending portions are mineralised. The Sandamap Noord shear zone parallels and lies within 10 km of the Welwitschia lineament zone which was considered by Corner (1983) to have been important in the localisation of late/post-tectonic uraniferous pegmatites such as are developed at the Rössing Uranium Mine. The discussion in Chapter 7.5 will show that late-tectonic pegmatites are thought to have played a key role in the concentration of gold mineralisation as well. One final point of note is that, in the vicinity of the Welwitschia lineament zone, an ap-

proximately 25-km-wide north-northeast-trending Karoo dolerite dyke swarm that extends from south of the Rössing Uranium Mine (Fig. 2.3) to Ketelbank (Fig. 4.1) in the north occupies deep-seated (early Proterozoic?) fractures that were reactivated during the Damaran  $D_4$  deformational phase.

4.3.2 Damaran deformation of the middle Swakop Group in NCZd

Because of the relatively poor exposure of schists in this area, the following description of Damaran deformation in NCZd is based largely on the study of 29 drillcores from the Otjua Tungsten Prospect (Steven, 1987). At this locality, situated on the southern side of the Schönfeld Dome (Map 1), the metasedimentary sequence is slightly overturned, strikes  $103^\circ$  and dips  $75^\circ$ - $85^\circ$  northwards. Although Steven (1987) states that "way-up structures are inconclusive", re-examination of the sequence by Badenhorst (1989, pers. comm.) has indeed indicated that the sequence youngs southwards. Metasediments possess a well-developed foliation,  $S_1$ , defined by biotite or hornblende, which is parallel to lithological contacts. Throughout the Schönfeld Dome area there is an absence of small- and medium-scale folds and there is very little direct evidence for two early phases of isoclinal or recumbent folding as suggested by Miller (1983a). The  $S_1$  fabric may have developed during an isoclinal  $F_1$  folding phase, but this cannot be proved. Three examples of very minor folds observed in biotite schist in drillcore may have resulted from soft-sediment deformation and be unrelated to the tectonism. Examination of a borehole core from the vicinity of the Epako Gold Prospect (Map 1) reveals the presence of one bedding-parallel schistosity,  $S_1$ . Kuyper (1984) contended that an  $S_2$  foliation is locally developed in the vicinity of the Schönfeld Dome, but, in the author's opinion, it is extremely localised.

The duplication of the sequence on Okongue at the western end of the Schönfeld Dome (Map 1) occurred as a result of the granite and pegmatite intrusion that accompanied the  $D_3$  deformation. Kuyper (1984) noted that small-scale structures in the Karibib Formation bear little relation to the overall structural pattern and considered decollement at the base of the carbonates to have been responsible for shearing out of synforms.  $D_3$  deformation and, more importantly, the large number of granite intrusions, have resulted in the formation of the elongate east-northeast-trending Schönfeld Dome. This dome has a long-axis of approximately 40 km and its axial plane dips steeply northwards. On the farms Tjirundo and Epako (Map 1)  $D_3$  deformation of the Karibib Formation carbonates has resulted in the development of doubly plunging domes and basins whose long axes strike east-northeast and whose axial planes are subvertical. At Otjua, calc-silicate rocks of the Spes Bona and Oberwasser Formations possess a prominent lineation that plunges  $68^\circ$ - $75^\circ$  on a bearing  $063^\circ$ , parallel to the  $D_3$  structures of Kröner (1984). This lineation is approximately parallel to the axes of minor, tight z-folds thought to be of  $D_3$  age.

Of particular interest in the Schönfeld Dome area is late-tectonic, semi-brittle deformation associated with lateral

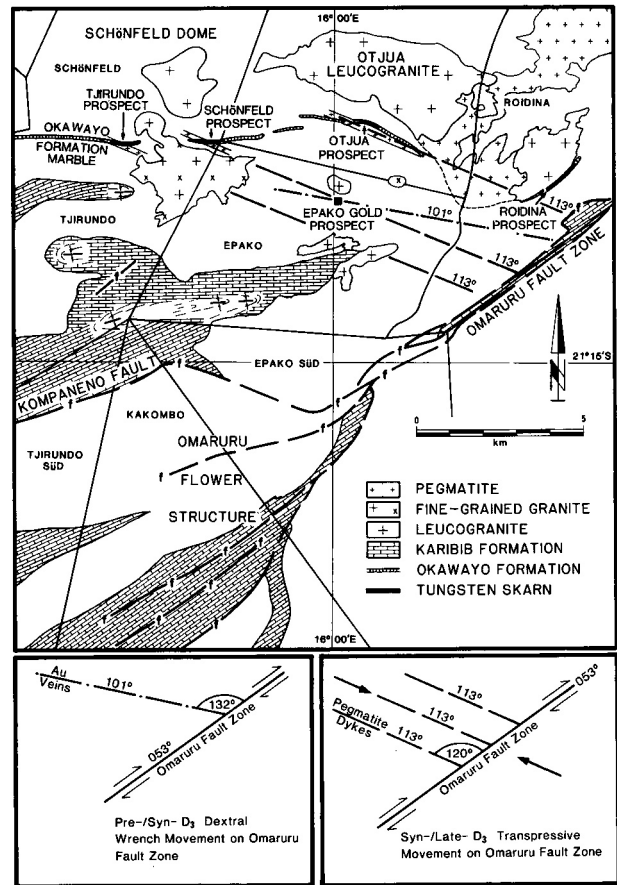


Figure 4.4: The relationship between dextral movement on the Omaruru fault zone, granitic intrusion and mineralisation in the Schönfeld Dome

displacement on the Omaruru Fault Zone and the subsequent development of the Omaruru flower structure. This probably occurred syn- to post- $D_3$ . Dextral motion on the Omaruru Lineament was believed by Steven (1987) to have played a key role in controlling the emplacement of late-tectonic granite, pegmatite dykes and associated tungsten skarn mineralisation at the Tjirundo, Schönfeld and Otjua Tungsten Prospects (Map 1) and the evidence for this will now be re-examined. The Schönfeld Dome is intruded by several types of granite including a late-tectonic, undeformed, fine-grained variety which crops out on southern Schönfeld, Tjirundo and Epako (Fig. 4.4). Where this granite transects the calc-silicate-rich formations of the middle Swakop Group, such as in the southeast corner of Schönfeld and the northeast corner of Tjirundo, this granite is confined to a series of east-southeast-trending dykes. Within these dykes this fine-grained granite is strongly foliated and most of the felsic minerals are fractured and show signs of having been strained. Pegmatites, thought to be derived from the leucogranites in the core of the Schönfeld Dome, have intruded the middle Swakop Group metasediments in a lit-par-lit manner. However, crosscutting portions of these subvertical pegmatites with a remarkably consistent orientation of  $113^\circ$  (east-northeast) are intimately associated with tungsten replacement skarns at Tjirundo, Schönfeld and Otjua and, significantly, are absent from those portions of the stratigraphy that are not skarned. Moreover, crosscutting pegmatites are confined to areas where the metasediments

strike between 090° and 105°. The above led Steven (1987) to suspect a large-scale tectonic control on the localisation of late-tectonic intrusions and associated mineralisation in the Schönfeld Dome. Noting that east-northeast-trending granite and pegmatite dykes lie at 60° to the Omaruru Fault Zone (Fig. 4.4), Steven (1987) suggested that dextral movement on this structure led to the formation of a series of zones of extension that became loci for granitic and pegmatitic intrusions. A review of the Riedel shears, faults and thrusts developed by strike-slip systems in sandbox experiments (Coward, 1990) shows that tensile fractures tend to develop at approximately 135° to the shear zone, parallel to <11 and perpendicular to 0'3. The fact that the felsic intrusions of the Schönfeld Dome lie at 120°, rather than 135° (Fig. 4.4), to the Omaruru Lineament suggests that transpressive forces directed from the northwest and southeast (probably related to D<sub>3</sub> doming as a result of granite intrusion) operated contemporaneously with the lateral displacement and thus rotated 0'1 and 0'3 in a clockwise direction.

Other evidence for the late-tectonic control on the localisation of mineralisation in NCZd comes from the Epako Gold Prospect. Late-Damaran auriferous quartz veins on average strike 101° and dip northwards at 70°–80°. The location of quartz veins, possibly in tensile fractures, is also attributed to dextral movement on the Omaruru Lineament. The fact that these auriferous veins lie at 135° to the major structure may suggest a pre-transpressive age of emplacement, i.e. pre- to syn-D<sub>3</sub> age. These ideas on the tectonic controls exerted on the localisation of mineralisation will be expanded upon in Chapter 8. One final feature of late-Damaran tectonism in NCZd is present at the intersection between the Omaruru Fault Zone and the Kompaneno Fault (Fig. 4.4) on Kakombo and Epako Süd. Intense shearing, brecciation and alteration, virtually unknown in Damaran rocks elsewhere in the CZ, are developed in metasomatised middle Swakop Group calc-silicate rocks. The riebeckite-bearing calc-silicate rocks (Thatcher, 1985, pers. comm.) are sheared, have a pink colouration due to iron staining, are cut by an anastomosing network of carbonate veins and contain minor fluorite in ferruginous vugs.

### 4.3.3 Damaran deformation of the upper Kuiseb Formation in NCZe

#### 4.3.3.1 Introduction

There is a marked reduction in deformational intensity and metamorphic grade on the northern side of the Tubussis Lineament-Kompaneno Fault (Fig. 4.1) in NCZe. This tectono-stratigraphic zone is bounded in the east by an inferred syn-sedimentary fault (Map 1: this is considered to be the best explanation for the sudden transition from carbonate sedimentation in Karibib times to the Kuiseb turbidite sedimentation) and the Tubussis Lineament in the south. Final movement on the latter structure, which has resulted in the juxtaposition of amphibolite and greenschist facies rocks in a similar manner to the Otjijhorongo Thrust (Fig. 4.1), may have resulted from the thrusting of NCZc over NCZe, possibly in Karoo times (see Cruickshank [1977] for it

discussion on Triassic and possible Jurassic movement on the Waterberg Thrust, the strike extension of the Tubussis Lineament). Because of the less intense tectonic history of NCZe, which contains sediments from the uppermost part of the Damara Sequence and is furthest from the Omaruru Lineament, deformational events cannot be correlated with the D<sub>1</sub>–D<sub>4</sub> phases of Kröner (1984). Folding phases discussed below do not correspond with phases described elsewhere in the field area.

The deformational characteristics of the Kuiseb Formation have been investigated on the farm Ohere 106 in NCZe (Fig. 4.1 and Map 2). The farm lies at the northeast end of the Nainais-Kohero tin belt, an east-northeast-trending graben structure filled with turbiditic sediments of the upper Kuiseb Formation. The metasedimentary sequence comprises phyllites, metaturbidites and biotite schists with subordinate calc-silicate rocks, unusual scheelite-vesuvianite skarnoid rocks, marble and very minor metasedimentary amphibolite. Sedimentary layering is defined by crossbedding in the more quartzitic components of the metaturbidites. Bouma sequences are well developed and fining-upward cycles, load structures, scoured bases and rip-up clasts have been identified. The best example of massive quartzites interpreted to represent proximal turbidites can be seen at Hill 1265 (Map 2). Younging directions are, however, frequently equivocal. Contradictory facing directions in the metaturbidites indicate local duplication of the sequence. The metasediments have undergone several phases of ductile deformation, greenschist-lower amphibolite facies metamorphism and have been intruded by late-tectonic granitic intrusions and stanniferous pegmatites. Four phases of folding have been identified on the farm, at least two of which are related to the intrusion of the granitoids.

#### 4.3.3.2 Regional deformation - F<sub>1</sub> structures

Throughout the farm an S<sub>1</sub> fabric, defined by micas, parallels the well-preserved sedimentary structures. On a regional basis, it is this S<sub>1</sub> foliation which has been deformed by, and hence wraps around, the granitoids (Map 1). Although younging directions indicate some duplication of the sequence, the F<sub>2</sub> synformal structure is essentially a syncline (Map 2). Few isoclinal folds have been identified and their interpretation is equivocal. In the northern corner of the farm isoclinal folds in schists with wavelengths of less than 10 cm and amplitudes of many metres are exposed in the Ohere River, but their development may well be related to the Salem granitoid. The rare isoclinal folds in the calc-silicate rocks may be considered evidence for an early phase of isoclinal folding (F<sub>1</sub>), but they are by no means widespread. No convincing evidence for recumbent folding on Ohere was found and the excellent preservation of sedimentary structures argues against it. This suggests that the S<sub>1</sub> fabric may have been derived by compaction of the metaturbidite sequence and not by a deformational event. Moreover, the localised duplication of the sequence may well be a result of large-scale syn-sedimentary slumping or have occurred as a result of granite intrusion and have nothing to do with an early isoclinal folding phase.

Bands of calc-silicate rocks on Ohere are boudinaged and have “broken up” to form prolate avoids or spindles tens of

centimetres in length. This contrasts markedly with the flattened, oblate calc-silicate lenses of the upper Kuiseb Formation closer to the Omaruru Lineament in NCZa. Calc-silicate rocks on Ohere define sedimentary layering, whereas on Sandamap Noord (Map 3) the long axes of calc-silicate lenses commonly define a transposition foliation. Quartz veins, up to 40 m long and up to tens of centimetres wide, that parallel  $S_1$  are present in the phyllites in the core of the  $F_2$  synform. Quartz blows or saddle reefs, up to several metres thick, are particularly concentrated in fold noses and predate the development of the  $S_2$  schistosity.

#### 4.3.3.3 Deformation related to granitoid intrusion - $F_2$ and $F_3$ structures

In NCZe, the emplacement of granitic plutons was synchronous with the later stages of regional tectonism in a similar manner to that described by Lagarde *et al.* (1990). The dome-and-basin structure of the area was undoubtedly related to the intrusion of the Ohere Oos Salem granite and the Ohere leucogranite as well as the regional tectonism. Because strain intensity increases towards the margin of the plutons, post- $F_1$  structures are best identified in the aureoles of intrusions and attention has been focused on the centre of Ohere. The major  $F_2$  structure is a broad, concentric synform that plunges at  $70^\circ$ – $80^\circ$  on a bearing of  $320^\circ$  (Map 2 and accompanying stereograms). On Ohere this  $F_2$  fold is clearly visible on the aerial photographs and is defined by the ground magnetic survey conducted by a mining company (Louwrens, 1986). One of the most noteworthy features of this  $F_2$  fold is the almost total absence of accompanying small-scale parasitic folds. Concentric folds probably originate by flexural slip folding and are typical of terrains that exhibit dome-and-basin structures (Hobbs *et al.*, 1976). The development of a pervasive axial-planar cleavage, an  $S_2$  fabric, is most intense in the core of the fold (Map 2 and accompanying stereograms). This  $S_2$  fabric is curvilinear and parallels the contact between the Kuiseb Formation and the Ohere leucogranite and has been locally refracted in the hinge zone. The  $S_2$  foliation has been locally refolded by a third folding phase,  $F_3$ , approximately coaxial with  $F_2$ .  $F_3$  folds plunge at approximately  $68^\circ$  on a bearing  $280^\circ$ . One of the few examples of an  $F_3$  fold is exposed on the south side of the Ohere River, one kilometre south of Hill 1265 (Map 2). An east-west trending, subvertical fracture cleavage ( $S_3$ ) is associated with the  $F_3$  folding phase (Map 2 and accompanying stereograms). In the author's opinion, the  $S_2$  and  $S_3$  fabrics on Ohere were formed primarily as the result of the intrusion of the Ohere leucogranite which has a 36 Ma younger Rb-Sr whole-rock date than the Salem intrusion. The  $S_2$  and  $S_3$  foliations appear to be analogous with the 'cleavage fronts' that surround syntectonic plutons in low grade terrains (Lagarde *et al.*, 1990).

#### 4.3.3.4 $F_4$ structures

A fourth folding phase ( $F_4$ ) is only locally developed, the fold axes plunging  $56^\circ$  on a bearing  $348^\circ$ . These small-scale, open folds rarely possess an accompanying fabric. However, a subvertical north-northwest-trending fracture cleavage on Grid 2 parallels  $F_4$  axial planes and is considered to be

an  $S_4$  fabric (Map 2 and accompanying stereograms). These structures may be the equivalent of Kröner's  $D_4$ .

## 4.4 CONCLUSION

The SCZ is underlain by an early Proterozoic inlier of granitic basement and evidence has been presented to show the complexity of its ductile and brittle deformational history. Of particular importance is the fact that, in common with other 1.7–2.0 Ga inliers in Namibia, this granitic basement is transected by numerous auriferous megashears that were possibly mineralised by a pre-Damaran event. Deep-seated east-northeast-trending fractures extending into the mantle controlled the localisation of pre-Damaran mafic dykes and Damaran continental volcanic rocks. These east-northeast-trending magnetite-bearing shear zones and metadolerite dykes are almost certainly responsible for the east-northeast-trending magnetic grain of the CZ to the east of the Welwitschia lineament zone (Corner's aeromagnetic composite, 1983). Major faults exerted a strong influence on Damaran sedimentation in the vicinity of the Omaruru Lineament. The intracontinental branch of the Damara probably occupied an ancient zone of weakness (Jacob *et al.*, 1983) and the distribution of Damaran sediments suggests that the structures along which rifting occurred were oriented northeast/east-northeast. Rifting is envisaged to have occurred along reactivated megashears similar to the ones on Abbabis and Narubis.

The Abbabis Inlier played a major role in partially shielding the lower part of the Damara Sequence, and the SCZ in particular, from Damaran deformation. The mechanically competent metasediments that drape the inlier also resulted in the SCZ appearing to undergo a relatively simple ductile deformational history. In contrast, close to the Omaruru Lineament in NCZa, the relatively incompetent Kuiseb Formation has undergone one, or maybe two phases of isoclinal to tight folding. The tectono-stratigraphic zone NCZa is intensely deformed along its strike length (Fig. 4. 1) in stark contrast to NCZe. Thus, although deformation in the highest stratigraphic levels (the tin belts) is generally less intense, Miller's (1983a, p. 459) assertion that the southern (Sandamap-Davib Ost) tin belt has a less complex structure is incorrect. This author believes that not only is there little evidence for recumbent folding at any stage, but that there is also little indication of directed tectonic transport in the early phases of the orogeny. This is an important point to remember when considering geodynamic models for the early deformational stages of the orogen. In the NCZ there is a decrease in deformational intensity away from the Omaruru Lineament. In the Omaruru area, in NCZd and NCZe in particular, there is little or no evidence for early isoclinal folding phases and the ductile deformation (northeast-trending  $D_3$  doming of Miller, 1983a) appears to be almost entirely related to the granitoid diapirs. The upper stratigraphic levels in NCZe are characterised by concentric folds which are found in regions that have undergone low overall shortening (Hobbs *et al.*, 1976).

The change in deformational style across the Omaruru Lineament must be emphasised. The SCZ is characterised by upright dome-and-basin structures. Diapirism, succes-

sive folding phases or folding in several directions during one deformational phase resulting in Type I interference patterns (Ramsay, 1967) have been invoked by various authors (Sawyer, 1981; Jacob *et al.*, 1983) to explain these phenomena. Within the field area, dome formation is the result of widespread granite intrusion in the manner envisaged by Kröner (1984). The southern portion of the NCZ is also characterised by dome-and-basin structures, but their nature changes significantly in a northward direction. On the northwest side of the Tubussis Lineament between Nainais and Ketelbank (Fig. 4.1), where the small amount or absence of granitic material precludes a diapiric mechanism for dome generation, NCZd is characterised by Type 2 mushroom-shaped interference patterns (Watson, 1982). These have resulted from the imposition of upright northeast-trending  $F_3$  structures on flat-lying earlier folds (op. cit., p.22). Approximately 130 km to the northwest in the Southern Kaoko Zone (SKZ), Coward (1981) has shown how early, tight, westward-verging north-south folds have been modified by upright east-northeast-trending  $F_3$  folds resulting in Type 2 interference structures. It is believed that the rigid nature of the Abbabis Inlier prevented the generation of early flat-lying recumbent folds in

the SCZ and the southern part of the NCZ. The confinement of northwestward-verging, flat-lying  $F_4$  folds on the northern edge of the SCZ to zones where the basement has undergone semi-brittle deformation such as the Welwitschia lineament zone, supports the argument that the Abbabis Inlier behaved as a relatively rigid block during the Damaran orogeny.

There is abundant evidence for a late-tectonic structural control on the localisation of epigenetic Damaran mineralisation. There is a spatial association between  $D_3$  domal structures and epigenetic mineralisation throughout the CZ. Gold skarn mineralisation in the SCZ and tungsten skarn mineralisation in the NCZ are commonly hosted by the lowest marble unit in the core of a  $D_3$  dome. Evidence has been presented for significant, late-tectonic, syn- $D_3$  dextral movement on the Omaruru Lineament and the associated localisation of tungsten skarns and gold veins in tensile structures on the northern side of the Kompaneno Fault and Omaruru Fault Zone (Map 1). There is also a strong localisation of both epigenetic carbonate-hosted and turbidite-hosted gold mineralisation, as well as zones of tourmaline alteration, in north-northeast - trending semi-ductile and brittle ( $F_4$ ?) structures on the NCZ/SCZ boundary in the Usakos-Karibib area.



## 5. METAMORPHISM

## 5.1 INTRODUCTION

There have been only two investigations aimed primarily at determining the metamorphic conditions that prevailed in the central portion of the CZ, both of which were essentially regional in nature (Miller, 1983a). In the SCZ, Puhan (1983) investigated the regional P/T conditions between Swakopmund and Karibib by examining dolomite-calcite solvus thermometry in dolomitic marbles. Much of Puhan's study area falls outside the area covered by this memoir. In the NCZ, information is available from a regional study of the aluminous pelites by Hoffer (1977). Hoffer was able to Map isoreactiongrads on a regional basis from the Okahandja Lineament in the south to the Kamanjab Inlier in the north (Fig. 5.1), but little detailed work has been completed in the Usakos-Karibib-Omaruru area. Information presented in this chapter will show that the metamorphic history of the CZ is considerably more complicated than Hoffer's (1977) pioneering study showed it to be. An examination of the metamorphic history of the area is beyond the scope of this memoir, but an understanding of the thermal history of the orogen has particular relevance to epigenetic deposits that are essentially hydrothermal in nature. Thus attention is focused on describing the nature of the metamorphism and determining the peak regional and thermal metamorphic conditions (in the NCZ in particular) and their relationship to late-tectonic mineralising events. The possible role played by metamorphic fluids and processes in mineralising events will be discussed in Chapter 7. Throughout the field area Damaran lithologies have been subjected to greenschist (300-500°C; Essene, 1989) to amphibolite (500-700°C; Essene, 1989) facies metamorphism. From Chapter 2, it is evident that the majority of metasediments have granoblastic textures and that retrogressive effects throughout the CZ were relatively minor. In general terms, the rocks of the SCZ were subjected to higher grade metamorphism than those of the NCZ. In both zones there is a broad increase in regional metamorphic grade from the east towards the high temperature zone on the coast (Fig. 5.1; Miller, 1983a). Immediately north of Karibib, peak regional metamorphic temperatures were in the lower amphibolite facies, while west of Usakos upper amphibolite facies assemblages and the products of associated partial melting are widespread. A feature of particular interest is the apparently higher regional metamorphic conditions that prevailed along the Omaruru Lineament in NCZa. Superimposed on the regional metamorphic assemblages are contact metamorphic effects associated with the numerous granite intrusions. This localised, but widespread, predominantly late-tectonic ( $D_3$ ), thermal overprinting, which is essentially Buchan type, is particularly evident in NCZd and NCZe.

Detailed information on Damaran metamorphic conditions can only be obtained from a small number of the lithostratigraphic units. Throughout that portion of the CZ under examination, amphibolites and metabasites are not present. The Nosib Group quartzites are of little help in elucidating the metamorphic history of the area on ac-

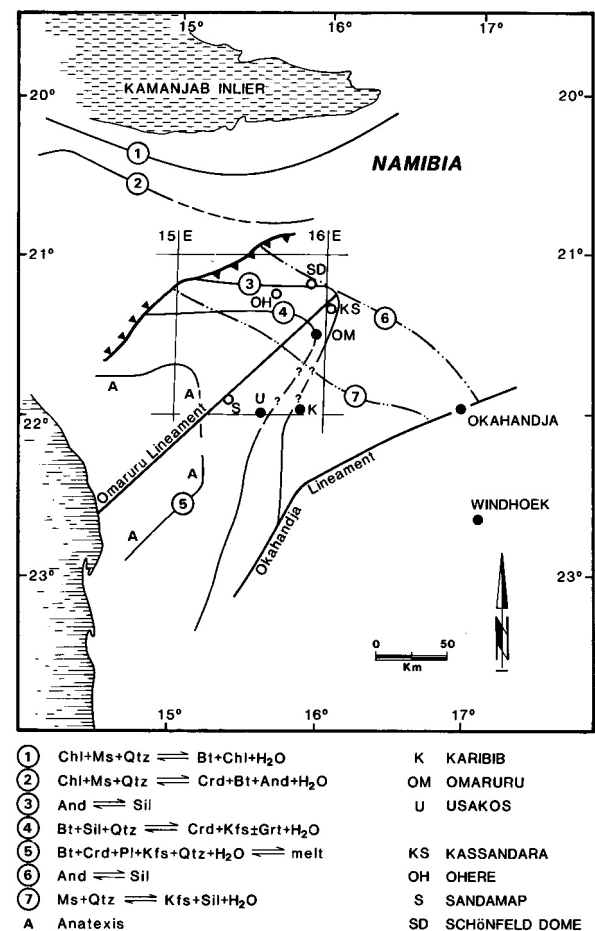


**Figure 5.1:** Isoreactiongrads in pelitic rocks in the Damaran Orogen (after Hoffer, 1977). Lower and upper sillimanite zones after Miller (1983a)

count of their composition and limited distribution in the NCZ. However, ellipsoids of sillimanite are present in the meta-arkoses of the Etusis Formation on Sandamap Noord in NCZb. Similarly, the mineral assemblages of the calc-silicate lithologies of the upper Nosib Group and lower Swakop Group are too uniform to be of assistance. The Karibib Formation carbonates rarely contain sufficient  $\text{SiO}_2$  to form silicate-dominated metamorphic assemblages, but in the immediate vicinity of Karibib, dolomitic marbles of the Karibib Formation in the SCZ commonly contain disseminated tremolite. In the NCZ, the highly calcareous nature of the Karibib Formation has resulted in the formation of virtually pure calcitic marble which is unsuitable for dolomite-calcite solvus thermometry. Calc-silicate rocks of the Kuiseb Formation commonly have an amphibole-rich reaction skarn, but are otherwise of little use in unravelling the metamorphic history of the area. As a result, work has concentrated on the metapelites of the Oberwasser Formation and the metapelites and metaturbidites of the Kuiseb Formation. Throughout the field area kyanite and staurolite are absent and garnet is extremely rare. The one record of staurolite in the SCZ was made by Nash (1971) from the Rössing Formation near the Rössing Uranium Mine (Fig. 1.2). Cordierite is very common in the area under investiga-

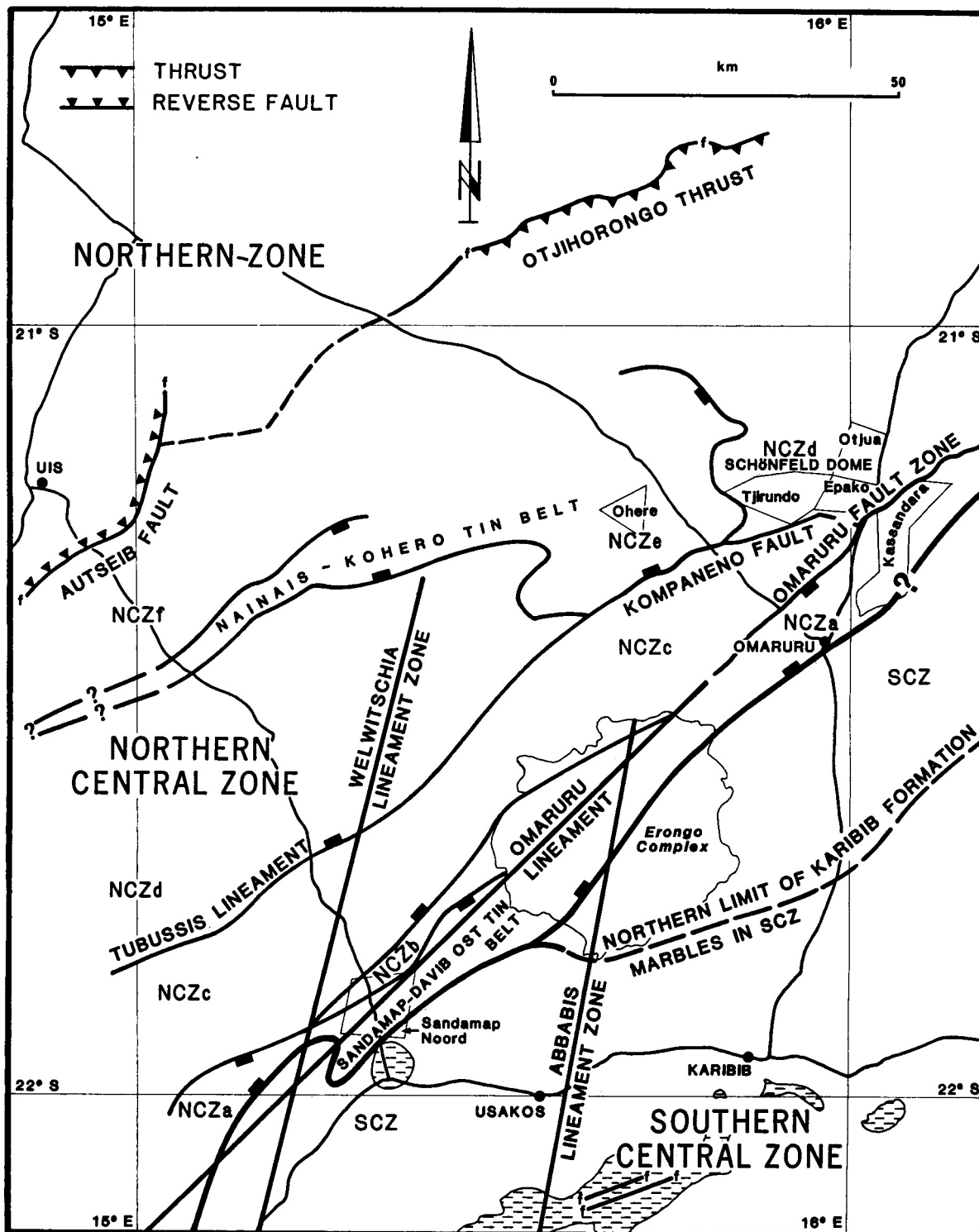


Figure 5.2: Localities referred to in Chapter 5

tion and sillimanite is widely distributed near granitic and pegmatitic intrusions. A discovery of note made during the course of field work is that andalusite-bearing assemblages are more widespread in the CZ than previously thought, but are notoriously difficult to identify in the field. It is thus apparent that both the regional and contact metamorphism in the CZ were of low-pressure/high-temperature type and provide an indication of a high geothermal gradient during the Damara orogeny.

Four areas (Fig. 5.2) have been chosen to illustrate the metamorphic histories of some of the tectono-stratigraphic

zones. The first two were chosen because of their intensely deformed nature close to the Omaruru Lineament. The second two examples are from less-deformed areas where both the tectonism and metamorphism were largely caused by late-tectonic granites. The four examples are:

- 1) The Kuiseb Formation pelites on Sandamap Noord in NCZa (Map 3)
- 2) The Kuiseb Formation pelites on Kassandara in NCZa (Map 1)
- 3) The Oberwasser Formation pelites from the Schönfeld Dome in NCZd (Map 1)

4) The Kuseb Formation pelites on Ohere in NCZe (Map 2)

The mineral abbreviations used are those suggested by Kretz (1983). The symbol "Als" has been used to denote the aluminium silicate polymorphs kyanite, sillimanite and andalusite and "Fib" for fibrolite. Porphyroblast-matrix relationships have been determined following the methods of Zwart (1962) and Spry (1969), although the author is aware that the assumptions on which these papers are based have recently been disputed by Bell (1985) and Bell *et al.* (1986).

## 5.2 METAMORPHISM ON THE FARM SANDAMAP NOORD 115 IN NCZa

### 5.2.1 Introduction

The Kuseb Formation is well exposed on Sandamap Noord and affords the opportunity to examine the various types of metamorphism that have affected the metasediments in NCZa. Aluminous schists at the base of the Kuseb Formation are overlain by more quartzitic metaturbidites in the core of the syncline on Sandamap Noord. As a result muscovite and aluminosilicate-dominated assemblages are particularly common in the schists immediately overlying the Karibib Formation (southwest corner of Map 3). In general, schists in the core of synformal structures have been metamorphosed to lower grades than their counterparts near stratigraphic or granitic domes. Because of the problem in distinguishing between regional and contact metamorphism in terrains where syn- and late-tectonic granitic intrusions are abundant, it has been assumed that the lowest grade schists are the products of regional metamorphism. This may not necessarily be true. Quartz is present at all localities except where mentioned.

### 5.2.2 Regional metamorphism

At a minimum distance of 800 m from the Sandamap Noord leucogranite and associated pegmatites (the  $D_3/D_4$  dome), the Kuseb Formation is most commonly represented by a fine-grained (<250  $\mu\text{m}$ ), finely laminated biotite schist with a lepidoblastic/granoblastic texture. The schist comprises the assemblage Qtz+Kfs+Olig+Bt $\pm$ Ms $\pm$ Crd $\pm$ Als. Accessories include tourmaline, apatite, zircon and opaque minerals, notably graphite. Tourmaline is abundant in all thin sections examined and locally constitutes two modal per cent. Traces of calcite, retrogressive chlorite and serpentine are also present. The schists usually possess a fairly pervasive schistosity defined by stubby (<250  $\mu\text{m}$ ) biotite. This fabric is parallel to lithological contacts on the outcrop scale, but in many instances is a transposed foliation. It is commonly poorly defined resulting in the schist having a granoblastic rather than a lepidoblastic texture. Locally the  $S_1$  schistosity is developed at up to 60° to a faint 100-300  $\mu\text{m}$  thick compositional layering that is almost certainly bedding. These beds are defined by alternating quartz and mica-rich layers. Within the more pelitic layers, the long axes of the biotite are oriented either parallel to or define the  $S_1$  schistosity. These  $S_1$  biotites are not strained and therefore represent a

new phase of mica growth. They are not rotated early biotites. Secondary and tertiary foliations in the schists are also defined by small biotites (Map 3). In general, biotite is much more common than muscovite in the  $S_1$  fabric. K-feldspar generally occurs as a fine-grained, granoblastic mineral in the groundmass, but is locally present in clusters of syn-/late-kinematic porphyroblasts. Coarse-grained (0.5 mm - 1.5 mm), randomly oriented, post-kinematic poikiloblasts of muscovite are common throughout the formation. Rare chlorite, growing retrogressively after biotite, is usually restricted to slip planes coplanar with the  $S_1$  fabric.

### 5.2.3 Early kinematic cordierite and late-kinematic andalusite growth in aluminous schists

Local occurrences of andalusite-cordierite schist are present in the core of the syncline in the centre of the farm and on the southern and northern sides of the Sandamap Noord Dome (Map 3). One kilometre northwest of the Sandamap Tin Mine the schists on either side of the main road are covered by a thin scree of andalusite pebbles. Outcrops are however rare. Porphyroblasts of the two minerals occur in the more aluminous biotite-muscovite schists where the two micas are present in approximately equal proportions. Yellow, pinitised poikiloblasts of cordierite up to 6 mm in diameter contain numerous inclusions of biotite and quartz. A fine-grained, planar  $S_1$  is usually oriented parallel to the coarser-grained  $S_2$  which wraps around the poikiloblasts indicating pre-/early kinematic growth of the cordierite. In some examples  $S_2$  extends into the cordierite suggesting synkinematic growth of the mineral. Cordierites are commonly overgrown, rimmed (Plate 5.1) and enveloped by large (up to 5 cm) subhedral poikiloblasts of late-kinematic andalusite.

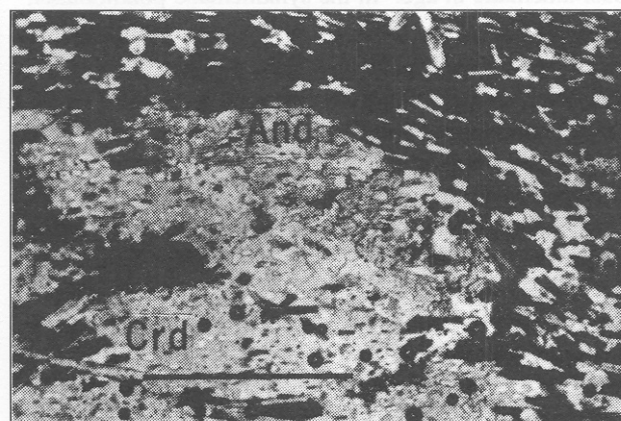


**Plate 5.1:** Andalusite (And) overgrowth on cordierite (Crd) poikiloblast in biotite schist from Sandamap Noord (SN340; PPL); scale bar = 1 mm

**For all plates:** PPL = Plane-polarised light; RL = Reflected light; XL = Crossed polars

In some porphyroblasts inclusions are so numerous that a sieve texture is developed. The planar, mica-defined  $S_1$  of the andalusite is coplanar with the  $S_1$  of the cordierite and  $S_2$ . Andalusite post-dates the cordierite, but the former is not post-kinematic because  $S_2$  not only curves around earlier cordierites overgrown by andalusite, but new rims of the aluminosilicate as well. Andalusite growth may however

be related to the intrusion of the granite/pegmatite dome (see discussion below). These aluminous schists are further characterised by traces of crosscutting (late/post-kinematic?) fibrolite and sillimanite. Retrogressive features include abundant post-kinematic poikiloblasts of muscovite and the overgrowth of pinitised cordierite by randomly oriented muscovite and biotite and coarser-grained quartz.

#### 5.2.4 Contact metamorphism associated with the $D_3/D_4$ leucogranite/pegmatite dome

The aureole around the leucogranite phacolith and associated pegmatites has been examined to study the thermal and mechanical effects of the intrusions (Map 3). Mineral assemblages of the Kuiseb Formation schists have been investigated along an 800-metre-long traverse on the southern side of the dome, but poor exposure prevented sampling at a regular spacing. Although there is a minor compositional variation of the schists along the traverse, all specimens have a single subvertical pervasive schistosity that wraps around the dome. This fabric is defined by biotite and, in most cases, muscovite. Eight hundred metres from the contact the assemblage Qtz+Bt+Kfs+Olig is present. The rock has a fine-grained ( $<1 \mu\text{m}$ ) lepidoblastic/granoblastic texture, the schistosity being defined by biotite. Muscovite is present as a post-kinematic poikiloblast. Closer to the intrusion (630 metres) the schistosity, defined by biotite and muscovite, is markedly more pervasive. Finely disseminated fibrolite is also present. Pinitised relicts of synkinematic cordierites are extensively altered to chlorite and serpentine. Four hundred and fifty metres from the contact the biotite-muscovite schist possesses abundant K-feldspar poikiloblasts. Some are synkinematic, but the majority do not disrupt the schistosity and thus are late-/post-kinematic in age. In the synkinematic poikiloblasts,  $S_i$  is commonly at a high angle to  $S_c$  and is locally slightly sinuous. This feature, which is interpreted as evidence for the rotation of porphyroblasts, is particularly prominent close to the domal structure. Four hundred and twenty metres from the contact the biotite-muscovite schists contain minor fibrolite; euhedral, post-kinematic K-feldspar porphyroblasts have overgrown pinitised cordierite relicts. The major mineral change in the thermal aureole occurs at 300 metres where fibrolite appears in 2-mm-long knots. At this point pinitised remnants of synkinematic cordierite porphyroblasts are overgrown by quartz, K-feldspar and randomly oriented mica. At 280 metres, fibrolite development is more extensive. Poorly defined, but discordant  $S_i$  in the synkinematic cordierites attests to rotation of the porphyroblasts. These cordierites are spatially associated with relict andalusite that is enveloped in muscovite. At 190 metres the mechanical effects associated with the intrusion of the granitic dome are readily apparent. The quartz-feldspar groundmass has more of an elongate than granoblastic texture and the relict cordierites are oval or elongate. One hundred metres from the contact there is a notable increase in size and abundance of the sillimanite mats and at 70 metres the schist contains up to 25 modal per cent fibrolite which is concentrated in knots and in folia (*sensu* Vernon, 1987). The development of the fibrolite knots, clusters and stringers around the aureole

of the domal structure is intriguing because there is no accompanying development of K-feldspar. Although the fibrolites are not universally nucleated on biotite as described by Kerrick (1987), they are localised in mica-poor domains suggesting their derivation from biotite precursors. Close to the contact, pinitised relicts of cordierites have been completely flattened.

On the northwest side of the dome, in contrast, in an area of abundant pegmatite intrusions (Map 3), sillimanite schists with second generation K-feldspar possessing a single pervasive mica schistosity are common. Andalusite is conspicuously absent and rare, pinitised early cordierite has been overgrown by fresh micas and quartz. Fibrolite and sillimanite are abundant in the schists. The deflection of the mica fabric around bulbous aggregates of fibrolite does not necessarily indicate synkinematic growth of the aluminosilicate; the aggregates may be pseudomorphs after andalusite. K-feldspar is present as synkinematic porphyroblasts where  $S_i$  is oriented parallel to  $S_c$ , but more commonly as post-kinematic perthitic poikiloblasts (Plate 5.2). In the immediate vicinity of pegmatitic intrusions the schists have a chaotic texture and quartz is absent, having probably been consumed in the reaction  $\text{Qtz} + \text{Ms} = \text{Kfs} + \text{Sil} + \text{H}_2\text{O}$ . A single late-kinematic garnet ( $<0.5 \text{ mm}$ ) was noted.

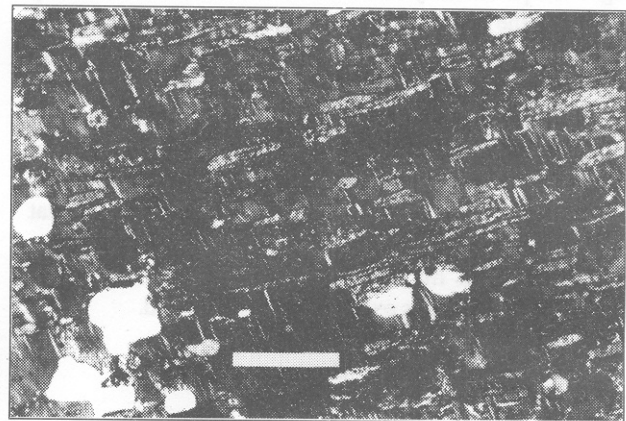
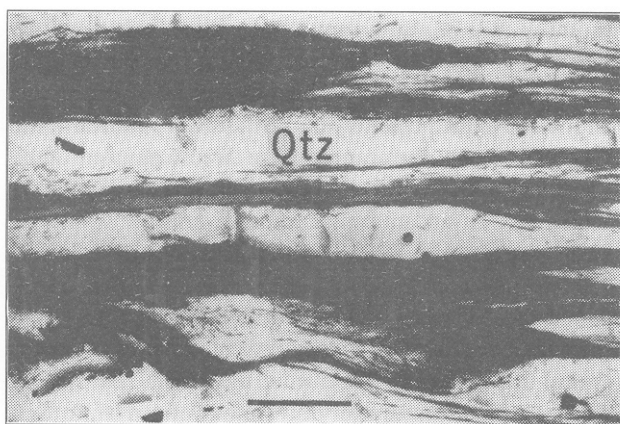


Plate 5.2: Post-kinematic perthitic poikiloblasts in biotite schist on Sandamap Noord (SN304; XL); scale bar = 200  $\mu\text{m}$

#### 5.2.5 Cataclastic metamorphism associated with the $D_3/D_4$ leucogranite/pegmatite dome

Intimately associated with the sillimanite schists of the aureole are some unusual quartz-sillimanite rocks. Subvertical, oblate spheroids of very hard, grey, streaky mylonite are up to several metres long and several tens of centimetres wide. Because of their hardness they form prominent outcrops. These mylonite lenses are concentrically arranged around the domal structure, their long axes running parallel to the contact between the intrusions and the metasediments (Map 3). They are best developed within 100 metres of the pegmatite-metasediment contact, but isolated occurrences are found up to 500 metres away. Mylonites are dominated by quartz ( $\pm 60\%$ ) and sillimanite ( $\pm 30\%$ ). The quartz crystals have sutured grain boundaries, undulose extinction and are commonly fractured. Fibrolite is present as radiating wisps, mats and streaks (plate 5.3), intergrown with sil-



**Plate 5.3:** Fibrolite segregations in mylonite, northwest margin of leucogranite-cored dome on Sandamap Noord (SN301; PPL); Qtz = quartzite; scale bar = 1 mm

limanite and overgrown by anhedral muscovite. Accessory minerals include garnet, K-feldspar, sericitised plagioclase, biotite altering to chlorite and graphite. The feldspar is commonly intergrown with quartz in a graphic intergrowth. Kerrick (1987) has described fibrolite accumulations in the contact aureoles of granitoid intrusions, attributing their development to the metasomatic alteration of biotite by fluids emanating from the intrusion and the removal of K, Mg and Fe by chloride complexes. Although this model may account for the origin of the closely associated fibrolite-bearing schists, it does not account for the commonly streaky, segregated quartz-mylonite rocks on Sandamap Noord. The latter is interpreted to be a type of high strain zone (Vernon, 1987), their development being related to the diapiric development of the domal structure (see discussion in section 5.2.7).

#### 5.2.6 Metamorphic effects associated with the $F_4$ folds

One of the notable features of the Kuiseb Formation on Sandamap Noord and, indeed throughout the NCZ, is that the growth of metamorphic minerals can rarely be attributed to a specific folding event. Biotites define various schistositys, but because of the lack of associated fold axes, there is uncertainty as to which deformational event caused their formation. A significant exception is the prominent sillimanite lineation which plunges shallowly, parallel to the axes of  $F_4$  folds in the southwest of the farm (Map 3 and Chapter 4). In this area, aluminous schists of the lower Kuiseb Formation possess a secondary foliation, interpreted as an axial planar  $F_4$  fabric ( $S_4$ ), that dips at  $20^\circ$ - $60^\circ$  to the east-south-east (Fig. 4.3, Stereos 4 and 5). The schists contain the assemblage Qtz+Kfs+Olig+Bt+Ms+Sil, tourmaline being very rare or absent. Plagioclase and K-feldspar are abundant, both as groundmass constituents and as elongate, late-/post-kinematic poikiloblasts. The linear fabric is defined by biotite, fibrolite mats, sillimanite and ribbon-like quartz. The fibrolite and sillimanite have nucleated on biotite and are particularly abundant in elongate monomineralic patches that define the lineation. Much of the biotite is highly strained and lies at a high angle to the plane of the secondary fabric. This mica is crosscut by the sillimanite fabric and is probably rotated, pre- $F_4$ , biotite.

Some of the sillimanite fibres are also oriented at right angles to the  $F_4$  sillimanite lineation suggesting pre- $F_4$  sillimanite growth. However, the confinement of poikiloblastic K-feldspar, much of it perthitic, to the  $F_4$  structures suggests that the majority of sillimanite was formed by the prograde reaction  $Ms+Qtz=Sil+Kfs+H_2O$  at  $F_4$  time. This indicates either that peak regional metamorphic conditions persisted until  $F_4$  times or the presence of a late-tectonic thermal event, possibly associated with the younger granite and pegmatite intrusions. Muscovite is present as large, post-kinematic poikiloblasts.

#### 5.2.7 Mylonitisation on the northwest side of the $D_3/D_4$ leucogranite/pegmatite dome

Mylonitisation of the Kuiseb metasediments is particularly intense on the northwest side of the domal structure (Map 3) in the immediate vicinity of a zone of Au-As-W mineralisation. Although some of the structural and metamorphic features present here can be recognised elsewhere around the dome, this unusually intense and longer-lived deformation is partly related to  $D_4$  movements on the Welwitschia lineament zone. In the immediate vicinity of the gold mineralisation, the ground is covered with distinctive, brown, elongate (2-6 cm), stubby segregations of fibrolite. Fibrolite aggregates are crenulated on a micro scale, though the crenulations are not systematically oriented. Fibrolite is commonly in contact with ragged deformed muscovite, but the temporal relationship between the two minerals is unclear. North-northeast-striking quartz-sillimanite mylonite rocks are developed as a swarm of laterally discontinuous, foliation-parallel lenses and veins traceable for several hundred metres across strike. Fibrolite/sillimanite comprises up to 30 modal per cent of these mylonites. The aluminosilicates are concentrated in linear rather than anastomosing zones which attests to the higher strain in this area. Much of the fibrolite overgrows xenoblastic K-feldspar.

Some north-northeast-trending mylonite zones cut otherwise undeformed late-tectonic tourmaline-bearing pegmatites attesting to very late Damaran movement. This relationship has not been observed elsewhere around the dome. In hand specimen, sheared pegmatites possess a subvertical, spaced foliation defined by fibrolite/sillimanite. Fibrolite is

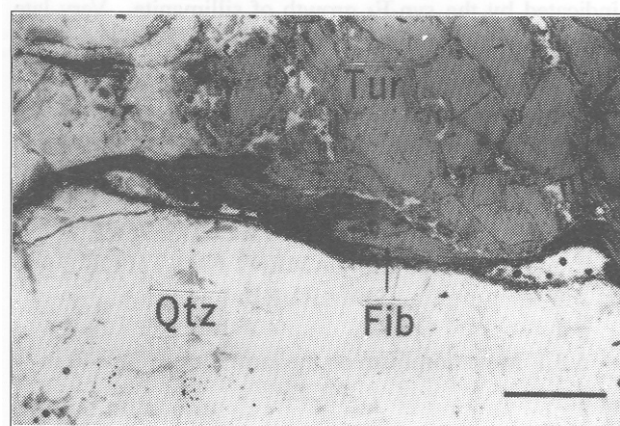


**Plate 5.4:** Fibrolite (Fib) segregation rimming zoned tourmaline (Tur) in sheared pegmatite, immediate vicinity of gold mineralisation, Sandamap Noord Gold Prospect, trench 22 (SN302; PPL); scale bar = 1 mm

confined to discrete zones (Plate 5.4), the folia anastomosing between lenticular grains of quartz and feldspar in the manner described by Vernon (1987, Fig.17). The fibrolite fibres are themselves locally crenulated and crosscut by later fibrolite and sillimanite. Sillimanite is disseminated in quartz and in radiating aggregates. The quartz has slightly undulose extinction and the K-feldspar has what appears to be structurally induced twinning. Graphite is concentrated in the fibrolite folia. There is little doubt that the anastomosing fibrolite fibres represent high strain zones as proposed by Vernon (1987). In his model, fibrolite crystals are localised in folia because of their ability to slide over one another during deformation and thus absorb shear strain. Quartz and feldspar crystallise in the intervening lower-strain domains.

### 5.2.8 Summary

Greywackes and turbidites of the Kuiseb Formation have been regionally metamorphosed during isoclinal and tight folding ( $F_1$  and  $F_2$ ) to form biotite±muscovite schists. The local presence of thin (several tens of centimetres) foliated quartz-feldspar-biotite rocks in the Kuiseb Formation suggests the presence of minor syntectonic (syn- $D_1$ ?) granite intrusions, which may have been partly responsible for the local growth of early-kinematic cordierite. A (regional?) rise in the temperature resulted in the coarsening of the mica fabric. Further flattening caused the wrapping of this new fabric around the slightly rotated cordierite porphyroblasts. During late  $D_3$ /early  $D_4$  compression, formation of the domal structures was largely caused by the intrusion of granites and associated pegmatites. The growth of late-kinematic andalusite after cordierite in the aluminous schists probably occurred at about this time, perhaps as a result of the associated thermal metamorphism. As the granite and pegmatites intruded, early-kinematic cordierite became further flattened and andalusite was replaced by fibrolite. Quartz-sillimanite mylonites mark high strain zones that formed concentrically around the dome. In the immediate vicinity (<50 metres) of pegmatite intrusions, sillimanite and perthitic K-feldspar were formed by the breakdown of muscovite and quartz. Persistence of these high temperature conditions until late Damaran times is indicated by the syn- $F_4$  growth of sillimanite. Very late Damaran movement on the Welwitschia lineament zone resulted in the formation of sillimanite mylonite rocks in late-tectonic pegmatites on the northwest side of the domal structure and suggests the persistence of a high geothermal gradient to the end of the Damaran orogeny.

## 5.3 METAMORPHISM ACROSS THE OMARURU LINEAMENT NORTH OF OMARURU

### 5.3.1 Metamorphism on the farm Kassandara 40 in NCZa

Intensely deformed aluminous schists of the Kuiseb Formation are well exposed on the farm Kassandara 40, 16 km northeast of Omaruru (Fig. 5.2, Map 1), on the southeast

side of the Omaruru Fault Zone. Although the metasediments in this portion of NCZa appear to have undergone early tectonic isoclinal-to-tight folding in a similar manner to their counterparts on the southwest side of the Erongo Complex, they cannot be the direct equivalent of the

Sandamap-Davib Ost tin belt. The Kuiseb Formation schists on Kassandara contain more K-feldspar porphyroblasts (see also Fig. 2.12), there are no associated calc-silicate rocks and the pegmatites are not stanniferous. Bands (channels?) of white, planar crossbedded quartzite up to several metres thick are locally present, but no sedimentological features can be identified in the schists. The steeply dipping schists possess a pervasive mica-defined fabric ( $S_1$ ). In the few instances where bedding has been observed,  $S_1$  is coplanar with  $S_0$ . The only other structural feature of note on the farm is a prominent sillimanite lineation which generally, but not exclusively, plunges southeast or south-southeast. Foliated, therefore syntectonic, leucogranites and associated leucopegmatites and undeformed, thus late-tectonic, muscovite-schorl pegmatites are widespread in this portion of NCZa. The mineral assemblages of schists at a distance of more than 1 km from the nearest visible granite intrusion have been examined.

The schists possess a lepidoblastic fabric defined by biotite. The most common mineral assemblage is Qtz+Kfs+Sil+Bt+Ms+Plag which corresponds to the upper sillimanite zone of Yardley (1989). The oligoclase, determined by the Michel-Lévy method, is a minor phase and accessory minerals include tourmaline, apatite, zircon and serpentine. In some samples, widespread secondary iron minerals appear to be weathering products after sulphide aggregates. The diagnostic feature of the schists on Kassandara is the presence of perthitic K-feldspar porphyroblasts up to 6 mm long. Within the majority of these elongate porphyroblasts, the  $S_1$  fabric diverges slightly and they are thus interpreted to be synkinematic. Quartz, biotite and tourmaline are common inclusions in the synkinematic K-feldspar: Si is usually parallel to  $S_0$ . Some K-feldspar porphyroblasts have a ribbon, poikiloblastic nature and are clearly post-kinematic overgrowths. Fibrolite is abundant in all thin sections, either nucleated on biotite or concentrated in 2-mm-long knotty segregations. Within these knots, fibrolite is randomly oriented. The widespread occurrence of sillimanite as an inclusion suggests some synkinematic growth of the mineral as well. One example of a circular knot of fibrolite, 250  $\mu$ m in diameter, was noted. The reaction that is considered to account for the observed assemblage is  $Ms+Qtz=Kfs+Sil+H_2O$ . There is no evidence for the formation of partial melts.

In the more nodular schists, the above-described assemblage occurs together with relict andalusite and pinitised cordierite. Blebs of andalusite in optical continuity are surrounded by K-feldspar and plagioclase; altered, prismatic andalusite is enveloped by fresh muscovite and the aluminosilicate occurs as rare blebs within altered cordierite. Yellowish, fractured cordierites with numerous inclusions, are elongate in the plane of schistosity,  $S_1$  tending to parallel  $S_0$ . However, the biotite fabric wraps around the cordierite indicating synkinematic growth of the porphyroblasts. The inclusions of andalusite within cordierite and K-feld-

spar suggest that prograde andalusite-forming reactions, such as  $Qtz+Chl+Ms=Crd+And+Bt+H_2O$ , were followed by reactions such as  $Qtz+Bt+Ms=Crd+Kfs+H_2O$ . The assemblage  $Qtz+Ms+Sil+Kfs$  is persistent to the highest grades of metamorphism. However, there is no evidence on Kassandara from the thin sections examined for the reaction  $Qtz+Sil+Bt=Grt+Crd+Kfs$  (Holdaway and Lee, 1977) as suggested by Hoffer (1977) for the Omaruru area (Fig. 5.1).

A notable feature of the Kuiseb Formation schists on Kassandara is the abundance of late-/post-kinematic hydrous minerals. In all samples examined, large, poikiloblastic muscovite, both conformable to and crosscutting  $S_1$ , is present. Biotite is locally extensively altered to chlorite and the K-feldspar is sericitised along cleavages. Biotite inclusions within the K-feldspar porphyroblasts have been largely shielded from this chloritisation. This large-scale retrogression is uncommon in the CZ and may well be related to late-/post-tectonic fluids that were channelled up the Omaruru Fault Zone and its associated splay faults (Map 1).

### 5.3.2 Metamorphism in the core of the Schönfeld Dome in NCZd

#### 5.3.2.1 Introduction

This section discusses the metamorphic assemblages in the pelitic and semi-pelitic biotite schists of the Oberwasser Formation on the farms Tjirundo 91 and Epako 38 in the core of the Schönfeld Dome (Map 1). In hand specimen, the schists possess a single pervasive schistosity defined by micas and have undergone amphibolite-facies metamorphism. In contrast to the Kuiseb Formation, muscovite rarely comprises more than 5% of the modal abundance of Oberwasser Formation schists. In the lower Oberwasser Formation, muscovite is usually absent; for example at the Otjua Prospect, the biotite schists contain neither muscovite nor aluminosilicate minerals (Steven, 1987). Middle Oberwasser Formation schists contain 3-5 wt%  $SiO_2$  less than their Kuiseb Formation counterparts (compare Tables 2.10, 2.13, 2.24, 2.25 and 2.26) and have considerable K-feldspar. One suspects that at least some of this K-feldspar was present prior to metamorphism and thus the Oberwasser Formation schists are not true pelites, but greywackes (Yardley, 1989, p.65). There appears to be an overall increase in metamorphic grade towards the centre of the Schönfeld Dome with localised thermal highs near granitic and pegmatitic intrusions. Spotted cordierite-bearing schists and the appearance of feldspar-rich blebs that disrupt the metamorphic banding and are suggestive of partial melting are widespread, but, due to the large number of intrusions with overlapping thermal aureoles, metamorphic assemblages cannot be mapped out in the field. However, four zones have been distinguished and samples have been selected from the middle and upper Oberwasser Formation to illustrate the late-tectonic thermal metamorphism superimposed on the regional metamorphic assemblages. Quartz is present in all the assemblages examined. None of the  $Al_2SiO_5$  polymorphs described is visible in hand specimen. Only one example of a garnetiferous schist was found and only traces of retrogressive chlorite were noted.

#### 5.3.2.2 Biotite zone

In the northern portion of Tjirundo 91, the metasediments of the Oberwasser formation are represented by a fine-grained (<1 mm), lepidoblastic  $Qtz+Bt+Kfs+Ms$  schist. Sample TJ2 was taken at least 1.2 km from the nearest exposed granite. K-feldspar is more abundant than quartz and accessories include plagioclase, tourmaline, opaque minerals and zircon. Biotite, up to 700  $\mu m$  long, comprises approximately 25% of the schist and defines an  $S_1$  fabric. However, much mica is oriented at a considerable angle to this schistosity suggesting several stages of biotite growth. The felsic grains are arranged in a granoblastic mosaic, their grain size being less than 100  $\mu m$ . The schist contains no porphyroblasts nor textures of note and appears to be an equilibrium assemblage. This nondescript biotite-K-feldspar schist is representative of the Oberwasser Formation in those portions of the Schönfeld Dome that do not appear to have been subsequently metamorphosed by a thermal event. No phyllites have been observed in NCZd and it is thus apparent that the regional metamorphism was at least of lower amphibolite facies grade.

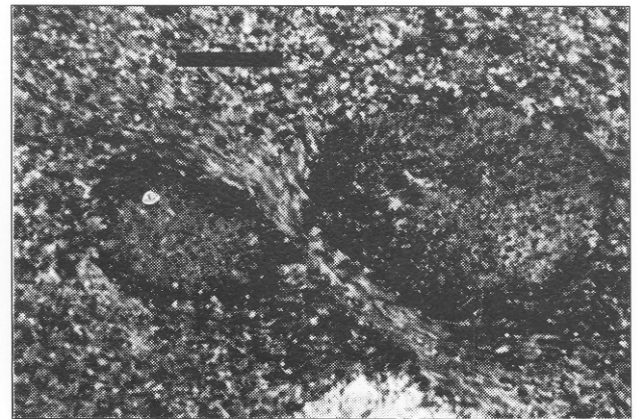
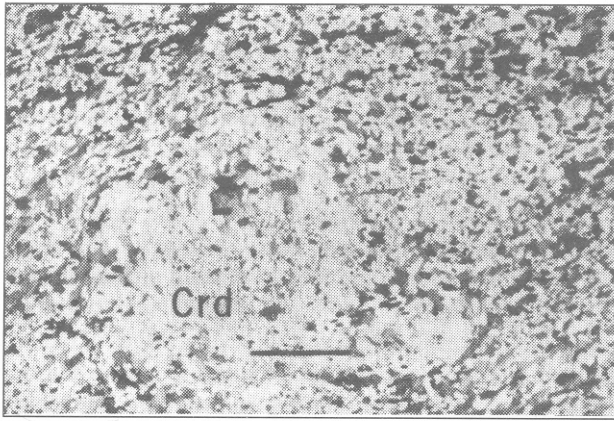


Plate 5.5: Synkinematic ( $D_3$ ) cordierite poikiloblasts in Oberwasser Formation schists from Lower Cordierite Zone on northeast Tjirundo (TJ1; XL); scale bar = 1 mm

#### 5.3.2.3 Lower cordierite zone

A sample of spotted schist from the middle Oberwasser Formation (TJ1) was taken from the northeast corner of Tjirundo 91 (Map 1), slightly closer to late-tectonic granite and pegmatite intrusions. The schist has a fine-grained lepidoblastic groundmass (less than 500  $\mu m$ ) with cordierite poikiloblasts up to 5 mm in diameter. The spotted schist comprises  $Qtz+Bt+Ms+Crd+Kfs+Plag$ ; accessories include tourmaline, opaque minerals (probably graphite), epidote and apatite. The  $S_1$  schistosity that parallels lithological contacts is defined by biotite (30%) and muscovite (5%) but, as with the biotite zone, much of the mica is randomly oriented. Poikiloblastic cordierite crystals full of inclusions are slightly elongate in the plane of schistosity and are pinitised. The  $S_1$  fabric is deflected around the syntectonic cordierite poikiloblasts with residues of biotite and muscovite concentrated on the rims (plate 5.5). The small proportion of mica within the poikiloblasts suggests that cordierite growth occurred as a result of mica breakdown. The  $S_1$  fabric of the cordierite is generally very poorly defined. In only two poikiloblasts is a well-defined  $S_1$  clearly



**Plate 5.6:** Late-/post-kinematic cordierite (Crd) poikiloblast in Middle Oberwasser Formation schist from Upper Cordierite Zone on Otjua/Epako boundary (EP3/1; XL). Note absence of biotite rim; scale bar = 1 mm

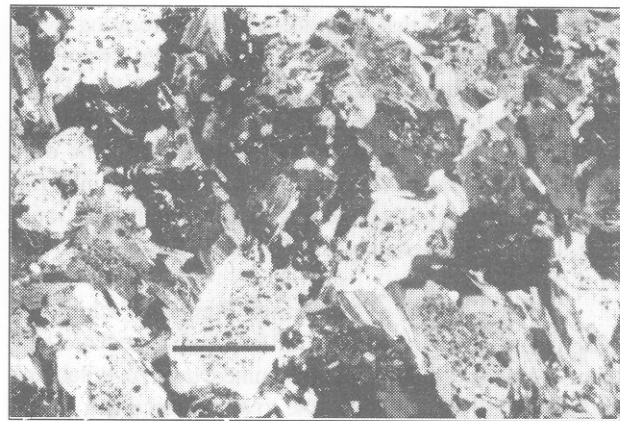


**Plate 5.7:** K-feldspar porphyroblasts in "schist" from sillimanite-K-feldspar zone at the Epako Gold Prospect (NS360; XL); scale bar = 1 mm

discordant to  $S_0$  and in one of these cordierites the micas are aligned parallel to the cleavage trace of the host. Other evidence for syntectonic cordierite growth is provided by the presence of rare pressure shadows around the porphyroblasts. The cordierites commonly possess nuclei of fresh, coarse-grained biotite, muscovite and quartz which appears to be forming from retrogressive reversal of the reaction  $Bt+Ms+Qtz=Crd+Kfs+H_2O$ .

#### 5.3.2.4 Upper cordierite zone

A sample from the middle Oberwasser Formation on the Otjua 37/Epako 38 boundary (EP3/1) has been selected to illustrate the higher metamorphic grade in the vicinity of granitic intrusions. The schist has a fine-grained (100-500  $\mu\text{m}$ ) groundmass, cordierite porphyroblasts up to 5 mm, a microscale gneissic banding rather than a schistosity and small (up to 7 mm in diameter) K-feldspar-rich blebs and lenses that disrupt the metamorphic layering. It is considered unlikely that these K-feldspar-rich segregations are derived from the granitic intrusions. The schist comprises  $Qtz+Bt+Ms+And+Crd+Kfs+Plag$  and accessories include tourmaline and opaque minerals (probably graphite). Thus the diagnostic feature of upper cordierite zone rocks is the presence of cordierite and K-feldspar poikiloblasts. The  $S_1$  fabric, which is defined by biotite (30%) and muscovite (2-3%), has been severely disrupted. Yellowish, pinitised cordierites contain numerous quartz and mica inclusions. In some syntectonic poikiloblasts, the micas are aligned in linear zones,  $S_1$  being discordant to  $S_0$  by up to  $70^\circ$ . Not all cordierites contain inclusion trails, suggesting several stages of cordierite growth. Evidence to support this is provided by the lack of biotite concentrations around the more elongate, late-tectonic cordierites (compare Plates 5.5 and 5.6). In the late-tectonic cordierites, inclusion alignment is crystallographically controlled by the host. This second generation of cordierite may well have formed from biotite breakdown by the reaction  $Bt+Al_2SiO_5+Qtz=Kfs+Crd+H_2O$ . This is supported by the relict nature of the andalusite. Blebs of the aluminosilicate in optical continuity over distances of 3-4 mm are enveloped by plagioclase and K-feldspar. The second generation K-feldspar has a poikiloblastic nature, enveloping quartz in particular, and can be distinguished from the earlier fine-

grained crystals in the matrix. Some tiny needles on the edge of biotite crystals may be fibrolite.

#### 5.3.2.5 Sillimanite-K-feldspar zone

The fourth sample was taken from borehole ED-1 (Epako Gold Prospect) collared in an area intruded by numerous pegmatite and small granite bodies in the northern portion of Epako 38 (Map 1). Sample NS360 was taken at a depth of 270 metres from surface. The "schist" has lost its lepidoblastic nature and has a granoblastic (150-500  $\mu\text{m}$ ) matrix (Plate 5.7). The assemblage  $Qtz+Bt+Ms+And+Sil+Kfs+Plag$  is present, the accessories comprising opaque minerals, zircon and considerable tourmaline. The randomly oriented, second generation K-feldspar (up to 3 mm long) is commonly perthitic and contains numerous inclusions. Oligoclase and andesine feldspar (determined by Michel-Lévy method) are present as inclusions and poikiloblasts. The aluminosilicate minerals comprise approximately 5% of the rock. Andalusite is present as relict blebs several tens of microns in diameter in optical continuity over distances of 3-4 mm. Fibrolite has grown directly from muscovite or on biotite where in contact with K-feldspar or perthite. Sillimanite is usually hosted by K-feldspar and plagioclase and is commonly in contact with biotite and, although present in the vicinity of andalusite, the two aluminosilicates are never in direct contact. The sillimanite is randomly oriented and there are no lineations nor fold axes in the area to which its growth can be related. The absence of muscovite in K-feldspar domains suggests that the mica has been consumed in the reaction  $Ms+Qtz=Kfs+Sil+H_2O(\pm\text{melt})$ . The appearance of "upper sillimanite zone" assemblages (Yardley, 1989) would thus appear to be unrelated to the regional metamorphism and be a result of the thermal metamorphism associated with the granite intrusions. Minor poikiloblastic muscovite is obviously late-/post-kinematic.

### 5.3.3 Metamorphism on the farm Ohere 106 in NCZe

#### 5.3.3.1 Introduction

On the farm Ohere (Fig. 5.2) biotite phyllites of the Kuiseb Formation have been thermally metamorphosed by granite

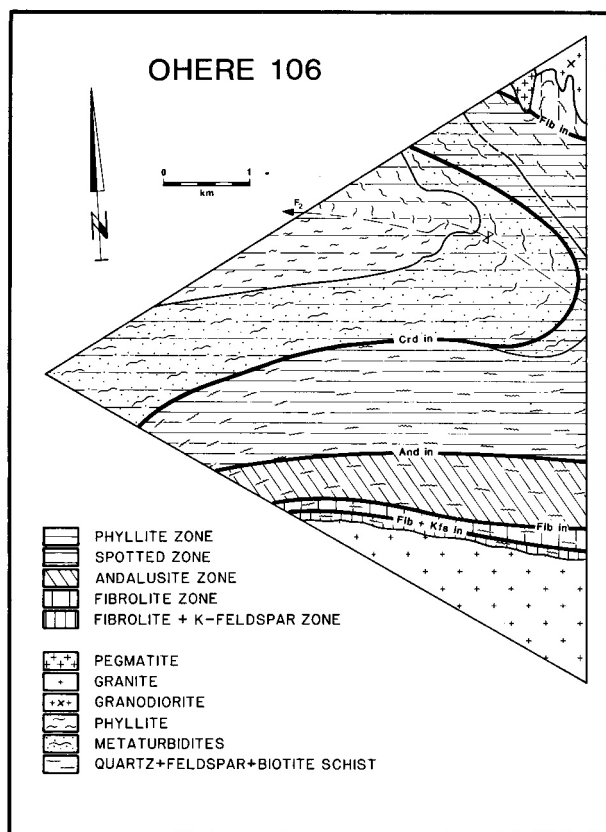


Figure 5.3: Metamorphic zones on Ohere 106

intrusions (Map 2). These are some of the best exposed examples of Buchan-type metamorphism in the NCZ and the metamorphic assemblages bear similarities with those described by Lagarde *et al.* (1990). A transition from green-schist facies phyllites in the core of the  $F_2$  syn-form through spotted schists to coarser-grained schistose hornfels on the granite contacts is clearly evident in the field. Metamorphic zones, based on field and petrographic studies have been mapped around the granites (Fig. 5.3) and will now be discussed in detail. Quartz is present in all the metamorphic assemblages examined. One of the few examples of garnetiferous schist in NCZe is exposed on the northern slope of Hill 1265 (Map 2). An unusual fluor-muscovite-spessartine garnet rock (OH-52) that crops out near a zone of tourmaline alteration and arseniferous gossan is thought to be an example of (hydrothermally?) altered schist. This rock is not suitable for biotite-garnet geothermometry (Ferry and Spear, 1978).

### 5.3.3.2 Phyllite Zone

The core of the synform on Ohere is underlain by phyllites and fine-grained schists characteristic of green-schist facies terrain. Milky quartz veins commonly parallel the essentially bedding-parallel schistosity ( $S_1$ ). In the hinge of the  $F_2$  fold, where a pervasive, axial planar  $S_2$  cleavage is developed, the quartz veins have a riffled surface indicating that their development predated granitoid intrusion. The phyllites are fine-grained (20-300  $\mu\text{m}$ ) and the  $S_1$  assemblage comprises  $\text{Qtz}+\text{Bt}+\text{Ms}\pm\text{Fsp}\pm\text{Chl}$ . Accessories include tourmaline, opaque minerals, zircon, apatite, calcite, epidote, sphene and serpentine. Only a few grains of fine-grained, fresh chlorite were noted in some thin sections, no-

tably defining secondary fabrics and replacing biotite. The  $S_1$  biotite is of regional metamorphic origin and unrelated to the intrusion of the granites. The undulose extinction and hence strained nature of some of the biotite is considered to be additional evidence for a pre- $F_2$  age. The  $S_1$  fabric is not always parallel to lithological contacts; for example in sample NS213 a faint compositional layering that is probably bedding is developed at  $30^\circ$  to the  $S_1$  foliation. The opaque minerals are commonly oxidised pyrite and arseno-pyrite porphyroblasts. Micas drape around these oxides and quartz is concentrated in the associated pressure shadows. In the core of the  $F_2$  fold (Map 2), the  $S_2$  foliation is defined by coarser-grained, commonly poikiloblastic, muscovite, fresh chlorite or brown-green biotite locally altered to a colourless, Mg-rich chlorite.

### 5.3.3.3 Spotted Zone

At a distance of approximately 2.2 km from the Ohere leucogranite and 1.5 km from the Ohere Oos Salem granite (Map 2) the phyllite is replaced by a fine-grained spotted or nodular schist. The thermal aureole is more easily identifiable around the younger Ohere leucogranite. The grain size of the matrix of spotted zone rocks varies between 40 and 200  $\mu\text{m}$ . The spots are either concentrations of muscovite or, more commonly, blue-grey avoids of cordierite up to 7 mm in diameter. Thus the mineral change that most clearly marks the boundary of a thermal aureole is the appearance of cordierite porphyroblasts. Spotted zone rocks comprise the assemblage  $\text{Qtz}+\text{Bt}+\text{Ms}+\text{Crd}\pm\text{Kfs}\pm\text{Plag}$ , the  $S_1$  fabric being defined by biotite. Accessories include tourmaline, graphite, apatite, opaque minerals and traces of chlorite. In the core of the  $F_2$  fold muscovite crystals are concentrated in ovoid clusters up to 2 mm in diameter. Within the clusters, muscovites are oriented in two principal directions, the long axes of the micas running parallel to the  $S_1$  and  $S_2$  cleavages in the area. This suggests that the thermally induced concentration of muscovite and the development of the  $F_2$  fold occurred contemporaneously. In sample NS218, a single crystal of undeformed, pinitised and altered cordierite has nucleated in the centre of a muscovite cluster. Cordierites are commonly strongly altered to chlorite and pinite on the rims, the latter imparting a characteristic yellow colour. Throughout the spotted zone the cordierite is notably poikiloblastic and has numerous inclusions, particularly of quartz. The relatively small number of mica inclusions suggests that muscovite and biotite were being consumed in the cordierite-forming reaction  $\text{Ms}+\text{Bt}+\text{Qtz}=\text{Crd}+\text{Kfs}+\text{H}_2\text{O}$ . The main problem with accepting that this was the primary cordierite-forming reaction is that very little K-feldspar has been observed in thin section. Miller (1980, p.55) experienced a similar difficulty in his study of cordierite zones that border Salem granite and was only able to identify K-feldspar by XRD analysis. It is considered unlikely that the reaction  $\text{Ms}+\text{Chl}+\text{Qtz}=\text{Crd}+\text{Bt}+\text{H}_2\text{O}$  took place because of the essential absence of chlorite in phyllite zone rocks. Micas, biotite in particular, wrap around some of the cordierite and are concentrated on the rims of the porphyroblasts in a similar manner to that described by Spry (1969, plate XIV). However, the timing of cordierite growth is problematico

Some samples (OH-46 and OH-56) possess poorly defined inclusion trails,  $S_1$  being developed at between  $10^\circ$  and  $20^\circ$  to  $S_2$ . The inclusion trails on their own are not considered to be convincing evidence for early kinematic cordierite growth because the muscovite in the clusters where cordierite nucleated is itself oriented parallel to the  $S_1$  and  $S_2$  foliations. Moreover, biotite wraps around and is concentrated at the muscovite clusters whose development would appear to be a result of thermal metamorphism. More convincing evidence for syntectonic cordierite growth is provided by the local presence of quartz-dominated pressure shadows around cordierite poikiloblasts in OH-36. Closer to the Ohere leucogranite (OH-56) cordierite crystals are flatter, indicating a higher ratio of compressive to shear strain or alternatively post-crystallisation deformation. Cordierites with inclusion-rich cores and inclusion-poor rims provide evidence for two stages of growth (OH-37). It is concluded that the majority of the cordierites are not the poikiloblastic overgrowths that one would expect in a post-tectonic thermal aureole. Their development is related to the thermal effects and syn- to late-tectonic deformation that accompanied the intrusion of the Salem granite and the leucogranite in particular (see Chapter 4 for a discussion on deformation and concomitant granite intrusion in NCZe). A faint  $S_2$  fabric defined by coarser-grained biotite and traces of chlorite is locally present in the spotted zone.

#### 5.3.3.4 Andalusite zone

The boundary of this zone is marked by the first appearance of small (1 mm) andalusite crystals that can only be identified in thin section. The schist is less fissile and coarser-grained (500  $\mu\text{m}$  - 1 mm) than in the spotted zone and is characterised by the assemblage Qtz+Crd+Bt+Ms+And $\pm$ Kfs $\pm$ Plag( $\pm$ Fib?). Accessories include opaque minerals (some of which are graphite), tourmaline, zircon, apatite and traces of chlorite. The cordierite poikiloblasts are notably flatter than in the spotted zone and are extensively pinitised, while the biotites are browner. There is a general, but by no means exclusive, spatial association between cordierite and andalusite. The poikiloblastic, subhedral andalusite has numerous inclusions (but no trails) and locally appears to be pseudomorphic after-cordierite. The close spatial association between cordierite and andalusite, the lack of muscovite in andalusite domains and the presence of slightly coarser-grained  $S_2$  biotite developed at a high angle to the  $S_1$  schistosity suggest that the prograde reaction  $\text{Ms} + \text{Crd} = \text{Qtz} + \text{And} + \text{Bt} + \text{H}_2\text{O}$  has occurred. The deflection of  $S_1$  biotite crystals around andalusite poikiloblasts is considered to be an inherited fabric derived from the spotted zone. There is enough evidence to relate the formation of andalusite on Ohere to the thermal metamorphism that accompanied the intrusion of the Ohere leucogranite rather than regional metamorphic processes. In several samples, tiny needles of possible fibrolite were observed indicating that the reaction  $\text{Ms} + \text{Crd} = \text{Qtz} + \text{Als} + \text{Bt} + \text{H}_2\text{O}$  occurred on the boundary with the sillimanite stability field (the lower sillimanite zone of Yardley, 1989). In a specimen taken close to the fibrolite-K-feldspar zone, cordierite has been retrogressively altered to coarse-grained chlorite and fine-grained, randomly oriented muscovite. Elsewhere coarse-

grained, post-kinematic muscovite overgrows the  $S_1$  fabric in a non-systematic manner. A local  $S_2$  fabric in andalusite zone rocks is defined by muscovite and chlorite after biotite. Pattison (1989) attributed the widespread occurrence of andalusite assemblages in graphitic schists in the Ballachulish aureole to a lowering of a  $\text{H}_2\text{O}$  by locally derived C-bearing fluid species. On Ohere this does not seem to have been the case: spotted zone rocks contain, if anything, more accessory graphite than andalusite zone schists.

#### 5.3.3.5 Fibrolite-K-feldspar zone

In the upper sillimanite zone on the borders of the Salem granite and the leucogranite, the schist loses its fissility and becomes more hornfelsic. A local, almost gneissic, segregation of the schist into leucocratic patches is evident. The zone is characterised in hand specimen by the development of coarse-grained (2 mm) aggregates of muscovite and in thin section by the assemblage Qtz+Bt+Ms+Als+Kfs+Crd. Accessories include plagioclase, tourmaline, opaque minerals and zircon. The diagnostic features of this zone are 1-mm-long fibrolite clusters and late-kinematic, elongate or poikiloblastic perthitic K-feldspar, though, somewhat surprisingly, the minerals are rarely in contact. Earlier, 'syntectonic cordierites (up to 3 mm long) with poorly defined inclusion trails are slightly pinitised. The biotite-dominated  $S_1$  fabric is deflected around the flattened cordierite porphyroblasts which lends the rock a knotty appearance. Preexisting corroded relicts of andalusite are commonly surrounded by quartz. Fibrolite needles have tended to nucleate on biotite and have replaced muscovite in particular, being concentrated in mats that are in contact with quartz and cordierite. Thus, in contrast to the aureole on Sandamap Noord where much of the fibrolite has grown from decomposed biotite and is not universally accompanied by K-feldspar growth, on Ohere the aluminosilicate growth has resulted from muscovite breakdown by the reaction  $\text{Ms} + \text{Qtz} = \text{Al}_2\text{SiO}_5 + \text{Kfs} + \text{H}_2\text{O}$  (the second sillimanite isograd; Evans and Guidotti, 1966) as well as andalusite decomposition. Large, second-generation muscovite poikiloblasts are randomly oriented and evenly distributed throughout the hornfels.

## 5.4 THERMOBAROMETRY

A petrogenetic grid for the pelitic metasediments of the Usakos-Karibib-Omaruru area has been constructed (Fig. 5.4). The  $\text{Al}_2\text{SiO}_5$  phase diagram of Holdaway (1971) with the triple point of  $501^\circ\text{C}$  and 3.76 kbar (Point H, Fig. 5.4) has been used. A discussion on the validity of this triple point has recently been given by Kerrick (1990), in which the "fibrolite problem" (Salje, 1986) and its influence on the  $\text{Al}_2\text{SiO}_5$  phase diagram is reviewed. It was, however, decided to retain Holdaway's (1971) value for the memoir. The curves for the reactions  $\text{Ms} + \text{Qtz} = \text{Als} + \text{Kfs} + \text{H}_2\text{O}$  (Chatterjee and Johannes, 1974),  $\text{Ab} + \text{Kfs} + \text{Qtz} + \text{H}_2\text{O} = \text{melt}$  (Luth *et al.*, 1964) and  $\text{Qtz} + \text{Bt} + \text{Ms} = \text{Kfs} + \text{Crd} + \text{H}_2\text{O}$  (Pattison and Harte, 1985) are also shown. The minimum biotite isograd is taken from Yardley (1989). The reaction  $\text{Ms} + \text{Chl} + \text{Qtz} = \text{Crd} + \text{Bt} + \text{H}_2\text{O}$  (Pattison, 1989) is shown for

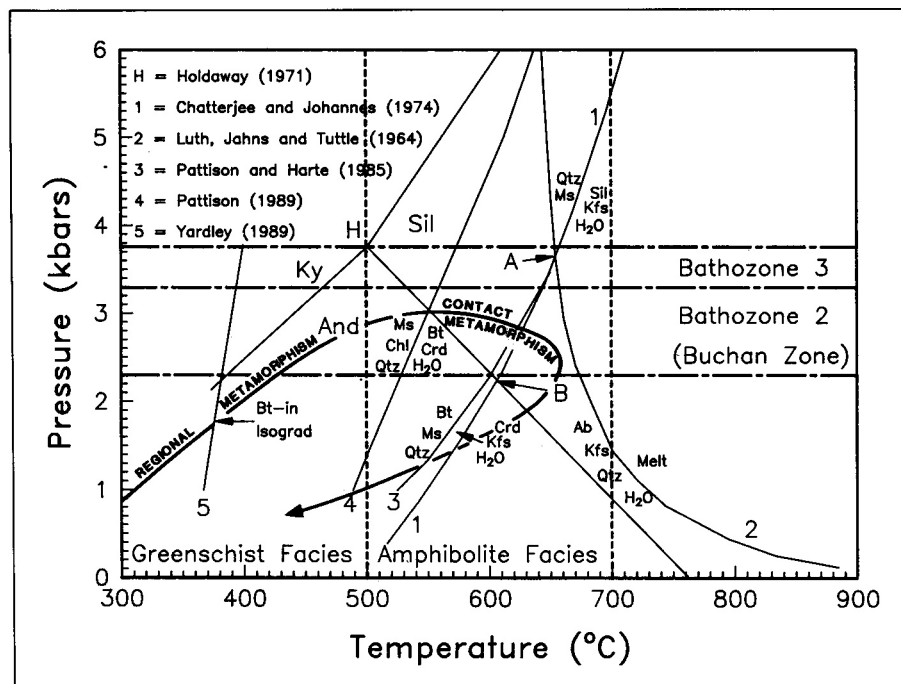


Figure 5.4: Petrogenic grid for pelitic metasediments in the CZ

completeness, but as discussed above, most of the cordierite in the CZ is believed to have formed from reaction 3. Because of the divariant nature of cordierite-forming reactions, the positions of curves 3 and 4 in Fig. 5.4 are for average cordierite compositions. Two of the relevant bathozones of Cannichael (1978), one of which corresponds to the Buchan Facies Series of Hietanen (1967), are also given. The greenschist-amphibolite facies boundary is taken from Essene (1989).

#### 5.4.1 Barometry

Kyanite has never been reported from the CZ and both andalusite and sillimanite are abundant. Because the sillimanite-bearing assemblages appear to have resulted from essentially isobaric heating, it is considered unlikely that peak metamorphic pressures at any stage in the evolution of the CZ exceeded the  $\text{Al}_2\text{SiO}_5$  triple-point value of  $3.76 \pm 0.3$  kbar (Holdaway, 1971). The absence of melt in most upper sillimanite zone assemblages indicates that the maximum pressure in the CZ during contact metamorphism was less than 3.65 kbar (Point A, Fig. 5.4). Throughout the field area the muscovite+quartz breakdown reaction yields fibrolite or sillimanite plus K-feldspar, but not andalusite (for the purposes of this memoir this reaction is considered to have occurred under the same conditions irrespective of whether fibrolite or sillimanite was produced). Thus confining pressures exceeded 2.2 kbar when this prograde reaction occurred (Point B, Fig. 5.4). Peak metamorphic pressures within the field area were thus between 2.2 and 3.6 kbar. These estimates are in good agreement with those obtained by other workers in central Namibia. Examination of metapelite assemblages in the southern SCZ near the Okahandja Lineament led Hoffer (1977) to suggest syntectonic pressures of 4 kbar, while values of between 4 (Sawyer, 1981) and 2.5 kbar (Hoffer, 1977) were estimated for the post-tectonic  $M_2$  peak. Puhan (1983) calculated total pressures

of between 2.6 and 3.4 kbar for the five-mineral assemblage forsterite+diopside+tremolite+dolomite+calcite for the area between Usakos and Swakopmund.

#### 5.4.2 Thermometry

There is a paucity of information on the regional and contact metamorphic temperatures that prevailed in the field area. Empirical observations indicate that the area underwent regional metamorphism in the greenschist-amphibolite facies (300°C-700°C). The lowest grade metamorphic rocks known to the author in the CZ are exposed on Ohere (Map 1) where the nearest granitoid intrusions are 3 km away. Biotite phyllites with only traces of mainly retrogressive chlorite are interpreted to have formed during regional metamorphism, prior to granitoid intrusion. Thus peak regional metamorphic temperatures in NCZe exceeded 400°C, the minimum temperature of biotite formation (Cliff, 1985; Yardley, 1989). In the other tectono-stratigraphic zones, regional metamorphic temperatures were possibly higher, certainly not less. Calcite-graphite geothermometry (Pineau *et al.*, 1976; Valley and O'Neil, 1981; Kreulen and Van Beek, 1983) has been used on marbles from the CZ by several authors. Valley and O'Neil (1981) applied their fractionation curve to four analyses from the Karibib area taken by Pineau *et al.* (1976) and found good agreement with temperatures obtained by Puhan (1976): 598°C by calcite-graphite isotope geothermometry as against 620°C by calcite-dolomite solvus thermometry. Steven (1987) subsequently used the same isotope geothermometer on calcitic marble from the Okawayo Formation to the north of Omaruru. Samples were taken from the core of the Okakombo Horst on Tjirundo Süd in NCZc and from the core of the Schönfeld Dome on NCZd (Map 1). Peak metamorphic temperatures of between 519°C and 626°C with an average of 586°C were indicated. This was considered to be consistent with the phase relations of the surrounding metasediments. These figures agree remark-

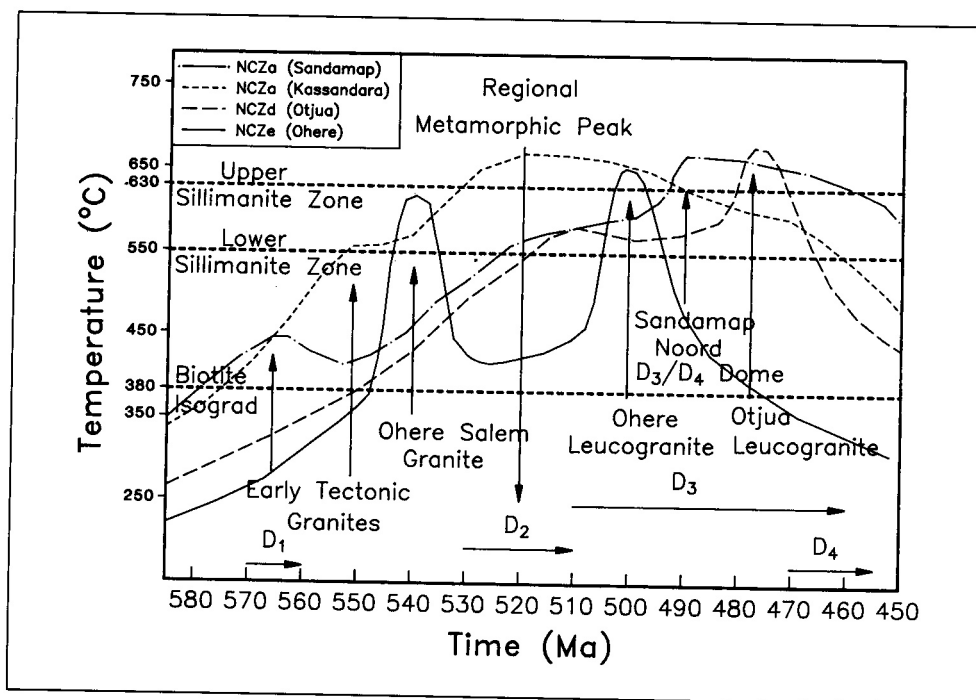


Figure 5.5: Deformation, metamorphism and granite intrusion in the CZ

ably well with those indicated by the petrogenetic grid (Fig. 5.4). Lower sillimanite zone rocks, which are common in the Schönfeld Dome, were stable between 500°C and 660°C (assuming a maximum confining pressure of 3.65 kbar). In the aureoles of granite intrusions (less than 200 metres from the contact), to which the upper sillimanite zone rocks are essentially confined, peak metamorphic temperatures exceeded 610°C (assuming a minimum confining pressure of 2.2 kbar). In general, the appearance of fibrolite without K feldspar in andalusite schists in the thermal aureoles of central Namibia supports Kerrick's (1987) contention that fibrolite growth occurred below the sillimanite stability field. Both the Irish and Namibian data contradict the experimental findings of Salje (1986) who determined that fibrolite is confined to a higher temperature field than sillimanite. The absence of wide-scale partial melting indicates that peak metamorphic temperatures in central Namibia did not exceed 700°C, even in the immediate vicinity of granitic plutons.

### 5.5 CONCLUDING COMMENTS ON THE DAMARAN TECTONOTHERMAL HISTORY OF THE FIELD AREA

A study of the metapelites of the Oberwasser and Kuiseb Formations was undertaken to illustrate the tectonothermal history of the field area. A generalised P-T-t loop for the various tectono-stratigraphic zones examined with the exception of NCZe is shown in Fig. 5.4. Peak metamorphic pressures in NCZe were lower, perhaps by as much as 0.5-1 kbar. A schematic diagram was constructed to show the relationship between deformation and metamorphism and the strong influence of the granite intrusions on the thermal history of the Central Zone at 3 kbar (Fig. 5.5). A confining pressure of 3 kbar was chosen because the value lies in the middle of the range given by the petrogenetic grid for pelitic meta-

sediments (Fig. 5.4) and is the average value determined by Puhan (1983). At 3 kbar, lower-sillimanite-zone conditions are attained at 550°C, upper-sillimanite-zone conditions at 630°C (Fig. 5.4). For the purposes of this diagram the Rb-Sr whole-rock dates of the granitoids are interpreted as ages of emplacement. The validity of this assumption will be discussed in Chapter 6.

Early deformation ( $D_1$  and  $D_2$ ) was marked by isoclinal ( $F_1$ ) and tight ( $F_2$ ) folding, but there is little evidence for recumbent folding as suggested by Miller (1983a). Accompanying regional metamorphism resulted in the widespread formation of biotite±muscovite schists in the northern SCZ and the southern NCZ and lower temperature assemblages, such as biotite phyllites, in NCZe (Fig. 5.5). The growth of metamorphic minerals can rarely be related to specific folding phases because of the paucity of fold closures and the superimposition of several generations of mica fabrics on one another. There is almost no indication of laterally directed tectonic transport in the early deformational phases in the Central Zone, in strong contrast to the Okahandja Lineament and Southern Zones in the southern portion of the orogen (Fig. 2.2; Miller, 1983a). The intrusion of early/syntectonic leucogranites in NCZa (Fig. 5.5) was partly responsible for the widespread formation of early/synkinematic cordierite in the pelitic units near the Omaruru Lineament. There is general agreement that the peak of regional metamorphism in the CZ occurred approximately syn- $D_2$  at ~520 Ma (Haack *et al.*, 1980; Miller, 1983a). In the vicinity of the Omaruru Lineament, the intrusion of syn- $D_2$  leucogranites resulted in the thermal overprinting of regional metamorphic assemblages, and localised partial melting in NCZa on Kassandara (Fig. 5.5) and in NCZb and NCZc. The  $D_3$  (510-460 Ma; Kröner, 1984) deformation ( $F_3$  folding) and concomitant granite intrusion were responsible for the northeast-trending structural grain and the northeast-trending oval to elongate, upright,

domal structures of the area. Rotation and further flattening of early/synkinematic cordierite porphyroblasts was related to this granite doming and associated folding. The intrusion of the post- $D_2$  granitoids had a major impact on the thermal history of NCZa, NCZd and NCZe in particular (Fig. 5.5), resulting in the progressive formation of second-generation cordierite, andalusite and sillimanite zones around thermal domes.  $D_4$  deformation resulted from movement on major lineament structures, such as the Welwitschia lineament zone, causing the localised formation of westward-verging  $F_4$  folds with north-northeast-trending axial traces. A prominent easterly or east-southeast-plunging sillimanite lineation is commonly associated with these  $F_4$  folds, supporting Miller's (1983a) contention that, in some parts of the CZ, such as on Sandamap Noord in NCZa, peak metamorphic conditions persisted until late-/post-tectonic times (Fig. 5.5).

In the NCZ deeper, apparently more deformed, crustal sections are in contact with shallower, less-deformed assemblages. In spite of the differences between the individual zones, there is a notable similarity in the mineral assemblages of the metapelites, which reflects the Buchan-style metamorphism to which the CZ was subjected. Along the Omaruru Lineament in NCZa, the intrusion of syntectonic granites resulted in the attainment of a regional metamorphic peak around  $D_2$  (~520 Ma) followed by  $D_3/D_4$  thermal overprinting. In NCZd and NCZe in contrast, where the evidence for one early isoclinal folding phase, let alone two, is not entirely convincing, the deformation and metamorphism occurred largely as a result of the syn- $D_3$  (510-460 Ma) intrusions. In general terms the intensity of metamorphism decreases to the northwest. Furthest from the collision zone in NCZe, rocks from the uppermost tectono-stratigraphic unit were regionally metamorphosed to greenschist grade only. They bear similarities to metasediments on the margins of the orogen in the Northern Zone (Fig. 2.2; Miller, 1980). This juxtaposition of tectono-stratigraphic zones with differing tectonothermal histories is not entirely a result of Damaran tectonism. Karoo/post-Karoo faulting was not inconsiderable in central Namibia.

The major conclusion that can be drawn from this study of four areas in the CZ is that the regional and contact metamorphism was of low-pressure/high-temperature type. However, there is a major problem in the CZ in separating regional from contact metamorphic effects in areas of abundant granitic intrusions as elsewhere (Holdaway *et al.*, 1982). One of the most surprising finds has been the recognition of thermal lows marked by greenschist facies rocks in an area traditionally thought to be underlain by sillimanite-cordierite assemblages and widespread partial melting (Miller, 1983a). The development of sillimanite-bearing assemblages is less common than indicated by Hoffer (1977) and is restricted to the aureoles of the, albeit numerous, syn-/late tectonic granite intrusions. In NCZb and NCZc in particular, these intrusions are so widespread that the appearance of sillimanite schists and the products of partial melting should be referred to as a regional contact metamorphic phenomenon. The number of metamorphic events that have affected the Damara Orogen has been the subject of much discussion. Jacob (1974), Hoffer (1977), Blaine (1977) and Puhan (1979) all argued for a single metamorphic event in the CZ that started syntectonically (during  $D_1$ ) and rose to a syn-/post-tectonic peak (Miller, 1983a). In contrast, Sawyer (1981) and Kasch (1983b) distinguished two peaks of metamorphism in the southern SCZ and Southern Margin Zone respectively. In a more recent study in the Southern Zone, east of Okahandja, Kasch (1987) recognised a single, prolonged event of prograde metamorphism. This author favours the existence of a single regional metamorphic peak, but has done insufficient work within the field area to determine whether the regional metamorphic peak in the NCZ was diachronous. However, the contact metamorphic effects clearly did not occur simultaneously; thus metamorphism in the NCZ, in general terms, was certainly diachronous. In a terrain such as the NCZ, where the influence on the timing and intensity of metamorphism has been so strongly influenced by syntectonic granite intrusions, it would seem pertinent to ask whether one can talk about a "peak of regional metamorphism" at all.



## 6. GEOCHRONOLOGY

### 6.1 INTRODUCTION

Most geochronological work in central Namibia has concentrated on Rb-Sr whole-rock determinations of the numerous granitic and pegmatitic intrusions. The data base for the field area largely rests on a detailed structural analysis of the planar fabrics within six granitoids and an accompanying Rb-Sr investigation (Haack *et al.*, 1980). This was the first attempt to unravel the relationship between the various granite intrusion types and the major folding phases in the Omaruru area. The regional synthesis conducted by Haack *et al.* (1983) provides Rb-Sr and  $\delta^{18}\text{O}$  information on the intrusions of the CZ, but at several localities the relationship between the intrusion and the local geology is either poorly exposed or poorly understood. Kröner and Hawkesworth (1977) were the first authors to provide geochronological evidence for late-tectonic emplacement of the uraniumiferous alaskites. A summary of the latest geochronological information available at the time was given by Miller (1983a). More recently, Haack and Gohn (1988) have dated mineralised pegmatites from the Uis Tin Mine and the Rubicon Lithium Mine (Fig. 1.3). Although the Donkerhuk granite, which intruded along the Okahandja Lineament (Fig. 2.1), lies well out of the field area, the work conducted by Blaxland *et al.* (1979) on this intrusion was important in constraining the geological history of the southern margin of the CZ.

It must be emphasised that only rarely does the stage in the evolution of a rock considered to be a geologically significant event coincide with the stage which is dated isotopically (Cliff, 1985). For example, mineral ages can record either a recrystallisation event or the cooling history of the orogen (Miller, 1983a), chemical and isotopic equilibration being stopped over a narrow temperature interval, commonly referred to as the "closure temperature" (Dodson, 1973). In spite of these cautionary comments it was considered nec-

essary to expand the geochronological data base for central Namibia, particularly in the NCZ. Because of the close spatial association between epigenetic mineralisation and the younger intrusions, attention was focused on the syn- to late-tectonic granitoids and pegmatites. Early tectonic granitoids and red granites have not been analysed. The Rb-Sr whole-rock ages of six Damaran granitoids and pegmatites considered, firstly, to be representative of the field area and, secondly, that host tin mineralisation or crop out in the immediate vicinity of epigenetic gold and tungsten mineralisation, have been determined. Mineral ages from one intrusion and the isotopic characteristics of three galena samples from the Sandamap Noord and Epako Gold Prospects have also been determined. Throughout the discussion a distinction between the terms "date" (a solution to an equation) and 'age' (a significant geological event) has been made (Faure, 1986).

### 6.2 Rb-Sr WORK

#### 6.2.1 Analytical Procedure

The analytical procedures that were followed are detailed in the Appendix.

#### 6.2.2 Rb-Sr whole-rock results

Results are listed and discussed in order of decreasing Rb-Sr age (Tables 6.1 and 6.2).

##### 6.2.2.1 Ohere Oos Salem granitoid

This intrusion has a granite core (samples NS233, NS234) and a granodiorite marginal phase (samples NS232, NS235; Map 1). Both phases are considered to belong to the same pluton (see discussion in Chapter 3). If the Sr-isotope results (Tables 6.1 and 6.2) from the two phases are placed on the

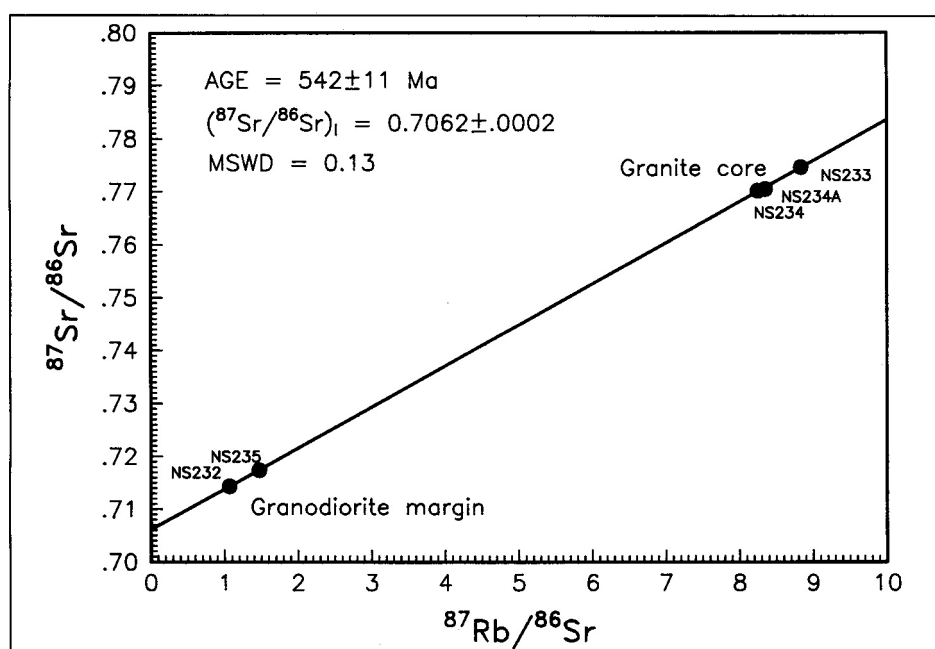


Figure 6.1: Rb-Sr whole-rock isochron for the Ohere Oos Salem granitoid

Locality and Lithology	Sample No.	Rb	Sr	Rb/Sr	$^{87}\text{Rb}/^{86}\text{Sr}$	$^{87}\text{Sr}/^{86}\text{Sr}^*$
Ohere Oos Salem granitoid	NS232	137	372	0.368	1.067	$0.71443 \pm 2$
	NS233	334	110	3.04	8.835	$0.77457 \pm 2$
	NS234	318	112	2.84	8.248	$0.77013 \pm 2$
	NS234A <sup>1</sup>	623.8	217.4	2.87	8.355	$0.77045 \pm 2$
	NS235	165	324	0.509	1.471	$0.71747 \pm 2$
Sandamap Noord leucogranite	NS292	286	68	4.21	12.354	$0.80652 \pm 2$
	NS293	282	47	6.00	17.524	$0.84475 \pm 2$
	NS293A <sup>1</sup>	482.7	82.1	5.88	17.241	$0.83936 \pm 2$
	NS294	285	52	5.48	16.049	$0.83147 \pm 2$
	NS295	229	82	2.79	8.106	$0.77417 \pm 2$
	NS295A <sup>1</sup>	244.9	87.1	2.81	8.192	$0.77521 \pm 2$
Ohere leucogranite	NS236	363	88	4.13	11.975	$0.79779 \pm 2$
	NS237	355	88	4.03	11.792	$0.79528 \pm 2$
	NS238	358	94	3.81	11.057	$0.78915 \pm 2$
	NS239	344	96	3.58	10.450	$0.78748 \pm 2$
	NS239A <sup>1</sup>	327.2	87.8	3.73	10.870	$0.78878 \pm 2$
Kohero Tin Mine stanniferous pegmatite	NST12-1	1056	1040	1.02	2.946	$0.74628 \pm 2$
	NST12-2	1766	968	1.82	5.412	$0.76341 \pm 2$
	NST12-2 <sup>1</sup>	1791	963	1.86	-	-
	NST12-3	422	1457	0.290	0.840	$0.73155 \pm 2$
	NST12-4	435	1308	0.333	0.964	$0.73225 \pm 2$
	NST12-5	953	1244	0.766	2.224	$0.74129 \pm 2$
Sandamap Noord non-stanniferous pegmatite	NST8-1	188	29.2	6.44	18.895	$0.85418 \pm 2$
	NST8-2	206	30.3	6.80	19.965	$0.86089 \pm 2$
	NST8-3	314	35.1	8.95	26.383	$0.90516 \pm 2$
	NST8-4 <sup>1</sup>	337.0	27.9	12.07	35.827	$0.96790 \pm 2$
	NST8-5	321	29.8	10.77	31.876	$0.94063 \pm 2$
	NST8-6 <sup>1</sup>	231.0	39.5	5.85	17.154	$0.84206 \pm 2$
Sandamap Tin Mine stanniferous pegmatite	NST9-1	45.4	6.1	7.44	21.879	$0.87157 \pm 2$
	NST9-2	31.2	6.0	5.20	15.212	$0.82138 \pm 4$
	NST9-4	83.6	6.0	13.93	41.462	$0.99920 \pm 5$
	NST9-5	15.8	5.6	2.82	8.220	$0.77905 \pm 4$
	NST9-6 <sup>1</sup>	68.04	12.8	5.30	19.090	$0.85352 \pm 2$

**Table 6.1:** Rb and Sr data for the three granitoids and the three pegmatites analysed

<sup>1</sup> Rb and Sr data obtained by isotope dilution

\*  $\pm$  S.E. (internal precision). Errors of 1.5% and 0.005% were applied to the  $^{87}\text{Rb}/^{86}\text{Sr}$  and  $^{87}\text{Sr}/^{86}\text{Sr}$  values respectively.

The two stanniferous pegmatites (NST9 and NST12) are relatively inhomogenous and large (20 kg) samples were selected. The non-stanniferous pegmatite on Sandamap Noord is relatively homogenous: the grain size rarely exceeds 5 mm.

same isochron (Fig. 6.1), the pluton has an Rb-Sr whole-rock age of  $542 \pm 11$  Ma ( $(^{87}\text{Sr}/^{86}\text{Sr})_1 = 0.7062$ ). This is considered to be the age of crystallisation and is almost identical to the emplacement age for the compositionally similar Otjozondjou pluton (Fig. 6.2), one of the best documented Salem granitoids in the CZ (Miller, 1980). The Otjozondjou intrusion also has a one-kilometre-wide marginal phase of quartz monzodiorite and diorite. The pluton has a U-Pb zircon age of  $546 \pm 30$  (Miller and Burger, 1983), an Rb-Sr whole-rock age of  $548 \pm 31$  Ma (Hawkesworth *et al.*, 1983) as well as a low  $(^{87}\text{Sr}/^{86}\text{Sr})_1$  ratio of 0.7054. The only other Salem Suite

granitoid that has been dated in the NCZ is the syn- $F_2$  Okombahe intrusion (Fig. 6.2) which has an Rb-Sr whole-rock age of  $553 \pm 22$  Ma ( $(^{87}\text{Sr}/^{86}\text{Sr})_1$  of 0.7056), also interpreted as a crystallisation event by Haack *et al.* (1980). Both the Otjozondjou and Okombahe intrusions, being syntectonic, are foliated on their margins. This marginal fabric is absent from the Ohere Oos intrusion because of the lower intensity of deformation in NCZe. In spite of its almost circular outcrop pattern, the author believes that the Ohere Oos granite intruded at the same time as, and is partly responsible for, the  $F_2$  folding in NCZe (Maps 1 and 2).

Locality	Lithology	Age (Ma)	$(^{87}\text{Sr}/^{86}\text{Sr})_i$	MSWD
Ohere Oos	Salem Granitoid	542 ± 11	0.7062 ± .0002	0.13
Sandamap Noord	Leucogranite Phacolith	512 ± 19	0.7153 ± .0030	0.67
Ohere	Leucogranite	506 ± 135	0.7107 ± .0214	1.14
Kohero Tin Mine	Stanniferous Pegmatite	492 ± 11	0.7256 ± .0002	1.10
Sandamap Noord	Pegmatite	473 ± 23	0.7267 ± .0072	0.05
Sandamap Noord	Stanniferous Pegmatite	468 ± 14	0.7238 ± .0028	3.17

**Table 6.2:** Rb-Sr whole-rock dates of granitoids and pegmatites. Errors in dates and  $(^{87}\text{Sr}/^{86}\text{Sr})_i$  ratios reported at 95% confidence level

#### 6.2.2.2 Sandamap Noord Leucogranite

The folded peraluminous leucogranite phacolith on Sandamap Noord (Map 3) has an Rb-Sr whole-rock date of 512 ± 19 Ma ( $(^{87}\text{Sr}/^{86}\text{Sr})_i = 0.7153$ ; Tables 6.1 and 6.2) which is taken to be the age of crystallisation of the intrusion (Fig. 6.3). This date coincides with the  $F_2$  folding in NCZa and the regional metamorphic peak (Fig. 5.5). This is supported by the fact that the leucogranite has a banding rather than a true foliation, indicating a post- $D_1$  age. The results support the contentions of Watson (1982) that the intrusion lies in the core of a domal structure which has deformed and been partly formed by the granite. The date for the Sandamap Noord intrusion is indistinguishable from the syn- $F_2$  "leucocratic granite" in the Omaruru River valley (Fig. 6.2; Haack *et al.*, 1980) which has an Rb-Sr whole-rock age of 514 ± 22 Ma ( $(^{87}\text{Sr}/^{86}\text{Sr})_i = 0.7123$ ). This is of note because the geochemical data (Chapter 3) showed that the Sandamap Noord intrusion is the most peraluminous granite examined in the CZ. One of the few other granites in the orogen to contain magmatic muscovite is the Donkerhuk granite for which Blaxland *et al.* (1979) determined Rb-Sr whole-rock ages of 523 ± 8 Ma ( $(^{87}\text{Sr}/^{86}\text{Sr})_i = 0.7074$ ) and 521 ± 15 Ma ( $(^{87}\text{Sr}/^{86}\text{Sr})_i = 0.7117$ ). Contemporaneous intrusion of peraluminous granites near major structural breaks such as the Omaruru and Okahandja Lineaments is therefore indicated.

#### 6.2.2.3 Ohere leucogranite

The Ohere leucogranite (Map 1) has an Rb-Sr whole-rock date of 506 ± 135 Ma ( $(^{87}\text{Sr}/^{86}\text{Sr})_i = 0.7107$ ; Tables 6.1 and 6.2 and Fig. 6.4) which is interpreted as a crystallisation event. The very homogenous nature of this intrusion (Table 3.7), and hence poorly constrained isochron, accounts for the large error. This result confirms that leucogranites with an oval to circular outcrop pattern within central Namibia (Fig. 6.2) have a late- to post-tectonic (post-  $D_2$ ) age.

#### 6.2.2.4 Pegmatites hosted by greenschist-facies rocks at the Kohero Tin Mine, west of Omaruru

The stanniferous pegmatite at the Kohero Tin Mine (Fig. 6.2 and Map 1), which does not contain any biotite, has an

Rb-Sr whole-rock date of 492 ± 11 Ma and a high  $(^{87}\text{Sr}/^{86}\text{Sr})_i$  ratio of 0.7256 (Tables 6.1 and 6.2 and Fig. 6.5). This date is indistinguishable from that determined for the morphologically similar, essentially unzoned, dyke-like pegmatite at the Uis Tin Mine (496 ± 30 Ma, Haack and Gohn, 1988; Fig. 6.2).

#### 6.2.2.5 Pegmatites hosted by amphibolite-facies rocks on Sandamap Noord, west of Usakos

Non-stanniferous pegmatite (with traces of biotite) from the margin of the Sandamap Noord  $D_3/D_4$  dome and stanniferous pegmatite (with no biotite) from the Sandamap Tin Mine have been investigated (Map 3). Surprisingly, Rb concentrations in the two pegmatites are considerably lower than the stanniferous pegmatites from the Kohero (see above) and Uis Tin Mines (Haack and Gohn, 1988), but the Rb/Sr ratios are higher (Table 6.1). Both pegmatites at Sandamap, which are essentially undeformed except for strained quartz, have late- to post-tectonic dates (473 ± 23 Ma and 468 ± 14 Ma respectively; Table 6.2, Figs. 6.6 and 6.7). The significance of these dates is unclear because of the well-documented sampling problems and the discordance of ages in zoned rare-element pegmatites (Clark, 1982). Open system behaviour of the Rb-Sr isotopic system has been documented by Clark (1982) in whole-rock samples - even in cases where there has been no subsequent metamorphism. Thus age differences may not necessarily reflect different crystallisation times. Because of the generally high concentration of Rb in these lithologies and subsequent (post-crystallisation?) migration of  $^{87}\text{Sr}$ , whole-rock and mineral dates are commonly anomalously low. This would appear to be the case at Sandamap Noord where the rare-element pegmatite, which is also enriched in volatiles, has a younger date. The pegmatites on Sandamap Noord have the high  $(^{87}\text{Sr}/^{86}\text{Sr})_i$  ratios that are so characteristic of this type of intrusion. The tin-bearing pegmatite on Sandamap Noord has an age which cannot be distinguished from the late-tectonic alaskite at the Rössing Uranium Mine (458 ± 8 Ma; Kröner and Hawkesworth, 1977; Hawkesworth *et al.*, 1983).



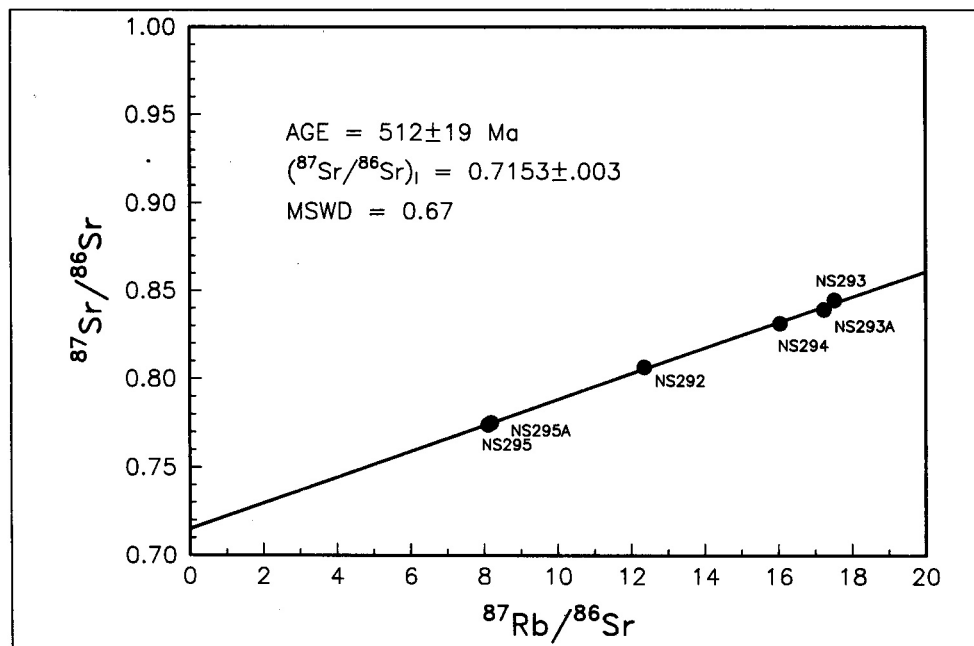


Figure 6.3: Rb-Sr whole-rock isochron for the Sandamap Noord leucogranite

intruded at 560-540 Ma. Secondly, sheet-like peraluminous leucogranites intruded along major structural breaks during  $F_2$  at the peak of regional metamorphism (~520 Ma). The third type of intrusion is the oval-shaped ~500-475 Ma (syn- $D_3$ ) leucogranites which are responsible for the northeast-trending elliptical outcrop pattern of the CZ. Fourthly, there are a number of late-/post-tectonic pegmatites concentrated near deep-seated crustal fractures such as the Welwitschia lineament zone or found in the tin belts.

The fact that intrusions hosted by greenschist-facies rocks on the northern side of the Tubussis Lineament-Kompaneno Fault (Fig. 6.2), such as the Ohere leucogranite and the Kohero pegmatite, have slightly older ages than leucogranites and pegmatites hosted by amphibolite-facies rocks suggests that, in general, Rb-Sr whole-rock dates in the CZ represent

cooling events, not the exact time of crystallisation. The data support the assertions made in Chapters 4 and 5 that the Tubussis Lineament represents a terrane boundary, possibly a major thrust. Similarly, on the northern boundary of the CZ, late-/post-tectonic intrusions such as the Uis pegmatites on the northern side of the Autseib Fault-Otjihorongu Thrust have older ages than essentially undeformed intrusions hosted by relatively higher grade metamorphic rocks to the south (Fig. 6.2).

#### 6.2.2.7 Rb-Sr mineral results

Biotites from the two phases of the Ohere Oos Salem granite were analysed. The two analyses define an isochron with an age of 435 Ma (Fig. 6.8). This is interpreted as the

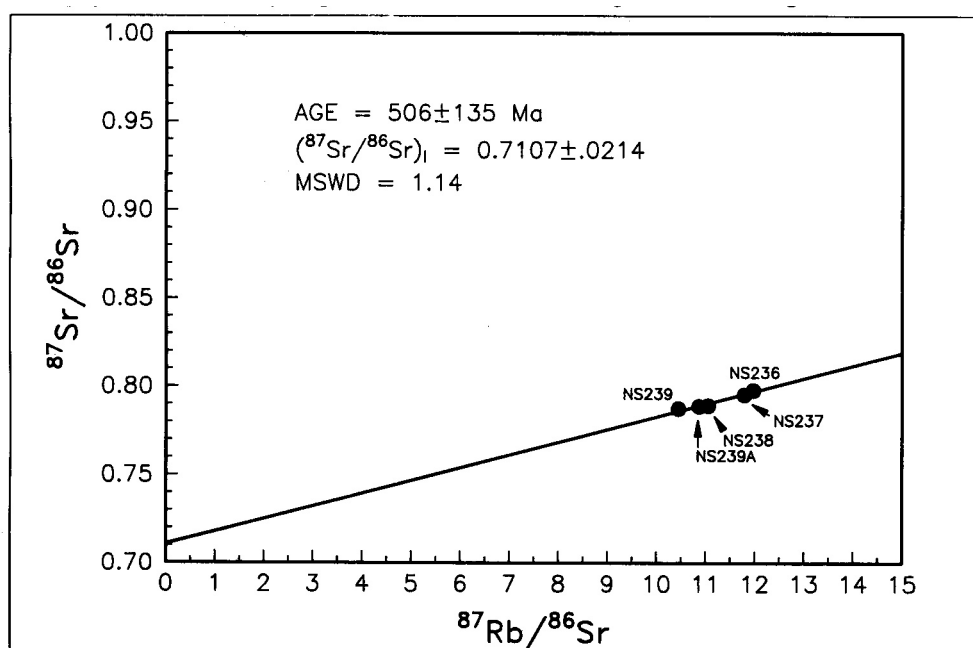


Figure 6.4: Rb-Sr whole-rock isochron for the Ohere leucogranite

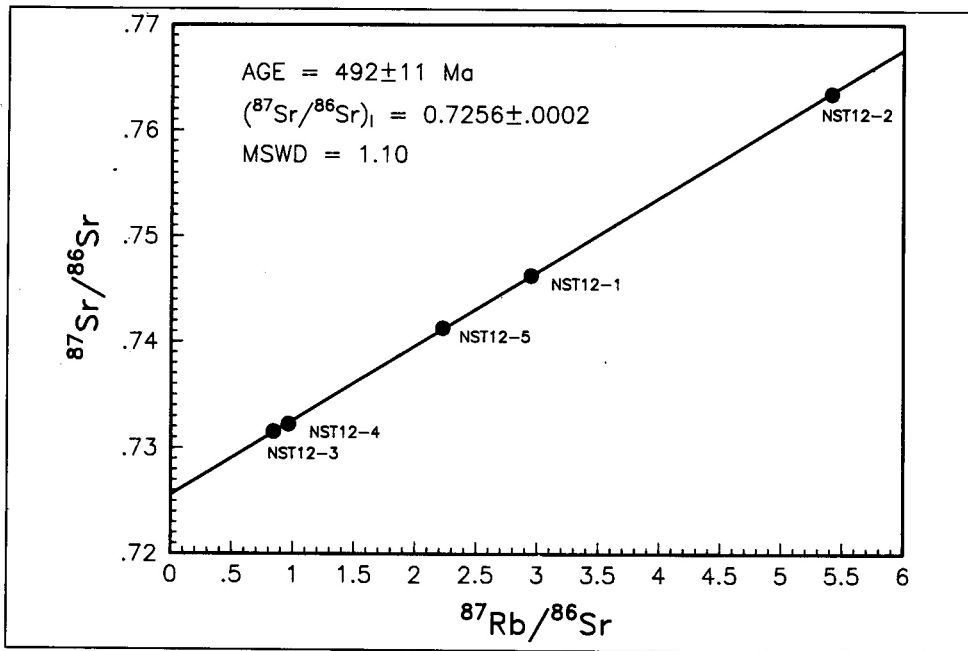


Figure 6.5: Rb-Sr whole-rock isochron for stanniferous pegmatite from Kohero Tin Mine

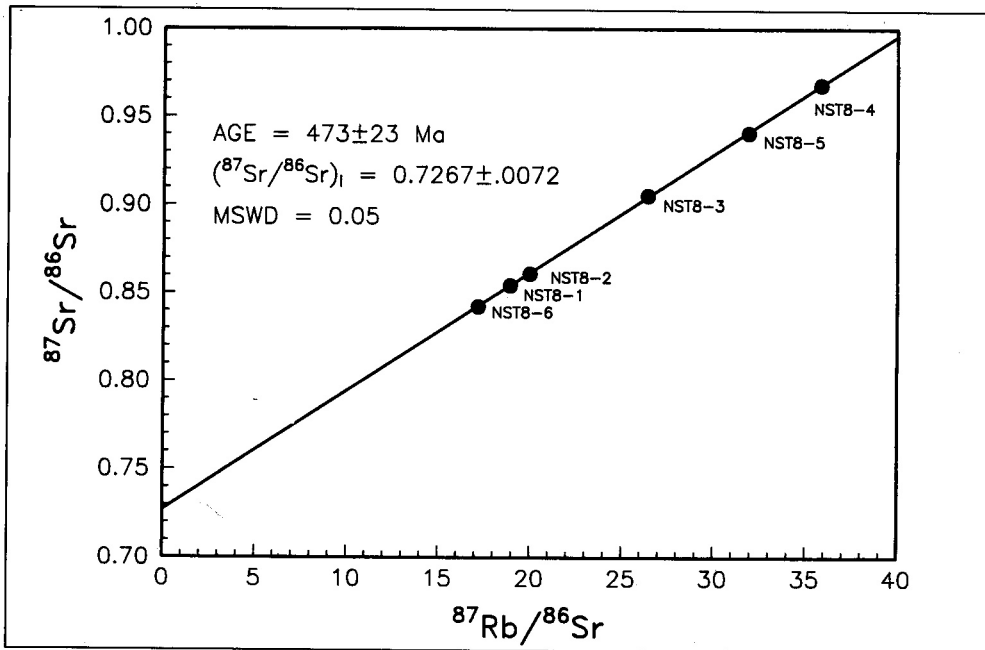


Figure 6.6: Rb-Sr isochron for non-stanniferous pegmatite from Sandamap Noord

time when the intrusion cooled through the blocking temperature for biotite of 300°C (Jäger *et al.*, 1967). This

compares with biotite ages of 475–442 Ma determined by Hawkesworth *et al.* (1983) for central Namibia.

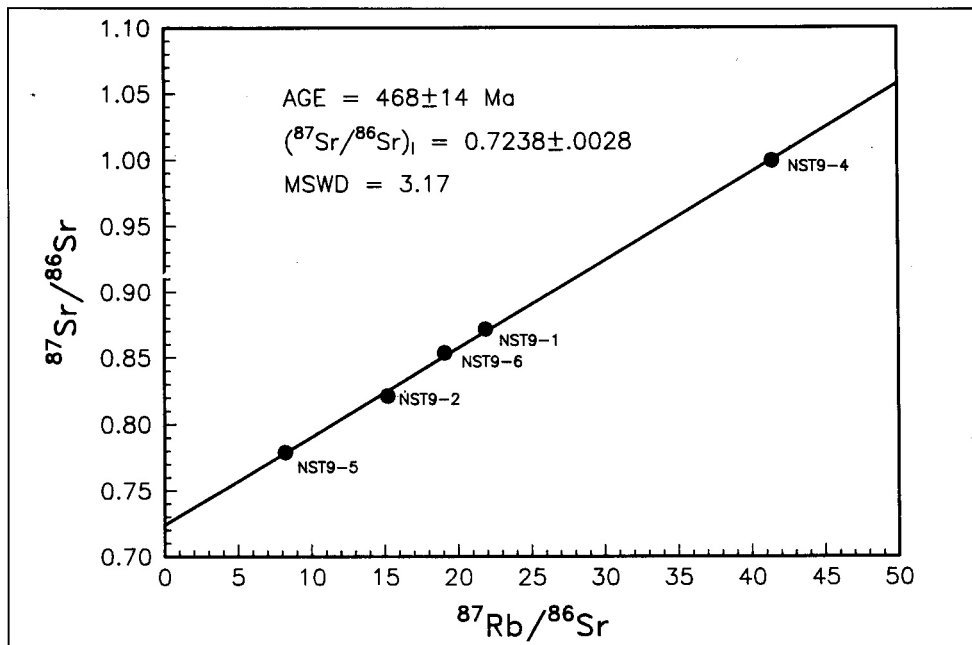


Figure 6.7: Rb-Sr whole-rock isochron for stanniferous pegmatite from Sandamap Tin Mine

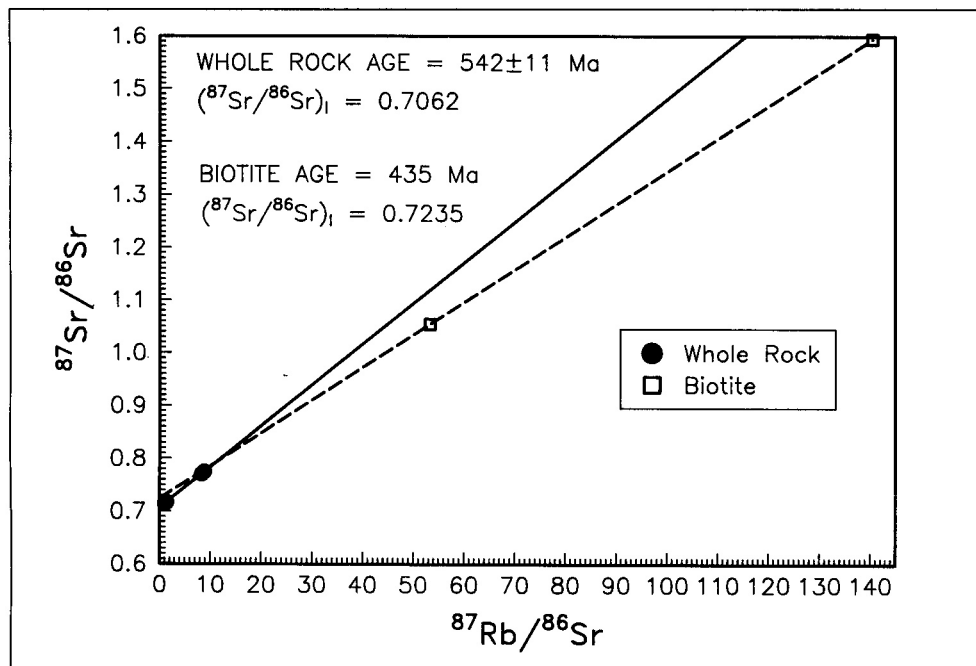


Figure 6.8: Rb-Sr isochrons (WR and minerals) for the Ohere Oos Salem granite

### 6.3 THE RELATIONSHIP BETWEEN LEUCOGRANITE AND PEGMATITES -

#### A POSSIBLE EXAMPLE OF THE DISRUPTION OF THE GEOTHERMAL GRADIENT BY GRANITE INTRUSION LEADING TO LARGE-SCALE PARTIAL MELTING OF METASEDIMENTS AT SANDAMAP NOORD

The intriguing spatial association between a leucogranite-cored dome and, successively, unzoned quartz-feldspar and zoned rare-element pegmatites concentrically arranged around the structure on Sandamap Noord (Map 3) requires

an explanation. This spatial relationship has been recorded elsewhere in the Sandamap-Davib Ost tin belt (Watson, 1982) and there is a possibility that similar processes produced other rare-element pegmatites in the orogen, notably the lithium pegmatites of the SCZ. Similar zones of ceramic and rare-element pegmatites around domal structures that mayor may not be cored by granite have been documented from Precambrian and Phanerozoic pegmatite fields (Cerny, 1982b). Because the example on Sandamap Noord is one of the best exposed in the CZ, a general model for stanniferous pegmatite generation in this tin belt can be proposed. More specifically the question as to whether the tin pegmatites are the products of the anatexis of Kuseib Formation schist or

late differentiates of the Sandamap Noord leuco-granite can be addressed. Section 6.3 should be read in conjunction with section 7.5.6 for an opposing argument based on the same evidence.

In spite of the uncertainty regarding the meaning of the Rb-Sr whole-rock dates for the intrusions on Sandamap Noord, textural evidence indicates that intrusion of the leucogranite considerably predated that of the pegmatites. The homogenous phacolith has a metamorphic banding and rounded, partially recrystallised grains; the pegmatites possess neither. This fact on its own is regarded as sufficient evidence that the pegmatites surrounding the domal structure are not differentiates that crystallised from a volatile-enriched residual melt of the leucogranite. It is envisaged that the leucogranite crystallised from granitic magma injected into strongly foliated schist resulting in the formation of a dyke-shaped (or possibly a sill-shaped) intrusion. The Rb-Sr whole-rock date of  $512 \pm 19$  Ma for the Sandamap Noord leucogranite is interpreted as a crystallisation event which places the time of emplacement at the peak of re-regional metamorphism. Subsequent incorporation of the granite into a domal structure resulted in the present outcrop pattern. The development of the Sandamap Noord domal structure may have occurred as a result of the ascent of partially molten granite to higher levels, as a result of late-tectonic Damaran compression about northeast- and north-northeast-trending fold axes ( $F_3$  and  $F_4$  respectively), diapirism associated with the pegmatite mass or a combination of these factors. The relatively small size of the phacolith suggests that, after its folding, diapiric effects associated with the ascent of the leucogranite could not have accounted for the formation of the  $D_3/D_4$  dome alone.

Whether the leucogranite was partly responsible for or merely incorporated in the dome, its intrusion would have perturbed the local geothermal gradient (De Yoreo *et al.*, 1989). It is envisaged that this increase in ambient temperature was sufficient to cause localised partial melting of the hydrous Kuiseb schists already being regionally metamorphosed in the amphibolite facies. The heat from the consolidating granite would have continued to cause localised partial melting of the metasediments as it rose through the earth's crust. Blobs of partial melt formed in the "thermal shadow" of the ascending diapir may have taken time to accumulate (Wickham, 1987), but once a "critical size" had been attained, ascended rapidly and crystallised around the dome. Wickham (1987) suggested that a drop of melt with a radius of 10 cm would rise at a rate of  $1 \text{ km Ma}^{-1}$ ; he modelled the ascent of large bodies using Stokes's Law which indicates that velocity is controlled most importantly by the size of the body and the viscosity of the country rock. Thus larger bodies rise faster because the higher thermal energy reduces drag.

The slow accumulation of small volumes of partial melt, the time taken for the partial melt to attain the critical melt fraction (CMF of Wickham, 1987; namely the point at which melt viscosity falls by as many as 14 orders of magnitude) and then coalesce into bodies up to several hundreds of metres long, and the problem of overcoming the viscosity of the country rock all contributed to a signifi-

cant time lag between the emplacement of the granite and the surrounding pegmatites at the presently exposed level. This would explain the close spatial association between the two types of intrusion yet the substantial discrepancy in ages and  $(^{87}\text{Sr}/^{86}\text{Sr})_i$  ratios between the leucogranite and the pegmatites. High  $(^{87}\text{Sr}/^{86}\text{Sr})_i$  ratios require a crustal precursor: partially melted hydrous schists are a possible candidate. This model helps to account for the small, internally zoned, blob-like nature of the stanniferous pegmatites of the Sandamap-Davib Ost Tin Belt and suggests that they segregated at low-melt fraction from metasediments in a similar manner to pegmatites derived from granites (McKenzie, 1985).

The above model is consistent with the conclusions of Roering and Gevers (1964) and Smith (1965) who also proposed that the tin-bearing pegmatites of the Central Damar are derived from the Kuiseb Formation. Stanniferous pegmatites at the Uis Tin Mine in the Strathmore-Uis Tin Belt were investigated by Haack and Gohn (1988) where the metasediments have not been as intensely metamorphosed as those at Sandamap. Richards (1986) noted that sillimanite is absent from the schists and estimates peak metamorphic conditions at  $600\text{--}650^\circ\text{C}$  and 4-5 kbars. The Uis pegmatite has an Rb-Sr whole-rock date of  $496 \pm 30$  Ma and an  $(^{87}\text{Sr}/^{86}\text{Sr})_i$  ratio of 0.734 (Haack and Gohn, 1988). These authors contended that the very high  $(^{87}\text{Sr}/^{86}\text{Sr})_i$  ratio could not be explained by equilibrium partial melting of basement, Etusis or Kuiseb Formation. One alternative considered by the authors for the origin of melts with such high  $(^{87}\text{Sr}/^{86}\text{Sr})_i$  ratios was a separation of melts in magma chambers for 1-2 Ma. Haack and Gohn (1988) rejected this possibility because such large volumes of liquid could not be kept in a magma chamber during rapid uplift.

The key question is what is meant by large? As previously discussed, the rate of ascent of diapirs is essentially dependent on the size of the pocket of melt and the viscosity of the enclosing rocks. It may well have taken several millions of years for spheres of partial melt with radii of 10 cm rising at  $1 \text{ km Ma}^{-1}$  to coalesce to form one body. Haack and Gohn (1988) instead favoured the breakdown of biotite (and possibly muscovite) as a mechanism of producing fluids with high concentrations of radiogenic strontium and high concentrations of rare metals. The Sandamap tin pegmatite has an  $(^{87}\text{Sr}/^{86}\text{Sr})_i$  ratio of 0.7238, considerably lower than that at Uis, and therefore equilibrium partial melting of the Kuiseb formation can still be considered as a possibility. Although this author agrees with Haack and Gohn (1988) that the stanniferous pegmatites of the CZ may have been derived from the Kuiseb Formation during the thermal event accompanying peak metamorphism, at Sandamap Noord the higher regional metamorphic grade and the disruption of the geothermal gradient by the intrusion of synmetamorphic peak peraluminous granites promoted more extensive (equilibrium?) partial melting than at the Uis Tin Mine. The idea that partial melting of metasediments can produce rare-metal pegmatites is not new: Stewart (1978) proposed this mechanism for the generation of lithium-rich and other rare-element pegmatites.

## 6.4 MINERALISATION AND THE YOUNGER INTRUSIONS

Throughout the CZ, mineralisation is either hosted by or spatially associated with the younger intrusions. Granitoids of the Salem Suite and the older, deformed ( $D_1$  and  $D_2$ ) leucogranites are generally not of economic interest. The only two examples of Salem Suite intrusions known to be partly responsible for epigenetic mineralisation are the Omangambo and Ohere Oos plutons (Fig. 6.2), in the aureoles of which massive skarns at the Ais Dome (Fig. 1.3; Miller, 1980) and the scheelite skarnoid rocks on Ohere (Map 2) are respectively developed. Uranium mineralisation in central Namibia is hosted by leucogranites and alaskites that are 510 Ma old or younger (Table 6.3). Tungsten skarn mineralisation on Stinkbank and at the Otjua Prospect (Fig. 6.2) is spatially associated with syn- $D_3$  leucogranites. Whole rock Rb-Sr dates for stanniferous pegmatites are now available for the Sandamap-Davib Ost (CZ), Nainais-Kohero (CZ) and Strathmore-Uis (NZ) tin belts (Table 6.3). In the NZ, the pegmatite at Uis and muscovite from cassiterite veins at the Gamigab prospect to the northwest of Uis (Walraven, 1988), also in the NZ, have Rb-Sr ages slightly older than the tin pegmatites hosted by amphibolite-facies rocks in the CZ (muscovite ages are identical to whole-rock ages elsewhere in the Damara, for example the Donkerhuk granite; Blaxland *et al.*, 1979). There is no

evidence from the results presented above and other recently reported data on stanniferous pegmatites (Haack and Gohn, 1988) for the modification of Damaran stanniferous pegmatites by post - Karoo "greisenising fluids" as suggested by Pirajno *et al.* (1988). Lithium-bearing pegmatite at the Rubicon Mine also has a late-tectonic Damaran age.

## 6.5 GRANITE AND PEGMATITE PETROGENESIS AND THE ISOTOPIC EVOLUTION OF THE CZ

The isotopic evolution of the orogen has already been addressed by Hawkesworth and Marlow (1983), but the small data set examined here emphasises some important points about the intrusions of the CZ. There is a general trend towards more evolved granite types and an increase in  $(^{87}\text{Sr}/^{86}\text{Sr})_I$  ratios with time, a fact Hawkesworth *et al.* (1983) attributed to the partial melting of crustal material at higher structural levels as the orogeny progressed. The new data confirm Hawkesworth *et al.*'s (1983) contention that the younger ages are concentrated in the centre of the orogen, that is the CZ. This tectono-stratigraphic zone is characterised by numerous post-collision ( $D_3$ ) granitoids, dome-like structures, thermal domes, low-pressure metamorphic assemblages and rapid uplift. Prograde metamorphism continued in the CZ 40-50 Ma after the margins of the orogen had started

Locality	Style of Mineralisation	Lithology Dated	Method	Age (Ma)	$(^{87}\text{Sr}/^{86}\text{Sr})_I$	Ref.
Rössing Mine	Uraniferous alaskite	Early alaskite	Rb-Sr (WR)	510	N.A.	1
Rössing Mine	Uraniferous alaskite	Late alaskite	Rb-Sr (WR)	458 ± 8	0.759	1,2
Stinkbank	Uraniferous leucogranite and scheelite skarn	Leucogranite	Rb-Sr (WR)	484 ± 25	0.739	3,4
Otjua Prospect	Scheelite skarn	Leucogranite	Rb-Sr (WR)	478 ± 4	0.7196	4, 5
Gamigab Prosp.	Cassiterite veins	Muscovite	Rb-Sr (Ms)	510	-	6,7
Uis Mine	Stanniferous pegmatite	Pegmatite	Rb-Sr (WR)	496 ± 30	0.734	8
Kohero Mine	Stanniferous pegmatite	Pegmatite	Rb-Sr (WR)	492 ± 11	0.7256	9
Sandamap Mine	Stanniferous pegmatite	Pegmatite	Rb-Sr (WR)	468 ± 14	0.7231	9
Rubicon Mine	Petalite (Li) pegmatite	Pegmatite	Rb-Sr (Amb, Kfs, Ms)	515 ± 36	0.736	8
Navachab Mine	Gold skarn	Biotite	Rb-Sr (Bt)	490	-	10

**Table 6.3:** Ages of late- to post-tectonic mineralised intrusions and mineralisation in the CZ

Amb - amblygonite; Bt - biotite; Kfs - k-feldspar; Ms - muscovite; WR - whole rock; N.A. - not available

References: 1 = Hawkesworth *et al.*, 1983; 2 = Kröner and Hawkesworth, 1977; 3 = Marlow, 1983;

4 = Steven, 1987; 5 = Haack *et al.*, 1983; 6 = Jacob, 1990, pers. comm.;

7 = Walraven, 1988; 8 = Haack and Gohn, 1988; 9 = Steven, 1992 (this work);

10 = Navachab Gold Mine Field Guide, 1989

Locality	Sample No.	$^{206}\text{Pb}/^{204}\text{Pb}$	$^{207}\text{Pb}/^{204}\text{Pb}$	Model Age (Ma)	Avg. Model Age (Ma)
Sandamap Noord Gold Prospect (northern side of dome)	NST13A	18.183	15.697	522	516
	NST13B	18.176	15.688	510	
Sandamap Noord Gold Prospect (north-western side of dome)	NST14A	18.178	15.676	486	503
	NST14B	18.196	15.701	520	
Epako Gold Prospect	NST15A	18.207	15.683	479	473
	NST15B	18.194	15.672	467	

**Table 6.4:** Galena analyses and Pb-Pb model ages from the CZ  
Pb-Pb model age: Start = 3.7 Ga,  $^{206}\text{Pb}/^{204}\text{Pb} = 11.152$ ,  $^{207}\text{Pb}/^{204}\text{Pb} = 12.998$  (Stacey and Kramers, 1975)  
NST13: Galena in quartz vein in Kuiseb Formation (trench 28)  
NST14: Galena in quartz vein running parallel to auriferous zone in Kuiseb Formation (trench 36)  
NST15: Galena in quartz vein in Oberwasser Formation (trench 4200)

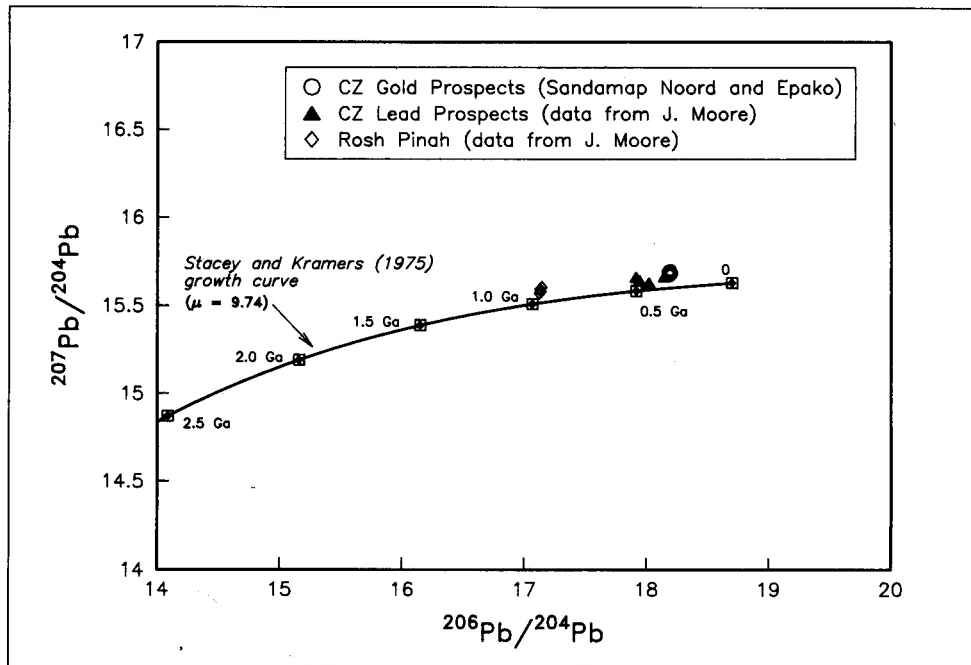


**Figure 6.9:** Galena analyses from the CZ and Rosh Pinah

to cool (Hawkesworth *et al.*, 1983). This Buchan-style metamorphism was responsible for the partial melting of basement and Nosib Group metaquartzites in the SCZ to form the uraniumiferous intrusions (Hawkesworth and Marlow, 1983) and perhaps Kuiseb Formation schists in the NCZ to form the stanniferous pegmatites. All granitic intrusions, with the exception of the  $D_2$  leucogranite on Sandamap Noord, have the trace element characteristics of intraplate or intracratonic intrusions (Figs 3.4 and 3.5).

Only the early tectonic Salem Suite granitoids have ( $^{87}\text{Sr}/^{86}\text{Sr}$ )<sub>1</sub> ratios similar to the magmas generated along destructive plate margins such as the Andes (Hawkesworth, 1982). These are the only intrusions in the CZ that could have been derived from the mantle or the lower crust. The post-collision (530-460 Ma) intrusions of the CZ are nearly all S-type granites, if not leucogranites, have a restricted compositional range (Fig. 3.3) and generally have high ( $^{87}\text{Sr}/^{86}\text{Sr}$ )<sub>1</sub> and  $\delta^{18}\text{O}$

values (Haack *et al.*, 1983). Only the synmetamorphic peak  $D_2$  leucogranites contain substantial magmatic muscovite. The pressure limitations on the ascent of peraluminous granite are well documented (Zen, 1988): pressures of 3-4 kbars were only attained during the regional metamorphic peak. The isotopic characteristics of the CZ intrusions indicate that the major portion of the magmatic arc of the orogen developed as the result of high-grade thermal metamorphism of metasediments and underlying granitic crust in an intracratonic setting, not as the result of subduction and subsequent partial melting of oceanic crust.

## 6.6 Pb-Pb WORK

Three samples of galena from the Sandamap Noord (Map 3) and Epako Gold Prospects (Map 1) have been isotopically

---

analysed in duplicate (Table 6.4; see Appendix for analytical details). The galenas are notably heterogeneous. Model ages have been calculated using the two-stage model of lead evolution (Stacey and Kramers, 1975; Fig. 6:9). Late Pan-African model ages for all the galenas are indicated. The samples from Sandamap Noord (Pb-Pb model ages 522-486 Ma) are similar to the Rb-Sr whole-rock dates of  $512 \pm 19$  Ma for the leucogranite and  $473 \pm 23$  Ma and  $468 \pm 14$  Ma for the pegm-

atites. The Pb-Pb model ages for the Epako galena (479-467 Ma) bracket the Rb-Sr whole-rock date of  $478 \pm 4$  Ma for the Otjua leucogranite, the only granitic intrusion in the Schönfeld Dome that has been dated. All three galena analyses plot above the Stacey and Kramers (1975) growth curve, in common with galenas from elsewhere in the Damara Orogen and southern Africa (Hawkesworth and Marlow, 1983).



## 7. MINERALISATION

## 7.1 INTRODUCTION

In this chapter six examples of Damaran epigenetic mineralisation (mineralisation formed after sedimentation and diagenesis) will be discussed. The occurrences are dealt with in the stratigraphic order of the host rocks. The first example is the Eureka monazite occurrence (Fig. 7.1) hosted by Etuis Formation quartzites. This monazite deposit has variously

been described as a skarn and a carbonatite and is the only known "hard-rock" rare earth deposit in central Namibia. The second and third types of epigenetic mineralisation are replacement skarns in carbonates. The scheelite skarn in the Okawayo Formation on the farm Otjua is the largest tungsten skarn known in central Namibia. The gold skarns, one a silicate-dominated system, the other a sulphide-dominated system are hosted by Karibib Formation marbles on the farm

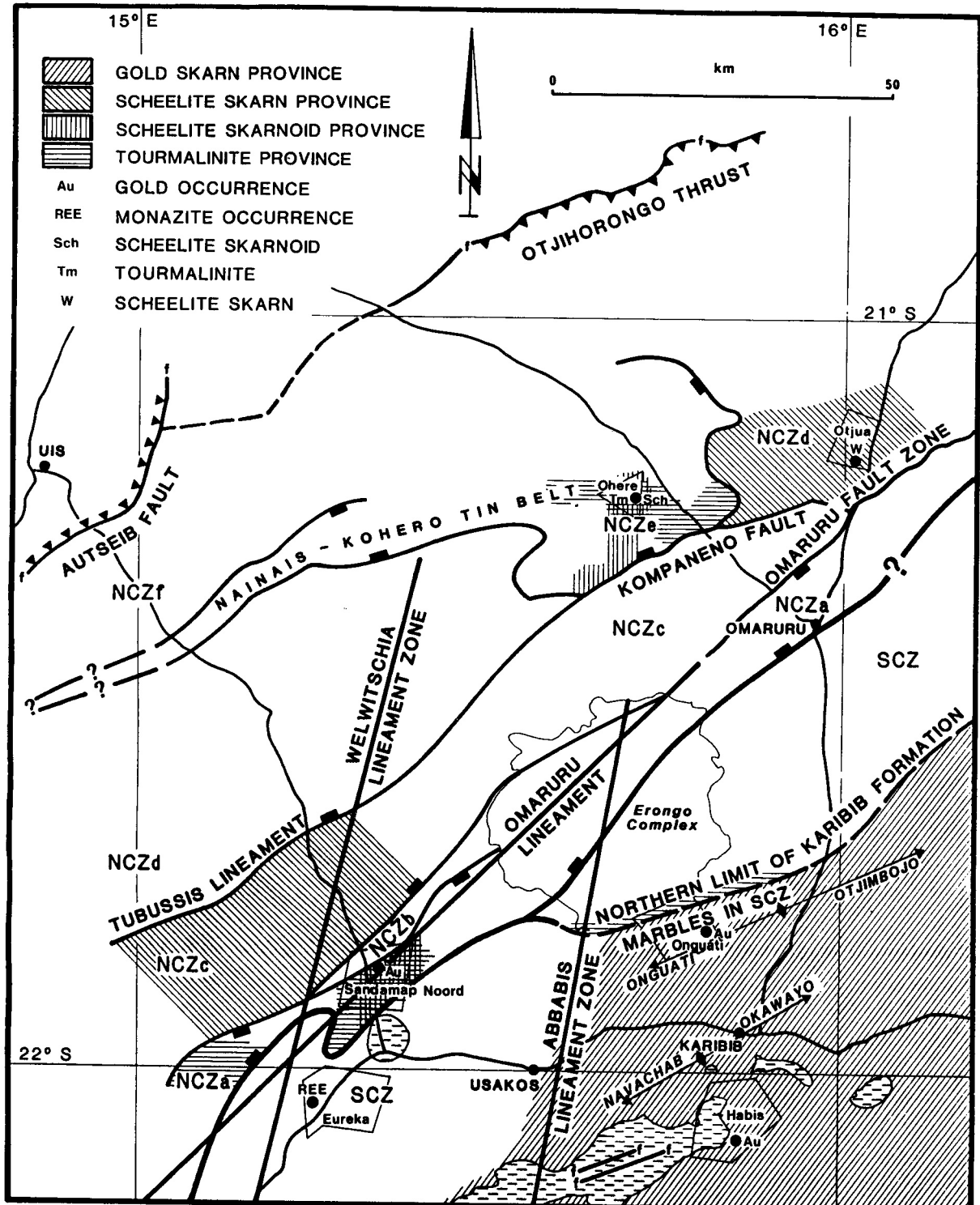


Figure 7.1: Localities referred to in Chapter 7

Habis and at the Onguati Copper Mine respectively. The fourth example of epigenetic mineralisation is a zone of recently discovered turbidite-hosted gold mineralisation in the Kuiseb Formation on Sandamap Noord. Tourmalinites and tourmaline alteration in Kuiseb Formation metaturbidities on Ohere comprise the fifth example of epigenetic mineralisation. Finally an unusual style of calc-silicate-hosted scheelite mineralisation in the Kuiseb Formation on Ohere, believed to be a metamorphogenic skarn, will be discussed. At those occurrences that have been investigated by other workers, attention is focused on features that have not previously been described. In each subsection the regional geology is briefly discussed. Many of the features have been addressed in detail in Chapters 2 to 6. It was felt, however, that many readers would want to place the examples of mineralisation in a regional context.

## 7.2 MAGNETITE-MONAZITE OCCURRENCE HOSTED BY THE ETUSIS FORMATION ON EUREKA

### 7.2.1 Introduction

An enigmatic dolomite-hosted monazite occurrence was discovered in an area of very poor exposure on the farm Eu-

reka 99 (Figs 1.3 and 7.1) in 1959 (Von Knorring and Clifford, 1960). The above authors' interpretation was that this represented a skarn deposit hosted by the "Marble Series" of the Damara Sequence. The development of the skarn was attributed to the regional phase of pegmatite emplacement. Subsequently, the identification of high strontium contents in the marble led Von Knorring (1964) to believe that the marble had a carbonatitic character. However, Burger *et al.* (1965) determined an age of 500 ± 20 Ma on a monazite from the occurrence, relating its development to the "regionally developed granitic pegmatites". Verwoerd (1967) attributed the origin of the mineralisation to hydrothermal solutions derivative of an alkalic subsilicic magma rather than the granite-pegmatites proposed by Von Knorring and Clifford (1960). Verwoerd did not dispute that the monazite is hosted by a marble. More recently, Dunai *et al.* (1989) conducted a Sr isotope study of the Eureka "carbonatite" occurrence and concluded that it had a magmatic origin. Because of the author's previous involvement in the exploration for monazite deposits in the CZ and the possibility that the Eureka monazite occurrence might represent an unusual type of skarn mineralisation, it was considered that the prospect was worthy of more work. The description that follows emphasises the relationship of the deposit to the regional geological setting for the first time. Three possible origins for this occurrence are reviewed.

Type Locality	Eureka 99, Usakos District
Host Formation	Top of Etusis (possibly base of Khan)
Host Lithology	Dolomitic (and Calcitic) Marble
Regional Geological Setting	Feldspathic Quartzites overlain by Marls (and Evaporites?)
Form of Mineralisation	Disseminated Monazite and Magnetite in Dolomitic Marble
Associated Volcanics	None Identified (Minor Rhyolites in Etusis Fmn. in Area [Jacob, 1974, p.10]).
Structural Features	Mineralisation in Core of D <sub>3</sub> Dome
Peak Metamorphic Facies	Upper Amphibolite
Damaran Intrusions	Late Damaran Leucogranites and Pegmatites
Age of Mineralisation	500 ± 20 Ma (Monazite Analysed by Burger <i>et al.</i> , 1965)
Geochemical Association	Anomalous Th, F, S
Ore Minerals	Monazite (0-30%), Magnetite (0-20%)
Gangue Minerals	Dolomite (±60%), Calcite (±10%), Iron Oxides other than magnetite (0-5%) Graphite (trace), Quartz (trace)
Associated Alteration	None Identified (finitisation described by Dunai <i>et al.</i> , 1989)
Classification	Monazite Skarn-possible carbonatite connection

Table 7/2.1: Monazite-magnetite occurrence in the Etusis Formation

## 7.2.2 Geological setting

The highly magnetic mineralisation is hosted by folded dolomitic marble in the core of the Eureka Dome (Fig. 4.3 and Map 5) on the northern margin of the SCZ. Due to the poor exposure, there is some uncertainty as to which stratigraphic unit hosts the mineralisation. The host marble horizon(s) is enclosed by feldspathic quartzites correlated with the Etusis Formation (Table 7/2.1), though the assemblage could be interpreted as the base of the Khan Formation. If the marble is a metamorphosed sedimentary rock, it is the lowermost carbonate horizon in the Damara Sequence. At the main monazite occurrence (Site C of Dunai *et al.*, 1989; Map 5) the relationship between the 7-m-thick carbonate and the enclosing country rocks is obscured by calcrete. Approximately 250 m south-southwest of locality C, minor monazite is hosted by a tightly folded magnetite-bearing dolomitic marble horizon (Site B of Dunai *et al.*, 1989; Map 5), which is enclosed by calc-silicate rocks and pinkish feldspathic quartzites. A prominent banding, which parallels lithological contacts, is present in the marble. Because of the poor exposure it is impossible to say with confidence that the marble is a folded carbonatitic dyke. A ground magnetic survey (50 metre line spacing, 25 metre reading interval) conducted over the main monazite occurrence (Site C) by the author whilst in the employ of a mining company revealed the presence of spotty anomalies. It was thought that these could be better explained by the presence of unevenly distributed magnetite in tightly folded marble than a late-/post-tectonic carbonatite plug or dyke. There is no evidence from the available aeromagnetic data for the presence of a hidden alkaline intrusion of any size.

## 7.2.3 Petrography of the monazite rock

The mineralogy of the monazite rock is presented in Table 7/2.1. Staining with Alizarin Red S revealed that fine-grained calcite is interstitial to the coarser dolomite. The carbonate grains are rimmed by goethite and limonite which lend the characteristic dark brown colour to the lithology. Monazite concentrations locally exceed 30% by volume and magnetite contents may be as high as 20%. The phosphate crystals vary in size from 50  $\mu\text{m}$  to ten centimetres. Very minor micro-

crystalline quartz is concentrated in interstices and crosscutting fractures. Minor relicts of a prismatic (ferromagnesian?) mineral filled with rhombs of iron carbonate and calcite are present. Several brown minerals, probably serpentine, were noted. No strontium phase was identified. The monazite crystals are either rounded prisms or oval shaped and are in contact at triple junctions with all other phases (Plate 7/2.1). Monazite inclusions occur in calcite and magnetite, while magnetite is locally an inclusion in monazite (Plate 7/2.2) and the carbonate. The monazite is an integral part of a high temperature assemblage (the enclosing rocks were metamorphosed under amphibolite-facies conditions) and the author disagrees with Verwoerd (1967) that monazite crystallised late. No petrographic differences between the monazite-bearing dolomite rock (Site C) and the dolomitic marble (Site B), other than the presence of the phosphate, were noted. Additional features of note are the presence of graphite and the lack of typical carbonatite silicate minerals.

## 7.2.4 Geochemistry of the monazite rock

Whole rock analyses of the dolomitic marble and the monazite rock (localities Band C respectively of Dunai *et al.*, 1989) are given in Table 7/2.2 (see Appendix for a note on the analytical methods employed). These results confirm the high Sr concentrations of the marbles and the low thorium contents of the monazite determined by Burger *et al.* (1965). However, no Zr was recorded (cf Von Knorring and Clifford, 1960) and the uranium and gold contents are also below the lower limit of detection. If these rocks are related to carbonatites, the low concentrations of Ba and Nb are striking.

## 7.2.5 Discussion

An interpretation of this occurrence is severely hampered by the poor exposure. The stratigraphic position of the host rock itself is not immediately apparent. However, the presence of Etusis Formation metasediments is indicated by the pink colour of the feldspathic quartzites and the presence of sillimanite spheroids in the core of the Eureka Dome (Map 5). The basic facts which require an explanation are: there are

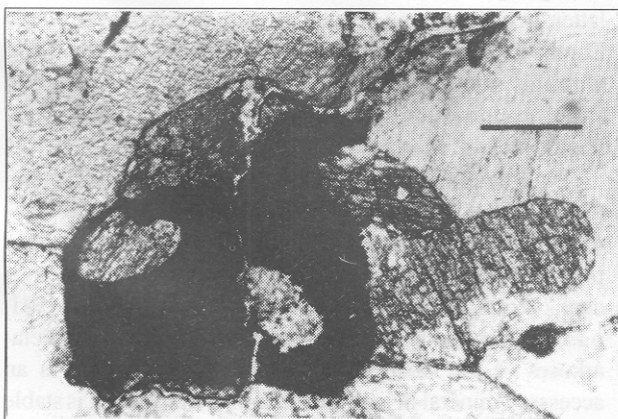


**Plate 7/2.1:** Oval-shaped monazite (high relief) and magnetite crystals surrounded by dolomite; monazite occurrence on Eureka (NS329; PPL); scale bar = 200  $\mu\text{m}$

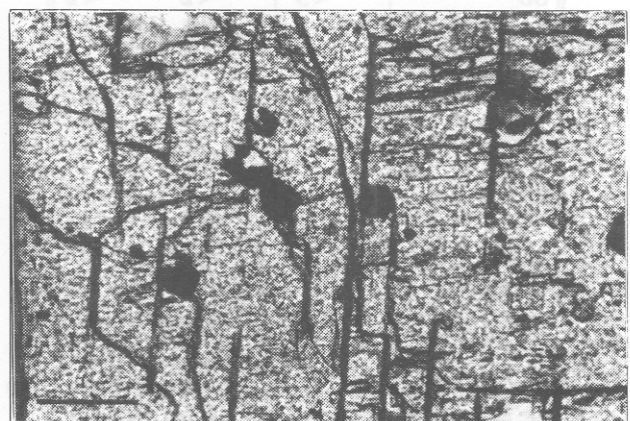


**Plate 7/2.2:** Magnetite inclusions in monazite; monazite occurrence on Eureka (NS329; PPL); scale bar = 100  $\mu\text{m}$

	NS329	NS346	NS347
SiO <sub>2</sub> (wt%)	1.21	.51	.07
TiO <sub>2</sub>	.03	<.01	<.01
Al <sub>2</sub> O <sub>3</sub>	.09	.00	<.01
Fe <sub>2</sub> O <sub>3</sub>	4.60	7.40	10.32
FeO	.73	2.54	2.48
MnO	.86	1.11	1.13
MgO	7.22	15.46	16.33
CaO	16.87	26.89	24.80
Na <sub>2</sub> O	<.02	<.02	<.02
K <sub>2</sub> O	.01	.00	.00
P <sub>2</sub> O <sub>5</sub>	10.20	.00	.01
SrO	2.09	2.74	2.82
La <sub>2</sub> O <sub>3</sub>	11.38	-	-
Ce <sub>2</sub> O <sub>3</sub>	17.45	-	-
Nd <sub>2</sub> O <sub>3</sub>	1.74	-	-
H <sub>2</sub> O-	.07	.07	.11
H <sub>2</sub> O+	.44	.84	1.14
CO <sub>2</sub>	25.35	41.21	39.79
TOTAL	100.33	98.82	99.02
F (ppm)	6216	613	523
S	685	91	191
Rb	<2	14	13
Ba	67	32	57
Th	2452	<4	<4
U	<5	<7	<7
Zr	<5	<13	38
Nb	30	31	30
Mo	12	60	55
Sn	36	8	2
W	<14	<7	<7
V	<6	<2	<2
Cr	64	12	11
Co	<3	24	103
Ni	<6	12	60
Cu	23	21	52
Zn	130	56	64
Ga	<3	<2	<2
Pb	109	<6	<6
Ge	<3	<1	<1
As	<3	3	3
Sb	<3	<2	<2
Bi	<8	<4	<4
Se	<3	1	2
Te	<4	<3	<3
Sc	<7	<2	<2
Y	72	66	66
La	-	230	221
Ce	-	519	478
Nd	-	220	199
Au (ppb)	<5	<5	<5

**Table 7/2.2:** Whole-rock analyses of monazite and strontium carbonate rocks on the farm Eureka 99, Usakos District  
 NS329: Site C of Dunai *et al.*, (1989), monazite carbonate rock  
 NS346: Site B of Dunai *et al.*, (1989), strontium carbonate rock  
 NS347: Site B of Dunai *et al.*, (1989), strontium carbonate rock

no carbonate horizons at this stratigraphic level elsewhere in the CZ; the monazite is an integral part of a high temperature assemblage; monazite mineralisation formed in a dolomite-calcite rock at  $500 \pm 20$  Ma (slightly after the peak of metamorphism); the carbonate enclosing the monazite has a mantle ( $^{87}\text{Sr}/^{86}\text{Sr}$ )<sub>i</sub> signature. Three possible models for the origin of the deposit are reviewed below.

#### 7.2.5.1 Metamorphogenic Skarn Model

The Eureka monazite occurrence may be an unusual type of metamorphogenic skarn formed by the local remobilisation and concentration of REE during the Damaran orogeny. Two possibilities are examined: firstly that marble horizons at the top of the Etusis Formation had an inherently high concentration of REE from which monazite crystallised during metamorphism and secondly that REE from detrital monazite in the enclosing Etusis Formation quartzites was remobilised and channelled into minor carbonate units.

The monazite-magnetite mineralisation is enclosed by feldspathic quartzites from the top of the Etusis Formation (Fig. 4.3). Thin (<5 -m-thick) marble horizons at this stratigraphic level and in the overlying Khan Formation are common on Eureka (Map 5). The presence of iron formations, sulphide mineralisation and graphite schists in the Khan Formation and at the base of the Rössing Formation (Chapter 2) indicates a shallow marine depositional environment for the upper Nosib and lower Swakop Group sediments. Miller (1983a) suggested an evaporitic origin for some of the calc-silicate rocks of the Khan Formation; Nash (1971) recorded anhydrite at this stratigraphic level at the Rössing Uranium Mine. Wedepohl (1978) noted concentrations of up to 11 300 ppm Sr for Holocene shallow-water limestones and dolomites from the Gulf of Mexico and Goldschmidt (1958) discussed the concentration of strontium in "evaporate sediments". Thus, the concentrations of 2.8 wt% SrO in the marble are high, but not incompatible with a sedimentary origin. It is possible that, with the change from clastic to chemical sedimentation in the Eureka area, minor, laterally impersistent carbonate horizons at the top of the Etusis Formation and the base of the Khan Formation acted as a sink for REE during sedimentation. Crystallisation of monazite would have occurred during regional or localised thermal metamorphism (the latter being possibly related to the development of the Eureka Dome) at approximately  $500 \pm 20$  Ma. The problem with this is that there are no known syn-sedimentary rare earth accumulations in chemical sediments (Neary and Highley, 1984; Mariano, 1989).

As an alternative to the above, low temperature metamorphic remobilisation of REE from Nosib Group sediments can be considered. The Etusis Formation sediments, primarily fluvial quartzites, are known to contain significant detrital concentrations of monazite (Marlow, 1981, p.226). Iron oxides are prominent accessories in the meta-arkoses of the Nosib Group. Although monazite is an accessory mineral in granitic rocks indicating that it is stable at magmatic temperatures, it is only moderately resistant to weathering (Deer *et al.*, 1962). Partially degraded monazite in the Etusis Formation can thus be considered to be a major reser-

voir of REE. The behaviour of REE during metamorphism is both variable (Humphris, 1984) and poorly understood (Grauch, 1989), but under certain circumstances they are highly mobile. REE mobility has been documented during low temperature alteration of basalts (Wood *et al.*, 1976), low-grade metamorphism of basic volcanic rocks (Hellman *et al.*, 1979), hydrothermal and supergene alteration of granites (Alderton *et al.*, 1980) and post-magmatic alteration of carbonatites (Andersen, 1986). Supergene and hydrothermal monazite derived from weathered calcite, dolomite and apatite in carbonatites is well documented (Mariano, 1989). Thus the derivation, of REE from degraded monazite and its mobilisation during prograde metamorphism into adjacent carbonate units must be considered a possibility. A similar metamorphic remobilisation model involving the breakdown of REE-bearing epidote was proposed by Moore and McStay (1990) for concentrations of allanite in calcic granofelses in the high-grade metamorphic terrain of the Namaqualand Metamorphic Complex.

#### 7.2.5.2 Magmatic Skarn Model

Metasomatic replacement of a metasedimentary carbonate unit by fluids emanating from felsic intrusions during the Damaran orogeny must also be considered as an alternative for the formation of the monazite. The lowermost marble horizon in the Damara Sequence would have acted as the ideal trap for vapours generated from the partial melting of the underlying Nosib Group and basement. Etusis Formation quartzites contain detrital concentrations of monazite and iron oxides (Marlow, 1981, p.226). Areas of the SCZ immediately underlain by granitic basement lithologies and clastic sediments of the Nosib Group (essentially derived from that basement) are intruded by red gneissic granite, uraniferous intrusions and associated igneous rocks (for example, at the Ida Dome, Stinkbank and Otjua in the Karibib district; Marlow, 1981, 1983). All the intrusions of the SCZ contain accessory monazite (Marlow, 1983). A good example of the nature of the SCZ intrusions is the undeformed magnetite-bearing pegmatite (section 3.6.1) cropping out over many square kilometres in the southeast portion of Eureka (Fig. 4.3). This lithology contains almost no hydrous phases. The magmas from which the SCZ intrusions formed (other than the Salem Suite) were water-poor because of the low water content of the parent rocks (Miller, 1974), but a small volatile-rich phase would undoubtedly have been present. Although the behaviour of phosphorus and rare earth elements in felsic melts is strongly influenced by the crystallisation of phosphorus compounds (usually apatite; Wedepohl, 1978), phosphorus is a volatile component of magmas (Wyllie and Tuttle, 1964) and can accumulate in the pegmatite stage. A  $P_2O_5$ -enriched vapour phase may have been exsolved during pegmatite evolution (Watson and Capobiano, 1981). As these magmas intruded the Damara Sequence these volatile-rich portions would have reacted with the country rock such as the lowermost carbonate horizon in the Eureka Dome. The age of 500:1:20 Ma for the Eureka monazite (Burger *et al.*, 1965) approximately coincides with the peak of metamorphism, when many of these anatectic melts were being generated.

If the magmatic skarn model is correct then this implies that firstly, this style of mineralisation is confined to the SCZ and secondly, that the monazite development is not related to the granitic pegmatites (Burger *et al.*, 1965), the majority of which are younger than 500 Ma.

#### 7.2.5.3 Carbonatite Model

The two pieces of evidence that support a carbonatitic model for the origin of the Eureka deposit are the chemistry of the monazite (specifically its high Ce and La and low thorium contents) and the juvenile  $^{87}Sr/^{86}Sr$  ratio of the "carbonatite". Four samples of the carbonate rock have  $^{87}Sr/^{86}Sr$  ratios between 0.70286 and 0.70318 (Dunai *et al.*, 1989) which can be considered good evidence for the presence of a mantle-derived fluid. However, in this author's opinion, Dunai *et al.* (1989) have not proved the presence of a carbonatitic intrusion. There is no field, aeromagnetic or petrographic evidence for the presence of a hidden carbonatite body of any size. In the field the carbonate rock can be interpreted as a folded marble or a folded carbonatitic dyke. The fenitisation arguments of Dunai *et al.* (1989) are not entirely convincing. For example, the authors state that metasomatism of the quartzites has occurred up to 20 metres from the carbonatite dyke citing the alteration of biotite to hydro-biotite and mobility of alkalis. Both of these processes could have occurred as the result of regional metamorphism. The calc-silicate gneiss that encloses the carbonate rock on Eureka is similar to other metamorphosed marls in central Namibia. The replacement of plagioclase by scapolite in the calc-silicate rocks described by Dunai *et al.* (1989) is common elsewhere in the CZ. The mantle signature of the carbonate could be explained by the interaction of a juvenile fluid with the lowermost carbonate in the Damara Sequence. Indeed Dunai *et al.* (1989) have mentioned that the  $^{87}Sr/^{86}Sr$  ratios of the carbonatite are slightly increased compared to the evolutionary path of a Rb-depleted mantle. One explanation offered by the authors to explain this phenomenon is that carbonatitic magma interacted with wall rock carbonates! There are no carbonates below this stratigraphic level in the Damara Sequence; the "carbonatite dykes" visible on Eureka thus could represent the wall rocks (marble) with which the magma interacted. If fluids emanating from this magma caused the formation of the monazite skarn, then the Eureka occurrence is a skarn related to alkaline/carbonatitic activity. It would seem unlikely that these alkaline/carbonatitic fluids were generated in the middle of the Damaran orogeny when geothermal gradients were elevated. The majority of carbonatitic intrusions are confined to a cratonic environment. This suggests a pre-/early Damaran age for the "mantle fluids", perhaps tapped during pre-/early Damaran rifting of the continental crust. (Re?) Crystallisation of the monazite would have occurred during the Damaran orogeny and would explain the morphology of the monazite and its (re?) crystallisation age of 500:1:20 Ma. Furthermore the mantle-derived fluid may not necessarily have carried the REE from which the monazite crystallised. REE may have been concentrated by sedimentary and metamorphic processes.

## 7.2.6 Conclusion

The author concedes that Dunai *et al.* (1989) have evidence for the presence of a mantle-derived fluid. There is, however, no field or petrographic evidence for the presence of a hidden, large carbonatite. The "carbonatite dykes" may just as well be marbles that have interacted with juvenile fluids. Indeed there are several laterally impersistent carbonate units without monazite mineralisation at the base of the Khan Formation on Eureka. There may well be a distinction between the fluid that is responsible for the low ( $^{87}\text{Sr}/^{86}\text{Sr}$ )<sub>i</sub> values and the fluid from which the monazite crystallised. The Eureka occurrence bears some similarities with the middle Proterozoic Bayan Obo iron-rare earth-niobium deposits in Inner Mongolia, China (Drew *et al.*, 1990), which are reported to be the largest REE deposits in the world (Mariano, 1989). These deposits were formed by the hydrothermal replacement of dolomite by fluids from a hidden alkaline-carbonatite in an intercontinental rift setting. No parent plutonic rocks have been identified. Although there is abundant Ba and Nb mineralisation and extensive K-metasomatism at Bayan Obo, the nature of the replacement, albeit on a much smaller scale, and the tectonic setting invite comparison with the Eureka occurrence. As with the Nosib Group, the host rocks at Bayan Obo are syn-rift sediments deposited in graben structures. If the fluid from which the monazite at Eureka crystallised is of juvenile origin, then monazite occurrences are probably confined to deep-seated major tectonic breaks. In this regard it is of note that the Eureka occurrence is located close to the intersection of the Omaruru Lineament and the Welwitschia lineament zone (Fig. 7.1).

## 7.3 TUNGSTEN SKARN MINERALISATION IN THE OKAWAYO FORMATION AT OTJUA

## 7.3.1 Introduction

Scheelite mineralisation was first discovered on the farm Otjua (Fig. 7.1) in the early 1980s by regional stream sediment sampling (Steven, 1987). During a subsequent exploration programme it became apparent that there are two different styles of scheelite mineralisation in the Schönfeld Dome (Map 1). The first style of mineralisation consists of fine-grained scheelite (<1 mm in diameter) hosted by quartz+plagioclase+scapolite+diopside calc-silicate rocks that are unrelated to carbonate units. These rocks were formed during regional metamorphism and are referred to as scheelite-bearing granofels (SBG). This lithology is also present in the calc-silicate rocks of the Okakombo Horst (Map 1) and its development is apparently unrelated to igneous intrusions (Steven, 1987). The second style of mineralisation is fine to coarse-grained (up to 4 cm in diameter) scheelite hosted by a coarse-grained, inequigranular calc-silicate gangue of scapolite, pyroxene, garnet and vesuvianite that replaces carbonate units. This second type of mineralisation is a replacement or metasomatic skarn, is clearly epigenetic and is only developed in close proximity to granitoid intrusions. The discontinuous, though volumetrically abundant, nature of the scheelite mineralisation in the granofels indicates that it may be considered as a very low-grade, large-tonnage tungsten resource. The skarn, possessing more evenly distributed tungsten within smaller ore bodies, is a moderate-grade, low-tonnage resource. At present, only the skarn-hosted scheelite mineralisation can be considered to be of economic interest. The discussion that follows describes and discusses the

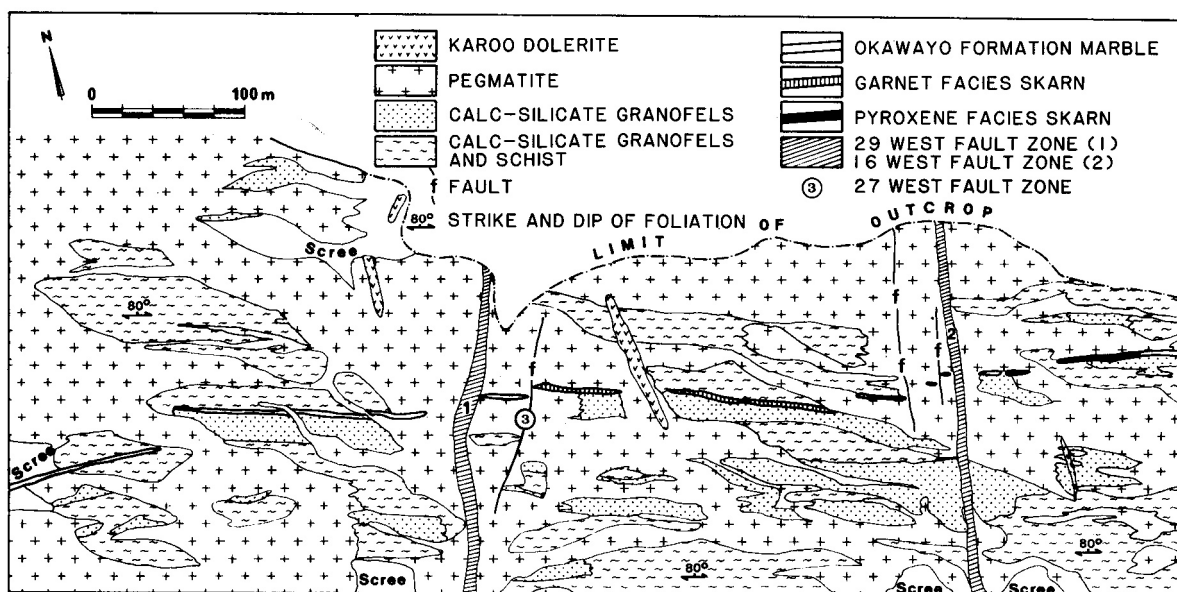


Figure 7/3.1: Simplified geological map of the Otjua Tungsten Prospect

Type Locality	Otjua Tungsten Prospect, Omaruru District
Host Formation	Okawayo
Host Lithology	Calcite marble
Regional Geological Setting	Shallow marine marls and carbonates
Form of Mineralisation	Lenses and pods of replacement skarn in calcite marble
Associated Volcanics	Minor sulphidic rhyolite may represent metamorphosed felsic volcanics
Structural Features	Mineralisation in core of D <sub>3</sub> dome; close proximity to Omaruru Fault Zone
Peak Metamorphic Facies	Amphibolite
Damaran Intrusions	Otjua Leucogranite Rb-Sr (WR) 478 ± 4 Ma, ( <sup>87</sup> Sr/ <sup>86</sup> Sr) <sub>I</sub> = 0.7196; δ <sup>18</sup> O = 15.1
Age of Mineralisation	Late Damara
Geochemical Association	W-F
Ore Minerals	Scheelite, fluorite, very minor pyrrhotite and chalcopyrite, traces of pyrite
Silicate Minerals	Grossular garnet, vesuvianite, hedenbergitic pyroxene, scapolite, c/zoisite
Classification	Tungsten Replacement Skarn
Comments	Skarnification Genetically Related to Granite Intrusion

**Table 7/3.1:** Scheelite skarn in the Okawayo Formation

genesis of one of the few documented tungsten replacement skarns on the African continent and the largest tungsten skarn discovered to date in the Damara Orogen: this section is a revised summary of the author's M.Sc. thesis (Steven, 1987). The term "skarn" is used to mean the large-scale transfer of components between hydrothermal fluids (which may be of magmatic origin) and carbonate rocks (Einaudi *et al.*, 1981).

### 7.3.2 Geological setting

The Otjua replacement skarn (Fig. 7/3.1) is one of four such bodies hosted by the Okawayo Formation marble (Table 7/3.1) on the southern side of the Schönfeld Dome (Map 1). Skarnification has only occurred where granite is proximal to the marble, though in none of the four examples is the contact between granite and marble exposed. However, at the Tjirundo, Schönfeld and Otjua replacement skarns, large masses of pegmatite, apparently derived from the granites, have extensively disrupted the metasediments.

#### 7.3.2.1 Metasediments and metavolcanic rocks

The Spes Bona and Oberwasser Formations comprise an alternating sequence of quartz-biotite schists, calc-silicate rocks, SBG and minor carbonate units. A minor, laterally impersistent, very fine-grained quartzo-feldspathic rock is interpreted as an altered felsic volcanic rock. The proportion

of calcareous units in both formations increases towards the contact with the Okawayo Formation. The schist is interpreted as representing metamorphosed muds, the calc-silicate rocks as marls and the marble as limestone. The fine intercalation of rocks composed of detrital material and chemical precipitates suggests that the sediments were laid down in a low energy environment. Skarnification of the minor carbonate horizons has occurred locally, especially in the Spes Bona Formation closer to the core of the dome. The Okawayo Formation is composed of a single, very pure, continuous calcareous marble unit, that varies in thickness from 0.7 to 4 metres.

#### 7.3.2.2 Structure and metamorphism

The metasediments at Otjua possess a single, bedding-parallel foliation defined by micas. The metasedimentary sequence strikes 103° and is overturned, dipping steeply northwards (Fig. 7/3.1). Calc-silicate rocks have a prominent lineation that plunges 68°-75° on a bearing 063° and is approximately parallel to the axes of minor, tight z-folds. Calcite-graphite isotope geothermometry conducted on marble samples from the vicinity of the Otjua Prospect and from the core of the Okakombo Horst on Tjirundo Süd revealed peak metamorphic temperatures between 519°C and 626°C with an average of 586°C (Map 1; Steven, 1987). These temperatures are in agreement with those indicated by the

petrogenetic grid for CZ pelites (Fig. 5.4). Lower sillimanite zone rocks, which are common in the Schönfeld Dome, were stable between 510°C and 660°C. In the aureoles of granite intrusions (less than 200 metres from the contact), to which the upper sillimanite zone rocks are essentially confined, peak metamorphic temperatures exceeded 610°C (assuming a minimum confining pressure of 2.2 kbars). The Otjua Prospect is disrupted by several north-north east-striking faults (Fig. 7/3.1) which are probably of Karoo age. All faulting appears to be in the same sense - minor sinistral horizontal displacements (1-20 metres) with considerable downthrows to the west.

### 7.3.2.3 Intrusive rocks

The Schönfeld Dome has been intruded and partially caused by a large number of granites and pegmatites (Map 1). The closest prominent intrusion to the Otjua prospect is the Otjua leucogranite which has an Rb-Sr whole-rock date of  $478 \pm 4$  Ma, an  $(^{87}\text{Sr}/^{86}\text{Sr})_1$  ratio of 0.7196 and an unusually high  $\delta^{18}\text{O}$  value of 15.1. The closest surface exposure of the Otjua leucogranite to the replacement skarn in the Okawayo Formation marble is 600 metres away. The second type of granite in the vicinity of the Otjua Prospect is a fine-grained variety, the closest exposure being 1.2 km to the south (Map 1). The age relationships between the fine-grained variety and the Otjua leucogranite are unknown, but they are thought to be cogenetic. On the southern side of the Schönfeld Dome in particular, the metasediments of the Spes Bona, Okawayo and Oberwasser Formations have been intruded by pegmatites in a passive or lit-par-lit manner. Crosscutting pegmatites with a consistent orientation of  $113^\circ$  are intimately associated with three of the four skarn prospects (Fig. 7/3.1). These transgressive pegmatites are absent from those portions of the Okawayo Formation that are unskarned. Contacts between the pegmatites and the metasediments are sharp and generally run parallel to the schistosity of the country rock. No thermal metamorphic effects have been observed on the pegmatite/metasediment contact. The Otjua Prospect is also transected by several north-south-trending Karoo dolerite dykes.

### 7.3.3 Morphology and petrography of the skarn

Metasomatic skarn is developed within several of the marble units at Otjua, but the most extensive and continuous skarn is hosted by the Okawayo Formation marble (Fig. 7/3.1). A strike length of 700 metres has been investigated by drilling to a depth of 370 metres below surface. The continuity and thickness of the skarn hosted by the Okawayo Formation combine to make it the most economically significant of all the skarns at the Otjua Prospect. The description that follows concentrates exclusively on skarn types occurring in this formation, though replacement skarns in the enclosing Spes Bona and Oberwasser Formations exhibit similar characteristics. The skarn can be subdivided into three zones or facies: vesuvianite-facies skarn which hosts minor scheelite mineralisation, garnet-facies skarn which hosts the majority of scheelite mineralisation and pyroxene-facies skarn which is essentially barren of tungsten. These three facies of skarn represent varying degrees of replace-

ment of marble (Fig. 7/3.2). Moreover, they appear to pass laterally into one another, but this cannot be proved due to the poor exposure. Transitional zones between the three facies have however been recognised. There is no evidence that one facies of skarn replaces, overprints or crosscuts another facies. Garnet-facies skarn constitutes more than 90% of the ore zone at Otjua. The vesuvianite-facies skarn is considered to be of limited commercial value: either the skarn is too thin or the tungsten grade is too low. No wolframite has been recorded at Otjua, either in the skarn or the associated intrusive rocks.

#### 7.3.3.1 Vesuvianite-facies skarn

This facies of skarn can be traced on surface for a distance of 325 metres west of the 27W Fault (Fig. 7/3.1) and drilling indicates that it extends at least 370 metres below surface. Replacement of the Okawayo Formation marble is incomplete, the skarn being especially well developed towards the structural footwall (Fig. 7/3.2). The marble-skarn contact is sharp, extending over a few millimetres. Mineral assemblages include vesuvianite (30-70%), clinopyroxene (5-30%), scapolite (10-30%), calcite (5-40%), garnet (0-5%), fluorite (0-2%), sphene (0-2%), plagioclase feldspar (0-2%), apatite (0-2%), clinozoisite (0-2%) and scheelite (0-1%). The prismatic vesuvianite contains numerous inclusions of very fine-grained calcite and altered scapolite.

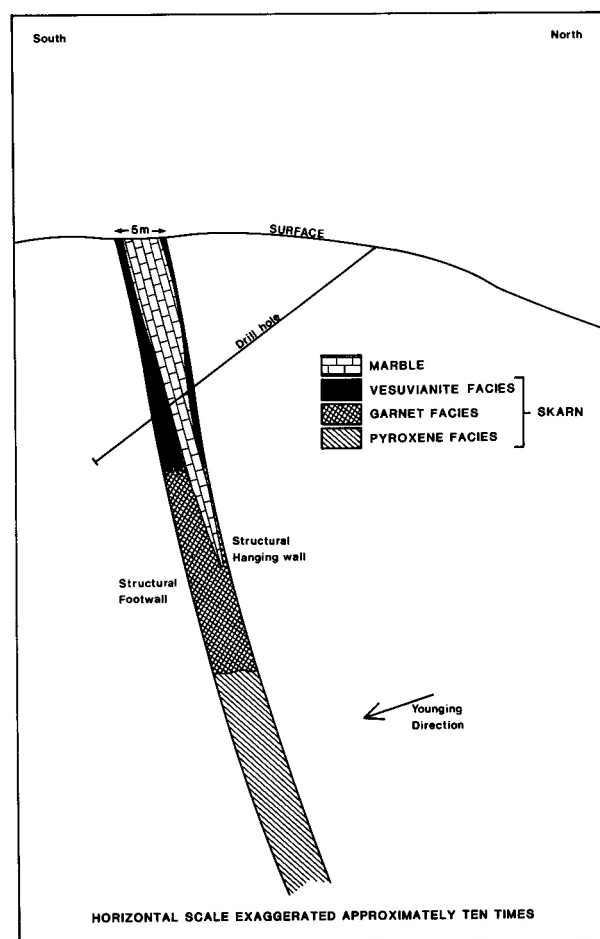


**Figure 7/3.2:** Schematic cross section through the Otjua Prospect showing direction of drillholes, overturning of sequence and varying degree of replacement of Okawayo Formation marble by skarn (after Steven, 1987)

Pyroxenes are usually less than 1 mm in diameter and occur in granoblastic clusters. Texturally, the assemblage is in equilibrium because all mineral phases are in contact with one another and there are no observable reaction relationships. Minor anhedral fluorite appears to have crystallised last.

### 7.3.3.2 Garnet-facies skarn

This facies of skarn can be traced sporadically for a distance of 270 metres between the 16W and 27W Faults and has been intersected at a depth of 350 metres below surface. Within this area large zones of unreplaced marble exist. However, the degree of replacement of marble is higher than in the vesuvianite facies (Fig. 7/3.2); skarn development is greatest on the structural footwall of the carbonate. Garnet-facies skarn comprises garnet (5-50%), hedenbergitic pyroxene (5-40%), scapolite (10-70%), fluorite (5-35%), carbonate (0-5%), scheelite (0-3%), plagioclase feldspar (0-3%), clinozoisite (0-3%), epidote (0-3%), hornblende (0-3%), chlorite (0-2%), pyrrhotite (0-2%), chalcopyrite (0-2%) and pyrite (0-1%). This facies of skarn generally has a granoblastic-poikiloblastic texture, but elsewhere the texture is chaotic. Poikiloblastic (up to 4 cm) and xenoblastic garnet (Plate 7/3.1) is commonly associated with and appears to overgrow scapolite. Pyroxene usually occurs with granoblastic scapolite or is surrounded by a groundmass of fluorite. Round to almost rectangular scheelite crystals range in size from 100  $\mu\text{m}$  to 4 mm in diameter (Plate 7/3.2). The scheelite is present at triple points in equilibrium with pyroxene and scapolite or poikiloblastically enclosed by garnet and, locally, fluorite. The fluorite is universally anhedral, forming rounded embayments into pyroxene and scapolite and appears to be a late-stage mineral. In summary, scheelite, scapolite and pyroxene all appear to have crystallised at about the same time, but poikiloblastic and interstitial garnet, the sulphides and some of the fluorite crystallised slightly later.

Garnet-facies skarn is usually zoned across its width, though no mineralogical zoning has been noted either down-dip or along strike. This zonation is by no means universally developed, but borehole intersections exhibit many of the

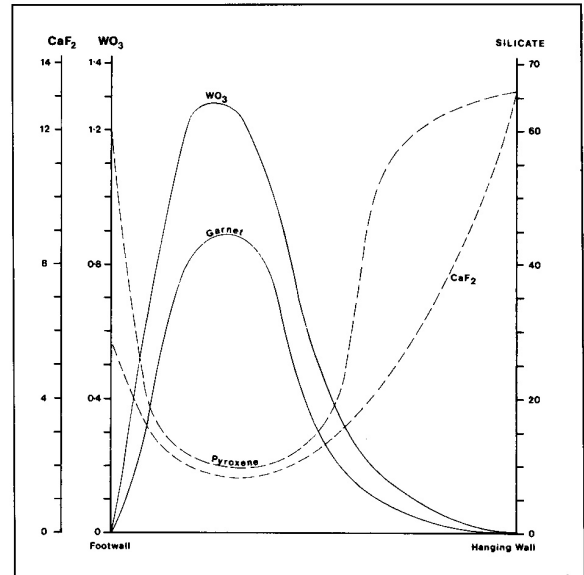


**Figure 7/3.3:** Schematic diagram showing mineralogical zonation and variations in wt%  $\text{CaF}_2$  and wt%  $\text{WO}_3$  contents across garnet-facies skarn (after Steven, 1987)

features which are summarised in Fig. 7/3.3: a concentration of fluorite towards the structural hanging wall of the skarn; a sympathetic relationship between garnet and scheelite; a tendency for scheelite to be concentrated on the footwall side of the core of the skarn, but a decrease in scheelite immediately on the footwall contact; an antipathetic relationship between pyroxene and garnet; a concentration of pyroxene towards the hanging and footwall contacts of the skarn.

### 7.3.3.3 Pyroxene-facies skarn

This facies can be traced on surface for a distance of approximately 90 metres on the eastern side of the 16W Fault and extends to at least 130 metres below surface. Pyroxene-facies skarn containing minor fluorite mineralisation has also been intersected in a borehole (OT14) at depth on the western side of the ore body. This skarn facies always replaces the entire width of the marble (Fig. 7/3.2) and comprises

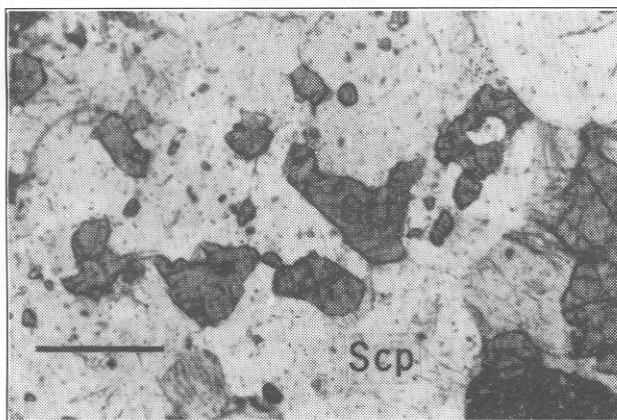


**Plate 7/3.1:** Garnet-facies skarn from Otjua Tungsten Prospect; xenoblastic garnet (Grt) and scapolite (Scp) (OT38998; PPL); scale bar = 0.5 mm

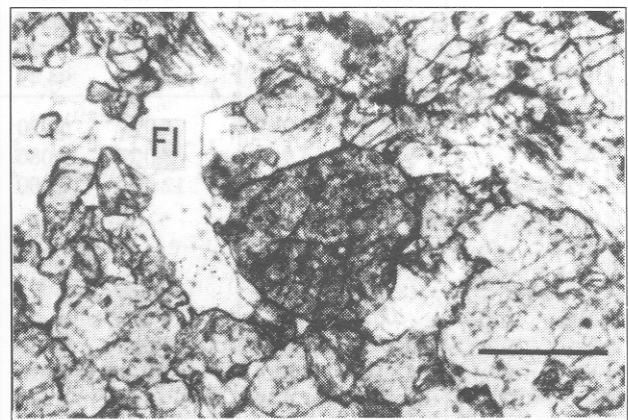


**Plate 7/3.2:** Garnet-facies skarn from Otjua Tungsten Prospect; scheelite crystal surrounded by scapolite and xenoblastic garnet (OT38998; PPL). Note fluorite (Fl) top left; scale bar = 0.5 mm

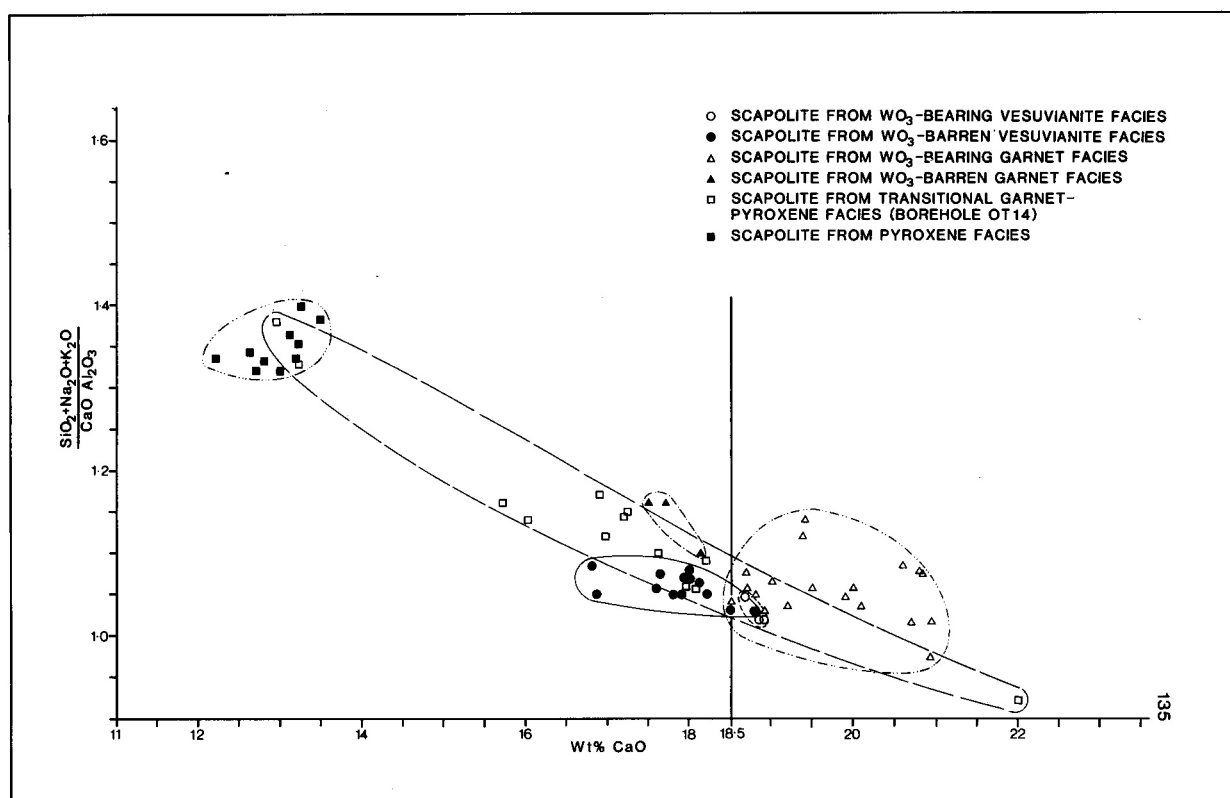


Figure 7/3.4:  $(\text{SiO}_2+\text{Na}_2\text{O}+\text{K}_2\text{O})/(\text{CaO}+\text{Al}_2\text{O}_3)$  versus wt% CaO for skarn scapolite analyses (after Steven, 1987)

hedenbergitic pyroxene (20-80%), scapolite (20-80%), hornblende (0-5%) and minor clay minerals, calcite, clinzoisite and opaque phases. Anhydral pyroxene and scapolite usually occur in a polygonal mosaic that is locally granoblastic, but

elsewhere there is a considerable range in grain size from 100  $\mu\text{m}$  to many centimetres. The scapolite is altered to clay minerals. Clinzoisite prisms are commonly associated with and may enclose scapolite, while hornblende rims pyroxene.

Facies	Vesuvianite		Vesuvianite-Garnet		Garnet		Garnet-Pyroxene		Pyroxene	
SiO <sub>2</sub> (wt%)	44.97	45.83	45.75	45.30	45.52	44.57	43.71	46.91	48.46	51.10
TiO <sub>2</sub>	ND	ND	.03	.02	ND	.01	.03	.03	.01	.02
Al <sub>2</sub> O <sub>3</sub>	27.40	27.35	27.81	28.22	25.65	26.29	27.49	26.73	25.78	27.46
FeO	.10	.10	.04	.12	.19	.12	.08	.19	.08	.02
MnO	ND	.01	.06	.01	.03	.03	.02	.02	ND	.03
MgO	.01	.03	.01	ND	.01	.01	ND	.01	ND	ND
CaO	18.91	18.68	17.96	17.79	20.90	20.99	18.35	16.92	13.25	13.47
Na <sub>2</sub> O	1.84	1.97	3.11	2.77	1.60	1.37	2.91	3.45	5.67	5.05
K <sub>2</sub> O	.38	.38	.33	.26	.17	.18	.47	.60	.53	.52
TOTAL	93.61	94.35	95.10	94.49	94.07	93.57	93.06	94.86	93.78	97.67
Si	6.984	7.045	6.991	6.920	7.211	7.079	6.892	7.179	7.376	7.347
Al	5.016	4.955	5.009	5.080	4.789	4.921	5.108	4.821	4.624	4.653
SUBTOTAL	12.000	12.000	12.000	12.000	12.000	12.000	12.000	12.000	12.000	12.000
Ti	-	-	.003	.002	-	.001	.004	.004	.001	.002
Fe	.013	.013	.005	.015	.025	.016	.011	.024	.010	.002
Mn	-	.001	.008	.001	.004	.004	.003	.003	-	.004
Mg	.002	.007	.002	-	.002	.002	-	.002	-	-
Ca	3.147	3.077	2.941	2.912	3.547	3.572	3.100	2.774	2.161	2.075
Na	.554	.587	.922	.820	.491	.422	.890	1.024	1.673	1.408
K	.075	.075	.064	.051	.034	.037	.095	.117	.103	.095
SUBTOTAL	3.791	3.760	3.945	3.801	4.103	4.054	4.103	3.948	3.948	3.586
%Me	83.4	82.4	75.0	77.1	87.2	88.7	76.0	71.1	55.0	58.1

Table 7/3.2: Representative analyses of skarn scapolite from the Otjua Tungsten Prospect  
N.B. Number of ions on the basis of 12(Si,Al)

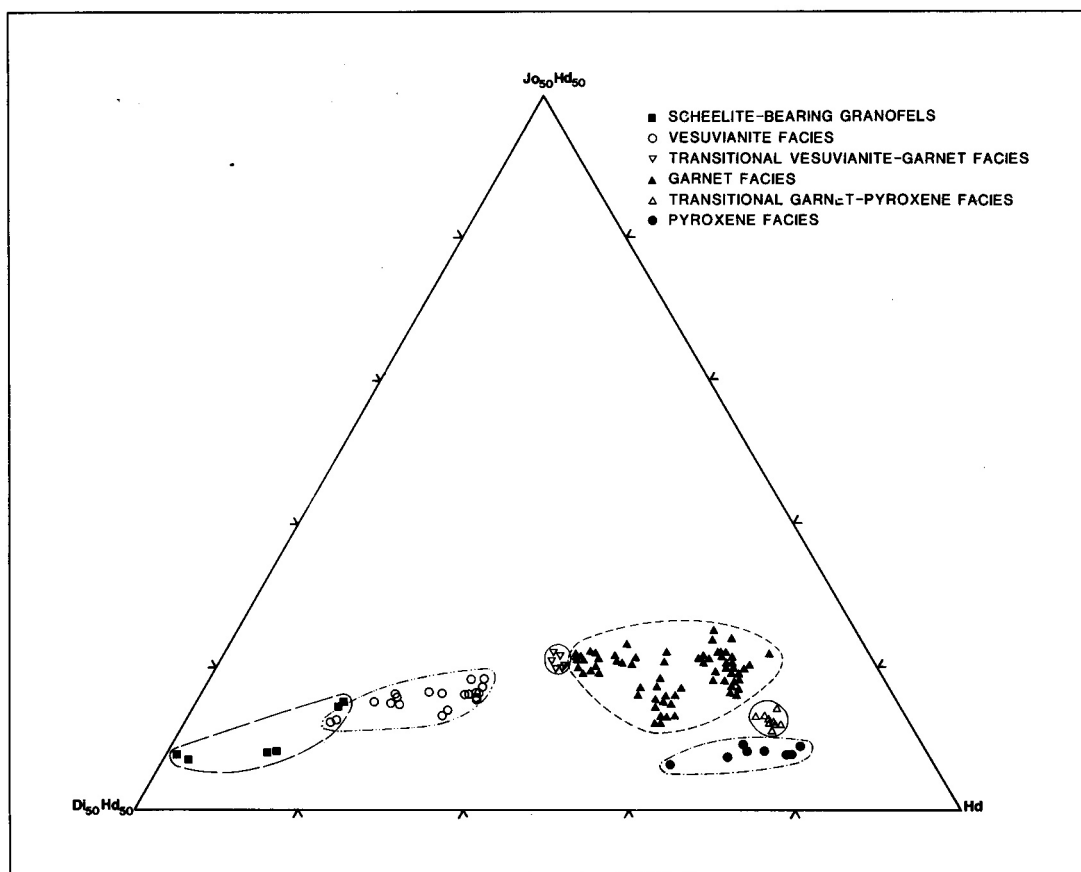


**Figure 7/3.5:** Compositions of pyroxene in granofels and skarn facies expressed as mole proportions of diopside (Di), Johannsenite (Jo) and Hedenbergite (Hd) (after Steven, 1987)

### 7.3.4 Skarn mineral chemistry

#### 7.3.4.1 Scapolite

Scapolite compositions for the three skarn facies as well as two intermediate assemblages are given in Table 7/3.2. In all three facies of skarn considerable compositional variations were noted both between scapolite grains and within single grains. No systematic variations from the core to the rim of crystals was observed, but where zoned, scapolite has a meionite-rich core. The main substitution in scapolite is  $\text{NaSi}=\text{CaAl}$  (Deer *et al.*, 1966) and a substitution index  $(\text{SiO}_2 + \text{Na}_2\text{O} + \text{K}_2\text{O})/(\text{CaO} + \text{Al}_2\text{O}_3)$  versus wt% CaO content is plotted for all scapolite analyses in Fig. 7/3.4. Scapolites from the garnet facies tend to be the most calcic, although there is an overlap in composition with those from the vesuvianite facies. Scapolites from pyroxene-facies skarn have a markedly different composition from the other two facies, possessing higher alkali contents. The large compositional variation of scapolite within a single microprobe section is exemplified by the sample from borehole OT14 where CaO contents of the scapolite vary from 12.9 to 22.1 wt%. Large variations in scapolite chemistry suggest either disequilibrium at the time of scapolite formation or that the scapolite crystallised from a fluid of rapidly changing composition.

Significantly, variations in scapolite composition are closely related to scheelite distribution in both the vesuvianite and garnet facies. Scapolites from the vesuvianite facies that contain more than 18.5 wt% CaO are associated with scheelite,

while portions of the skarn containing less calcic scapolites are essentially devoid of scheelite. Similarly, scapolites from scheelite-bearing garnet facies skarn are more meionitic. This suggests that scheelite formation and scapolite chemistry were controlled by the availability of calcium ions throughout the skarn system. The local development of scapolite with Ca-rich cores and the textural evidence indicating early crystallisation of scheelite and scapolite suggests that  $(a_{\text{Ca}^{2+}})$  was highest during the earliest stage of skarn formation.

#### 7.3.4.2 Pyroxene

Representative analyses of pyroxene from the various skarn facies are listed in Table 7/3.3 and a summary of pyroxene composition within the skarn system is given in Fig. 7/3.5. None of the pyroxenes from any of the skarn facies exhibits systematic compositional zoning from rim to core. Pyroxenes show considerable compositional variation within each facies, but each facies possesses pyroxene of characteristic composition. An evolutionary trend towards Fe enrichment with progressive replacement of the marble is evident in Fig. 7/3.5. The presence of pyroxene with intermediate composition in the transitional zones demonstrates a genetic link between the facies. The tendency towards ferrous and manganese-enriched pyroxene in the later stages of prograde growth of calcic tungsten-bearing skarn is a common worldwide phenomenon (Einaudi *et al.*, 1981). Fig. 7/3.5 illustrates the point that on the deposit scale the skarn system has developed in a broadly systematic manner, but on the local

Facies	Vesuvianite		Vesuvianite-Garnet		Garnet		Garnet-Pyroxene		Pyroxene	
SiO <sub>2</sub> (wt%)	48.92	49.24	48.46	49.19	49.42	48.58	47.40	47.75	48.23	48.34
TiO <sub>2</sub>	ND	ND	ND	ND	ND	ND	ND	.04	ND	ND
Al <sub>2</sub> O <sub>3</sub>	.40	.29	.32	.28	.45	.40	.30	.29	.28	.12
Cr <sub>2</sub> O <sub>3</sub>	ND	ND	ND	ND	ND	ND	ND	ND	ND	ND
FeO	19.17	18.43	21.28	21.45	21.75	22.61	25.36	25.13	25.83	25.90
MnO	2.47	2.26	2.93	2.98	3.13	3.17	1.81	1.90	1.18	1.24
MgO	4.72	5.42	3.31	3.25	3.07	2.04	1.37	1.54	1.86	1.64
CaO	23.58	23.93	23.48	23.44	22.31	22.89	23.16	23.02	22.75	22.89
Na <sub>2</sub> O	.07	.11	.07	.07	.07	.05	.11	.11	.09	.08
K <sub>2</sub> O	ND	ND	ND	ND	ND	ND	ND	ND	ND	ND
TOTAL	99.33	99.68	99.85	100.66	100.10	99.74	99.51	99.78	100.22	100.21
Si	1.969	1.967	1.965	1.975	1.989	1.982	1.960	1.965	1.971	1.977
Ti	-	-	-	-	-	-	-	.001	-	-
Al	.019	.014	.015	.013	.021	.019	.015	.014	.013	.006
Cr	-	-	-	-	-	-	-	-	-	-
Fe	.645	.616	.722	.720	.732	.771	.877	.865	.883	.886
Mn	.084	.076	.101	.101	.107	.110	.063	.066	.041	.043
Mg	.283	.323	.200	.194	.184	.124	.084	.094	.113	.101
Ca	1.017	1.024	1.020	1.009	.962	1.001	1.026	1.015	.996	1.003
Na	.005	.009	.006	.005	.005	.004	.009	.009	.007	.006
K	-	-	-	-	-	-	-	-	-	-
SUM	4.022	4.029	4.029	4.017	4.000	4.011	4.034	4.029	4.024	4.022

**Table 7/3.3:** Representative analyses of skarn pyroxene from the Otjua Tungsten Prospect  
N.B. Number of ions on the basis of 6 oxygens

scale considerable chemical disequilibrium during skarn formation is indicated. Note that pyroxene in the SBG is more diopsidic than any of the skarn pyroxene (Fig. 7/3.5).

#### 7.3.4.3 Garnet

Representative analyses of grossular garnet from the Otjua skarn are given in Table 7/3.4. Unlike the other silicate minerals in the Otjua skarn, garnet occurs as anhedral grains or intergrown, anastomosing masses, making it impossible to distinguish between early and late-crystallising phases of the garnet. Large compositional variations were noted within individual grains over very short distances (<50µm) as well as between garnet grains. These variations are non-systematic; garnets showing no compositional variation are commonly in contact with grains showing marked oscillatory zoning. Garnet almost certainly crystallised from a fluid of changing composition; the late-stage nature of the garnet suggests that it formed from a residual fluid. Substantial variations in skarn garnet have been noted by Burton *et al.* (1982) and Mathieson and Clark (1984) and thus the situation at Otjua is not atypical of skarn deposits.

#### 7.3.4.4 Summary of skarn mineral chemistry

Skarn minerals from the three facies have compositions that are typical of metasomatic tungsten skarn deposits (Einaudi *et al.*, 1981). The variations in pyroxene chemistry are similar to those observed at other metasomatic tungsten skarns, for example the Strawberry Mine (Nokleberg, 1981). The compositions of the two minerals that are common to all three facies of skarn show that the three facies are genetically

related. The first skarn minerals to form show considerably more homogeneity than is common in skarns, but on the local scale the skarn system possesses disequilibrium assemblages with garnet in particular exhibiting extensive compositional variation. The few scapolite grains that are zoned have a calcium-rich core: scapolite chemistry and scheelite distribution are closely linked in the skarn system. In terms of the mineralogical guidelines for the classification of skarns suggested by Newberry (1979) and listed by Einaudi *et al.* (1981) the Otjua skarn is a reduced tungsten skarn because the pyroxene-garnet ratio is approximately 2:1; the pyroxene composition at Otjua is in the range 58.5-88.1 mol% Hd, 3.2-12.5 mol% Jo; the garnet at Otjua is andradite poor and the diagnostic opaques at Otjua are pyrrhotite and chalcopyrite. Newberry (1979) suggested that reduced skarns were either formed in carbonaceous host rocks or at great depth.

#### 7.3.5 Marble and skarn bulk rock chemistry

The calcitic nature of the Okawayo Formation marble is shown in Table 2.7 and the large-scale introduction of material into the carbonate unit during metasomatism is clearly evident from the whole-rock chemistry of the three skarn facies (Fig. 7/3.6). Systematic changes in major and minor element concentrations with progressive metasomatism of the Okawayo Formation can be accounted for by the presence or absence of certain minerals and by changes in mineral chemistry. The decrease in total Ca content of the Okawayo Formation with increasing metasomatism is matched by a corresponding increase in SiO<sub>2</sub> concentration. With progres-

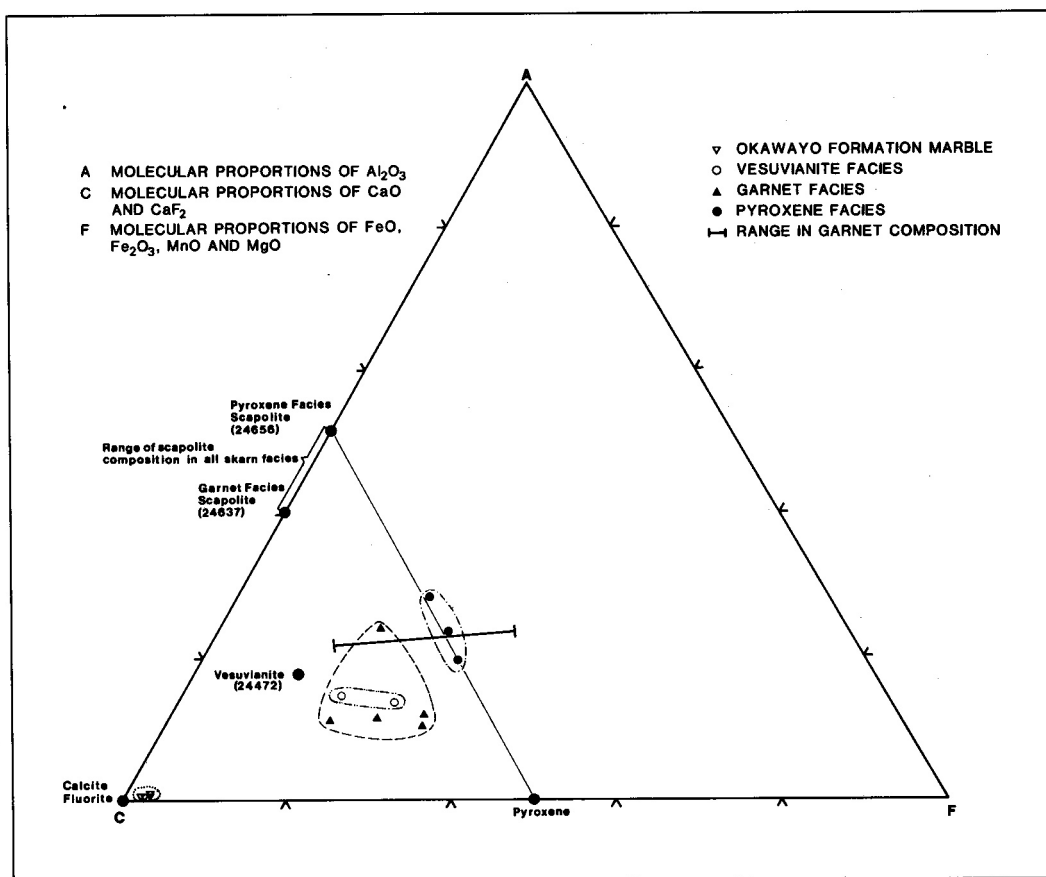


Figure 7/3.6: Modified ACF plot for marble and skarn analyses (modified after Steven, 1987)

sive replacement of the carbonate unit, the proportion of calcite in the mineral assemblages declines (vesuvianite facies: 5-40% calcite; garnet facies: 0-5% calcite; pyroxene facies: none). Changes in mineral assemblages and mineral composition to show the progressive metasomatism are shown in the modified ACF plot (Fig. 7/3.6). Only major minerals are shown on this diagram. The introduction of magnesium, iron and manganese that accompanied metasomatism results in the vesuvianite and garnet-facies skarns plotting well away from the marble. The garnet-facies skarn exhibits considerable compositional variation and encloses the vesuvianite facies field, emphasising their similar bulk composition. The

pyroxene facies skarn plots furthest from the Ca apex along the relevant scapolite-pyroxene tie line.

### 7.3.6 Genesis of the Otjua skarn

#### 7.3.6.1 Timing of skarnification

The metasediments enclosing the skarn are foliated, have a fine-grained, equigranular texture and their minerals are unzoned, suggesting equilibration under peak metamorphic conditions at 520 Ma. In contrast, skarns hosted by the Okawayo Formation lack a tectonic fabric, exhibit replacement features, a diverse range of textures and some skarn minerals possess a wide range in composition over short distances. Skarn formation clearly postdated the peak of regional metamorphism. The purity of the marble and the large proportion of exotic elements in the skarn compared to the carbonate make it extremely improbable that the skarn formed *in situ* from a mineralised dolomitic precursor. Skarnification occurred as the result of large-scale metasomatic replacement of calcitic marble by Ca-Fe-Mg-Mn silicates. One fact in particular shows that there was only a small difference in temperature between the skarn-forming fluid and the carbonate: there is no contact metamorphic effect between skarn and marble, in contrast to many North American examples (Newberry, 1982). The meta-sediments and skarn are disrupted and transected by late-tectonic pegmatitic dykes, apparently derived from the Otjua leucogranite. No contact metamorphic effects are developed in the rocks that these pegmatite bodies intrude, indicating that ambient rock temperatures could not

SiO <sub>2</sub> (wt%)	37.65	37.87	37.81	38.73	37.40	38.03
TiO <sub>2</sub>	.17	ND	.08	.12	.05	.14
Al <sub>2</sub> O <sub>3</sub>	19.56	20.39	19.98	20.23	20.74	20.17
Cr <sub>2</sub> O <sub>3</sub>	ND	ND	ND	ND	ND	ND
FeO	9.24	12.44	12.08	6.41	13.83	10.70
MnO	4.54	6.64	6.58	3.40	8.38	7.77
MgO	ND	.04	.04	.04	.16	.09
CaO	27.89	22.18	23.00	31.11	19.61	23.28
TOTAL	99.05	99.56	99.57	100.04	100.17	100.18
Si	2.979	2.996	2.996	2.998	2.963	2.992
Ti	.010	-	.005	.007	.003	.008
Al	1.824	1.901	1.866	1.846	1.937	1.870
Cr	-	-	-	-	-	-
Fe <sup>3+</sup>	.176	.099	.134	.154	.063	.130
Fe <sup>2+</sup>	.436	.724	.667	.261	.853	.574
Mn	.304	.445	.442	.223	.562	.518
Mg	-	.005	.005	.005	.019	.011
Ca	2.365	1.880	1.953	2.580	1.665	1.962
SUM	8.094	8.050	8.068	8.074	8.065	8.065

Table 7/3.4: Representative analyses of skarn garnet from the Otjua Tungsten Prospect  
N.B. Number of ions on basis of 12 oxygens

	OT102	OT103	OT104	OT105	OT106	OT107	OT108	OT109	OT110	OT111
SiO <sub>2</sub> (wt%)	38.77	41.84	46.20	45.10	40.66	42.42	29.50	49.68	48.37	49.94
TiO <sub>2</sub>	.84	.52	.03	.05	.10	.04	.11	.04	.02	.03
Al <sub>2</sub> O <sub>3</sub>	12.79	11.06	7.53	8.64	18.67	9.48	10.18	16.91	12.57	14.75
Fe <sub>2</sub> O <sub>3</sub>	.89	1.45	1.75	1.40	1.10	1.78	1.22	-	-	-
FeO	5.92	9.65	11.67	9.31	7.30	11.89	8.12	8.75	12.93	11.06
MnO	.52	.81	2.17	2.29	2.26	2.12	2.49	.42	.64	.47
MgO	2.84	2.10	1.07	.84	.38	1.51	.89	.61	.75	.90
CaO	29.65	25.05	16.09	14.88	22.99	20.76	12.14	15.82	17.68	16.75
Na <sub>2</sub> O	.29	.96	.47	.45	1.02	.55	.30	3.42	1.99	2.86
K <sub>2</sub> O	.01	.19	.09	.18	.17	.12	.09	.60	.41	.51
P <sub>2</sub> O <sub>5</sub>	.22	.15	.09	.07	.11	.12	.08	.17	.15	.10
H <sub>2</sub> O-	.06	.07	.09	.10	.03	.01	.11	.04	.14	.05
LOI	4.64	4.35	1.82	1.89	3.19	2.19	2.01	3.58	3.63	3.87
CaF <sub>2</sub>	3.10	2.10	11.30	16.40	1.90	6.80	32.00	-	-	-
TOTAL	100.54	100.30	100.37	101.60	99.88	99.79	99.24	100.04	99.28	101.29
F (ppm)	-	-	-	-	-	-	-	584	<490	<490
S	122	42	56	<7.0	<6.0	<7.0	13	<6.0	141	<6.0
Rb	<2.0	16	8	20	10	8	14	19	14	21
Ba	7	11	7	10	7	23	14	77	37	34
Sr	182	159	128	161	158	157	158	189	168	167
Th	30	29	30	25	<5.0	<5.0	159	<5.0	<5.0	100
U	13	44	<4.0	6	<4.0	7	<4.0	10	<4.0	7
Zr	126	62	19	25	21	19	25	15	11	12
Nb	17	29	27	26	23	4	34	42	19	25
Mo	8	16	56	14	13	13	18	4	6	4
Sn	110	26	70	52	37	<4.0	20	<4.0	14	<4.0
W	722	3783	2835	444	6526	5511	5416	23	21	29
V	137	101	9	12	51	39	28	8	10	12
Cr	75	51	15	15	11	12	15	6	0	6
Co	17	18	14	14	8	18	12	11	20	16
Ni	36	22	6	8	<1.7	13	6	4	8	6
Cu	<1.7	<1.9	<1.7	<1.6	<1.6	<1.6	4	2	7	5
Zn	480	677	375	391	260	538	169	232	247	272
Pb	8	10	<5.0	<5.9	8	<5.8	7	29	11	23
As	27	10	<7.0	<7.0	<7.0	<7.0	<7.0	<7.0	<7.0	<7.0
Sb	<5.0	<5.0	<5.0	<5.0	<5.0	<5.0	<5.0	<5.0	<5.0	<5.0
Sc	15	17	9	8	14	8	5	20	8	11
Y	71	194	8	9	85	18	38	31	26	25
Au (ppb)	<5	<5	15	10	<5	<5	46	<5	<5	<5

**Table 7/3.5:** Whole-rock analyses of skarns from the Otjua Tungsten Prospect

OT102: Vesuvianite facies skarn; RUL grid 41W/38S

OT103: Vesuvianite facies skarn; RUL grid 31W/10N

OT104: Garnet facies skarn; RUL grid 26W/27-30N

OT105: Garnet facies skarn; RUL grid 27W/29-33N

OT106: Garnet facies skarn; RUL grid 24W/28-29N

OT107: Garnet facies skarn; RUL grid 22W/22-24N

OT108: Garnet facies skarn; RUL grid 17W/35-36N

OT109: Pyroxene facies skarn; RUL grid 12W/52-55N

OT110: Pyroxene facies skarn; RUL grid 12W/51-55N

OT111: Pyroxene facies skarn; RUL grid 13W/50-52N

N.B. FeO ratio for vesuvianite and garnet facies skarn selected at 0.15 on basis of estimation of Fe<sup>3+</sup> in vesuvianite and garnet. All iron reported as FeO for pyroxene facies skarn (after Steven, 1987)

have been far below those attained at 520 Ma. Skarn formation occurred after the peak of metamorphism (520 Ma) and before the final crystallisation of the Otjua leucogranite (478±4 Ma).

### 7.3.6.2 The mechanism of skarn formation

#### 7.3.6.2.1 "Bimetasomatic exchange" "with the country rocks

Some or all of the elements required to form the silicate minerals in the skarn could have been provided by the wall rocks and it is necessary to examine the evidence that the various skarn facies developed as a result of "bimetasomatic exchange". Although diffusion models can explain a number of thin reaction zones (Thompson, 1959; Vidale, 1969), it is widely accepted that they cannot account for the large thicknesses of skarn in most metasomatic deposits (Einaudi *et al.*, 1981). Several features argue against an exchange of elements between the carbonate and the wall rocks at Otjua. Firstly, drillhole intersections of marble indicate that there has been no reaction between the marble and the enclosing country rocks in areas away from the skarn. Marble-schist contacts do not contain unusual metamorphic assemblages (Thompson, 1959). Secondly, if the skarn was derived from an exchange of elements between marble and the enclosing wall rocks, different mineral assemblages would have developed where the marble is in contact with schist and with calc-silicate rocks. This is clearly not the case: all three facies of skarn are in contact with both lithologies. Thirdly, there is no visible alteration or depletion of the wall rocks that immediately enclose the skarn. At Otjua, models of skarn formation invoking exchange of elements with the country rocks by metasomatic diffusion (Korzhinskii, 1965) can unequivocally be rejected.

#### 7.3.6.2.2 Infiltrational metasomatism

The systematic changes in mineralogy, mineral chemistry and whole-rock compositions of the facies of skarn indicate that the subvertical Okawayo Formation marble acted as a reactive conduit for a channelised mineralising fluid that progressively metasomatised the carbonate. Skarnification of the Okawayo Formation occurred as the result of infiltrational metasomatism as envisaged by Korzhinskii (1965). The localisation of vesuvianite-facies skarn on the country rock-marble contact suggests that this was a zone of higher permeability and was important in channelling the fluid. It would appear that the facies development along the "metasomatic column" resulted from three main variables (Steven, 1987)? variations in the ratio of activity of calcium ions ( $a_{Ca^{2+}}$ ) from the decomposing marble to the activity of elements introduced by the incoming fluid; the fluid/rock ratio; and temperature. This is the best explanation for the petrographic evidence which shows that facies of skarn do not crosscut or replace another facies. Where transitional skarn assemblages have been identified, mineral compositions are also transitional, indicating that one pulse of fluid could account for the skarn. The strong control on mineral chemistry is attributed to the temperature dependent partitioning of major, minor and trace elements in the fluid. It

would thus appear that the various skarn facies developed at broadly the same time.

### 7.3.6.3 Source of the skarn-forming fluid

Carbonate-hosted tungsten skarn mineralisation is spatially associated with late-tectonic granite stocks and pegmatitic intrusions both within the Schönfeld Dome and elsewhere in the CZ (Steven, 1987). This author considered the Otjua leucogranite to be the source of the fluid from which the skarn formed. He argued that the highly anomalous ( $^{87}Sr/^{86}Sr$ )<sub>1</sub> and  $\delta^{18}O$  values of the intrusion indicated that it was an anatectic melt derived from scheelite-bearing lower Swakop Group metasediments. Geochemical studies conducted by Steven (1987) showed the widespread distribution of scheelite mineralisation in the metamorphosed marls of the lower Swakop Group in the Omaruru area. Major and trace element geochemistry showed that the granofels (SBG) is a type of marl with anomalous concentrations of W (up to 1.4 wt%) and F (up to 6500 ppm). In other respects the granofels is indistinguishable from Calc-silicate rocks suggesting that the two lithologies were derived from similar sedimentary precursors. SBG are not a type of replacement skarn formed by metasomatism of a calc-silicate rock, nor are they spatially associated with granites or pegmatites. Thus calc-silicate rocks and granofels constitute a major sediment-hosted tungsten reservoir that existed prior to skarn formation and late-tectonic granite intrusion.

One of the major problems in resolving the source of the skarn-forming fluid is the obscure relationship between the granite, the pegmatite and the skarn. Interpretation is hampered by the poor exposure. The closest outcrop of the Otjua leucogranite to the replacement skarn is 600 metres away. The massive pegmatite appears to have been derived from the leucogranite, but the geochemical data thought to link the intrusions is equivocal. Fragments of skarn in the pegmatite immediately west of the 16W Fault (Fig. 7/3.1) indicate that skarnification predated pegmatite intrusion.

I Steven (1987) envisaged that the three facies of skarn, the pegmatite and the granite were a continuum that crystallised from an anhydrous granite magma. Tungsten and fluorine were concentrated in the volatile-rich part of the system farthest from the magma. These volatiles reacted with marble to produce skarn. Subsequently the leucogranite crystallised releasing a pegmatitic phase that disrupted the metasediments and the skarn. However, as pointed out by Moore (1989, pers. comm.), in a more classical interpretation, the cooling Otjua leucogranite would have first exsolved a pegmatite melt phase and only subsequently a hydrothermal phase rich in F and W. This issue will not be resolved without a detailed radiometric investigation of the intrusions.

The complete replacement of the marble by a metasomatic fluid over hundreds of metres clearly indicates the introduction of large volumes of fluid from a point source at depth. This implies the accumulation and temporary storage of a large amount of fluid: a magma chamber is the most obvious possibility. If the fluid did not come from the intrusion, it may well have come from the metasediments and merely

have been focused by the intrusion. It is possible that the intruding Otjua leucogranite caused partial melting of the F-bearing Spes Bona Formation as it ascended. The role of fluorine in the lowering of the solidus to temperatures below 600°C is well documented (Manning and Pichavant, 1983). Temperatures in the aureoles of granitoids and pegmatites in the Schönfeld Dome exceeded 660°C (Fig. 5.4). Thus as an alternative to the model proposed by Steven (1987), the Otjua granite, rather than being the source of the fluids, may merely have acted as a “heat-engine” and mobilised fluids in the metasediments within its thermal aureole. In this respect the importance of Buchan-type metamorphism and of thermal domes in the tectonothermal history of the CZ was not fully appreciated by Steven (1987) because of the lack of  $\text{Al}_2\text{SiO}_5$  polymorphs in the metasediments that enclose the Otjua skarn. Three examples of thermal domes in the CZ have now been documented (see Chapter 5).

### 7.3.7 Conclusion

The Otjua tungsten replacement skarn formed within the thermal aureole of the Otjua leucogranite. It cannot be classified as a contact skarn because no igneous contact is exposed (and may not be present), nor has any endoskarn (altered intrusion) been recognised. The Otjua skarn has many similarities with other replacement tungsten skarns, the majority of which are associated with calc-alkaline intrusions of mid-Palaeozoic to late Cretaceous age in the Circum-Pacific region (Einaudi *et al.*, 1981). Firstly, skarn is developed within a thin carbonaceous marble horizon in an intercalated pelite/calc-silicate granofels/marble sequence. Secondly, a series of skarn facies with a vesuvianite periphery is developed. These facies represent progressive replacement of the marble. Mineral chemistry studies indicate that certain of the skarn facies minerals crystallised from a fluid of fluctuating composition. Hence evidence of chemical disequilibrium in the skarn system is widespread. Thirdly, the silicate minerals in the later skarn facies show a tendency towards Fe and Mn enrichment. Fourthly, the garnet facies hosts the majority of scheelite mineralisation. Finally, the alteration of the enclosing country rock is minimal.

The major differences between the Otjua skarn and those tungsten skarns documented by Einaudi *et al.* (1981) are as follows: the granite deemed to be responsible for the mineralisation (and indeed all the intrusions in the Schönfeld Dome) is highly fractionated (in Damaran terms), exhibiting S-type characteristics and is relatively anhydrous; there is an absence of Mo in the scheelite in the skarn and in the associated intrusions; the skarn system is relatively Fe-poor and lacks significant sulphide mineralisation; the absence of a retrogressive/hydrated skarn facies containing biotite or hornblende makes the deposit unusual; in contrast to many other replacement skarns, there is evidence for a strong structural control on the localisation of skarn deposits in the Schönfeld Dome.

The similarities between the Otjua skarn and other tungsten skarns suggest that skarn development occurred in a similar manner to other replacement skarns. Skarn formation processes associated with Cretaceous intrusions in the

Circum-Pacific were already in operation in the early Phanerozoic. Not only is the Otjua skarn one of the oldest examples, it is also one of the few tungsten skarns to have been formed synorogenically while the country rocks were undergoing amphibolite facies metamorphism. The important differences between the Otjua skarn and other Phanerozoic tungsten skarns are thought to be the result of the different source areas of the tungsten and the intrusions. If the Otjua leucogranite is an anatectic melt derived from tungsten-bearing Damaran metasediments or alternatively the Otjua granite merely acted as a heat source and scavenged tungsten from the scheelite-bearing granofels, then the low sulphide and Mo contents of the skarn are a reflection of the geochemistry of lower Swakop sediments and the overall ensialic nature of the Damara Orogen. In this regard it is of note that the Otjua skarn has more similarities to the continental, postorogenic or anorogenic tin-tungsten skarns (Einaudi and Burt, 1982) in spite of its lack of tin.

## 7.4 GOLD SKARN MINERALISATION IN THE KARIBIB FORMATION IN THE KARIBIB DISTRICT

### 7.4.1 Introduction

Mineral exploration in the Karibib area in the mid to late 1980s resulted in the discovery of epigenetic carbonate-hosted auriferous quartz veins and associated alteration of presumed hydrothermal origin. At the Navachab Gold Mine the veins are sufficiently well mineralised and closely spaced that they can be commercially exploited by bulk mining methods (Navachab Gold Mine Field Guide, 1989). Gold mineralisation is essentially confined to the Okawayo and Karibib Formation marbles in the core of the east-north-east-trending Navachab-Okawayo and Onguati-Otjimbojo anticlines (Fig. 7.1; Pirajno *et al.*, 1991). Because the majority of veins are hosted by calcitic and dolomitic marble, this style of mineralisation has been referred to as an example of a distal gold skarn. Strictly speaking the term skarn refers to the silicate gangue of ore deposits that have replaced carbonate sediments (Bates and Jackson, 1987). In recent years economic geologists have, perhaps regrettably, extended the term “skarn deposits” to include examples that “result from the interaction of hot silicate magmas and cooler sedimentary rocks” (Meinert, 1987). In this section the term skarn is confined to those rocks produced by the metasomatic replacement of a carbonate unit, unless specifically stated. At many of the gold occurrences in the Karibib area there is an absence of silicate gangue and the mineralisation can equally well be described as mineralised hydrothermal veins, usually with a quartz gangue. In most examples the base metal sulphide component is small and the geochemical association is Au-Bi-As-Te. At all the prospects discovered so far, mineralisation is hosted by exoskarn (replaced carbonate rock). No endoskarn (replaced intrusion) has yet been identified. The gold mineralisation is not spatially associated with a particular type of igneous rock. At the Navachab Gold Mine there is a small outcrop of a two-mica granite within the mine area, while north of Karibib, lithium

pegmatites are the only intrusions to crop out within several kilometres of the gold mineralisation. Immediately south of Karibib a number of dioritic plutons, andesitic plugs, granites and lithium pegmatites are spatially associated with the gold mineralisation. In this section, two examples of gold skarn mineralisation considered to be representative of the Karibib area are discussed. Emphasis has been placed on presenting new data. A sulphide-bearing system with minor silicate alteration from the Onguati Copper Mine and a sulphide-poor system with extensive silicate alteration from the Habis Gold Prospect (Fig. 7.1) will be examined. Petrographic studies, reflected-light microscopy and geochemical data have been used to classify this poorly known style of mineralisation.

#### 7.4.2 Onguati Copper Mine

##### 7.4.2.1 General geology

A general description of the marble-hosted sulphide and gold mineralisation at the Onguati Copper Mine has been given by Pirajno *et al.* (1990a, 1991) and the salient geological features of the occurrence are listed in Table 7/4.1. Massive chalcopyrite ore was last mined at Onguati during the 1970s. The sulphide skarn ore is developed in a swarm of quartz veins hosted by Karibib Formation marbles in the

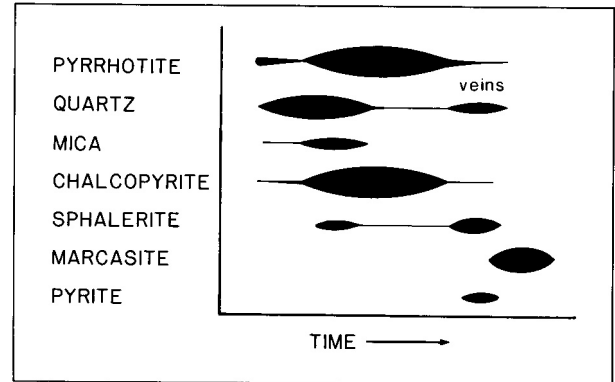


**Figure 7/4.1:** Paragenetic summary of semi-massive chalcopyrite-pyrrhotite ore from the Onguati Copper Mine

core of the Onguati-Otjimbojo anticline (Fig. 7.1). There is a strong structural control on the orientation of the mineralised veins which have a north-northeast/northeast orientation and a shallow ( $-35^\circ$ ) eastward or southeastward dip. This is not a stockwork of randomly oriented veins. There is a close genetic relationship between southeastwardly dipping gold veins and similarly oriented late-tectonic thrust faults. The auriferous veins are almost entirely hosted by intensely deformed calcitic marble. In contrast, spatially associated dolomitic carbonates and metavolcanic and pyroclastic rocks of

<b>Regional Geological Setting</b>	<b>Monoclinial downfold of Damara Sequence (over ENE-trending basement fault?) on the northern margin of the SCZ. Mineralisation hosted by marbles in the ENE-trending Onguati-Otjimbojo anticline</b>
<b>Host Formation</b>	<b>Karibib</b>
<b>Host Lithology</b>	<b>Calcitic marble</b>
<b>Form of Mineralisation</b>	<b>Shear zones, quartz veins, skarn veinlets</b>
<b>Associated Volcanics</b>	<b>Continental, alkaline volcanics of the Daheim Formation</b>
<b>Structural Features</b>	<b>Swarm of shallow SE-dipping quartz veins parallel to late-tectonic thrust faults</b>
<b>Peak Metamorphic Facies</b>	<b>Amphibolite</b>
<b>Intrusions within 1 km</b>	<b>Late-/post-tectonic lepidolite pegmatites</b>
<b>Age of Mineralisation</b>	<b>Late Damara</b>
<b>Highest Fire Assay (g/t)</b>	<b>&gt;50.0</b>
<b>Geochemical Association</b>	<b>Au-Cu-As-W-Bi-Te-Sn-Se(-Sb)</b>
<b>Ore Minerals</b>	<b>Chalcopyrite, pyrrhotite, sphalerite, bismuth, hessite, pyrite</b>
<b>Gangue Minerals</b>	<b>Quartz, malachite (vesuvianite, Frommurze <i>et al.</i>, 1942)</b>
<b>Classification</b>	<b>Distal gold skarn</b>
<b>Comments</b>	<b>Auriferous megashear zones in the underlying basement are considered to be a significant reservoir of gold</b>

**Table 7/4.1:** Carbonate-hosted gold mineralisation at the Onguati Copper Mine

	NMSL1296	NMSL1295
F	<173	<128
Rb	4	<1.8
Sr	26	29
Th	<5.6	<4.3
U	<6.6	<4.9
Zr	<4.4	3
Nb	<4.3	<3.2
Mo	<4.5	<3.4
Sn	28	5
W	726	93
Ni	<6.2	<3.2
Cu	17230	269
Zn	2389	20
Ga	<2.5	3
Pb	9	23
Ge	<2.3	<1.5
As	800	1104
Sb	<2.6	4
Bi	<6.9	47
Se	370	<1.4
Te	<4.2	<3.1
Y	12	<3.4
Au	.2	.4

**Table 7/4.2:** Partial analyses of auriferous gossans from the Onguati Copper Mine and the Habis Gold Prospect, Karibib District

N.B. All values, including gold, in ppm

NMSL1296: Onguati Copper Mine gossan

NMSL1295: Habis Gold Prospect gossan, HKB4 borehole site

the Daheim Formation have not been as intensely deformed because of their stronger mechanical properties (Heard, 1976). The north-northeast/northeast orientation and shallow southeastward dip of the thrust faults and gold veins suggest that late-tectonic west-north-west-directed compression about the north-northeast-trending Abbabis lineament zone (ALZ) played an important role in the localisation of auriferous fluids. The first detailed petrographic description of the ore is given below. A silver telluride is described for the first time from central Namibia. No silicate minerals other than quartz were observed in hand specimen on the margins of ore veins at Onguati, though Frommurge *et al.* (1942) mention the presence of vesuvianite.

#### 7.4.2.2 Petrographic description of chalcopyrite-pyrrhotite skarn

A piece of strongly magnetic, semi-massive chalcopyrite-pyrrhotite ore (NSP18) from the margin of one of the veins at the Onguati Copper Mine was examined microscopically. A partial analysis of gossan from the main ore zone is given for comparison in Table 7/4.2. Approximately half of the skarn is comprised of opaque minerals. Chalco-pyrite (30%), pyrrhotite (10%) and marcasite-pyrite intergrowths (10%) after pyrrhotite are the major sulphides. The chalcopyrite contains dendritic intergrowths of an exsolved mineral, inclusions of elongate sphalerite (usually less than 200  $\mu\text{m}$  in length) and

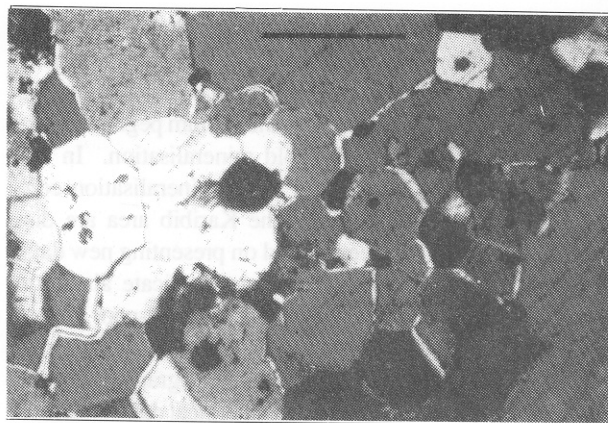


**Plate 7/4.1:** Granoblastic quartz in chalcopyrite-pyrrhotite (opaque phases) skarn from Onguati Copper Mine (NSP18; XL); scale bar = 0.5 mm

small (less than 350  $\mu\text{m}$ ) aggregates of sphalerite, pyrrhotite, bismuth and silver tellurides. The non-opaque minerals comprise quartz (10-25%), carbonate (20-40%), biotite (0-3%), chlorite (0-3%), a colourless mica which may be muscovite, and a minor amount of an unidentified, olive-brown pleochroic mineral (possibly serpentine) upon which it was not possible to obtain an optic figure. Some of the biotites are up to 600  $\mu\text{m}$  long and should be suitable for radiometric age determinations.

A paragenetic summary of the Onguati ore is given in Fig. 7/4.1 (the bismuth and silver tellurides are discussed in detail in section 7.4.2.3). Minor amounts of pyrrhotite (<5% vol.%) are present as inclusions within the quartz. Small pyrrhotite crystals are developed at triple junctions between quartz grains, but the majority of the sulphides are usually interstitial to and envelop the aggregates of silicates. The chalcopyrite and pyrrhotite are present as an anhedral, interlocking, interstitial mass and appear to have crystallised together. Biotite, altering to chlorite, and very minor muscovite are developed on the edge of the sulphide network, but not exclusively with pyrrhotite. The concentration of some of the sphalerite and pyrite in elongate stringers suggests their crystallisation late in the paragenetic sequence. The pyrrhotite is extensively altered ("bird's eye" texture) to pyrite and marcasite and the sulphides have locally been cut by quartz veins.

The major textural feature of the quartz is its annealed nature which has resulted in the widespread development of triple junctions (Plate 7/4.1). This texture is an indication of a high-temperature of formation for the early skarn minerals (i.e. > 400°C) or alternatively that the ore has been metamorphosed. The latter interpretation is considered unlikely because the sulphides do not exhibit a similar texture. Geochemical studies show that the Karibib Formation marble at Onguati contains less than 1.5 wt%  $\text{SiO}_2$  (Table 2.19), but it is possible that the quartz was concentrated in veins (which were subsequently replaced by sulphides) during metamorphism and hence has a metamorphic texture. However, it is considered more likely that the granoblastic texture formed as the result of slow cooling of the ore and that the quartz is an integral part of a high-temperature ore assemblage.

### 7.4.2.3 Exsolution features and inclusions in the chalcopyrite-pyrrhotite skarn

Examination of a polished section (NSP21) of massive chalcopyrite ore (Table 7/4.3) in reflected light revealed the presence of a number of exsolved phases and inclusions which comprise less than two volume per cent of the ore. The exsolution lamellae are of a Co-rich pyrrhotite (Table 7/4.4), which has a dendroid or locally herringbone morphology. Some examples are strongly pleochroic (cream to blue-grey) and have the morphological appearance of stibnite. Similar pyrrhotite lamellae, considered to be decomposition products after cubanite, have been described in high-temperature chalcopyrite by Ramdohr (1969, p.530, Fig. 253). More than half of the inclusions are somewhat elongate, rounded crystals of sphalerite (Table 7/4.3), usually less than 200  $\mu\text{m}$  in diameter, though some may be up to 500  $\mu\text{m}$  long. They almost universally contain blebs of chalcopyrite. Sphalerite is locally concentrated in stringers that lend a vein-like appearance to their distribution (Plate 7/4.2).

The second major type of inclusion is aggregates of sphalerite, Co-poor pyrrhotite, silver tellurides and native bismuth. These inclusions are of particular interest because the gold skarns of the Karibib area are characterised by a strong correlation between bismuth and gold. At the Navachab Gold Mine, one of the main ore minerals is maldonite,  $\text{Au}_2\text{Bi}$  (Navachab Mine Field guide, 1989). At Onguati the aggregates range in size from 100-400  $\mu\text{m}$ . Rounded and somewhat elongate sphalerite and pyrrhotite enclose anhedral hessite which itself envelops anhedral bismuth (Plates 7/4.3 and 4).

	Chalcopyrite		Sphalerite	
S (wt%)	34.30	34.44	33.95	34.27
Fe	30.36	30.41	11.32	10.13
As	.01	ND	ND	ND
Cu	34.78	34.33	2.52	.62
Zn	ND	ND	51.65	54.31
Sb	ND	ND	ND	ND
Sn	.07	.07	ND	ND
Pb	ND	ND	ND	ND
Bi	ND	ND	.01	ND
TOTAL	99.52	99.25	99.45	99.33

**Table 7/4.3:** Representative analyses of chalcopyrite and sphalerite from the Onguati Copper Mine

In plane-polarised light the dark-grey sphalerite with "chalcopyrite disease", the pinkish-brown pyrrhotite and the creamy-white, anhedral bismuth are relatively easy to identify. The bismuth grains rarely exceed 100  $\mu\text{m}$  in length. The pyrrhotite inclusions, in contrast to the exsolution lamellae in the chalcopyrite, are Co-poor (Table 7/4.4). The hessite, which contains up to 1.7 wt% Se and minor Sb (Table 7/4.5), is grey with a bluish tint (Plate 7/4.3). Locally, hessite is intergrown with a lighter phase (Plate 7/4.3, centre right). These lamellae are too small (less than 1  $\mu\text{m}$  thick) to resolve with the electron beam. A microprobe analysis of the central area revealed the presence of

	Pyrrhotite lamellae in chalcopyrite								A
S (wt%)	34.97	34.62	36.09	35.82	35.68	35.69	35.26	38.55	
Fe	55.67	56.45	56.65	54.68	57.03	52.56	51.76	60.31	
As	.04	.04	.02	ND	.05	ND	.03	.07	
Cu	3.42	1.02	.73	1.13	1.87	.80	.57	.03	
Zn	ND	.08	ND	ND	ND	ND	.04	.22	
Ni	ND	ND	ND	ND	ND	ND	ND	.03	
Co	4.78	5.83	5.92	7.40	3.92	9.14	10.41	ND	
Sb	ND	ND	ND	ND	ND	.01	ND	.01	
Sn	.12	.11	.08	.08	.08	.12	.08	ND	
Pb	ND	ND	ND	ND	ND	ND	ND	ND	
Bi	ND	ND	ND	ND	ND	ND	ND	ND	
Mn	ND	ND	ND	ND	.01	.01	ND	ND	
TOTAL	99.00	98.15	99.49	99.11	98.64	98.33	98.15	99.22	

**Table 7/4.4:** Representative analyses of pyrrhotite from the Onguati Copper Mine. A: Co-poor pyrrhotite inclusion

a 'mineral' with a composition similar to hessite with Bi contents of up to 6.8% and Se contents of up to 6.6% (Table 7/4.5, analysis 5). On the edge of one bismuth grain, a very pale-blue phase was analysed with the electron microprobe. The geochemical analysis reveals the presence of a bismuth selenide whose composition approximates to  $\text{Bi}_4\text{Se}$  (Table 7/4.6). On the contact between chalcopyrite and hessite, a cobalt antimony sulphide with minor arsenic contents was noted (Plate 7/4.4). The mineral is a member of the ullmanite family (Table 7/4.6), either costibite or paracostibite (L. Cabri, 1990, pers. comm.). Some of the native bismuth contains traces of gold (Table 7/4.6), but no gold phase was identified. The enclosure of anhedral silver, tellurium and bismuth minerals within sphalerite and pyrrhotite suggest the late crystallisation of the former.

	1	2	3	4	5	6
S (wt%)	.03	.24	.02	.07	.07	.03
Fe	.17	.44	.09	.54	.10	.15
As	ND	ND	ND	ND	ND	ND
Cu	.19	.35	.05	.16	.10	.18
Zn	.48	1.14	.29	.06	.19	.14
Sb	.17	.26	.25	.24	.17	.19
Sn	ND	ND	ND	ND	ND	ND
Bi	.07	.22	.07	ND	6.83	.17
Pb	ND	ND	.03	.02	.02	ND
Au	ND	.03	.02	ND	ND	.01
Ag	60.19	60.35	58.57	58.91	56.22	59.11
Te	35.16	34.52	38.02	37.86	30.06	36.52
Se	1.65	1.70	.97	.83	6.63	1.68
TOTAL	98.11	99.25	98.38	98.69	100.39	98.18

**Table 7/4.5:** Representative analyses of hessite from the Onguati Copper Mine

The third group of inclusions is pyrite, which locally contains minor arsenic (Table 7/4.7). A few anhedral grains are evenly distributed throughout the massive chalcopyrite, but are seldom larger than 75  $\mu\text{m}$ . Some of the pyrite is present in veins that appear to postdate the sphalerite stringers (Plate 7/4.2). The majority of subhedral-euhedral pyrite is, however, concentrated near or in crosscutting veinlets. Locally, subhedral pyrites are crosscut (rather than replaced) by goethite veins. Pyrite crystals may be up to 0.4 mm in diameter and, where incipiently altered, appear a creamy-white colour in plane-polarised light. Twinning is locally

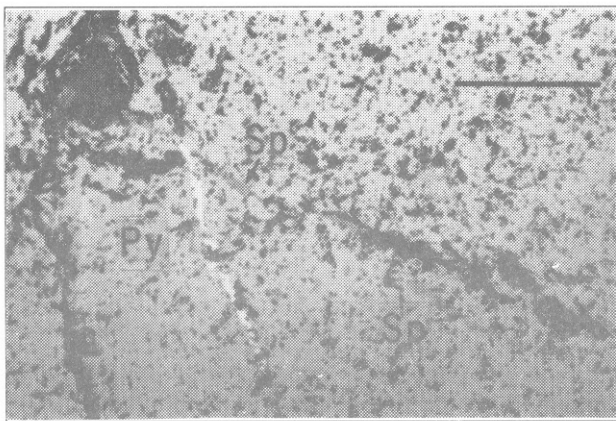


Plate 7/4.2: Sphalerite (Sp) stringers and pyrite (Py) vein in massive chalcopyrite ore from Onguati Copper Mine (NSP21; RL); scale bar = 0.5 mm

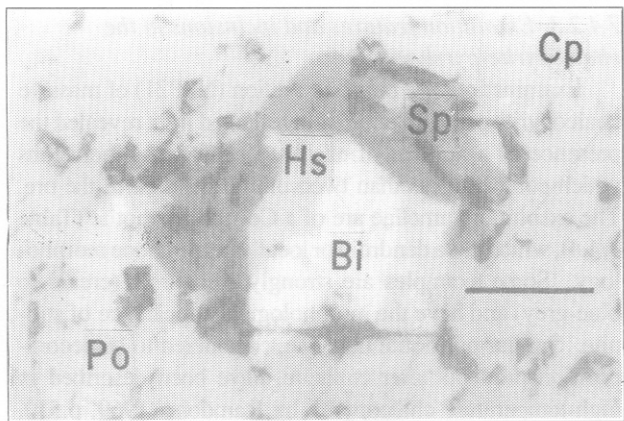


Plate 7/4.3: Bismuth (Bi), hessite (Hs), sphalerite (Sp) and pyrrhotite (Po) aggregates in massive chalcopyrite (Cp) ore from Onguati Copper Mine (NSP21; RL); scale bar = 50 µm

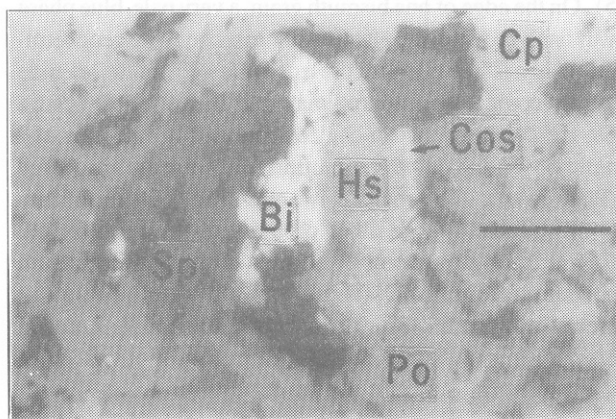


Plate 7/4.4: Bismuth (Bi), hessite (Hs), sphalerite (Sp), costibite (Cos) and pyrrhotite (Po) aggregates in massive chalcopyrite (Cp) ore from Onguati Copper Mine (NSP21; RL); scale bar = 50 µm

S (wt%)	52.65	52.46	52.36	52.68
Fe	46.49	46.59	46.61	46.72
As	ND	.04	.04	.03
Cu	.17	.15	.09	.84
Zn	.04	.03	ND	ND
Ni	.01	ND	.02	.06
Co	ND	ND	ND	ND
Sb	ND	ND	.02	ND
Sn	.05	.07	.04	.13
Pb	ND	ND	ND	ND
Bi	ND	ND	ND	ND
Mn	ND	ND	.01	.01
TOTAL	99.41	99.34	99.19	ND.47

Table 7/4.7: Representative analyses of pyrite from the Onguati Copper Mine

	Bi-selenide	Costibite	Native bismuth	
S (wt%)	.20	14.30	.02	.06
Fe	1.53	.49	.26	.52
As	ND	2.00	ND	ND
Cu	.44	.36	.42	.54
Zn	.86	ND	.47	.42
Sb	ND	55.34	ND	ND
Sn	ND	ND	ND	.05
Bi	86.47	ND	98.10	96.93
Pb	.47	ND	ND	ND
Au	.04	ND	.09	ND
Ag	ND	ND	.01	.46
Te	.27	ND	ND	.37
Se	9.39	ND	.04	.42
Co	.01	26.70	ND	ND
Ni	.01	.11	ND	ND
TOTAL	99.69	99.87	99.41	99.77

Table 7/4.6: Representative analyses of Bi-selenide, costibite and bismuth from Onguati Copper Mine

present. A pale-blue pleochroic mineral, too small to analyse with the electron microprobe, is probably covellite.

7.4.2.4 Summary of Onguati Copper Mine sulphide skarn assemblage

It is considered highly unlikely that the complex intergrowths of the silver tellurides would have survived metamorphism and deformation. They represent a primary exsolution feature that postdates the Damaran tectonism. It is possible that the sulphides were emplaced at an earlier stage in the orogeny and that only the ex solution is late-/post-tectonic in age. This is considered unlikely because of the confinement of mineralisation to late-stage, cross-cutting fractures. Moreover, geochemical analyses reveal that concentrations of Bi, Te and Se of unaltered Karibib Formation marble are below the LLD (Table 2.19). The skarn mineralisation is thus clearly epigenetic. Several textural features indicate a high-temperature of formation for the early minerals of this skarn (i.e. > 400°C). The quartz,

<b>Regional Geological Setting</b>	<b>Dolomitic marbles overlying Abbabis basement inlier</b>
<b>Host Formation</b>	<b>Karibib</b>
<b>Host Lithology</b>	<b>Dolomitic marble</b>
<b>Form of Mineralisation</b>	<b>Quartz-tremolite veins with sulphide mineralisation</b>
<b>Associated Volcanics</b>	<b>Minor amphibolite may be tuffaceous equivalent of Daheim Formation</b>
<b>Structural Features</b>	<b>Mineralisation in core of domal structure</b>
<b>Peak Metamorphic Facies</b>	<b>Amphibolite</b>
<b>Intrusions within 1 km</b>	<b>Red gneissic granite, minor andesite plug, lepidolite pegmatites</b>
<b>Age of Mineralisation</b>	<b>Late Damara</b>
<b>Highest Fire Assay (g/t)</b>	<b>0.4</b>
<b>Geochemical Association</b>	<b>Au-As-W-Bi-Cu</b>
<b>Ore Minerals</b>	<b>None identified in oxidised material</b>
<b>Associated Alteration</b>	<b>Massive tremolite, quartz-tremolite veins, gossan (after sulphides)</b>
<b>Classification</b>	<b>Gold skarn</b>
<b>Comments</b>	<b>The very close proximity of auriferous basement rocks is considered to be highly significant</b>

**Table 7/4.8:** Carbonate-hosted gold mineralisation at the Habis Gold Prospect

which crystallised early in the paragenetic sequence, has a classic polygonal texture. After crystallisation of the higher temperature sulphides such as chalcopyrite, the Co-rich pyrrhotite (which may be a replacement after cubanite) was ex solved. Concentrations of elements that were incompatible in the crystallising chalcopyrite clustered together to form aggregates of sphalerite, Co-poor pyrrhotite, bismuth and silver-tellurium minerals. Sphalerite and pyrrhotite crystallised first because they envelop the other minerals. Upon further cooling Se-bearing hessite crystallised. Hessite subsequently ex solved bismuth and selenium which resulted in the local formation of a myrmekitic intergrowth. Bismuth appears to have been the last mineral to crystallise and seems to have been involved in subsolidus reactions with selenium. The concentration of pyrite euhedra near fractures indicates a very late position in the paragenetic sequence for this mineral. Minor late-stage alteration of the ore assemblage included the development of "bird's eye" texture in the pyrrhotite and oxidation of the chalcopyrite and pyrite to goethite near fractures. In summary, early quartz was succeeded by the high-temperature sulphides chalcopyrite, pyrrhotite and sphalerite, the lower-temperature tellurides and lastly native bismuth. The late crystallisation of tellurides, and to a lesser extent bismuth, is a characteristic of skarn-type and gold quartz vein deposits (Boyle, 1979).

#### 7.4.3 Habis Gold Prospect silicate skarn

The Habis Gold Prospect is located at the northeast end of the Abbabis Inlier (Fig. 7.1) and the geology of the prospect is summarised in Table 7/4.8. Zones of massive tremolite alteration intimately associated with auriferous gossan are hosted by grey dolomitic marble (upper marble) on a low hill approximately 500 metres north-northeast of the Habis farmhouse. No sulphide mineralisation is exposed on surface. Partial analyses of the auriferous gossan from the vicinity of the Randex HKB4 borehole collar are given in Table 7/4.2. Although the Habis gossan is depleted in metals relative to the Onguati gossan, they have similar geochemical profiles, having anomalously high concentrations of As, W, Cu and Zn. The tremolite zones, which may be many metres thick, tend to be concentrated in layers parallel to the bedding of the marble, but are locally crosscutting. Sheaves of light-grey tremolite form rosettes which lend a distinctive appearance to the alteration zone. In thin section the tremolite rocks comprise radiating aggregates of colourless clin amphibole (80-90%), scapolite (0-20%), carbonate (0-5%), diopside (0-3%) and minor sphene and opaques. More massive, prismatic amphiboles, many centimetres in length, have a pale green colour which attests to their more actinolitic nature (confirmed by XRD).

A clear distinction can be made between tremolite associated with auriferous alteration zones and tremolite which

grew as a result of prograde regional metamorphism in the dolomitic marble. Minor poikiloblastic tremolite is a common phase in the lower and upper marbles of the Karibib Formation on the farm Habis (as it is elsewhere in the dolomitic portions of the Karibib Formation), but the amphibole does not comprise more than five per cent of the rock (Table 2.16). In contrast the zones of massive tremolite grew as the result of the large-scale metasomatic decarbonation of the dolomitic marble. There is a close association between tremolite alteration and epigenetic gold mineralisation throughout the Karibib district (Badenhorst, 1989, pers. comm.).

#### 7.4.4 Summary of the gold skarns of the Karibib area

Gold skarn mineralisation in central Namibia is essentially confined to the SCZ and the majority of occurrences are located to the east of the Abbabis lineament zone (Fig. 7.1) in an area that has undergone lower amphibolite facies metamorphism. The mineralisation is subtle, usually comprising a poorly developed stockwork or swarm of carbonate-hosted veins of hydrothermal origin or zones of quartz-tremolite alteration. Gold mineralisation is hosted by both dolomitic and calcitic marble and, to a lesser extent, calc-silicate lithologies. Other than tremolite which was produced by the large-scale decarbonation of dolomitic marble, none of the skarns has a major development of silicate minerals. Garnet-pyroxene skarn assemblages on the margins of quartz veins have been described from the Navachab Gold Mine, but are seldom more than several centimetres in width (Navachab Gold Mine Field Guide, 1989). At the Onguati Copper Mine and the Habis Gold Prospect, the mineralisation lacks a tectonic fabric and clearly crosscuts unmineralised metasediments. In the Onguati-Otjimbojo anticline there is a close relationship between mineralisation and late-tectonic brittle deformation structures such as thrust faults. Textural evidence indicates high-temperatures of formation for the early minerals such as quartz. With the exception of the Onguati Copper Mine, the base metal sulphide component of the gold skarns is negligible; pyrrhotite predominates over pyrite in all known skarns. The field and petrographic evidence from the two prospects examined clearly indicate that the mineralisation is epigenetic and of late Damaran age. The style of mineralisation and the geochemical association (Au-Bi-As-Te) bear certain similarities to the gold skarns of the western United States (Meinert, 1987), where skarn development is attributed to the interaction between magmatic fluids and sediments. Low-temperature (< 250°C) bismuth and telluride minerals are especially characteristic of gold skarns and are usually absent from the more proximal base metal- or sulphide-rich systems where silicate gangue is abundant. The term distal skarn for the gold mineralisation of the CZ is thus particularly appropriate.

#### 7.4.5 Origin of the gold mineralisation

Because of the recent discovery of gold skarns in central Namibia and the lack of published data, comments on their

origin are of necessity speculative. However, various relevant features and some models are discussed below.

##### 7.4.5.1 Previous work on the gold skarns of the Karibib area

Little has been published on the genesis of the “hydrothermal copper-gold” (Miller, 1983b) and gold skarn mineralisation in the Karibib area. Some comments on the only model proposed so far (Pirajno *et al.*, 1990a, 1991) are required. These authors proposed a general three-stage model involving deposition of gold and sulphide-bearing alkaline basaltic lavas in Daheim times, followed by the generation of metamorphic fluids during the Damaran orogeny. These fluids are envisaged to have leached ore metals from the volcanic rocks and caused dolomitisation of the overlying marble units. Finally, granites generated large-scale convective cells resulting in the formation of mineralised quartz vein systems. The author agrees with Pirajno *et al.* (1990a, 1991) that the mafic volcanic rocks of the Daheim Formation could be a major source of gold and base metals, but suggests that there are a number of problems with their model. Firstly, Pirajno (1990, pers. comm.) believes that the mafic volcanic rocks were erupted along an east-northeast-trending fissure vent. Scoria, spatter cone material, trifurcate structures, base surge deposits and pillow lavas can be seen in the pristine Daheim Member. Although the magma undoubtedly came from the mantle, it was intruded along major fractures presumably similar to the ones exposed on Abbabis and Narubis (Fig. 2.1). When were these structures mineralised? The evidence from the basement inliers of central Namibia points to a pre-Damaran gold mineralising event. Thus the precious metal mineralisation in the mafic volcanic rocks could result from “crustal contamination”. The importance of the auriferous basement is discussed in the next section. Secondly, the distribution and nature of the metavolcanic rocks of the Daheim Formation are not well known: no geochemical data have been published. Nowhere in the Karibib area do the mafic volcanic rocks of the Daheim Member comprise more than 25% of the Karibib Formation; in large areas volcanic rocks are absent. It is doubtful whether they could have provided all the gold present in the skarn and quartz veins of the Karibib district. Thirdly, there is no evidence for substantial deformation, shearing, chloritisation or devolatilisation of the Daheim Member volcanic rocks at the present erosion level. At the Onguati Copper Mine, dolomite, which encloses the metavolcanic rocks and pyroclastics, has largely protected the Daheim Formation from intense deformation because of its strong mechanical properties (Heard, 1976). Large-scale leaching of ore metals from metavolcanic rocks would surely have resulted in some visible modification. Fourthly, Pirajno *et al.* (1990a) have not made a good case for the “extensive dolomitisation” (op. cit., p.444) or the “regional-scale selective hydrothermal alteration” (Pirajno and Jacob, 1991) of the carbonate units by metamorphic fluids that leached Mg out of mafic volcanic rocks. In the Karibib area near the Abbabis Inlier, the Karibib Formation is dolomitic in nature (Smith, 1965; Chapter 2). Dolomites are certainly not restricted to areas of gold skarn minerali-

sation. This entire stratigraphic unit cannot have been dolomitised on a regional basis by metamorphic fluids from a volumetrically small pile of mafic volcanic rocks which are pristine in nature: a simple mass balance calculation reveals there was insufficient Mg present in the volcanic rocks for the process to have occurred, even allowing for massive alteration. No geochemical data for the Daheim Member is available, but basanites from the East African Rift (the most mafic members of a suite from a comparable tectonic setting) contain 10.5 wt% MgO (Wilson, 1989). Dolomite marble at the Habis Gold Prospect, where the carbonate: volcanic rock ratio exceeds 5: 1, contains approximately 21 wt% MgO. There is evidence for *late* Damaran dolomitisation of Karibib Formation carbonate rocks in the vicinity of the Onguati Copper Mine and at the Navachab Gold Mine (Jacob, 1992, pers. comm.) but, in this author's opinion, the fluid responsible for this was not necessarily derived from the metavolcanic rocks.

#### 7.4.5.2 Gold in the underlying basement

None of the models presented so far for the origin of the gold skarn mineralisation in the Karibib area (Pirajno *et al.*, 1990a, 1991) has taken cognisance of the large amount of gold in the underlying Abbabis Inlier. This is of particular relevance because the Karibib area is one of the few places in the CZ where carbonate lithologies locally lie unconformably on basement lithologies. The first record of gold in Abbabis Complex lithologies was given by Smith (1965), who mentioned auriferous quartz veins in "Abbabis gneiss". During the course of this study anomalous gold contents (> 300 ppb Au) were recorded within shear zones (Fig. 2.1), chlorite-magnetite rocks and cupriferous quartz veins in the Abbabis Complex. Gold mineralisation is concentrated in east-northeast-trending megashears which themselves are cut by undeformed, presumably late-Damaran pegmatites. Arguments were presented in section 4.2.4 to support the idea that final strike-slip movement on these structures occurred in pre-Damaran times. Were these structures mineralised in pre-Damaran or Damaran times or both? The evidence from the other basement inliers in Namibia (Fig. 2.2) points to a pre-Damaran gold-mineralising event (see discussion in chapter 4). Some auriferous copper veins containing up to 1 g/t Au crosscut undeformed pegmatite sills. The best example of the latter crops out 100 metres north of the Navachab/Narubis/Abbabis corner beacon (Fig. 2.1). These auriferous veins are very late Damaran at the oldest. A calculation of the amount of gold contained in one of the megashears is enlightening. The main shear zone on the farms Abbabis and Narubis is in excess of 6 km long, at least 10 metres wide, probably has a specific gravity of 2.8 and is estimated to extend at least one kilometre into the earth's crust. This segment of the shear zone contains 168 x 10<sup>6</sup> metric tons of rock. If the average *in situ* gold content of the shear zone is 150 ppb gold (and sampling has revealed up to 2 g/t Au), then this segment of a single megashear alone contains 810 x 10<sup>3</sup> ounces of gold. This is only slightly less than the published ore reserve of the Navachab Gold Mine (62 500 ounces of gold to be produced for fifteen years giving a combined total of 938 x 10<sup>3</sup> ounces of gold). These megashear zones in the Abbabis Inlier there-

fore represent a significant reservoir of gold. The age of the Abbabis Inlier is particularly intriguing. The U-Pb age determination on zircons from granite-gneiss of the Narubis Granitoid Complex of the Abbabis Inlier yielded a concordia age of 1925-280 +330 Ma (Jacob *et al.*, 1978). This is a minimum age for one of the youngest lithologies in the inlier. The metasedimentary and metavolcanic rocks (many of which are mafic and hence could represent a substantial gold reservoir) may be considerably older.

#### 7.4.5.3 A possible relationship between felsic intrusions and gold mineralisation

At the majority of the marble-hosted gold occurrences in the Karibib area, there is no igneous intrusion in the immediate vicinity to which the mineralisation can be attributed. Thus a genetic relationship between the gold mineralisation and felsic intrusions can only be inferred. However, the gold-bismuth association of the gold skarns is considered to be particularly important because bismuth is commonly present in pegmatitic and granitic melts (Wedepohl, 1978). There is a worldwide association between felsic intrusions and Au-Bi-Te-S mineralisation (Meinert, 1989; Pulz *et al.*, 1991). The most likely sources for the mineralising fluids are hidden, late-/post-tectonic felsic intrusions or, alternatively, magmatically modified metamorphic fluids derived from the Abbabis Inlier. In the vicinity of the Habis Prospect there are diorites, granites and lithium pegmatites, while further away from the Abbabis Inlier, at Onguati, the only exposed intrusions within ten kilometres of the gold mineralisation are late-/post-tectonic lithium pegmatites. Of all the intrusions in the SCZ, only these pegmatites contain a (very minor) sulphide phase. These lithium pegmatites, which are a type of rare-element pegmatite (Cerny, 1982a), are notably concentrated in the Karibib area (De Kun, 1965) and are restricted to areas where the overlying Damaran rocks have undergone lower amphibolite facies metamorphism. The gold skarns of the SCZ are spatially associated, on a regional basis, with the most extensive development of these intrusions (compare Figs. 3.1 and 7.1). These pegmatites are known to contain a variety of arsenic, antimony, bismuth, and phosphate minerals such as bismuth lead phosphate at the Rubicon Mine (Von Knorring, 1962), triphylite-lithiophyllite in the Ricksburg Farm area (Von Knorring, 1963 p.34) and at Rubicon Mine (Von Knorring, 1985), the copper-iron phosphate, chalcociderite (Von Knorring, 1967, p.36), the bismuth carbonate mineral, kettnerite (Von Knorring, 1971, p.63) and bismutite, minor bismuthinite and a possible bismuthian variety of mimetite at Rubicon Mine (Von Knorring, 1972, p.53). The pegmatites of the Karibib area locally contain masses of loellingite and an iron-arsenic species, karibibite (Von Knorring *et al.*, 1973). Bismuth ochre from the Rubicon Lithium Mine is known to contain anomalous gold concentrations (11.2 g/t Au) and the major ore phase at the Navachab Gold Mine is maldonite (Au<sub>2</sub>Bi). This large variety of bismuth minerals in the Karibib area and a possible gold-bismuth association were discussed sometime ago by Von Knorring (1975).

Lithium pegmatites in pre-Damaran and Damaran rock types are confined to an area underlain by 1.7-2.0 Ga base-

ment. These intrusive rocks are particularly hosted by the Karibib Formation because the damming effect of the carbonate units prevented their intrusion to higher stratigraphic levels. The origin of lithium pegmatites in general is enigmatic, with models invoking anatexis of Li-rich sediments (Stewart, 1978), mixing of Li-enriched fluids from metasediments with pegmatitic melts and direct derivation from a residual volatile-rich granite melt (Cerny, 1982b) having been proposed. On isotopic grounds Haack and Gohn (1988) argued that the lithium pegmatites of the Karibib area could not be derived from basement granitic gneisses nor Etusis Formation quartzites nor could they be differentiates of nearby Salem granites. They proposed that they were formed from the decomposition of biotite-rich metasediments. The only biotite-rich metasediments below the Karibib Formation in the SCZ are in the basement; for example in the Tsawis and Naob Formations (Brandt, 1987a). However, Haack and Gohn's (1988) objections to a magmatic as opposed to a metamorphic origin hinge on the fact that the  $(^{87}\text{Sr}/^{86}\text{Sr})_1$  ratio of the pegmatite is too high. High  $(^{87}\text{Sr}/^{86}\text{Sr})_1$  are a feature of pegmatites which are notorious for extremely high Rb/Sr ratios and  $^{87}\text{Sr}$  mobility (Clark, 1982).

#### 7.4.6 Conclusion

In the mid to late 1980s, a regionally extensive style of epigenetic gold mineralisation was discovered in central Namibia that has similarities with distal gold skarn and auriferous quartz vein deposits of the western United States. A magmatic origin is commonly inferred for this relatively low-temperature Au-Bi-As-Te-S mineralisation. In the

Karibib area the mineralisation cannot be directly attributed to a particular type or age of igneous rock. However, the evidence suggests that the sources for the gold-bismuth mineralisation are hidden, late-/post-tectonic felsic intrusions, specifically lithium pegmatites, and hydrothermal fluids derived from the Abbabis Inlier. There is no evidence for the presence of the well-documented porphyry-related gold association (Bonham, 1989; Sillitoe and Bonham, 1990) in the CZ, either within an intrusion or as a peripheral skarn. The SCZ is floored by granitic basement (the 1.7-2.0 Ga Abbabis Inlier) which possesses significant quantities of gold and can be considered to be a major gold reservoir. There is a close spatial relationship in the CZ between epigenetic gold mineralisation hosted by Damaran rocks and proximity to the Abbabis basement (Martin, 1963). It is considered significant that only in the vicinity of Karibib do carbonate units directly overlie the auriferous basement lithologies. The lithium pegmatites and gold skarn mineralisation are seen as a magmatic-hydrothermal continuum (see London, 1986, for a discussion on the transition between magmatic and hydrothermal regimes). If the pegmatites were not derived from the partial melting of basement, they would at least have interacted with fluids in the basement inlier as they ascended. The numerous east-northeast-trending auriferous megashears and east-northeast-trending metadolerite dykes would have provided ideal pathways for Damaran hydrothermal fluids. In the Damaran cover rocks, gold mineralisation is concentrated in east-northeast-trending  $D_3$  structures such as the Onguati-Otjimbojo and Na-

vachab-Okawayo anticlines. Elsewhere in Namibia, early Proterozoic basement inliers are known to be auriferous. In the Kamanjab Inlier, where there are no Damaran intrusions and surrounding Damaran rocks were subjected to greenschist facies metamorphism, east-northeast-trending megashears that displace the Huab Formation are host to gold mineralisation (Martin, 1963). A pre-Damaran gold mineralising event is indicated for the inliers that floor the intracontinental branch of the orogen.

### 7.5 TURBIDITE-HOSTED GOLD MINERALISATION

#### IN THE KUISEB FORMATION ON SANDAMAP NOORD

##### 7.5.1 Introduction

In early 1987, the author conducted a literature study to identify favourable environments for gold mineralisation in central Namibia. Woodall (1979) noted that the majority of Australian Proterozoic gold deposits was hosted by orogenic sequences, namely successions containing abundant turbidites or where deformation had been intense. The upper Kuiseb Formation represents a highly deformed late Proterozoic flysch succession that comprises thick (4-10 km) accumulations of metagreywackes and graphitic metaturbidites deposited in east-northeast/northeast-trending graben structures (the tin belts of NCZa and NCZe). In

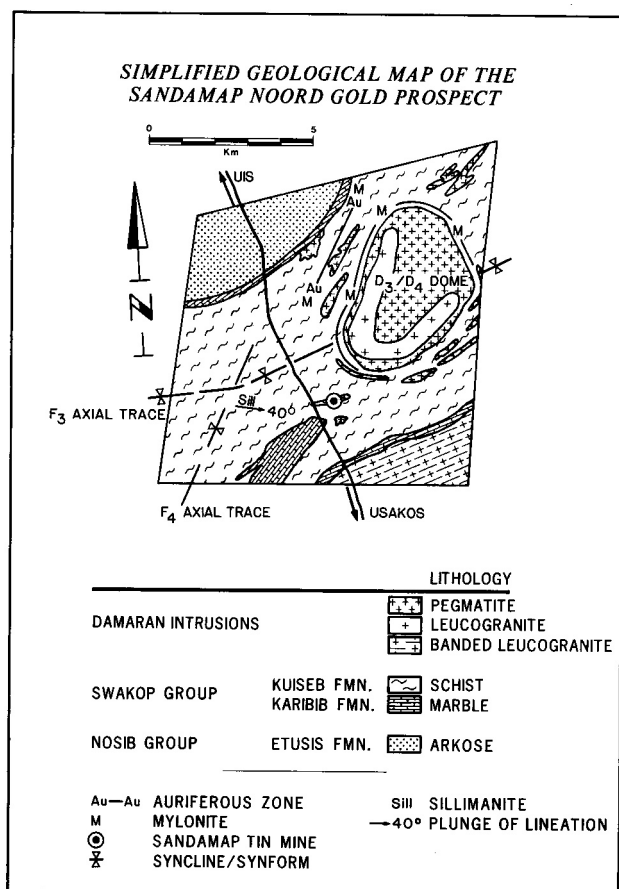


**Figure 7.5.1:** Simplified geological map of the Sandamap Noord Gold Prospect

<b>Regional Geological Setting</b>	<b>Tin belt graben, immediate vicinity of Omaruru Lineament</b>
<b>Host Formation</b>	<b>Kuiseb</b>
<b>Host Lithology</b>	<b>Quartz + biotite + sillimanite + K-feldspar (<math>\pm</math> garnet) schist (metaturbidite)</b>
<b>Form of Mineralisation</b>	<b>NNE-trending ferruginous quartz veins, gossan stringers and mylonite rocks</b>
<b>Associated Volcanics</b>	<b>None identified</b>
<b>Structural Features</b>	<b>Mineralisation on edge of D<sub>3</sub>/D<sub>4</sub> dome; related to Welwitschia lineament zone</b>
<b>Peak Metamorphic Facies</b>	<b>Upper amphibolite</b>
<b>Damaran Intrusions</b>	<b>Late Damaran leucogranites, pegmatites and cassiterite-ferberite pegmatites</b>
<b>Age of Mineralisation</b>	<b>Late Damara</b>
<b>Highest Fire Assay (g/t)</b>	<b>45.8</b>
<b>Geochemical Association</b>	<b>Au-As-W-Pb-F(-Cu-Bi-Ag-Te)</b>
<b>Ore Minerals</b>	<b>Gold, loellingite and arsenopyrite (scorodite), pyrrhotite, pyrite and galena</b>
<b>Gangue Minerals</b>	<b>Tourmaline, graphite, calcite, kaolinite, alunite, jarosite, brookite</b>
<b>Associated Alteration</b>	<b>Massive calcite-graphite-tourmaline rocks, auriferous grunerite rocks</b>
<b>Tentative Classification</b>	<b>Turbidite-hosted gold of magmatic origin</b>
<b>Comments</b>	<b>Concentration of auriferous fluids in high strain zone</b>

**Table 7/5.1:** Turbidite-hosted gold mineralisation on Sandamap Noord

early 1987, it was thought that this stratigraphic unit was prospective for gold mineralisation of eugeosynclinal type (Hutchinson, 1987) and, more specifically, for turbidite-hosted gold mineralisation (Boyle, 1986). Gold mineralisation in turbidite sequences occurs in quartz veins and segregations, being concentrated in dilational structures in particular. These deposits are characterised by a simple mineralogy (pyrite, arseno-pyrite, tourmaline, minor scheelite and carbonate) and minimal wallrock alteration. Attention was focused in the vicinity of recently identified tourmaline alteration and late-tectonic lineament structures such as the Welwitschia lineament zone (Fig. 7.1). In early 1988, a sample of limonite-impregnated ferruginous schist from Sandamap Noord was found to contain 18.6 g/t Au. Further sampling revealed the presence of a 2500-metre-long zone of auriferous, ferruginous and jarositic schist, ferruginous quartz veins, gossan stringers and zones of alteration (Fig. 7/5.1). The style of late Proterozoic/early Palaeozoic gold mineralisation on Sandamap Noord is believed to be previously unknown in southern Africa (Steven, 1991).

### 7.5.2 Geological setting

The Sandamap Noord gold prospect is located in the Sandamap-Davib Ost tin belt, immediately north of the Omaruru Lineament and approximately 10 km east of the north-north-east-trending Welwitschia lineament zone (Fig. 7.1, Table 7/5.1). The latter structure was considered by Corner (1983) to have played an important role in the localisation of late-tectonic uraniumiferous pegmatitic granites such as are developed at the Rössing Uranium Mine.

#### 7.5.2.1 Metasediments and metavolcanic rocks

The farm Sandamap Noord (Fig. 7/5.1) is underlain by Nosib Group meta-arkoses (Etusis Formation) and Swakop Group marine carbonates and metaturbidites (Karibib and Kuiseb Formations). Gold mineralisation is hosted by sheared biotite-sillimanite-K-feldspar schists of the upper Kuiseb Formation. Biotite $\pm$ cordierite $\pm$ andalusite schists without sillimanite are present in the core of the syncline (Map 3) in locations furthest removed from domal structures and granitic intrusions. Rapidly alternating layers of coarse- and fine-grained schists suggest the presence of graded bedding, but no unequivocal sedimentary features can be identi-

fied. However, elsewhere in the NCZ diagnostic features of turbidites such as rip-up clasts, flame structures and scours are preserved in the upper Kuiseb Formation. There is one example of a thin (<2 metres) horizon of green biotite schist in the Kuiseb Formation in the northwest of the farm (Map 3). This is a retrogressively metamorphosed biotite schist, not a metavolcanic rock. There are no mafic lavas nor pyroclastic rocks within the Damara Sequence on Sandamap Noord.

#### 7.5.2.2 Structure and metamorphism

The metasediments have been folded and deformed during four deformational events ( $D_1$ - $D_4$ ). The  $F_1$  and  $F_2$  folds are respectively isoclinal and tight. Peak regional metamorphic conditions (~3.0 kbar, 650°C) were attained syn- $F_2$  at ~520 Ma. The  $D_3$  deformation and concomitant granite intrusion were responsible for the northeast-trending  $F_3$  folds and the northeast-trending oval to elongate domal structures of the area (Fig. 7/5.1). Reclined  $F_4$  folds with north-northeast-trending axial traces and eastward-dipping axial planes are present in the southwestern part of the farm (Map 3), but on a regional basis are restricted to the vicinity of the Welwitschia lineament zone. A prominent east-southeast-plunging sillimanite lineation parallel to  $F_4$  fold axes indicates that peak metamorphic conditions persisted until the  $D_4$  deformational event.

#### 7.5.2.3 Syntectonic granite intrusions, leucogranite phacolith and pegmatite intrusions of the $D_3/D_4$ dome

On Sandamap Noord the local presence of thin, foliated quartz-feldspar-biotite rocks tens of centimetres wide in the Kuiseb Formation suggest the presence of minor syntectonic granite intrusions. This type of intrusion is common at this stratigraphic level elsewhere in the CZ (Miller, 1983a). A folded, 8-kilometre-long leucogranite phacolith lies in the core of the  $D_3/D_4$  dome (Map 3) possessing a banding rather than a true foliation. Mineral grains are rounded nature and lobate suggesting minor metamorphic recrystallisation. The leucogranite comprises quartz, microcline, oligoclase, magmatic muscovite, biotite, garnet, tourmaline, zircon and chlorite. The feldspars are universally fresh, though slight sericitisation of the microcline has occurred locally. The muscovite in the Sandamap Noord leucogranite is magmatic according to the criteria of Miller *et al.* (1981). Geochemical analyses of the leucogranite are given in Table 3.3: the intrusion is unmineralised (apart from local concentrations of apatite), peraluminous and has an uncorrected ASI value (Zen, 1988) of 1.12. The leucogranite is surrounded by a mass of undeformed, late-/post-tectonic non-stanniferous pegmatite (Map 3), though the exact relationship between the intrusions is obscured by the poor exposure. The pegmatite from the edge of the domal structure contains quartz, microcline and oligoclase with minor primary muscovite, garnet and traces of tourmaline and biotite altering to chlorite. The majority of the muscovite is primary, but some small white micas overgrow sericitised microcline. However, feldspar alteration is generally very minor. The pegmatite has an igneous texture and has not been recrystallised by metamorphic processes.

#### 7.5.2.4 Metamorphic effects associated with the $D_3/D_4$ Dome

Fibrolite in the schist surrounding the dome is concentrated in knots and in folia (*sensu* Vernon, 1987) for a distance of several hundred metres (Map 3). Brown, elongate (2-6 cm), stubby segregations of fibrolite have weathered out of the schist and cover the ground. Mylonitic rocks that run parallel to the contact between the intrusions and the metasediments comprise quartz, sericitised feldspar, biotite and muscovite, while fibrolite/sillimanite is concentrated in folia. These high-strain zones are related to the diapiric intrusion of the domal structure and concomitant pegmatite intrusion. Mylonite zones near the north-northeast-trending gold zone cut unfoliated tourmaline pegmatites, attesting to late Damaran movement. In sheared pegmatite, fibrolite also tends to be concentrated in discrete, anastomosing zones.

#### 7.5.2.5 Stanniferous pegmatites

Zoned, elongate or blob-like stanniferous pegmatites, up to 1 km long, cluster around the  $D_3/D_4$  domal structure, particularly on the southern side (Map 3). The largest bodies at the Sandamap Tin Mine have been mined for tin. Stanniferous pegmatites have a quartz core which is surrounded by a cassiterite-bearing Li-rich greisen which contains purperite, petalite, triphylite and lithiophylite (Von Knorring, 1984, pers. comm.). The outer zone of the pegmatite comprises quartz, albitised microcline and oligoclase, minor tourmaline, lepidolite and muscovite and traces of chlorite. In contrast to the unzoned non-stanniferous pegmatite, the oligoclase is cloudy and extensively altered, being overgrown by tiny muscovite (or perhaps zinnwaldite or lepidolite; Von Knorring, 1985) laths, which are concentrated in fractures. The stanniferous pegmatites have an unequivocal igneous texture and locally contain ferberite and minor pockets of auriferous (determined by fire assay) arsenic mineralisation. Large (3 mm) crystals of loellingite have largely been replaced by scorodite and are commonly surrounded by a skeletal framework of small, euhedral arseno-pyrite rhombs.

### 7.5.3 The auriferous zone

The north-northeast-trending, 2500-metre-long auriferous zone (Map 3) is largely obscured by gravel, calcrete and scree. The mineralisation is hosted by sheared quartz+biotite+sillimanite+K-feldspar schists, which contain minor muscovite and plagioclase, accessory cordierite, tourmaline, apatite and zircon and traces of garnet. Garnet-fibrolite mylonites are confined to the immediate vicinity of the gold mineralisation. Subhedral, slightly elongate almandine garnets (up to 1 cm long), that deflect the fibrolite-defined mylonitic fabric, contain fibrolite inclusions at growth fronts. Garnet cores contain numerous anhedral quartz inclusions indicating that garnet grew as a syn- to late-kinematic porphyroblast/poikiloblast. There is no evidence for the rotation of garnet crystals. Other minerals in the mylonite include strained quartz, plagioclase, perthite and traces of biotite, muscovite, graphite and zircon. The

	NS241	NS303	NS317	NS321	NS323
SiO <sub>2</sub> (wt%)	50.22	22.06	38.76	53.46	37.58
TiO <sub>2</sub>	.01	.39	.96	.98	1.20
Al <sub>2</sub> O <sub>3</sub>	.47	7.42	4.94	24.03	21.56
Fe <sub>2</sub> O <sub>3</sub>	11.53	2.89	33.08	.85	4.94
FeO	26.60	1.41	.52	1.92	7.23
MnO	.71	.03	.51	.31	3.13
MgO	4.87	1.88	.29	.28	.90
CaO	.16	30.14	.97	4.10	1.65
Na <sub>2</sub> O	.03	.07	.32	2.31	1.00
K <sub>2</sub> O	.05	.61	1.89	.75	1.80
P <sub>2</sub> O <sub>5</sub>	.01	.09	.16	.15	.18
As <sub>2</sub> O <sub>3</sub>	-	-	.51	.08	.30
H <sub>2</sub> O-	.61	.26	1.74	1.17	1.02
H <sub>2</sub> O+	.83	.87	6.13	4.44	7.09
CO <sub>2</sub>	3.03	31.77	.78	1.07	.59
SO <sub>3</sub>	-	-	7.43	4.35	10.40
TOTAL	99.12	99.88	98.98	100.27	100.56
F (ppm)	147	1400	<112	1400	2800
S	145	105	-	-	-
Rb	<1.3	64	7.4	3.3	12.3
Ba	223	149	405	606	536
Sr	15.1	117	183	286	461
Th	5.3	8.0	61	17	18.2
U	3.8	4.2	3.3	7.2	8.2
Zr	<1.0	65	229	218	265
Nb	<1.0	8.7	16.5	18.3	19.0
Mo	<.9	1.0	1.3	<.5	1.5
Sn	3.2	16.1	19.8	12.8	15.2
W	18.7	12.9	93	57	282
V	40	68	359	117	220
Cr	7.4	51	122	101	140
Co	<4.8	4.3	11.2	4.0	4.0
Ni	<4.0	7.2	17.8	18.3	18.8
Cu	26	27	124	18.3	84
Zn	140	69	5.0	3.2	9.6
Ga	<1.8	11.9	27	38	33
Pb	<3.7	6.8	<3.5	32.0	3.1
Ge	1.8	<1.0	8.8	1.0	8.4
As	1945	19.0	-	-	-
Sb	<2.1	<1.4	5.9	<1.2	<1.5
Bi	18.0	<3.3	200	<2.9	42
Se	<1.5	<1.0	<1.5	<.9	<1.2
Te	<3.4	<2.3	<3.1	<1.9	<2.5
Sc	9.5	<2.6	16.5	18.8	25
Y	3.7	16.4	7.9	42	63
La	7.4	10.4	56	41	62
Ce	<8.3	21	92	98	107
Nd	<5.1	15.7	40	60	45
Au (ppm)	0.27	N.D.	45.8	.4	.8

**Table 7/5.2:** Whole-rock analyses of alteration/mineralisation at the Sandamap Noord Gold Prospect

NS241: Massive grunerite rock, trench no. 9

NS303: Massive calcite-graphite-tourmaline rock, trench no. 6

NS317: Gossanous jarositic schist, trench no. 15

NS321: Kaolinite-alunite-garnet rock, trench no. 15

NS323: Kaolinite-alunite-garnet rock, trench no. 15

anhedral, elongate feldspars are universally enveloped by the characteristically lenticular quartz.

The auriferous zone comprises a series of foliation-parallel ferruginous quartz veins, gossan stringers and anastomosing zones of alteration and bleaching. The zone is 3-10 metres wide and dips steeply eastwards at 50-800. Three main types of alteration/mineralisation have been identified. The most common type, which contains minor gold mineralisation (usually < 1 g/t Au; Table 7/5.2, samples NS321 and NS323),

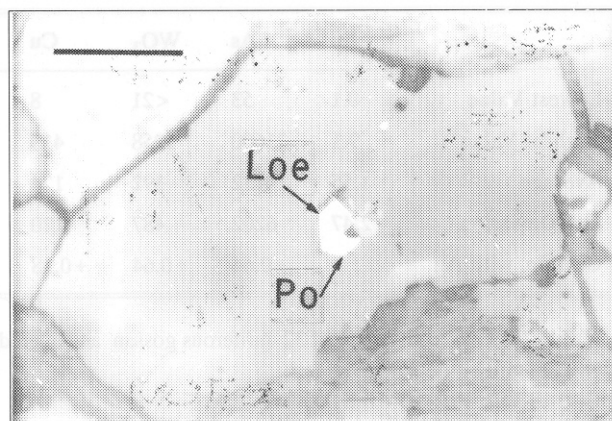


**Plate 7/5.1:** Inclusions of loellingite (Loe) and pyrrhotite (Po) in angular quartz at the Sandamap Noord Gold Prospect (NS241B; RL); scale bar = 100  $\mu$ m

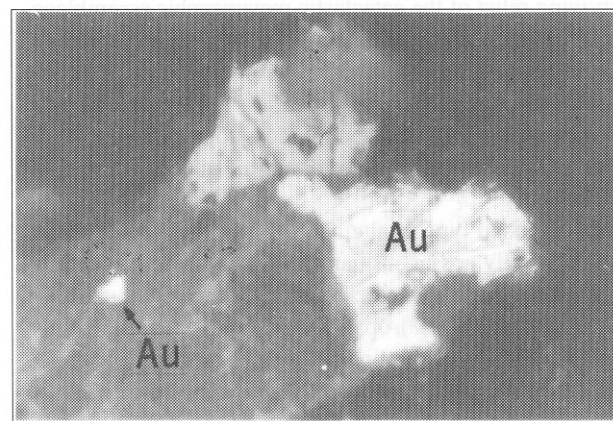


**Plate 7/5.2:** Gold (Au) grains in ferruginous, jarositic schist at the Sandamap Noord Gold Prospect (NSP8; RL); largest grain 0.1 mm across

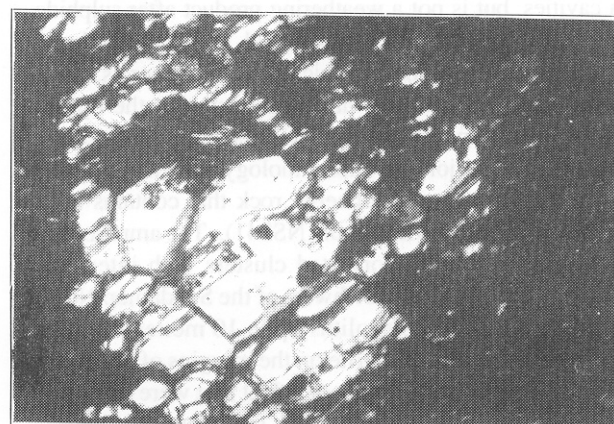


**Plate 7/5.3:** Calcite-graphite-tourmaline rock from alteration zone at the Sandamap Noord Gold Prospect (NS303; PPL). Note angular nature of quartz. Horizontal field of view is 2.25 mm

is a cream yellow-light brown kaolinite-alunite-garnet rock that locally has a planar fabric defined by coarse-grained clay minerals. Elsewhere the texture is fine-grained and chaotic being dominated by angular (hydraulically fractured?) quartz (< 300  $\mu$ m). Some quartz grains contain small (< 30  $\mu$ m) inclusions of nickeliferous loellingite and pyrrhotite (Plate 7/5.1). The altered interstitial alunite was only identified by

	Au	As	WO <sub>3</sub>	Cu	Pb	Zn	Bi	Sn	Ag	Mo
<b>Lowest Value</b>	0.1	53	<21	8	5	3	<20	<20	<1	<20
<b>Highest Value</b>	9.1	21600	1958	413	>1000	>1000	432	99	66	78
<b>Average</b>	1.55	4182	392	124	100	77	Too	Few	Values	Above
<b>Std. Deviation</b>	2.47	6202	487	120	223	186	LLD			
<b>Correln. with Au</b>		+0.64	+0.64	+0.18	-0.11	-0.08				

**Table 7/5.3:** Geochemistry of 32 auriferous gossan and altered schist samples from the Sandamap Noord Gold Prospect (values in ppm)

XRD and microprobe analysis. Almandine garnet (up to 5 mm in diameter) may make up to 25% of the mineral assemblage in the kaolinite zones and has a similar composition to the garnet in the mylonite. The garnet in the alteration zone is thus interpreted as a surviving relict of the cataclastic metamorphic assemblage and is not an alteration mineral. It is inferred that kaolinite development was most intense where fibrolite was concentrated. Minor amounts of plagioclase are present and accessory minerals include iron oxides, tourmaline, zircon, jarosite, finely disseminated graphite and a trace of possible gypsum.

The second type of alteration is a yellow-brown ferruginous, locally gossanous, jarosite schist that is crosscut by veinlets of calcite. The rock comprises (natro)jarosite (30-50%), quartz (20-30%), opal (10-25%) and opaque minerals (up to 60%). Minor minerals include grunerite, calcite, altered feldspar and muscovite. Gold is concentrated in this rock (up to 46 g/t Au; Table 7/5.2, sample NS317). The largest grain of native gold found in a sample of gossanous schist was 0.1 mm in diameter (Plate 7/5.2). Bright yellow jarosite is present in stringers, veinlets and as encrustations in cavities, but is not a weathering product after sulphide. Optically negative, grey-white opal has completely replaced and pseudomorphed mica and clay minerals. Electron microprobe analysis has confirmed that the opaque minerals are iron and titanium oxides such as brookite.

The third major alteration lithology, which is the least common, is a massive grunerite rock that contains up to 0.5 g/t Au (Table 7/5.2, sample NS241). The amphibole is arranged in randomly oriented clusters with interstitial quartz. One kilometre northwest of the Sandamap Noord farmhouse (Map 3), xenoliths up to 10 metres across of massive auriferous grunerite on the margins of pegmatite are interpreted as fragments of schist that were caught up during pegmatite intrusion and subsequently metasomatised. Grunerite is locally present in jarosite schist, but not kaolinite-alunite rocks, suggesting the presence of higher temperature alteration assemblages on the contact with pegmatites and in the centre of the auriferous zone (Map 3).

A distinctive, apparently unmineralised, lithology, which is intimately associated with the gold zone and is interpreted as wallrock alteration, is an unfoliated, massive calcite-graphite-tourmaline rock (Plate 7/5.3), which comprises calcite ( $\pm 50\%$ ), graphite ( $\pm 20\%$ ), tourmaline ( $\pm 10\%$ ), quartz ( $\pm 10\%$ ), muscovite ( $\pm 5\%$ ), biotite (2.3%) and minor iron oxides (Table 7/5.2, sample NS303). The grain size is usually

less than 200  $\mu\text{m}$ . The relationship between this lithology and the auriferous zone is obscured by scree. A 100-metre-long zone of north-northeast-trending galena and pyrite-bearing quartz veins runs parallel to the auriferous zone (Map 3), but may be unrelated to the gold mineralisation. However, the presence of mimetite (lead chloro-arsenate) with some of the galena mineralisation suggests a genetic relationship.

#### 7.5.4 Gold and the “pathfinder” elements

A suite of 32 gossanous and altered schist samples was collected on surface and geochemically analysed by a commercial laboratory (Table 7/5.3). Gold was analysed by fire assay, Cu, Pb, Zn and Ag by atomic absorption spectroscopy and Sn, W, Mo, As, Sb and Bi by XRF. Sb contents of both gossanous and altered schist are universally below the detection limit. Gold concentrations correlate positively with arsenic (Pearson’s correlation coefficient: +0.64;) and tungsten (Pearson’s correlation coefficient: +0.64) in both rock types. There is a large surficial secondary arsenic dispersion halo (as defined by Rose *et al.*, 1979, p.17) around the gold mineralisation at Sandamap Noord. A further point of interest is that several samples of auriferous gossan from Sandamap Noord contain slightly elevated tellurium contents (3-5 ppm). A full geochemical analysis of a gossanous jarositic schist that contains 45.8 g/t Au is given in Table 7/5.2 (Sample NS317).

#### 7.5.5 Summary

Gold mineralisation is hosted by altered schist, quartz veins and mylonite rocks in the aureole of a leucogranite-cored D<sub>3</sub>/D<sub>4</sub> dome. Some of the high-strain zones surrounding the domal structure formed during the diapiric intrusion of the granites and pegmatites and are thus unrelated to the regional tectonism. Only the north-northeast-trending portions of these zones are mineralised with gold. The altered schist and graphite-tourmaline rocks do not possess pervasive metamorphic fabrics and thus cannot be older than -520 Ma. The possibility that the occurrence represents a metamorphosed syngenetic gold deposit intruded by granites and pegmatites is therefore rejected. The intensive alteration of the Kuiseb Formation schist in the auriferous zone is most unusual in the Damara Orogen and a magmatic fluid or a magmatically modified metamorphic fluid is favoured as being responsible for the gold mineralisation. It is considered highly unlikely that a metamorphic fluid alone could give

rise to such intensive alteration. The only post - Damaran intrusions in the area are unmineralised, unaltered Karoo dolerite and quartz-feldspar porphyry dykes (Map 3). A genetic relationship between these lithologies and the gold mineralisation is deemed improbable.

The sulphates alunite and jarosite are not weathering products after sulphide minerals (Bladh, 1982) and are present only in pervasively altered Kuiseb Formation schist. The gangue assemblage of kaolinite, alunite, jarosite and opal is characteristic of advanced argillic and alunitic alteration caused by hydrothermal solutions at less than 300°C (Siems, 1984). On account of the weathering, it has not been possible to determine whether some of the alunite has formed by weathering of kaolinite as suggested by Siems (1984). Alunite and jarosite alteration assemblages are produced under acid oxidising conditions in hypogene porphyry copper and epithermal gold deposits (Scott, 1990). Thus, one of the intriguing features is that, although the alteration assemblage is characteristic of an *epithermal* (< 200°C) gold deposit, the prospect exhibits many of the features of Archaean *mesothermal* gold deposits that have been reviewed by Groves *et al.* (1990): the mineralising event postdated the metamorphic peak; the mineralisation is epigenetic and structurally controlled in late-tectonic ( $D_3/D_4$ ) structures; the wallrock alteration is retrograde with respect to peak metamorphism; the mineralisation is “gold-only” with high gold-enrichment factors ( $10^3$ - $10^4$ ), moderate enrichments of As, Band Wand low enrichments in Cu, Zn and Pb.

#### 7.5.6 Genesis of the gold mineralisation

The gold mineralisation on Sandamap Noord is considered to be epigenetic and of late Damaran age. Auriferous loellingite-arsenopyrite-scorodite phases within the stanniferous pegmatites suggest that these intrusions were intimately related to, if not responsible for, the gold mineralising event. The “soil” that covers the stanniferous pegmatites on the southern side of the dome has an anomalously high arsenic content (Keenan, 1982). This arsenic anomaly has a strike length of 5 km and a width of one km, extending from the vicinity of the Sandamap Tin Mine in the west to the eastern boundary of the farm (Map 3). Anomalous arsenic concentrations were also recorded in the “soil” on the northern side of the dome away from gold mineralisation. The Kuiseb Formation calc-silicate rocks (Table 2.30) and schists (Table 2.24) have arsenic contents only slightly above average abundances in shale (Levinson, 1974): arsenic mineralisation is restricted to pegmatites and hydrothermal veins. Thus rare-element pegmatites (defined as pegmatites enriched in Li, Rb, Cs, Be, Ta, Sn, Nb; Cerny, 1982a) and arsenic mineralisation are concentrically arranged around a domal structure, while galena and auriferous quartz veins and hydrothermal alteration are confined to the northwestern side. The situation on Sandamap Noord invites comparison with other rare-element pegmatites (REP) which are spatially associated with leucogranites in andalusite-sillimanite terrains (Cerny, 1982b). The REP “provide the most convincing evidence for a genetic link [between pegmatites and] granites” (Cerny, 1982a), being

generated from the fractionation of differentiated, allochthonous intrusions.

On Sandamap Noord, in contrast, the relationship between the leucogranite and the pegmatites is not clear. The homogenous leucogranite phacolith has a banding, rather than a foliation, and rounded, partially recrystallised grains; the pegmatites possess neither of these. If the banding is interpreted as a fabric resulting from tectonism ( $D_2$  deformation), then the leucogranite considerably predated pegmatite intrusion and the latter are unlikely to be differentiates of the leucogranite. If, however, the banding is interpreted as a fabric that developed during the diapiric development of the dome, then the leucogranite may not be so different in age from the pegmatite. Moreover, the meaning of the Rb-Sr whole-rock dates of the pegmatite is equivocal. The leucogranite has a Rb-Sr whole rock date of  $512 \pm 19$  Ma which is interpreted to be the age of crystallisation. The pegmatites have significantly younger dates ( $473 \pm 23$  Ma and  $468 \pm 14$  Ma), but their ages of emplacement may be considerably older (see discussion in chapter 6.2.2.5). The large difference in  $(^{87}\text{Sr}/^{86}\text{Sr})_1$  ratio between the leucogranite (0.7153) and the pegmatites (0.7267 and 0.7238) seems to preclude the possibility that either of the pegmatite types are differentiates of the phacolith, but the significance of this can only be discussed once the ages of crystallisation are more accurately known. Anomalous, and particularly high,  $(^{87}\text{Sr}/^{86}\text{Sr})_1$  values are a feature of pegmatites worldwide (Clark, 1982).

In Chapter 6 it was argued that the stanniferous pegmatites were derived from the large-scale partial melting of biotite and muscovite from Kuiseb Formation schists during and slightly after the peak of regional metamorphism. This process is believed to have been enhanced by the Buchan-style metamorphism associated with the large number of syn-/late-tectonic granitic intrusions. It would seem unlikely that this happened at the present-day erosional level because peak metamorphic conditions (~3 kbar, 650°C) were not high enough for partial melting to have occurred (Fig. 5.4). In general, REP are not formed by regional metamorphic processes, but are thought to have been generated at intermediate depths (3.5-7 km, i.e. 0.9-2.2 kbar) from the differentiation of granites (Cerny, 1982a, 1982b). Cerny distinguished between the “sterile” granitoids, which comprise the bulk of a batholithic assemblage, and the rarer, predominantly S-type “fertile” granites which are the parents to REP. The two-dimensional exposure on Sandamap Noord precludes an examination of the leucogranite to determine whether the intrusion is as compositionally in homogenous as most REP-generating granites. The two pieces of evidence that indicate that it is a “fertile” granite, at least in Damaran terms, are the presence of magmatic muscovite and the rare stringers of apatite. It is thought that auriferous fluids were mobilised by, and probably expelled from, rare-element pegmatites in the aureole of a diapiric dome that is cored by a syntectonic peraluminous granite. Whether the pegmatites and hydrothermal alteration are derived from residual fluids in the leucogranite or from the large-scale anatexis of Kuiseb Formation metasediments cannot be determined because of the depth of erosion, poor exposure and ambiguous isotopic data. However, the strong stratigraphic

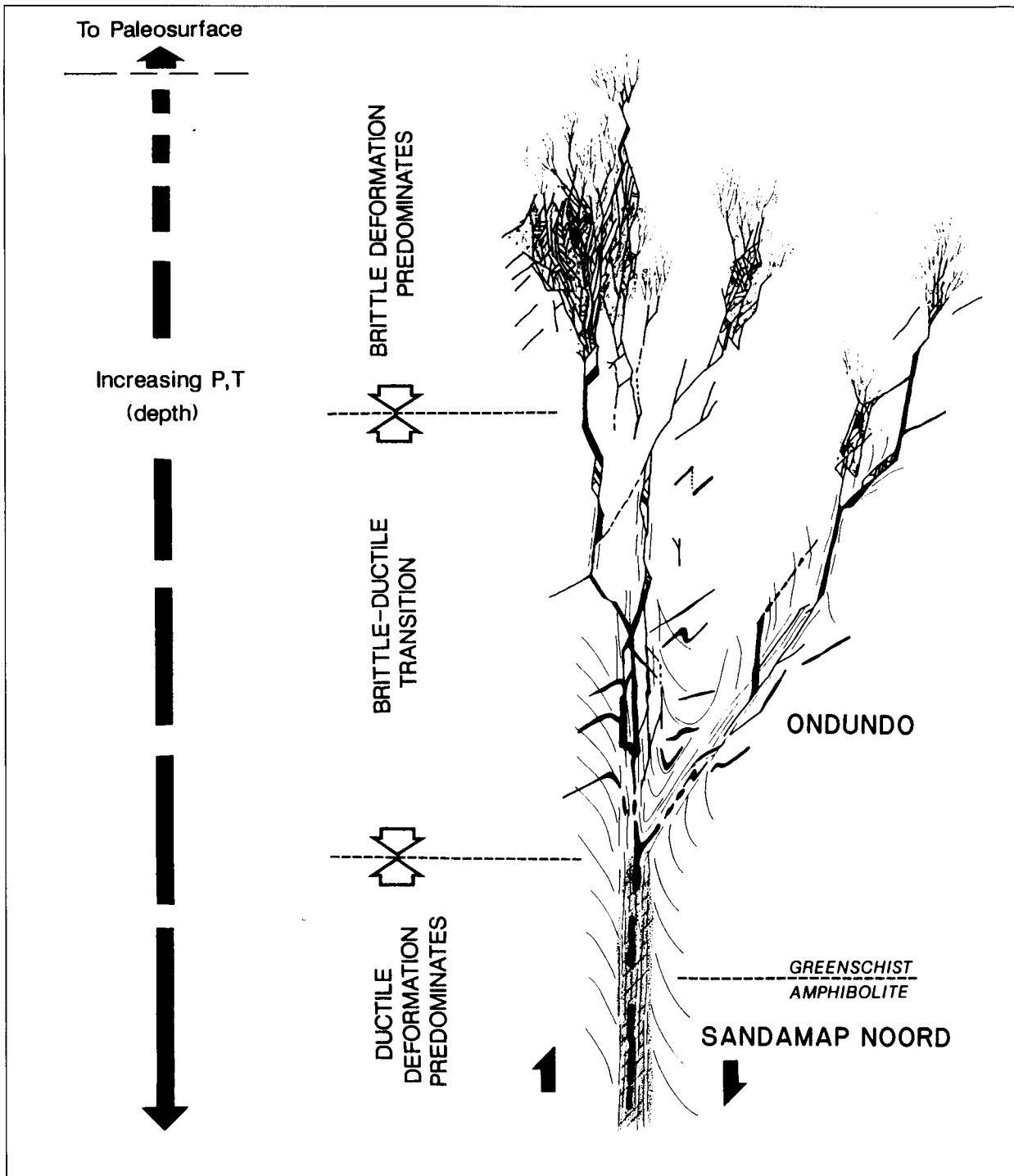


Figure 7/5.2: An idealised Archaean gold ore zone (after Colvine *et al.*, 1988)

control on the types of pegmatite in the CZ, and in particular the restriction of particular types of REP to specific stratigraphic levels (chapter 3), indicates that, even if the REP of the CZ are the products of igneous fractionation of granitic melts and not the products of anatexis, there has been considerable interaction with fluids in the country rock.

In spite of the above uncertainties, the following sequence of events is envisaged for the formation of the Sandamap Noord gold zone:

1) The presence of abundant disseminated graphite and fine-grained sulphide mineralisation throughout the upper Kuiseb Formation combined with the great thickness of this

stratigraphic unit point to rapid, anoxic sedimentation within graben structures during late Kuiseb times. Diagenesis and greenschist facies metamorphism of numerous carbon and sulphur-rich layers led to the crystallisation of graphite, pyrite and arsenopyrite-rich layers. Some of these pyritic phylites and schists (for example on Ohere 106) are known to have elevated gold contents (100-130 ppb Au). The upper Kuiseb Formation therefore represents a major reservoir of Au, As and S.

2) These sediments were further deformed and metamorphosed to amphibolite facies grade during the Damaran orogeny. Localised partial melting of Kuiseb Formation

metasediments below the present-day erosional level occurred slightly after the peak of regional metamorphism. This process was facilitated by the thermal effects associated with the numerous syn- to late-tectonic granite intrusions such as the leucogranite in the core of the Sandamap Noord dome.

3) The diapiric intrusion of the leucogranite-cored dome and accompanying pegmatites (which may or may not have been derived from the leucogranite) resulted in the development of unmineralised mylonitic high-strain zones in the enclosing schists. Au-As fluids, either mobilised from the metasediments by and/or expelled from the stanniferous pegmatites, were concentrated in north-northeast-trending structures. These structures parallel major, deep-seated structural breaks such as the Welwitschia lineament zone. The angular nature of loellingite-bearing quartz grains in the auriferous zone suggests significant brittle deformation either during or after the formation of the Au-As mineralisation.

4) Regional, west-northwest-directed  $D_4$  compression resulted in the development of  $F_4$  folds with north-northeast-trending axial traces and semi ductile deformation of otherwise undeformed pegmatites in the vicinity of the Welwitschia lineament zone.

#### 7.5.7 Conclusion

Epigenetic gold mineralisation on Sandamap Noord is hosted by metaturbidites that have been extensively sheared. However, the essentially two-dimensional rock exposure and the lack of drillcore hamper interpretation. For example, the exact relationship between the mineralisation and the shear is obscured by scree. Moreover, as far as can be ascertained, the mineralisation is not cut by Damaran granitic or pegmatitic intrusions that would be suitable for radiometric determinations. The evidence indicates that stanniferous pegmatites in the aureole of a leucogranite-cored dome have released a hydrothermal gold-bearing phase that has altered the Kuiseb Formation schist. The present erosion surface has exposed the roots of the system: most of the pegmatite aureole and hydrothermal veins have been eroded away. There is a coregionality between gold mineralisation and late-tectonic pegmatites elsewhere in the Central Zone of the Damara Orogen (section 7.4). The Sandamap Noord gold zone lies within 10 km of the north-northeast-trending Welwitschia lineament zone which was considered by Corner (1983) to have played an important role in the localisation of late- to post-tectonic uraniumiferous alaskites. The tin-bearing pegmatite at the Sandamap Tin Mine has a Rb-Sr whole-rock date which cannot be distinguished from the age of the late-tectonic alaskite at the Rössing Uranium Mine (458±8 Ma; Kröner and Hawkesworth, 1977; Hawkesworth *et al.*, 1983).

At the Ondundo Gold Prospect (Fig. 1.3), the only other known turbidite-hosted gold deposit in central Namibia, gold-pyrite-arsenopyrite mineralisation is hosted by a series of bedding-parallel quartz veins (Reuning, 1937). Wallrock alteration is minimal. Relatively open folding and green-schist facies metamorphism, so typical of the Northern Zone (Fig. 2.2), characterise the deposit. The nearest Damaran intrusions are more than 20 km away. The deposit is similar to the turbidite-hosted gold deposits reviewed by

Boyle (1986). At the Sandamap Noord Gold Prospect, in contrast, wallrock alteration is extensive, the Kuiseb Formation sediments have been isoclinally folded, subjected to upper amphibolite facies metamorphism and the area has been intruded by granites and pegmatites. Although poor exposure precludes an assessment as to whether the mylonitic structures actually host the mineralisation, they are absent at Ondundo. The Sandamap Noord and Ondundo turbidite-hosted gold occurrences appear to be late Proterozoic/early Palaeozoic analogues of Archaean lode gold occurrences (Fig. 7/5.2; Colvine *et al.*, 1988). The former is hosted by rocks that have undergone essentially ductile deformation, the latter deposit possesses features characteristic of the brittle-ductile transition.

## 7.6 TOURMALINITE MINERALISATION IN THE KUISEB FORMATION ON OHERE

### 7.6.1 Introduction

Tourmalinites (defined as a stratabound rock containing 20% or more of tourmaline; Bates and Jackson, 1987) have been the subject of much interest in recent years because of their close spatial relationship with a number of types of stratiform mineralisation (Slack, 1982; Slack *et al.*, 1984; Taylor and Slack, 1984; Plimer, 1988; Palmer and Slack, 1989). Plimer (1986, 1988), in particular, has described tourmalinite mineralisation from several localities and has frequently invoked an exhalative model to explain the origin of such large accumulations of boron. However, a syn-genetic origin for tourmalinites is not universally accepted. At many localities structural and textural studies are lacking and the role of metamorphic fluids has been ignored (Davies, 1985). Steven (1987) mapped stratiform scheelite-bearing tourmalinites on the farms Ohere, Ohere Oos, Gross Okandjou and Kompaneno in the core of a major regional syncline (Map 1) and on the basis of relatively little evidence suggested an exhalative origin for this style of mineralisation. Badenhorst (1988a) has discussed the nature of the tourmalinites on Ohere in more detail and proposed an early diagenetic replacement or possibly an exhalative origin. However, neither of these authors discussed the relationship of the tourmalinites to the local structure. A discussion on the origin of the tourmalinites is of interest because of the recent discovery of a zone of scorodite-tourmaline alteration on the north of Ohere 106 (Map 2). Moreover, massive, unfoliated tourmaline-graphite rocks, which could broadly be referred to as tourmalinites, are intimately associated with the gold-arsenic mineralisation on Sandamap Noord 115 (Map 3). The present study focuses on a structural and geochemical investigation of the best exposed tourmalinite mineralisation on Ohere which it is believed can resolve the syngenetic/epigenetic argument. Emphasis has again been placed on presenting new data.

### 7.6.2 Geological setting

The farm Ohere 106 lies at the northeast end of the Nainais-Kohero tin belt (Fig. 7.1). Tourmalinites are hosted by

metasediments of the Kuiseb Formation that have undergone at least four phases of ductile deformation, greenschist-lower amphibolite facies metamorphism and have been intruded by syn-/late-tectonic granitic intrusions and late-/post-tectonic stanniferous pegmatites (Map 2). The metasediments 'comprise phyllites, metaturbidites and biotite schists with subordinate calc-silicate rocks, unusual scheelite-vesuvianite skarnoid rocks, marble and very minor para-amphibolite. The metamorphic grade increases from the western portion of Ohere 106 towards the contacts with the granites where sillimanite schists are developed (Fig. 5.3). Throughout the farm an  $S_1$  fabric defined by micas runs parallel to the well-preserved sedimentary structures. Although younging directions indicate some duplication of the sequence, the  $F_2$  synformal structure is essentially a syncline (Map 2) that plunges at  $70^\circ$ - $80^\circ$  on a bearing  $320^\circ$ . The fold has a pervasive axial planar cleavage, an  $S_2$  fabric, whose development is most intense in the hinge zone. The  $S_2$  foliation has been locally refolded by a third folding phase,  $F_3$ , that is approximately coaxial with  $F_2$ . The  $F_2$  and  $F_3$  folds developed as the result of the intrusion of the Ohere Oos Salem granite and the Ohere leucogranite. A fourth folding phase ( $F_4$ ) is only locally developed, the fold axes plunging steeply north-northwest.

#### 7.6.3 Nature and petrography of the tourmalinite

Tourmalinite on Ohere is a stratiform (i.e., it has the form of a layer or bed; Bates and Jackson, 1987), fine-grained, hard, black lithology with a glossy sheen. It is a finely laminated rock that occurs in lenses up to 50 metres long and several decimetres wide. Tourmalinites are prominent at certain stratigraphic levels in the upper Kuiseb Formation in NCZe and zones in which the lithology is present can be traced for many kilometres (Map 1). On Ohere the tourmalinites are hosted by metaturbidites and cordierite schists and, to a lesser extent, phyllites in the core of the synform. Sedimentary structures such as graded beds, Bouma sequences and load structures characteristic of turbidites are abundant in tourmalinites and have been described in detail by Badenhorst (1988a). Tourmaline is rarely visible in hand specimen, but is readily identified as a strongly pleochroic granular mass or aggregate of stubby prisms in thin section. The tourmalinites are characterised by a simple mineralogy dominated by approximately equal proportions of quartz and tourmaline. The Ohere tourmalinites commonly contain very minor plagioclase, disseminated scheelite, traces of pyrite, zircon, sphene, rutile, iron oxides and scorodite and local concentrations (up to 10 volume per cent) of graphite. One intriguing but rare rock type noted on Ohere is a tourmalinite breccia rock. No outcrop of this lithology was discovered. Angular fragments of graphitic tourmalinite up to several centimetres long are set in a matrix of fine-grained quartz. The annealed and granoblastic nature of the quartz indicates that brecciation occurred before the peak of metamorphism. A similar lithology was noted by the author on a visit to the Ondundo Gold Prospect (Fig. 1.3).

#### 7.6.4 Structural investigation of tourmalinite mineralisation

The tourmalinite mineralisation on Ohere was mapped revealing that a substantial proportion of the lithology is crosscutting, not stratiform. The tourmalinites were divided on a morphological basis into three types: Type 1 tourmalinite is a finely laminated rock conformable with the  $S_1$  foliation for distances of up to several tens of metres. It is this type of tourmalinite which on first examination appears to have formed from the metamorphic recrystallisation of a syndepositional accumulation of boron; Type 2 tourmalinite is a fine-grained variety which crosscuts the  $S_1$  foliation and generally occupies kink bands, but preserves the fine laminations of  $S_1$ ; and Type 3 tourmalinites, crosscutting quartz-tourmaline veins, which possess a banding parallel to the vein. The three types of tourmalinite are intimately associated on Ohere. Six localities around the  $F_2$  fold were selected for a detailed structural investigation (Fig. 7/6.1). The four foliations ( $S_1$  to  $S_4$ ), quartz-tourmaline joints and the orientation direction of the Type 2 tourmalinites from the various grids have been plotted on equal-area stereographic projections.

In the core of the syncline on Grid 1, the majority of the tourmalinite is conformable with the  $S_1$  fabric. It is in this area that the stratiform nature of the tourmalinite suggests the original presence of a boron-rich precursor. The  $S_1$  foliation dips steeply to the northwest, the  $S_2$  cleavage is subvertical, oriented northwest/southeast and the  $S_3$  fracture cleavage dips steeply northwards. The  $S_4$  fracture cleavage dips steeply west-southwest. Proportionally fewer Type 2 tourmalinites are oriented  $134^\circ$ , axial planar to the  $F_2$  structure. Quartz-tourmaline joints are also oriented approximately parallel to the  $S_2$  fabric.

On the northern side of the hinge zone (Grid 2) crosscutting tourmalinites are more prominent. The  $S_1$  foliation dips steeply west-southwest, but in the Type 2 tourmalinites this fabric has been rotated and dips westward to northwestward. Thus Type 2 tourmalinites which run parallel to the  $S_2$  foliation are located within z-shaped kink bands. The fabrics  $S_3$  and  $S_4$  have similar orientations to those described from Grid 1. Quartz-tourmaline joints that intrude the metasediments show a fairly wide scatter in their orientation, but in general are parallel to  $S_2$ .

On the southern limb of the  $F_2$  fold (Grid 3), the  $S_1$  fabric in the schist dips steeply northwards. Type I tourmalinites are poorly developed. Type 2 tourmalinites are confined to s-shaped kink bands where the  $S_1$  foliation dips at a shallower angle to the northwest. The  $S_2$  fabric, the Type 2 tourmalinites and quartz-tourmaline joints have a similar subvertical east-southeast orientation.

On the northern limb of the  $F_2$  fold (Grid 4) the tourmalinite is clearly transgressive, Type 2 mineralisation predominating by far over Type 1. The subvertical  $S_1$  foliation strikes northwest in the schist but north-south in the tourmalinite. The Type 2 tourmalinites occupy kink bands that have a z-shaped morphology. The  $S_2$  fabric, the Type 2 tourmalinites and transgressive quartz-tourmaline joints have a similar east-west orientation.

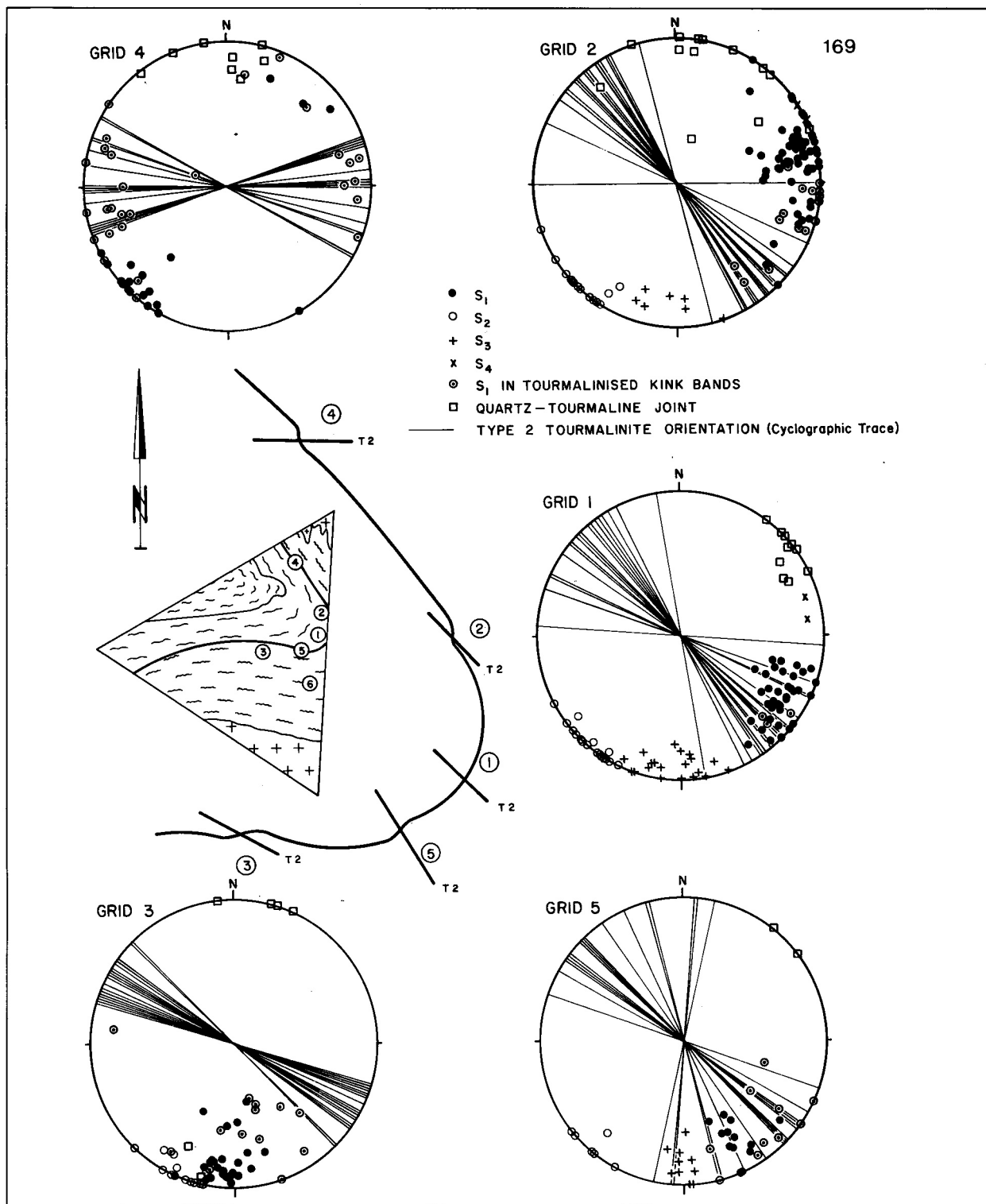


Figure 7/6.1: Structural summary of the tourmalinites and associated alteration on Ohere 106

On Grid 5 conformable and crosscutting tourmalinites are equally abundant. The  $S_1$  fabric dips steeply north-north-west, while the  $S_2$  and  $S_3$  fabric orientations are similar to those on Grid 1. Type 2 tourmalinites occupy kink bands with an s-shaped morphology where  $S_1$  dips steeply north-west. As at Grids 1, 2 and 3, the  $S_2$  fabric, Type 2 tourmalinites and the quartz-tourmaline joints all have a similar east-southeast/southeast orientation.

On Grid 6 Type 3 tourmalinites are present in an area that has been intruded by pegmatites. These intrusions have caused local tourmalinisation of the enclosing schist.

#### 7.6.5 Structural summary

The  $F_2$  syncline on Ohere 106 is a concentric fold that originated by flexural slip folding. This style of folding is typical of terrains that exhibit dome-and-basin structures (Hobbs *et al.*, 1976), such as NCZe. There is a very strong structural control on the localisation of tourmalinite mineralisation on the farm: stratiform tourmalinite mineralisation (Type 1) is essentially confined to the hinge of the  $F_2$  structure. At all the mapped localities Type 2 tourmalinites are oriented parallel to the  $S_2$  fabric, regardless of the orientation of the latter. Thus the major proportion of the tourmalinite,

	NS225	NS226	NS227	NS228	NS229	NS230	NS231	1	2
SiO <sub>2</sub> (wt%)	55.74	49.98	54.56	57.76	57.25	61.08	53.41	75.43	72.16
TiO <sub>2</sub>	.81	.72	.79	.89	1.04	.96	.51	0.48	0.46
Al <sub>2</sub> O <sub>3</sub>	18.59	18.79	16.30	19.44	21.12	14.07	22.39	12.72	14.77
Fe <sub>2</sub> O <sub>3</sub>	All		Iron		as		FeO	0.74	0.76
FeO	5.49	4.82	3.68	4.19	4.68	4.67	5.41	3.19	3.62
MnO	.03	.04	.03	.04	.03	.04	.05	0.02	0.07
MgO	4.30	4.89	3.95	4.86	4.86	3.01	5.70	3.30	1.44
CaO	.85	1.14	.76	1.08	.76	.61	1.13	0.27	0.39
Na <sub>2</sub> O	.88	.96	.81	.95	1.07	.73	1.08	0.71	0.95
K <sub>2</sub> O	.02	.06	.02	.02	.03	.02	.03	0.10	0.99
P <sub>2</sub> O <sub>5</sub>	.09	.16	.16	.18	.07	.08	.06	0.00	0.20
H <sub>2</sub> O-	.12	.09	.05	.06	.05	.09	.05		
H <sub>2</sub> O+	.82	.44	.33	.40	.32	.40	.46	1.48	1.97
CO <sub>2</sub>	3.97	9.14	10.50	2.59	.42	6.94	.55		
B <sub>2</sub> O <sub>3</sub>	5.94	6.19	5.49	6.03	6.39	4.73	7.23	1.57	2.14
TOTAL	97.64	97.42	97.43	98.49	98.09	97.43	98.06	100.04	99.96
F (ppm)	1600	2100	2500	1600	3400	3100	5200		
S	1689	125	132	47	993	868	519		
Rb	1	3	.7	1	1	<.7	2		
Ba	49	14	41	7	34	241	49		
Sr	182	198	171	145	193	131	208		
Th	14	12	13	14	13	15	5		
U	4	2	4	3	4	4	<1.3		
Zr	173	172	182	186	187	242	69		
Nb	12	9	13	12	16	22	<.6		
Mo	.7	<.5	<.5	.6	<.5	1	<.5		
Sn	96	154	119	85	99	84	171		
W	8	6	15	7	23	39	496		
V	226	238	170	218	228	154	280		
Cr	135	115	119	136	155	116	78		
Co	7	6	8	21	8	7	9		
Ni	24	39	30	64	18	19	22		
Cu	97	9	17	5	8	154	16		
Zn	74	129	64	74	75	101	116		
Ga	27	33	26	29	31	20	37		
Pb	8	10	5	10	8	6	7		
Ge	1	2	1	<.8	2	4	2		
As	66	70	21	35	3	7	36		
Sb	<1.2	<1.2	<1.1	<1.2	<1.2	<1.2	<1.2		
Bi	<2.7	<2.6	<2.5	<2.6	<2.6	2.7	<2.7		
Se	<.8	<.8	<.7	<.8	<.8	.8	<.8		
Te	<1.9	<1.8	<1.8	<1.8	<1.9	<1.9	<1.9		
Sc	29	32	23	30	36	20	36		
Y	32	33	35	38	36	45	8		
La	38	35	17	29	46	39	8		
Ce	73	62	31	59	88	82	10		
Nd	40	38	19	33	47	50	7		
Au (ppb)	<5	<5	<5	<5	<5	<5	<5		

**Table 7/6.1:** Whole-rock analyses of tourmalinites from Ohere 106, Omaruru District, and Australia

NS225: Ohere 106, grid 1, type 2 tourmalinite

NS226: Ohere 106, grid 1, type 1 tourmalinite

NS227: Ohere 106, grid 2, type 1 tourmalinite

NS228: Ohere 106, grid 2, type 2 tourmalinite

NS229: Ohere 106, grid 2, type 1 tourmalinite

NS230: Ohere 106, grid 2, type 2 tourmalinite

NS231: Ohere 106, grid 2, type 3 tourmalinite

1: Average of 5 analyses from the Golden Dyke Dome, Northern Territory, Australia (Plimer, 1988)

2: Tourmalinite from Mt Howden, Willyama Subgroup, Broken Hill, NSW, Australia (Plimer, 1988)

	Schist	Tourmalinite	Gain (+)/Loss (-)
	n=3	n=6	in wt%/ppm
SiO <sub>2</sub> (wt%)	61.62	57.11	-4.51
TiO <sub>2</sub>	.86	.88	+0.02
Al <sub>2</sub> O <sub>3</sub>	17.26	18.39	+1.13
Fe <sub>2</sub> O <sub>3</sub>	5.05	4.19	-0.86
FeO	1.40	.91	-0.49
MnO	.06	.04	-0.02
MgO	3.11	4.39	+1.28
CaO	.27	.88	+0.61
Na <sub>2</sub> O	.55	.92	+0.37
K <sub>2</sub> O	5.51	.03	-5.48
P <sub>2</sub> O <sub>5</sub>	.14	.13	-0.01
H <sub>2</sub> O-	.36	.08	-0.28
H <sub>2</sub> O+	2.71	.46	-2.25
CO <sub>2</sub>	1.04	5.70	+4.66
B <sub>2</sub> O <sub>3</sub>	.05	5.90	+5.85
TOTAL	100.00	100.00	
F (ppm)	775	2383	+1608
S	355	642	+287
Rb	276	1	-275
Ba	760	64	-696
Sr	37	170	+133
Th	15	14	-1
U	4	4	NC
Zr	186	190	+4
Nb	16	14	-2
Mo	ND	ND	-
Sn	33	106	+73
W	7	16	+9
V	158	205	+47
Cr	116	130	+14
Co	17	9	-8
Ni	34	32	-2
Cu	12	48	+36
Zn	106	86	-20
Ga	25	28	+3
Pb	6	8	+2
Ge	ND	2	-
As	37	34	-3
Sb	ND	ND	-
Bi	ND	ND	-
Se	ND	ND	-
Te	ND	ND	-
Sc	22	28	+6
Y	34	36	+2
La	33	34	+1
Ce	66	66	NC
Nd	36	38	+2

**Table 7/6.2:** Normalised average analyses of schist and tourmalinite used in mass balance calculation

NC = no change

ND = not detected

although stratiform on the centimetre to decimetre scale, is actually transgressive. In an area intruded by pegmatites (Grid 6), Type 3 tourmalinites predominate over Type 2s. Even here, the latter are also located in kink band zones. It is believed that the subvertical S<sub>2</sub> cleavage provided a channel way for boron-rich fluids resulting in the formation of the Type 2 tourmalinites. Subsequent replacement of the metaturbidites along the essentially bedding-parallel S<sub>1</sub> fabric in the hinge zone led to the formation of the stratiform Type 1 tourmalinites. Bedding-plane slip is an important feature in the development of concentric folds and would have provided channels for the migration of tourmalinising fluids. Quartz-tourmaline veins are also oriented parallel to the S<sub>2</sub> fabric.

#### 7.6.6 Geochemistry of the tourmalinites

Because of the well-documented association between tourmalinites and various styles of exhalative ores (Plimer, 1988), seven whole-rock analyses of tourmalinite were completed. It was also hoped that whole-rock geochemistry

would distinguish between Type 1 and Type 2 tourmalinite and could indicate whether the latter was a remobilisation product of the former. The results are listed in Table 7/6.1 where the variable SiO<sub>2</sub> concentrations (50-61 wt%) and very high B<sub>2</sub>O<sub>3</sub> contents are evident. The geochemical association B-F-W-Sn is of note, but no tin or fluorine phases were identified in thin section. Scheelite is a common accessory mineral in the tourmalinites on Ohere and accounts for the anomalous tungsten contents. The tourmalinites from Ohere are slightly anomalous in arsenic. There is no systematic variation in major element contents between Type 1 and Type 2 tourmalinites. Petrographic work also failed to distinguish between the two types of tourmalinite. It is therefore considered unlikely that the transgressive tourmalinite is a remobilisation product of stratiform tourmalinite mineralisation. Plimer (1988) is the only person to have published geochemical analyses for tourmalinites with which the Ohere data can be compared (Table 7/6.1). The Australian tourmalinites come from lower/lower-middle Proterozoic assemblages and are intimately associated with iron formations and base metal sulphide mineralisation. An exhalative origin for these tourmalinites is envisaged by Plimer (1988). The Australian examples are more siliceous (> 72 wt% SiO<sub>2</sub>) and contain less than a third B<sub>2</sub>O<sub>3</sub> of the Ohere tourmalinites. The significance of this is discussed below. Gold concentrations in the tourmalinites examined on Ohere are below the LLD. Elsewhere in the CZ, for example on Sandamap (northwest corner of Map 4) and on Hakskeen (Fig. 1-3), auriferous tourmalinites with minor As-Bi mineralisation are developed.

#### 7.6.7 Genesis of the tourmalinites

##### 7.6.7.1 Timing of tourmalinisation

The majority of the tourmalinite is oriented parallel to the S<sub>2</sub> foliation and is only stratiform in the core of the fold. Moreover, in thin section many of the tourmaline prisms can be seen to lie in the plane of the S<sub>2</sub> schistosity. Type 2 tourmalinite formation clearly postdated the initiation of the S<sub>2</sub> fabric-forming event. The confinement of crosscutting tourmalinites to kink bands suggests that zones of relatively competent tourmalinised schist acted as "structural resisters" during the final stages of F<sub>2</sub> fold formation. Thus tourmalinisation occurred before the end of F<sub>2</sub> folding. The field and geochemical evidence show that Type 2 tourmalinites are not remobilisation products of Type 1 tourmalinites. Various models for the origin of the tourmalinites are reviewed below.

##### 7.6.7.2 Exhalative/diagenetic model

The first question that must be answered is whether some of the tourmalinites could have been derived from a syn-sedimentary concentration of boron. The Type 2 and Type 3 tourmalinites can be excluded from this discussion. Type 1 tourmalinites exhibit many of the sedimentary structures that are so characteristic of turbidites (Badenhorst, 1988a). As far as the author is aware, the tourmaline only occupies the position of the clay-sized material, that is at the top of the fining-upward cycles; Exhalative tourmalinites from

	X <sup>α</sup>	X <sup>β</sup>	R	k	e	Change	Transfer
						V/D(X <sup>β</sup> )-X <sup>α</sup>	μmol g <sup>-1</sup>
Si	.288	.267	1.079	1.015	k*	-	-
Ti	.00516	.00528	.977	.92	n	-	-
Al	.0913	.0973	.938	.883	i	+ .0131	+486
Fe	.0462	.0364	1.269	1.194	r	-.0071	-128
Mn	.00047	.00031	1.516	1.427	n	-	-
Mg	.0188	.0265	.709	.668	i	+ .0096	+396
Ca	.00193	.00629	.307	.289	i	+ .0048	+120
Na	.00408	.00683	.597	.562	i	+ .0033	+141
K	.0457	.00025	182.80	172.01	r	-.0454	-1162
P	.00061	.00057	1.070	1.007	n	-	-
H	.00341	.0006	5.68	5.35	r	-.0028	-2766
C	.00284	.0155	.183	.172	i	+ .0138	+1149
B	.00016	.01832	.0087	.008	i	+ .0195	+1803
F	.00078	.00238	.328	.308	i	+ .0018	+93
S	.00036	.00064	.563	.529	i	+ .0003	+10
Rb	.00028	.000001	280.0	263.5	r	-.0003	-3
Ba	.00076	.00006	12.67	11.92	r	-.0007	-5
Sr	.00004	.00017	.235	.221	i	+ .0001	+2
Zr	.00019	.00019	1.00	.941	q*	-	-
V	.00016	.00021	.762	.717	i	+ .0001	+1
Cr	.00012	.00013	.923	.867	n	-	-
Zn	.00011	.00009	1.222	1.15	n	-	-

**Table 7/6.3:** Boron metasomatism: mass balance calculation

α = parent (unaltered) rock, i.e. schist; β = product (altered) rock, i.e. tourmalinite;

d<sup>α</sup> = average density of schist = 2.71; d<sup>β</sup> = average density of tourmalinite = 2.88;

D = density ratio, d<sup>α</sup>/d<sup>β</sup> = 0.941;

X<sup>α</sup> = mass fraction of element in schist; X<sup>β</sup> = mass fraction of element in tourmalinite;

R = concentration ratio X<sup>α</sup>/X<sup>β</sup>;

k = density corrected concentration ratio = product RD;

k\* = selected uniform k value = 1.01;

e = element classification: q\* = stationary, i = introduced, r = removed, n = indeterminate;

V = volume change, i.e. volume of product relative to parent = 1.01

the Golden Dyke Dome Broken Hill commonly have tourmaline-rich bases (Plimer, 1986, 1988). Badenhorst (1988a) described the presence of rip-up clasts of tourmalinite in tourmalinite, but has not documented the presence of rip-up clasts of tourmalinite in a tourmaline-free matrix similar to those from Broken Hill (Slack *et al.*, 1984). This is an important point because, if the Ohere tourmalinites have resulted from large-scale metasomatism, the rip-up clasts may well have been tourmalinised after sedimentation. A further point of note is that the Ohere tourmalinites do not have the thin laminations characteristic of exhalites. Finely laminated transitional rock types between schist without tourmaline and massive tourmalinite are not present on Ohere. If one accepts that Type 1 tourmalinites are exhalative or diagenetic in origin, the strong structural control on their localisation requires an explanation. A further major problem with accepting that any of the tourmalinites on Ohere are chemical sediments derived from exhalative fluids is that they are essentially hosted by (not just associated with) turbidites, which by definition were deposited in a high energy submarine environment.

These two processes generally do not operate at the same time.

#### 7.6.7.3 Replacement model

The evidence for a selective replacement (epigenetic) origin for the tourmalinite mineralisation on Ohere is overwhelming. The structural evidence indicates that tourmalinitisation occurred syn-S<sub>2</sub> formation, contemporaneous with the intrusion of the leucogranite. Several hand specimens on the margins of kink bands exhibit evidence of the replacement of schist by a boron front (see also Badenhorst, 1988a; Fig. 6).

##### 7.6.7.3.1 Boron metasomatism on Ohere: mass balance calculation

The replacement of Qtz+Bt+PlagKfs schists by Qtz+Tur assemblages (tourmalinites) on Ohere invites comparison with similar rocks elsewhere. Boron metasomatism in quartz-mica schists on the margins of pegmatite in South Dakota has been investigated by Shearer *et al.* (1984). The breakdown of

feldspar and biotite by “alkali leaching” during boron metasomatism resulted in the formation of tourmaline+quartz assemblages whose modal compositions are similar to the Ohere tourmalinites. Kretz *et al.* (1989) are the only authors to have conducted mass balance calculations (MBC) on tourmaline alteration zones on the margins of pegmatites in the Yellowknife Supergroup, Canada: the MBC shown below follows the methods and uses the same symbols as these authors (*op. cit.*, Table 1). The average of three analyses of Kuiseb Formation schist from the immediate vicinity of the tourmalinites (Table 2.26; NS218, NS219, NS220) was normalised to 100 (Table 7/6.2). The average modal percentage tourmaline in the three schists was 0.5 vol%. Thus the B<sub>2</sub>O<sub>3</sub> content of the schists was estimated at 0.05 wt% because the B<sub>2</sub>O<sub>3</sub> content of tourmaline is -10 wt% (Deer *et al.*, 1966). Six analyses of Type 1 and Type 2 tourmalinite (Table 7/6.1; NS225-230) were averaged and normalised. The gains and losses in wt% or ppm that occurred during tourmalinisation of the schist are shown in Table 7/6.2. Mass fractions of the elements were calculated and are listed in Table 7/6.3. Average densities for the schist and tourmalinite were determined by measuring the displacement in water of samples of known weight. There is no field evidence to suggest that replacement was not a “constant-volume” process (*i.e.* V=1). However, a value for V of 1.0 I was selected after examining the k values as suggested by Kretz *et al.* (1989). The calculation (Table 7/6.3) reveals that the elements Si and Zr remained stationary during boron metasomatism, there was a net introduction of the elements B, C, Al, Mg, Na, Ca, F, S, Sr and V and a net loss of the elements H, K, Fe, Ba and Rb: it is not possible to comment on the behaviour of Ti, Mn, P, Cr and Zn. Slightly different elements were introduced and removed at Ohere than reported in South Dakota (introduction of B, Na, Fe, Al, removal of K, Si, Rb, Li, Ba) and Yellowknife (introduction of B, H, Ca, Zn, removal of K, Na, Fe, Rb, Sr and Ba), but the style of the alteration, namely massive introduction of boron and significant removal of potassium, was similar. Moreover, the amount of transfer of elements (in  $\mu\text{mol g}^{-1}$ ) during the tourmalinisation on Ohere was not too dissimilar from the quantities recorded by Kretz *et al.* 1989: average removal of 406  $\mu\text{mol g}^{-1}$  of potassium and an average introduction of 1090  $\mu\text{mol g}^{-1}$  of boron. This suggests a fluid of similar composition was responsible for the two processes. The potassium discrepancy is accounted for by the lower K<sub>2</sub>O content of the Yellowknife schists which contain less than 3.7 wt% K<sub>2</sub>O. The discrepancy in the transfer of boron is believed to result from the fact that the metasomatism recorded by Kretz *et al.* (1989) occurred on the lateral margins of a pegmatite; tourmalinisation on Ohere was most probably caused by a fluid derived from a granitic or pegmatitic melt, but at the apex of the system.

#### 7.6.7.3.2 Source of the boron fluid

That some sedimentary rocks such as fine-grained marine clays are a major reservoir of boron is well documented (Wedepohl, 1978). Boron is commonly absorbed onto clay minerals; illite may contain up to 2000 ppm boron (Harder, 1959). The Kuiseb Formation in NCZe is estimated to be at

least 4 kilometres thick (Map 1) and was almost certainly a major reservoir of boron. Evidence for this is provided by the fact that tourmaline, the major reservoir of boron in metamorphic rocks, is a widespread accessory in the pelitic schists of the Kuiseb Formation in the CZ (Chapter 2) and the NZ (Miller, 1980). On Ohere, tourmaline is a common accessory in the greenschist-facies phyllites, indicating that the mineral was stable at less than 400°C (Fig. 5-4). On Sandamap Noord, tourmaline comprises up to two volume per cent of the amphibolite-facies schists in areas well away from the nearest exposed granite or pegmatite.

These observations confirm the fact that tourmaline has a wide stability range during metamorphism and may be stable in the granulite facies (Werdning and Schreyer, 1984). Thus, although prograde metamorphism resulted in the release of a considerable volume of H<sub>2</sub>O (average Ohere phyllite/schist has 3 wt% H<sub>2</sub>O, average Sandamap Noord schist has 1.4 wt% H<sub>2</sub>O; Tables 2.24 and 2.26), tourmaline did not break down to release boron into the “significant quantities of aqueous fluid” that accompany regional metamorphism (Symmes and Ferry, 1991). Instead, the major cause of tourmalinisation on Ohere appears to be a fluid derived from a granitic or pegmatitic melt. The mass balance calculation has revealed the similarities between boron metasomatism on Ohere and on the margins of pegmatites in North America. Investigation of the metamorphic aureoles surrounding the granitic intrusions on Ohere (Chapter 5) show that the peak regional metamorphic conditions were only of greenschist facies grade. Thus the bulk of dehydration reactions, that is basin dewatering, occurred at the time of, and as a result of, granite intrusion. Metamorphic fluids may well have mixed with a hydrothermal phase derived from the leucogranite and were then channelised into S<sub>2</sub> structures. It would seem unlikely in these circumstances that the metasomatising fluid was exclusively magmatic in origin. The contribution of metamorphic fluids in tourmalinisation processes has been recognised elsewhere. Decimetre-thick tourmalinites that formed during regional metamorphism have been described by Abraham *et al.* (1972). These authors noted a depletion of potassium in the tourmaline-rich layers which resulted from tourmalinisation of the phyllosilicates. Moreover, the role of metamorphic fluids in mineralising processes has been emphasised by Maiden (1981) who noted that tin and tungsten could be mobilised without the metals having entered the magma phase.

#### 7.6.7.3.3 Tourmalinisation and stanniferous pegmatites

Boron enrichment is not confined to the tourmalinites on Ohere. Apart from the large number of quartz-tourmaline veins oriented parallel to the S<sub>2</sub> foliation, there are several randomly oriented crosscutting tourmaline veins which may be related to the pegmatites in the area. Furthermore, some tourmalinisation is developed on the margins of pegmatite intrusions (Grid 6), but the alteration seldom persists laterally for a distance of more than several tens of centimetres into the enclosing schist. The two-dimensional exposure precludes an assessment as to whether the tourmalinisa-

tion extends vertically. Tourmalinisation on the margins of stanniferous pegmatites can also be observed at the Kohero Tin Mine (Map 1) and has been reported from the Uis Tin Mine (Richards, 1986). It is possible that fluids streaming off deep-seated pegmatite intrusions led to the development of proximal Type 3 tourmalinites and more distal Type 2s and Type 1s. Thus the tourmalinites on Ohere may have resulted from large-scale tourmalinisation of the Kuiseb Formation at the apex of a pegmatite system. Higher structural levels of the Nainais-Kohero tin belt where metasediments predominate over pegmatites are exposed on Ohere, Ohere Oos and Gross Okandjou. At the southwestern end of the tin belt (Fig. 7.1) stanniferous intrusions are larger and more numerous at the presently exposed level suggesting that either the intrusions have migrated further from their source area (as a result of a higher geothermal gradient during the orogeny?) or a higher degree of uplift in the Nainais area. The main problem with accepting that large-scale tourmalinisation of the Kuiseb Formation is related to the pegmatites is the evidence suggesting that the tourmalinising event occurred before the end of  $F_2$  folding. Although it has obviously not been possible to date every stanniferous pegmatite, it is widely accepted that they are late-/post-tectonic in age (Miller, 1983a and Chapter 6). Pegmatite intrusion occurred considerably after the formation of the  $F_2$  folds.

#### 7.6.8 Conclusion

Metamorphism of a clay with a maximum boron content of 2000 ppm (Harder, 1959) could produce an Al-silicate/feldspar-quartz-tourmaline rock with a maximum of 4 volume per cent tourmaline (Plimer, 1988). Thus an alternative explanation is required for the origin of tourmalinites in the Kuiseb Formation, some of which contain in excess of 50 volume per cent tourmaline. At most occurrences in central Namibia, the tourmalinites are conformable with the enclosing mica-defined schistosity and have a stratiform nature. Because of poor exposure, the tectonic history and the age of the mica fabric can rarely be determined with confidence. The tourmalinites on Ohere in contrast are some of the best exposed in the CZ and relationships with the enclosing rocks can clearly be seen. These tourmalinites do not have the thin laminations that are characteristic of exhalites. An exhalative model cannot explain the essentially transgressive nature of the tourmalinites. There is no field evidence for shearing or remobilisation of the Ohere tourmalinites, though the Type 2 and Type 3 tourmalinites are closely related on Grid 2. Type I and Type 2 tourmalinites cannot be distinguished by geochemical means, which would be surprising if the transgressive portions represented remobilised portions of stratiform exhalative horizons. As far as can be ascertained, the tourmalinites on Ohere are not associated with mafic volcanic rocks, banded iron formations or massive sulphide mineralisation. The tourmalinites are certainly not associated with evaporites, another environment of deposition that has been proposed for this rock type (Behr *et al.*, 1983; Slack *et al.*, 1984).

A replacement model can adequately explain the development of the tourmalinite mineralisation on Ohere 106. Lo-

cal tourmalinisation of the schist was undoubtedly caused by pegmatitic intrusions. However, the bulk of the tourmalinites on Ohere are believed to have formed by the selective replacement of schist and metaturbidite by boron-rich fluids derived from the Ohere leucogranite. These fluids, which probably interacted with the Kuiseb Formation metasediments, caused channelised boron metasomatism of the schist in  $S_2$  structures. Boron partitions preferentially into the vapour phase of crystallising granites (Pichavant and Manning, 1984) and is commonly involved in post-magmatic hydrothermal processes (Benard *et al.*, 1985). There is a worldwide association between tourmaline and tin and, to a lesser extent tungsten, in greisens and altered granitic rocks (Plimer, 1980). Although the Ohere leucogranite does not have the specialised geochemical or mineralogical characteristics of the mineralised tourmaline and topaz granites (Pichavant and Manning, 1984), this may partly be a result of the deep erosion. Compared to other Damaran granites the Ohere leucogranite is highly fractionated (Table 3.7), in common with most granites associated with Sn-W mineralisation (Plimer, 1980). Interestingly, the element sodium is preferentially leached from granitic melts that coexist with  $B_2O_3$  vapour phases (Pichavant, 1981): this could explain the somewhat surprising introduction of Na during the feldspar breakdown that accompanied boron metasomatism (Table 7/6.3). Tourmalinites are localised in the core of  $F_2$  folds elsewhere in the CZ. Approximately one kilometre southwest of the Sandamap Tin Mine (Map 3) stratiform and crosscutting tourmalinites have been mapped in the hinge zone of an  $F_2$  fold (see Steven, 1992 for a map of the tourmalinisation on Sandamap Noord).

### 7.7 SCHEELITE-VESUVIANITE SKARNOID ROCKS IN THE KUISEB FORMATION ON OHERE

#### 7.7.1 Introduction

Scheelite-vesuvianite-garnet rocks in the Kuiseb Formation were first discovered on the farm Ohere 106 (Map 1) during a regional exploration programme in early 1985. Similar lithologies were noted at the same stratigraphic level during the course of field work on Sandamap Noord (Map 3). The presence of stratiform regional skarns or skarnoid (as defined by Einaudi and Burt, 1982) rocks that on first inspection are apparently unrelated to the granitic plutons in the area is of interest because this assemblage is atypical of the Kuiseb Formation. Barnes (1983) has described similar stratabound tungsten mineralisation from a number of localities in the vicinity of Broken Hill, Australia. Moreover, Plimer (1983) has suggested that such lithologies represent the distal equivalent of exhalative massive sulphide mineralisation. On a visit to Ohere 106, Slack (1987, pers. comm.) commented on the similarities between the scheelite-vesuvianite skarnoid rocks and Corruga-type scheelite mineralisation in the Broken Hill district (Barnes, 1983). The present work concentrates on describing the mineralisation and discussing its origin.

<b>Type Locality</b>	<b>Ohere 106 and Ehuuro 120, Omaruru District</b>
<b>Host Formation</b>	<b>Upper Kuiseb</b>
<b>Regional Geological Setting</b>	<b>North-east end of Nainais-Kohero tin belt graben</b>
<b>Form of Mineralisation</b>	<b>Disseminated scheelite in skarnoid/calc-silicate rocks</b>
<b>Associated Volcanics</b>	<b>None identified</b>
<b>Structural Features</b>	<b>Associated calc-silicate rocks may have spindle-shaped geometry with long axes parallel to F<sub>2</sub> folds</b>
<b>Peak Metamorphic Facies</b>	<b>Greenschist-amphibolite</b>
<b>Damaran Intrusions</b>	<b>Salem granite, leucogranite, cassiterite-bearing pegmatites</b>
<b>Age of Mineralisation</b>	<b>Damara</b>
<b>Geochemical Association</b>	<b>W-Sn-F-Zn(-Bi)</b>
<b>Ore Minerals</b>	<b>Scheelite, traces of pyrrhotite, pyrite, chalcopyrite and stanniferous rutile</b>
<b>Silicate Minerals</b>	<b>Vesuvianite, quartz, garnet, pyroxene, clinozoisite and plagioclase</b>
<b>Associated Alteration</b>	<b>Pyritic calc-silicate rocks, tourmalinites and tourmalinised metasediments</b>
<b>Classification</b>	<b>Synsedimentary/metamorphogenic concentration of tungsten in a skarnoid</b>
<b>Comments</b>	<b>Morphologically similar to calc-silicate bearing scheelite mineralisation that may be distal equivalent of Broken Hill, Australia. Namibian examples are not metamorphosed cotecules</b>

**Table 7/7.1:** Scheelite-vesuvianite skarnoid rocks in the Kuiseb Formation

### 7.7.2 Geological setting

Scheelite-bearing skarnoid rocks are traceable for over 30 km around the Ehuuro Salem granite and the Ohere leucogranite (Map 1). The stratigraphic unit which hosts these calc-silicate lithologies is locally up to 2 km thick, but has been duplicated by isoclinal folding. A complex deformational history has obscured the stratigraphy in the Nainais-Kohero tin belt, but on Ohere these calcareous lithologies are underlain by nondescript quartz-biotite schist and overlain by turbidites in the upper Kuiseb Formation (Map 2). The vesuvianite skarnoid rocks are developed at the same stratigraphic level as calcitic marble, scheelite-bearing garnetiferous calc-silicate granofels and garnetiferous chert-like rocks (Table 7/7.1). The associated calc-silicate rocks host finely disseminated sulphide mineralisation such as pyrite, pyrrhotite and chalcopyrite. Thus during upper Kuiseb times there was a not insignificant period of chemical sedimentation. In certain areas, for example on Ohere, there is a spatial association between vesuvianite skarnoid rocks and tourmalinites, which, in 1985, was regarded as particularly interesting in the light of Plimer's (1983) work. The grade of metamorphism in this part of the tin belt was greenschist/lower amphibolite facies, but was of upper am-

phibolite grade in the aureoles of granitoids.

### 7.7.3 Characteristics of vesuvianite skarnoid rocks

The term skarnoid was chosen for the vesuvianite rocks because of their coarse-grained calc-silicate gangue which is so characteristic of skarns, but the lack of metasomatically altered marble and the apparent absence of any direct genetic relationship with granitic plutons. In short, they are regional metamorphic rocks with a skarn-like mineral assemblage. After a night survey with a hand-held ultra-violet lamp, four areas on Ohere were selected for detailed mapping (Map 2, Grids 7 to 10). The vesuvianite rocks occur as poorly layered to massive, discontinuous lenses up to 12 metres wide and several hundreds of metres long. The horizons form prominent outcrops and can be traced at the same stratigraphic level for many kilometres. In some areas the skarnoid rocks grade laterally into quartz-feldspar-diopside calc-silicate rocks (Grid 8). Elsewhere they are enclosed by thin (< 1 m) amphibolites (Grid 9; Fig. 7/7.1) which are interpreted as metamorphosed calcareous pelites (see Chapter 2). The vesuvianite skarnoid rocks are locally stained with malachite (Grid 9; Fig. 7/7.1), associated with local gossan (Grid 10) and cut by tension gashes filled with quartz (Grid

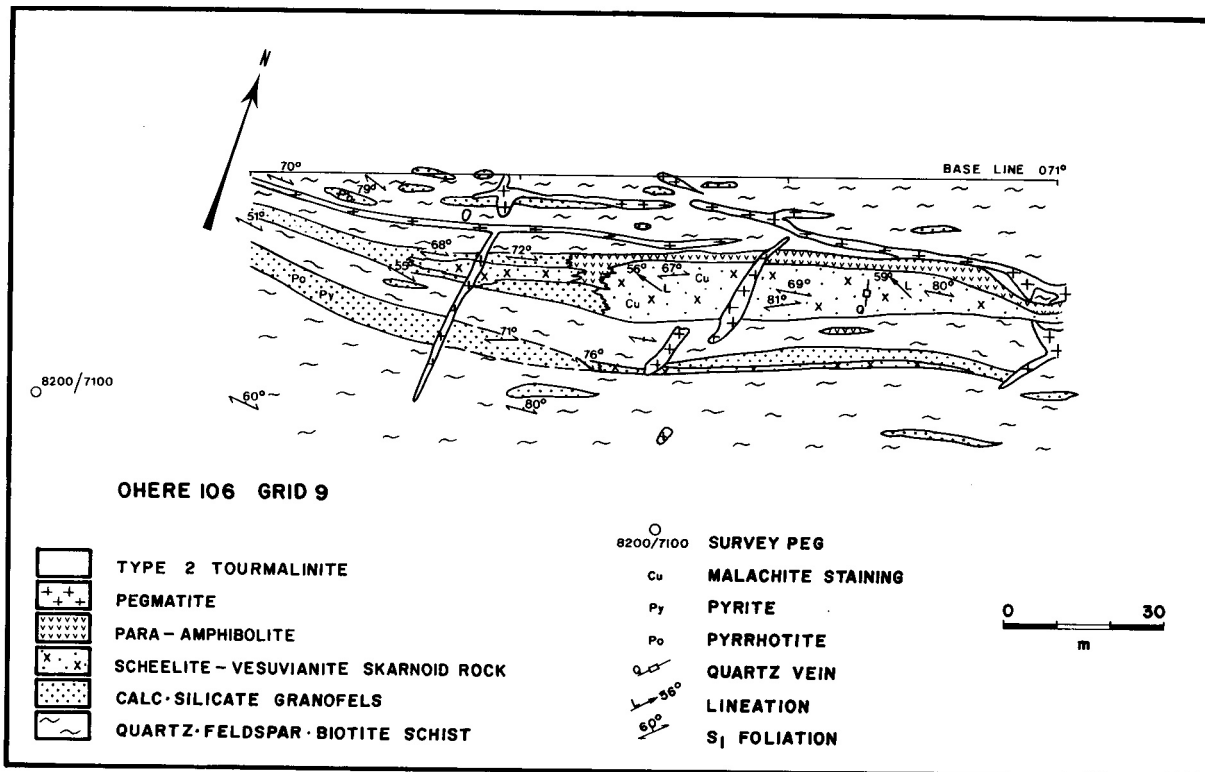


Figure 7/7.1: Geological map of scheelite-vesuvianite skarnoid rocks on Ohere 106 (grid 9)

7; Fig. 7/7.2). The scheelite, which fluoresces blue-white (indicating a low Mo content), is irregularly distributed, occurring as fine disseminations or as coarse-grained aggregates up to 2 cm in diameter.

7.7.4 Petrography of the vesuvianite skarnoid rocks

The vesuvianite skarnoid rocks on Ohere have mineral assemblages dominated by vesuvianite and quartz which together commonly comprise 80 modal per cent. Other major minerals are diopsidic pyroxene (10-50%) and garnet (0-20%); minor minerals (<5% modal per cent) are clinozoisite,

plagioclase and traces of sphene, scapolite, scheelite, sericite, epidote and iron oxides. The ore minerals that have been identified are traces of pyrite, pyrrhotite and chalcopyrite. The vesuvianite skarnoid rocks do not exhibit a lateral mineralogical zonation or facies development, unlike the skarns at Otjua. The skarnoid is characterised by a rather chaotic inequigranular texture that is dominated by prismatic (up to 5 cm) or poikiloblastic vesuvianite and granular aggregates of strained quartz. The vesuvianite may also be anhedral and is commonly in contact with anhedral/subhedral garnet. Vesuvianite has numerous inclusions most notably interstitial calcite and subhedral clinozoisite (with distinctive anomalous

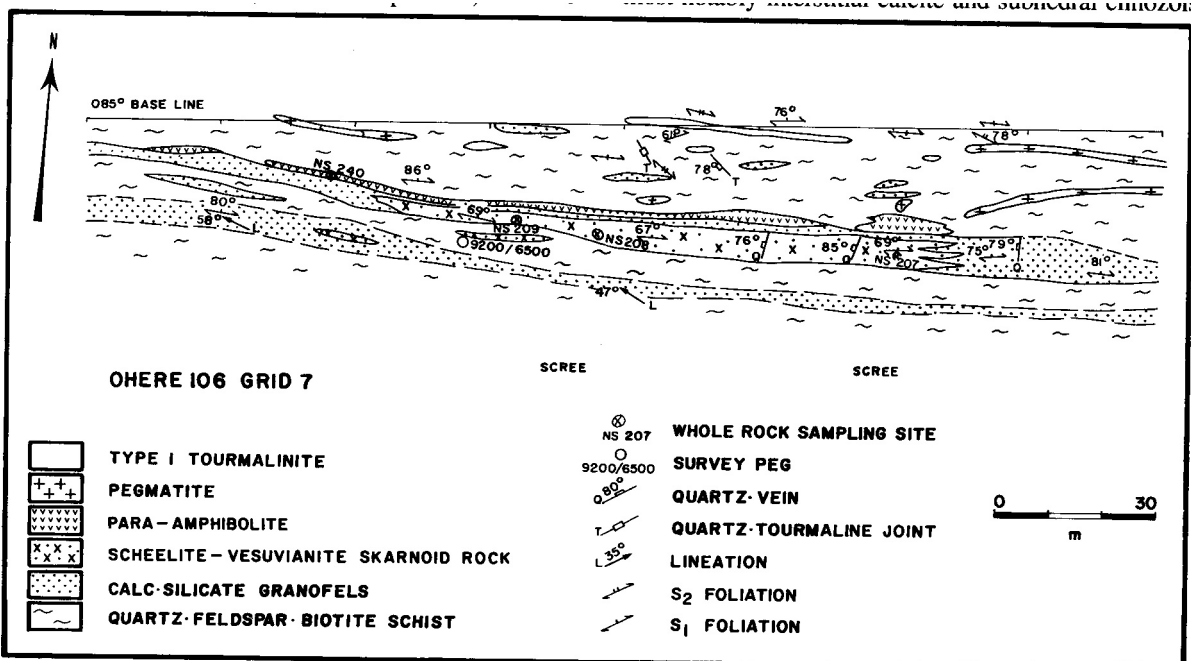


Figure 7/7.2: Geological map of scheelite-vesuvianite skarnoid rocks on Ohere 106 (grid 7)

	NS207	NS208	NS209	NS210	NS211	NS212	A	B
SiO <sub>2</sub> (wt%)	60.26	65.58	54.02	45.75	50.43	47.81	48.83	63.75
TiO <sub>2</sub>	.64	.57	.51	.63	.41	.36	.99	1.10
Al <sub>2</sub> O <sub>3</sub>	8.24	10.14	12.01	13.44	13.33	14.23	19.77	18.67
Fe <sub>2</sub> O <sub>3</sub>	.71	.29	.00	.00	4.41	.66	.47	.47
FeO	4.47	3.51	5.88	4.59	3.05	6.71	.70	.54
MnO	.46	.30	1.46	.58	1.54	1.34	24.63	8.32
MgO	1.58	1.31	.88	1.05	1.13	1.83	.72	.61
CaO	19.83	15.73	21.25	29.11	23.21	24.41	.54	.62
Na <sub>2</sub> O	.07	.40	.31	.04	.21	.25	.36	1.42
K <sub>2</sub> O	.00	.30	.03	.00	.09	.04	1.12	1.75
P <sub>2</sub> O <sub>5</sub>	.14	.13	.09	.17	.11	.35	.08	.29
H <sub>2</sub> O-	.13	.10	.14	.07	.07	.08	As	H <sub>2</sub> O+
H <sub>2</sub> O+	.23	.49	.41	.21	.43	.22	1.13	2.12
CO <sub>2</sub>	1.30	1.92	2.78	2.09	1.70	2.06	<.04	.00
TOTAL	98.07	100.76	99.77	97.73	100.12	100.34	99.38	99.66
F (ppm)	7440	6200	9800	9000	4600	3700		
S	935	163	1392	81	98	33		
Rb	<.9	24	2	<.9	10	4		
Ba	<3.5	52	9	<3.3	6	19		
Sr	104	238	70	99	96	125		
Th	19	15	4	35	13	12		
U	3	3	<1.8	<1.8	3	<1.9		
Zr	206	185	121	106	103	117		
Nb	6	8	21	2	6	8		
Mo	<.6	<.6	<.6	1	24	.7		
Sn	383	272	717	268	221	234		
W	19	14	7	1387	1419	62		
V	35	45	110	44	72	101		
Cr	54	65	32	35	39	49		
Co	8	7	5	5	7	9		
Ni	15	18	6	11	12	21		
Cu	11	8	20	<1.6	<1.7	<1.7		
Zn	730	315	295	266	280	380		
Ga	12	13	19	30	38	39		
Pb	11	16	13	7	<2.8	6		
Ge	6	3	27	19	30	28		
As	24	20	3	35	14	7		
Sb	5	3	<1.5	7	2	<1.6		
Bi	30	21	4	112	26	16		
Se	<1.0	<.9	<1.0	<1.1	<1.1	<1.1		
Te	<2.4	<2.2	<2.5	<2.5	<2.6	<2.6		
Sc	9	9	9	6	9	12		
Y	29	41	31	33	23	27		
La	31	35	7	31	24	12		
Ce	57	68	15	70	48	18		
Nd	32	40	13	40	27	14		
Au (ppb)	<5	<5	<5	<5	<5	8		

Table 7/7.2: Whole-rock analyses of scheelite-vesuvianite rocks and cotiules from Ohere 106, Omaruru District

NS207: Grid 7

NS208: Grid 7

NS209: Grid 7

NS210: Grid 10

NS211: Grid 10

NS212: Grid 10

A: Metamorphosed cotiule from Stavelot massif, Belgium (Lamens *et al.*, 1986)B: Metamorphosed cotiule from Stavelot Massif, Belgium (Lamens *et al.*, 1986)

blue interference colours). Both minerals appear to be minor breakdown products of vesuvianite. Clinopyroxene is present as small (< 0.4 mm) rounded grains or an anhedral granular mass. The pale colour and strong pleochroism of the sphene indicate that it is a low-iron variety. Plagioclase feldspar is extensively altered to sericite. The fine-grained scheelite is locally euhedral. Electron microprobe analysis of small (< 50 µm) reddish-brown inclusions (grey with moderate reflectance in reflected light) in sphene revealed the presence of stanniferous rutile and an unidentified zirconian titanium mineral. No sphalerite, gahnite or cassiterite has been positively identified.

#### 7.7.5 Geochemistry

Six whole-rock analyses of vesuvianite skarnoid are given in Table 7/7.2. The scheelite-vesuvianite rocks have very low alkali contents and are less siliceous (45.8-65.6 wt% SiO<sub>2</sub>) and more calcareous (15.7-29.1 wt% CaO) than the associated calc-silicate rocks (58-72.7 wt% SiO<sub>2</sub>, 6.6-15.8 wt% CaO; Table 2.31). MgO concentrations in the vesuvianite skarnoid rocks (0.9-1.8 wt%) are lower than those of the calc-silicate rocks (1.5-2.5 wt%). The scheelite-vesuvianite rocks have anomalous contents of F, Sn, W, Zn and Bi. The fluorine is located in vesuvianite which locally has 2 wt% F. A soil geochemistry survey conducted by a mining company revealed a coincidence between copper and tungsten anomalies in the vicinity of some vesuvianite skarnoid rocks. Although minor chalcopyrite was noted in some polished sections, the bulk rock analyses reveal that copper contents are generally less than 20 ppm (Table 7/7.2). Disseminated chalcopyrite mineralisation and anomalous copper contents are a feature of the associated calc-silicate rocks (Table 2.31). The data base is too small to determine whether tungsten concentrations correlate with other components. Scheelite mineralisation is known to be patchy and irregularly distributed, though concentrations locally exceed several wt% WO<sub>3</sub>. Only one sample has a gold concentration above the LLD.

#### 7.7.6 Discussion

It was initially thought that the scheelite-vesuvianite rocks with their substantial proportion of garnet might be a type of coticule rock. Coticule is a fine-grained metasedimentary rock consisting of quartz and manganiferous garnet (Bates and Jackson, 1987) for which volcanoclastic and volcanic exhalative origins have recently been proposed (Kramm, 1976; Lamens *et al.*, 1986). The lithology has been described from the vicinity of exhalative mineralisation such as Broken Hill (Plimer, 1988). The characteristic features of coticule rocks are a very fine grain size, a very fine laminated structure and high Mn concentrations. Two analyses of lower Ordovician coticules from Belgium (Lamens *et al.*, 1986) are given in Table 7/7.2. The vesuvianite skarnoid rocks on Ohere clearly do not exhibit either the morphological nor the geochemical characteristics of coticule rocks. No manganese phase such as piemontite has been identified in the skarnoid. Moreover, the Mn contents of the vesuvianite rocks and associated calc-silicate litholo-

gies on Ohere are only slightly more than the average values for deep-sea sediments quoted by Turekian and Wedepohl (1961). The Ba concentrations of the calcareous lithologies on Ohere are considerably lower than the Ba contents for marine sediments listed by these authors. There is therefore no evidence for an exhalative or volcanic exhalative origin for the vesuvianite rocks on Ohere.

The second alternative considered was a metamorphogenic model. Vesuvianite is found both as a contact metasomatic and a regional metamorphic mineral in metamorphosed limestones and marls (Deer *et al.*, 1982) and has a very large stability range (Winkler, 1976) from greenschist to granulite facies grade (Hochella *et al.*, 1982). The mineral is chemically and structurally closely related to grossular garnet 'and the controlling factor as to which mineral will actually crystallise may be related to the presence or absence of fluorine or other volatile constituents' (Deer *et al.*, 1982). Vesuvianite from the Ohere skarnoid contains up to 2 wt% F and has a composition similar to the vesuvianites at Otjua (Steven, 1987). However, there is no evidence for the metasomatic replacement of a carbonate unit by infiltrational metasomatism such as at Otjua. The evidence suggests that the calc-silicate rocks on Ohere, and indeed throughout the upper Kuiseb Formation, are calcareous sediments that formed at the same time as the laterally impersistent thin marbles. The close spatial association between these lithologies suggests that the vesuvianite rocks are a metamorphosed calcareous sediment. The scheelite-vesuvianite rocks in NCZe are considered to be a type of metamorphogenic skarn whose development is related to the Buchan-style metamorphism that affected the area. It is envisaged that metamorphic fluids from the surrounding schist and to a lesser extent from the calc-silicate lithologies were mobilised during this thermal metamorphism resulting in the local skarnification of calcareous metasediments and calc-silicate rocks. This is to a certain extent supported by the work of Hochella *et al.* (1982) who indicated that the growth and stability of vesuvianite require a fluid phase with a very high H<sub>2</sub>O.

#### 7.7.7 Conclusion

The scheelite-vesuvianite rocks of the upper Kuiseb Formation represent a significant stratiform tungsten reserve that bears certain similarities with the scheelite-bearing bedded calc-silicate lithologies of the Broken Hill district (Barnes, 1983). However, the presence of only very minor accompanying amphibolites, derived from impure calcareous sediments, indicates that they are different from Coruga-style mineralisation. Moreover, the vesuvianite rocks are not associated with iron formations, manganiferous cherts or mafic volcanic rocks. There is little evidence for the existence of volcanic exhalative processes during upper Kuiseb times. The vesuvianite rocks are thought to be regional metamorphogenic skarns whose formation was related to the Buchan-style metamorphism associated with the granitoid intrusions. Because of the influence of the large number of granitic plutons, it has not been possible to determine whether the skarn-forming process was the re-

sult of regional metamorphism alone. Unlike Otjua, skarn formation occurred primarily as the result of the redistribution of volatiles (F, H<sub>2</sub>O, CO<sub>2</sub>) and was not accompanied by large-scale infiltrational metasomatism.

For some reason that is not entirely clear, the calc-silicate lithologies and vesuvianite skarnoid rocks in the Nainais-Kohero tin belt possess finely disseminated scheelite mineralisation. There is no tungsten mineralisation in the enclosing schists nor, with the possible exception of the structurally controlled tourmalinites, has scheelite been remobilised into structural traps. The tungsten may have been in the calcareous lithologies since diagenesis or the metal (or possibly scheelite) may have been mobilised and precipitated during greenschist-facies metamorphism (Foster, 1977). Plimer (1980) has described several calc-silicate-hosted scheelite occurrences within metamorphosed, thick, deep-water sequences. In many examples the stratiform tungsten deposits are associated with mafic volcanic rocks

and Plimer (1980) has invoked an exhalative origin for the mineralisation. In the NCZ there is no obvious relationship between scheelite mineralisation and exhalative processes, let alone mafic volcanism. These conclusions are of note because both the tourmalinites (for which a replacement origin is now favoured) and the scheelite-bearing calc-silicate lithologies of the NCZ have superficial characteristics in common with supposedly exhalative mineralisation at Broken Hill. A detailed re-examination of the two styles of mineralisation on Ohere has shown that epigenetic processes involving magmatic and metamorphic fluids derived from granitoids and basin dewatering are more tenable. The pelite-dominated Kuiseb Formation in NCZe is at least 4000 metres thick and 9800 metres thick in the NZ (Miller, 1980). Basin dewatering processes that occurred as the result of compaction, tectonism and Buchan-type metamorphism would have produced large volumes of fluid that must also be taken into consideration.



## 8. SYNTHESIS

### 8.1 CENTRAL ZONE MINERALISATION IN THE LIGHT OF GEODYNAMIC CONSIDERATIONS

Various geodynamic models have been proposed for the evolution of the intracratonic branch of the Damara Orogen. These range from ensialic orogenic evolution in an aulacogen (Martin and Porada, 1977) to ensialic development followed by subduction as a result of delamination of the lower crust (Kröner, 1982) to the development of an intracratonic basin behind a zone of subduction in South America (Hawkesworth *et al.*, 1986). More mobilist models envisage plate-tectonic evolution with development and closure of a narrow ocean analogous to the Red Sea during northward subduction of the Kalahari Craton below the Congo Craton (Miller, 1983a), or complete separation of continental plates by a wide ocean followed by continental collision and subduction (Barnes and Sawyer, 1980; Kasch, 1983a; Hoffman, 1990). Hartnady *et al.* (1985) suggested that the collision phase occurred as the result of the clockwise rotation of the Kalahari Craton relative to the Congo Craton (Fig. 8.1). More recently, Stanistreet *et al.* (1991) have explained the development of the Damara Orogen and Nama Foreland in terms of Wilson-cycle plate-tectonic history. The most contentious proposal of these authors, based on no new geochronological data, is that the Sesfontein thrust belt (Fig. 2.2) in the northern coastal branch developed syn-Central Zone D<sub>3</sub> deformation (Fig. 8.1).

Coward (1983) indicated that the development of the Sesfontein thrust belt predated deformation in the intracratonic branch. Stanistreet *et al.*'s map has however been retained for this memoir because it is the most recent synthesis of the Pan-African belts in Namibia. All authors, whether mobilist or not, however accept that the CZ represents some form of volcanic/magmatic arc and that Damaran intrusion-hosted mineralisation is confined to this tectono-stratigraphic zone. To what extent can the epigenetic, metasediment-hosted mineral occurrences examined in this memoir make a contribution to the geodynamic discussion?

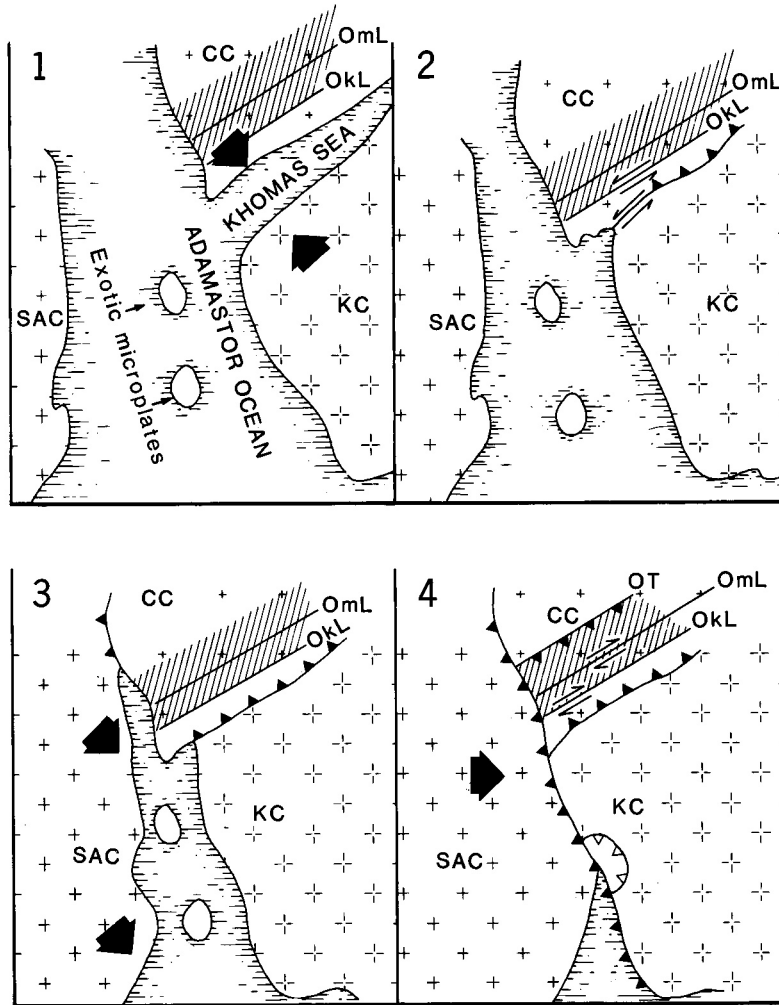
The first, and in many ways most crucial point, is that there is a paucity of epigenetic mineral deposits formed in the "orogenic phase" of the Damara Orogen (Martin, 1978) in spite of the large volumes of granites and pegmatites. There is an almost complete lack of intrusion-hosted base and precious metal mineralisation with the exception of uranium and tin. Metallic sulphide mineralisation, either within an intrusion or within contact metasomatic deposits or the aureoles of intrusions, is rare in the CZ, in spite of excellent exposure and a long prospecting history. In almost all of the examples a late-tectonic, highly fractionated granite or pegmatite is considered to be responsible for the development of the mineralisation, though in many cases the source of the metals may well have been the Damaran metasediments. The geochemical signature of the intrusion-related deposits is ensialic, i.e. sulphur poor. Moreover, where present, the amount of epigenetic mineralisation is small in comparison to that present in active continental margin batholiths. For example, the largest tungsten skarn deposit discovered to date in the Damara

Sequence, namely Otjua, has a drill-indicated ore reserve of a few hundred thousand tons (Steven, 1987). Published ore reserves of tungsten skarns from the Circum-Pacific region are one to two orders of magnitude larger (Einaudi, *et al.*, 1981). As emphasised by Martin (1978), the rarity and small size of the deposits cannot simply be a result of the deep erosional level that is exposed: the intrusions of the CZ, being largely crustal remelts (Haack *et al.*, 1983; Hawkesworth *et al.*, 1986) are dominated by granites (*sensu stricto*) and pegmatites, not calc-alkaline intrusions.

The most intensely studied subduction - related intrusions and associated magmato-hydrothermal ore deposits are those of the Circum-Pacific region (Einaudi *et al.*, 1981; Ishihara, 1981; Titley and Beane, 1981; White *et al.*, 1981; Sillitoe, 1989; Richards *et al.*, 1991). The characteristic style of mineralisation in this tectonic setting is calc-alkaline, locally alkaline, porphyry-hosted copper, molybdenum and copper-gold mineralisation. Other mineralisation associated with continental margin orogenic belts are tungsten and base metal (Cu-Zn-Pb-Mo) sulphide skarns associated with I-type intrusions. In stark contrast, there is no copper and molybdenum porphyry mineralisation in the magmatic arc of the Damara Orogen. Andesitic volcanic rocks and their parent intrusions are absent in the CZ, at least at the tectonic level exposed at present. Stanistreet *et al.* (1991) interpreted 'pre-main deformation' I-type tonalites in the SCZ near Karibib (documented by Brandt, 1987b) as subduction - related intrusions, but these barren intrusions form only 5% of the plutonic suite. These intrusions are not present elsewhere in the CZ. The diorites and granodiorites of the Salem Suite, the only intrusions that could credibly be called calc-alkaline, have mantle (<sup>87</sup>Sr/<sup>86</sup>Sr)<sub>1</sub> ratios, but not a single Salem intrusion contains base or precious metal mineralisation. The silicate skarns and skarnoids of the CZ have a W-F±Sn±Zn signature which is more characteristic of a continental setting (Einaudi *et al.*, 1981), while molybdenite and lead-zinc skarns are unknown in central Namibia. The gold vein/skarn mineralisation in the Karibib area could be interpreted as part of a distal epithermal system related to a porphyry copper (Colley *et al.*, 1989), but there is no exposed intrusion-hosted gold mineralisation in the CZ, except for minor segregations in pegmatites. There are no precious metal deposits in the CZ that can be compared with the epithermal Au-Ag ores of North America (Berger and Henley, 1989). A regional investigation of the δ<sup>18</sup>O characteristics of granitoid intrusions of the CZ (Haack *et al.*, 1983) revealed that the sort of deep circulation of meteoric ground waters and interaction with granitic plutons described by Taylor (1977) did not occur during the Damaran orogeny (Steven, 1987).

Current thinking clearly favours a Wilson-type plate-tectonic history for the intracratonic branch of the Damara (Hoffman, 1990; Stanistreet *et al.*, 1991). This author concedes that the sedimentological and structural evidence from the Okahandja Lineament, Southern and Southern Margin Zones (Fig. 2.2) is convincing for crustal shortening across the Khomas trough as a result of continental collision (Fig. 8.1). However, the mineral deposits of the magmatic arc generated during the supposed subduction of oceanic crust have

- 1 CZ D<sub>1</sub> DEFORMATION - CLOSURE OF KHOMAS SEA
- 2 CZ D<sub>2</sub> DEFORMATION - SINISTRAL MOTION IN SCZ
- 3 CZ Early D<sub>3</sub> DEFORMATION - WIDESPREAD GRANITE INTRUSION AND DOMING
- 4 CZ Late D<sub>3</sub> /D<sub>4</sub> DEFORMATION - DEXTRAL MOTION ON OKAHANDJA AND OMARURU LINEAMENTS



CRATONIC MOVEMENTS AND CZ DEFORMATION  
(MODIFIED AFTER STANISTREET ET AL., 1991)

CC	CONGO CRATON	OkL	OKAHANDJA LINEAMENT
KC	KALAHARI CRATON	OmL	OMARURU LINEAMENT
SAC	SOUTH AMERICAN CONTINENT	OT	OTJIHORONGO THRUST
	CENTRAL ZONE (CZ)		

Figure 8.1: Cratonic movements and CZ deformation (modified after Stanistreet *et al.*, 1991)

very little in common with those in the Circum-Pacific. On the contrary, the mineral occurrences of the CZ have a strong intracratonic signature and have some characteristics in common with the Sn, W, Mo and U deposits of back-arc magmatic belts such as are developed in the Eastern Cordillera of Bolivia and the Western Tin Belt of Thailand and Burma (Mitchell and Garson, 1981). These deposits are characterised by the presence of silicic and peraluminous

granites with crustal (<sup>87</sup>Sr/<sup>86</sup>Sr) ratios. The generation of these melts was related to melting of continental crust and only indirectly to subduction of oceanic material. Thrusting is also a feature of back-arc magmatic belts (Mitchell and Garson, 1981) and intriguingly, the northern boundary of the CZ is the Otjijhorongo Thrust (Figs. 2.1 and 8.1) where partially melted biotite schist has been thrust over

greenschist facies rocks (Miller, 1980). Evidence has been presented in this memoir for post- $D_3$  thrusting elsewhere in the CZ, near the Omaruru Lineament in particular. In summary, the epigenetic and intrusion-hosted mineral deposits of the CZ provide little support for the concept of Andean-type subduction of oceanic crust during the orogeny. Partial melting of pre-Damaran crust and the mobilisation of fluids from these inliers and the Damaran metasediments played the most important role in producing the relatively small epigenetic gold, tin and tungsten deposits of the CZ.

## 8.2 REGIONAL STRUCTURAL CONTROLS ON THE LOCALISATION OF EPIGENETIC MINERALISATION IN THE CZ

One of the main reasons cited by Martin (1978) for the absence of sizeable hydrothermal deposits in the CZ was the paucity of syn- and post-tectonic faulting. Detailed work has revealed that what little epigenetic mineralisation is present is structurally controlled. Major structural breaks or lineaments are believed to have played a role in localising mineralisation in central Namibia in the manner envisaged by O'Driscoll (1986). There is clear evidence for a broad northeast/east-northeast-trending zone of crustal weakness in the rocks that floor the intracratonic branch of the orogen (Fig. 8.2). The pre-Damaran basement is transected by numerous subvertical, east-north east-trending megashears which probably extend to the base of the crust. These megashears exerted an influence on late Proterozoic dyke emplacement, Damaran rifting, sedimentation, alkaline volcanism and the localisation of hydrothermal fluids. An east-northeast-trending mafic dyke swarm intruded along these megashears at the time of early Damaran rifting and is partly responsible for the northeast/east-northeast-trending aeromagnetic grain of the Abbabis Inlier. Northeast/east-northeast-trending faults are envisaged to have been responsible for the rifting that initiated the Damaran episode. Major structures such as the Omaruru and Tubussis Lineaments controlled sedimentation resulting in the deposition of fluvial arkoses, feldspathic quartzites and shallow-marine limestones close to the Abbabis Inlier (SCZ) and calcareous limestones and deeper water pelites and turbidites to the north (NCZ). Evidence for the existence of deep-seated fractures which tapped mantle fluids in early Damaran times is provided by the juvenile isotopic signature of the carbonate at the Eureka monazite occurrence. The Daheim Member volcanic rocks were erupted along east-northeast-trending structures that also extended into the mantle on the northern margin of the SCZ. During the orogenic phase, the distribution of basement and sediments with contrasting competencies resulted in the development of different deformational styles in the NCZ and SCZ. In both subzones,  $D_3$  domal structures (in particular the marble horizons) and linear, north-northeast-trending  $D_4$  structures acted as physico-chemical traps for late-tectonic magmas and mineralising fluids such as uraniumiferous alaskites at Rössing, scheelite skarn mineralisation in the Schönfeld Dome and gold skarn/vein mineralisation at Navachab, Habis and Onguati-Otjimbojo. There is thus a

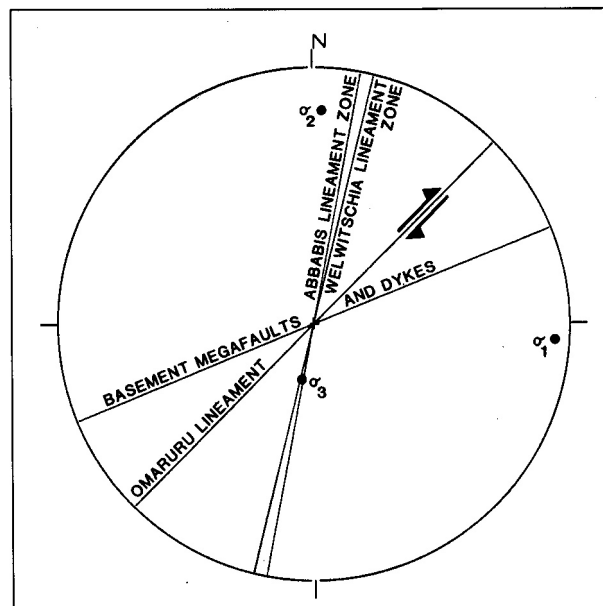


**Figure 8.2:** Principal stress axes during  $D_4$  deformation in the SCZ. Note dextral motion on Omaruru Lineament

unifying theme to these apparently diverse mineralisation types.

Late-tectonic dextral movement on the Omaruru Lineament, in much the same manner as dextral motion on the Okahandja Lineament (Stanistreet *et al.*, 1991), is believed to have been the underlying control on the localisation of late- $D_3$ / $D_4$  epigenetic mineralisation. In the SCZ, the Abbabis Inlier and overlying Nosib Group quartzites behaved as a relatively rigid block during early Damaran tectonism. In contrast, the thin skin of overlying incompetent marble (calcitic members of the Karibib Formation) has been extensively deformed. Towards the end of  $D_3$  folding and doming, subhorizontal, east-southeast/west-northwest-directed  $D_4$  compression, which Stanistreet *et al.* (1991) have related to the closure of the Adamastor Ocean (Fig. 8.1), caused uplift of basement and lower Damaran stratigraphy near the north-northeast-trending Welwitschia and Abbabis lineament zones (Corner, 1983). In the basement inlier south of Karibib,  $\sigma_1$  was horizontal and  $\sigma_3$  was subvertical (Fig. 8.2). This stress field was responsible for the localisation of late-/post-tectonic pegmatite sills in the Abbabis Complex. Contemporaneously, westward-verging  $F_4$  folds with shallow, eastward-dipping axial planes and east-southeast-plunging extension lineations were formed near major tectonic breaks such as the Welwitschia lineament zone (Fig. 8.3). Auriferous fluids were concentrated in north-northeast-trending high strain zones (ductile structures) on Sandamap Noord and north-northeast-trending zones of tourmalinisation on Hakskeen. Tungsten skarn mineralisation is hosted by lower Kuiseb Formation marbles at a strike change (in a dilational jog?) near the Welwitschia lineament zone on Pforte. To the north and east of Karibib, epigenetic gold skarn/vein mineralisation was emplaced in brittle/ductile and brittle structures in rocks that had undergone greenschist/lower amphibolite facies metamorphism. Auriferous hydrothermal fluids were dammed up by the Karibib Formation marbles in the east-north east-trending Onguati-Otjimbojo anticline. Gold skarn mineralisation was concentrated

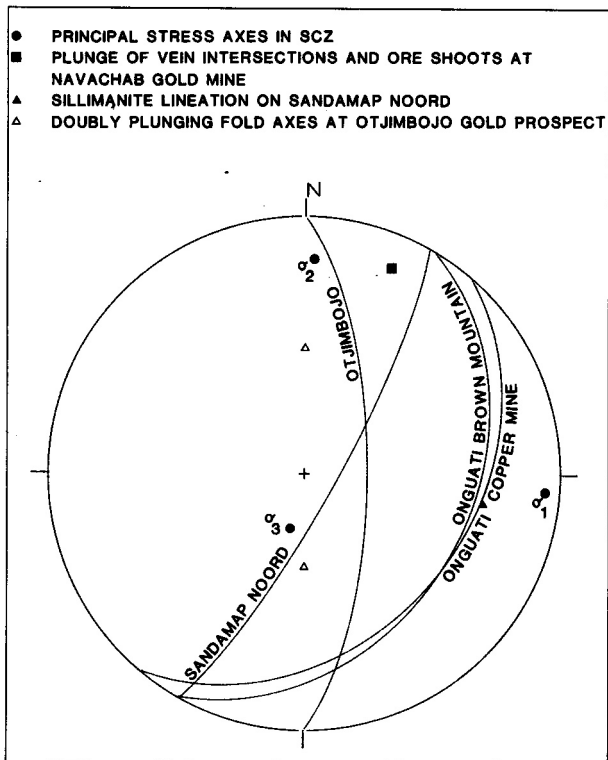


**Figure 8.3:** Late-tectonic ( $D_4$ ) structures hosting gold mineralisation in the CZ

where this east-northeast-trending structure is cut by, firstly, eastward- and southeastward-dipping thrust faults at Onguati and secondly, *en echelon* doubly plunging north/south second generation folds which drape over north/south (strike-slip?) faults at Otjimbojo (Fig. 8.3). These subvertical north/south faults parallel the Abbabis lineament zone (Figs. 8.2 and 8.3) and are a feature of the SCZ as far east as the Waldau Ridge near Okahandja (Fig. 1.1). Thus megashear zones, faults and dykes in the basement acted as access points and channel ways for hydrothermal fluids. Reactivation of east-northeast-trending megafaults in the SCZ possibly occurred because these structures lie parallel to Riedel fractures that were synthetic to the Omaruru Lineament (Fig. 8.2).

In the NCZ, where no Abbabis Complex and only minor Nosib Group sediments are developed, mechanically incompetent marbles and schists were multiply deformed, attenuated and subsequently intruded by numerous granitic plutons during  $D_3$  doming. Late-tectonic, (late- $D_3/D_4$ ) west-north west-directed compression on the Omaruru and Tubussis Lineaments resulted in dextral movement on these structures and the development of the Omaruru flower structure. Due to the absence of a rigid basement inlier,  $\sigma_3$  was oriented north-northeast, but was essentially horizontal (cf Abbabis Inlier; compare Figs. 8.2 and 8.4). This wrench movement on deep-seated structures may have acted as a trigger for the magmas that formed the Pforte/Ketelbank, Okarundu Nord, Ohere and Otjua leucogranites: this type of granite is confined to within 10 km of the Tubussis Lineament/Kompaneno Fault/Omaruru Fault Zone. Late-tectonic, epigenetic mineralisation is concentrated in a number of apparently pinnate, west-northwest-trending, (tensile?) structures at a number of stratigraphic levels on the northwest side of the Kompaneno Fault/Omaruru Fault Zone. In ascending stratigraphic order

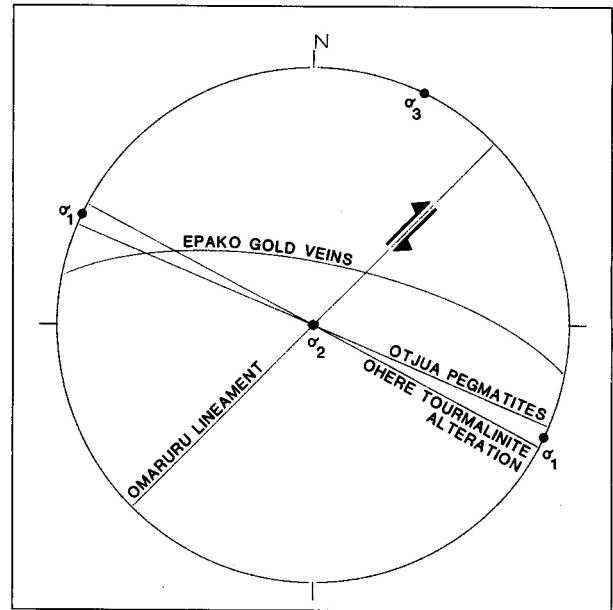


**Figure 8.4:** Principal stress axes during late- $D_3/D_4$  deformation in the NCZ. Note dextral motion on the Omaruru Lineament

these are the Otjua tungsten skarn deposit (Okawayo Formation), the Epako Gold Prospect (Oberwasser Formation), the Crystal Tin Mine (Karibib Formation) and the Ohere tourmalinite occurrences (Kuisseb Formation). Several widely spaced west-north west-trending photo lineaments in the NCZ, which are visible on LANDSAT images, may have developed at this time. The Omaruru River (Map 1) appears to follow the path of one such structure to the west of Omaruru.

### 8.3 CONCLUDING THOUGHTS ON GOLD METALLOGENESIS IN CENTRAL NAMIBIA

The data base on gold mineralisation in general is so large (Keppie *et al.*, 1986; Keays *et al.*, 1989; Ladeira, 1991) that meaningful comparisons can be made between the gold deposits of central Namibia and better-documented districts, in spite of the lack of detailed isotopic and fluid inclusion studies in the former. The most important conclusion to be drawn is that the gold mineralisation in the Damaran rocks of the CZ is epigenetic in nature and of late- Damaran age. In common with Archaean gold deposits (Groves *et al.*, 1990), gold mineralisation is structurally controlled and is hosted by late-tectonic,  $D_3$  or  $D_4$  ductile/brittle structures and, locally, thrust faults. The Au-Bi-Te association in the skarn assemblages and the alunite-kaolinite-jarosite alteration assemblage in the metatubidite mineralisation is indicative of low temperature (< 250°C), almost epithermal fluids. The preservation of undeformed assemblages, which are retrograde with respect to peak metamorphic conditions, indicates that the gold mineralising event occurred towards the end of the orogeny when the CZ was being uplifted. Low temperature (:S; 300°C), epigenetic gold mineralising events in the waning stages of an orogeny are now documented from terrains as disparate as Archaean greenstone belts (De Ronde *et al.*, 1991) and the Tertiary Alpine event (Diamond, 1990). The evidence from the described gold occurrences in Namibia points to the op-

eration of magmatic-hydrothermal processes in the aureoles of late-tectonic granitic intrusions: rare-element pegmatites are implicated as a possible source of hydrothermal fluids.

Three hypotheses for the origin of gold mineralisation which have attracted widespread attention during the 1980s can be ruled out for the CZ gold occurrences. The first of these involves the mobilisation of gold during the metamorphic dewatering/devolatilisation of mafic volcanic rocks near the greenschist/amphibolite transition (Phillips and Groves, 1983; Groves *et al.*, 1985; Phillips *et al.*, 1987). There are no mafic volcanic rocks within 20 km of the metaturbidite-hosted gold occurrence on Sandamap Noord. Alkaline volcanic rocks are developed near the Karibib skarn-hosted gold occurrences, but they comprise a volumetrically insignificant part of the Abbabis Inlier and the Damaran stratigraphy (< 5%); where exposed, they are pristine and unsheared. Mass balance calculations reveal that alteration of the volcanic rocks did not play a prominent role in dolomitisation of the Karibib Formation. Moreover, the Au-Bi-Te association in the spatially associated skarns is more suggestive of a magmatic fluid derived from a granitoid. In a recent review, Groves *et al.* (1990) conceded that in greenstone belt terrains where granitoid domes are abundant, models for gold mobilisation that invoke metamorphic devolatilisation of mafic volcanic rocks alone, are untenable. The second model that can be discounted is one involving the large-scale leaching of low concentrations of gold from country or volcanic rocks by meteoric fluids in convection cells in the aureoles of granitoid intrusions (Berger and Henley, 1989). One of the notable features of CZ granitoids is their anhydrous nature and their lack of visible alteration (Steven, 1987). The limited  $\delta^{18}\text{O}$  data available for the CZ (Haack *et al.*, 1983; Steven, 1987) provide no evidence for interaction between magmas and meteoric waters. The upper portions of the CZ, where this process may have occurred, have long since been eroded. The third model, the lamprophyre-mesothermal gold one of Rock *et al.* (1989), is believed to have played no role in the generation of the CZ gold deposits. There is no evidence for an association, either genetic or spatial, between skarn- or metaturbidite-hosted gold deposits and alkaline intrusions in the CZ.

The potential of the four major lithostratigraphic units underlying central Namibia, namely the basement granitic gneisses, the feldspathic quartzites of the Nosib Group, the carbonates and very subordinate mafic volcanic rocks of the Karibib Formation and the pelagic sediments of the Kuiseb Formation, to have acted as sources for auriferous fluids and as subsequent hosts for gold mineralisation can now be assessed. Two gold provinces can be distinguished in the CZ, both of which are defined geochemically. In the SCZ, neither the Nosib Group nor the Karibib Formation meta-sediments can be considered as significant gold reservoirs. In contrast, the Abbabis basement inlier possesses significant quantities of gold, at least some of which appears to have been emplaced during a pre-Damaran mineralising event. Gold mineralisation was locally remobilised within the inlier during the Damaran orogeny, but more importantly was channelled by hydrothermal fluids via major crustal fractures and dykes into the overlying metaquartz-

ites and the marbles. Au-Bi-Te mineralisation was concentrated near lithium pegmatites or in veins along major lineament systems. The lithium pegmatites interacted with and were possibly derived from the 1.7-2.0 Ga Abbabis Inlier. The marble-hosted mineralisation in the overlying Karibib Formation can be referred to as skarn mineralisation only in the broadest sense of the word. The proportion of skarn (silicate gangue) at these prospects is either very small (Navachab) or non-existent (Onguati). In the NCZ, in contrast, Au-As-W mineralisation, possibly higher temperature than the Au-Bi-Te of the SCZ, was localised in highly deformed metaturbidites and, to a lesser extent, marbles. The original source of the gold, arsenic and tungsten may have been the pelitic sediments of the Oberwasser and Kuiseb Formations. Metals were concentrated in the aureoles of late-tectonic granitic and pegmatitic intrusions. Some of these intrusions, the pegmatites in particular, were possibly derived from the partial melting of the metapelites, itself another gold concentrating mechanism. Particularly favourable sites for gold deposition were late-tectonic high strain zones which resulted from movement on major structures such as the Welwitschia and Abbabis lineament zones.

#### 8.4 PELITE/TURBIDITE-HOSTED GOLD MINERALISATION IN THE DALRADIAN AND THE DAMARAN CZ COMPARED

Because of the paucity of gold mineralisation in Proterozoic rocks (Woodall, 1979), there are a limited number of ensialic terrains of similar age with which the CZ gold deposits can be compared. An exception is the well-documented late Proterozoic Dalradian Series in Scotland and Ireland that was deformed and metamorphosed during the early Palaeozoic Caledonian orogeny (Fettes *et al.*, 1986, 1991). Moreover, comprehensive regional geochemical studies of the Dalradian Series are available (Plant *et al.*, 1989). The Dalradian Series has many features in common with the Damara Sequence, both comprising late Proterozoic, predominantly sedimentary, sequences laid down on continental basement. In the Dalradian, initial fluvial clastic development was followed by the development of shallow-marine carbonates and glaciogenic tillites. Further carbonate deposition was followed by the accumulation of turbiditic sediments in fault-bounded basins. Localised rupture of the crust resulted in the extrusion of tholeiitic lavas towards the top of the sequence in a similar manner to the Matchless Member basalts and volcanic rocks. In the Dalradian Series there is a strong association between late felsic porphyries intruded along lineament systems and Au-As-Bi mineralisation. The main control on the distribution of As appears to be turbidite facies sediments deposited in fault-bounded basins associated with crustal extension. Anomalous arsenic is associated with all centres of gold mineralisation. The distribution of arsenic around gold centres generally suggests that arsenic was derived from the metasediments. Sb is commonly enriched over shales and muddy clastics. In contrast bismuth is thought to be derived from magmatic sources. Elongate bismuth anomalies may follow lineament systems in which Bi is concentrated in

hydrothermal solutions.

The tectonic setting of the Dalradian Series and Damara Sequence is similar, namely tectonised, extensional (volcano)-sedimentary basins into which a late-/post-tectonic series of felsic intrusions was emplaced. Hutchinson (1987) discussed gold metallogeny in Precambrian rocks and emphasised the eugeosynclinal nature of the Archaean greenstone belts and the late Proterozoic/early Palaeozoic turbidite-hosted deposits. This author considers a Kuiseb Formation-filled graben (a tin belt) to be the ensialic analogue of an Archaean greenstone belt, where turbidites were deposited in listric-faulted basins. In such a setting the economically significant gold mineralisation is late (i.e. epigenetic), postdating peak metamorphism and most magmatic events of the orogenic cycle. Mineralisation is spatially associated with late-/post-tectonic suites of felsic intrusions that were emplaced along discordant lineaments. The concentration of Au-As-W mineralisation within high strain zones in the Kuiseb Formation is reminiscent of Archaean greenstone belts (Colvine *et al.*, 1988).

Plant *et al.* (1989) considered that the genesis of the Dalradian gold deposits is consistent with a "modified metamorphic model". For some reason, possibly syn-sedimentary, arsenic became enriched in turbidite/shale sequences. Gold (within disseminated pyrite and arseno-pyrite) may also have become enriched as a result of low-level hydrothermal circulation related to the high geothermal gradient that accompanied rifting. The rapid deposition of turbidites under anoxic conditions resulted in the preservation of kerogens. The author considers that this was particularly important in the tin belts of central Namibia. The Dalradian gold deposits occur mainly where across-strike lineaments cut listric-faulted sedimentary basins. A direct analogy is present at Sandamap Noord where the east-northeast-trending Sandamap-Davib Ost tin belt is cut by the north-northeast-trending Welwitschia lineament zone. In the Dalradian Series gold was concentrated by high-level hydrothermal activity around felsic porphyries. In the Damara Sequence the equivalent felsic intrusions were pegmatites in the aureoles of granites. The source of the gold, sulphur, As and Sb in the Dalradian (and the Damaran tin belts?) was the organic and sulphur-enriched sediments (Plant *et al.*, 1989). In contrast, Bi was concentrated in igneous centres. Thus the identification of regional As and Bi enrichment is an important prerequisite for the identification of gold mineralisation in the Damara, as it is in the Dalradian.

### 8.5 CONCLUDING COMMENTS

Examined in isolation from the other tectono-stratigraphic zones, the CZ shows little evidence for continental collision in common with other low-pressure/high-temperature terrains (Wickham and Oxburgh, 1985). The epigenetic mineral deposits of the CZ possess an intracratonic signature.

An Andean-type collision model for the inland branch of the orogen is unsuccessful in explaining the continental nature and the paucity of the CZ magmato-hydrothermal deposits. The distribution of the metasediments, the tectonic evidence and the confinement of various granitoid and pegmatoid types to particular tectono-stratigraphic zones argue against significant lateral displacement within the CZ. There is evidence for extensive crustal shortening across the orogen, but tectono-stratigraphic zones have remained essentially where they evolved (Stanistreet *et al.*, 1991). The major variations in lithostratigraphy in the CZ are perpendicular to the north-east-strike of the intracontinental branch of the Damara Orogen. Thus original sedimentary facies belts, of which the tin belts are the best example, are subparallel to the subsequent structures. Regional metamorphic isograds are broadly oriented perpendicular to these lithostratigraphic zones, peak metamorphic conditions increasing from northeast to southwest. Superimposed on the regional metamorphism are the contact effects of the numerous granitic domes. Although deeper crustal levels are undoubtedly exposed on the present-day Namibian coast as a result of more extensive uplift, pressure is not considered to have varied as much as temperature along the length of the CZ. The Usakos-Karibib-Omaruru area lay within the 400°C-700°C "window", spanning the greenschist-amphibolite facies transition. Thermal conditions were ideal for the preservation of late-tectonic pegmatites and high temperature skarns (400-650°C; Einaudi *et al.*, 1981) and at a later stage, because of the rapid uplift, lower temperature ( $\leq 300^\circ\text{C}$ ), epigenetic vein-type mineralisation.

Why does the CZ host the epigenetic deposits? This can be directly attributed to the large number of granitic plutons and the accompanying low-pressure metamorphism (Barton and Hanson, 1989). That the epigenetic mineral deposits are commonly far removed from their parent/causative intrusion should come as no surprise. The large number of granitic intrusions led to the development of overlapping thermal domes and a high geothermal gradient (55-65°C/km). The confinement of specific types of epigenetic mineralisation to certain tectono-stratigraphic levels suggests that the original sources of the metals were the pre-existing basement and the Damaran sediments. Ascending granitoid and pegmatite magmas interacted with the metasediments to assimilate-and/or leach certain elements. Loss of metals from Damaran sediments undoubtedly occurred during regional metamorphism (Haack *et al.*, 1984), but it was the granitoid intrusions that were most effective in focusing fluid and raising ambient temperatures (Connolly and Thompson, 1990) in the latter stages of the orogeny.

## REFERENCES

- Abraham, K., Mielke, H. and Povondra, P. 1972. On the enrichment of tourmaline in metamorphic sediments of the Arzberg Series, W.- Germany (NE-Bavaria). *Neues Jahrbuch für Mineralogie. Monatshefte*, 209-219.
- Alderton, D.H.M., Pearce, J.A and Potts, P.J. 1980. Rare-earth element mobility during granite alteration; evidence from south-west England. *Earth and Planetary Science Letters*, **49**, 149-165.
- Andersen, T. 1986. Compositional variation of some rare earth minerals from the Fen complex (Telemark, SE Norway): implications for the mobility of rare earths in a carbonatite system. *Mineralogical Magazine*, **50**, 503-509.
- Badenhorst, F.P. 1986a. 'n Voorlopige petrografiese studie van die granitiese gesteentes van Gebied 2115B in die noordelike Sentrale Sone van die Damara-orogeen. *Communications of the Geological Survey of S.W.A./Namibia*, **2**, 13-26.
- Badenhorst, F.P. 1986b. *The Omaruru Lineament, a major tectono-stratigraphic boundary in the Central Zone of the Damara Orogen, S.W.A./Namibia*. Unpublished Report of the Geological Survey of SWA/Namibia, Windhoek, 16 pp.
- Badenhorst, F.P. 1987. Lithostratigraphy of the Damara Sequence in the Omaruru area of the northern Central zone of the Damara Orogen and a proposed correlation across the Omaruru Lineament. *Communications of the Geological Survey of S.W.A./Namibia*, **3**, 3-8.
- Badenhorst, F.P. 1988a. A note on stratiform tourmalinites in the Late Precambrian Kuiseb Formation, Damara Sequence. *Communications of the Geological Survey of S.W.A./Namibia*, **4**, 67-70.
- Badenhorst, F.P. 1988b. The lithostratigraphy of the Chuos mixtite in part of the southern Central Zone of the Damara Orogen, South West Africa. *Communications of the Geological Survey of S.W.A./Namibia*, **4**, 103-110.
- Baird, A.K. 1961. A pressed specimen die for the Norelco Vacuum-Path X-ray spectrograph. *Norelco Report*, **8**, 108-109
- Barnes, R.G. 1983. Stratiform and stratabound tungsten mineralisation in the Broken Hill Block, N.S.W. *Journal of the Geological Society of Australia*, **30**, 225-239.
- Barnes, S.J. and Sawyer, E.W. 1980. An alternative model for the Damara mobile belt: ocean crust subduction and continental convergence. *Precambrian Research*, **13**, 297-336.
- Barton, M.D. and Hanson, R.B. 1989. Magmatism and the development of low-pressure metamorphic belts: implications from the western United States and thermal modeling. *Geological Society of America Bulletin*, **101**, 1051-1065.
- Bates, R.L., and Jackson, J.A 1987. *Glossary of Geology*, American Geological Institute, Alexandria, Virginia, 788 pp.
- Behr, H.-J., Ahrendt, H., Martin, H. Porada, H. Rohrs, J. and Weber, K. 1983. Sedimentology and mineralogy of Upper Proterozoic playa-lake deposits in the Damara Orogen, 577-610. In: Martin, H. and Eder, F.W., Eds., *Intracontinental Fold Belts*, Springer-Verlag, Berlin, Heidelberg, 945 pp.
- Bell, T.H. 1985. Deformation partitioning and porphyroblast rotation in metamorphic rocks: a radical re-interpretation. *Journal of Metamorphic Geology*, **3**, 109-118.
- Bell, T.H., Fleming, P.D. and Rubenbach, M.J. 1986. Porphyroblast nucleation, growth and dissolution in regional metamorphic rocks as a function of deformation partitioning during foliation development. *Journal of Metamorphic Geology*, **4**, 37-67.
- Benard, F., Moutou, P. and Pichavant, M. 1985. Phase relations of tourmaline leucogranites and the significance of tourmaline in silicic magmas. *Journal of Geology*, **93**, 271-291.
- Bence, A.E. and Albee, A.L. 1968. Empirical correction factors for the electron microanalysis of silicates and oxides. *Journal of Geology*, **76**, 382-403.
- Berger, B.R. and Henley, R.W. 1989. Advances in understanding of epithermal gold-silver deposits, with special reference to the Western United States, 405-423. In: Keays, R.R., Ramsay, W.R.H. and Groves, D.L, 1989, Eds., *The Geology of Gold Deposits: The perspective in 1988*. Economic Geology Monograph 6, Economic Geology Publishing Company, New Haven, 667 pp.
- Berning, J., Cooke, R., Hiemstra, S.A. and Hoffman, U. 1976. The Rössing uranium deposit, South West Africa. *Economic Geology*, **71**, 351-368.
- Bhatia, M.R. 1983. Plate tectonics and geochemical composition of sandstones. *Journal of Geology*, **91**, 611-627.
- Bladh, K.W. 1982. The formation of goethite, jarosite and alunite during the weathering of sulphide-bearing felsic rocks. *Economic Geology*, **77**, 176-184.
- Blaine, J.L. 1977. Tectonic evolution of the Waldau Ridge structure and the Okahandja Lineament in part of the Central Damara Orogen, west of Okahandja, South West Africa. *Bulletin of the Precambrian Research Unit, University of Cape Town*, **21**, 99 pp.
- Blatt, H., Middleton, G. and Murray, R. 1972. *Origin of sedimentary rocks*. Prentice-Hall Inc., New Jersey, 634 pp.
- Blatt, H., Middleton, G. and Murray, R. 1980. *Origin of sedimentary rocks*. Prentice-Hall Inc., New Jersey, 782 pp.
- Blaxland, A., Gohn, E., Haack, U. and Hoffer, E. 1979. Rb/Sr ages of late-tectonic granites in the Damara Orogen, South West Africa/Namibia. *Neues Jahrbuch für Mineralogie Monatshefte*, **11**, 498-508.
- Bonham, H.F. 1989. Bulk mineable gold deposits of the western United States, 193-207. In: Keays, R.R., Ramsay, W.R.H. and Groves, D.L, 1989, Eds., *The Geology of Gold Deposits: The perspective in 1988*. Economic Geology Monograph 6, Economic Geology Publishing Company, New Haven, 667 pp.
- Botha, P.J. 1978. *Die geologie in die omgewing van die benedene-Omarururivier, Suidwes-Afrika*. Unpublished M.Sc. thesis, University of the Orange Free-State, 157 pp.
- Boyle, R.W. 1979. The geochemistry of gold and its deposits. *Geological Survey of Canada, Bulletin 280*, 584 pp.
- Boyle, R.W. 1986. Gold deposits in turbidite sequences: Their geology, geochemistry and history of the theories of their origin, 1-13. In: Keppie, J. Duncan, Boyle, R.W. and Haynes, S.J., Eds., *Turbidite-Hosted Gold Deposits*. Geological Association of Canada Special Paper 32.
- Brandt, R. 1985. Preliminary report on the stratigraphy of the Damara Sequence and the geology and geochemistry of Damara granites in an area between Walvis Bay and Karibib. *Communications of the Geological Survey of S.W.A./Namibia*, **1**, 31-43.
- Brandt, R. 1987a. A revised stratigraphy for the Abbabis Complex in the Abbabis inlier, Namibia. *South African Journal of Geology*, **90** (3), 314-323.
- Brandt, R. 1987b. Evolution of the Pan-African granitic rocks of the Damara Orogen, Namibia, 121-125. In: Matheis, G. and Schandelmeier, H.S., Eds. *Current research in African earth sciences*. Balkema, Rotterdam, Holland.
- Brisbin, W.C. 1986. Mechanics of pegmatite intrusion. *American Mineralogist*, **71**, 644-651.
- Burger, A.J., Von Knorring, O. and Clifford, T.N. 1965. Mineralogical and radiometric studies of monazite and sphene occurrences

- in the Namib desert, South West Africa. *Mineralogical Magazine*, **35**, 519-528.
- Burger, A.J., Clifford, T.N. and Miller, R.McG. 1976. Zircon U-Pb ages of the Fransfontein granitic suite, northern South West Africa. *Precambrian Research*, **3**, 415-431.
- Burton, J.C., Taylor, L.A. and Chou, I.-M., 1982, The  $f_{O_2}$ -T and  $f_{S_2}$ -T stability relations of hedenbergite and of hedenbergite-johannsenite solid solutions. *Economic Geology*, **77**, 764-783.
- Carmichael, D.M. 1978. Metamorphic bathozones and bathograds: a measure of the depth of post-metamorphic uplift and erosion on a regional scale. *American Journal of Science*, **278**, 769-797.
- Cerny, P. 1982a. Anatomy and classification of granitic pegmatites, 1-39. In: Cerny, P., Ed., *Granitic pegmatites in science and industry*. Mineralogical Association of Canada Short Course Handbook Volume 8, Winnipeg, 555 pp.
- Cerny, P. 1982b. Petrogenesis of granitic pegmatites, 405-461. In: Cerny, P., Ed., *Granitic pegmatites in science and industry*. Mineralogical Association of Canada Short Course Handbook Volume 8, Winnipeg, 555 pp.
- Chamber of Mines of SWA/Namibia report. 1985. *What mining means to SWA/Namibia*.
- Chappell, B.W. and White, A.J.R. 1974. Two contrasting granite types. *Pacific Geology*, **8**, 173-174.
- Chatterjee N.D. and Johannes, W. 1974. Thermal stability and standard thermodynamic properties of synthetic  $2M_1$ -muscovite  $KAl_2(AlSi_3O_{10}(OH)_2)$ . *Contributions to Mineralogy and Petrology*, **48**, 89-114.
- Clark, G.S. 1982. Rubidium-strontium isotope systematics of complex granitic pegmatites, 347-371. In: Cerny, P., Ed., *Granitic pegmatites in science and industry*. Mineralogical Association of Canada Short Course Handbook Volume 8, Winnipeg, 555 pp.
- Clarke, D.B. 1981. The mineralogy of peraluminous granites: a review. *Canadian Mineralogist*, **19**, 3-17.
- Cliff, R.A. 1985. Isotopic dating in metamorphic belts. *Journal of the Geological Society of London*, **142**, 97-110.
- Colley, H., Treloar, P.J. and Diaz, F. 1989. Gold-silver mineralisation in the El Salvador Region, Northern Chile, 208-217. In: Keays, R.R., Ramsay, W.R.H. and Groves, D.I., Eds., *The Geology of Gold Deposits: The perspective in 1988*. Economic Geology Monograph 6, Economic Geology Publishing Company, New Haven, 667 pp.
- Colvine, A.C., Fyon, J.A., Heather, K.B., Marmont, S., Smith, P.M. and Troop, D.G. 1988. Archean lode gold deposits in Ontario. *Ontario Geological Survey, Miscellaneous Paper*, **139**, 136 pp.
- Connolly, J.A.D. and Thompson, A.B. 1990. Focused fluid movement in the lower crust: thermal consequences and silica transport. *EOS, Transactions of the American Geophysical Union*, **71**, 642.
- Corner, B. 1981. *An interpretation of the aeromagnetic data covering the western portion of the Damara Orogenic Belt with special reference to the occurrence of uraniferous granite*. Unpublished Ph.D. thesis, University of the Witwatersrand, 100 pp.
- Corner, B. 1983. An interpretation of the aeromagnetic data covering the western portion of the Damara Orogen in S.W.A./Namibia. *Special Publication of the Geological Society of South Africa*, **11**, 339-354.
- Coward, M.P. 1981. The junction between the Pan-African mobile belts in Namibia: its structural history. *Tectonophysics*, **76**, 59-73.
- Coward, M.P. 1983. The tectonic history of the Damaran belt. *Special Publication of the Geological Society of South Africa*, **11**, 409-421.
- Coward, M.P. 1990. *Extensional Tectonics and Basin Development*. Course Notes, Seminar at SOEKOR, Bellville, RSA.
- Cruickshank, A.R.I. 1977. The Waterberg thrust fault in South West Africa: is it a failed arm of a triple junction? *Transactions of the Geological Society of South Africa*, **80**, 29-30.
- Dana, E.S. 1944. *System of mineralogy, Volume I: Elements, sulphides, sulfosalts and oxides*. Seventh edition, John Wiley, New York, 834 pp.
- Davies, B.M. 1985. Tourmalines from Appalachian-Caledonian massive sulphide deposits: textural, chemical and isotopic relationships - a discussion. *Economic Geology*, **80**, 2038-2046.
- Deer, W.A., Howie, R.A. and Zussman, J. 1962. *Rock-Forming Minerals, Volume 5: Non-Silicates*. Longmans, London, 371 pp.
- Deer, W.A., Howie, R.A., and Zussman, J. 1966. *An introduction to the rock-forming minerals*. Longmans, London, 528 pp.
- Deer, W.A., Howie, R.A. and Zussman, J. 1982. *Rock-forming minerals, Volume 1A, Orthosilicates*. Longmans, London, 919 pp.
- De Kock, G.S. 1985. Die geologie van 'n gebied suidoos van Karibib. *Communications of the Geological Survey of S.W.A./Namibia*, **1**, 45-55.
- De Kun N. 1965. *Mineral Resources of Africa*. Elsevier, 740 pp.
- De Ronde, C.E.J., de Wit, M.J., Spooner, E.T.C. and Bray, C.J. 1991. Mafic-ultramafic hosted, shear zone related, Au-quartz vein deposits in the Barberton greenstone belt, South Africa: Structural style, fluid properties and light stable isotope geochemistry, 279-286. In: Ladeira, E.A., Ed., *Proceedings of Brazil Gold '91, An International Symposium on the Geology of Gold: Belo Horizonte, 1991*. Balkema, Rotterdam, Holland 823 pp.
- De Yoreo, J.J., Lux, D.R. and Guidotti, C.V. 1989. The role of crustal anatexis and magma migration in the thermal evolution of regions of thickened continental crust, 187-202. In: Daly, J.S., Cliff, R.A. and Yardley, B.W.D., Eds, *Evolution of Metamorphic Belts*. Geological Society Special Publication No. 43, Blackwell Scientific Publications, Oxford, 566 pp.
- Diamond, L.W. 1990. Fluid inclusion evidence for P-V-T-X evolution of hydrothermal solutions in Late-Alpine gold-quartz veins at Brusson, Val D'Ayas, northwest Italian Alps. *American Journal of Science*, **290**, 912-958.
- Diehl, M. 1986. Preliminary report on the Cape Cross-Uis pegmatite field. *Communications of the Geological Survey of S.W.A./Namibia*, **2**, 39-46.
- Dodson, M.H. 1973. Closure temperatures in cooling geochronological and petrological systems. *Contributions to Mineralogy and Petrology*, **40**, 259-274.
- Drew, L.J., Meng Qingrun and Sun Weijun 1990. The Bayan Obo iron-rare earth-niobium deposits, Inner Mongolia, China. *Lithos*, **26**, 43-65.
- Dunai, T., Stoessel, G.F.U. and Ziegler, U.R.F. 1989. Note: A Sr isotope study of the Eureka carbonatite, Damaraland, Namibia. *Communications of the Geological Survey of Namibia*, **5**, 89-90.
- Eglington, B.E. and Harmer, J.E. 1991. GEODATE (Version 2.2): a program for the processing and regression of isotope data using IBM-compatible microcomputers. *CSIR Manual EMA-H9101*, 57 pp.
- Einaudi, M.T. and Burt, D.M. 1982. Introduction-terminology, classification, and composition of skarn deposits. *Economic Geology*, **77**, 745-795 pp.
- Einaudi, M.T., Meinert, L.D. and Newberry, R.J. 1981. Skarn deposits. *Economic Geology 75th Anniversary Volume*, 317-391.

- El Bouseily, A.M. and El Sökkary, A.A. 1975. The relation between Rb, Ba and Sr in granitic rocks. *Chemical Geology*, **16**, 207-219.
- Essene, E.J. 1989. The current status of thennobarometry in metamorphic rocks, 1-44. In: Daly, J.S., Cliff, R.A. and Yardley, B.W.D., Eds., *Evolution of Metamorphic Belts*. Geological Society Special Publication No. 43, Blackwell Scientific Publications, Oxford, 566 pp.
- Evans, B.W. and Guidotti, C.V. 1966. The sillimanite-potash feldspar isograd in western Maine, USA. *Contributions to Mineralogy and Petrology*, **12**, 25-62.
- Exley, C.S. 1957. Magmatic differentiation and alteration of the St. Austell granite. *Quarterly Journal of the Geological Society of London*, **114**, 197-230.
- Faure, G. 1986. *Principles of isotope geology*. John Wiley and Sons, New York, 589 pp.
- Ferry, J.M. and Spear, F.S. 1978. Experimental calibration of the partitioning of Fe and Mg between biotite and garnet. *Contributions to Mineralogy and Petrology*, **66**, 113-117.
- Fettes, D.J., Graham, C.M., Harte, B. and Plant, J.A. 1986. Lineaments and basement domains: an alternative view of Dalradian evolution. *Journal of the Geological Society of London*, **143**, 453-464.
- Fettes, D.J., Leslie, A.G., Stephenson, D. and Kimbell, S.F. 1991. Disruption of Dalradian stratigraphy along the Portsoy Lineament from new geological and magnetic surveys. *Scottish Journal of Geology*, **27**, 1,57-73.
- Fleischer, R. and Routhier, P. 1973. The 'consanguineous' origin of a tounnaline-bearing gold deposit: Pas sagen de Mariana (Brazil). *Economic Geology*, **68**, 11-22.
- Folk, R.L. 1968. *Petrology of sedimentary rocks*. Hemphills Book Store, Austin, Texas, 170 pp.
- Foster, R.P. 1977. The solubility of scheelite in hydrothermal chloride solutions. *Chemical Geology*, **20**, 27-43.
- Frommurze, H.F., Gevers, T.W., Rossouw, P.J. 1942. *The geology and mineral deposits of the Karibib area, South West Africa*. Explanation to Sheet 79, Geological Survey of South Africa, 172 pp.
- Gevers, T.W. 1931. *The fundamental complex of western Damara-land, South West Africa*. Unpublished D.Sc. thesis, University of Cape Town, 163 pp.
- Goldschmidt, V.M. 1958. *Geochemistry*. Oxford University Press, Oxford, 730 pp.
- Grauch, R.I. 1989. Rare earth elements in metamorphic rocks, 147-167. In: Lipin, B.R. and Mckay, G.A., Eds; *Geochemistry and mineralogy of rare earth elements*. Reviews in Mineralogy, Volume 21, 348 pp.
- Groves, D.I., Phillips, G.N., Ho, S.E., and Houstoun, S.M. 1985. The nature, genesis and regional controls of gold mineralisation in Archean greenstone belts of Western Australian shield: a brief review. *Transactions. of the Geological Society of South Africa*, **88**, 135-148.
- Groves, D.I., Barley, M.E., Cassidy, K.F., Fare, R.J., Hagemann, S.G., Ho, S.E., Hronsky, J.M.A., Mikucki, E.J., Mueller, A.G., McNaughton, N.J., Ridley, J.R. and Vearncombe, J.R. 1990. Sub-greenschist to granulite-hosted Archean lode-gold deposits: a depositional continuum from deep-sourced hydrothermal fluids in crustal-scale plumbing systems? *Third Archean Symposium, Perth, Australia*.
- Haack, U. and Gohn, E. 1988. Rb-Sr Data on some pegmatites in the Damara Orogen. *Communications of the Geological Survey of SWA/Namibia*, **4**, 13-18.
- Haack, U., Gohn, E. and Klein, J.A. 1980. Rb/Sr ages of granitic rocks along the middle reaches of the Omaruru River and the timing of orogenic events in the Damara belt (Namibia). *Contributions to Mineralogy and Petrology*, **74**, 349-360.
- Haack, U., Hoefs, J. and Gohn, E. 1983. Genesis of Damaran granites in the light of Rb/Sr and  $\delta^{18}\text{O}$  data, 847-872. In: Martin, H. and Eder, F.W., Eds, *Intracontinental Fold Belts*. Springer Verlag, Berlin, Heidelberg, 945 pp.
- Haack, U., Heinrichs, H., Boness, M. and Schneider, A. 1984. Loss of metals from pelites during regional metamorphism. *Contributions to Mineralogy and Petrology*, **85**, 116-132.
- Harder, H. 1959. Beitrag zur Geochemie des Bors. III Bor in Sedimenten. *Nach. Acad. Wissen. Göttingen II, Math-Phys Klasse*, **6**, 123-175.
- Hartnady, C.J.H., Joubert, P. and Stowe, C.W. 1985. Proterozoic crustal evolution in southwestern Africa. *Episodes*, **8**, 236-244.
- Hartnady, C.J.H., von Veh, M. and Ransome, I.G.D. 1990. *Gariiep Excursion Guide, 23<sup>rd</sup> Earth Science Congress of the Geological Society of South Africa*, 49 pp.
- Hatch, F.H., Wells, A.K. and Wells, M.K. 1972. *Petrology of the igneous rocks*. George Allen and Unwin Ltd., London, 551 pp.
- Haughton, S.H., Frommurze, H.F., Gevers, T.W., Schwellnus, C.M. and Rossouw, P.J. 1939. *The geology and mineralogy of the Omaruru area, South West Africa*. Explanation to Sheet 71, Geological Survey South Africa, 151 pp.
- Hawkesworth, C.J. 1982. Isotopic characteristics of magmas erupted along destructive plate margins, 549-571. In: Thorpe, R.S., Ed., *Orogenic andesites*. Wiley Intersciences, New York, 724 pp.
- Hawkesworth, C.J. and Marlow, A.G. 1983. Isotope evolution of the Damara Orogenic Belt. *Special Publication of the Geological Society of South Africa*, **11**, 397-408.
- Hawkesworth, C.J., Gledhill, A.R., Roddick, J.C., Miller, R. McG. and Kröner, A. 1983. Rb-Sr and  $^{40}\text{Ar}/^{39}\text{Ar}$  studies on models for the thermal evolution of the Damara belt, Namibia. *Special Publication of the Geological Society of South Africa*, **11**, 323-338.
- Hawkesworth, C.J., Menzies, M.A. and Van Calsteren, P. 1986. Geochemical and tectonic evolution of the Damara Belt, Namibia, 305-319. In: Coward, M.P. and Ries, A.C., Eds., *Collision Tectonics*. Geological Society Special Publication No. 19.
- Heard, H.C. 1976. Comparison of the flow properties of rocks at crustal conditions. *Philosophical Transactions of the Royal Society of London*, **A283**, 173-186.
- Heinrich, K.F.J. 1966. X-ray Absorption Uncertainty, 296-377. In: Mckinley, T.D., Heinrich, K.F.J. and Wittry, D.B., Eds., *The Electron Microprobe*. John Wiley and Sons, New York, 1035 pp.
- Hellman, P.H., Smith, R.E. and Henderson, P. 1979. The mobility of the rare earth elements: evidence and implications from selected terrains affected by burial metamorphism. *Contributions to Mineralogy and Petrology*, **71**, 23-44.
- Henry, G., Stanistreet, I.G. and Maiden, K.J. 1986. Preliminary results of a sedimentological study of the Chuos Formation in the Central Zone of the Damara Orogen: Evidence for mass flow processes and glacial activity. *Communications of the Geological Survey of S.W.A./Namibia*, **2**, 75-92.
- Henry, G., Clendenin, C.W., Stanistreet, I.G. and Maiden, K.J. 1990. Multiple detachment model for the early rifting stage of the late Proterozoic Damara orogen in Namibia. *Geology*, **18**, 67-71.
- Herron, M.M. 1988. Geochemical classification of terrigenous sands and shales from core or log data. *Journal of Sedimentary Petrology*, **58**, 820-829.
- Hietanen, A. 1967. On the facies series in various types of metamorphism. *Journal of Geology*, **75**, 187-214.
- Hine, R., Williams, B.W. and White, A.J.R. 1978. *Journal of the Geological Society of Australia*, **25**, 219-234.
- Hobbs, B.E., Means, W.D. and Williams, P. F. 1976. *An Outline of Structural Geology*. Wiley, New York, 571 pp.

- Hochella, M.F., Liou, J.G., Keskinen, M.J. and Kim, H.S. 1982. Synthesis, and stability relations of magnesium idocrase. *Economic Geology*, **77**, 798-808 pp.
- Hoffer, E. 1977. *Petrologische Untersuchungen zur Regional-metamorphose Al-reicher Metapelite im Südlichen Damara-Orogen (Südwest-Afrika)*. Habilitationsschrift, University of Göttingen, 150 pp.
- Hoffman, K.H. 1989. New aspects of lithostratigraphic subdivision and correlation of late Proterozoic to early Cambrian rocks of the southern Damara Belt and their correlation with the central and northern Damara Belt and the Gariiep Belt. *Communications of the Geological Survey of S.W.A./Namibia*, **5**, 59-67.
- Hoffman, K.H. 1990. Sedimentary depositional history of the Damara belt related to continental breakup, passive to active margin transition and foreland basin development. *23rd Earth Science Congress of the Geological Society of South Africa*, 250-253.
- Holdaway, M.J. 1971. Stability of andalusite and the aluminium silicate phase diagrams. *American Journal of Science*, **271**, 97-131.
- Holdaway, M.J. and Lee, S.M. 1977. Fe-Mg cordierite stability in high grade pelitic rocks based on experimental, theoretical and natural observations. *Contributions to Mineralogy and Petrology*, **63**, 175-198.
- Holdaway, M.J., Guidotti, C.V., Novak, J.M. and Henry, W.E. 1982. Polymetamorphism in medium- to high-grade pelitic metamorphic rocks, west-central Maine. *Geological Society of America*, **93**, 572-584.
- Humphris, S.E. 1984. The mobility of the rare earth elements in the crust, 317-342. In: Henderson, P., Ed., *Rare earth geochemistry*. Elsevier, Amsterdam, 510 pp.
- Hutchinson, R.W. 1987. Metallogeny of Precambrian gold deposits: Space and time relationships. *Economic Geology*, **82**, 1993-2007.
- Ishihara, S. 1981. The granitoid series and mineralisation. *Economic Geology 75<sup>th</sup> Anniversary Volume*, 458-484.
- Jacob, R.E. 1974. Geology and metamorphic petrology of part of the Damara Orogen along the lower Swakop River, South West Africa. *Bulletin of the Precambrian Research Unit, University of Cape Town*, **17**, 185 pp.
- Jacob, R.E., Kröner, A. and Burger, A.J. 1978. Areal extent and first U-Pb age of the pre-Damara Abbabis complex in the central Damara belt of South West Africa. *Geologische Rundschau*, **67(2)**, 706-718.
- Jacob, J.E., Snowden, P.A. and Bunting, F.J.L. 1983. Geology and structural development of the Tumas Basement Dome and its cover rocks. *Special Publication of the Geological Society of South Africa*, **11**, 157-172.
- Jäger, E., Niggli, E. and Wenk, E. 1967. Rb-Sr Altersbestimmungen an Glimmern der Zentralalpen. *Beitrag zur geologische Karte Schweiz*, **NF134**, Bern, 1-67.
- Kasch, K.W. 1983a. Continental collision, suture progradation and thermal relaxation: a plate tectonic model for the Damara Orogen in central Namibia. *Special Publication of the Geological Society of South Africa*, **11**, 423-429.
- Kasch, K.W. 1983b. Tectonothermal evolution of the southern Damara Orogen. *Special Publication of the Geological Society of South Africa*, **11**, 255-265.
- Kasch, K.W. 1987. Metamorphism of pelites in the Upper Black Nossob River area of the Damara Orogen. *Communications of the Geological Survey of Namibia*, **3**, 63-82.
- Keays, R.R., Ramsay, W.R.H. and Groves, D.J. 1989. Eds, *The Geology of Gold Deposits: The perspective in 1988*. Economic Geology Monograph 6, Economic Geology Publishing Company, New Haven, 667 pp.
- Keenan, J.H.G. 1982. *Final prospecting report on Sandamap grant M46/3/973*. Anglo American Prospecting Services.
- Keppie, J.D., Boyle, R.W. and Haynes, S.J., Eds. 1986. Turbidite-Hosted Gold Deposits. *Geological Association of Canada Special Paper*, **32**, 186 pp.
- Kerrick, D.M. 1987. Fibrolite in contact aureoles of Donegal, Ireland. *American Mineralogist*, **72**, 240-254.
- Kerrick, D.M. 1990. The Al<sub>2</sub>SiO<sub>5</sub> polymorphs. *Reviews in Mineralogy, Volume 22*.
- Klein, J.A. 1980. *Unpublished geological report on area 2115A*. Geological Survey of S.W.A./Namibia.
- Korzhiinskii, D.S. 1965. The theory of systems with perfectly mobile components and processes of mineral formation. *American Journal of Science*, **263**, 193-205.
- Kramm, U. 1976. The coticule rocks (spessartine quartzites) of the Venn-Stavelot Massif, Ardennes, a volcanoclastic meta-sediment? *Contributions to Mineralogy and Petrology*, **56**, 135-155.
- Kretz, R. 1983. Symbols for rock-forming minerals. *American Mineralogist*, **68**, 277-279.
- Kretz, R., Hartree, R. and Jones, P. 1989. Metasomatic crystallisation of muscovite in granite and tourmaline in schist related to pegmatite emplacement near Yellowknife, Canada. *Contributions to Mineralogy and Petrology*, **1021**, 191-204.
- Kreulen, R. and van Beek, P.C.J.M. 1983. The calcite-graphite isotope thermometer; data on graphite bearing marbles from Naxos, Greece. *Geochimica et Cosmochimica Acta*, **47**, 1527-1530.
- Kröner, A. 1982. Rb-Sr geochronology and tectonic evolution of the Pan-African Damara Belt of Namibia, Southwestern Africa. *American Journal of Science*, **282**, 1471-1507.
- Kröner, A. 1984. Dome structures and basement reactivation in the Pan-African Damara belt of Namibia, 191-206. In: Kröner, A. and Greiling, R., Eds., *Precambrian Tectonics Illustrated*. E., Schweizerbart'sche Verlagsbuchhandlung, Stuttgart, Germany, 419 pp.
- Kröner, A. and Hawkesworth, C. 1977. Late Pan-African emplacement ages for Rössing alaskitic granite (Damara belt) and Rooi Lepel bostonite (Gariiep belt) in Namibia and their significance for the timing of metamorphic events. *Twentieth Annual Report of the Research Institute for African Geology, University of Leeds*, 14-17.
- Kuyper, J.L. 1984. *Report on the regional 1:10,000 mapping of the Omaruru Tungsten Prospect*. Unpublished Company Report for Johannesburg Consolidated Investment Company.
- Ladeira, E.A. 1991. Ed., *Proceedings of Brazil Gold '91, An International Symposium on the Geology of Gold: Belo Horizonte*, 1991. Balkema, Rotterdam, Holland 823 pp.
- Lagarde, J.L., Ait Omar, S. and Roddaz, B. 1990. Structural characteristics of granitic plutons emplaced during weak regional deformation: examples from late Carboniferous plutons, Morocco. *Journal of Structural Geology*, **12**, 805-822.
- Lamens, J., Geukens, F. and Viaene, W. 1986. Geological setting and genesis of coticules in the Lower Ordovician of the Stavelot Massif, Belgium. *Journal of the Geological Society*, **143**, 253-258.
- Leake, B.E. 1990. Granite magmas: their sources, initiation and consequences of emplacement. *Journal of the Geological Society*, **147**, 579-589.
- Levinson, A.A. 1974. *Introduction to exploration geochemistry*. Applied Publishing Ltd., Illinois, U.S.A.
- London, D. 1986. Magmatic-hydrothermal transition in the Tanco rare-element pegmatite: evidence from fluid inclusions and phase-equilibrium experiments. *American Mineralogist*, **71**, 376-395.
- Louwrens, D.J. 1986. *Final prospecting report on grant M46/3/1515*. Rössing Uranium Limited.

- Luth, W.D., Jahns, R.H. and Tuttle, O.F. 1964. The granite system at pressures of 4 to 10 kilobars. *Journal of Geophysical Research*, **69**, 659-773.
- Maiden, K.J. 1981. A discussion of the paper by I.R. Plimer 'Exhalative Sn and W deposits associated with mafic volcanism as precursors to Sn and W deposits associated with granites': *Mineralium Deposita*, **16**, 455-456.
- Manning, D.A.C. and Pichavant, M. 1983. The role of fluorine and boron in the generation of granitic melts, 94-109. In: Atherton, M.P. and Gribble, C.D., Eds., *Migmatites, melting and metamorphism. Proceedings of the Geochemical Group of the Mineralogical Society*. Shiva Publishing Limited, Cheshire, U.K., 326 pp.
- Mariano, A.N. 1989. Economic geology of rare earth minerals, 309-337. In: Lipin, B.R. and McKay, G.A., Eds., *Geochemistry and mineralogy of rare earth elements*. Reviews in Mineralogy, Volume **21**, 348 pp.
- Marlow, A.G. 1981. *Remobilisation and primary uranium genesis in the Damara Orogenic Belt, Namibia*. Unpublished Ph.D. thesis, University of Leeds, 277 pp.
- Marlow, A.G. 1983. Geology and Rb-Sr Geochronology of mineralised and radioactive granites and alaskites, Namibia. *Special Publication of the Geological Society of South Africa*, **11**, 289-298.
- Martin, H. 1963. Geological map of South West Africa (1:1,000,000).
- Martin, H. 1978. The mineralisation of the ensialic Damara orogenic belt, 405-415. In: Verwoerd, W.J., Ed., *Mineralisation in metamorphic terranes*. Special Publication of the Geological Society of South Africa, **4**, 552 pp.
- Martin, H. 1983. Alternative geodynamic models for the Damara Orogeny. A critical discussion, 913-945. In: Martin, H. and Eder, E.W., Eds., *Intracontinental Fold Belts*. Springer Verlag, Berlin, Heidelberg, 945 pp.
- Martin, H. and Porada, H. 1977. The intracratonic branch of the Damara Orogen in South West Africa. I. Discussion of geodynamic models. *Precambrian Research*, **5**, 311-338.
- Martin, H., Porada, H. and Walliser, O.H. 1985. Mixite deposits of the Damara Sequence, Namibia: Problems of interpretation. *Palaeogeography, Palaeoclimatology and Palaeoecology*, **51**, 159-196.
- Mathieson, G.R. and Clark, A.H. 1984. The Cantung E Zone scheelite skarn orebody, Tungsten, Northwest Territories: A revised genetic model. *Economic Geology*, **79**, 883-901.
- Mawson, S.A. 1984. *Geochemical exploration for gold with particular reference to southern Africa*. Unpublished M.Sc. Dissertation, University of Rhodes.
- McArdle, P., Fitzell, M., Oosterom, M.G., O'Connor, P.J. and Kennan, P.S. 1989. Tourmalinite as a potential host for gold in the Caledonides of southeast Ireland. *Mineralium Deposita*, **24**, 154-159.
- McCarthy, T.S. and Hasty, R.A. 1976. Trace element distribution patterns and their relationship to the crystallisation of granite melts. *Geochimica et Cosmochimica Acta*, **40**, 1351-1358.
- McKenzie, D.P. 1985. The extraction of magma from the crust and mantle. *Earth and Planetary Science Letters*, **74**, 81-91.
- Meinert, L.D. 1987. *Gold in skarn deposits - a preliminary overview*. Proceedings of the 7<sup>th</sup> Quadrennial IAGOD Symposium, E. Schweizerbart'sche Verlagsbuchhandlung, Stuttgart.
- Meinert, L.D. 1989. Gold skarn deposits - geology and exploration criteria, 537-552. In: Keays, R.R., Ramsay, W.R.H. and Groves, D.I., 1989, Eds., *The Geology of Gold Deposits: The perspective in 1988*. Economic Geology Monograph 6, Economic Geology Publishing Company, New Haven, 667 pp.
- Miller, C.E., Stoddard, E.F., Bradfish, L. and Dollase, W.A. 1981. Composition of plutonic muscovite: genetic implications. *Canadian Mineralogist*, **19**, 25-34.
- Miller, R.McG. 1969. The geology of the Etiro pegmatite, Kari-bib District, S.W.A. *Annals of the Geological Survey of South Africa*, **7**, 125-130.
- Miller, R.McG. 1973. The Salem granite suite, South West Africa: genesis by partial melting of the Khomas schist. *Memoir of the Geological Survey of South Africa*, **64**, 106 pp.
- Miller, R.McG. 1974. Some economic aspects of the crystallisation of the Damara granites, South West Africa. *Bulletin of the Precambrian Research Unit, University of Cape Town*, **15**, 184-192.
- Miller, R.McG. 1979. The Okahandja Lineament, a fundamental tectonic boundary in the Damara Orogen of South West Africa/Namibia. *Transactions of the Geological Society of South Africa*, **82**, 349-361.
- Miller, R.McG. 1980. Geology of a portion of Central Damara-land. *Memoir of the Geological Survey of South Africa, South West Africa Series*, **6**, 78 pp.
- Miller, R.McG. 1983a. The Pan-African Damara Orogen of S.W.A./Namibia. *Special Publication of the Geological Society of South Africa*, **11**, 431-515.
- Miller, R.McG. 1983b. Economic implications of plate tectonic models of the Damara Orogen. *Special Publication of the Geological Society of South Africa*, **11**, 385-395.
- Miller, R.McG. 1983c. Tectonic implications of the of the contrasting geochemistry of Damara mafic volcanic rocks, S.W.A./Namibia. *Special Publication of the Geological Society of South Africa*, **11**, 115-138.
- Miller, R.McG. and Burger, A.J. 1983. U-Pb zircon ages of members of the Salem granitic suite along the northern edge of the central Damara granite belt. *Special Publication of the Geological Society of South Africa*, **11**, 273-280.
- Miller, R.McG. and Grote, W. 1988. Geological Map of the Damara Orogen, 1:500,000. *Map accompanying Evolution of the Damara Orogen of S.W.A./Namibia, Special Publication of the Geological Society of South Africa, No. 11*. Geological Society of South Africa, Johannesburg, 515 pp.
- Mitchell, A.H.G. and Garson, M.S. 1981. *Mineral deposits and global tectonic settings*. Academic Press Geology Series, London, 405 pp.
- Moore, J.M. 1989. A comparative study of metamorphosed supracrustal rocks from the western Namaqualand Metamorphic Complex. *Bulletin of the Precambrian Research Unit, University of Cape Town*, **37**, 370 pp.
- Moore, J.M. and McStay, J.H. 1990. The formation of allanite-(Ce) in calcic granofels, Namaqualand, South Africa. *Canadian Mineralogist*, **28**, 77-86.
- Nash, C.R. 1971. *Metamorphic petrology of the SJ area, Swakopmund District, South West Africa*. Unpublished M.Sc. thesis, University of Cape Town, 77 pp.
- Navachab Gold Mine Field Guide, 1989. Prepared for the Geological Society of Namibia by Erongo Mining and Exploration Company.
- Neary, C.R. and Highley, D.E. 1984. The economic importance of the rare earth elements, 423-466. In: Henderson, P., Ed., *Rare earth element geochemistry*. Elsevier, Amsterdam, 510 pp.
- Newberry, R.J. 1979. Systematics in W-Mo-Cu skarn formation in the Sierra Nevada: An overview (abstract). *Geological Society of America, Abstracts with Programs*, **11**, 486.
- Newberry, R.J. 1982. Tungsten-bearing skarns of the Sierra Nevada. I. The Pine Creek Mine, California. *Economic Geology*, **77**, 823-844.

- Nockolds, S.R. and Allen, R. 1953. The geochemistry of some igneous rock series. I., Calc-alkali igneous trends. *Geochimica et Cosmochimica Acta*, **4**, 105-142.
- Nokleberg, W.J. 1981. Geologic setting, petrology and geochemistry of zoned tungsten-bearing skarns at the Strawberry mine, Central Sierra Nevada, California. *Economic Geology*, **76**, 111-133.
- Norrish, K. and Hutton, J.T. 1969. An accurate X-ray spectrographic method for the analysis of a wide range of geological samples. *Geochimica et Cosmochimica Acta*, **33**, 431-453.
- O'Driscoll, E.S.T. 1986. Observations of the lineament-ore relation. *Philosophical Transactions of the Royal Society of London*, **A 317**, 195-218.
- Palmer, M.R. and Slack, J.F. 1989. Boron isotopic composition of tourmaline from massive sulfide deposits and tourmalinites. *Contributions to Mineralogy and Petrology*, **103**, 434-451.
- Pattison, D.R.M. 1989. P-T conditions and the influence of graphite on pelitic phase relations in the Ballachulish Aureole, Scotland. *Journal of Petrology*, **30**, 1219-1244.
- Pattison, D.R.M. and Harte, B. 1985. A petrogenetic grid for pelites in the Ballachulish and other Scottish thermal aureoles. *Journal of the Geological Society of London*, **142**, 7-28.
- Pearce, J.A., Harris, N.B.W. and Tindle, A.G. 1984. Trace element discrimination diagrams for the tectonic interpretation of granitic rocks. *Journal of Petrology*, **25**, 4, 956-983.
- Pettijohn, F.J., Potter, P.E. and Siever, R. 1972. *Sand and sandstone*. New York, Springer Verlag, 306 pp.
- Phillips, G.N. and Groves, D.J. 1983. The nature of Archean gold-bearing fluids as deduced from gold deposits of Western Australia. *Journal of the Geological Society of Australia*, **30**, 25-39.
- Phillips, G.N., Groves, D.I. and Brown, I.S. 1987. Source requirements for the Golden Mile; Kalgoorlie: significance to the metamorphic replacement model for Archean gold deposits. *Canadian Journal of Earth Science*, **24**, 1643-1651.
- Pichavant, M. 1981. An experimental study of the effect of boron on a water-saturated haplogranite at 1 kbar pressure: geological applications. *Contributions to Mineralogy and Petrology*, **76**, 430-439.
- Pichavant, M. and Manning, D. 1984. Petrogenesis of tourmaline granites and topaz granites; the contribution of experimental data. *Physics of the Earth and Planetary Interiors*, **35**, 31-50.
- Pineau, F., Latouche, L. and Javoy, M. 1976. L'origine du graphite et les fractionnements isotopiques du carbone dans les marbres métamorphiques des Gours Oumelalen (Ahaggar, Algérie), des Adirondacks (New Jersey, U.S.A.) et du Damara (Namibie, Sud-Ouest africain). *Bulletin de Societe de Geologique de France*, **XVIII**, 1713-1723.
- Pirajno, F. 1990. Geology, geochemistry and mineralisation of the Erongo Volcanic Complex, Namibia. *South African Journal of Geology*, **93(3)**, 485-504.
- Pirajno, F. and Schlögl, H.U. 1987. The alteration-mineralisation of the Krantzberg tungsten deposit, South West Africa/Namibia. *South African Journal of Geology*, **90**, 499-508.
- Pirajno, F. and Jacob, J. 1991. Gold mineralisation in the intracontinental branch of the Damara Orogen, Namibia: a preliminary survey. *Journal of African Earth Sciences*, **13**, 305-311.
- Pirajno, F., Petzel, V.F.W., and Jacob, R.E. 1988. Geology and alteration-mineralisation of the Brandberg West Sn-W deposit, Damara Orogen. *South African Journal of Geology*, **90 (3)**, 256-269.
- Pirajno, F., Jacob, R.E. and Petzel, V.F.W. 1990a. Marble-hosted sulphide and gold mineralisation at Onguati-Brown Mountain, southern central zone of the Damara Orogen, Namibia. *23<sup>rd</sup> Earth Science Congress of the Geological Society of South Africa*, 443-446.
- Pirajno, F., Roesner, H. and Petzel, V.F.W. 1990b. The volcanic history of the Paresis igneous complex. *23<sup>rd</sup> Earth Science Congress of the Geological Society of South Africa*, 447-450.
- Pirajno, F., Jacob, R.E. and Petzel, V.F.W. 1991. Distal skarn-type mineralisation in the Central Zone of the Damara Orogen, Namibia, 95-100: In: Ladeira, E.A., Ed., *Proceedings of Brazil Gold '91, An International Symposium on the Geology of Gold: Belo Horizonte*, 1991. Balkema, Ratterdarn, Holland 823 pp.
- Plant, J.A., Breward, N., Forrest, M.D. and Smith, R.T. 1989. The gold pathfinder elements As, Sb and Bi - their distribution and significance in the southwest Highlands of Scotland. *Transactions of the Institute of Mining and Metallurgy*, **98**, B91-101.
- Plimer, I.R. 1980. Exhalative Sn and W deposits associated with mafic volcanism as precursors to Sn and W deposits associated with granites. *Mineralium Deposita*, **15**, 275-289.
- Plimer, I.R. 1983. *The association of B- and F- rich rocks with stratiform mineralisation*. Course notes, Department of Geology, University of Witwatersrand.
- Plimer, I.R. 1986. Tourmalinites from the Golden Dyke Dome, Northern Australia. *Mineralium Deposita*, **21**, 263-270.
- Plimer, I.R. 1988. Tourmalinites associated with Australian submarine exhalative ores, 255-283. In: Friedrich, G.H., Herzig, P.M., Eds., *Base Metal Sulphide Deposits in Sedimentary and Volcanic Environments*. Springer Verlag, Berlin, 290 pp.
- Plimer, I.R. and Elliot, S.M. 1979. The use of Rb/Sr ratios as a guide to mineralisation. *Journal of Geochemical Exploration*, **12**, 21-34.
- Puhan, D. 1976. Metamorphic temperature determined by means of the dolomite-calcite solvus geothermometer - examples from the Central Damara Orogen (South West Africa). *Contributions to Mineralogy and Petrology*, **58**, 23-28.
- Puhan, D. 1979. *Petrologische und geothermometrische Untersuchung an silikatförmigen Dolomit-Caldt Marmoren zur Ermittlung der Metamorphosebedingungen im zentralen Damara-Orogen (Südwest-Afrika)*. Habilitationsschrift. University of Göttingen, 76 pp.
- Puhan, D. 1983. Temperature and pressure of metamorphism in the Central Damara Orogen. *Special Publication of the Geological Society of South Africa*, **11**, 219-224.
- Pulz, G.M., Michel, D., Jost, H. and Giuliani, G. 1991. The Archean Maria Lazara gold deposit, Goias, Brazil: An example of Au-Bi-Te-S metallogeny related to shear zones intruded by synkinematic granitoids, 385-387. In: Ladeira, E.A., Ed., *Proceedings of Brazil Gold '91 An International Symposium on the Geology of Gold: Belo Horizonte*, 1991. Balkema, Rotterdam, Holland 823 pp.
- Ramdohr, P. 1938. Die Khan-Grube bei Arandis, Südwestafrika. *Zeitschrift für Praktische Geologie*, **46**, 41-50.
- Ramdohr, P. 1969. *The ore minerals and their intergrowths* (Second Edition, Two Volumes). Pergamon Press, Oxford
- Ramsay, J.G. 1967. *Folding and Fracturing of Rocks*. McGraw-Hill Book Company, London, 568 pp.
- Reuning, E. 1937. Die Goldfelder von Ondundo, Südwestafrika. *Geologische Rundschau*, **28 (3-4)**, 229-239.
- Richards, J.P., Chappell, B.W., McCulloch, M.T. and McDougall, I. 1991. The Porgera gold deposit, Papua New Guinea, I: Association with alkalic magmatism in a continent-island-arc col-

- lision zone, 307- 312. In: Ladeira, E.A., Ed., *Proceedings of Brazil Gold '91 An International Symposium on the Geology of Gold: Belo Horizonte*, 1991. Balkema, Rotterdam, Holland 823 pp.
- Richards, T.E. 1986. Geological characteristics of rare-metal pegmatites of the Uis type in the Damara Orogen, South West Africa/Namibia, 1845-1862. In: Anhaeusser, C.R. and Maske, S., Eds., *Mineral Deposits of Southern Africa, II*. Geological Society of South Africa, 2335 pp.
- Rock, N.M.S., Groves, D.I., Perring, C.S. and Golding, S.D. 1989. Gold, lamprophyres, and porphyries: what does their association mean?, 609-625. In: Keays, R.R., Ramsay, W.R.H. and Groves, D.I., 1989, Eds., *The Geology of Gold Deposits: The perspective in 1988*. Economic Geology Monograph 6, Economic Geology Publishing Company, New Haven, 667 pp.
- Roering, C. 1963. *Pegmatite investigations in the Karibib District, South West Africa*. Unpublished Ph.D. thesis, University of the Witwatersrand, 130 pp.
- Roering, C. 1966. Aspects of the genesis and crystallisation sequence of the Karibib pegmatites, South West Africa. *Economic Geology*, **61**(6), 1064-1089.
- Roering, C. and Gevers, T.W. 1964. Lithium and beryllium bearing pegmatites in the Karibib District, South West Africa, 463-496. In: Haughton, S.H., Ed., *Some Ore Deposits in Southern Africa*. Geological Society of South Africa, Johannesburg.
- Rose, A.W., Hawkes, H.E. and Webb, J.S. 1979. *Geochemistry in Mineral Exploration*. Academic Press, London, 657 pp.
- SACS (South African Committee for Stratigraphy), 1980, Stratigraphy of South Africa. Part I (Comp. L.E. Kent). Lithostratigraphy of the Republic of South Africa, South West Africa/Namibia, and the Republics of Bophuthatswana, Transkei and Venda. *Handbook of the Geological Survey of South Africa*, No. 8.
- Salje, E. 1986. Heat capacities and entropies of andalusite and sillimanite: The influence of fibrolitisation on the phase diagram of the  $Al_2SiO_5$  polymorphs. *American Mineralogist*, **71**, 1366-1371.
- Sawyer, E.W. 1981. Damaran structural and metamorphic geology of an area south-east of Walvis Bay, S.W.A./Namibia. *Memoir of the Geological Survey of South-West Africa*, **7**, 94 pp.
- Schermerhorn, L.I.G. 1974. Late Precambrian mixtites: glacial and/or nonglacial? *American Journal of Science*, **274**, 673-824.
- Scott, K.M. 1990. Origin of alunite- and jarosite-group minerals in the Mt. Leyshon epithermal gold deposit, northeast Queensland, Australia. *American Mineralogist*, **75**, 1176-1181.
- Shand, S.J. 1943. *Eruptive rocks*. George Allen and Unwin, London, 444 pp.
- Shearer, C.K., Papike, J.J. and Simon, S.B. 1984. Pegmatite/wall-rock interactions, Black Hills, South Dakota: Progressive boron metasomatism adjacent to the Tip Top pegmatite. *Geochimica et Cosmochimica Acta*, **48**, 2563-2579.
- Siems, P.L. 1984. *Hydrothermal alteration for mineral exploration workshop*. University of Witwatersrand, 528 pp.
- Sillitoe, R.H. 1989. Golddeposits in western Pacific island arcs, 274-291. In: Keays, R.R., Ramsay, W.R.H. and Groves, D.I., 1989, Eds., *The Geology of Gold Deposits: The perspective in 1988*. Economic Geology Monograph 6, Economic Geology Publishing Company, New Haven, 667 pp.
- Sillitoe, R.H. and Bonham, H.F. 1990. Sediment-hosted gold deposits: Distal products of magmatic-hydrothermal systems. *Geology*, **18**, 157-161.
- Slack, J.F. 1982. Tourmaline in Appalachian-Caledonian massive sulphide deposits and its exploration significance. *Transactions of the Institute for Mining and Metallurgy*, **91** (B), 881-89.
- Slack, J.F., Herriman, N., Barnes, R.G. and Plimer, I.R. 1984. Stratiform tourmalinites in metamorphic terranes and their geologic significance. *Geology*, **12**, 713-716.
- Smith, D.A.M. 1965. The geology of the area around the Khan and Swakop Rivers in S.W.A. *Memoir of the Geological Survey of South Africa, South West Africa Series*, **3**, 113 pp.
- Spry, A. 1969. *Metamorphic textures*. Pergamon Press, Oxford.
- Stacey, J.S. and Kramers, J.D. 1975. Approximation of terrestrial lead isotope evolution by a two-stage model. *Earth and Planetary Science Letters*, **26**, 207-221.
- Stanistreet, I.G., Kukla, P.A. and Henry, G. 1991. Sedimentary basinal responses to a Late Precambrian Wilson Cycle: the Damara Orogen and Nama Foreland, Namibia. *Journal of African Earth Sciences*, **13**, 141-156.
- Steven, N.M. 1987. *Tungsten mineralisation at the Otjua Prospect: A geological and geochemical investigation*. Unpublished M.Sc. thesis, University of Cape Town, 152 pp.
- Steven, N.M. 1988. *Intermediate report on grant M46/3/1614: Exploration conducted on thefms Sandamap Noord 115, Sandamap 64 and Eureka 99, central Namibia*. Goldfields Namibia.
- Steven, N.M. 1991. Turbidite-hosted gold mineralisation at the Sandamap Noord prospect, central Namibia, 567-574. In: Ladeira, E.A., Ed., *Proceedings of Brazil Gold '91, An International Symposium on the Geology of Gold: Belo Horizonte, 1991*. Balkema, Rotterdam, Holland 823 pp.
- Steven, N.M. 1992. *A study of epigenetic mineralisation in the Central Zone of the Damara Orogen, Namibia with special reference to gold, tungsten, tin and rare earth elements*. Unpublished Ph.D. thesis, University of Cape Town, 221 pp.
- Steven, N.M. and Badenhorst, F.P. 1988. *Field Guide to the Otjua Tungsten Prospect and the Okawayo Stratigraphic Section*. Unpublished Report of the Geological Survey of Namibia.
- Steven, N.M. and Kuyper, J.L. 1985. Reconnaissance geological map of the western peripheral area (1:100,000; B and O - Rössing Uranium Joint Venture)
- Steven, N.M., Armstrong, R.A. and Moore, J.M. 1992. New Rb-Sr data from the Central Zone of the Damara Orogen, Namibia. *Communications of the Geological Survey of Namibia*, in press.
- Stewart, D.B. 1978. Petrogenesis of lithium-rich pegmatites. *American Mineralogist*, **63**, 970-980.
- Streckeisen, A. 1976. *To each plutonic rock its proper name*. *Earth Science Reviews*, **12**, 1-33.
- Sweeney, R.I. 1988. *Geochemistry of the Sabie River Basalt Formation in the central Lebombo. Karoo Igneous Province*. Unpublished Ph.D. thesis, University of Cape Town.
- Symmes, G.H. and Ferry, J.M. 1991. Evidence from mineral assemblages for infiltration of pelitic schists by aqueous fluids during metamorphism. *Contributions to Mineralogy and Petrology*, **108**, 419-438.
- Talbot, C.J. 1977. Inclined and asymmetric upward-moving gravity structures. *Tectonophysics*, **42**, 159-181.
- Taylor, B.E. and Slack, J.F. 1984. Tourmaline from Appalachian-Caledonian massive sulphide deposits: textural, chemical and isotopic relationships. *Economic Geology*, **79**, 1703-1726.
- Taylor, H.P. 1977. Water/rock interactions and the origin of  $H_2O$  in granitic batholiths. *Journal of the Geological Society of London*, **133**, 509-558.
- Thompson, J.B. 1957. The graphical analysis of mineral assemblages in pelitic schists. *American Mineralogist*, **42**, 842-858.

- Thompson, J.B. 1959. Local equilibrium in metasomatic processes, 437- 457. In: Abelson, P.H., Ed., *Researches in Geochemistry*. John Wiley and Sons, New York.
- Titley, S.R. and Beane, R.E. 1981. Porphyry copper deposits: part I. Geologic settings, petrology and tectogenesis. *Economic Geology - 75<sup>th</sup> Anniversary Volume*, 214-235.
- Turekian K.K. and Wedepohl, K.H. 1961. Distribution of the elements in some major units of the earth's crust. *Bulletin of the Geological Society of America*, **72**, 175-192.
- Valley, J.W. and O'Neil, J.R. 1981. <sup>13</sup>C/<sup>12</sup>C exchange between calcite and graphite: a possible thermometer in Grenville marbles. *Geochimica et Cosmochimica Acta*, **45**, 411-419.
- Van Loon. 1984. Accurate determination of the noble metals I: Sample decomposition and methods of separation. *Trends in Analytical Chemistry*, **3**, 10, 272-275.
- Vernon, R.H. 1987. Growth and concentration of fibrous sillimanite related to heterogenous deformation in K-feldspar-sillimanite metapelites. *Journal of Metamorphic Geology*, **5**, 51-68.
- Verwoerd, W.J. 1967. The carbonatites of South Africa and South West Africa. *Handbook 6, Geological Survey of South Africa*.
- Vidale, R. 1969. Metasomatism in a chemical gradient and the formation of calc-silicate bands. *American Journal of Science*, **267**, 857-874.
- Von Knorring, O.V. 1962. On the mineralogy of pegmatites in the Karibib and Usakos area of South West Africa. *Sixth Annual Report of the Research Institute for African Geology, University of Leeds*, 9-10.
- Von Knorring, O.V. 1963. Report on mineralogical research. *Seventh Annual Report of the Research Institute for African Geology, University of Leeds*, 33-37.
- Von Knorring, O.V. 1964. Report on mineralogical Research. *Eighth Annual Report of the Research Institute for African Geology, University of Leeds*, 11-13.
- Von Knorring, O.V. 1967. Pegmatite mineral studies. *Eleventh Annual Report of the Research Institute for African Geology, University of Leeds*, 36-37.
- Von Knorring, O.V. 1971. Notes on minerals from the Karibib area in South West Africa. *Fifteenth Annual Report of the Research Institute for African Geology, University of Leeds*, 63.
- Von Knorring, O.V. 1972. On the occurrence of bismuth minerals in some African pegmatites. *Sixteenth Annual Report of the Research Institute for African Geology, University of Leeds*, 53-55.
- Von Knorring, O.V. 1975. Bismuth mineralisation in some African pegmatites. *Nineteenth Annual Report of the Research Institute for African Geology, University of Leeds*, 19-21.
- Von Knorring, O.V. 1985. Some mineralogical, geochemical and economic aspects of lithium pegmatites from the Karibib-Cape Cross pegmatite field in South West Africa/Namibia. *Communications of the Geological Survey of S.W.A./Namibia*, **1**, 79-84.
- Von Knorring, O. and Clifford, T.N. 1960. On a skarn monazite occurrence from the Namib desert near Usakos, S.W.A. *Mineralogical Magazine*, **32**, 650-653.
- Von Knorring, O.V., Sahama, T.H. and Rehtijarvi, P. 1973. Karibibite, a new FeAs mineral from South West Africa. *Lithos*, **6**, 265-272.
- Wagener, G.E. 1989. Systematic variation in the tin content of pegmatites in western central Namibia. *Journal of Geochemical Exploration*, **34**, 1-19.
- Walraven, F.C. 1988. Geology and alteration-mineralisation in the Gamigab area, north of Brandberg. *Communications of the Geological Survey of Namibia*, **4**, 83-88.
- Watson, E.B. and Capobiano, C.J. 1981. Phosphorus and the rare earth elements in felsic magmas: an assessment of the role of apatite. *Geochimica et Cosmochimica Acta*, **45**, 2349-2358.
- Watson, N.I. 1982. *Unpublished report on the geology of area 2115C*. Geological Survey of S.W.A.
- Weber, K., Ahrendt, H. and Hunziker, J.C. 1983. Geodynamic aspects of structural and radiometric investigations on the northern and southern margins of the Damara Orogen, South West Africa/Namibia. *Special Publication of the Geological Society of South Africa*, **11**, 307-320.
- Wedepohl, K.H., Ed. 1978. *Handbook of geochemistry*. Springer Verlag.
- Werdning, G. and Schreyer, W. 1984. Alkali-free tourmaline in the system MgO-Al<sub>2</sub>O<sub>3</sub>-B<sub>2</sub>O<sub>3</sub>-SiO<sub>2</sub>-H<sub>2</sub>O. *Geochimica et Cosmochimica Acta*, **48**, 1331-1344.
- White, W.H., Bookstrom, A.A., Kamilli, R.J., Ganster, M.W., Smith, R.P., Ranta, D.E. and Steininger, R.C. 1981. Character and origin of Climax-type molybdenum deposits. *Economic Geology 75<sup>th</sup> Anniversary Volume*, 270-316.
- Wickham, S.M. 1987. The segregation and emplacement of granitic magmas. *Journal of the Geological Society of London*, **144**, 281-297.
- Wickham, S.M. and Oxburgh, E.R. 1985. Continental rifts as a setting for regional metamorphism. *Nature*, **318**, 330-333.
- Willis, J.P., Ahrens, L.H., Danchin, R.V., Erlank, A.J., Gurney, J.J., Hofmeyr, P.K., McCarthy, T.S. and Orren, M.J. 1971. Some interelement relationships between lunar rocks and fines and stoney meteorites. In: *Proceedings of the Second Lunar Scientific Conference*, 1123-1138.
- Willis, J.P., Erlank, A.J., Gurney, J.J., Theil, R.H. and Ahrens, L.H. 1972. Major, minor and trace element data for some Apollo II, 12, 14 and 15 samples. In: *Proceedings of the Third Lunar Scientific Conference*, 1269-1273.
- Wilson, M. 1989. *Igneous Petrogenesis*. Unwin Hyman Ltd. London, 466 pp.
- Winkler, H.G.E. 1976. *Petrogenesis of metamorphic rocks*. Springer Verlag, New York, 334 pp.
- Wood, D.A., Gibson, I.L. and Thompson, R.N. 1976. Elemental mobility during zeolite facies metamorphism of the Tertiary basalts of eastern Iceland. *Contributions to Mineralogy and Petrology*, **55**, 241-254.
- Woodall, R. 1979. *Gold - Australia and the World*. Nedland, University of Western Australia Geology Department, University Extension Publication, 3,1-34.
- Woodcock, N.H. and Fischer M. 1986. Strike-slip duplexes. *Journal of Structural Geology*, **8**, 725-735.
- Wyllie, P.J. and Tuttle, O.F. 1964. Experimental investigation of silicate systems containing two volatile components; Part III: The effects of SO<sub>3</sub>, P<sub>2</sub>O<sub>5</sub>, HCl and Li<sub>2</sub>O, in addition to H<sub>2</sub>O, on the melting temperatures of albite and granite. *American Journal of Science*, **262**, 930.
- Yardley, B.W.D. 1989. *An introduction to metamorphic petrology*. Longman Scientific and Technical, Singapore, 248 pp.
- Zen, E-an 1986. Aluminium enrichment in silicate melts by fractional crystallisation: some mineralogic and petrographic constraints. *Journal of Petrology*, **27**, 1095-1117.
- Zen, E-an 1988. Phase relations of peraluminous granitic rocks and their petrogenetic implications. *Annual Review of Earth and Planetary Science*, **16**, 21-51.
- Zwart, H.J. 1962. On the determination of polymetamorphic mineral associations, and its application to the Bosost Area (Central Pyrenees). *Geologische Rundschau*, **52**, 38-65.

## APPENDIX: ANALYTICAL METHODS

### 1. Whole-rock geochemical data

#### 1.1 General

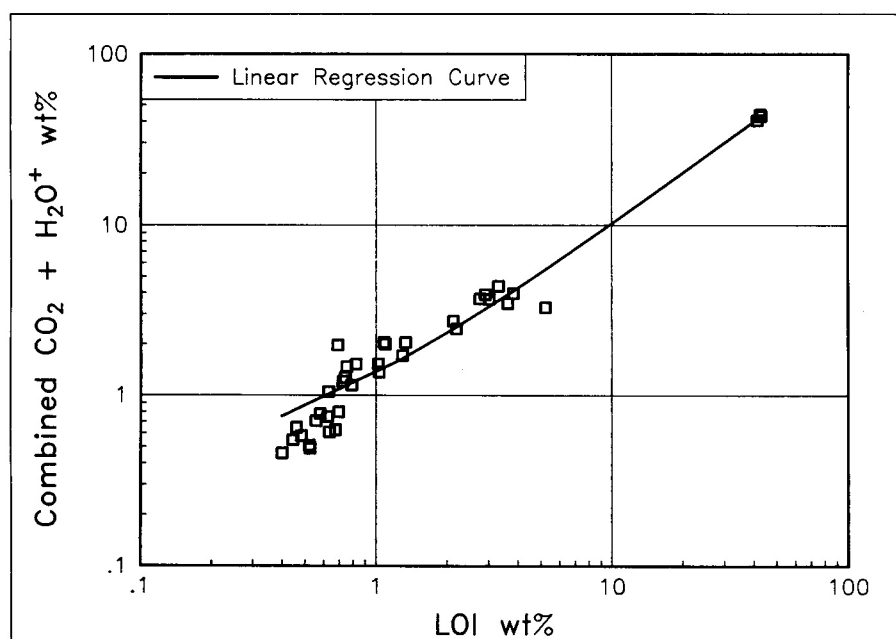
Samples were analysed by X-ray fluorescence spectrometry (XRF) in the Department of Geochemistry, University of Cape Town (UCT). Operating conditions have been described by Willis *et al.* (1971 and 1972; see also Course Notes on XRF Spectrometry, Dept. of Geochemistry, 1989 edition). Certain elements were analysed by commercial laboratories (see below).

#### 1.2 Preparation of samples

Five-kilogram samples were collected in the field or from drillcore. All weathered or oxidised surfaces were removed in the field or, in the case of siliceous samples, by sawing. Sawn surfaces were lapped with corundum grit to remove impurities that had been smeared onto the samples by the diamond saw blade. Samples were then split, crushed and milled to -300 mesh in a carbon steel vessel. Three 'runs' of cleaning quartz were milled between samples to ensure that the vessel was clean. The vessel was then precontaminated with 60 g of sample.

#### 1.3 Water and carbon dioxide determinations

Samples were placed in platinum crucibles, weighed, heated in the oven at 110°C overnight and reweighed to determine H<sub>2</sub>O-. Samples were then roasted at 850°C (carbonate rocks at 1000°C) overnight and reweighed to determine the Loss on Ignition (LOI). The LOI was not determined on those samples known to contain high concentrations of fluorine, boron, sulphur (either in the form of sulphide or sulphate) and arsenic because of the possibility of causing contamination of the furnaces. H<sub>2</sub>O-, H<sub>2</sub>O+, SO<sub>3</sub> and CO<sub>2</sub> determinations were subsequently conducted by infrared spectroscopy on all samples by the Geological Survey, Pretoria. In this technique, SO<sub>3</sub> and CO<sub>2</sub> were determined with a LECO CS244 analyser while H<sub>2</sub>O- and H<sub>2</sub>O+ were measured with a LECO RM100 analyser. Good agreement was obtained for those samples for which the LOI and combined CO<sub>2</sub> and H<sub>2</sub>O+ contents had been independently measured (Appendix Fig. 1).



Appendix Figure 1: Combined CO<sub>2</sub> + H<sub>2</sub>O<sup>+</sup> (GS) vs LOI (UCT)

#### 1.4 The analysis of boron

Boron concentrations were determined by Inductively Coupled Plasma-Optical Emission Spectroscopy (ICP-OES) in the Department of Analytical Chemistry, UCT. Dried samples were dissolved in HNO<sub>3</sub> and HF in teflon containers. These containers were heated at 130°C to facilitate sample digestion. Samples were then read at the appropriate wavelength on the ICP-OES. The final result is the mean of duplicate samples. Boron is recorded as wt% B<sub>2</sub>O<sub>3</sub>.

#### 1.5 The analysis of fluorine

Because of the high costs involved in analysing fluorine by the Specific Ion Electrode method (S.I.E.), concentrations of the element were determined by XRF. Those samples containing high concentrations of fluorine (NS207-NS212, NS225-231, OT102-108) were reanalysed by S.I.E. after alkaline fusion by Scientific Services Pty. For the abovementioned samples the S.I.E. value is quoted because it is considered to be more accurate.

#### 1.6 The analysis of sulphur

Sulphur was analysed by infra-red spectroscopy at the Geological Survey, Pretoria. Those samples containing high sulphur contents were examined microscopically to determine in what phase the element was located. Sulphur contents are reported as S except for the sulphate-rich samples where the element is reported as wt% SO<sub>3</sub> (Table 7/5.2).

#### 1.7 FeO determinations

FeO was determined by the normal redox titration method at the Geological Survey, Pretoria.

#### 1.8 Pellet preparation for XRF analysis

Pressed pellet briquettes were prepared using the method of Baird (1961).

#### 1.9 Wavelength scanning

Prior to quantitative analysis, all samples from mineralised areas and associated alteration zones were scanned on a Siemens SRS 303 X-ray spectrometer between 0.387Å and 2.103Å.

#### 1.10 Major element analysis

All major elements, except B, F, Na, As, La, Ce, Nd and Sr, were determined using the lithium tetraborate fusion methods of Norrish and Hutton (1969). Sodium was analysed by XRF using pressed powder briquettes prepared using the method of Baird (1961). The As concentrations in the auriferous gossan from Sandamap Noord and the rare earth contents in sample NS329 from Eureka were determined by Scientific Services Pty. MINTEK standards that covered the appropriate concentration ranges were used. The strontium concentrations in samples NS329, NS346 and NS347 were determined on pressed powder briquettes.

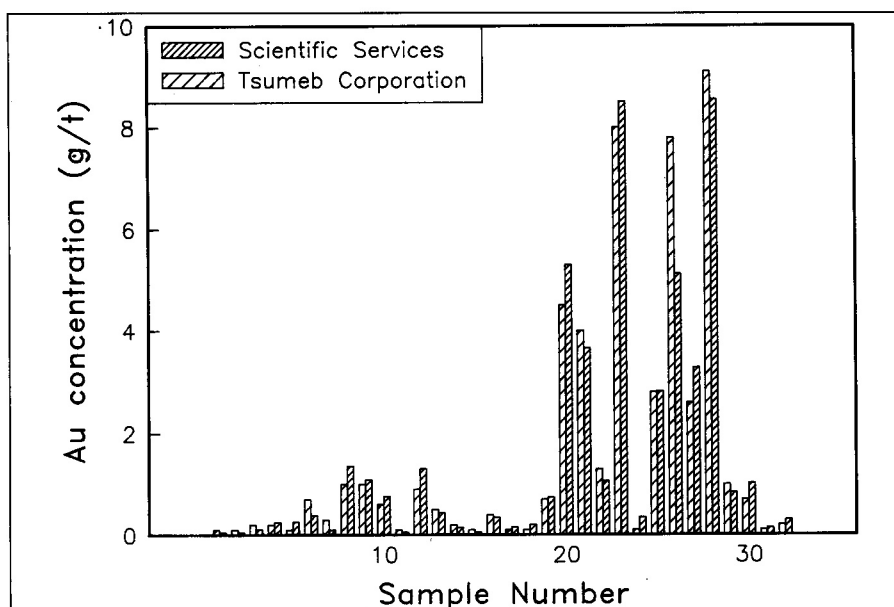
#### 1.11 The analysis of trace elements

Trace elements were analysed using the command programs commonly used in the Department of Geochemistry at UCT.

#### 1.12 Mass absorption coefficients (MACs) and trace element reduction

For those rocks containing only trace concentrations of economic elements, the MACs used in the reduction of trace element data were as follows: for those elements with analyte wavelengths shorter than the Fe K-absorption edge, matrix effects were corrected using MACs that had been determined from the intensity of the Rh K<sub>α</sub> Compton peak from a Rh anode X-ray tube and calculated at the Mo K<sub>α</sub> wavelength. For those elements with analyte wavelengths on the long wavelength side of the Fe K-absorption edge, MACs were calculated from the major element compositions using Heinrich's (1966) values for elemental MACs.

For those samples containing arsenic, strontium, tungsten and rare earth concentrations in excess of 0.2 wt%, MACs were also calculated at the W L<sub>β</sub> wavelength. This was because of the presence of the respective major



Appendix Figure 2: Sandamap Noord fire assay results laboratory comparison

element absorption edge between the Compton peak wavelength and the wavelength of some of the analyte lines of the trace elements. For example, in the case of samples containing major concentrations of arsenic, the analyte lines of Pb, Se, Bi, Ge, Ga, Zn, Cu, Ni and W lie on the long wavelength side of the arsenic absorption edge and were reduced with MACs calculated at W  $L_{\beta}$ . Elements with analyte lines on the short wavelength of the arsenic absorption edge, e.g. Rb, Sr, Y, etc were reduced with MACs calculated at Mo  $K_{\alpha}$  in the normal manner.

### 1.13 The analysis of the monazite carbonate rock from Eureka

Considerable attention was paid to the sample of monazite skarn. A wavelength scan was completed on sample NS329 on a Philips PW1500 X-ray spectrometer using a Cr tube run at 60kV and 45mA and a LIF220 detector crystal between  $10^{\circ}$  and  $86^{\circ} 2\theta$ . The presence of minor concentrations (i.e., several hundred ppm) of Pr and Sm, and possibly Gd, is indicated. Of interest is the absence of uranium and zirconium in this sample. Von Knorring and Clifford (1960) recorded traces of Zr in the monazite from this locality. It is possible that they mistook the Sr  $K_{\beta}$  line for the Zr  $K_{\alpha}$  line. Wavelength scans were conducted on NS329 on a Siemens SRS 303 X-ray spectrometer between  $0.387\text{\AA}$  and  $2.103\text{\AA}$ . These results confirm the light rare earth enriched nature of the monazite skarn, and its relatively low thoria contents and very low yttrium, zirconium and uranium concentrations (cf the monazites listed in Deer, Howie and Zussman, 1962, 342-343). La, Ce and Nd concentrations were determined on pressed powder briquettes by Scientific Services Pty using MINTEK standards. Trace element concentrations were determined in the normal manner in the Department of Geochemistry, UCT.

### 1.14 The analysis of gold

In the early stages of the project, when areas needed to be identified for more detailed work, gold was analysed by the Atomic Absorption Spectrometry Scan (AAS Scan) method by Scientific Services Pty (see Mawson, 1984, for a review of the techniques used for analysing for gold in southern Africa). Scientific Services Pty claimed a LLD of 30 ppb Au for these analyses. This modified AA technique (Aqua Regia leach followed by DIBK Extraction prior to AA determination) for the analysis of gold concentrations of up to 2000 ppb Au in rocks worked well (see Van Loon, 1984, p.275, for a description of the technique). Samples containing in excess of 300 ppb Au were reanalysed by fire assay by Scientific Services Pty and some samples were checked by McLachlan and Lazar CC. Scientific Services Pty claimed a LLD of 50 ppb Au for their fire assay results. Thirty-two samples containing gold mineralisation from Sandamap Noord were submitted to Scientific Services Pty and Tsumeb Corporation for an inter-laboratory comparison. Excellent agreement was obtained (Appendix Fig. 2).

Those samples for which major and trace element data were obtained were subsequently analysed for gold by atomic absorption spectrometry (AAS) by the author at the Geological Survey, Pretoria. Samples were selected

from localities proximal to known epigenetic base and precious metal mineralisation. 10 g samples were roasted to remove sulphur and organic matter and then decomposed with hydrobromic acid, containing bromine. The gold was extracted into a solution of a quaternary ammonium salt in DIBK and gold concentrations were determined by AAS. The Geological Survey claimed a LLD of 5 ppb Au, though 30 ppb seemed to be more realistic.

## 2. Mineral chemistry

Mineral grains were analysed using a Cameca electron microprobe in the Department of Geochemistry, UCT. The size of each polished section was approximately 2 cm by 3 cm. The operating conditions have been discussed by Sweeney (1988) and are summarised below.

### 2.1 Silicate minerals

Beam current: 40 nA

Accelerating voltage: 15 kV

Analysing crystals: LiF (200) for the elements Fe and Mn  
 PET for the elements Ca, K, Ti, Cr  
 TLAP for the elements Si, Al, Mg, Na

Detection: Flow counters with Ar/CH<sub>4</sub> gas mixture

Calibration standards: CHRO: Stillwater Chromite (Natural Standard)  
 DIOP: Pure Diopside Glass (Synthetic Standard)  
 FLUR: Fluorite (Natural Standard)  
 K-H: Kakanui Hornblende (Natural Standard)  
 K-P: Kakanui Pyrope (Natural Standard)  
 LACO: Labradorite (Natural Standard)  
 NUNI: Nunivak Anorthoclase (F-10, Natural Standard)  
 OR-1: Orthoclase (F-7, natural Standard)  
 RHOD: Rhodonite (Synthetic Standard)  
 RUT: Rutile (Synthetic Standard)

Standards used

Cordierite: K-P, RUT, RHOD  
 Garnet: K-P, RUT, CHRO, RHOD, K-H  
 Pyroxene: DIOP, K-P, CHRO, RUT, RHOD, K-H  
 Scapolite and Feldspar: K-P, RUT, RHOD, K-H, latterly NUNI, OR-1, LACO  
 Sphene: DIOP, RUT, K-P, CHRO, RHOD, K-H  
 Vesuvianite: K-P, RUT, CHRO, RHOD, K-H

Nominal concentrations were corrected using the methods of Bence and Albee (1968) and in certain cases by the ZAF program.

## 2.2 Sulphide and oxide minerals

Beam current: 40 nA

Accelerating voltage: 15-30 kV

Analysing crystals:

TLAP for the elements As, Se  
 PET for the elements S, Sb, Sn, Bi, Pb, Ag, Te, Mn  
 LiF (200) for the elements Fe, Cu, Zn, Au, Co, Ni

Detection: Flow counters with Ar/CH<sub>4</sub> gas mixture

Calibration standards:

RUT: Rutile (Synthetic Standard)  
 RHOD: Rhodonite (Synthetic Standard)  
 K-P: Kakanui Pyrope (Natural Standard)  
 CHRO: Stillwater Chromite (Natural Standard)  
 ILMT: Ilmenite (Natural Standard)  
 GAHN: Gahnite (Natural Standard)  
 CHAL: Chalcopyrite (Natural Standard)  
 SPHA: Sphalerite (Natural Standard)  
 SM-3: Troilite (Natural Standard)  
 As, Sn, Bi, Sb, Pb, Au, Ag, Te, Se, Co, Ni: Spec Pure metals from Johnson Mathey

Nominal concentrations were corrected using the ZAF program.

## 3. Radiogenic isotope work

### 3.1 Rb-Sr work

Whole-rock Sr isotope analyses were performed on 100-150 mg splits of powdered samples in the Department of Geochemistry, UCT. Following dissolution in HF/HNO<sub>3</sub>, Sr was separated and concentrated for mass spectrometric analysis using standard ion-exchange procedures. Samples were loaded on single Ta filaments with phosphoric acid and Sr isotope ratios were measured using triple-collector or quadruple-collector configurations (for isotope dilution analyses) in dynamic mode. The isotopic fractionation correction factor  $^{87}\text{Sr}/^{86}\text{Sr}=0.1194$  was used. During the course of this study, a mean  $^{87}\text{Sr}/^{86}\text{Sr}$  value of  $0.71026 \pm 2$  ( $2\sigma$ ) was obtained for the NBS standard SRM-987 ( $n=30$ ). Rb and Sr elemental concentrations were determined by XRF. For checking purposes, Rb and Sr concentrations were determined by isotope dilution on one sample (NST12-2): concentrations of 963 ppm Sr (968 ppm by XRF) and 1791 ppm Rb (1766 ppm by XRF) were recorded. This results in a difference of only 1.9% in the Rb/Sr ratio.

Isotope ratios were measured on a VG Sector multicollector mass spectrometer. Dates were calculated using the statistical package GEODATE (Version 2.2; Eglington and Harmer, 1991). Analytical errors of 1.5% and 0.005% were applied to the  $^{87}\text{Rb}/^{86}\text{Sr}$  and  $^{87}\text{Sr}/^{86}\text{Sr}$  values respectively. Errors in dates and  $(^{87}\text{Sr}/^{86}\text{Sr})_t$  ratios are reported at the 95% confidence level. The Rb decay constant value of  $1.42 \times 10^{-11} \text{y}^{-1}$  was used. The MSWD value was  $<2.5$  in all but one case, with isochron/errorchron definition based on F parameters assuming 20 replicates.

### 3.2 Pb-Pb work

Untarnished specimens of galena were dissolved in HCl. A small aliquot of the resulting solution was dried down and then re-dissolved in a drop of HNO<sub>3</sub> and diluted to 3 ml. The lead was purified by electrodeposition on a platinum electrode. The anode was stripped with a solution of HNO<sub>3</sub> and H<sub>2</sub>O<sub>2</sub>. The samples were loaded on single Re filaments with silica gel and phosphoric acid. Pb isotopes ratios were corrected for mass fractionation by normalising to values obtained by repeated analysis of the NBS common lead standard SRM-981. The bias-correction factors were 0.03% amu<sup>-1</sup>(<sup>206</sup>Pb/<sup>204</sup>Pb), 0.03% amu<sup>-1</sup>(<sup>207</sup>Pb/<sup>204</sup>Pb) and 0.04% amu<sup>-1</sup>(<sup>208</sup>Pb/<sup>204</sup>Pb) for the analysis period.